Chapter 14: Climate Phenomena and their Relevance for Future Regional Climate Change

Coordinating Lead Authors: Jens Hesselbjerg Christensen (Denmark), Krishna Kumar Kanikicharla (India)

Lead Authors: Edvin Aldrian (Indonesia), Soon-Il An (Korea), Iracema Fonseca Albuquerque Cavalcanti (Brazil), Manuel de Castro (Spain), Wenjie Dong (China), Prashant Goswami (India), Alex Hall (USA), Joseph Katongo Kanyanga (Zambia), Akio Kitoh (Japan), James Kossin (USA), Ngar-Cheung Lau (USA), James Renwick (New Zealand), David Stephenson (UK), Shang-Ping Xie (USA), Tianjun Zhou (China)

Contributing Authors: Tercio Ambrizzi, Bruce Anderson, Osamu Arakawa, Raymond Arritt, Mark Baldwin, Mathew Barlow, David Barriopedro, Michela Biasutti, Sebastien Biner, David Bromwich, Josephine Brown, Wenju Cai, Leila V. Carvalho, Ping Chang, Ole Bøssing Christensen, Clara Deser, Kerry Emanuel, Hirokazu Endo, David Enfield, Amato Evan, Belen Rodriguez de Fonseca, Alessandra Giannini, Annamalai Hariharasubramanian, Ashok Karumuri, Jack Katzfey, Erik Kjellström, Jeff Knight, Thomas Knutson, Ashwini Kulkarni, Ashok Karumuri, William K. Lau, Geert Lenderink, Chris Lennard, Renping Lin, Neil Mackellar, Victor Magnana, Gareth Marshall, Linda Mearns, Jerry Meehl, Claudio Menendez, Hiroyuki Murakami, David Neelin, Geert Jan van Oldenborgh, Martin Olesen, Jan Polcher, Yun Qian, Paulo Ruti, James Screen, Jan Sedlacek, Silvina Solman, Martin Stendel, Izuru Takayabu, John Turner, Caroline Ummenhofer, Kevin Walsh, Bin Wang, Chunzai Wang, Ian Watterson, Matthew Widlansky, Andrew Wittenberg, Tim Woollings, Sang-Wook Yeh, Chidong Zhang, Lixia Zhang, Xiaotong Zheng, Liwei Zou

Review Editors: John Fyfe (Canada), Won-Tae Kwon (Korea), Kevin Trenberth (USA), David Wratt (New Zealand)

Date of Draft: 5 October 2012

Notes: TSU Compiled Version

Table of Contents

Executive Summary

Regional climates emerge from the complex interaction of large-scale climate phenomena such as monsoons, tropical convergence zones, ENSO and other dominant modes of climate variability, and local physical processes. Climate phenomena therefore provide a useful scientific basis for the understanding and assessment of regional climate change. For example, past changes in regional climate are often interpreted in terms of changes in dominant modes of climate variability (see Chapters 2, 3, 4, 7 and 10). Large-scale climate phenomena are also increasingly well simulated by global climate models, and so provide a useful basis for evaluating regional processes in such models (see Chapter 9). Credibility in regional climate change projections is gained by the ability of climate models to represent relevant phenomena and the processes that drive them (see Chapter 9), and model agreement in future projections of the phenomena (see Chapters 11 and 12). These criteria form the scientific basis for this recent assessment of future changes in climate phenomena and regional climate, which is summarised below:

Future Changes in Climate Phenomena

Monsoon Systems [14.2]

There is *medium to high confidence* that global monsoon precipitation is *likely* to strengthen in the 21st century with increase in its area and intensity while the monsoon circulation weakens. In high emission scenarios, global monsoon area and global monsoon total precipitation are *very likely* to increase by the end of the 21st century. Monsoon onset dates are *likely* to be early or not to change much and the monsoon retreat dates are *very likely* to delay, resulting in lengthening of the monsoon season. There is *high confidence* in the assessment that future increase in precipitation extremes is *very likely* in the South Asian and the East Asian monsoon regions. Precipitation extremes are also *very likely* to increase in the North and South African monsoon regions as well as in the Australian monsoon region. There is *medium confidence* that interannual rainfall variability is *likely* to increase in the future and the relationship between monsoon and El Niño is also *likely* to strengthen. [14.2.1]

There is *medium to high confidence* that overall precipitation associated with the Asian-Australian monsoon system is *likely* to increase but with a north-south asymmetry: the Indian monsoon rainfall increases while the changes in the Australian summer monsoon rainfall are small. *Medium confidence* in that the Indian summer monsoon circulation weakens, but compensated by increased atmospheric moisture content *likely* leading to more rainfall. For the East Asian summer monsoon region, both monsoon circulation and rainfall will *likely* increase. It is *likely* that rainfall will increase due to enhanced monsoon circulation and increased water vapour, but there is *low confidence* in the spatial distribution of such rainfall change. There is *medium confidence* that over the Maritime continent monsoon the austral summer precipitation is *likely* to increase. There is *high confidence* that the Australian summer monsoon over the Java archipelago and northernmost Australia will very likely to be delayed and shortened while there is a *medium confidence* in the delay of monsoon over the interior of Australia. *Medium confidence* in that the Western North Pacific monsoon is *likely* to weaken, but compensating moisture effects will enhance precipitation. [14.2.2]

There is *low confidence* in projections of the American monsoon precipitation changes. It is *likely* that precipitation associated with the NAMS will arrive later in the annual cycle, and persist longer. Future changes in the timing and duration of the SAMS are also *likely*, but details of these changes remain uncertain. [14.2.3]

There is *medium confidence* that a small delay in the development of the West African mean rainy season is *likely*; but with an intensification of late-season rains. The limitations of model simulations in the region suggest a cautious approach towards future projections. [14.2.4]

Tropical Phenomena and Modes of Variability [14.3]

There is low to medium confidence that an increase in precipitation along the ITCZ and a decrease in precipitation in the subtropics are likely in the future. There is *medium confidence* in assessing that the frequency of zonally-oriented SPCZ events is *likely* to increase, with the SPCZ lying well to the northeast of its average position. There is *medium confidence* that rainfall change over tropical oceans is *likely to* follow a 'warmer-get-wetter' pattern, increasing where the SST warming exceeds the tropical mean and vice versa. There is *medium confidence* that SACZ is *likely* to shift southwards, leading to an increase in precipitation

over southeastern South America. A reduction of precipitation associated with the SACZ, or southward shifting of the precipitation band, in future projections is *likely*. [14.3.1]

There is low confidence in assessing the future changes in MJO due to the poor skill in simulating MJO and its sensitivity to SST warming patterns that are subject to large uncertainties in their future projection. [14.3.2]

There is *medium to high* confidence that the tropical Indian Ocean is *likely* to feature a zonal pattern with reduced (enhanced) warming and decreased (increased) rainfall in the east (west), a pattern especially pronounced during August to November. There is *high confidence* that the Indian Ocean dipole mode will *likely* remain active, with interannual variability unchanged in SST but decreasing in thermocline depth. [14.3.3]

The observed SST warming in the tropical Atlantic represents a reduction in spatial variations in climatology: the warming is weaker in north compared to south of the equator; and the equatorial cold tongue weakens both in the mean and interannual variability. There is *low confidence* in the projections over the tropical Atlantic - both for the mean and interannual modes, because of large errors in model simulations of current climate. [14.3.4]

El Nino-Southern Oscillation [14.4]

ENSO shows considerable inter-decadal modulations in amplitude and spatial pattern both in the instrumental record and in model simulations. There is *high confidence* that ENSO *very likely* remains as the dominant mode of interannual variability in the future. However, natural modulations of the variance and spatial pattern of ENSO are so large that it is *as likely as not* whether any projected change in the 21st century is attributable to changes in atmospheric composition. There is *high confidence* that both El Niño and La Niña-induced teleconnection patterns over the extra-tropical Northern Hemisphere are *likely* to move eastwards in the future. There are indications that the central Pacific type of El Niño will become more frequent in a warmer climate but the confidence is *low* because of large natural modulations of El Niño patterns.

Annular and Dipolar Modes of Variability [14.5]

There is *high confidence* that future boreal wintertime NAO is *very likely* to exhibit large natural variations and trends of similar magnitude to those observed in the past; is *very likely* to be differ quantitatively from individual climate model projections; is *likely* to become slightly more positive (on average) due to increases in greenhouse gases. There is high confidence that the austral summer/autumn positive trend in SAM is *very likely* to continue but is *likely* to weaken considerably as ozone depletion recovers through to the mid-21st century. There is *medium confidence* from recent studies that projected changes in NAO and SAM are sensitive to boundary processes, which are not yet well represented in many climate models currently used for projections e.g., stratosphere-troposphere interaction, ozone chemistry, solar forcing, and atmospheric response to Arctic sea ice loss.

Additional Phenomena of Relevance [14.6]

PNA – no future assessment available. [14.6.1]

There is *medium confidence* that the PSA pattern is *likely* to change due to tropical convection changes in the Pacific/Indonesia regions. The changes are *likely* to be in intensity and position of the anomalous centres and may affect precipitation over South America. [14.6.2]

Low to medium confidence that it is likely that the frequency of NH and SH blocking will decrease under increasing GHG concentrations, while trends in blocking intensity and persistence are uncertain. Future strengthening of the zonal wind and meridional jet displacements may partially account for the projected decrease in blocking frequency. [14.6.3]

There is low to medium confidence that TBO strengthens in the future but the internally generated decadal timescale variability complicates the interpretation of such future changes. [14.6.4]

On the basis of the recent literature, it is as likely as not that the QBO may weaken in future, and its period may increase slightly. [14.6.5]

Future changes in the PDO/IPO are uncertain and have not been investigated in any depth. It is presently *as likely as not* that the PDO/IPO will change its form or temporal behaviour in future. [14.6.6]

It is *unlikely* that the AMO will change its behaviour as the mean climate changes. However, natural fluctuations in the AMO over the coming few decades are *likely* to influence regional climates at least as strongly as will human-induced changes. [14.6.7]

Tropical Cyclones [Box 14.2]
The influence of climate change on tropical cyclones is *likely* to vary by region, but the specific characteristics of the changes are not yet well quantified. Data quality provides only *low confidence* in the detection of century-scale trends in tropical cyclone activity and their attribution to CO_2 forcing. However, there is *medium confidence* that shorter-term forcing by natural and anthropogenic aerosols have had a measurable effect on tropical cyclone activity in certain regions. Projections for the 21st century indicate that it is *likely* that the global frequency of tropical cyclones will either decrease or remain essentially unchanged, concurrent with a *likely* increase in both global mean tropical cyclone maximum wind speed and rainfall rates, but there is *lower confidence* in region-specific projections. The frequency of the most intense storms will *more likely than not* increase substantially in some basins.

Extra-tropical Cyclones [Box 14.3]
There is *high confidence* that the global number of extra-tropical cyclones is *unlikely* to decrease by more than a few percent due to global warming and that future changes in storms are *likely* to be small compared to natural interannual variability and substantial variations between model simulations of storms. There is *high confidence* that a small poleward shift is *likely* in the Southern Hemisphere storm track, but the magnitude is model-dependent. There is *medium confidence* that a poleward shift in the N. Pacific storm track is *more likely than not* and that it is *unlikely* that the response of the N. Atlantic storm track is a simple poleward shift. There is *low confidence* in the impact of storm track changes on regional climate at the surface especially for extreme events.

Future Changes in Regional Climate

Arctic
There is high confidence that future temperature evolution of Arctic climate on decadal time scales and longer will likely continue to be dominated by the signals of anthropogenic climate change. It is likely the pan-Arctic region will experience a statistically-significant increase in precipitation by mid-century. [14.7.2]

North America
There is high confidence that very likely the anthropogenic warming signal will be large compared to internal variability in all NA regions throughout the year by mid-century. There is medium confidence that it is likely that the northern half of NA will experience an increase in precipitation over the 21st century, while Mexico and Central America will experience a decrease. [14.7.3]

Central America and Caribbean
It is virtually certain that temperatures are very likely to increase in Central America and the Caribbean and likely that precipitation will decrease in most of the Central America and Caribbean regions. [14.7.4]

South America
It is very likely that the precipitation will increase in La Plata basin and northwestern coast of South America and will decrease in Northeastern Brazil, eastern Amazonia and Chile. There is medium confidence in extreme precipitation trends in Northeast, northern sector of Southeast and west coast of tropical South America. It is very likely that the temperature will increase in the whole continent, but the highest temperatures are projected in southern Amazonia. It is very likely that there is an increase of warm days and nights and reduction of cold days and nights in most regions of South America. It is likely that the heat waves become more frequent in Amazonia, Northeast and west coast of South America. [14.7.5]

Europe and Mediterranean

There is medium confidence in models ability to project regional temperature changes, particularly for a specific climate scenario. It is therefore virtually certain that temperatures will show a positive trend throughout the century over all of Europe and the Mediterranean region and will be enhanced with the intensity of the anthropogenic radiative forcing. It is very likely that winter temperature will rise more in NE than in CE or MD subregions, while in summer the warming will be more intense in MD and CE than in NE. The length, frequency, and/or intensity of warm spells or heat waves are assessed to be very likely to increase throughout the region. There is medium confidence in an annual increase in NE and CE, while a decrease is likely in MD during the summer half year. It is very likely that the frequency and intensity of winter precipitation will increase in the 21st century over NE and CE but there is a notably inconsistency and low confidence over the MD since changes depend on region and model considered. [14.7.6]

Africa

There is high confidence that it is virtually certain that all of Africa will continue to warm during the 21st century. Sahara already very dry is very likely to remain dry. But because of models' overall inability to capture the physical processes of the monsoonal rain in West Africa and large model spread in the projections, there is low confidence in projection statements about drying or wetting of Sahel and the rest of West Africa. There is medium confidence in projections with likely little change in mean precipitation in East Africa, while Southern Africa is likely to receive reduced precipitation in Austral winter. There is a high confidence of a likely increase in rainfall for the East African short rainy season, but low confidence in projections regarding drying or wetting in the long rainy season. There is medium confidence of a likely decrease in spring and summer rainfall over much of Southern Africa. [14.7.7]

Central and North Asia

A stronger warming trend is projected for northern Asia during winter. For central Asia, warming magnitude is similar between winter and summer. Precipitation in northern Asia will very likely increase, whereas the precipitation trend over central Asia is less certain. Extreme precipitation events will likely increase in both regions. [14.7.8]

East Asia

It is very likely that temperatures will increase by the end of the century, more in summer than in winter, related to a decrease in soil moisture, and that there will be a decrease in precipitation, mainly in winter, since there is very little precipitation in summer under present-day conditions. As a consequence, it is likely that there will be more pronounced drought periods. There is medium confidence, that an increase of East Asian summer monsoon intensity throughout the 21st century and of summer precipitation over the whole of East Asia is likely. Precipitation increase is likely over the Yangtze River Valley, Korean peninsula and Japan during the Meiyu-Changma-Baiu season in May-July. Precipitation extremes are very likely to increase over most of southeastern China in all seasons, and over Japan in summer. There is high confidence that surface air temperature over East Asia virtually certain will increase significantly by the end of the 21st century, with larger magnitude over northern China and in winter. [14.7.9]

West and South Asia

There is high confidence in assessment of temperature projections. It is virtually certain that temperatures will increase in both sub-regions. Projected regional rainfall changes are broadly consistent with physical arguments of 'wet gets wetter and dry becomes drier' over these two contrasting rainfall regions of West and South Asia. However, large uncertainties in the projected amplitude changes make the assessment difficult. There is low to medium confidence in quantitative assessment of precipitation changes, but it is likely that West Asia will receive less precipitation in the April to September half year and South Asia will receive more than at present. [14.7.10]

Southeast Asia

There is high confidence that warming is very likely to continue trough this century. It is likely that the warming will show substantial sub-regional differences. It is very likely that there will be a greater warming at night-time than daytime for all seasons. It is very likely that the rising temperatures will continue to be manifested in a rising number of hot days and warm nights, and a decline in cooler weather. There is medium confidence that rainfall is likely to increase averaged across the region, but the direction of change has strong geographical variations. [14.7.11]

Australia and New Zealand

There is high confidence that it is likely that cool season precipitation will continue to decrease over southern Australia, with dry spells likely to become more persistent over southern Australia. It is very likely that the Australian continent will continue to warm through the 21st century, at a rate similar to the global land-surface mean. The frequency of very warm days is virtually certain to increase through this century, across the whole country. There is also high confidence that it is very likely that temperatures will continue to rise over New Zealand, at less than the global rate through the 21st century. There is moderate confidence that precipitation is likely to increase in western regions of New Zealand in winter and spring. In summer and autumn, it is as likely as not that precipitation amounts will change. [14.7.12]

Pacific Islands Region

It is very likely that temperatures, including the frequency and magnitude of extreme high temperatures, will continue to increase through the 21st century. Rainfall is likely to increase in equatorial regions (e.g., Kiribati). However, in regions directly affected by the SPCZ and western portion of the ITCZ, the rainfall outlook is uncertain and it is as likely as not that rainfall will increase in many Pacific Island nations. [14.7.13]

Antarctic

There is moderate confidence that it is very likely that Antarctic temperatures will continue to increase, but more slowly than the global mean rate of increase. As temperatures rise, it is likely that precipitation will increase, but the magnitude and the spatial pattern of change are uncertain. The form of future changes in Antarctic sea ice extent and in surface climate change over the continent will depend strongly on the future evolution of the SAM and the ENSO teleconnection, both of which remain uncertain. [14.7.14]

14.1 Introduction

Regional climates, including their mean state and variability[1], are the complex outcome of local physical processes, and the non-local response to large-scale phenomena such as the El Niño-Southern Oscillation (ENSO) and other dominant modes of climate variability. This chapter assesses the physical basis of future regional climate change in the context of changes in the following types of phenomena: *regional-scale convergence zones* (i.e., monsoons, tropical convergence zones), large-scale *modes of climate variability,* and *tropical and extra-tropical cyclones*. More generic processes relevant to regional climate change, such as thermodynamic processes and land-atmosphere feedback processes are assessed in Chapter 12. Local processes such as snow-albedo feedback, moisture feedbacks due to local vegetation, effects of steep complex terrain etc. can be important for changes but are beyond the scope of this chapter. Our focus here is on large-scale atmospheric phenomena rather than more local feedback processes or impacts such as floods and droughts.

The following two subsections provide a general introduction on regional-scale convergence zones and modes of climate variability, before specific phenomena are assessed in Sections 14.2–14.6. Each section briefly describes a climate phenomenon, provides a summary of key findings from the Fourth Assessment Report, AR4 (IPCC, 2007b), assesses process understanding and how well models simulate the phenomenon, and then presents an assessment of future projections for the phenomenon. Section 14.7 then uses these phenomena to interpret projected future changes for regions defined in previous regional climate change assessments (IPCC, 2007a; IPCC, 2007b; IPCC, 2012). An assessment of Regional Climate Models (RCMs) and other downscaling tools required for local impact assessments is presented in Section 9.5. Section 14.1.3 discusses the important cross-cutting topic of cyclones, and Section 14.1.5 concludes with a summary of findings from AR4 relevant for this assessment.

14.1.1 Regional-Scale Convergence Zones

The dynamics of regional climates are determined by local weather systems that control the net transport of heat, moisture, and momentum into the region. For example, the major monsoon systems where the seasonal movement of convergence zones over land leads to profound changes in local hydrological cycles. Monsoon systems are well-known climate phenomena that affect the lives of billions of people particularly in Asia, Africa, Australia, and the Americas. Section 14.2 assesses current understanding of monsoonal behaviour in the present and future climate, how monsoon characteristics are influenced by the large-scale tropical modes of variability and their potential changes, and how the monsoons in turn affect regional extremes. Convergence zones over the tropical oceans also play a fundamental role in determining both regional climates and the global atmospheric circulation. Section 14.3 presents an assessment of these and other important tropical phenomena.

[START BOX 14.1 HERE]

Box 14.1: Conceptual Definitions and Impacts of Modes of Climate Variability

This box briefly defines key concepts used to interpret modes of variability (below) and summarises regional impacts associated with well-known modes (Box 14.1, Table 1 and Box 14.1, Figure 1). The terms below are used to describe variations in time series variables reported at a set of geographically-fixed spatial locations e.g., a set of observing stations or model grid points[2].

Climate indices
Time series constructed from climate variables that provides an aggregate summary of the state of the climate system. For example, the difference between sea-level pressure in Iceland and the Azores provides a simple yet useful historical NAO index (see Box 2.4 for definitions of this and other well-known observational indices). Because of their maximum variance properties, climate indices are often defined using *principal components*.

[1] Regional climate is understood here in the widest sense to mean the whole joint probability distribution of climate variables for a region including the time-mean state, the variance and co-variance, and the extremes.
[2] Based on the more complete statistical and dynamical interpretation in Stephenson et al. (2004).

Principal component
A linear combination of a set of time series variables that has maximum variance subject to certain normalisation constraints. Principal components are widely used to define optimal *climate indices* from gridded datasets (e.g., the AO index defined as the principal component of gridded NH sea-level pressure).

Climate pattern
A set of coefficients obtained by "projection" (regression) of climate variables at different spatial locations onto a *climate index* time series.

Empirical Orthogonal Function
The *climate pattern* obtained when choosing the *climate index* to be a principal *component*. It is an eigenvector of the covariance matrix.

Teleconnection
A statistical association between climate variables at widely separated, geographically-fixed spatial locations. Teleconnections are caused by large spatial structures such as basin-wide coupled modes of ocean-atmosphere variability, Rossby wave-trains, mid-latitude jets and storm-tracks, etc.

Teleconnection pattern
A correlation map obtained by calculating the correlation between variables at different spatial locations and a climate index. It is the special case of a *climate pattern* obtained for standardised variables and a standardised *climate index* i.e., the variables and index are each centred and scaled to have zero mean and unit variance. One-point teleconnection maps are made by choosing a variable at one of the locations to be the climate index.

Mode of climate variability
Underlying space-time structure with preferred spatial pattern and temporal variation that helps account for the gross features in variance and for *teleconnections*. A mode of variability is often considered to be the product of a spatial *climate pattern* and an associated *climate index* time series.

Climate regime
A set of similar states of the climate system that occur more frequently than nearby states due to either more persistence or more often recurrence. In other words, a cluster in climate state space associated with a local maximum in the probability density function.

[INSERT BOX 14.1, TABLE 1 HERE]
Box 14.1, Table 1: Regional impacts of modes of variability.

[INSERT BOX 14.1, FIGURE 1 HERE]
Box 14.1, Figure1: Global distribution of average annual rainfall (in cm/year) from 1979–2010 GPCP data base, monsoon precipitation domain (white contours) as defined by (Kim et al., 2011a) and winter storm-tracks in both hemispheres (black contours) depicted by contours of band-pass filtered root-mean-square of 500 hPa geopotential height in m (as proposed by (Blackmon et al., 1977) from 1979–2010 NCEPv1 reanalysis (reference here). In left (right) column seasonal correlation maps of NAO, SOI (the atmospheric component of ENSO) and SAM mode indexes vs. monthly temperature (precipitation) anomalies in boreal winter (DJF) and austral winter (JJA) or spring (SON). Grey contours indicate a 99% significance level. The mode indexes were taken from NOAA (http://www.esrl.noaa.gov/psd/data/climateindices/list/), global temperatures from NASA GISTEMP (http://data.giss.nasa.gov/gistemp/) and global precipitations from GPCP (http://www.esrl.noaa.gov/psd/data/gridded/data.gpcp.html).

[END BOX 14.1 HERE]

14.1.2 Modes of Climate Variability

This chapter assesses future changes in modes of climate variability that are known to be relevant for regional climate (see Box 14.1 for definitions of mode, regime, and teleconnection). Phenomena of interest include large-scale tropical modes of variability, such as ENSO (Section 14.4), modes of variability affecting

the mid-latitudes that are influenced by tropical variability, such as the Pacific-North American (PNA) pattern (Section 14.6), and modes that represent mid- and high-latitude dynamical variability, such as the NAO/NAM and SAM (Section 14.5). Many of these modes are described in previous IPCC reports (e.g., Section 3.6 of AR4) and a recent assessment of observed historical behaviour can be found in Section 2.6 of this report. Climate models are generally able to simulate the gross features of many of the modes of variability (see Chapter 9), and so provide useful tools for understanding how modes might change the future (e.g., Handorf and Dethloff, 2009; Müller and Roeckner, 2008).

Modes and regimes provide a simplified description of variations in the climate system. In the simplest paradigm, variations in local climate variables are described by linear projection onto a set of mode indices (Baldwin et al., 2009; Baldwin and Thompson, 2009; Hurrell and Deser, 2010). For example, a large fraction of interannual variance in Northern Hemisphere sea-level pressure is accounted for by linear combinations of the NAM and the PNA modes (Quadrelli and Wallace, 2004). Furthermore, four climate modes account for much of the variation in global atmospheric mass: the two annular modes (SAM and NAM), a global ENSO-related mode and a fourth mode related to the Pacific Decadal Oscillation (PDO), which in turn is closely related to ENSO and the PNA pattern (Trenberth et al., 2005b). The non-linear regime paradigm considers the probability distribution of local climate variables to be a multi-modal mixture of distributions related to a discrete set of regimes/types (Cassou and Terray, 2001; Monahan et al., 2001; Palmer, 1999). Individual modes are prone to misinterpretation (Monahan et al., 2009) and there is debate on the relevance of the different paradigms (Ambaum, 2008; Christiansen, 2005; Fereday et al., 2008; Stephenson et al., 2004).

Modes of climate variability may respond to climate change in one or more of the following ways:

- *Index changes* – the probability distributions of the mode indices may change (e.g., shifts in the mean and/or variance, or more complex changes in shape such as changes in local probability density e.g., frequency of regimes);

- *Spatial changes* – the spatial patterns associated with the modes may change (e.g., new flavours of ENSO, see Section 14.4.4) or regional teleconnections may alter (e.g., enhanced precipitation for a given change in index; (Bulic and Kucharski, 2012);

- *Structural changes* – the types and number of modes and their mutual dependencies may change – completely new modes could in principle emerge.

Assessment of changes in modes of variability can be problematic for several reasons. Firstly, interpretation depends on how one separates modes of variability from forced changes in the time mean or variations in the annual cycle (Compo and Sardeshmukh, 2010; Pezzulli et al., 2005). Modes of variability are generally defined using indices based on either detrended anomalies (Deser et al., 2010a) or anomalies obtained by removing the time mean over a historical reference period (see Box 2.4 in Chapter 2). The mode index in the latter approach will include changes in the mean, whereas by definition there is no trend in a mode index when it is based on detrended anomalies. Secondly, it can be difficult to separate natural variations from forced responses, for example, 20th Century warming trends in the N. Atlantic that may be due to trends in aerosol and other forcings rather than natural internal variability (see Sections 14.6.1 and Box 14.3). Finally, modes of climate variability are non-linearly related to one another (Hsieh et al., 2006) and this relationship can change in time (e.g., trends in correlation between ENSO and NAO indices).

Even if a climate mode index does not contribute greatly to mean regional climate change, a climate mode may still play a very important role in regional natural variability. This is especially so for changes in the extremes of regional climate, which are likely to be sensitive to small changes in variance or shape of the distribution of the mode indices or the mode spatial patterns (Coppola et al., 2005; Scaife et al., 2008). Therefore, in addition to being a major source of uncertainty for future regional climate projections (Deser et al., 2012), changes in the variance and extremes of mode indices are relevant for future regional climate.

14.1.3 Tropical and Extra-Tropical Cyclones

Tropical and extra-tropical cyclones are important weather phenomena intimately linked to regional climate phenomena and modes of climate variability. Because of their cross-cutting nature, they are assessed here in

Boxes 14.2 and 14.3 separately from other climate phenomena. Both types of cyclone can produce extreme wind speeds and precipitation (see Section 3.4, SREX (IPCC, 2012)) and are a major source of natural catastrophe risk. Boxes 14.2 and 14.3 assess the recent progress in scientific understanding of how these weather systems are likely to change in the future.

14.1.4 Summary of Large-Scale Climate Phenomena and their Impacts

Box 14.1, Figure 1 illustrates the large-scale climate phenomena assessed in this Chapter. Many of the climate phenomena are evident in the map of annual mean rainfall (central panel). The most abundant annual rainfall occurs in the tropical convergence zones: ITCZ over the Pacific, Atlantic and African equatorial belt (see Section 14.3.1.1), SPCZ over central South Pacific (see Section 14.3.1.2) and SACZ over Southern South America and Southern Atlantic (see Section 14.3.1.3). In the global monsoon domain (white contours on the map), large amounts of precipitation occur but only in certain seasons (see Section 14.2). Local maxima in precipitation are also apparent over the major storm track regions in mid-latitudes (see Box 14.3). Box 14.1 Figure 1 also illustrates surface air temperature (left panels) and precipitation (right panels) teleconnection patterns for ENSO (in December to February and June to August; see Section 14.4), NAO (in December to February; see Section 14.5.1), and SAM (in September to November; see Section 14.5.2). The teleconnection patterns were obtained by taking the correlation between monthly gridded temperature and precipitation anomalies and indices for the modes (see Box 14.1 definitions). It can be seen that all three modes have far-reaching effects on temperature and precipitation in many parts of the world. Box 14.1, Table 1 briefly summarises the main regional impacts of different well-known modes of climate variability.

14.1.5 Previous IPCC Assessment of Climate Phenomena

The assessment of regional climate change in AR4 was largely based around General Circulation Model (GCM) projections of surface temperature and precipitation. The present chapter introduces a new way to assess future regional climate in terms of changes in phenomena. Although little direct information was provided in AR4 about the role in controlling future regional climates, the information about the projected changes in regional-scale convergence zones and modes of climate variability were assessed in Chapter 10 in AR4. In brief, the findings relevant to this chapter can be summarized as follows:

Monsoons: An increase in precipitation is projected in the Asian monsoon (along with an increase in interannual season-averaged precipitation variability) and the southern part of the west African monsoon with some decrease in the Sahel in northern summer, as well as an increase in the Australian monsoon in southern summer in a warmer climate. The monsoonal precipitation in Mexico and Central America is projected to decrease in association with increasing precipitation over the eastern equatorial Pacific through Walker Circulation and local Hadley Circulation changes. However, the uncertain role of aerosols in general and carbon aerosols in particular, complicates the nature of future projections of monsoon precipitation, particularly in the Asian monsoon.

Mean Tropical Pacific Climate Change: Multi-model averages show a weak shift towards average background conditions which may be described as ‘El Niño-like’, with sea surface temperatures in the central and east equatorial Pacific warming more than those in the west, weakened tropical circulations and an eastward shift in mean precipitation.

El Niño: All models show continued ENSO interannual variability in the future no matter what the change in average background conditions, but changes in ENSO interannual variability differ from model to model. Based on various assessments of the current multi-model data set, there is no consistent indication of discernible changes in projected ENSO amplitude or frequency in the 21st century.

Annular Modes: Sea level pressure is projected to increase over the subtropics and mid-latitudes, and decrease over high latitudes associated with an expansion of the Hadley Circulation and annular mode changes (NAM/NAO and SAM). A positive trend in the NAM/NAO as well as the SAM index is projected by many models. The magnitude of the projected increase is generally greater for the SAM, and there is considerable spread among the models.

Tropical Cyclones (Hurricanes and Typhoons): Results from embedded high-resolution models and global models project a likely increase of peak wind intensities and notably, where analysed, increased near-storm precipitation in future tropical cyclones. Studies investigating tropical storm frequency simulate a decrease in the overall number of storms, though there is less confidence in these projections and in the projected decrease of relatively weak storms in most basins, with an increase in the numbers of the most intense tropical cyclones.

Extra-tropical Cyclones (mid-latitude windstorms): Storm tracks are projected to move pole ward, with consequent changes in wind, precipitation and temperature patterns outside the tropics, continuing the broad pattern of observed trends over the last half Century. Some studies suggest fewer storms in mid-latitude regions.

14.2 Monsoon Systems

14.2.1 Global Overview

Monsoons are seasonal phenomena and are responsible for the majority of summer rainfall within the tropics. In the classical view, the monsoon is driven by the seasonal cycle of solar heating and difference in thermal inertia of land and ocean that establish a land-sea temperature difference. This contrast, with the land being warmer than the surrounding ocean in late spring and summer, gives favourable conditions for the occurrence of convection in the summer hemisphere, allowing the monsoon to be viewed as a seasonal migration of the ITCZ. As the monsoon season matures, latent heat released by convection high above the land surface helps to pull in additional moisture from nearby oceans over the land, maintaining the wet season. This thermal forcing depends on large-scale orography and controls the regional monsoon domain and intensity (Wu et al., 2012). The land-sea temperature difference is projected to become larger in the summer season as seen from larger warming over land than ocean (Section 12.4.3.1 and Atlas Figure AI.4-5). However, this does not lead to generally stronger monsoon circulations in the future. Changes in regional monsoon characteristics are rather complex.

Figure 14.1 shows the time series of boreal summer meridional temperature difference in the upper troposphere between the Tibetan Plateau region and the Indian Ocean region. Most of CMIP5 models underestimate the present-day meridional temperature gradient compared to reanalysis data. The CMIP5 multi-model mean shows a gradual decrease in the meridional temperature gradient in the 20th Century. Reanalysis data show different trends and therefore it is not possible to evaluate the simulated trend. Future projections show a smaller decrease (–0.3°C difference between 2080–2099 and 1986–2005) in RCP4.5 and a larger (–0.8°C) decrease in RCP8.5, implying a weakening South Asian summer monsoon circulation throughout the 21st Century, which is related to a weakening of tropical overturning circulation (Section 12.4.4.2).

[INSERT FIGURE 14.1 HERE]

Figure 14.1: Time series of meridional temperature difference of June to August mean 300 hPa temperature between 50°E–100°E, 20°N–40°N and 50°E–100°E, 0°N–20°N (20 years running mean). Thin black, dark blue, warm blue, warm yellow and bright red lines denote each CMIP5 model results of historical, RCP2.6, RCP4.5, RCP6.0 and RCP8.5 runs, respectively. Thick lines are ensemble means of 16 CMIP5 models. 90%-range (±1.65 standard deviation) is also plotted. Four reanalysis data are shown by green (ERA40), yellow-green (NRA1), purple (JRA25) and oragne (ERA-Int) lines.

From a global point of view, t precipitation characteristics over South Asia, East Asia, Australia, Africa and Americas can be viewed as an integrated global monsoon system, associated with a global-scale persistent atmospheric overturning circulation (Trenberth et al., 2000). Wang and Ding (2008) demonstrated that the global monsoon is the dominant mode of annual variation of the tropical circulation, characterizing the seasonality of Earth's climate in tropical latitudes. The monsoon-affected region is, however, not uniform in the historical record (Conroy and Overpeck, 2011), and it could vary in the future. Examination of historical precipitation records over monsoon regions throughout the globe reveals a decreasing trend in the global *land* monsoon precipitation over the last half Century, with primary contributions from weakening of the summer monsoon systems in the Northern Hemisphere (Wang and Ding, 2006). When the oceanic monsoon is combined with the land monsoon, the global monsoon precipitation has intensified for the 1979–2008 epoch mainly due to the statistically significant upward trend in the northern hemisphere summer monsoon

precipitation (Hsu et al., 2011; Wang et al., 2012a; Zhou et al., 2008c). When changes in monsoon domain are considered, the fractional increase in monsoon area is greater than that in total precipitation, so that the ratio of these two measures (which serves as an index of the global monsoon intensity) exhibits a decreasing trend (Hsu et al., 2011). Multi-model ensemble generally reproduces the observed global monsoon, but the disparity between the best and poorest models is very large (Section 9.5.2.3). It is still difficult to detect observed change in global monsoon circulation from climate model simulations (Section 10.3.3.7) and the models with finer resolution does not seem to produce trends that better match observed trends in tropical monsoon circulation (Kim et al., 2008).

The global monsoon area (GMA), the global monsoon total precipitation (GMP), and the global monsoon precipitation intensity (GMI) are all projected to increase by the end of the 21st century (Hsu et al., 2012a; Kitoh et al., 2012), where the monsoon precipitation domain is defined as the region where the annual range is >2.5 mm day^{-1} in summer season (MJJAS in the NH, and NDJFM in the SH). CMIP5 model projections show an expansion of GMA mainly over the central to eastern tropical Pacific, the southern Indian Ocean, and eastern Asia (Figure 14.2a and b). The rates of change of GMP are large, with 0 +9 and +13% (+5, +17 and +27%) change at the 10th, 50th and 90th percentile, respectively for RCP4.5 (RCP8.5), suggesting that monsoon-related precipitation could increase markedly in a warmer climate (Figure 14.2c). GMA, GMI and GMP are all likely to increase in the RCP4.5 scenario. In the RCP8.5 scenario, GMA and GMP are very likely and GMI is likely to increase at the end of the 21st Century. Changes in indices of precipitation extremes such as simple daily precipitation intensity index (SDII), annual maximum 5-day precipitation total (R5d), and dry days (DD) consistently indicate that intense precipitation will increase with larger increase rates than those of mean precipitation (Figure 14.2d). It is apparent that the change rates for SDII, R5d, and DD depend more on the emission scenario than do those for mean precipitation. The GMP experiences a large interannual variation, being strongly negatively correlated with the Nino3.4 index averaged over a typical monsoon year (defined from May to the following April) in the observations and the present-day simulations. Such rainfall variability is projected to intensify in future warmer climates and the relationship between the monsoons and ENSO is projected to strengthen (Hsu et al., 2012b).

[INSERT FIGURE 14.2 HERE]

Figure 14.2: (a) Monsoon precipitation domain based on 29 CMIP5 multi-model mean precipitation during 1986–2005 and 2080–2099 for RCP4.5 scenario, based on the definition by Wang et al. (2011). Warm Yellow (dark blue) shading: monsoon domain only in the present (future). Blue shading: monsoon domain in the both periods. (b) As in (a), but for RCP8.5. (c) Future change ratio (%) in global monsoon area (GMA), global monsoon total precipitation (GMP), and global monsoon intensity (GMI), defined by Hsu et al. (2012), over monsoon domain defined by every model and scenario, based on monthly data by the 29 models. Left (right) sides: RCP4.5 (RCP8.5) scenario. Red line: 10th, 50th, and 90th percentile. (d) As in (c), but for simple precipitation daily intensity index (SDII), annual maximum 5-day precipitation total (R5d), and dry days (DD), based on daily data by 21 CMIP5 models. All these indices are calculated for the summer season (NH: MJJAS, SH: NDJFM).

Projected future increases of global monsoon precipitation are attributed to increases in moisture convergence due to increased water vapour in the air column and increased surface evaporation due to warmer surface temperatures, offset to a certain extent by the weakening of the monsoon circulation. Despite the response to a warmer climate in terms of the global monsoon system, monsoons may differ in the local response both in terms of precipitation and circulation features because the mechanisms at work may be different (Cherchi et al., 2011). Besides warming by greenhouse gases, climate change in monsoon regions may be strongly affected by the increased aerosol forcing and induced feedback processes (Ramanathan et al., 2005). The aerosol direct forcing (heating) in the atmosphere and negative forcing (cooling) at the surface alters atmospheric stability and sets up horizontal pressure gradients, which modulate the large-scale circulation and hence monsoon rainfall (Lau et al., 2008). However, the representation of aerosol forcing in climate change simulations differs among models, and remains an important source of uncertainty (Chapter 9).

Time series of summer precipitation anomalies in each regional monsoon domain over land are displayed in Figure 14.3. As indicated by the 10th and 90th percentile lines, model scatter is very large. Only in SAS do models project statistically significant increase with 90th percentile value crossing zero line around 2040s. Figure 14.4 shows the different behaviour of changes in precipitation indices for each regional monsoon domain between 2080–2099 and 1986–2005. Mean precipitation (Pav) is generally projected to increase over all regional monsoon domains, but the 90th percentile value shows the opposite change in most regions.

Model median increase rates for precipitation over the Asian monsoon domains (SAS and EAS) are larger than those over the other monsoon domains. Projected changes in precipitation extremes are highly consistent among the different monsoon domains. Heavy precipitation indices are projected to increase much more than the mean precipitation over all monsoon domains. Future increase in the precipitation extremes (SDII and R5d) is virtually certain in the South Asian monsoon region, and is very likely in the East Asian monsoon region. R5d is also very likely to increase in North and South African monsoon regions and in the Australian monsoon region.

[INSERT FIGURE 14.3 HERE]

Figure 14.3: Time series of observed and simulated summer precipitation anomalies (%; 20 years running mean) relative to the base period average (1986–2005, except GPCC VASClimO (1986–2000)) over land global monsoon domain. The monsoon domains defined for the base period are fixed for the whole period. For the time series of simulations, Historical (grey), RCP4.5 (blue), and RCP8.5 (red) simulations by 29 CMIP5 model ensembles are shown in 10th and 90th percentile (shading), and in all model average (thick line). For the time series of observations, CRU TS3.1 (dark blue), APHRODITE (light blue), and GPCC v.6 (deep green with solid line) are calculated using only grid boxes (2.5 degree in lon./lat.) where at least an observation site exists for more than 80% of the whole period (1921–2005 for CRU TS3.1 and GPCC v.6; 1951–2005 for APHRODITE); GPCC VASClimO (light green), GPCC v.6 (deep green with dot), GPCP (black) and CMAP (black with dot) are calculated using all grids for the period (1901–2010 for GPCC v.6; 1951-2000 for GPCC VASClimO; 1979–2010 for GPCP and CMAP). (a) Land monsoon domains with regional division. (b) EAS. (c) NAM. (d) NAF. (e) SAS. (f) SAM. (g) SAF. (h) AUS.

[INSERT FIGURE 14.4 HERE]

Figure 14.4: Change ratio (%) in averaged precipitation (Pav), simple precipitation daily intensity index (SDII), annual maximum 5-day precipitation total (R5d), and dry days (DD) over each regional land monsoon domain, based on daily data by 21 CMIP5 models. All these indices are calculated over monsoon domains determined by each model and each scenario for the summer season (NH: MJJAS, SH: NDJFM). Left (right) side plots are for RCP4.5 (RCP8.5) scenario. Red lines indicate 10th, 50th, and 90th percentile. (a) Land monsoon domains with regional division. (b) EAS. (c) NAM. (d) NAF. (e) SAS. (f) SAM. (g) SAF. (h) AUS.

Timings of monsoon onset date, retreat date and thus monsoon duration will change in the future (Figure 14.5). Overall, CMIP5 models project that the onset dates will come earlier or not change much and that monsoon retreat dates will delay, resulting in a lengthening of the monsoon season. In particular, such features are commonly projected in SAS, where onset date will *likely* come earlier in both RCP4.5 and RCP8.5 scenarios, retreat date will *very likely* delay in both RCP4.5 and RCP8.5 scenarios, and duration will *likely* be longer in RCP4.5 and *very likely* longer in RCP8.5 scenario. In EAS and AUS, onset will *likely* be earlier in RCP4.5 and *very likely* in RCP8.5, with *likely* longer monsoon duration. In NAF, both onset and retreat are *likely* to become delayed. Other monsoon regions show inconsistent projections.

[INSERT FIGURE 14.5 HERE]

Figure 14.5: As for Figure 14.4, but for future changes (days) in monsoon onset date, retreat date and duration. The calculation is based on the definition by Wang and LinHo (2002)using daily precipitation climatology (filtered with 12 harmonics) averaged over regional monsoon domain. It is noted that for EAS the threshold value of the relative precipitation is adjusted from 5.0 to 4.0 mm day^{-1}.

In summary, in the RCP4.5 scenario, global monsoon precipitation is likely to strengthen in the 21st century with an increase in the area affected and in intensity, while the monsoon circulation weakens. In the RCP8.5 scenario, global monsoon area and global monsoon total precipitation is very likely to increase by the end of the 21st century. Generally, monsoon onset dates will come earlier or not change much and monsoon retreat dates will become delayed, resulting in a lengthening of the monsoon season.

14.2.2 Asian-Australian Monsoon

The seasonal variation in the thermal contrast between the large Eurasian landmass and the Pacific-Indian Oceans drives the powerful Asian-Australian monsoon system, which consists of four major subsystems: Indian, East Asian (EA), Western North Pacific (WNP), and Indo-Australian. The Asian Australian monsoon (AAM) is a major climate system in the tropics, with the west Pacific monsoon as its eastern extension (Webster, 2006).

Interannual variability of the AAM system strongly depends on the seasonal evolution of ENSO (Wang et al., 2008a). Seasonal reforecast experiments have demonstrated that atmosphere-ocean coupling in the monsoon regions is critical for successful simulation of the leading mode of AAM variability (Wang et al., 2008a). On interdecadal time scales, it is unclear to what extent the regional monsoons in the AAM system vary in a cohesive manner. There is evidence of strengthened correlation between the AAM system and ENSO since the late 1970s (Wang et al., 2008a), although the Indian summer monsoon–ENSO relationship appears to have weakened (Kumar et al., 1999).

Emissions and atmospheric loading of aerosols over Asian monsoon regions have increased (Che et al., 2007; Ramanathan and Carmichael, 2008; Sahu et al., 2008). These aerosols are made up of a complex mixture of sulphate, black carbon (BC) or soot, organic carbon and dust from both natural and anthropogenic sources. Since AR4, simulations with general circulation models indicate a wide variety of aerosol effects on monsoon climate. These include a reduced north-south sea surface temperature gradient due to "solar dimming" (Chung and Ramanathan, 2006; Ramanathan et al., 2005); and a slowdown of the meridional overturning circulation (Bollasina et al., 2011) leading to weakening of monsoon rainfall. On the other hand, atmospheric moist convergence feedback induced by heating of elevated dust and black carbon accumulated over the Indo-Gangetic Plain (Collier and Zhang, 2009; Flanner et al., 2011; Krishnamurti et al., 2009; Lau and Kim; Lau et al., 2006b; Lau et al., 2010; Mahmood and Li, 2012; Qian et al., 2011; Randles and Ramaswamy, 2008; Wang et al., 2009a; Yasunari et al., 2011)is shown to increase monsoon rainfall during May-June. Besides atmospheric feedback, aerosol forcing in monsoon regions may also be associated with strong atmosphere-surface hydrology feedback (Bollasina and Nigam, 2009). Rotstayn et al (2007) and Cai et al (2011)suggested that through long-range transport, Asian anthropogenic aerosols may have increased Australian rainfall, especially in the northwest. However, the possible scenarios and pathways by which aerosols may interact and alter monsoon rainfall and climate are still poorly understood (Turner and Annamalai, 2012).

Future changes of the AAM system projected by 20 CMIP5 models (Wang et al., 2012b) suggest an increase (about 7%) in the total AAM precipitation (the land as well as the oceanic components) by the end of the 21st century, mainly due to increases in Indian Summer Monsoon (ISM) and East Asian Summer Monsoon (EASM) rainfall (by 9–10%). There is a strong north-south asymmetry: Indian monsoon rainfall is projected to increase by 9 % but the Australian summer monsoon rainfall increases only slightly (1.7%). However, large uncertainties remain in the projections as indicated by inter-model spread.

The dynamics of the monsoons is governed by ocean-atmosphere-land interactions and various associated modes of climate variability (Webster, 2006) (Chapter 12; Box 14.1, Table 1) as well as static factors like orography. The monsoon is generally characterized by precipitation metrics, although wind and other variables are also used (see also Chapter 2); each regional monsoon has characteristic land-ocean configuration and involves different land-ocean-atmosphere interaction processes. These regional monsoons are discussed below.

14.2.2.1 Indian Monsoon

Over much of India, the summer monsoon (June-September) rainfall accounts for nearly 80% of the annual rainfall; both the ISM and the winter monsoon (or northeast: October to December) exhibit variability on a wide spectrum of scales. The precipitation during the summer monsoon is characterized by a maximum along the monsoon trough extending to the North Bay of Bengal and a secondary maximum south of the equator (between 0° and 10°S). Changes in forcings, such as reduction of the land-ocean thermal gradient (Figure 14.6) can lead to reduction of the Indian monsoon, even though the large-scale monsoon may not change.

[INSERT FIGURE 14.6 HERE]

Figure 14.6: Inter annual variability and linear trend in the difference between area averaged surface temperature over the Indian land mass and the adjoining seas (Indian Ocean, Arabian sea and Bay of bengal) for the period 1951–2010 (adopted from, Ramesh and Goswami, 2007a). The linear trends have been expressed as % of standard deviation over the period.

There are multiple lines of evidence that the Asian monsoon, and perhaps therefore the Indian monsoon as well, had undergone abrupt shifts and weakening in the past, giving rise to prolonged and intense droughts (Meehl and Hu, 2007; Cook et al, 2010, Sinha et al. 2011; see also Chapter 9).

At sub-seasonal time scales, monsoon rainfall is modulated by intense intraseasonal oscillations (ISOs; Maloney and Shaman, 2008; Lau and Wu, 2009, see also 14.6.4) associated with fluctuations of the inter-tropical convergence zone (ITCZ) (Lau and Wu, 2010; Maloney and Shaman, 2008, see Section 14.3.1.1). CMIP3 models' inability to simulate the space-time evolution of monsoon ISOs (Lin et al., 2008a; Sperber and Annamalai, 2008) and monsoon synoptic systems (Stowasser et al., 2009), perhaps due to coarse resolution (Klingaman et al., 2011) and misrepresentation of processes (Levine and Turner, 2011), remains a major source of errors in assessing their skill on the simulation of sub-seasonal variations. The multi-model mean of CMIP5 models, however, demonstrates a substantial improvement in representing the evolution of monsoon ISOs (Sperber et al., 2012). Over India, CMIP5 models simulate an overall delay in monsoon onset, timing in the peak intensity and duration, suggesting systematic errors in representing the seasonal cycle (Sperber et al., 2012).

At interannual timescales, strong (>1.5 standard deviation) deficits in monsoon rainfall over South Asia including India appear to be associated with ENSO (Prasanna and Annamalai, 2012). The ENSO-ISM relationship waxes and wanes at decadal time scales with a weakening around 1980 (Kumar et al., 1999). Long integrations with coupled models suggest that these decadal swings are largely due to internal variability of the coupled climate system (Meehl et al., 2012). In contrast, a strengthening of the relationship between ENSO and the northeast monsoon (NEM) covering south peninsular India and Sri Lanka is reported (Kumar et al., 2007; Zubair and Ropelewski, 2006). In a given year the seasonal mean rainfall is also related to the total number of active and break days. While these sub-seasonal variations are largely determined by internal dynamics their statistics are partially conditioned by ENSO, suggesting accurate projections of future monsoon variability require the simulation of both the ENSO–monsoon association (Annamalai et al., 2007) and the complex space–time evolution of intraseasonal variations. At decadal time scales, ISM variability has been linked to similar variations in SST over the Atlantic (Kucharski et al., 2006).

The recent weakening tendency in seasonal monsoon rainfall has been attributed to factors including black carbon and/or sulphate aerosol (Bollasina et al., 2011; Chung and Ramanathan, 2006, as discussed above), SST rises over the Indo-Pacific warm pool (Annamalai et al., 2012) and land-use changes (Niyogi et al., 2010, see also Chapter 10). Analysis of gridded rainfall data indicates an increase in extreme rainfall events at the expense of weaker rainfall events (Dash et al., 2007; Goswami et al., 2006) over the central Indian region, and in many other areas (Krishnamurthy et al., 2009). While the number of monsoon depressions is declining (Krishnamurthy and Ajayamohan, 2010), the upward trend in extreme rainfall events may be due to enhanced moisture availability (Goswami et al., 2006) or warmer SST in the tropical Indian Ocean (Rajeevan et al., 2008). However, observed variability of extreme rainfalls can depend on the scale of the analysis (Ghosh et al., 2009). Observations at higher spatial and temporal resolutions available for the last 5-6 decades suggest that the spatial and temporal extent of continental monsoon rainfall is changing (reducing) even though at larger scale the total rainfall may not change, or even increase (Ramesh and Goswami, 2007b).

There is growing evidence that the monsoon and its variations may be affected by anthropogenic forcing (Turner and Annamalai, 2012). A shared feature in many CMIP3 models is suppressed rainfall over the Ocean (Cai et al., 2011d; Turner and Annamalai, 2012); such a suppressed equatorial precipitation can weaken cross-equatorial monsoon flow and alter air-sea interaction (Stowasser et al., 2009). Another feature of many model projections is an increase in 'time-mean' rainfall over India (Annamalai et al., 2007; Kumar et al., 2011a; Sabade et al., 2011; Turner et al., 2007a; Ueda et al., 2006). These results are generally reproducible in CMIP5 (Chaturvedi et al., 2012; Wang et al., 2012b). While intensity changes are model- or scenario-dependent (Annamalai et al., 2007; Kumar et al., 2011a), agreements in the 'sign' are consistent with the expected changes due to thermodynamic effects in a warmer climate (Held and Soden, 2000; Held and Soden, 2006).

Model projections using UK Met Office Hadley Centre's high resolution regional climate model PRECIS (Providing REgional Climates for Impact Studies) and using the IPCC-SRES A1B emission scenario indicate an increase of 9–16% in summer monsoon precipitation over India in the 2080s compared to the

baseline (1961–1990), with less frequent but more intense rain days (Krishna Kumar et al., 2006; Kumar et al., 2011b). High-resolution (~ 20 km) future scenarios with the MRI/JMA 20-km mesh AGCM (Rajendran and Kitoh, 2008) shows widespread but spatially-varying increases in rainfall over the interior ISM region and substantial reduction in orographic rainfall over the west coast of Kerala. On the contrary, simulations with a different regional model indicate a suppression of ISM precipitation under the A2 scenario, mainly due to the weakening of large-scale monsoon flow and suppression of intraseasonal oscillations (Ashfaq et al., 2009).

Despite current uncertainty over the stability of the monsoon–ENSO teleconnection, one emerging result from modelling studies is that this association remains intact in a warmer world (Annamalai et al., 2007; Kumar et al., 2011a; Turner et al., 2007a). An examination of CMIP5 models confirms the results from CMIP3 models (Annamalai et al., 2012). While large uncertainty exists in the projection of ENSO amplitude (Collins et al., 2011); enhanced evaporation variability resulting from the warmer mean state could enhance monsoon interannual variability. A probability distribution (Figure 14.7) of drought and flood years in present and future climates simulated by a suite of models that display reasonable ENSO–monsoon relationships (Turner and Annamalai, 2012) suggests normal monsoon years are likely to become less frequent in a warmer planet; however, there is no clear consensus about the occurrence of extreme years.

[INSERT FIGURE 14.7 HERE]

Figure 14.7: Spatial distribution of ERE of different categories accumulated over five years (2001–2005). The high density of ERE over the west coast and along the flanks of the monsoon trough is prominent.Inter-annual variations in the percentage contribution of ERE (light grey shaded)/ WRE (dark grey shaded) to seasonal (June-September) rainfall over India (black) and the linear trend line (red). The percentage contribution of ERE has grown in the recent years; the linear trend of ERE component is +0.042% yr^{-1} (inset). The analysis is based on daily rainfall data from IMD for the period 1951–2004 (adopted from, Goswami and Ramesh, 2008; Ramesh and Goswami, 2007a).

The ability of CMIP3 models to simulate monsoon rainfall is limited by the models' ability to correctly simulate strongly localised rainfall events, quite likely due to the relatively low horizontal resolution and therefore deficient topography of the CMIP3 models (Qian and Zubair, 2010). Simulation of localized extreme rainfall events also affects the interannual variability in monsoon precipitation (Goswami and Ramesh, 2008; Kim et al., 2008); about 35% of the interannual variability of the Indian monsoon comes from heavy rainfall events (Figure 14.8, Goswami and Ramesh, 2008).

[INSERT FIGURE 14.8 HERE]

Figure 14.8: Climate scenarios. Normalized probability of occurrences (number of occurrences divided by the total number of years) of interannual variability of South Asian monsoon rainfall from four CMIP3 models that depict realistic mean monsoon precipitation and ENSO–monsoon association. a, gfdl_cm2_0. b, gfdl_cm2_1. c, mpi_echam5. d, mri_cgcm2_3_2a. Pre-industrial control probability density function (PDF; solid line) and future climate (1% per year increase in carbon dioxide experiments, 1pctto2x) PDF (dashed line) are shown. The future variations are scaled by the pre-industrial control interannual standard deviations whose values (in mm) are also shown (std). The differences in the shape of the PDFs have been tested for significance based on a Kolmogorov–Smirnov test. Although all models suggest a reduction in the occurrence of normal monsoon years (± one standard deviation in monsoon rainfall) the changes in the tails of the distribution are significant in only one model, mri_cgcm2_3_21 (d). The caveat is that this particular model has the least agreement in terms of mean and interannual standard deviation with observed rainfall). In the model that has the best agreement with observations, gfdl_cm2_1 (b), changes in the tails are not significant.

Although most CMIP5 coupled models have explicit treatment of direct and indirect aerosol effects, the uncertainties involved in representing the processes and spread in model simulations make any definitive assessment rather difficult. Similarly, uncertainties related to sensitivity of model resolution (Cherchi and Navarra, 2007; Klingaman et al., 2011, see also Chapter 9) and model biases (Levine and Turner, 2011) make definitive conclusions from model simulations difficult at the regional level.

14.2.2.2 East Asian Monsoon

East Asia is located on the lee side of the Tibetan Plateau between the Eurasian continent and the Pacific Ocean, and it is affected by humid and warm southerly flow in summer and dry cold northerly air outbreaks in winter. The seasonal reversal of wind and the associated precipitation is defined as the East Asian monsoon, which is a system involving both tropical and subtropical fluctuations (Ding and Chan, 2005; Zhou et al., 2009c). East Asia experiences early summer heavy rainfall events along the quasi-stationary

Meiyu-Changma-Baiu rain band and the occurrence of typhoons, and is subject to large interannual variability, mostly related to ENSO.

For the past 60 years, the East Asian summer monsoon (EASM) has been weakening (Figure 14.9a-b) which has resulted in a tendency toward increased droughts in northern China and floods in the Yangtze River Valley (Figure 14.10 a); a pattern usually termed as "wetter southern China and drier northern China" (Gong and Ho, 2002; Hu, 1997; Wang, 2001; Yu et al., 2004). During the 20th Century the EASM was subject to no substantial trends (Zhou et al., 2009c). The EASM weakening shows distinct three-dimensional structures with a tropospheric cooling trend over East Asia during July and August (Yu and Zhou, 2007). The cooling trend is most prominent at the upper troposphere around 300 hPa and is connected to northern hemispheric interdecadal climate change (Zhou and Zhang, 2009). The western Pacific subtropical high, which controls the water vapour supply for monsoon rainfall, has extended westward and thus prevents the northward penetration of water vapour transport (Zhou et al., 2009b). At upper levels, the South Asian High has experienced a zonal expansion (Gong and Ho, 2002; Zhou et al., 2009b). The East Asian subtropical westerly jet, which has strong effects on Asian-Pacific climate (Zhang et al., 2006c), has become enhanced south of its normal position (Yu and Zhou, 2007). The surface wind speed over China has substantially weakened in both winter and summer during 1969–2000 (Xu et al., 2006). The EASM has begun to recover since the early 1990s, although its strength is still less than that in the period of 1965-1980 (Liu et al., 2012; Zhu et al., 2011).

[INSERT FIGURE 14.9 HERE]

Figure 14.9: Time series of EASM indices (bars) and their trend line (dashed line) from NCEP/NCAR reanalysis, (b) ERA-40 reanalysis, (c) GOGA run of CAM3, (d) difference between GOGAI and GOGA run of CAM3. Also shown are the slope of the trends (b, change per 50-year). The EASM index is defined as the normalized zonal wind shear between 850 and 200 hPa averaged over 20°N–40°N and 110°E–140°E. GOGA run is forced by observed monthly SSTs over the global oceans from 1950 to 2000, while GOGAI is driven by global SST plus IPCC 20th century atmospheric (primarily greenhouse gases and direct aerosol) forcings (Li et al., 2010b).

Precipitation changes since 1950 due to the weakening tendency of the EASM are evident in both mean and extreme precipitation (Zhai et al., 2005). A strongly decreasing trend over the North China is found in SDII, R95, R5D and CWD (Figure 14.9 b-f), while an increasing trend over South China is evident in R5D and CWD (Figure 14.9d and f). Observational data shows both the frequency and amount of light rain have decreased in eastern China during 1956–2005, with high spatial coherency, attributable in part to the warm rain suppression by aerosols (Qian et al., 2009a; R et al., 2011) (Liu et al., 2011a). Recent analysis of hourly data finds that rainfall intensity has decreased (increased) in the mid-lower reaches of the Yangtze River valley (North China).The "wetter South-drier North" pattern of mean precipitation is mostly attributed to moderate and low intensity rainfall (≤10 mm/hour) rather than the extreme rainfall (≥20 mm/hour) (Yu et al., 2010c), although the frequency of extreme rain events has substantially increased along the Yangtze River (Qian et al., 2007a; Qian et al., 2007b). The drier North China is dominated by long duration (lasting longer than 12-hour) rainfall events, especially those occurring between midnight and morning, while the wetter South China is associated with both the substantially increased frequency and amount of long duration precipitation (Li et al., 2011c).

For the whole 20th century, the total summer precipitation over East Asia shows no clear trend (Zhang and Zhou, 2011b). The June-September precipitation amount in Seoul and numbers of torrential rain (>75 mm) days, highest one-day rainfall amount, number of extremely wet days, and the precipitation amount falling in extremely wet days, all have a trend significant at the 99% confidence level for 1778–2004 (Wang et al., 2006). The increasing trend is statistically significant for heavy rainfall intensity in Hong Kong during 1885 to 2008 (Ginn et al., 2010; Wong et al., 2011) and in Japan during 1901–2004 (FUJIBE et al., 2006). The interannual variability of precipitation in Japan has gradually increased since the 1970s, but the annual precipitation trend is not clear (JMA, 2011).

[INSERT FIGURE 14.10 HERE]

Figure 14.10: Linear trend for summer (a) total precipitation (b) SDII, (c) R95 (summer total precipitation when PR >95th percentile), (d) R5d, (e) CDD (maximum number of consecutive days with PR <1 mm)and (f) CWD (maximum number of consecutive days with PR >1mm) in percent per 50-year for summer precipitation from the APHRODITE data set for 1951–2000. The trends statistically significant at 5% level are dotted.

Understanding of climate change in the East Asian monsoon regions has been a challenge. The "wetter South-drier North" trend may be mainly dominated by natural decadal variability, while the rainfall intensity and frequency could be partially of anthropogenic origin (Lei et al., 2011; Zhu et al., 2012). The weakening tendency of the EASM is reasonably reproduced by AGCMs driven by historical tropical SSTs (Figure 14.9c, Li et al., 2010b). The combination of recent warming in the tropical ocean (Li et al., 2010b; Zhou et al., 2008b; Zhou and Zou, 2010) and weakening of atmospheric heating over the Tibetan Plateau leads to a reduction of land-sea thermal contrast, thus favours the weakening of the East Asian summer monsoon during 1950-2002 (Ding et al., 2009; Ding et al., 2008; Duan and Wu, 2008). The decreased heating over the Tibetan Plateau is caused by the increased snow cover and depth over the Tibetan Plateau in preceding winter and spring (Ding and Wang, 2009; Zhang et al., 2004), which may be related to the enhanced winter NAO (Xin et al., 2010) and enhanced coupling between the SST warming in the northern Indian Ocean and the tropical convective maximum (Zhang et al., 2004).

Numerical model experiments demonstrate that the greenhouse gas plus aerosol forcing (direct effect) increases the land-sea thermal contrast and thus enhances rather than weakens the EASM circulation (Figure 14.9d, (Li et al., 2010c)). Global warming may bring about a change of monsoon rain band position rather than precipitation intensity (Hori et al., 2007; Li et al., 2010b). The large-scale warming might prolong (shorten) the duration of dry spells in the northern (southern) China by decreasing the zonal temperature gradient in the eastern China (Wang et al., 2010b). Global warming may result in a weakened East Asian winter monsoon though a weakened Aleutian Low and Siberian High (Hori and Ueda, 2006).

The aerosol effect on EASM circulation and precipitation changes during the past 60 years has large uncertainties. The combined effect of BC and sulphate aerosols is largely dominated by sulphates, which might produce a weakened EASM but enhanced precipitation over South China (Liu et al., 2009a). Sulphate aerosol may reduce the surface heating over land and diminish land-sea thermal contrast (Li et al., 2007; Qian et al., 2006; Qian et al., 2007b). GCM experiments have shown that increased AOD in China causes a noticeable increase in precipitation in the southern part of China in July, through induced surface cooling in mid-latitude leading to strengthening of the Hadley circulation (Gu et al., 2006). However, the inclusion of black carbon in the simulations does not necessarily produce the observed "north drought/south flood" precipitation pattern in China during the past 50 years (Wang and Zhou, 2005). Sulphate aerosols have been show to affect rainfall redistribution over East Asia in late spring and early summer, and weaken monsoon rainfall through direct (Kim et al., 2007; Liu et al., 2009b) or semi-direct (Zhang et al., 2009) effects. However, these results contradict the observations of the north/dry and south/wet pattern in East Asia in recent decades.

The mean EASM circulation, and the associated surface air temperature pattern, south Asian high, and east Asian jet, is well captured by CMIP3 CGCMs and AGCMs (Boo et al., 2011; JIANG et al., 2005; Lin et al., 2006; Zhou and Yu, 2006). However, the climatological mean precipitation over eastern China is underestimated by CMIP3 models (Li and Zhou, 2011; Lin et al., 2008b), and its simulation is sensitive to convection schemes (Chen et al., 2010). Higher-resolution models show better performance in reproducing the location and amount of orographic rainfall (Gao et al., 2006; Kobayashi and Sugi, 2004) and Baiu frontal structure (Kitoh and Kusunoki, 2008). A reasonable simulation of the Meiyu rain band depends on the realistic representation of the low-level jet to the south of the Yangtze River valley and the upper-level East Asian jet (Wang et al., 2011a). The main features of the Asian-Australian monsoon are reasonably simulated by CMIP3 AGCMs, suggesting the dominance of remote El Niño forcing in producing the predictable portion of AAM rainfall variability (Zhou et al., 2009d). However, East Asian summer monsoon rainfall is poorly modelled, which is mainly due to sparse historical SST data resulting in not capturing the zonal land-sea thermal contrast change across East Asia (Li and Zhou, 2011; Zhou et al., 2008a; Zhou and Zou, 2010). Low resolution CMIP3 AGCMs are unable to reproduce the observed variability of East Asian summer monsoon rainfall (Li and Zhou, 2011), while improvements areevident in high resolution models (Kitoh and Kusunoki, 2008).

[INSERT FIGURE 14.11 HERE]

Figure 14.11: Time series of summer monsoon indices (21-year running mean) relative to the base period average (1986-2005). Historical (gray), RCP4.5 (blue) and RCP8.5 (Red) simulations by 15 CMIP5 model ensembles are shown in 10th and 90th (shading), and 50th (thick line) percentile. (a) East Asian monsoon zonal thermal contrast index, (b) East Asian summer monsoon meridional thermal contrast index, (c) Indian monsoon index, (d) western North Pacific summer monsoon index, (e) Australian monsoon index (see Zhou et al. (2009) for indices definitions)

CMIP3 multi-model ensembles show large uncertainty in future projections of monsoon precipitation and circulation (Ding et al., 2007; Kripalani et al., 2007a). The EASM precipitation in CMIP3 models under the SRES A1B scenario increases strongly (~ 9%) by the 2040s due to an increase in both monsoon circulation and water vapour (Sun and Ding, 2010), but the mean precipitation along the Yangtze River may decrease under theA2 scenario (Tao et al., 2012). CMIP5 projections indicate a likely increase of EASM circulation (Figure 14.11a, b) and rainfall (Figure 14.11b) throughout the 21st century under both RCP4.5 and RCP8.5 stabilization scenario. This is different to other parts of the Asian-Australian monsoon which may weaken in monsoon circulation (Figure 14.11c-e) but increase in monsoon rainfall (Figure 14.3e, f, h).

14.2.2.3 The Maritime Continent Monsoon

A widespread interaction between land and water characterizes the region between the Asian continent and Australia. In meteorological terms, this region made up of thousands of islands of various sizes and numerous shallow bodies of sea water is often referred to as the Maritime Continent. Multi-scale climate processes contribute to climate variability and change over the Maritime Continent. On the interannual time scale, ENSO affects the intensity of the Asian-Australian monsoon (Aldrian and Susanto, 2003), (Tangang et al., 2007) (Juneng and Tangang, 2005)) and the monsoon affects the intensity of the diurnal cycle of land-sea and mountain-valley breezes which the modulate the spatial distribution of precipitation over the islands in the Maritime Continent (Qian et al., 2010a; Robertson et al., 2011).

The continent provides a land bridge along which maximum convection marches from the Asian summer monsoon regime (generally peaking in June, July, August, or JJA) to the Australian summer monsoon system (generally peaking in December, January and February, or DJF) (Hung et al., 2004). The onset, retreat and duration of the monsoon in these regions are of particular importance for the agriculture sector in many countries in the region, and monsoon-related droughts and floods have an enormous social and economic impact (Naylor et al., 2007). In many countries (e.g., Indonesia) variability of the monsoon together with its coherence with ENSO contributes to a large portion (up to 72% in Indonesia) of the total climate variance (Aldrian and Djamil, 2008). The monsoon also affects the intensity of regional diurnal cycle of land-sea and mountain-valley breezes, modulating the spatial distribution of precipitation over the islands of the Maritime Continent (Qian et al., 2010a; Robertson et al., 2011).

The retreat of the Asian summer monsoon in boreal fall (generally during September, October, November, SON) is associated with the onset process of the Australian monsoon system, and vice versa. During SON, the convection maximum occurs in the eastern Indian Ocean, Malay Peninsula and Sumatra, and southern South China Sea. This general area is the midpoint of the path of the southeastward progression of convection from the Asian summer monsoon to the Australian summer monsoon. However, during March to May, the maximum convection does not retrace that path but stays near and south of the equator (Chang et al., 2005). Several mechanisms have been proposed to explain such an asymmetry (Hung et al., 2004).

Multiple factors affect the onset and retreat of the Maritime Continent monsoon hence the system experiences considerable variability. The influence of ENSO is better understood than most other factors. The weakening of SST gradients along the equator during El Niño leads to a seasonal march in September to November that is slower than normal, and hence a delay in the onset of the Australia summer monsoon (Moron et al., 2010). The delay is often associated with an increase in the frequency of dry extremes (Curtis et al., 2007). A spatial and temporal rainfall analysis of a catchment area in East Java based on 40 rainfall stations from 1955 to 2005 showed a decrease in accumulated rainfall but the ratio between the wet and dry season rainfall has increased (Aldrian and Djamil, 2008). There have been no obvious trends in extreme rainfall indices in Indonesia, but there has been a substantial decrease in the number of rain days at many stations in the Philippines including that at Daet, along the east coast (Manton et al., 2001).

Although the Asian and Australian summer monsoon regimes intertwine across the equator, regions situated at least five degrees latitude north (south) of the equator generally experience a predominant influence from the Asian (Australian) summer monsoon regimes, recording clear wet and dry seasons (Aldrian and Susanto, 2003; Giannini et al., 2007). The latitudinal extent of the intrusion by the Australian summer regime into the Northern Hemisphere appears to be greater than that of the Asian summer monsoon into the Southern Hemisphere (Chang et al., 2005). As such, most locations in the Maritime Continent tend to experience their

annual maximum during Austral summer. The exact month of the rainfall peak at a given location, however, depends on many factors such as the orientation of terrain with respect to wind directions and complex island topography and local sea-land-air interactions (Aldrian et al., 2005; Aldrian and Susanto, 2003; Chang et al., 2005).

Recent literature confirms that drought and flooding in the Maritime continent are strongly influenced by rainfall variability, which is closely related to the diurnal change (Qian, 2008; Ward et al., 2011), intraseasonal variations such as the Madden-Julian Oscillation (Hidayat and Kizu, 2010; Salahuddin and Curtis, 2011) (Tangang et al., 2008), annual monsoon variability (Chang et al., 2005; Moron et al., 2009; Moron et al., 2010), and interannual large-scale phenomena such as ENSO (Aldrian et al., 2007; Juneng et al., 2007; Moron et al., 2010). Complex island topography and local sea-land-air interactions cannot adequately be represented in large scale GCMs or RCMs nor can they be fully resolved in remotely-sensed data such as the Tropical Rainfall measuring Mission (TRMM) data set (Aldrian and Djamil, 2008; Qian, 2008).

ENSO has a large impact on the climate variability of the Maritime continent. Warm ENSO events usually cause delayed onsets of the austral summer monsoon over Indonesia (Moron et al., 2010) and are associated with an increase in frequency of dry extremes (Curtis et al., 2007). Based on simulations with a single GCM (ECHAM5/MPI-OM), Müller and Roeckner (2008) concluded that future changes in the mean state are El Nino-like.

Diurnal and interannual variability of rainfall over Indonesia and Malaysia in austral summer (October to April) is strongly affected by the MJO passage (Hidayat and Kizu, 2010; Rauniyar and Walsh, 2011; Salahuddin and Curtis, 2011). Although the impact is largely inhomogeneous over the islands, analysis of precipitation gauges and wind observations suggest that the state of the MJO can be used to forecast climate extremes (dry and wet) in the Maritime continent (Moron et al., 2010; Salahuddin and Curtis, 2011).

Modelling the Maritime Continent monsoon is one of the greatest challenges of climate science. Representation of each element of the system (the Asian summer monsoon, the Australian summer monsoon, ENSO, the ITCZ, convection processes over the Maritime continent) is in itself a non-trivial task, but a realistic simulation involves getting right their complex relationships including the seasonal march and the asymmetry in the cross-hemisphere transition. These tasks are made even more difficult because of the coarse resolution of the contemporary large-scale CGCMs. As such, complex island topography and local sea-land-air interactions cannot be adequately represented, affecting simulations of the seasonal and diurnal cycle over the islands (Aldrian and Djamil, 2008; Qian, 2008). In addition, large-scale CGCMs tend to systematically underestimate the precipitation over the Maritime Continent, and the deficient rainfall is a driver of other systematic errors beyond the Maritime Continent (Neale and Slingo, 2003).

Climate change projections of the Maritime Continent monsoon therefore carry large uncertainties. Among the many sources are uncertainties in changes of each of the elements such as ENSO, the onset, retreat, and intensity of the Asian and Australian summer monsoon, in addition to regional rainfall distribution and the associated seasonal and diurnal cycle that large-scale CGCM simulate poorly. In general, most CGCMs tend to simulate increasing precipitation in the tropical central Pacific but declining trends over the Maritime Continent for June to August (Ose and Arakawa, 2011), consistent with a decreasing zonal SST gradient across the equatorial Pacific and a weakening Walker circulation (Collins et al., 2010).

In no other region is the need for high-resolution or downscaling to resolve the complex terrain as compelling as over the Maritime Continent. An increasingly common approach is to use outputs from large-scale CGCMs as boundary conditions for forcing high-resolution regional circulation models that incorporate a more realistic representation of local characteristics. Such a study (Kitoh et al., 2010) suggested that the summer monsoon in Indonesia is projected to increase. By the end of 21st century under the SRES A1B scenario, rainfall increases of about 20% in summer are projected, consistent with the “wet regions getting wetter” mechanism (Seager et al., 2012).

In another effort, several such downscaling simulations have been performed using the CSIRO Conformal Cubic Atmospheric Model (CCAM). These downscaling experiments were carried out with progressively higher resolution in several stages, from a quasi-uniform global resolution of 200km to 60km, for six host

CMIP3 CGCMs (CSIRO Mk3.5, GFDL 2.0, GFDL 2.1, ECHAM5, HadCM3, and Miroc-Medres) under the A2 emissions scenario to the year 2100 (Katzfey et al., 2009). While the uncertainties in large-scale model projections carry over, biases associated with the annual cycle of climatological SSTs were corrected to produce a more realistic climatology (Nguyen et al., 2012). Although there are major inter-model differences, the ensemble mean of these downscaling experiments (Figure 14.12) indicates a general increase in summer (December to February) rainfall over much of the Borneo and Celebes areas, as well as much of northeast Philippines (Figure 14.12, top right panel). Over much of the Java region, the increase is surrounded by a general reduction over the ocean. In the Austral winter (June to August), there is an increase over northern Sumatra but a decrease over Java and southern Sumatra, with a general agreement between projections based on the host CGCMs and the downscaling models.

[INSERT FIGURE 14.12 HERE]

Figure 14.12: Multi-model mean rainfall change in DJF (upper row) and JJA (lower row) (mm day^{-1}) in global climate models (left) and a regional downscaling model 60 km simulations (right, (Nguyen et al., 2012)), each consisting of the same six models, for the 30-year period centred on 2055, relative to a 30-year period centred on 1990, using the A2 (high) emissions scenario.

In many places, the projected change from the downscaling models is opposite in direction to that from the host CGCMs, for example, December to February rainfall over northern Borneo and northern Philippines. At a given location, the projected change might be interpreted as a net balance between two opposing mechanisms: "wet regions getting wetter" versus "warmest regions getting wetter." The latter occurs as circulation changes advect increased moisture to locations where the surface temperature is warmest. The SST bias correction results in a shift of the location of the warmest temperatures. It is not clear what the threshold resolution is, beyond which the balance would not change further.

14.2.2.4 Australian Monsoon

The Australian summer monsoon is commonly described using a wind index, an average of east-west tropospheric winds at 850 mb over a broad area north Australia. An index over northeast Australia (120°E-150°E, 0°–10°S) (Wang et al., 2004) shows a clear post-1980 reduction, which is also confirmed by other studies (e.g., Li et al., 2012b). A new index described by Kajikawa (2010) using an average over a region northwest of Australia (110°E–130°E, 15°S–5°S) captures a higher percentage of the variance of northern Australia summer rainfall, but does not fully exhibit the post-1980 reduction. Such an average hides substantial regional variations. For example, over northwest Australia, summer rainfall has increased by more than 50% (Rotstayn et al., 2007; Shi et al., 2008a; Smith et al., 2008), whereas over northeast Australia, summer rainfall has decreased markedly since around 1980.

For northwest Australia, the increasing rainfall trends are mainly a result of similar trends in average rainfall intensity, which appear independent of ENSO, suggesting that the increasing rainfall trends are largely unrelated to ENSO (Smith et al., 2008). Climate model results suggest that an increasing level of northern hemispheric aerosols is responsible for the rainfall increase (Rotstayn et al., 2007), but another study suggests that this is a model specific result (Shi et al., 2008a). Indeed, there is no consensus among CMIP3 models (Cai et al., 2011a).

There is also a lack of consensus on rainfall reductions over southeast Australia. One suggestion regards the reduction as a part of the monsoon rainfall decrease as described in the Wang et al. (2004) index, with consistent differential warming rates in the regional ocean (Li et al., 2012b). However, an alternative explanation points to a modulation on the ENSO-rainfall teleconnection by the Pacific Decadal Oscillation (PDO): during the post-1976 positive PDO phase, the decadal mean position of convection was situated farther east, so even with a La Niña-induced westward shift, the convection centre was still situated too far east to impact on Australia (Cai and van Rensch, 2012; Cai et al., 2010).

Simulation of the Indo-Australian monsoon has improved substantially, and despite model errors and biases in simulating monsoon intensity and location, models in general show skill in representing gross spatial summer precipitation characteristics (Moise et al., 2005). Further, atmospheric GCMs forced by SST anomalies could skilfully reproduce the monsoon-related zonal wind variability over recent decades (Wang et al., 2004; Zhou et al., 2009a). Recent analysis of the skill of a suite of CMIP3 models in reproducing the

broad features of observed rainfall, temperature and circulation variations over northern Australia shows a major divergence, with half the models overestimating the tropical rainfall and the other half underestimating it (Colman et al., 2011). The seasonal reversal of the monsoon circulation in the region and the location, orientation and seasonal progression of the low level monsoon ‘‘shear line’’ (the line of zero east-west winds) are found to be reasonable in terms of the model ensemble mean, but with vastly varying skill in individual models (Colman et al., 2011). An examination of monsoon onset and retreat dates, diagnosed using both the 850 hPa wind and atmospheric volumetric precipitable water (Zhang, 2010; Zhang et al., 2012), showed that a majority of the models capture the northwest–southeast evolution of the summer monsoon, but large biases exist not only in the modelled onset/retreat dates but also in the extent of the monsoon inland penetration into Australia. Most CMIP models have biases in monsoon season duration, but CMIP5 models generally perform better than CMIP3 (Jourdain et al., 2012).

Under global warming, the overall changes in rainfall in tropical Australian rainfall are small, and the simulated changes carry substantial uncertainties (Moise et al., 2012). A small increase in March and April is projected, but it is not certain if the increase is an indication of a prolonged monsoon season> The increase is largely due to thermodynamic effects associated with enhanced atmospheric moisture content, with dynamic effects contributing to a weakened monsoon circulation. Using a group of CMIP5 “best” models under the RCP8.5 scenario, most projections produced five to 20% more monsoon rainfall over the 21st century than during the pre-industrial period (Jourdain et al., 2012). In terms of onset and retreat dates, the agreement among CMIP3 models varies across the domain. In between the Sumatra-Java archipelago and the north end of the Australian continent, over 80% of the models simulate delayed monsoon onset and a shortened duration by about 10 days associated with a reduction of simulated westerlies (Zhang et al., 2012). A large proportion of CMIP3 models show relatively less warming in the eastern Indian Ocean, contributing to the reduction of simulated westerlies, thus suggesting that the warming pattern in the Indian Ocean contributes to the simulated delayed onset and shortened duration under global warming. A weaker model agreement is seen over the interior of the Australian continent, where model ensembles show an approximate 7-day delay of both the onset and retreat with little change in duration (Zhang et al., 2012).

14.2.2.5 Western North Pacific Monsoon

The Western North Pacific summer Monsoon (WNPSM) is an oceanic monsoon system. The prominent circulation features of the WNPSM that affect the summer climates in marine East Asia (specifically, the region comprised by the South China Sea, Philippine Sea and surrounding domains) and the western North Pacific are the western North Pacific monsoon trough and the subtropical anticyclonic ridge (Zhou et al. 2011). The onset of the WNPSM occurs in mid-summer, later than monsoon onsets in Southeast Asia, East Asia and South Asia, due to the weak meridional sea surface temperature and pressure gradient (Zhang and Wang, 2008). The onset of WNPSM in late July is characterized by a sudden northward shift of convective activity in the western Pacific, an abrupt strengthening of monsoon trough and a northward shift of subtropical anticyclonic ridge from 20°N to 35°N. Both the heat-induced teleconnection and air-sea interaction are involved in the monsoon development processes (Ueda et al., 2009).

The WNPSM does not show any clear trend during 1950–1999. Since the late 1970s the overall coupling between the western North Pacific monsoon system and ENSO has strengthened (Wang et al., 2008a; Xie et al., 2009), overriding the weakening of the Indian monsoon-ENSO anti-correlation during the developing phase (Wang et al., 2008a). CMIP5 models project a weakening tendency of WNPSM circulation under RCP4.5 and RCP8.5 scenarios (Figure14.11e) but with enhanced precipitation due to the convergence of moisture. In the global warming scenarios, the intense cyclonic activity over the WNP declines, while weak cyclone activity increases (Deo et al., 2011).

When forced by observed historical sea surface temperatures, the interannual variability of the western North Pacific summer monsoon is reasonably well modelled (Zhou et al., 2009b). CMIP3 models have difficulties in reproducing the stepwise eastward progress of convection, probably related to a poor SST distribution and poor representation of the monsoon trough over the warm pool area in GCMs (Inoue and Ueda, 2009). Accurate simulation of WNPSM variability needs the inclusion of air-sea coupling. Regional ocean-atmosphere coupled models generally show a cold bias of simulated SST over the WNP (Zou and Zhou, 2012), which partly stems from the overestimation of convection frequency by the atmospheric model (Zou and Zhou, 2011). The 1-month lead hind cast of ENSEMBLES models (a coordinated multi-model effort in

Europe)successfully predicted the interannual variation of WNPSM, but with large prediction spread mainly arising from the internal dynamics of air-sea interaction over the WNP and Indian Ocean (Li et al., 2012a). The interannual variability of WNPSM can even influence ENSO evolution. Due to the asymmetry of the atmospheric circulation anomalies over the WNP during ENSO-mature winters, El Niño decays much faster than La Niña (Okumura et al., 2011; Wu et al., 2010). CMIP5 model results indicate that if a model can reproduce the asymmetry of the WNP atmospheric circulation anomalies, it can simulate the asymmetric evolution of ENSO (Wu and Zhou, 2012).

14.2.3 AmericanMonsoons

Although the American monsoons, including the North America Monsoon System (NAMS) and the South America Monsoon System (SAMS) do not change wind directions from summer to winter, as do other monsoon systems, there are large inter-seasonal differences in precipitation, humidity, and atmospheric circulation (Marengo et al., 2010a; Vera et al., 2006a). For this reason, the NAMS and SAMS indices are often defined in terms of precipitation characteristics (Wang and LinHo, 2002) rather than a wind reversal, permitting the use of a comparable index for all monsoon regions. While there was a downward trend in global land monsoon rainfall accumulation from 1950 to 2004, this was mainly caused by the North African and South Asian monsoon (Zhou et al., 2008c), and the long-term trend of the Southern Hemisphere Monsoon, including the SAMS, was not statistically significant (Zhang and Zhou, 2011a). Meanwhile, between 1979 and 2008, a positive trend in global monsoon precipitation and global monsoon area was found. Both the SAMS and NAMS regions contribute to the increase (Hsu et al., 2011). In CMIP3 future climate projections, the areas of both the SAMS and NAMS increase (Hsu et al., 2012a). The CMIP5 models project an even larger expansion of NAMS than SAMS in the future scenarios (Kitoh et al., 2012). Although the CMIP5 models project increases in precipitation extremes in the NAMS and SAMS, the changes are larger in the NAMS. Increased precipitation and expansion of monsoon area have been associated with a warming-induced expansion of the Hadley cell towards higher latitudes.

14.2.3.1 North America Monsoon System

The warm season precipitation in northern Mexico and the southwestern USA is strongly influenced by the NAMS. While seasonal-mean precipitation in this region is generally controlled by the establishment of a continental-scale upper-level anticyclone and a lower-level thermal low (Higgins et al., 1997; Vera et al., 2006a), it is also under the influence of factors operating at multiple spatial and temporal scales, including propagating waves and troughs in the tropics, synoptic disturbances and fronts entering the domain from the mid-latitudes, and land falling tropical cyclones (Douglas and Englehart, 2007). It is fed by two distinct, relatively narrow low-level moisture sources—the Great Plains Low-Level Jet (LLJ) to the east of the Sierra Madres, which is approximately 200–400 km in width, and the narrower Gulf of California LLJ to the west of the Sierra Madres, which is approximately 100km in width. Further, the large-scale circulation features—including the upper-tropospheric monsoon ridge, the North Atlantic subtropical (or Bermuda) high, the Intertropical Convergence Zone, and the subtropical jet stream—in which these phenomena develop are modified by slowly evolving coupled climate features associated with the PDO, the AMO, and solar activity (Arias et al., 2012; Feng and Hu, 2008; Metcalfe et al., 2010; Seager et al., 2009; van Loon et al., 2004). As such, it is relatively difficult to simulate many of the important rainfall-producing phenomenon within the global climate models typically used for climate-change analysis (Castro et al., 2007; Cerezo-Mota et al., 2011; Lin et al., 2008a), although these models do seem to capture gross-scale features associated with its seasonal cycle (Gutzler, 2009; Liang et al., 2008b).

Historical trends provide little guidance as to the future state of the system. In the core of the monsoon region—centred over western Mexico, Arizona and western New Mexico—no distinct trends have been discerned with regard to overall precipitation over the last half of 20th Century (Anderson et al., 2010); (Arriaga-Ramirez and Cavazos, 2010) due to countervailing trends in intensity (increasing) and frequency (decreasing) of events, as well as length of the monsoon season (decreasing) itself (Englehart and Douglas, 2006). However, monsoonal stream flow in western Mexico has been decreasing, possibly as a result of changing precipitation characteristics or antecedent hydrological conditions rather than overall precipitation amounts (Gochis et al., 2007). Additional analyses indicate there has also been a systematic delay in onset, peak, and termination of the monsoon (Grantz et al., 2007) as well as an increase in extreme precipitation events associated with land falling hurricanes (Cavazos et al., 2008). Finally, positive trends in NAMS

precipitation have been detected in areas north of the "core" monsoon area of Arizona and western New Mexico (Anderson et al., 2010), in agreement with the northward expansion of the summertime North American monsoon during relatively warm periods within the Holocene (Harrison et al., 2003; Metcalfe et al., 2010; Mock and Brunelle-Daines, 1999; Petersen, 1994; Poore et al., 2005).

Over the coming century, CMIP5 simulations tend to show a reduction in precipitation in the core zone of the monsoon (Annex I), but this signal is not reproducible across models, even under the RCP8.5 scenario. Thus the evidence for current or future anthropogenic influence on NAMS precipitation is very limited and hence confidence in projections of monsoon precipitation changes is currently low. However, projections of monsoon timing indicate it is likely that the monsoon rains will arrive later in the annual cycle but will persist later as well (Seth et al., 2011), in agreement with already-observed changes. Further, projected increases in temperatures are reproducible across models (Annex I), which are very likely to increase the frequency of extreme summer temperatures (Anderson, 2011; Diffenbaugh and Ashfaq, 2010; Duffy and Tebaldi, 2012), likely to reduce stream flow (Das et al., 2011) and likely to enhance droughts (Cayan et al., 2010; Weiss et al., 2009) during the monsoon period.

14.2.3.2 South America Monsoon System

The South American Monsoon System (SAMS) onset occurs around the end of October and the demise happens roughly between end of March and end of April (Silva and Carvalho, 2007); (Raia and Cavalcanti, 2008). The SAMS cycle comprises three stages: rainfall beginning over north western South America, South Atlantic Convergence Zone (SACZ) establishment, and precipitation increase over the mouth of the Amazon River (Nieto-Ferreira and Rickenbach, 2010). As with the NAMS, global climate models generally capture the gross elements of the SAMS, but miss important regional features. The overall annual cycle of precipitation in the SAMS region is generally well-represented by CMIP3 models (Bombardi and Carvalho, 2009); (Seth et al., 2011). However, analyses of ten CMIP3 models show that most models represent the current climate's annual cycle of precipitation over the Amazon and northwest South America poorly (Bombardi and Carvalho, 2009). SAMS onset dates are reasonably simulated by AGCMs and CMIP3 models, with the exception of south eastern Brazil, where the rainy season duration is underestimated in some areas and overestimated in others (Bombardi and Carvalho, 2009; Liebmann et al., 2007).

In spite of difficulties in simulating SAMS, credible mechanisms leading to anthropogenically-forced changes in the monsoon regions, including the SAMS region, have been identified. Idealized experiments with a coupled atmospheric-ocean model subjected to increasing CO_2 show intensification of the precipitation difference between summer and winter in the global monsoon regions, including the SAMS region (Cherchi et al., 2011). During the wet season, regional mechanisms including increased evaporation and decreased stability act to increase precipitation. Increased stability (see Chapter 12 and (Chou and Chen, 2010)) acts remotely to decrease SAMS precipitation in the dry season. Some CMIP3 models mimic this behaviour, projecting a precipitation increase in austral summer (Seth et al., 2011).

Previously-established analytical techniques to obtain SAMS indices (Raia and Cavalcanti, 2008; Silva and Carvalho, 2007) (Jones and Carvalho, 2012) indicate that six CMIP5 models show a 50% increase in amplitude of the wet/dry season contrast under the RCP8.5 emissions scenario. However, the competing effects in wet and dry seasons identified above create ambiguous outcomes in the transition between dry and wet seasons. For example, in the Seth et al. (Seth et al., 2011)) study of CMIP3 models, precipitation was projected to decrease in austral spring in the SAMS region. This transition season effect could indicate a future shifting in the SAMS cycle. However, other studies conflict with one another and with these results: The median onset and demise in the future projections (2080-2100) of CMIP3 models under the A1B emissions scenario are similar to the 20th Century (1979-2000) in the central monsoon region (Bombardi and Carvalho, 2009). Most projections by 21 CMIP5 models in (Kitoh et al., 2012)) indicate a delayed onset and small changes in the demise date. Meanwhile, the (Jones and Carvalho, 2012)) study of the CMIP5 models under RCP8.5 shows earlier onsets by 24 days, later demises by 21 days, and thus noticeably longer durations of the SAMS by the end of the 21st century. Therefore, unlike the increase in precipitation of some areas and decrease in other areas within the SAMS region, during the wet season, and a general precipitation decrease in the dry season, which are all likely to occur in association with anthropogenic climate change, these simulated future changes in SAMS onset and demise must be viewed with caution.

Until very recently, literature on changes in the SAMS over the past few decades has been sparse. There is observational evidence that the duration and amplitude of the wet/dry season contrast have increased in the last 62 years (Carvalho et al., 2012), though the confidence in such changes is higher in the last 30 years. Ten CMIP5 models subjected to historical forcing consistently show increases in the amplitude, earlier onset, later demise and longer duration of the SAMS during the 1951–2005 period (Jones and Carvalho, 2012), consistent with the observational evidence and CMIP5 ensemble behaviour noted above for the 21st century. Statistical tests comparing linear trends from these simulations and pre-industrial control experiments with no external forcing support the hypothesis that these changes in SAMS characteristics are linked to anthropogenic forcing and modifications in land-cover and land-use in South America.

In summary: There is evidence for current or future anthropogenic influence on NAMS and SAMS precipitation; however, it is mixed, and overall confidence in projections of monsoon precipitation changes is currently low. It is likely precipitation associated with the NAMS will arrive later in the annual cycle, and persist later, consistent with recent trends. Future changes in the timing and duration of the SAMS are also likely, but exactly what these changes will be remains uncertain.

14.2.4 African Monsoon

West African climate is dominated by the West African monsoon (WAM) system. The monsoon develops during northern spring and summer, with a rapid northward jump of the rainfall belt from along the Gulf of Guinea at 5°N in May to June to the Sahel at 10°N in July to August. The WAM brings the rainfall maxima to their northernmost location in August and then withdraws to the south. Multiple scales, from convective organization to intraseasonal waves, strongly interact with the seasonal evolution and the interannual variability of the monsoon (Gu et al., 2004; Lebel et al., 2010; Ruti and Dell'Aquila, 2010). Anomalies in tropical Atlantic (Hoerling et al., 2006) and Mediterranean (Jung et al., 2006; Rowell, 2003). SST influence the flow into the Sahel and the moistening of the boundary layer, so that a colder northern tropical Atlantic (especially relative to the southern) or a cold Mediterranean induces negative rainfall anomalies. Warm anomalies in the Indian Ocean or in the Pacific during the growth phase of ENSO tend to increase vertical stability elsewhere and induce subsidence and dry near-surface flow over North Africa (Bader and Latif, 2003; Hagos and Cook, 2008; Janicot et al., 1996; Lu, 2009; Rowell, 2001).

Given the importance of SST forcing on the region, the uncertainty in future change in West African monsoon rainfall may be attributed to model biases, most notably the failure to reproduce the climatological east-west gradient in equatorial Atlantic SST, or to differences in the patterns of projected SST that influence the monsoon; alternatively, uncertainty in land processes and the direct response to radiative forcing may be dominant (Biasutti et al., 2008; Giannini et al., 2008; Rowell, 2011; Xue and others, 2010). Qualitatively, the CMIP3 ensemble simulates a more reproducible response during the pre-onset and the demise portion of the rainy season (Biasutti and Sobel, 2009; Biasutti et al., 2009; Seth et al., 2010). Rainfall is projected to decrease during spring—implying a small delay in the development of the mean rainy season; but to increase in fall—implying an intensification of late-season rains. The limitations of model simulations in the region, from lacking convective organization (Kohler et al., 2010) to the underestimation of interannual variability (Scaife et al., 2009) suggests a cautious attitude towards future projections.

14.2.5 Assessment Summary

There is *medium to high confidence* that global monsoon precipitation is *likely* to strengthen in the 21st century with increase in its area and intensity while the monsoon circulation weakens. Precipitation extremes such as simple daily precipitation intensity index (SDII), annual maximum 5-day precipitation total (R5d), and dry days (DD) are likely to increase with larger rates than those of mean precipitation. Future increase in SDII and R5d is very likely in the South Asian and the East Asian monsoon regions. R5d is also very likely to increase in North and South African monsoon regions and in the Australian monsoon region. Interannual rainfall variability is likely to intensify in the future warmer climate and the relationship between monsoon and El Niño is also likely to strengthen. Overall, CMIP5 models project that the monsoon onset will be earlier or not change much and the monsoon retreat dates will delay, resulting in a lengthening of the monsoon season. Such features are likely to occur in most of Asian-Australian Monsoon regions.

There is medium to high confidence that the total Asian-Australian monsoon precipitation is likely to increase but with a north-south asymmetry: the Indian monsoon rainfall increases significantly while the changes in the Australian summer monsoon rainfall are small. There is a medium confidence that the Indian summer monsoon circulation to weaken, but more abundant moisture in the atmosphere overwhelms weakened circulation, resulting in more rainfall. In case of East Asia summer monsoon, both the rainfall and circulation are likely to increase in the future. It is *likely* that rainfall will increase due to enhanced monsoon circulation and increased water vapour, but there is *low confidence* in the spatial distribution of such rainfall change. There is *medium confidence* that over the Maritime continent monsoon in the austral summer precipitation is *likely* to increase. There is *high confidence* that the Australian summer monsoon over the Java archipelago and northernmost Australia will very likely to be delayed and shortened while there is a *medium confidence* in the delay of monsoon over the interior of Australia. *Medium confidence* in that the Western North Pacific monsoon is *likely* to weaken, but compensating moisture effects will enhance precipitation.

There is *low confidence* in projections of the American monsoon precipitation changes. It is *likely* that precipitation associated with the NAMS will arrive later in the annual cycle, and persist longer. Future changes in the timing and duration of the SAMS are also *likely*, but details of these changes remain uncertain. There is *medium confidence* that a small delay in the development of the West African mean rainy season is *likely*; but with an intensification of late-season rains. The limitations of model simulations in the region suggest a cautious approach towards future projections.

14.3 Tropical Phenomena and Modes of Variability

14.3.1 Convergence Zones

Tropical convection over the oceans, averaged for a month or longer, is organized into long and narrow convergence zones, often anchored by SST structures. A radiative perspective of convection change is presented in Chapter 7.6, while the emphasis here is on regional change. In model experiments where spatially-uniform SST warming is imposed, precipitation increases in these tropical convergence zones (Xie et al., 2010b), following the 'wet-get-wetter' paradigm (Held and Soden, 2006). On the flanks of a convergence zone, rainfall may decrease because of the increased horizontal gradient in specific humidity and the resultant increase in dry advection into the convergence zone (Neelin et al., 2003).

While these arguments based on moist atmospheric dynamics call for tropical convective change to be organized around the climatological rain band, evidence is emerging that changes of tropical convection in a warmer climate depend on the spatial pattern of SST warming. As a result of the SST pattern effect, rainfall change does not generally project onto the climatological convergence zones. In CMIP3/5 model projections, annual-mean rainfall change over tropical oceans follows a 'warmer-get-wetter' pattern, increasing where the SST warming exceeds the tropical mean and vice versa (Sobel and Camargo, 2011; Xie et al., 2010b). The correlation between regional patterns of SST warming and precipitation in 20°S–20°N is positive in CMIP5 models, with the median at 0.5 (Figure 14.13). Differences among models in the SST warming pattern are an important source of uncertainty in rainfall projections, accounting for a third of inter-model variability in tropical precipitation change (Ma and Xie, 2012).

Figure 14.13 presents selective indices tracking major SST warming patterns for RCP8.5. Reproducible patterns of SST change among CMIP5 models include: greater warming in the Northern than Southern Hemisphere, a pattern favouring rainfall increase (decrease) at locations north (south) of the equator (Friedman et al., 2012); enhanced equatorial warming (Liu et al., 2005) that anchors a pronounced rainfall increase in the equatorial Pacific; reduced warming in the subtropical Southeast Pacific that weakens convection there; decreased zonal SST gradient across the equatorial Pacific (see Section 14.4) and westward zonal SST gradient change across the equatorial Indian Ocean (see Section 14.3.3) that together help weaken the strength of the Walker Cells.

[INSERT FIGURE 14.13 HERE]

Figure 14.13: Upper panel: Annual-mean precipitation percentage change (δP/P in green/gray shade and white contours at 20% intervals), and relative SST change (color contours at intervals of 0.2°C; negative dashed) to the tropical (20°S–20°N) mean warming in RCP8.5 projections, shown as 23 CMIP5 model ensemble mean. Lower panel: SST warming

pattern indices in 23-model RCP8.5 ensemble, shown as the 2050–2099 minus 1900–1949 difference. From left: Northern (EQ-60°N) minus Southern (60°S-EQ) Hemisphere; equatorial (120°E–60°W, 5°S–5°N) and Southeast (130°W–70°W, 30°S–15°S) Pacific relative to the tropical mean warming; zonal SST gradient in the equatorial Pacific (120°E–180°E minus 150°W–90°W, 5°S–5°N) and Indian (50°E–70°E, 10°S–10°N minus 90°E–110°E, 10°S-EQ) Oceans. Rightmost: spatial correlation between relative SST change and precipitation percentage change (δP/P) in the tropics (20°S–20°N). (The spatial correlation for the multi-model ensemble mean fields in the upper panel is 0.61). The circle and error bar indicate the ensemble mean and ±1 standard deviation, respectively.

14.3.1.1 Inter-Tropical Convergence Zone

The Inter-Tropical Convergence Zone (ITCZ) is generally identified as a region of persistent low-level convergence, upper-level divergence with strong upward motion, cloudiness and precipitation, located immediately north of the equator, characterized by distinct seasonal migration across the equator. The characteristics of the ITCZ vary noticeably with longitude; it is narrow in the central and eastern Pacific, but becomes broader in the western Pacific due to strong monsoon flows. The ITCZ axis in the Indo-Pacific region can be partitioned into three sections: the continental monsoon trough in India, the Bay of Bengal, and Indo-China; the oceanic monsoon trough in the Pacific warm pool; and the trade wind trough in the central Pacific.

The ITCZ exhibits variability at different spatial-temporal scales, and affects the climate through redistribution of convective forcing; it thus plays a crucial role in the water and energy cycles, air-sea interaction, monsoon evolution, and planetary teleconnections (Cheng et al., 2007; Chiang et al., 2008). The variability of the ITCZ results from a host of processes, from long-term orbital forcing to anthropogenic forcing in recent times (Delworth and Dixon, 2006; Joseph and Nigam, 2006). A northward shift of the ITCZ has been suggested as the trigger of abrupt shifts of Northern Hemisphere atmospheric circulation (Steffensen et al., 2008). Southward shifts of the Atlantic ITCZ and its relation to Atlantic thermohaline circulation have been noted in CMIP/PMIP simulations (Stouffer et al., 2006).
There is some observational evidence (Mann and Emanuel, 2006) that anthropogenic aerosols cooled the tropical North Atlantic over the 20th Century; model studies (Chang et al., 2011) indicate that this cooling alters the tropical Atlantic inter-hemispheric temperature gradient, with implications for the Atlantic ITCZ; however, there are indications of decreasing aerosol forcing in the North Atlantic in the recent years (Chapter 2). Analysis of ship reports shows an increase in cloud cover in the central equatorial Pacific over the past six decades (Tokinaga et al., 2012), which suggests a southward shift of the tropical rain band.

Modelling studies have shown that cooling from the mid-to-high latitude of the Northern Hemisphere can affect the northern tropics through an equatorward shift in the ITCZ (Broccoli et al., 2006; Kang et al., 2008). Variations of the Atlantic meridional overturning circulation (AMOC) can affect the tropical Atlantic ITCZ (Chang et al., 2008; Cheng et al., 2007). Simulation of the AMOC, and hence simulations of shifts in the ITCZ, have been found to be sensitive to processes such as cloud feedback (Zhang et al., 2010). Improvement of the estimated response of the ITCZ and consequent impact on regional climate will also depend on the representation of aerosol effects in models, especially with regards to their impacts on inter-hemispheric asymmetric warming (Kiehl, 2007; Ramanathan and Carmichael, 2008). Recent studies with climate models have demonstrated the power of extratropical forcing in causing the ITCZ to shift northward or southward (Kang et al., 2008). Slab ocean model simulations from different modelling centres show a wide range of ITCZ shifts in response to doubling carbon dioxide concentrations (Kang et al., 2009). Other processes that can be important are positive feedbacks within the tropics due to increasing water vapour content and high clouds in the new ITCZ location, which amplify changes due to other forcings.

Although most models reproduce the observed broad patterns of precipitation and year-to-year variability associated with the ITCZ (Braconnot et al., 2007; Newton et al., 2006), many models (especially those without flux corrections) still show an unrealistic double-ITCZ pattern over the tropical Pacific (Brown et al., 2011; Dai, 2006; De Szoeke and Xie, 2008; Lin, 2007) (Zhang et al., 2007b). The “double ITCZ” model bias applies predominantly to the eastern Pacific, where a band of precipitation is simulated near the equator in the Southern Hemisphere that is not seen in observations except briefly in March/April (Chapter 9, De Szoeke and Xie, 2008). Sensitivity experiments with individual CGCMs showed that the bias can be alleviated by modifying the atmospheric models (e.g., Zhang and Wang, 2006).

Most models project an increase in precipitation along the ITCZ and a decrease in precipitation in the subtropics. In the northern hemisphere winters the precipitation in the ITCZ is enhanced, while it decreases in the subtropical belt, thus reinforcing the deserts. However, there is some evidence of reversal of this trend in the last two decades (Parker et al., 2007; Thompson et al., 2010). Inter-hemispheric asymmetry in warming, under the influence of anthropogenic sulphate emissions (Ming and Ramaswamy, 2009) can affect north-south SST gradients and the future behaviour of ITCZ.

14.3.1.2 South Pacific Convergence Zone

The South Pacific Convergence Zone (SPCZ) (Vincent, 1994; Widlansky et al., 2011) extends south-eastward from the tropical warm pool of the western Pacific to French Polynesia and the Southern Hemisphere mid-latitudes. It is a key feature of the climate of the southwest Pacific, contributing most of the yearly rainfall to the many South Pacific island nations under its influence. Regional rainfall follows the seasonal migration of the warm pool and the SPCZ, reaching greatest intensity during austral summer (DJF). The position of the SPCZ varies on interannual to decadal time scales, shifting northeast or southwest in response to ENSO and the IPO/PDO (Folland et al., 2002) (Vincent et al., 2011).

At the time of the AR4, the basic physical processes maintaining the SPCZ were documented, but it was not well modelled. Many GCMs tended to simulate the SPCZ as lying east-west, giving a 'double-ITCZ' structure and missing the southeastwards orientation. Since the AR4, several studies (Takahashi and Battisti, 2007; Vincent et al., 2011) (Lintner and Neelin, 2008; Widlansky et al., 2011) have made progress on explaining the detailed physical mechanisms of SPCZ orientation and variability. These mechanisms are associated with zonal and meridional SST gradients, trade wind strength, and subsidence over the eastern Pacific. Recent work (Vincent et al., 2011) (Cai et al., 2012) suggests a non-linear relationship between ENSO and SPCZ position. Strong El Niño events induce a zonally-oriented SPCZ located well northeast of its average position, while more moderate ENSO events are associated with movement of the SPCZ to the northeast or southwest, without a change in its orientation.

While some models have improved their simulation of the SPCZ, many still have major shortcomings (Brown et al., 2012a). An analysis of CMIP5 results (Cai et al., 2012) showed that less than half (8 of 20) the models were able to reproduce the non-linear ENSO-related behaviour discussed above. However, models from both CMIP3 and CMIP5 that do simulate the SPCZ well show a consistent tendency towards much more frequent zonally-oriented SPCZ events (Figure 14.14) in future (using the SRES A2 emissions scenario for CMIP3 and RCP8.5 for CMIP5). The mechanism appears to be associated with a reduction in near-Equatorial meridional SST gradient, a consistent feature of modelled SST response to anthropogenic forcing. An increased frequency of zonally-oriented SPCZ events would have major implications for regional climate in the southwest Pacific, leading to increased interannual variability of rainfall in many areas and possibly to more frequent drought in the south western part of the region.

[INSERT FIGURE 14.14 HERE]

Figure 14.14: (a) and (b) – the two leading principal component patterns of rainfall (Global Precipitation Climatology Project version 2) in the SPCZ region (Eq.–30°S, 160°E–80°W), during December to February (units are mm day^{-1}). Lines superimposed in (a) show the average SPCZ position during El Niño (green), La Niña (blue) and neutral (black) states. The red line in (b) shows the average SPCZ position during zonal-SPCZ events. The SPCZ position is defined as the position where the maximum of rainfall greater than 6 mm per day5 is situated and a linear fit is applied. (c) illustrates the nonlinear relationship between the leading principal component time series. La Niña, neutral and moderate El Niño years are indicated with blue, black and green dots, respectively. A zonal SPCZ event (red dots) is defined as when the first principal component is greater than one standard deviation, and when the second principal component is positive. (from Cai et al., 2012).

In summary, based on analysis of models that successfully simulate the location and variability of the SPCZ, it is likely that the frequency of zonally-oriented SPCZ events will increase, with the SPCZ lying well to the northeast of its average position during those events.

14.3.1.3 South Atlantic Convergence Zone

The South Atlantic Convergence Zone (SACZ) is a band of cloud and precipitation extending from the Amazon region towards southeastern Brazil and Atlantic Ocean during summertime. Floods in many

locations and landslides in mountainous areas of southeastern Brazil are often related to this feature. Weakening or displacement of the SACZ leads to drier than normal conditions in these regions. The dominant mode of austral summer precipitation variability over South America exhibits a dipole pattern, with one centre over SACZ region and another one over Southeastern South America (SESA). Precipitation associated with the SACZ is reproduced by some CMIP3 models (Vera and Silvestri, 2009; Vera et al., 2006b) and CMIP5 (Cavalcanti and Shimizu, 2012).

Decreased precipitation in central and eastern Brazil, a region affected by the SACZ, was projected by 6 out of 10 CMIP3 models under A1B scenario (Bombardi and Carvalho, 2009). The reduction is also noted by the study of (Seth et al., 2010), which projects a southward displacement of the SACZ and the Atlantic Subtropical High during SON and DJF. The shifting of the South Atlantic Subtropical High has been related to the southward expansion of the Hadley Cell, (Lu et al., 2007) and is consistent with the positive trend of the AAO index (Section 14.5.2) and poleward shifting of the stormtracks (Previdi and Liepert, 2007). The reduced precipitation in the SACZ is also consistent with the increased precipitation over SESA in the second half of 21st century, in CMIP3 models that simulated the dipole precipitation pattern in present and future (A1B) climate scenarios (Junquas et al., 2011).

Pacific SST warming and strengthening of the PSA-like wave train (Section 14.6.2) in the second half of 21st century compared to the first half were considered as potential mechanisms contributing to the changes in the dipole pattern (Junquas et al., 2011). Another important result, also consistent with precipitation reduction in the SACZ region, is the intensification of northerly wind at low levels over South America in future projections (Seth et al., 2010). This circulation change can be associated with an increase in the Low Level Jet (LLJ) occurrences (Section 14.7.5). Increased moisture flux from the Amazon Basin to the La Plata Basin is in accord with the precipitation increase in the southern regions and a decrease in the SACZ. Results from HADGEM2-ES-CMIP5, a model which reproduces the main features of precipitation and atmospheric circulation over South America, show intensification and extension towards the ocean of the southern dipole centre and weakening of the northern centre associated with the SACZ in the last 26 years of the 21st century (Cavalcanti and Shimizu, 2012). This result is consistent with the shifting of the SACZ southwards, as projected by CMIP3 models (Seth et al., 2010), and also with the precipitation increase over southeastern South America, projected by CMIP5 models (Figure AI50-Atlas).

14.3.2 Madden Julian Oscillation

The Madden-Julian Oscillation (MJO, Madden and Julian, 1994) is the dominant component of tropical intraseasonal (20–100 days) variability. It consists of pairs of convectively active and suppressed phases defined by positive and negative anomalies in precipitation, respectively, over large areas of up to approximately 20,000 km^2. Associated with this is an east-west (zonal) overturning circulation with ascending motion in the active phase and descending motion in the suppressed phase. This convection-circulation coupled pattern propagates eastward along the equator normally from the Indian Ocean to the western and central Pacific at an average speed of ~5 ms^{-1} (Zhang, 2005). In boreal summer, there is a northward propagation of the MJO in conjunction with its eastward propagation. The MJO modulates tropical cyclone activity (Frank and Roundy, 2006), contributes to intraseasonal fluctuations of the monsoons (Maloney and Shaman, 2008), and modulates the ENSO cycle (Lengaigne et al., 2004). The MJO also excites teleconnection patterns outside the tropics in both hemispheres (L'Heureux and Higgins, 2008) (Lin et al., 2009).

At the time of the AR4, the MJO was well-described and the mechanisms that maintain it were understood to involve coupling between the atmospheric circulation and deep convection, as well as air-sea interaction. Yet the MJO was not well modelled, nor could deficiencies in model simulations of the MJO be explained based on physical understanding at that time (Zhang, 2005), although model representation of convection and air-sea fluxes were known to be important factors (see also Chapter 9).

Simulation and prediction of the MJO by GCMs remains challenging, although progress has been made in recent years (Benedict and Randall, 2009; Weare et al., 2012; Xavier et al., 2010; Zhang et al., 2006a). Because of the close connections between the MJO and extreme events, the inability of climate models to properly simulate the MJO and its potential response to climate change seriously limits the application of these models to project the statistics of extreme events in the future, especially in the tropics.

Possible changes in the MJO in a future warmer climate have just begun to be explored. In the MPI Earth System Model, MJO variance based on a multi-variant index increases appreciably in global warming(Schubert et al., 2012). The change in MJO variance is highly sensitive to the spatial pattern of SST warming. In an atmospheric GCM with the boreal winter SST climatology, precipitation variance increases in response to a spatially uniform SST warming while it decreases under a warming pattern taken from a coupled global warming simulation (Maloney, 2012a). In the latter case, the SST warming in the Eastern Hemisphere south of the equator is weak relative to the tropical mean, causing a decrease in the mean precipitation. Change in wind variability is mediated by the increase in tropospheric static stability due to the SST warming. The poor skill in simulating MJO, and the sensitive to SST warming pattern, which is itself subject to large uncertainties, makes it challenging to assess how MJO will change under global warming.

14.3.3 Indian Ocean Modes

The tropical Indian Ocean (TIO) is part of the Indo-western Pacific warm pool anchoring strong atmospheric convection. TIO SST exhibits two distinct modes of interannual variability, as extracted from an EOF analysis. The Indian Ocean basin (IOB) mode, explaining more than 30% of the total variance, features a nearly uniform structure while the Indian Ocean dipole (IOD) mode, explaining less than 15% of the variance, has a heavy loading in the eastern equatorial Indian Ocean off Indonesia, with weaker anomalies of the opposite polarity over the rest of the basin. See recent reviews by Schott et al. (2009), Deser et al. (2010a), and discussions in Chapters 2 and 9. Both modes are statistically significantly correlated with ENSO. IOB peaks in the boreal spring of the ENSO decay year while IOD peaks in the fall of the ENSO developing year.

14.3.3.1 Mean State

The basin-mean SST of TIO has risen steadily for much of the 20th Century, especially since the 1950s. Coupled ocean-atmosphere GCMs generally simulate this SST trend very well under the observed radiative forcing (Alory et al., 2007), suggesting the forced nature of the trend. The SST increase over the North Indian Ocean is noticeably weaker than the rest of the basin since 1930s, a difference suggested due to reduced surface solar radiation by Asian brown clouds with important effects on Indian and African monsoons (Chung and Ramanathan, 2006) and Arabian Sea cyclones (Evan et al., 2011b).

Over the equatorial Indian Ocean, coral isotope records off Indonesia for 1858–1997 indicate a reduced SST warming and/or suppressed freshening of salinity (Abram et al., 2008), in support of an IOD-like pattern in SST. Historical ship measurements suggest an easterly wind change for the past six decades especially during July to October, a result consistent with a reduction (increase) of marine cloudiness in the east (west), a decreasing trend at many stations over the maritime continent, and a thermocline shoaling in the east (Tokinaga et al., 2012). Ocean GCMs forced by atmospheric reanalyses, however, point to changes of opposite sign (Han et al., 2010). This discrepancy could be due to the modest magnitude of the forced changes compared to natural variability and spurious change in reanalyses.

In many CMIP3 models, the response of the equatorial Indian Ocean to global warming is characterized by easterly wind change, with a shoaling thermocline (DU and XIE, 2008; Vecchi and Soden, 2007b) and reduced SST warming in the east (Stowasser et al., 2009) (Figure 14.15). The change in zonal SST gradient, in turn, reinforces the easterly wind change, indicative of Bjerknes feedback (Xie et al., 2010b). While the deceleration of the Walker circulation occurs under global warming even in the absence of any change in zonal SST gradient (Held and Soden, 2006), models with strong Bjerknes feedback tend to produce an IOD-like zonal pattern with reduced SST warming and suppressed convection in the eastern equatorial Indian Ocean (Cai et al., 2011b). This coupled pattern is most pronounced during July to November.

[INSERT FIGURE 14.15 HERE]

Figure 14.15: September to November changes in a 22-model CMIP5 ensemble (2050–2099 in RCP8.5 minus 1900–1949 in historical run). (a) SST (colour contours at 0.1°C intervals) relative to the tropical mean (20°S–20°N), and precipitation (shading and white contours at 20 mm per month intervals). (b) Surface wind velocity (m/s), and SSH deviation from the global mean (contours, cm). Over the equatorial Indian Ocean, ocean-atmospheric changes are in positive Bjerknes feedback, with the reduced SST warming and suppressed convection in the east.

14.3.3.2 Indian Ocean Basin Mode

The IOB mode forms in response to ENSO via the atmospheric bridge and surface heat flux adjustment (Alexander et al., 2002; Klein et al., 1999). Recent studies show that ocean dynamics and ocean-atmosphere interaction within the TIO basin are important for the long persistence of IOB (Du et al., 2009; Izumo et al., 2008; Wu et al., 2008). In the summer following El Nino, the persistent basin-wide SST warming induces coherent atmospheric anomalies (Xie et al., 2009), known as the TIO capacitor effect that includes a weakened Northwest Pacific monsoon (Wang et al., 2003), suppressed tropical cyclone (TC) activity (Du et al., 2011) over the Northwest Pacific, and anomalous rainfall over East Asia (Huang et al., 2004).

For a 60-year period since 1950, the IOB mode intensified markedly across the 1970s, a change most pronounced in the summer following ENSO (Xie et al., 2010a). This interdecadal change in IOB explains the intensification of correlation between the Northwest Pacific summer monsoon and ENSO (Wang et al., 2008a), a change reproduced in atmospheric GCM simulations forced by observed SST (Huang et al., 2010). Observations along a busy ship track across the North Indian Ocean and South China Sea reveal another epoch of strong IOB variability during 1880-1910 in addition to the current epoch after the 1970s, and a 60-year lull in between (Chowdary et al., 2012). Both epochs of intensified IOB variability coincide with those of enhanced ENSO activity, suggesting the importance of the Pacific forcing.

How the IOB mode responds to global warming depends in part on how ENSO will change (Section 14.4). In an OAGCM, (Zheng et al., 2011) found that the IOB mode and its capacitor effect persist longer, through summer into early fall in global warming (Figure 14.16). This increased persistence may intensify ENSO's influence on Northwest Pacific tropical cyclones. It also suggests that the recent intensification of IOB variability may be partly due to global warming. This response to global warming is not reproducible in a large CMIP5 ensemble, with the IOB persistence increasing in some models but decreasing in some others (Figure 14.3.4).

[INSERT FIGURE 14.16 HERE]

Figure 14.16: Scatter plot comparing the IOB mode in 22 CMIP5 models between the 20th century historical and 21st century RCP8.5 simulations: regression of North Indian Ocean (40°E–100°E, 0–20°N) SST during July to September upon the preceding November to January Nino3.4 (170°W–120°W, 5°S–5°N) SST. The red dot denotes the multi-model ensemble mean, and the error bar the standard deviation of inter-model variability.

14.3.3.3 Indian Ocean Dipole Mode

IOD develops in July to November and involves Bjerknes feedback among zonal SST gradient, zonal wind and thermocline tilt along the equator, much akin to ENSO in the Pacific (Saji et al., 1999; Webster et al., 1999). Besides inducing precipitation over oceanic regions, a positive IOD event (with negative SST anomalies off Sumatra) is associated with droughts in Indonesia, reduced rainfall over Australia, intensified Indian summer monsoon, floods in East Africa, hot summers over Japan, and anomalous climate in the extratropical Southern Hemisphere (Yamagata et al., 2004).

IOD variability is high around 1850, and after the 1970s (Abram et al., 2008). A major IOD event occurred in 2006, and the dipole mode index remains positive for 2007 and 2008. Such a prolonged IOD-like state is very rare, which, along with the increase in IOD activity since the 1970s, prompts the suggestion that global warming might be a culprit (Abram et al., 2008; Behera et al., 2008; Cai et al., 2009a).

The IOD variability in SST remains nearly unchanged in global warming (Ihara et al., 2009) (Figure 14.17a) despite the easterly wind change that shoals the thermocline (Figure 14.17b) and intensifies thermocline feedback on SST in the eastern equatorial Indian Ocean. (Zheng et al., 2010) show that the global increase in atmospheric dry static stability weakens atmospheric response to zonal SST gradient, countering the enhanced thermocline feedback. On balance, IOD amplitude in SST does not change much in global warming simulations, suggesting that the recent intensification of IOD activity is part of natural variability. This is consistent with a decrease in thermocline variability associated with IOD (Figure 14.17b).

One important property of IOD does change in global warming. IOD in the current climate is strongly skewed, with cold events off Indonesia much stronger than warm ones. This skewness originates from a deep

thermocline in the equatorial Indian Ocean that is subcritical for thermocline/Bjerknes feedback. In global warming, the shoaling thermocline weakens the asymmetry in thermocline feedback between cold and warm events (Zheng et al., 2010) (Figure 14.17c). The strong skewness in the current climate and its projected decrease have important implications for IOD's climatic influences. In current climate, climate anomalies are pronounced only at the positive phase of IOD. They may become strong at the negative phase in a warmer climate.

[INSERT FIGURE 14.17 HERE]

Figure 14.17: Scatter plots comparing IOD properties in 22 CMIP5 models between the 20th century historical and 21st century RCP8.5 simulations: (a) standard deviation and skewness of the dipole mode index defined as the western (50°E–70°E, 10°S–10°N) minus eastern (90°E–110°E, 10°S–0°) SST difference; and (b) SSH standard deviation in the eastern equatorial Indian Ocean (90°E–110°E, 10°S–0°). September to November interannual anomalies are used. The red dot denotes the multi-model ensemble mean, and the error bar the standard deviation of inter-model variability. Most models show little change in IOD variance but a decrease in both SSH variance and IOD skewness.

The change in the mean state of the tropical Indian Ocean is likely to feature an IOD-like pattern during July to November, with reduced warming and suppressed rainfall in the eastern basin including Indonesia. Many CMIP3 models project such a pattern in response to increased GHG, with support from limited observations for the past six decades. Under global warming, the IOD mode of interannual variability is likely to remain unchanged in amplitude despite a shoaling thermocline in the mean state of the eastern equatorial Indian Ocean but the negative skew of SST variability off Sumatra is likely to weaken as a result of the mean thermocline change. There are indications that in a warmer climate, the IOB mode persists longer following the decay of an ENSO event, strengthening ENSO's influence on summer rainfall and tropical cyclone activity over the Northwest Pacific and East Asia. This IOB change is not reproducible among CMIP5 models, however.

14.3.4 Atlantic Ocean Modes

The Atlantic features a northward-displaced ITCZ, and a cold tongue that develops in boreal summer. Climate models generally fail to simulate these characteristics of tropical Atlantic climate (Chapter 10). In these models, a double ITCZ develops during boreal spring astride the equator, and zonal SST gradient on the equator is often opposite to observations (Richter and Xie, 2008). These biases severely limit their skills in simulating modes of climate variability and in projecting future climate change in the Atlantic sector.

14.3.4.1 Mean State

Over the past century, the Atlantic has experienced the most pronounced and persistent warming trend of all the tropical oceans (Deser et al., 2010b; Tokinaga and Xie, 2011). The warming pattern, captured as the leading mode of an empirical orthogonal function (EOF) analysis on the observed 20th Century SST (Figure 14.18), shows a clear hemispheric asymmetry with stronger warming trends in the tropical South than North Atlantic, particularly in the east equatorial south Atlantic and off the coast of Angola. The pattern is a part of the global warming EOF (Parker et al., 2007). The associated time variation, which displays a well-defined warming trend superimposed on a multidecadal variation, is highly correlated with the globally averaged SST ($r = 0.89$). The multidecadal variation, obtained by removing the linear trend, is statistically significantly correlated with the monthly mean Atlantic Multidecadal Oscillation (AMO) index ($r = 0.53$) (not shown). The warming has brought detectable changes in atmospheric circulation and rainfall pattern in the region. In particular, the ITCZ has shifted southward and land precipitation has increased (decreased) over the equatorial Amazon, equatorial West Africa, and along the Guinea coast (over the Sahel) (Deser et al., 2010b; Tokinaga and Xie, 2011) .

[INSERT FIGURE 14.18 HERE]

Figure 14.18: The leading EOF (left) of a gridded observed monthly mean SST record from Hadley Centre sea ice and SST version 1 (HadISST1) data set (Rayner et al., 2003), which explains 36% of the SST variance, and the associated monthly mean time series (right) normalized by its maximum absolute value (blue) overlaid by the globally averaged SST (red). The middle and bottom panel show the observed and modeled linear trend values for SST averaged in the tropical Atlantic basin and for an interhemispheric SST index, respectively, in the 20th century simulation (cyan) and the A1B simulation (magenta).

CMIP3 20th century climate simulations generally capture the warming trend of the basin-averaged SST over the tropical Atlantic. A majority of the models also seem to capture the secular trend in the tropical Atlantic SST interhemispheric gradient and, as a result, the southward shift of the Atlantic ITCZ over the past Century (Chang et al., 2011). However, none of the models reproduces the intense warming trend observed off the coast of Angola, and only a few models simulate the substantial warming trend in the east equatorial South Atlantic. Modelling studies show that the interhemispheric SST gradient is responsive to changes in the Atlantic Meridional Overturning Circulation (AMOC) (Chang et al., 2008; Cheng et al., 2007), and to anthropogenic aerosol cooling that is strong over the Northern Hemisphere (Biasutti and Giannini, 2006; Ming and Ramaswamy, 2009; Rotstayn and Lohmann, 2002; Williams et al., 2001).

CMIP3 model future climate projections under the A1B scenario show an accelerated SST warming over much of the tropical Atlantic. Projections of the interhemispheric SST gradient change within the basin, however, are not consistent among the models (Figure14.18). Many models display little or no hemispheric asymmetry in the future SST warming trend (Figure14.18), and show little change in the position of the ITCZ (Breugem et al., 2006). Interestingly, a few models that exhibit the largest displacement of the ITCZ project a northward shift of the ITCZ over the 21st century (Breugem et al., 2006), in contrast to the southward shift for the past decades. One explanation is that GHG increase dominates in the future over the anthropogenic aerosol effect, the latter possibly being responsible for the recent southward shift in the Atlantic ITCZ (Chang et al., 2011; Tokinaga and Xie, 2011).

14.3.4.2 Atlantic Meridional Mode

On decadal time scales, the interhemispheric SST variation emerges more clearly as a “dipole-like” pattern revealed by the 2nd EOF (Figure 14.19), referred to as the Atlantic meridional mode (AMM) (Chiang and Vimont, 2004; Servain et al., 1999; Xie and Carton, 2004). A thermodynamic feedback between surface winds, evaporation, and SST (WES; XIE and PHILANDER, 1994) is fundamental (Chang et al., 1997). Despite the importance of the local air-sea feedback, AMM variability is strongly influenced by other modes of climate variability, particularly El Niño/Southern Oscillation (ENSO) and the North Atlantic Oscillation (NAO) (Chang et al., 2006b) as the record warming of the tropical North Atlantic in 2009–2010 illustrates (Hu et al., 2011).

Not much research has been done on the long-term variation of the AMM. An examination of the time series associated with the 2nd SST EOF suggests that the AMM amplitude appeared to modulate over multidecadal time scales during the past Century. AMM activities were relatively strong in the early and late decades of the 20th century and weak in the mid-Century. Interestingly, this variation in AMM activity seems to coincide with the multidecadal modulation of ENSO in the tropical Pacific, raising the possibility that the two phenomena may be interrelated. Some recent studies suggest that the interhemispheric SST anomaly in the tropical Atlantic can alter ENSO strength in the tropical Pacific through an atmospheric bridge (Dong et al., 2006; Timmermann et al., 2007). The long-term variation of the AMM in the CMIP3 20th century climate simulations shows little consistency among the models. Only a few IPCC models capture the observed intensification of AMM variability during the late decades of the 20th century.

Many IPCC model simulations with the A1B emission scenario show only minor changes in the SST variance associated with the AMM, resulting in a negligible change in the multimodel mean variances. However, the few models that give the best AMM simulation over the 20th century project a weakening in future AMM activity (Breugem et al., 2006), possibly due to the northward shift of the ITCZ (Breugem et al., 2007). At present, model projections of future change in AMM activity is considered highly uncertain because of the poorly simulated Atlantic ITCZ by the models. In fact, uncertainty in projected changes in Atlantic meridional SST gradient has been identified as an important source of uncertainty for regional climate projection surrounding the tropical Atlantic Ocean (Good et al., 2008). Several physical factors are likely to affect the future state of the AMM. One is the position of the Atlantic ITCZ, which affects the strength and duration of WES feedback (Breugem et al., 2006; Breugem et al., 2007; Chang et al., 2006b), and thus AMM variability. Other factors include future changes in ENSO and the NAO, both exerting a substantial remote influence on the AMM. Understanding future changes in AMM bears important implications for extreme climate changes, such as hurricane, under global warming in the tropical Atlantic sector, as the AMM is tightly coupled with ITCZ and has a profound impact on the regional atmospheric circulation. Atlantic hurricane activity correlates highly to the AMM on both interannual and decadal time

scales, and this AMM-hurricane relationship provides a dynamic framework for understanding the impact of climate variability/change on Atlantic hurricanes (Smirnov and Vimont, 2011; Vimont and Kossin, 2007).

[INSERT FIGURE 14.19 HERE]

Figure 14.19: Same as Figure 14.18, except for the 2nd EOF (left), which explains 14% of the monthly mean SST variance. The associated time variation(blue in right panel) is overlaid by a detrended interhemispheric SST gradient index derived by differencing the SSTs averaged in the two boxes shown in the left panel. The two time series are correlated at r = 0.86. The yellow shade and black lines show the amplitude modulation of the PC time series using a 21-year moving window. Standard deviations of the observed and modeled March-April-May interhemispheric SST gradient time series are shown in the bottom panel for the 20th century simulation (cyan) and the A1B simulation (magenta), respectively.

14.3.4.3 Atlantic Niño

On interannual time scales, a phenomenon akin to ENSO occurs in the tropical Atlantic. This Atlantic Niño mode is captured by the 3rd EOF of the observed SST (Figure 14.20). It occurs more sporadically than ENSO and is typically phase-locked to boreal summer (ZEBIAK, 1993), although a secondary occurrence is noted in November to December (Okumura and Xie, 2006). Along the west coast of southern Africa, episodes of warm and cold SSTs, known as Benguela Niños and Niñas, occur irregularly during boreal spring, sometimes connected to equatorial Atlantic Niños (Luebbecke et al., 2010; Reason et al., 2006). Collectively, these interannual climate fluctuations in the tropical Atlantic have been shown to affect regional climate and marine ecosystem, including the West Africa Monsoon (Giannini et al., 2003; Vizy and Cook, 2002), rainfall in the coastal region (Rouault and Richard, 2003) and local fish populations (Boyer et al., 2001). Bjerknes feedback is considered important for energizing the Atlantic Niño mode (ZEBIAK, 1993) (CARTON and HUANG, 1994; Keenlyside and Latif, 2007) although quantifying it has been difficult because of the mode's weak amplitude and sporadic nature (Chang et al., 2006a).

Although the above discussion about the AMM and Atlantic Niño is presented in terms of EOF decomposition, which may bear potential pitfall of over-interpretation of pure statistical analysis results, their existence has been independently confirmed by other statistical analyses, such as composite analysis (e.g., Chiang and Vimont, 2004 for AMM and Chang et al., 2006a for Atlantic Niño). Furthermore, a large body of theoretical, modelling and observational work shows that these modes are dynamically consistent with ocean-atmospheric feedbacks in the region.

The interannual component of Atlantic variability Nino has weakened by 40% in amplitude from 1960 to 1999, associated with a weakening in the equatorial cold tongue (Tokinaga and Xie, 2011). This weakened Atlantic Nino might be a response to the combined forcing of increased GHG and aerosols, but could also be due in part to natural variability. The equatorial Atlantic warming in the early 20th century did not produce a decrease in Atlantic Niño variability while the peak of Atlantic Niño activity in 1960s (Figure 14.20) does not seem to be fully explained by the anthropogenic forcing. CMIP3 models generally fail to simulate the recent decline in Atlantic Nino variability.

Majority of the models forced with the A1B emission scenario project no major change in Atlantic Niño activity in the 21st century with the exception of a couple of models that project a sizable decrease in future Atlantic Niño activity. But because the Atlantic Niño mode is so poorly simulated by the models, there is little confidence in their projection of future Atlantic Niño activity (Breugem et al., 2006). In the absence of reliable model projection, several factors are identified that could have a major influence on future change in Atlantic Niño variability. First, the equatorial thermocline and the SST distribution along the equator are fundamentally important for the Bjerknes feedback. Any long-term changes in the upper ocean thermal structure can cause changes in Atlantic Niño activity. Second, remote influence of ENSO can trigger Atlantic Niño with the help of local Bjerknes feedback mechanism (Chang et al., 2006a; Latif and Grotzner, 2000). Third, modelling studies show that a weakening in the AMOC may result in a weaker upper ocean stratification in the eastern equatorial Atlantic Ocean, which in turn leads to a weakened annual cycle and Atlantic Niño activity (Chang et al., 2008). Last but not least, sulphate aerosol forcing in concert with other GHG forcing may impact both the mean climate and Atlantic Niño. It remains to be seen whether the reduced effect of aerosol-induced cooling in the future will cause a rebound in Atlantic Niño activity, as hypothesized by (Tokinaga and Xie, 2011).

[INSERT FIGURE 14.20 HERE]

Figure 14.20: Same as Figure 14.18, except for the 3rd EOF (upper left), which explains 9% of the monthly mean SST variance. The associated time series (blue in upper right panel) is overlaid by a detrended Atl-3 index derived by averaging the monthly mean SST in the box shown in the left panel. The two time series are correlated at r = 0.5. The yellow shade and black lines show the amplitude modulation of the Atl-3 index using a 21-year moving window. Standard deviations of the observed and modeled September-October-November detrended Atl-3 SST time series are shown in the bottom panel for the 20th century simulation (cyan) and the A1B simulation (magenta).

The observed SST warming in the tropical Atlantic represents a reduction in spatial variations in climatology: the warming is weaker north than south of the equator; and the equatorial cold tongue weakens both in the mean and interannual variability. The confidence of the projections over the tropical Atlantic—both for the mean and interannual modes—is low because of large errors in model simulations of current climate.

14.3.5 Assessment Summary

There is low to medium confidence that an increase in precipitation along the ITCZ and a decrease in precipitation in the subtropics are likely in the future. There is *medium confidence* in assessing that the frequency of zonally-oriented SPCZ events is *likely* to increase, with the SPCZ lying well to the northeast of its average position during those events. The mechanism appears to be associated with a reduction in near-Equatorial meridional SST gradient, a consistent feature of modelled SST response to anthropogenic forcing. There is low to *medium confidence* that rainfall change over tropical oceans is *likely to* follow a 'warmer-get-wetter' pattern, increasing where the SST warming exceeds the tropical mean and vice versa. There is *medium confidence* that SACZ is *likely* to shift southwards, leading to an increase in precipitation over southeastern South America. A reduction of precipitation associated with the SACZ, or southward shifting of the precipitation band in future projections is *likely*.

There is *medium to high* confidence that the tropical Indian Ocean is *likely* to feature a zonal pattern with reduced (enhanced) warming and decreased (increased) rainfall in the east (west), a pattern especially pronounced during August to November. There is *high confidence* that the Indian Ocean dipole mode will *likely* remain active, with interannual variability unchanged in SST but decreasing in thermocline depth resulting in the reduction of negative skew of SST variability off Sumatra. There is low confidence that in a warmer climate, the IOB mode persists longer following the decay of an ENSO event, strengthening ENSO's influence on summer rainfall and tropical cyclone activity over the Northwest Pacific and East Asia.

The observed SST warming in the tropical Atlantic represents a reduction in spatial variation in climatology: the warming is weaker in north compared to south of the equator; and the equatorial cold tongue weakens both in the mean and interannual variability. There is *low confidence* in the projections over the tropical Atlantic - both for the mean and interannual modes, because of large errors in model simulations of current climate.

There is low confidence in assessing the future changes in MJO due to the poor skill in simulating MJO and its sensitivity to SST warming patterns that are subject to large uncertainties in their future projection.

14.4 El Niño Southern Oscillation

The El Niño-Southern Oscillation (ENSO) is a coupled ocean-atmosphere phenomenon naturally occurring at the inter-annual time scale. El Niño involves abnormal warming of tropical eastern-to-central Pacific sea surface temperature (SST) usually peaking at the end of the calendar year, which leads to a weakening of zonal SST contrast between the tropical western Pacific 'warm pool' and the tropical eastern Pacific 'cold tongue' (Figure 14.21). It is closely linked to its atmospheric counterpart, the Southern Oscillation, s surface pressure seesaw between Darwin and Tahiti or more comprehensively the equatorial zonal-overturning called the 'Walker circulation'. El Niño and Southern Oscillation are two different aspects of the same phenomenon and are caused by a positive feedback between the atmosphere and the tropical Pacific Ocean referred to as Bjerknes feedback (Bjerknes, 1966; Bjerknes, 1969). The opposite phase to El Niño, when the eastern equatorial Pacific cools, has been named La Niña.

[INSERT FIGURE 14.21 HERE]

Figure 14.21: Idealized schematic showing atmospheric and oceanic conditions of the tropical Pacific region and their interactions during normal conditions, El Niño conditions, and in a warmer world. a, Mean climate conditions in the tropical Pacific, indicating SSTs, surface wind stress and associated Walker circulation, the mean position of convection, and the mean upwelling and position of the thermocline. b, Typical conditions during an El Niño event. SSTs are anomalously warm in the east; convection moves into the central Pacific; the trade winds weaken in the east and the Walker circulation is disrupted; the thermocline flattens and the upwelling is reduced. c, The likely mean conditions under climate change derived from observations, theory and CGCMs. The trade winds weaken; the thermocline flattens and shoals; the upwelling is reduced although the mean vertical temperature gradient is increased; and SSTs (shown as anomalies with respect to the mean tropical-wide warming) increase more on the equator than off. Diagrams with absolute SST fields are shown on the left, diagrams with SST anomalies are shown on the right. For the climate change fields, anomalies are expressed with respect to the basin average temperature change so that blue colors indicate a warming smaller than the basin mean, not a cooling (Collins et al., 2010).

14.4.1 Tropical Pacific Mean State

Patterns of tropical Pacific SST change under global warming are uncertain. The tropical Pacific west-east SST contrast apparently strengthened during the 20th century, possibly as a result of the 'ocean dynamic thermostat', as upwelling/cooling of surface waters in the eastern Pacific overcompensates against increased surface radiative warming (Cane et al., 1997; Clement et al., 1996; Seager and Murtugudde, 1997). This change was observed in many gridded data sets (An et al., 2011; Cane et al., 1997; Hansen et al., 2006; Karnauskas et al., 2009) and was simulated by most CMIP3 models (An et al., 2011),. However, raw SST data without interpolation or bias-correction showed the opposite result of a decreases east-west SST contrast (Deser et al., 2010b; Tokinaga et al., 2012). Therefore, estimated trends of zonal SST gradient depend on the data used and the period chosen, even during the most recent few decades, because of observational uncertainties associated with limited data sampling, changing measurement techniques, and analysis procedures (Section 2.6.8). Nevertheless, a warming of the western tropical Pacific, up to 0.75°C per 50 years, and the expansion of warm pool are in agreement across many studies (Cane et al., 1997; Cravatte et al., 2009; Curtis and Hastenrath, 1999; Huang and Liu, 2001; Knutson and Manabe, 1998; Latif et al., 1997; Lau and Weng, 1999; Liu and Huang, 2000), while the warming over the eastern tropical Pacific for the last century is proposed as ENSO-related trend (Compo and Sardeshmukh, 2010; Wang and Lee, 2008). The tropical Pacific mean response to global warming has been suggested to be neither El Niño-like nor La Niña-like (Collins et al., 2010; DiNezio et al., 2009; Tung and Zhou, 2010) since the mechanisms for these changes are different from that of ENSO events – the Bjerknes feedback (Figure 14.1).

Apart from changes in the zonal SST gradient, the ocean surface warms more near the equator than in the subtropics in CMIP3 and CMIP5 projections (Gastineau and Soden, 2009; Liu et al., 2005) because of the difference in evaporative cooling (Xie et al., 2010b). Other oceanic changes include a basin-wide thermocline shoaling (Collins et al., 2010; DiNezio et al., 2009; Vecchi and Soden, 2007b), a weakening of the surface current, and a slight upward shift of the equatorial undercurrent (Luo and Rothstein, 2011). A weakening of tropical atmosphere circulation during the twentieth Century has been documented in observational and reanalysis data (Bunge and Clarke, 2009; Karnauskas et al., 2009; Tokinaga et al., 2012; Vecchi and Soden, 2007b; Vecchi et al., 2006; Yu and Zwiers, 2010; Zhang and Song, 2006) and in CMIP3 (Gastineau and Soden, 2009; Vecchi and Soden, 2007b). However, apart from the long-term trends, the intensification of tropical atmosphere circulation during the recent 2-3 decades was reported in several observational and reanalysis data (Li and Ren, 2011; Liu and Curry, 2006; Mitas and Clement, 2005; Mitas and Clement, 2006; Sohn and Park, 2010; Zahn and Allan, 2011; Zhang et al., 2011a).

14.4.2 Variance Changes over the Recent Decades and Future

The amplitude modulation of El Niño at longer timescales has been observed in reconstructed instrumental records (An and Wang, 2000; Gu and Philander, 1995; Mitchell and Wallace, 1996; Power et al., 1999a; Power and Smith, 2007; Wang, 1995; Wang and Wang, 1996; Yeh and Kirtman, 2005) and in various proxy records (Braganza et al., 2009; Cobb et al., 2003; Li et al., 2011d; Yan et al., 2011), and was also simulated by CGCMs (Lau et al., 2008; Wittenberg, 2009). The modulation was believed to relate to changes in mean climate conditions of the tropical Pacific (An and Wang, 2000; Fedorov and Philander, 2000; Li et al., 2011d; Wang and An, 2001; Wang and An, 2002), which indeed occurred between the pre-1980s and the post-1980s (An and Jin, 2000; An and Wang, 2000; Fedorov and Philander, 2000; Kim and An, 2011). An increasing trend in ENSO amplitude was also observed during the past Century (Li et al., 2011d), possibly

caused by global warming (Kim and An, 2011; Zhang et al., 2008a) although other reconstructions in this data-sparse region dispute that trend (Giese and Ray, 2011).

However, long-term CGCM simulations demonstrated that the decadal and even centennial timescale modulations of ENSO could be generated without invoking change in any external forcing (Wittenberg, 2009; Yeh et al., 2011). The modulation could result from nonlinear processes in the tropical climate system (Timmermann et al., 2003) or the interactive feedback between the mean climate state and ENSO (Choi et al., 2011; Choi et al., 2012; Choi et al., 2009b; Ye and Hsieh, 2008), or from truly random changes in ENSO activity from decade to decade linked to chaotic variability in the atmosphere (Power and Colman, 2006; Power et al., 2006). Thus, it is uncertain whether the decadal modulation of ENSO properties (amplitude, frequency, location of maximum loading, propagation , etc.) that occurred during recent decades is related to anthropogenic effects or to natural variability. Furthermore, because the change in tropical mean conditions under global warming is quite uncertain even over the past few decades (see Sections 14.4.1 and 14.4.5), it is hard to say whether ENSO will intensify, weaken, or remain unchanged in future (Hu et al., 2012a; Solomon and Newman, 2011) (Vecchi and Wittenberg, 2010). It is virtually certainly however that ENSO will not disappear in future (Collins et al., 2010).

[INSERT FIGURE 14.22 HERE]

Figure 14.22: Intensities of El Niño and La Niña events in the eastern equatorial Pacific (Niño3 region; upper) and in the central equatorial Pacific (Niño4 region; lower) the estimated linear trends, obtained from ERSST and HadISST (upper). Red and blue lines from ERSST, and dark red and dark blue lines from HadISST. EP and CP events are selected based on B case of Table 14.1.

The multi-model mean obtained from seven CMIP5 models that are best at simulating strong El Niño events shows a gradual increase of the intensity of the central Pacific El Niño (see Section 14.4.4) through pre-industrial, historical, and RCP simulations (Kim and Yu, 2012). CMIP3 models also suggested a westward shift of the strongest SST variability in their future projections (Boer, 2009; Yeh et al., 2009b). However, modelled future changes in the variability of El Niño in CMIP5 models (Figure 14.23) is model- and scenario-dependent (Guilyardi et al., 2012; Kim and Yu, 2012; Stevenson et al., 2012), and thus 21st century change to El Niño amplitude based on the multi-model mean is statistically insignificant (Stevenson, 2012).

[INSERT FIGURE 14.23 HERE]

Figure 14.23: Sea surface temperature anomalies and anomalous surface wind vectors on January 1998 and January 2010. Former and latter events are one of the biggest Eastern Pacific El Nino and Central Pacific El Nino in 20th century, respectively. Contour intervals are 0.5 degrees. Courtesy of TOGA TAO.

14.4.3 Teleconnections

ENSO events influence severe weather, ecosystems, agriculture, freshwater supplies, and tropical cyclone activity worldwide. The ENSO signal travels all over the globe through atmospheric waves, and this is called the ‘atmospheric ENSO teleconnection’. The global teleconnection pattern of ENSO depends on the heating sources associated with the location and amplitude of SST anomalies, and the atmospheric wave pathway that is influenced by the background atmospheric circulation (HOREL and WALLACE, 1981). The wave paths associated with ENSO are not limited to the troposphere but expand into the lower stratosphere, even to the Arctic region, where a warming and weakening polar vortex is recorded during an El Niño year, and even more strongly the following year (Bell et al., 2009; Cagnazzo and Manzini, 2009; Li and Lau, 2012b; Randel et al., 2009; Ren et al., 2012).

Scenario projections in CMIP3 and CMIP5 showed a systematic eastward shift in both El Niño and La Niña-induced teleconnection patterns over the extratropical Northern Hemisphere (Meehl and Teng, 2007; Meehl et al., 2007b; Stevenson et al., 2012), which might be due to the eastward migration of tropical convection centres associated with the expansion of the warm pool under global warming (Cravatte et al., 2009; Kug et al., 2010a; Müller and Roeckner, 2008; Muller and Roeckner, 2006) or a shift in the mid-latitude mean circulation (Meehl and Teng, 2007). Furthermore, some models produced an intensified ENSO pattern over the North Atlantic region in a warmer climate (Bulic et al., 2012; Müller and Roeckner, 2008) while weakening the ENSO teleconnection pattern over the North Pacific (Stevenson, 2012). It is unclear whether the eastward shift of tropical convection is related to longitudinal shifts in El Niño maximum SST anomaly (see 14.4.4). Nevertheless, some CGCMs, which do not simulate more central Pacific warming events (see

14.4.4) in response to global warming, do not produce a substantial change in the zonal shift of the convection (Müller and Roeckner, 2008; Yeh et al., 2009b).

14.4.4 Different Flavours of El Niño

Beyond the classical view of the El Niño pattern, another structure of anomalous warm SST, i.e., the warming in the equatorial central Pacific (CP) sandwiched by anomalous cooling to the east and west (hereafter referred to as CP El Niño) (Figure 14.24) (Larkin and Harrison, 2005; Trenberth and Tepaniak, 2001), has been frequently observed in the tropical Pacific since the 1990s (Ashok et al., 2007; Kao and Yu, 2009; Kug et al., 2009; Yeh et al., 2009b) (also see Sections 2.6.8, 9.5.3.4.1, 14.4.3) (Table 14.1). CP El Niño shows no basin-wide features or distinct propagation of SST anomalies and it occurs rather episodically in comparison with the conventional El Niño (Yu et al., 2010b). Many indices of CP El Niño have been proposed, but no clear and agreed definition has yet emerged to identify both CP El Niño and conventional El Niño (see Table 14.1). Furthermore, several studies using other classification methods do not find such a distinction between CP and 'conventional' El Niño events (Lian and Chen, 2012; Newman et al., 2011) (Lian and Chen; Lian and Chen, 2012; Newman et al., 2011), seeing changes in the location of El Niño from the western to the eastern Pacific as part of a random distribution (Giese and Ray, 2011). Hence, CP El Niño and conventional El Niño may not be different phenomena but rather a nonlinear evolution of the ENSO phenomenon (Takahashi et al., 2011).A debate remains as to whether the CP El Niño is intrinsically different to the conventional El Niño or if every event is a varying mix of these two patterns.

[INSERT TABLE 14. 1 HERE]
Table 14.1: Lists of years for Eastern Pacific and Central Pacific El Nino events.

[INSERT FIGURE 14.24 HERE]
Figure 14.24: SST (°C) averaged over the Niño3 region (150°W–90°W, 5°S–5°N), for (a) the ERSST.v3 historical reconstruction of Smith et al. (2008), and (b) the 20 consecutive centuries (numbered) from the GFDL CM2.1 pre-industrial control run. Red/blue shading highlights departures of the running annual-mean SST from the multidecadal background state, where the latter is obtained via a 211-month triangle smoother which transmits (25, 50, 75)% of the time series amplitude at periods of (15, 20, 30) year. Unshaded time series ends in Figure 14.24 indicate the half-width of the triangle smoother; ends of the observed time series in panel (a) are zero-padded prior to smoothing. The top of the grey bar is the long-term mean, indicated at the bottom right of each plot (Wittenberg, 2009).

The global impacts of central Pacific warming (CP El Niño) are different to those of the eastern Pacific warming (conventional El Niño) (Ashok et al., 2007; Hu et al., 2012b; Kao and Yu, 2009), including monsoonal rainfall over China and Korea (Feng and Li, 2011; Feng et al., 2010; Kim et al., 2012) and over Australia (Ashok et al., 2007; Taschetto and England, 2009; Taschetto et al., 2009; Wang and Hendon, 2007), United States air temperature and rainfall (Mo, 2010), winter temperature over the North Atlantic and Eurasian regions (Graf and Zanchettin, 2012), typhoon activity in the western North Pacific (Guanghua and Chi-Yung, 2010; Hong et al., 2011; Kim et al., 2011b), and the warming in western Antarctica (Ding et al., 2011; Lee et al., 2010b). The influence of CP El Niño on Atlantic hurricanes may also be different from the conventional El Niño (Kim et al., 2009), but it has been shown that the anomalous atmospheric circulation in the hurricane main development region during CP El Niño is similar to that during conventional El Niño (Lee et al., 2010a).

Changes in the impacts from conventional El Niño to CP El Niño are possibly due to the change in the location of tropical atmospheric heating source (Hoerling et al., 1997; Kug et al., 2010a). For example, conventional El Niño leads to the Pacific North American (PNA)-like atmospheric pattern along with changes in the Aleutian low strength (Müller and Roeckner, 2008), while CP El Niño is more linked to the atmospheric variability over the North Pacific such as the North Pacific Oscillation (NPO), which represents a meridional shift of the Aleutian low pressure centre (Di Lorenzo et al., 2010).

Some studies argue that more frequent occurrence of CP El Niño events during recent decades is related to the changes in the tropical Pacific mean state in response to increased greenhouse gas forcing (Yeh et al., 2009a). In particular, a flattening of thermocline depth in the equatorial Pacific and a weakened Walker circulation under global warming modulate the relative importance of feedback processes associated with El Niño dynamics (Yeh et al., 2009a). A heat budget analysis in the ocean mixed layer reveals that zonal advection is a major dynamical feedback process in developing of CP El Niño and the anomalous surface

heat flux in the decaying of CP El Niño (Kug et al., 2010b; Yu et al., 2010b). On the other hand, other studies (Lee and McPhaden, 2010; McPhaden et al., 2011) further showed that the future climate condition change associated with the increased occurrence of CP El Niño is not consistent with the observed climate condition that leads to more frequent occurrence of CP El Niño. Thus, whether the mean climate state change leads to more frequent emergence of CP El Niño or the other way around is not yet known. The increase in the frequency of CP El Niño during recent decades may be a manifestation of natural climate variability (Na et al., 2011; Yeh et al., 2011).

14.4.5 Sources of Uncertainty in ENSO Projections

The future of ENSO remains uncertain for several reasons: (1) the past behaviour and sensitivities of ENSO are poorly known; (2) ENSO is difficult to simulate in comprehensive GCMs (see Section 9.5.3.4.1); (3) ENSO may be subject to spontaneous random fluctuations on decadal-to-centennial timescales; (4) the future of the tropical Pacific mean state is uncertain; and (5) sensitivities of ENSO to changes in mean state are uncertain.

Improvements in ENSO simulations and projections have been hindered by uncertainties in the past behaviour of ENSO (see Section 9.5.3.4.1). Past behaviour must be inferred from short and incomplete instrumental records of tropical Pacific climate, along with indirect records from paleo proxies like corals, tree rings, lake sediments, and ice cores from tropical mountain glaciers (Vecchi and Wittenberg, 2010). Attempts to reconstruct past ENSO behaviour, using model assimilation of historical data (Giese and Ray, 2011) and paleo proxies over the past millennium (Li et al., 2011d), have met with mixed success. Although instrumental SST records for the tropical Pacific are available back to the 1850s, observations of the crucial coupled air-sea feedbacks that control ENSO behaviour -- including subsurface temperature and current fluctuations, and air-sea exchanges of heat, momentum, and water -- are available only after the advent of widespread buoy, ship, and satellite observations of the tropical Pacific in the late 1970s. Thus historical variations in ENSO feedback strengths and patterns remain highly uncertain (Chen, 2003; Wittenberg, 2004). In addition, paleo proxies of ENSO must be calibrated using the uncertain instrumental reconstructions, which imparts downstream uncertainties in paleo reconstructions.

Even if the global mean state could be projected perfectly into the future, there would remain uncertainties in the projection of ENSO behaviour, due to the intrinsic modulation of ENSO. The modulation arises from both nonlinearities in ENSO feedbacks and stochastic driving by near-equatorial winds, and has been documented in observations (An and Wang, 2000) and in GCMs (Stevenson et al., 2012; Wittenberg, 2009). In particular, (Wittenberg, 2009) showed that an unforced pre-industrial GCM simulation can spontaneously generate epochs of extreme ENSO behaviour lasting decades or even centuries, many of which mimic the 150 year observational record (Figure 14.25). Thus it is possible that (1) historically observed variations in ENSO behaviour might have been dominated by intrinsic modulation, and (2) the historical record might not have covered the full repertoire of ENSO behaviour, leaving open the possibility that ENSO could exhibit new behaviour in the future even without responding to changes in external forcings.

[INSERT FIGURE 14.25 HERE]

Figure 14.25: Standard deviation of Niño3 (upper) and Niño4 (lower) SST anomalies for CMIP5 model experiments. Blue bars, pre-industrial control experiments, dark red bars, last half of 21 century from the RCP4.5 experiments, yellow green bars, last half of 21 century from RCP8.5 experiments. Calculations are performed for the models indicated on the x-axis, and the linear trend has been removed in RCP4.5 and RCP8.5. The black 'error bar' indicates the minimum and maximum of 50-year windowed standard deviation of Niño index anomalies computed from the pre-industrial control experiments.

As described in Section 14.4.1, both the past and future changes in tropical Pacific mean state are uncertain, due to short and intermittent historical records and a wide diversity of model simulations and projections. Given that ENSO feedbacks depend strongly on the background mean state of the tropical Pacific, uncertainties in the projected mean state—whether due to scenario uncertainty, model uncertainty, or intrinsic changes in the mean state—contribute directly to uncertainties in future projections of ENSO.

Studies have shown that ENSO has a complex, nonlinear, coupled relationship with changes in the Pacific mean state (Fedorov et al., 2003; Fedorov and Philander, 2001; Rodgers et al., 2004; Sun, 2003; Sun and Zhang, 2006; Sun and Liu, 1996), and that even in the absence of changes in ENSO, mean state changes can

alter the remote teleconnections and impacts of ENSO (Meehl et al., 2006). Projections of future ENSO behaviour depend on competing changes in feedbacks, whereby increased wind-SST coupling, and zonal temperature gradients act to amplify ENSO, while decreased upwelling and increased surface heat flux damping of SST anomalies act to diminish ENSO (Philip and Van Oldenborgh, 2006; Vecchi and Wittenberg, 2010). Due to these competing changes in feedbacks, the ENSO response to future climate changes can depend sensitively on the dynamical regime of the model remains quite diverse in CMIP3 and CMIP5. However, the competition of feedback changes, while contributing to model diversity, may also reduce the total sensitivity of ENSO to mean state changes (DiNezio et al., 2012). This may explain why none of the SRES.A2 projections in CMIP3 exhibited more than a 40% change in ENSO amplitude by 2075 (van Oldenborgh et al., 2005).

14.4.6 Assessment summary

ENSO shows considerable inter-decadal modulations in amplitude and spatial pattern on the instrumental record. Because models with constant radiative forcing display similar modulations, it is not possible to attribute the observed change to external forcing.

There is *high confidence* that

- It is *very likely* that ENSO will remains the dominant mode of interannual variability in future. However natural modulations of variance and spatial pattern of ENSO are so large that it is not possible to tell with confidence if the projected change in the 21st century is due to human-induced changes in atmospheric composition
- Based on model projections, it is *likely* there will be a systematic eastward shift in both El Niño and La Niña-induced teleconnection patterns over the extratropical Northern Hemisphere.

There is *medium confidence* that

- The intensity of central Pacific warming (CP El Niño) is *likely* to increase with increased greenhouse warming.

[START BOX 14.2 HERE]

Box 14.2: Tropical Cyclones

The potential for regional changes in future tropical cyclone frequency, track and intensity is of great interest, not just because of the associated risk of damage and loss of life, but also because tropical cyclones can play a major role in maintaining regional water resources (Jiang and Zipser, 2010; Lam et al., 2012). Past and projected increases in exposure to tropical cyclones in many regions (Peduzzi et al., 2012) heightens the interest further. Detection of past trends in various measures of tropical cyclone activity is constrained by the quality of the historical data records and uncertain quantification of natural variability in these measures (Knutson et al., 2010; Seneviratne et al., 2012), (see also Chapters 2 and 10). Consideration of global trends as well as trends in specific regions is further complicated by substantial regional differences in data quality, collection protocols, and record length (Knapp and Kruk, 2010; Song et al., 2010). Annual-mean global tropical cyclone frequency since 1980 (within the modern geostationary satellite era) has remained roughly steady at about 90 per year, with a standard deviation of about 10% (9 storms). Standard deviations of annual frequency in individual ocean basins, however, can be greater than 40% of the means in those basins, which reduces the signal-to-noise ratio and introduces substantial uncertainty into regional tropical cyclone frequency trend detection.

Attempts to detect trends in even smaller intra-basin regions such as those defined by islands or archipelagos are further constrained by the reduced data sample size associated with finely subdividing the global data. Intra-basin regional trend detection is also substantially challenged by variability in tropical cyclone tracks (Kossin and Camargo, 2009). This variability is driven largely by random fluctuations in atmospheric steering currents, but also is observed across a broad range of time-scales in response to more systematic modes of climate variability such as the El Niño – Southern Oscillation (ENSO), Pacific Decadal Oscillation, North Atlantic Oscillation, Atlantic Meridional Mode, and Madden-Julian Oscillation (Camargo et al., 2008; Camargo et al., 2007; Chand and Walsh, 2009; Chu et al., 2012; Ho et al., 2004; Kossin et al., 2010; Tu et al., 2009; Wang et al., 2010a; Wu et al., 2005). Even modest tropical cyclone track variability can lead to

large differences in associated impacts at a specific location. For example, small islands can be affected by multiple tropical cyclones in one season (e.g., the Philippines in 2009) and then remain largely unaffected for multiple subsequent years even while the total number of storms in the larger, but immediate surrounding region exhibits normal variability. This type of "temporal clustering" can occur randomly or via systematic modulation by climate variability, and can also strongly affect the impact of tropical cyclones on ecosystems such as coral reefs (Mumby et al., 2011). The combination of data issues (quality and sample size), signal-to-noise issues, and the natural variability of tropical cyclone tracks introduce substantial uncertainties into detection-attribution studies as well as disaster and mitigation planning aimed at specific intra-basin regions. Furthermore, while theoretical arguments have been put forward linking tropical cyclone intensity and genesis with anthropogenic climate change (Emanuel, 1987; Rappin et al., 2010), there is little theoretical guidance available to help elucidate the relationships between climate and tropical cyclone track variability.

Regional analyses of Century-scale variability and trends of various measures of tropical cyclone activity provide mixed results from which robust conclusions are difficult to establish (also see Chapter 2). Regional trends in tropical cyclone frequency have been identified in the North Atlantic, with storm frequency increasing sharply over the past 20-30 years. Over longer time-periods, especially since the late 19th Century, the fidelity of the reported trends is debated (Holland and Webster, 2007; Landsea, 2007; Mann et al., 2007a). Different methods for estimating undercounts in the earlier part of the North Atlantic tropical cyclone record provide mixed conclusions (Chang and Guo, 2007; Kunkel and al., 2008; Mann et al., 2007b; Vecchi and Knutson, 2011; Vecchi and Knutson, 2008). Trends in cyclone frequency have also been identified over the past 50-60 years in the North Indian Ocean and may be due to changes in the strength of the tropical easterly jet (Krishna, 2009; Rao et al., 2008) but again uncertainties in the regional tropical cyclone data quality substantially limit reliability, particularly when attempting to detect Century-scale trends (Mohapatra et al., 2011). Furthermore, metrics based solely on storm frequency can be strongly influenced by weak and/or short-lived storms (Landsea et al., 2010), which are arguably of much lesser physical relevance than stronger and/or longer-lived storms. This limits the usefulness of such metrics that do not take storm intensity or duration into account. Regional trends in the frequency of very intense tropical cyclones can be identified in the historical data over the past 30–40 years (Webster et al., 2005), although confidence in the amplitude of these trends is compromised by data homogeneity uncertainties (Kossin et al., 2007; Landsea et al., 2006). There has been a sharp increase in annual tropical cyclone power dissipation (which represents an amalgamation of frequency, intensity, and storm duration) in the Atlantic since 1970 (Emanuel, 2005), but longer-term trends are more uncertain because of data heterogeneities, particularly in the records of storm intensity (Hagen and Landsea, 2012; Hagen et al., 2012; Landsea et al., 2012). Upward regional and global trends in the intensity of the strongest storms have been identified in a more homogeneous data record by Elsner et al. (2008), but their analysis was necessarily limited to the modern geostationary satellite period and only spans about 30 years. Increasing trends in the frequency of landfalling tropical cyclones have not been identified in any region (Chan and Xu, 2009; Kubota and Chan, 2009; Wang and Lee, 2008; Weinkle et al., 2012) although Callaghan and Power (2010) identified a statistically significant downward trend in the number of severe tropical cyclones making landfall over north-eastern Australia since the late 19th century. Measurements of tropical cyclone landfall frequency are generally considered to be more reliable than those of storms that remain at sea throughout their lifetimes, particularly in the earlier parts of the historical records. But as described above, confining storm counts to any pre-defined region cannot discriminate between basin-wide frequency variability and track variability, and it remains uncertain whether the trend reported by Callaghan and Power (2010) is driven by natural processes or whether some part is driven by global warming. When data uncertainties due to past changes in observing capabilities are taken into account, confidence in the fidelity of any reported basin-wide trends in tropical cyclone activity on time-scales longer than about 50 years is substantially compromised. Shorter term increases, such as observed in the Atlantic since 1970, appear to be robust (Kossin et al., 2007), and have been hypothesised to be related, in part, to regional external forcing by greenhouse gasses and aerosols (discussed below), but the more steady century-scale trends that may be expected from CO_2 forcing are much more difficult to assess given the data uncertainty in the available tropical cyclone records. This presents a confounding factor to formal detection of trends that may be attributed to anthropogenic effects because the expected natural variability on multi-decadal time-scales is not yet well quantified in the various regions.

While there is evidence that sea surface temperature (SST) in the tropics has increased due to increasing greenhouse gases (Gillett et al., 2008; Karoly and Wu, 2005; Knutson et al., 2006; Santer et al., 2006) and there is a theoretical expectation that increases in potential intensity will lead to stronger tropical cyclones

(Elsner et al., 2008; Emanuel, 2000; Wing et al., 2007), the relationship between SST and potential intensity under CO_2 warming has not yet been fully elucidated (see also Chapter 10). Potential intensity describes the theoretical limit to how strong a tropical cyclone can become based on the three-dimensional thermodynamic environment that the storm moves through (Emanuel, 1987). Observations demonstrate a strong positive correlation between SST and potential intensity, but it is known that this relationship is not unique. For example, raising SST by reducing surface wind speed produces a much more rapid increase in potential intensity with SST than does raising it by increasing CO_2 because other factors that control potential intensity will vary differently according to each process (Emanuel et al., 2012). Similarly, vertical wind shear, which affects tropical cyclone genesis and intensification, is apparently modulated differently by internal variability versus external radiative forcing of regional SST (e.g., Zhang and Delworth 2009).

While it is generally agreed that regional projections of SST by themselves are not a useful proxy for future tropical cyclone potential intensity, there is a growing body of research since the IPCC Fourth Assessment Report suggesting that the difference between regional SST and spatially averaged SST in the tropics can serve as a useful proxy for regional potential intensity (Camargo et al., 2012; Ramsay and Sobel, 2011; Vecchi and Soden, 2007a; Xie et al., 2010b). The hypothesis is largely phenomenological and based on observed correlation, but has some physical basis in the theory that upper-tropospheric temperatures are sensitive to mean tropical SST (Sobel et al., 2002), while regional lower-tropospheric temperatures are more sensitive to local SST. This combination of factors affects regional lapse rates, which in turn affects potential intensity. In this case, localized SST changes are hypothesized to be more effective at altering potential intensity than a more globally uniform tropical SST change (e.g., as would be expected from forcing by well-mixed greenhouse gases) of the same magnitude. Since projections of 21st century tropical SST change tend to show relative SST changes (i.e., regional average changes relative to the tropical mean) that can be quite different from the absolute SST warming in regions where storms form and track (Vecchi and Soden, 2007a), this recent research suggests that increasing SST due to greenhouse warming, by itself, does not yet have a fully reconciled physical link to increasingly strong tropical cyclones. However, it has been argued (Emanuel 2010; Emanuel et al. 2012) that the physical link between relative SST and potential intensity is only valid on time-scales shorter than about two years. On longer time-scales, which allow the ocean mixed layer to equilibrate to surface forcing, Emanuel et al. (2012) argue that potential intensity is mostly controlled by local surface radiative balance and ocean heat flux convergence and in general, SST cannot be considered an external control on potential intensity, but merely a co-factor. By this argument (and the assumptions that it is based on), projections of SST by themselves, whether absolute SST or relative SST, cannot uniquely determine future potential intensity changes, and hence they cannot uniquely determine future tropical cyclone changes. Still, the studies of Camargo et al. (2012), Ramsay and Sobel (2011), Vecchi and Soden (2007a), Xie et al. (2010b), and others have demonstrated that the correlation between relative SST and potential intensity is in fact consistently evident on multi-decadal and longer time-scales. Thus, while the presumptive theoretical arguments of Emanuel (2010) and Emanuel et al. (2012) suggest that there is no reason to expect such a relationship (and therefore there is no physical justification for using 21st century relative SST projections to statistically infer future potential intensity), both data and model projections support the existence of a useful relationship between relative SST and potential intensity on decadal and longer timescales. While the balance of relevant literature supports the hypothesis that long-term relative SST projections can serve as a useful proxy for future tropical cyclone potential intensity, this remains an active area of research (and debate) without a clear consensus yet.

The distinction between the competing hypotheses described above is a critical one because while tropical SST is expected to continue to increase under global warming, there is much more uncertainty in how regional SST is expected to change relative to the tropical mean (Vecchi et al., 2008; Villarini et al., 2011). In general, future relative SST changes forced by increasing well-mixed greenhouse gas in the tropics are not expected to be large (Vecchi and Soden, 2007a) and thus if relative SST is a useful proxy for potential intensity, there would not be an expectation for large increases in future tropical cyclone intensity (Vecchi et al., 2008). The results of Emanuel (2010) and Emanuel et al. (2012) do not provide alternative projections of potential intensity, but only state that they are not constrained by any measure of future SST alone. As an example of the ramifications of the differences, the present 20-30 year period of heightened tropical cyclone activity in the North Atlantic, concurrent with comparative recent quiescence in most other ocean basins (Maue, 2011), is apparently related to differences in the rate of SST increases, as global tropical SST has been rising steadily but at a slower rate than the Atlantic (Holland and Webster, 2007). The present period of relatively enhanced warming in the tropical North Atlantic has been proposed to be due to internal variability

(Camargo et al., 2012; Ting et al., 2009a; Zhang and Delworth, 2009), and both direct (dimming) and indirect (cloud-albedo) effects of radiative forcing by anthropogenic tropospheric aerosols (Booth et al., 2012; Mann and Emanuel, 2006) and mineral (dust) and volcanic aerosols (Evan et al., 2012; Evan et al., 2011a; Evan et al., 2009). None of these proposed mechanisms provide a clear expectation that North Atlantic SST will continue to increase at a greater rate than the tropical-mean SST and thus if future potential intensity can be described by relative SST, the present steep upward trend in tropical cyclone intensity in the North Atlantic would be expected to abate.

Observed regional climate variability generally represents a complex convolution of factors, both natural and anthropogenic, and the response of tropical cyclones to each factor is not yet well elucidated. For example, the steady long-term secular increase in tropical Atlantic SST due to increasing greenhouse gas (e.g., Santer et al. (2006)) can be dominated by shorter-term decadal variability forced by both external and internal factors (Booth et al., 2012; Camargo et al., 2012; Chang et al., 2011; Evan et al., 2011a; Evan et al., 2009; Mann and Emanuel, 2006; Solomon et al., 2011; Ting et al., 2009a; Villarini and Vecchi, 2012; Zhang and Delworth, 2009). Similarly, tropical upper-tropospheric temperatures, which modulate tropical cyclone potential intensity (Emanuel, 2010), can be forced by slowly-evolving secular changes in the stratospheric circulation of ozone (Brewer-Dobson circulation) due to climate change with occasional large amplitude and persistent changes forced by volcanic eruptions (Emanuel et al., 2012; Evan, 2012; Thompson and Solomon, 2009). In addition to greenhouse warming scenarios, tropical cyclones can also respond to anthropogenic forcing via different and possibly unexpected pathways. For example, increasing anthropogenic emissions of black carbon and other aerosols in South Asia has affected SST gradients in the Northern Indian Ocean (Chung and Ramanathan, 2006; Meehl et al., 2008), which has in turn led to a weakening of the vertical wind shear in the region. Evan et al. (2011b) linked the reduced wind shear to the observed increase in the number of very intense storms in the Arabian Sea, including five very severe cyclones that have occurred since 1998 killing over 3500 people and causing over $6.5 billion in damages (in 2011 U.S. dollars). Furthermore, it is possible that much of the multi-decadal variability of North Atlantic SST is radiatively forced, via the cloud albedo effect, by what are essentially pollution aerosols emitted from North America and Europe (Booth et al., 2012). Note that in the North Atlantic, the evidence suggests that the *reduction* of pollution aerosols since the United States Clean Air Act of 1970 (with further contribution from the European Commission's Air Quality Framework Directive) is linked to tropical SST increases, while in the northern Indian Ocean, *increases* in aerosol pollution have been linked to reduced vertical wind shear. Both of these effects have been observed to be related to increased tropical cyclone activity. Finally, in addition to interannual-to-multidecadal forcing of tropical Atlantic SST via radiative dimming (Evan et al., 2011a; Evan et al., 2009), dust aerosols have a large and more immediate *in situ* effect on the regional thermodynamic and kinematic environment (Dunion, 2011; Dunion and Marron, 2008), and Saharan dust storms—whose frequency has been linked to atmospheric CO_2 concentration (Mahowald, 2007)—have also been linked to reduced strengthening of tropical cyclones (Dunion and Velden, 2004; Wu, 2007). Direct *in situ* relationships have also been identified between aerosol pollution concentrations and tropical cyclone structure and intensity (Khain et al., 2008; Khain et al., 2010; Rosenfeld et al., 2011). Thus, when assessing changes in tropical cyclone activity, it is clear that detection and attribution aimed simply at long-term linear trends forced by increasing well-mixed greenhouse gasses is not adequate to provide a complete picture of the potential anthropogenic contributions to the changes in tropical cyclone activity that have been observed.

Similar to observational analyses, confidence in numerical simulations of tropical cyclone activity (summarised in Box 14.2, Tables 1–4) is reduced when model spatial scale is reduced from global to region-specific (IPCC SREX Box 3.1). Projections based on the SRES A1B warming scenario through the late 21st century indicate that it is *likely* that the global frequency of tropical cyclones will either decrease or remain essentially unchanged while mean intensity increases by +2 to +11% and tropical cyclone rainfall rates increase by about 20% within 100 km of the cyclone centre (Knutson et al., 2010). However, inter-model differences in regional projections lead to lower confidence in basin-specific projections, and confidence is particularly low for projections of frequency within individual basins (Knutson et al., 2010). Still, the available modelling studies that are capable of producing very strong cyclones typically project substantial increases in the frequency of the most intense cyclones and it is *more likely than not* that this increase will be substantially larger than 10% in some basins (Bender et al., 2010; Emanuel et al., 2008; Knutson et al., 2010; Murakami et al., 2012; Yamada et al., 2010). It should be emphasized that this metric is generally more important to physical and societal impacts than overall frequency or mean intensity.

As seen in Box 14.2 Tables 1–4, the numerical model projections introduced in the literature often vary substantially in the details of the models and the experiments performed, and it is difficult to objectively assess their combined results to form a common consensus. Still, it is useful to perform this exercise after normalising the models and their output using a combination of objective and subjective expert judgements. The results of this exercise are shown in Box 14.2, Figure 1, and are based on a subjective normalisation of the model output to four common metrics under a common future scenario projected through the 21st century. The annual frequency of tropical cyclones is generally projected to decrease or remain essentially unchanged in the next Century in most regions although as noted above, the confidence in the projections is lower in specified regions than global projections. The decrease in storm frequency is apparently related to projected changes in tropical middle-troposphere convective mass flux associated with global warming (Emanuel et al., 2012; Emanuel et al., 2008; Held and Zhao, 2011; Murakami et al., 2012; Sugi et al., 2009; Zhao et al., 2009). A number of experiments that are able to simulate intense tropical cyclones project increases in the frequency of these storms in some regions, although there are presently only limited studies to assess and there is insufficient data to draw from in most regions to make a confident assessment there. The models generally project an increase in mean lifetime-maximum intensity of simulated storms, which is consistent with a projected increase in the frequency in the more intense storms since an increase in the mean intensity is expected to manifest as a greater increase in the upper extremes of intensity (Elsner et al., 2008). The projected increase in intensity concurrent with a projected decrease in frequency can be theoretically argued to result from a difference in scaling between projected changes in surface enthalpy fluxes and the Clausius-Clapeyron relationship associated with the moist static energy of the middle-troposphere (Emanuel et al., 2012). The increase in rainfall rates associated with tropical cyclones is a consistent feature of the numerical models under greenhouse warming as atmospheric moisture content in the tropics and tropical cyclone moisture convergence is projected to increase (Allan and Soden, 2008; Knutson et al., 2010; Trenberth et al., 2007a; Trenberth et al., 2005a).

A number of studies since the IPCC Fourth Assessment Report have attempted to project future changes in tropical cyclone tracks and genesis at inter- or intra-basin scale (Emanuel et al., 2008; Lavender and Walsh, 2011; Leslie et al., 2007; Li et al., 2010d; Murakami and Wang, 2010; Murakami et al., 2011b; Vecchi and Soden, 2007c; Yokoi and Takayabu, 2009; Zhao et al., 2009). These studies suggest that projected changes in tropical cyclone activity are strongly correlated with the projected changes in the spatial pattern of tropical SST (Murakami et al., 2011a; Sugi et al., 2009; Zhao and Held, 2012) and associated weakening of the Pacific Walker circulation (Vecchi and Soden, 2007b). However, assessing qualitative changes in regional tropical cyclone frequency is still limited because confidence in projections critically depend on the performance of control simulations (Murakami and Sugi, 2010), and current climate models still fail to simulate observed temporal and spatial variations in tropical cyclone frequency (Walsh et al., 2012a). As noted above, tropical cyclone genesis and track variability is modulated in most regions by known modes of atmosphere/ocean variability. The phenomenological details of the relationships vary by region (e.g., El Niño events tend to cause track shifts in western North Pacific typhoons and tend to suppress Atlantic storm genesis and development). Similarly, it has been demonstrated that accurate modelling of tropical cyclone activity fundamentally depends on the model's ability to reproduce these modes of variability (e.g., Yokoi and Takayabu, 2009). Reliable projections of future tropical cyclone activity, both global and regional, will then depend critically on reliable projections of the behaviour of these modes of variability (e.g., ENSO) under global warming, as well as an adequate understanding of their physical links with tropical cyclones. At this time, however, there is still uncertainty in their projected behaviours (e.g., Collins et al., 2010).

The reduction in signal-to-noise ratio that accompanies changing focus from global to regional scales also lengthens the emergence time-scale (i.e., the time required for a trend signal to rise above the natural variability in a statistically significant way). Based on changes in tropical cyclone intensity predicted by idealized numerical simulations with CO_2-induced tropical SST warming, Knutson and Tuleya (2004) suggested that clearly detectable increases may not be manifest for decades to come. The more recent high-resolution dynamical downscaling study of Bender et al. (2010) supports this argument and suggests that the predicted increases in the frequency of the strongest Atlantic storms may not emerge as a clear statistically significant signal until the latter half of the 21st century under the SRES A1B warming scenario. Other studies that have considered projected changes in tropical cyclone-related damage and loss under A1B warming (Crompton et al., 2011; Emanuel, 2011; Mendelsohn et al., 2012) predict a broad range of emergence time-scales from decades to centuries. However, it should again be emphasized that regional forcing by agents other than greenhouse gas, such as anthropogenic aerosols, is known to affect the regional

climatic conditions differently (e.g., Zhang and Delworth, 2009), and there is evidence that tropical cyclone activity has changed in some regions because of effects from anthropogenic aerosol pollution. The fidelity of the emergence time-scales projected under A1B warming thus depends on the fidelity of A1B aerosol projections, which are known to be highly uncertain (Forster et al., 2007; Haerter et al., 2009).

In summary, detection and attribution of trends as well as agreement among numerical simulations is substantially compromised when the scale of focus is reduced from global to regional. This is particularly severe when intra-basin regions such as island chains or specific sections of coastline are considered and tropical cyclone track variability plays a much larger role. The influence of past and future climate change on tropical cyclones is *likely* to vary by region, but the specific characteristics of the changes are not yet well understood, and the substantial influence of ENSO and other known climate modes on global and regional tropical cyclone activity emphasizes the need for more reliable assessments of future changes in the characteristics of these modes. When data uncertainties due to past changes in observing capabilities are taken into account, confidence in the fidelity of any reported regional trends in tropical cyclone activity on time-scales longer than about 50 years is substantially compromised. However, recent advances in understanding and phenomenological evidence for shorter-term effects on tropical cyclones from aerosol forcing are providing increasingly greater confidence that anthropogenic forcing has had a measurable effect on tropical cyclone activity in certain regions. Shorter term increases such as those observed in the Atlantic over the past 30–40 years appear to be robust and have been hypothesised to be related, in part, to regional external forcing by greenhouse gasses and aerosols, but the more steady Century-scale trends that may be expected from CO_2 forcing are much more difficult to assess given the data uncertainty in the available tropical cyclone records. While projections under 21st century greenhouse warming indicate that it is *likely* that the global frequency of tropical cyclones will either decrease or remain essentially unchanged, concurrent with a *likely* increase in both global mean tropical cyclone maximum wind speed and rainfall rates, there is *lower confidence* in region-specific projections of frequency and intensity. Still, based on high-resolution modeling studies, the frequency of the most intense storms, which is particularly relevant to physical and social impacts, will *more likely than not* increase substantially in some basins under projected 21st century warming. Two important questions that have not been reconciled but continue to motivate active research are 1) whether tropical cyclone potential intensity is and will continue to be correlated with future changes in relative SST, which is generally not shown to increase substantially in the next Century (Vecchi and Soden, 2007a), and 2) what portion of the observed multi-decadal climate variability in the tropical Atlantic (which tropical cyclones are observed to substantially respond to) is due to natural variability versus external forcing by greenhouse gasses and anthropogenic aerosols.

[INSERT BOX 14.2, FIGURE 1 HERE]

Box 14.2, Figure 1: General consensus assessment of the numerical experiments described in Box 14.2, Tables 1-4. All values represent *expected percent change* (year 2100 relative to 2000) under an A1B-like scenario, based on expert judgment after subjective normalisation of the model projections. Four metrics were considered: the percent change in 1) the total annual frequency of tropical storms, 2) the annual frequency of Category 4 and 5 storms, 3) the mean Lifetime Maximum Intensity (LMI; the maximum intensity achieved during a storm's lifetime), and 4) the precipitation rate within 200 km of storm center at the time of LMI. For each metric, the first numeric value is the best guess of the expected percent change, and the range in parentheses is the 67% (*likely*) confidence interval for this value. There are nine regions considered: Global, Northern Hemisphere, Southern Hemisphere, Eastern North Pacific, North Atlantic, Northern Indian, Southern Indian, Western North Pacific, and South Pacific.

[INSERT BOX 14.2, TABLE 1 HERE]

Box 14.2, Table 1: Projections of tropical storm frequency. Projected change in frequency of tropical storms in warm climate runs relative to control run in percent. Red and blue numbers/text denote projected increases and decreases, respectively. Bold text denotes where a statistical significance test was reported that showed significance. The frequency projections from Emanuel et al. (2008) been computed slightly differently from those shown in Figure 8 of the original paper in order to facilitate intercomparison with projection results from other studies.

[INSERT BOX 14.2, TABLE 2 HERE]

Box 14.2, Table 2: Projections of intense TC frequency. Projected change in frequency of intense tropical cyclones (i.e., more intense than tropical storms) in warm climate runs relative to control run in percent. The rows of reported results are ordered from top to bottom generally in order of decreasing model horizontal resolution. Red and blue numbers/text denote projected increases and decreases, respectively. Bold text denotes where a statistical significance test was reported that showed significance.

[INSERT BOX 14.2, TABLE 3 HERE]
Box 14.2, Table 3: Tropical cyclone intensity change projections (percent change in maximum wind speed or central pressure fall, except as noted in the table. The dynamical model projections are ordered from top to bottom in order of decreasing model horizontal resolution. Red and blue colors denote increases and decreases, respectively. Pairs of numbers in parentheses denote ranges obtained using different models as input to a downscaling model or theory. The potential intensity change projections from Emanuel et al. (2008), Knutson and Tuleya (2004), and Vecchi and Soden (2007) in the table include some results that are adapted from the original papers but have been modified in order to facilitate intercomparison of methods and projection results from different studies. In some cases, ACE or PDI changes are reported, which depend on intensity, frequency, and lifetime.

[INSERT BOX 14.2, TABLE 4 HERE]
Box 14.2, Table 4: Tropical cyclone-related precipitation projected changes (%) for the late 21st century (relative to present day).

[END BOX 14.2 HERE]

14.5 Annular and Dipolar Modes

This section assesses the following dominant modes of variability in the extra-tropics: the North Atlantic Oscillation (NAO), the North Pacific Oscillation (NPO), and the Northern and Southern Annular Modes (NAM and SAM). These modes are the focus of much research attention, especially in impact studies, where they are often used as aggregate descriptors of past regional climate trends and variations over many parts of the world[3]. This assessment focuses on recent research on these modes that is most relevant for future regional climate change. Past behaviour of these modes inferred from observations is assessed in Section 2.7.

14.5.1 Northern Modes

The North Atlantic Oscillation is a well-established dipolar mode of climate variability having opposite-polarity variations in sea-level pressure between two centres (poles) of action: the Atlantic subtropical high and the Iceland/Arctic low (Budikova, 2009; Hurrell et al., 2003; Wanner et al., 2001). The NAO is associated with substantial variation in the tropospheric jet, storms (see Box 14.3), and blocking that influence climate over the North Atlantic and surrounding continents (Hurrell and Deser, 2009). The NAO exists in boreal summer as well as in boreal winter, albeit with different physical characteristics (Folland et al., 2009).

The NAO has been interpreted as the regional manifestation of an annular mode in sea-level pressure known as the Arctic Oscillation (AO) (Thompson and Wallace, 1998) or the Northern Annular Mode (NAM) (Thompson and Wallace, 2000). The AO index (and NAM at 1000hPa) is very similar to the NAO index (see Chapter 2: Box 2.4, Table 1) but the spatial climate patterns differ considerably over the N. Pacific (Ambaum et al., 2001; Feldstein and Franzke, 2006). The AO is more zonally symmetric than the NAO and so resembles the NAM in the lower stratosphere (Baldwin and Thompson, 2009). The NAM is a Northern Hemisphere analogue of the Southern Annular Mode (Section 14.5.2). In what follows, the term NAO is used to denote NAO, AO and NAM in boreal winter unless further distinction is required.

The Pacific basin analogue of the NAO, the North Pacific Oscillation, is a prominent wintertime mode of variability characterized by a north-south dipole in sea level pressure over the N. Pacific (Linkin and Nigam, 2008; Rogers, 1981; Walker, 1924). The NPO and its upper air signature, the West Pacific (WP) teleconnection pattern, are associated with north-south displacements of the Asian-Pacific jet stream and the Pacific storm track. The NPO/WP substantially influences winter air temperature and precipitation over much of western North America as well as sea ice over the Pacific sector of the Arctic, more so than either ENSO or the PNA (Linkin and Nigam, 2008). The NPO/WP also affects the strength of the North Pacific Ocean gyre-scale circulation, with consequences for upper ocean temperature, salinity, nutrients, and marine biology (Ceballos et al., 2009; Cloern et al., 2010; Di Lorenzo et al., 2009). By affecting the strength of the Trade Winds, which subsequently alter sea surface temperatures over the subtropical Pacific, the NPO contributes to the excitation of ENSO events via the "Seasonal Footprinting Mechanism" (SFM) (Alexander

[3] For example, since IPCC (2007) more than 2000 scientific articles have been published, which include NAO, AO, or NAM in either the title or abstract.

et al., 2010; Anderson, 2003; Vimont et al., 2009). Some studies indicate that warm events in the central tropical Pacific Ocean may in turn excite the NPO/WP (Di Lorenzo et al., 2009).

Recent multi-model studies of NAO (Hori et al., 2007; Karpechko, 2010; Zhu and Wang, 2010) reconfirm the small positive response of boreal winter NAO indices to greenhouse gas forcing noted in earlier studies reported in AR4 (Kuzmina et al., 2005; Miller et al., 2006; Stephenson et al., 2006). Projected trends in wintertime NAO indices are generally found to have small amplitude compared to natural internal variations (Deser et al., 2011). Furthermore, there is substantial variation in NAO projections from different climate models. For example, one study found no substantial NAO trends in two simulations with ECHAM4/OPYC3 (Fischer-Bruns et al., 2009), whereas another study found a strong positive trend in NAO in the ECHAM5/MPI-OM SRES A1B simulations (Müller and Roeckner, 2008). The model-dependence of the response is an important source of uncertainty in the regional climate change response (Karpechko, 2010). A multi-model study of 24 climate model projections suggests that there are no major changes in the NPO due to greenhouse warming (Furtado et al., 2011).

Figures 14.26a-b) summarise the NAO and NAM indices simulated by models participating in the CMIP5 experiment. The multi-model mean of the NAO and NAM indices are similar and exhibit small linear trends in agreement with those shown for the NAM index in AR4 (AR4, Figure 10.17a). The multi-model mean projected increase of around 1-2 hPa from 1850 to 2100 is smaller than the spread of around 2-4 hPa between model simulations (Figure 14.26b)

Some differences in model projections can be accounted for by changes in the NAO spatial pattern, for example, northeastward shifts in NAO centres of action have been found to be important for estimating the trend in the NAO index (Hu and Wu, 2004; Ulbrich and Christoph, 1999). Individual model simulations have shown the spatial extent of NAO influence decreases with greenhouse gas forcing (Fischer-Bruns et al., 2009), a positive feedback between jet and storm tracks that enhances a pole ward shift in the NAO pattern (Choi et al., 2010), and changes in the NAO pattern but with no changes in the propagation conditions for Rossby waves (Brandefelt, 2006). One modelling study found a trend in the correlation between NAO and ENSO during the 21st century (Muller and Roeckner, 2006). Any changes in the structure of NAO and its association with other modes of variability would have consequences for the impact of NAO on regional climate change.

The NAO may be a preferred pattern of response to climate change (Gerber et al., 2008). However, this is not supported by a detailed examination of the vertical structure of the simulated global warming response (Woollings, 2008). Hori et al. (2007) noted that NAO variability did not change substantially in the SRES-A1B and 20th century scenarios and so concluded that the trend in the NAO index (defined relative to a historical mean state) is a result of an anthropogenic trend in the basic mean state rather than due to changes in NAO variability. However, other research indicates that there is a coherent two-way interaction between the trend in the mean state and the NAO-like modes of variability – the mode and/or regime structure change due to changes in the mean state (Barnes and Polvani, 2012; Branstator and Selten, 2009).

Climate models are generally able to simulate the gross features of NAO and NPO (see Section 9.5.3.2). However, model simulations have underestimated the magnitude of the large positive trend from 1960-2000 in NAO observations, which now appears to be more likely due to natural variability rather than anthropogenic influences (see Section 10.3.3.4). Detection and attribution of trends in sea-level pressure due to greenhouse gas, aerosol and ozone changes is more conclusive on global spatial fields than on NAO indices (Gillett and Fyfe, 2012). Some studies have even considered NAO to be a source of natural variability that needs to be removed before detection and attribution of anthropogenic changes (Zhang et al., 2006b). Detection of regional surface air temperature response to anthropogenic forcing has been found to be robust to the exclusion of model-simulated AO and PNA changes (Wu and Karoly, 2007). Model projections of wintertime European precipitation have been shown to become more consistent with observed trends after removal of trends due to NAO (Bhend and von Storch, 2008). Underestimation of trends in NAO can lead to biases in projections of regional climate e.g., Arctic sea ice (Koldunov et al., 2010).

Underestimation of NAO long-term variability may be due to missing or poorly represented processes in climate models. Recent observational and modelling studies have helped to confirm that the lower stratosphere plays an important role in explaining recent more negative NAO winters and long term trends in

NAO (Dong et al., 2011; Ouzeau et al., 2011; Scaife et al., 2005; Schimanke et al., 2011). This is supported by evidence that seasonal forecasts of NAO can be improved by inclusion of the stratospheric QBO (Boer and Hamilton, 2008; Marshall and Scaife, 2010). Other studies have found that observed changes in stratospheric water vapour changes from 1965–1995 led to a substantial impact on NAO simulated by a model, and have suggested that changes in stratospheric water vapour may be another possible pathway for communicating tropical forcing to the extra-tropics (Bell et al., 2009; Joshi et al., 2006). There is growing evidence that future NAO projections are sensitive to how climate models resolve stratospheric processes and troposphere-stratosphere interactions (Scaife et al., 2011a).

Several recent studies of historical data have found a negative association between solar forcing and NAO (Haigh and Roscoe, 2006; Kodera et al., 2008; Lockwood et al., 2010), while other studies have found little imprint of solar and volcanic forcing on NAO (Casty et al., 2007). Negative associations between NAO and solar forcing have been reproduced in several recent modelling studies (Ineson et al., 2011; Lee et al., 2008).

Observational studies have noted weakening of NAO during periods of reduced Arctic sea-ice (Strong et al., 2009; Wu and Zhang, 2010). Several modelling studies have also shown a negative NAO response to the partial removal of sea-ice in the Arctic or high-latitudes (Deser et al., 2010c; Kvamsto et al., 2004; Magnusdottir et al., 2004; Screen et al., 2012; Seierstad and Bader, 2009). However, the strength and timing of the response to sea ice loss varies considerably between studies, and can be hard to separate from common responses to warming of the troposphere and from natural climate variability. The impact of sea ice loss in individual years on NAO is small and hard to detect (Bluthgen et al., 2012). Reviews of the emerging literature on this topic can be found in (Budikova, 2009) and (Bader et al., 2011).

[INSERT FIGURE 14.26 HERE]

Figure 14.26: Summary of multi-model ensemble simulations of wintertime mean NAO, NAM and SAM sea-level pressure indices for historical and RCP4.5 scenarios produced by 30 climate models participating in CMIP5. Panels a-c) show time series of the ensemble mean (black line) and inter-quartile range (grey shading) of the mean index for each model. Panels d-f) show scatter plots of individual model 2070–2099 time means versus 1975–2004 time means (black crosses) together with (–2,+2) standard error bars. The NAO index is defined here as the difference of regional averages: (90°W–60°E, 20°N–55°N) minus (90°W–60°E, 55°N–90N) (Stephenson and Pavan, 2003). The NAM and SAM are defined as zonal indices: NAM as the difference in zonal mean SLP at 35°N and 65°N (Li and Wang, 2003) and SAM as the difference in zonal mean SLP at 40°S and 65°S (Gong and Wang, 1999). All indices have been centered to have zero time mean from 1861–1900. Comparison of simulated and observed trends from 1961–2011 is shown in Figure 10.11.

14.5.2 Southern Annular Mode

The Southern Annular Mode[4] (SAM), is the leading mode of climate variability in the Southern Hemisphere extra-tropics, comprising co-varying sea-level pressure or geopotential height anomalies of opposite sign in middle and high latitudes, extending through the depth of the troposphere, which are related to fluctuations in the latitudinal position and strength of the mid-latitude jet. When pressures/heights are below (above) average over Antarctica the SAM is defined as being in its positive (negative) phase and the circumpolar westerly winds are stronger (weaker) than average. Associated with this, the storm tracks move poleward during the positive SAM and equatorward during the negative SAM. Although broadly annular in nature, hence its name, the spatial pattern of the SAM includes a substantial non-annular component in the Pacific sector (Figure 14.27) (Fogt et al., 2012; Kidston et al., 2009). SAM variability has a major influence on the climate of Antarctica, Australasia, southern South America and South Africa (Thompson et al., 2011 and references therein; Watterson, 2009).

The SAM exhibits marked seasonal variability in both its structure and in its effects on regional climate. For example, correlations between the SAM and temperature at some Antarctic Peninsula stations change sign between seasons (Marshall, 2007) while the effect of the SAM on temperature and rainfall over New Zealand (Kidston et al., 2009) and on regional Australian rainfall (Hendon et al., 2007) changes markedly through the year. Moreover, non-linearities in the structure of the positive and negative polarities of the SAM result in polarity-specific changes in surface climate impacts (Fogt et al., 2012).

[4] also known as the Antarctic Oscillation (AAO)

[INSERT FIGURE 14.27 HERE]

Figure 14.27: Left – the annual mean pattern of the positive SAM in the 850 hPa monthly height anomaly field (average height anomalies when the amplitude time series is +1 standard deviation). Positive contours are red, negative are blue and zero is black. The contour interval is 5 m. Right – the seasonal-mean amplitude of the SAM pattern, taken from station data (courtesy G. Marshall, British Antarctic Survey, http://www.antarctica.ac.uk/met/gjma/sam.html). The black line illustrates the long-term trend, calculated by heavily smoothing the raw seasonal amplitude time series with seven applications of a 13-point binomial filter (Trenberth et al., 2007b, Appendix 3A).

Silvestri and Vera (2009) discussed decadal variability in the effects of the SAM on regional climate, emphasising broad-scale changes in the sign of precipitation relationships over southern South America and temperature relationships over Australia during 1958–1979 and 1983–2004. Marshall et al. 2011) examined a regional change in the sign of a SAM-temperature relationship in part of East Antarctica and demonstrated that changes in the phase and magnitude of the zonal wave-number 3 pattern, superimposed upon the annular structure of the SAM, were responsible for the reversal. Using ice-core data they also showed that such changes occurred throughout the 20th century and hence were likely to reflect internal natural variability rather than an anthropogenic forcing. Such changes in coastal Antarctica will impact the role of the SAM in driving the formation of Antarctic Bottom Water, a central component of the global thermohaline circulation (McKee et al., 2011). Others have shown that the impact of the SAM on Antarctic climate also depends upon how it interacts with other modes of circulation variability, such as those related to ENSO (e.g., Fogt and Bromwich, 2006).

The physical mechanisms of the SAM are generally well-understood, and the SAM is well-represented in many climate models, although the detailed spatial and temporal characteristics vary between models (Raphael and Holland, 2006). In the past few decades the SAM index has exhibited a positive trend in austral summer and autumn (e.g., Jones et al., 2009; Marshall, 2007; Figure 14.6.1), a change attributed primarily to the effects of ozone depletion and, to a lesser extent, the increase in greenhouse gases (Thompson et al., 2011, see also Chapter 10, section 10.3.3.5), thus demonstrating that ozone depletion has had a direct effect on surface climate in the Southern Hemisphere, through its influence on the SAM trend. It is likely that these two factors will continue to be the principal drivers into the future, but as the ozone hole recovers they will be competing to push the SAM in opposite directions (Arblaster et al., 2011; Bracegirdle et al., 2012; Thompson et al., 2011), at least during late austral spring and summer, when ozone depletion has had its greatest impact on the SAM. The SAM is also influenced by teleconnections to the tropics, primarily associated with ENSO (Carvalho et al., 2005; L'Heureux and Thompson, 2006). Changes to the tropical circulation, and to such teleconnections, as the climate warms could further affect SAM variability (Karpechko et al., 2010).

The AOGCMs used for the AR4 projected a continuing positive trend in the SAM in both summer and winter (Miller et al., 2006). However, those models generally had very poor simulations of stratospheric ozone, with some not including it at all while others kept it constant into the future rather than having a recovery. In 20th century simulations with many of these models, the austral spring and autumn SAM development showed an underestimation of natural variability in austral autumn, and substantial austral spring trends that are not present in observations and reconstructions, indicating that care should be taken in interpretation of future SAM projections in these seasons (Fogt et al., 2009). In addition, Arblaster et al. (2011) showed that there can be large differences in the sensitivity of these models to CO_2 increases, which affects their projected trends in the SAM.

Since the AR4 a number of chemistry-climate models (CCMs) have been run that have fully interactive stratospheric chemistry, although unlike the AOGCMs they are usually not coupled to the oceans (see also Chapter 9, Sections 9.1.3.3.6, 9.4.1.3). The majority of these CCMs, which generally compare well to reanalyses (Gerber et al., 2010) although many exhibit biases in their placement of the Southern Hemisphere eddy-driven jet (Bracegirdle et al., 2012; Wilcox et al., 2012), indicate that through to at least the mid-21st century the current observed SAM changes are neutralised or reversed during austral summer (Bracegirdle et al., 2012; Perlwitz et al., 2008; Polvani et al., 2011; Son et al., 2010). Figure 14.26 shows the projected ensemble-mean future SAM index evolution from a suite of CMIP5 models, suggesting that the recent positive trend will weaken as stratospheric ozone concentrations recover over southern high latitudes. The currently-observed positive SAM trend is not projected to return before the end of the century. In such CCMs, the impact of the ozone recovery in coming decades often has a greater effect than further increases in greenhouse gases on the SAM during austral summer. In austral winter, weak positive trends in the SAM

are projected to continue through the 21st century (see also Chapter 11, Section 11.4.2.4.2; Chapter 12, Section 12.4.4.1).

14.5.3 Assessment Summary

There is *high confidence* that future boreal wintertime NAO is *very likely* to exhibit large natural variations and trends of similar magnitude to those observed in the past; is *very likely* to be differ quantitatively from individual climate model projections; is *likely* to become slightly more positive (on average) due to increases in greenhouse gases. There is high confidence that the austral summer/autumn positive trend in SAM is *very likely* to continue but is *likely* to weaken considerably as ozone depletion recovers through to the mid-21st century. There is *medium confidence* from recent studies that projected changes in NAO and SAM are sensitive to boundary processes, which are not yet well represented in many climate models currently used for projections e.g., stratosphere-troposphere interaction, ozone chemistry, solar forcing, and atmospheric response to Arctic sea ice loss. There is *low confidence* in projections of other modes such as the NPO due to the small number of modelling studies.

[START BOX 14.3 HERE]

Box 14.3: Extra-Tropical Cyclones

Background

Extra-tropical cyclones (ETCs) are pervasive features of mid-latitude weather, with a typical scale of 1000 km and lifetimes of 1–5 days (Hoskins and Hodges, 2002). These storms grow on the baroclinic instability of the large-scale atmospheric flow, extracting potential energy from the meridional temperature gradients which arise from the contrast in solar heating between high and low latitudes. ETCs preferentially occur over the ocean basins where surface friction is low and heat and moisture are readily available, forming the midlatitude storm tracks (Brayshaw et al., 2009; Gerber and Vallis, 2009). ETCs have a dual importance in climate; not only do they constitute many of the most extreme weather events in the midlatitudes (e.g., Liberato et al., 2011) but they are also key components of the global climate system, acting as eddies which transport heat, momentum and vorticity and shape the large scale atmospheric circulation itself.

In the past there has been little agreement on how ETCs will respond to anthropogenic forcing (Cubasch et al., 2001). The generation of climate models which contributed to the CMIP3 project began to show more agreement, with many models in particular projecting a poleward shift of the storm tracks (Yin, 2005) and an expansion of the tropics (Lu et al., 2007). As stated in AR4 (Meehl et al., 2007b) this response is particularly clear in the Southern Hemisphere, where the poleward jet shift associated with the Southern Annular Mode is more reproducible and coherent(Miller et al., 2006). In the Northern Hemisphere, however, the poleward shift is less clear. It is evident to some extent in zonal mean fields (Yin, 2005) but regional responses differ widely from this in many models (Ulbrich et al., 2008). Shifts in the locations of the storm tracks are closely associated with shifts in the westerly jet streams (Athanasiadis et al., 2010; Raible, 2007). In fact the transient eddies of the storm tracks are increasingly taken as the starting point for theories explaining the variability and change of the jets (e.g., Benedict et al., 2004). However, the coupling between the storm track and the large scale flow is intrinsically two-way in nature (Gerber and Vallis, 2007; Lorenz and Hartmann, 2003; Robinson, 2006), which often confounds the search for simple chains of cause and effect.

Competing Influences on Future ETC Change

The key challenge in predicting future storm track change is the balancing of several different competing dynamical influences (Held, 1993; O'Gorman, 2010; Woollings, 2010). It is becoming more apparent that the relatively modest storm track response in many models does indeed reflect the partial cancelling of opposing tendencies (Butler et al., 2010; Lim and Simmonds, 2009; Son and Lee, 2005). A key factor which has received much attention is the contrast in the meridional gradient of warming at upper and lower levels. In the upper troposphere the meridional temperature gradient is projected to increase due to both the latent heat-related enhanced warming in the tropics and the stratospheric cooling which extends down to around 200 hPa at high latitudes (Meehl et al., 2007b). In the lower troposphere, in contrast, warming is enhanced over the polar regions, in particular over the Arctic in winter, which results in a decrease in the meridional

temperature gradient. In this way the potential energy available for storm growth is expected to increase at upper levels but decrease at lower levels, and it is still unclear whether this will lead to an overall increase or decrease in ETC activity. The outcome can appear as an increase in eddy activity at upper levels and a decrease at lower levels (Hernandez-Deckers and von Storch, 2010), although in other models changes in low level eddy activity are more in line with the upper level wind changes (Mizuta, 2012; Mizuta et al., 2011; Wu et al., 2011). While the influence of the warming pattern is most often described in terms of the associated horizontal gradients, several recent studies have considered the implications of the vertical temperature gradients. These are related to the static stability which also has an important influence on baroclinicity and hence storm growth. The pattern of warming reflects increased stability in the tropics and subtropics and decreased stability at higher latitudes, and there is some modelling evidence that this may be a strong factor in the response (Kodama and Iwasaki, 2009; Lim and Simmonds, 2009; Lu et al., 2008; Lu et al., 2010). The increase in the depth of the troposphere as it warms may also be important (Lorenz and DeWeaver, 2007), as may structure in the pattern of sea surface temperature change (Graff and LaCasce, 2012).

Irrespective of whether the horizontal or vertical gradients dominate it is clear that the considerable uncertainties in the tropical and polar warming lead to uncertainty in the storm track response (Rind, 2008). Given the two-way nature of the coupling between the storm tracks and the large scale circulation, it is also possible that the storm track response itself is partly responsible for the changes in the large-scale temperature distribution. However, there is some evidence that this is not the case and that the atmospheric poleward heat fluxes are largely determined by regional processes which set the amplitude of the tropical and polar warming (Hwang and Frierson, 2011). Several specific mechanisms have been proposed to explain how the storm tracks respond to the large scale changes, including changes in eddy phase speed (Chen et al., 2007; Chen et al., 2008; Lu et al., 2008), eddy source regions (Lu et al., 2010) and eddy length scales (Kidston et al., 2011) with a subsequent effect on wave-breaking characteristics (Riviere, 2011), and the issue is still widely discussed.

There are also regional processes which could prove very important for the storm track response in certain regions. Sea-ice loss is a particular example which has been shown to influence midlatitude storm activity in some modelling studies (Bader et al., 2011; Deser et al., 2010c; Seierstad and Bader, 2009)). The land-sea contrast in warming also has a local influence on baroclinicity along the eastern continental coastlines (Long et al., 2009; McDonald, 2011). There is some disagreement over whether the storm track response to a combination of forcings combines linearly, with some studies suggesting relatively linear behaviour (Lim and Simmonds, 2009) but others suggesting otherwise (Butler et al., 2010). However, it has been suggested that model simulations are often too short to allow a quantitative assessment of the linearity, especially in idealised models with unrealistically long timescales of variability (Simpson et al., 2010).

The increase of moisture content in a warmer atmosphere is also likely to have competing effects. Latent heating has been shown to play a role in invigorating individual ETCs, and this may be particularly important for cyclones developing over the eastern ocean basins which are likely to lead to downstream impacts (Dacre and Gray, 2009; Fink et al., 2012; Fink et al., 2009). However, there is evidence that the overall effect of moistening is to weaken eddy activity by improving the efficiency of poleward heat transport and hence reducing the dry baroclinicity (Frierson et al., 2007; Lucarini and Ragone, 2011; O'Gorman and Schneider, 2008; Schneider et al., 2010). Consistent with this, Bengtsson et al. (2009) and (Zappa et al., 2012b) showed that while the precipitation does increase along the storm tracks this does not lead to an increase in cyclone intensity in other measures such as wind speed or vorticity.

Projected ETC Changes and their Relevance for Regional Climates

The response of ETCs in the latest projections is described in Section 12.4.4.3. Here we summarise the most coherent aspects of this and assess the implications for regional climate change. In general, there remains low confidence in the implications of storm track change for future regional climate. Individual models often show regional storm track changes which are comparable with the magnitude of natural variability and so can be expected to have societal impact. However, it is rare that the majority of models agree on a response of this magnitude at any given location, especially over land (Harvey et al., 2012). It is also apparent that there can be considerable disagreement between different cyclone/storm track identification methods (Raible et al., 2008; Ulbrich et al., 2009), which can lead to different conclusions even when applied to the same

data. Conversely, when the same method is applied to different models the spread between the model responses is often larger than the ensemble mean response, especially in the Northern Hemisphere (Laine et al., 2009; Ulbrich et al., 2008). There are systematic storm track biases common to many models, and these appear to have some influence on the projected storm track response to forcing (Chang et al., 2012a; Chang et al., 2012b).

A poleward shift of the Southern Hemisphere storm track remains one of the most reproducible projections, yet even here there is considerable quantitative uncertainty. This is associated partly with the varied model biases in jet latitude (Kidston and Gerber, 2010) and partly with a lack of confidence in the cloud response (Trenberth and Fasullo, 2010). Many models also project a similar poleward shift in the North Pacific (Bengtsson et al., 2006; Catto et al., 2011; Ulbrich et al., 2008), although this is weaker compared to natural variability and often varies considerably between ensemble members (McDonald, 2011; Pinto et al., 2007). The poleward shifts are generally less clear at the surface than at upper levels (Chang et al., 2012a; McDonald, 2011; Yin, 2005), reducing the regional impacts. However, Gastineau and Soden (2009) still find a poleward shift in extreme surface wind events in the CMIP3 models, with the strongest changes in the subtropics and the Southern high latitudes. Several models project a particular weakening of the Mediterranean storm track (Donat et al., 2011; Loeptien et al., 2008; Pinto et al., 2007; Ulbrich et al., 2009) in which increasing static stability is very important (Raible et al., 2010).

Several studies have noted that the response of the North Atlantic storm track is quite different from a poleward shift in many models, comprising instead an increase in storm activity and a downstream extension of the storm track into Europe (Bengtsson et al., 2006; Catto et al., 2011; McDonald, 2011; Pinto et al., 2007; Ulbrich et al., 2008). In some models this regional response is very important (Ulbrich et al., 2009), with storm activity over Western Europe increasing by 50% (McDonald, 2011) or by an amount comparable to the natural variability (Pinto et al., 2007; Woollings et al., 2012). The return periods of intense cyclones are shortened (Della-Marta and Pinto, 2009) with clear effects on measures of wind damage (Donat et al., 2011; Leckebusch et al., 2007) and economic losses (Pinto et al., 2012). This response is related to the local minimum in warming in North Atlantic SSTs, which serves to increase the meridional temperature gradient on its southern side (Catto et al., 2011; Laine et al., 2009). The minimum in warming in turn arises due to the weakening of northward ocean heat transports by the meridional overturning circulation (MOC), and the varying MOC responses of the models can account for a large fraction of the uncertainty in the Atlantic storm track response (Woollings et al., 2012). CMIP5 models show a similar, albeit weaker extension of the storm track towards Europe, flanked by reductions in cyclone activity on both the northern and southern sides (Harvey et al., 2012; Zappa et al., 2012b) with reasonable agreement between models (Sansom et al., 2012).

Most models and studies are in agreement on a global reduction in ETC numbers (Ulbrich et al., 2009), although only by a few percent which would have little impact. In individual regions there can be much larger changes which are comparable to natural variations, but it is rare that these changes are seen reproducibly in the majority of models (e.g., Donat et al., 2011). ETC intensities are particularly sensitive to the method and quantity used to define them, so there is little consensus on changes in intensity (Ulbrich et al., 2009). While there are indications that the absolute values of pressure minima deepen in scenario simulations (Lambert and Fyfe, 2006), this is often associated with large-scale pressure changes rather than changes in the pressure gradients or winds associated with ETCs (Bengtsson et al., 2009; McDonald, 2011; Ulbrich et al., 2009). The CMIP5 models continue to show little change in the intensity of winds associated with ETCs (Zappa et al., 2012b)

Some models with improved representation of the stratosphere have shown a markedly different anthropogenic response in the Northern Hemisphere which resembles the negative phase of the Northern Annular Mode (Morgenstern et al., 2010), with consequences for Atlantic / European storm activity in particular (Scaife et al., 2011a). Concerns over the skill of CMIP3 models in representing both the stratosphere and the MOC mean that confidence in Northern Hemisphere storm track projections remains low. Higher horizontal resolution can improve ETC representation, yet there are still relatively few high-resolution global models which have been used for storm track projections (Bengtsson et al., 2009; Catto et al., 2011; Geng and Sugi, 2003; Zappa et al., 2012a). Several studies have used Regional Climate Models (RCMs) to simulate storms at high resolution in particular regions. In multi-model experiments over Europe the storm response is more sensitive to the choice of driving GCM than the choice of RCM (Donat et al.,

2011; Leckebusch et al., 2006), highlighting the importance of large-scale circulation uncertainties. There has been little work on potential changes to mesoscale storm systems, although it has been suggested that polar lows may reduce in frequency due to an increase in static stability (Zahn and von Storch, 2010).

Summary

There is *high confidence* that the global number of extra-tropical cyclones is *unlikely* to decrease by more than a few percent due to global warming and that future changes in storms are *likely* to be small compared to natural interannual variability and substantial variations between model simulations of storms. There is *high confidence* that a small poleward shift is *likely* in the Southern Hemisphere storm track, but the magnitude is model-dependent. There is *medium confidence* that a poleward shift in the N. Pacific storm track is *more likely than not* and that it is *unlikely* that the response of the N. Atlantic storm track is a simple poleward shift. There is *low confidence* in the impact of storm track changes on regional climate at the surface especially for extreme events.

[END BOX 14.3 HERE]

14.6 Additional Phenomena of Relevance

14.6.1 Pacific-North American Pattern

The term 'Pacific-North American' (PNA) pattern was coined by (Wallace and Gutzler, 1981) to refer to a mode of atmospheric variability in the mid-tropospheric geopotential height field. This pattern, as defined on the basis of the index given in Box 2.4, Table 1, is prevalent over the North Pacific and the North American land mass (see regression chart in Box 2.4, Figure 2), particularly during the winter season. Variations in the strength and polarity of the PNA patterns are accompanied by prominent shifts in the jet stream and storm tracks over the Pacific and North American sectors, and thus exert notable influences on the temperature and precipitation in these regions on intermonthly and interannual periods (e.g., Nigam, 2003). The data records indicate a significant positive trend in the wintertime PNA index over the past 60 years (see Table 2.14 and Box 2.4, Figure 1).

Observational evidence presented by (Horel and Wallace, 1981) and others indicate that the PNA pattern is linked to ENSO events in the tropical Pacific (see Section 14.4). However, (Straus and Shukla, 2002) and (Nigam, 2003) pointed out that the teleconnection pattern related to ENSO variability exhibits some notable differences from the PNA pattern.

More recent diagnoses (see review by Bronnimann, 2007) show that ENSO may impact European climate through modulation of the North Atlantic Oscillation (NAO), especially during late winter and early spring. The observational and model results reported by Li and Lau (2012b) and Li and Lau (2012a) illustrate that one possible mechanism for this connection is related to the ENSO-forced teleconnection pattern in the North Pacific-North American sector. Specifically, this response pattern is accompanied by systematic changes in the position and intensity of the storm tracks over that region. The transient disturbances along the storm tracks propagate farther eastward and reach the North Atlantic. The ensuing dynamical interactions between these storm track eddies and the local quasi-stationary circulation lead to changes in the NAO. In addition to tropospheric processes, Ineson and Scaife (2009), Bell et al. (2009) and Cagnazzo and Manzini (2009) have demonstrated a stratospheric link between ENSO and NAO in late winter.

Stoner et al. (2009) have made a comprehensive assessment of the capability of 22 coupled atmosphere-ocean GCMs contributing to IPCC AR4 in replicating the essential temporal and spatial aspects of the observed PNA pattern. Their results indicate that a majority of the models overestimate the fraction of variance explained by the PNA pattern, and that the spatial characteristics of PNA patterns simulated in 14 of the 22 models are in good agreement with the observations.

14.6.2 Pacific-South American Pattern

The Pacific-South American pattern (PSA) is a teleconnection prominent on intraseasonal to interannual time scales. Anomalous convection in the tropical Pacific triggers circulation anomalies which propagate as

Rossby wave trains toward the extra-tropics and then towards the tropics again (Mo and Higgins, 1998) (Figure 14.28). The PSA has a similar configuration to the Pacific North American (PNA) pattern. This pattern induces atmospheric circulation anomalies over South America and has influences on extreme precipitation over the continent. The observed extreme precipitation anomalies display a dipole configuration, with opposite anomalies between southeastern Brazil and southern Brazil/Uruguay/northeastern Argentina. This dipole is associated with enhancement or weakening of the South Atlantic Convergence Zone (Section 14.3.1) and is supported by the anomalous circulation, which is part of the PSA (Nogués-Paegle et al., 2000; Carvalho et al., 2002; Cunningham and Cavalcanti, 2006). As this pattern is related to anomalies in tropical Pacific /Indonesia convection, changes in these anomalies due to global warming could change the intensity, frequency, phase and position of the present pattern, with impacts on South America precipitation. Along with the Southern Annular Mode (Section 14.5.2), the PSA has been shown to influence the surface climate across the South Pacific, including the west Antarctic (Schneider et al., 2011).

[INSERT FIGURE 14.28 HERE]

Figure 14.28: (a) PSA1 in DJF from zonal asymmetric geopotential anomaly at 500 hPa (Era Interim); (b) C1 amplitudes series (1979–2004); (c) PSA2 in DJF from zonal asymmetric geopotential anomaly at 500 hPa (Era Interim); (d) PC2 amplitudes series (1979–2004).

The two PSA modes, calculated from the second and third PC analyses show positive trends from 1979 to 2008 (Chapter 2), but as mentioned in Chapter 2, robustness of the trends needs further investigations. The PSA pattern has been reproduced in a number of model simulations (Solman and Le Treut, 2006; Bates, 2010; Grainger et al., 2011; Cavalcanti and Shimizu, 2012), although some CMIP3 models do not reproduce the PSA associated with ENSO events (Vera and Silvestri, 2009; Chapter 9). The PSA patterns simulated by HADGEM2-CMIP5 compare well with the observed patterns obtained from reanalyses ERA-Interim (Figure 14.29).

[INSERT FIGURE 14.29 HERE]

Figure 14.29: (a) PSA1 in DJF from zonal asymmetric geopotential anomaly at 500 hPa (HADGEM2-historical); (b) PC1 amplitudes series (1979–2004); (c) PSA2 in DJF from zonal asymmetric geopotential anomaly at 500 hPa (HADGEM2-historical); (d) PC2 amplitudes series (1979–2004).

The increase in frequency and intensity of positive SST anomalies in the tropical Pacific was suggested to be related to PSA-type wave train intensification by the end of the 21st century associated with the precipitation dipole over South America in the summer season (Junquas et al., 2011). Besides changes that can occur associated with tropical convection, changes in the PSA centres could also occur in relation to the Atlantic Meridional Overturning Circulation (AMOC), which is projected to weaken in the 21st century (Chapter 12, Section 12.4.7.2). An experiment with a coupled model simulating the AMOC weakening (Timmermann et al., 2010) showed intensification of the negative PSA phase (low pressure anomaly close to Antarctica). Analysis from CMIP5 HADGEM2-ES results showed the PSA pattern displaced eastward in relation to its present mean position (Figure 14.30; Cavalcanti and Shimizu, 2012). In the mean, the pattern is projected to shift eastward, while for cases of extreme precipitation over southeastern South America, the pattern is projected to intensify and to shift westward (Junquas et al., 2011). The few studies on projections of this pattern are still not enough to assess the reliability of projected changes. However, PSA pattern is likely to change due to tropical convection changes in the Pacific/Indonesian regions.

[INSERT FIGURE 14.30 HERE]

Figure 14.30: (a) PSA1 in DJF from zonal asymmetric geopotential anomaly at 500 hPa (HADGEM2-CP8.5); (b) PC1 amplitudes series (2073–2098); (c) PSA2 in DJF from zonal asymmetric geopotential anomaly at 500 hPa (HADGEM2-RCP8.5); (d) PC2 amplitudes series (2073–2098).

14.6.3 Blocking

Atmospheric blocking is associated with persistent, slow-moving high-pressure systems that obstruct the prevailing westerly wind of middle and high latitudes and the normal eastward progress of extra-tropical transient storm systems. Atmospheric blocking is an important component of the intraseasonal climate variability in the extra-tropics and can also be responsible of long-lived extreme weather conditions, such as cold spells in winter (e.g., Buehler et al., 2011) and summer heat waves (e.g., 2010 Russian heat-wave, Dole

et al., 2011). Blocking frequency is higher in the Northern Hemisphere and reaches a maximum (minimum) in winter-spring (summer-autumn), usually persists from a few days to some weeks and shows preferred locations (Barriopedro et al., 2010; Berrisford et al., 2007; Tyrlis and Hoskins, 2008). The most consistent long-term observed trends are a reduced winter activity over the North Atlantic (e.g., Croci-Maspoli et al., 2007), which is in harmony with recurrent positive phases of the NAO in the second half of 20th century (see Section 2.6.8.), and a decrease in the Southern Hemisphere (e.g., Dong et al., 2008) which seems to agree with the observed AAO upward trend (see Table 2.14).

Since the AR4, climate models have made some progress in the simulation of NH blocking activity (Scaife et al., 2010; Vial and Osborn, 2011). Some of the updated CMIP5 models are capable of simulating long-lived blocking with the observed frequency (see Figure 14.31), though an underestimation over the Euro-Atlantic sector still remains. In the SH, blocking frequency and duration is also underestimated, particularly over the Australia-New Zealand sector (Matsueda et al., 2010). Such blocking underestimation is mainly attributed to the limited horizontal resolution in the atmospheric component of AOGCMs (e.g., Matsueda et al., 2009; Scaife et al., 2011b; Scaife et al., 2010), along with systematic equatorward biases in jet stream latitude (Barnes et al., 2011; Vial and Osborn, 2011) and tropical SSTs biases in the North Pacific case (e.g., Hinton et al., 2009).

[INSERT FIGURE 14.31 HERE]

Figure 14.31: Annual mean blocking frequency in the Northern Hemisphere (expressed in % of time, i.e., 1% means ~4 days per year) as simulated by a suite of CMIP5 models (color lines) for the 1961–1990 period of one run of the historical simulation. Grey shading shows the mean model result plus/minus one standard deviation. Black thick line indicates the observed blocking frequency derived from the NCEP/NCAR reanalysis. Only CMIP5 models with available 500 hPa geopotential height daily data at http://pcmdi3.llnl.gov/esgcet/home.htm have been used. Blocking is defined as in (Barriopedro et al., 2006), which uses a modified version of the (Tibaldi and Molteni, 1990) index. Daily data was interpolated to a common regular 2.5° × 2.5° longitude-latitude grid before detecting blocking.

Future model projections of blocking activity are generally constrained by the relatively poor model performance in accurately simulating blocking signatures, as well as by the lack of agreement in defining blocking (see Section 9.5.2.2.1), hence they must be treated with caution. It is likely that the frequency of NH and SH blocking will decrease under increasing GHG concentrations (Barnes et al., 2011; Dong et al., 2008; Wiedenmann et al., 2002), while trends in blocking intensity and persistence are uncertain. Future strengthening of the zonal wind and meridional jet displacements (see Section 11.4.2.4) may partially account for the projected decrease in blocking frequency. How the location and frequency of blocking events will evolve in future are both critically important for understanding regional climate change. For example, (Sillman et al., 2011) found that a northward shift in north Atlantic blocking location would reduce the cooling effect of wintertime blocking in northeastern Europe.

14.6.4 Tropospheric Biennial Oscillation

It has long been noted that there is a biennial tendency of many phenomena in the Indo-Pacific region that affects droughts and floods over large areas of south Asia and Australia (e.g., Mooley and Parthasarathy, 1983; Nichoolls, 1978; Trenberth, 1975; Troup, 1965). Brier (1978) suggested a possible central role of air-sea coupling, and Meehl (1987) proposed a mechanism involving large-scale dynamically coupled interactions across the Indo-Pacific to account for the biennial tendency, termed the Tropospheric Biennial Oscillation (TBO, Meehl, 1997). There was also a role for atmospheric circulation anomalies over south Asia and consequent land surface temperature anomalies that contributed to anomalous meridional temperature gradients and biennial monsoon variability (Meehl, 1994a; Meehl, 1994b), thus giving rise to explanations of the TBO that involved processes in the Indian sector (Chang and Li, 2000; Li et al., 2001). SST anomalies in the equatorial eastern Pacific Ocean in the TBO tend to transition from positive to negative (or vice versa) in northern spring, so the seasons leading up to those transitions are crucial to the TBO (e.g., Meehl and Arblaster, 2002a; Meehl and Arblaster, 2002b). The fundamental nature of the dynamically coupled processes involved with the TBO have been additionally documented in a number of global coupled climate model simulations (e.g., Loschnigg et al., 2003; Meehl and Arblaster, 2011; Meehl, 1997; Nanjundiah et al., 2005; Ogasawara et al., 1999).

Regional patterns of SST anomalies in the TBO in the Indian Ocean during the northern fall season following the south Asian monsoon subsequently became known as the Indian Ocean Dipole (IOD, e.g., Saji

et al., 1999; Webster et al., 1999, Section 14.3.3). Thus, a "negative IOD" in northern fall (negative SST anomalies in the western tropical Indian Ocean, and positive SST anomalies in the eastern tropical Indian Ocean), with negative SST anomalies in the equatorial eastern Pacific, transition to basin-wide negative SST anomalies across the Indian Ocean in northern winter, with positive SST anomalies in the eastern equatorial Pacific in the following northern spring and summer in the TBO (Meehl et al., 2003).

Izumo et al. (2010) made use of these transition processes in the TBO to document El Nino forecast skill by monitoring the state of the IOD in northern fall. Additionally, convective heating anomalies in the Pacific (Wu and Kirtman, 2004), or in the Indian Ocean associated with the IOD (e.g., Annamalai et al., 2005), or a combination from the southeastern Indian Ocean and western Pacific (Clarke et al., 1998; Li et al., 2006; Li et al., 2001) affect the southeastern Indian Ocean and western north Pacific anticyclones. The resulting wind stress anomalies in the equatorial western Pacific contribute to TBO SST transitions in the eastern equatorial Pacific (Lau and Wu, 2001; Turner et al., 2007a). Such consecutive annual SST anomaly and anomalous monsoon transitions from one sign to another characterize the TBO. Thus, the TBO provides the fundamental framework for understanding coupled processes across the Indo-Pacific region involving the Asian-Australian monsoon, the IOD, and ENSO.

The processes that produce the TBO are affected by internally generated decadal-timescale variability. Just as the Interdecadal Pacific Oscillation (IPO) influences the nature of interannual variability in the Australia-Pacific region (Power et al., 1999a), so does the IPO affect the decade-to-decade strength of the TBO (Meehl and Arblaster, 2011). During periods of positive IPO (warmer SSTs in the tropical Pacific on the decadal timescale, e.g., from the 1970s to 1990s), the TBO was weak, and vice versa for negative IPO with a stronger TBO (post-1990s, Meehl and Arblaster, 2012). Thus, prediction of decadal timescale variability assessed in Ch. 11 that can be associated, for example, with the IPO (e.g., Meehl et al., 2010) can influence the accuracy of shorter-term predictions of interannual variability associated with the TBO across the entire Indo-Pacific region (Turner et al., 2011). This set of regional processes from interannual to decadal is of great relevance for decadal climate prediction and the short-term climate change problem (Chapter 11).

With regards to possible future behaviour of the TBO, an analysis of a multi-model dataset that stratified models to focus on those that more accurately simulated the TBO in present-day climate showed that, for those models, the TBO strengthens in a future warmer climate (Nanjundiah et al., 2005). However, as with ENSO and IOD, internally generated decadal timescale variability complicates the interpretation of such future changes.

14.6.5 Quasi-Biannual Oscillation

The quasi-biennial oscillation (QBO) is a near-periodic, large-amplitude, downward propagating oscillation in zonal (westerly) winds in the equatorial stratosphere (e.g., Baldwin et al., 2001). The QBO is associated with the variability of the largest jet feature in the atmosphere, and is evident in time series of the zonal mean zonal wind near the equator, which changes from strong easterlies to strong westerlies through each QBO cycle (approximately 28 months). It is driven by vertically propagating internal waves that are generated in the tropical troposphere (Plumb, 1977).

The QBO has substantial effects on the global stratospheric circulation, in particular the strength of the northern stratospheric polar vortex as well as the extratropical troposphere (e.g., Boer, 2009; Marshall and Scaife, 2009) (Garfinkel and Hartmann, 2011). These extratropical effects occur primarily in winter when the stratosphere and troposphere are strongly coupled (e.g., Anstey and Shepherd, 2008; Garfinkel and Hartmann, 2011).

It has been unclear how the QBO will respond to future climate change related to greenhouse gas increase and recovery of stratospheric ozone. Climate models assessed in the AR4 did not simulate the QBO as they lacked the necessary vertical resolution (Kawatani et al., 2011). However, recent model studies without using gravity wave parameterization (Kawatani et al., 2012; Kawatani et al., 2011) showed that the QBO period and amplitude may become longer and weaker, and the downward penetration into the lowermost stratosphere may be more curtailed in a warmer climate. This finding is attributed to the effect of increased equatorial upwelling (stronger Brewer-Dobson circulation) (Butchart et al., 2006; Garcia and Randel, 2008; McLandress and Shepherd, 2009; Okamoto et al., 2011) dominating the effect of increased wave forcing

(more convective activity). Similar studies with gravity wave parameterization (Watanabe and Kawatani, 2012) gave conflicting results depending on the simulated changes in the intensity of the Brewer-Dobson circulation.

There are limited published results on the behaviour of the QBO in future climates, using CMIP5 models. On the basis of the recent literature, it is as likely as not that the QBO may weaken in future, and its period may increase slightly.

14.6.6 Pacific Decadal Oscillation/Inter-Decadal Pacific Oscillation

The "Pacific Decadal Oscillation" (PDO, Box 14.1) refers to the leading Empirical Orthogonal Function (EOF) of monthly Sea Surface Temperature (SST) anomalies over the North Pacific (north of 20°N) from which the globally-averaged SST anomalies have been subtracted (Mantua et al., 1997). It exhibits anomalies of one sign along the west coast of North America and of opposite sign in the western and central North Pacific (see also Chapter 9, Section 9.5.3.4.4, and Chapter 11). The PDO is closely linked to fluctuations in the strength of the wintertime Aleutian Low Pressure System, an index of which is the North Pacific Index (NPI) defined as the average sea level pressure over the region 30°N–65°N, 160°E–140°W (Trenberth and Hurrell, 1994). The timescale of the PDO is around 20-30 years, with changes of sign between positive and negative polarities in the 1920s, the late 1940s, the late 1970s, and around 2000.

The extension of the PDO to the whole Pacific basin is known as the "Inter-decadal Pacific Oscillation" (IPO, Power et al., 1999b). The IPO is nearly identical in form to the PDO in the Northern Hemisphere but is defined globally, as the 3rd EOF (principal component) of 13-year lowpass-filtered global SST anomalies and has substantial amplitude in the tropical and southern Pacific. The time series of the PDO and IPO are very highly correlated on an annual basis. The PDO/IPO pattern is considered to be the result of internal climate variability (Alexander, 2010; Schneider and Cornuelle, 2005) and has not been observed to exhibit a long-term trend. Variability associated with the PDO/IPO has a modulating influence on ENSO, with more El Niño activity during the positive PDO/IPO and more La Niña activity during the negative PDO/IPO.

At the time of the AR4, little had been published on modelling of the PDO/IPO or of its evolution in future. In a recent study, Furtado et al. (2011) found that the PDO/IPO did not exhibit major changes in spatial or temporal characteristics under greenhouse gas warming in most of the 24 coupled climate models used for the IPCC AR4, although some models indicated a weak shift toward more occurrences of the negative phase of the PDO/IPO by the end of the 21st century (Lapp et al., 2011). However, given that the models strongly underestimate the PDO/IPO connection with tropical Indo-Pacific SST variations (Furtado et al., 2011; Lienert et al., 2011), the credibility of the projections remains uncertain.

In summary, future changes in the PDO/IPO are uncertain and have not been investigated in any depth. It is presently as likely as not that the PDO/IPO will change its form or temporal behaviour in future.

14.6.7 Atlantic Multi-Decadal Oscillation

The Atlantic Multidecadal Oscillation (AMO, Box 14.1, see also Chapter 9, Section 5.3) is a multidecadal fluctuation (superimposed on the rising trend) seen in the instrumental SST record throughout the North Atlantic Ocean. Area-mean North Atlantic SST shows variations with a range of about 0.4°C (see Chapter 2, Box 2.4) and warming of a similar magnitude since 1870. The AMO has a quasi-periodicity of about 70 years, although the approximately 150-year instrumental record possesses only a few distinct phases – warm during approximately 1930–1965 and after 1995, and cool between 1900–1930 and 1965–1995. The phenomenon has also been referred to as 'Atlantic Multidecadal Variability' (AMV) to avoid the implication of temporal regularity. Along with secular trends and Pacific variability, the AMO or AMV is one of the principal features of multidecadal variability in the instrumental climate record.

The AR4 highlighted a number of important links between the AMO and regional climates. Subsequent research using observational and palaeo-climate records, and climate models, has confirmed and expanded upon these connections, such as West African Monsoon and Sahel rainfall (Mohino et al., 2011), summer climate in North America (Feng et al., 2011b; Seager et al., 2008) and Europe (Folland et al., 2009; Ionita et al., 2012) and Atlantic major hurricane frequency (Chylek and Lesins, 2008; Zhang and Delworth, 2009).

Further, the list of AMO influences around the globe has been extended to include decadal variations in many other regions (e.g., Huss et al., 2010; Kucharski et al., 2009a; Kucharski et al., 2009b; Marullo et al., 2011a; Wang et al., 2011b; Zhang and Delworth, 2009). Future AMO variability could be an important contributor to regional climate change over the next few decades across a wide range of regions. Assessing future AMO activity relates to the questions of whether it is a long-lived fluctuation or peculiar to the instrumental period, its physical origins and predictability.

The fact that palaeo-reconstructions of Atlantic temperatures trace AMO-like variability back before the instrumental era was noted in AR4 WG1. This has been confirmed by further analyses, although these suggest potential for intermittency in AMO variability (Saenger et al., 2009; Zanchettin et al., 2010). Control simulations of climate models run for hundreds or thousands of years also show long-lived Atlantic multidecadal variability (Menary et al., 2012). These lines of evidence suggest the likelihood that AMO variability will continue into the future, and no fundamental changes in the characteristics of North Atlantic multidecadal variability in the 21st century are seen in the CMIP3 models (Ting et al., 2011).

Many studies have diagnosed a trend towards a warm North Atlantic in recent decades additional to that implied by global climate forcings (Knight, 2009; Polyakov et al., 2010). It is unclear exactly when the current warm phase of the AMO will terminate, but it is likely to occur within the next few decades, leading to a cooling influence in the North Atlantic and offsetting some of the effects of global warming (Keenlyside et al., 2008; see also Chapter 11). A shift towards the negative phase of the AMO as part of a future cycle could have effects that include further drying of the African Sahel, reduction of Indian monsoon rainfall, increased wet season rainfall in North East Brazil, wetter summers in central North America, drier summers in North Western Europe, and a possible reduction in major Atlantic hurricane activity.

Some similarity in the shape of the instrumental time series of global and northern hemisphere mean surface temperatures and the AMO has long been noted. By removing an estimate of the effect of interannual variability phenomena like ENSO, AMO transitions have been shown to have the potential to produce large and abrupt changes in hemispheric temperatures (Thompson et al., 2010). Estimates of the AMO's contribution to recent climate change are uncertain, however, as attribution of the observed AMO requires a model (physical or conceptual), whose assumptions are nearly always difficult to verify (Knight, 2009).

In summary, it is unlikely that the AMO will change its behaviour over coming decades as the mean climate changes. However, natural fluctuations in the AMO over the coming few decades are likely to influence regional climates at least as strongly as will human-induced changes.

14.6.8 Assessment Summary

There is low to *medium confidence* that the PSA pattern is *likely* to change due to tropical convection changes in the Pacific/Indonesia regions. The changes are *likely* to be in intensity and position of the anomalous centres and may affect precipitation over South America. No current literature exists to assess the future behaviour of PNA.

Low to medium confidence that it is likely that the frequency of NH and SH blocking will decrease under increasing GHG concentrations, while trends in blocking intensity and persistence are uncertain. Future strengthening of the zonal wind and meridional jet displacements may partially account for the projected decrease in blocking frequency.

There is low to medium confidence that TBO strengthens in the future but the internally generated decadal timescale variability complicates the interpretation of such future changes. On the basis of the recent literature, it is as likely as not that the QBO may weaken in future, and its period may increase slightly.

Future changes in the PDO/IPO are uncertain and have not been investigated in any depth. It is presently *as likely as not* that the PDO/IPO will change its form or temporal behaviour in future. It is *unlikely* that the AMO will change its behaviour as the mean climate changes. However, natural fluctuations in the AMO over the coming few decades are *likely* to influence regional climates at least as strongly as will human-induced changes.

14.7 Future Regional Climate Change

14.7.1 Overview

The sections below assess future climate projections of surface air temperature and precipitation for several continental-scale regions, and interpret them, where possible, in terms of projected changes in the major *climate phenomena* assessed in Sections 14.2–14.6. The regions are similar to those used for impact assessment in AR4 WGI and WGII. The sections refer to the appropriate CMIP5 (Taylor et al., 2011c) projection maps presented in Annex I: Atlas of Global and Regional Climate Projections. Annex I uses smaller sub-regions similar to those first proposed by Giorgi and Francesco (2000) and Giorgi et al. (2001) but with modifications introduced by SREX (Seneviratne et al., 2012) and are summarised in Figure 14.32. Table 14.2 presents a quantitative summary of the regional area-averages for three projection periods (near future, middle century and end of century) in the RCP4.5 scenario (Similar tables for RCP2.6, RCP6.0 and RCP8.5 are found in the Chapter 14 Supplementary Material).

Uncertainty in future regional climate change arises from several sources similar to those identified for global mean temperature (see Chapters 8, 11, and 12). However, there is generally more uncertainty in regional climate projections than for global mean projections and the relative importance of the sources differs (Deser et al., 2012). Sampling uncertainty due to natural variability is much larger for regional area-averages than for global means, which makes detection and attribution less tractable at the regional scale (Chapter 10). Spatial variations in aerosol forcing (Chapter 7) and land use/cover changes (DeFries et al., 2002; Moss et al., 2010) become more important forcings and sources of uncertainty on regional scales. Model uncertainty in regional climate responses is also large and depends on the variable, for example, climate models agree more readily on the sign and magnitude of temperature changes than for precipitation changes (IPCC, 2007b). Despite all these sources of uncertainty, credibility in regional climate change projections may be improved by identifying key drivers of the change and then evaluating how well climate models simulate such processes.

This regional assessment aims to assess the scientific basis for future regional climate change by interpreting regional projections in terms of projected changes in large-scale climate phenomena. The assessment has several caveats. Firstly, it focuses on surface air temperature and precipitation changes and so does not provide all the information required for subsequent impact studies, e.g., other less certain aspects of the water cycle (see Chapter 12) such as evapo-transpiration required for hydrological impacts. Secondly, it only attempts to interpret changes in terms of the large-scale phenomena assessed in Sections 14.2–14.6. Other processes can also be important for regional climate change (see Sections 14.1.2 and the attribution assessment in Section 10.6.1). Thirdly, this assessment is based primarily on multi-model ensemble projections from general circulation models (e.g., CMIP5 output shown in Annex I) with no attempt to bias correct or downscale climate model output to match observations. The model spread shown in Annex I takes no account of model discrepancies and so is neither a complete nor reliable estimate of the uncertainty in future observables. Regional climate assessments involve additional uncertainty due to the use of a cascade of uncertainty through the hierarchy of models needed to generate local information (e.g., calibration uncertainty due to choice of downscaling scheme). Climate model discrepancies and regional downscaling methods are evaluated in Chapter 9.

[INSERT FIGURE 14.32 HERE]

Figure 14.32: Spatial extent of 26 sub-regions covering different climate zones. Analyses in this chapter are performed for land grid points only, unless stated otherwise in the text. Region names and coordinates are given in Table 14.2. See also Seneviratne et al. (2012). [To be updated and confirmed with Atlas].

[INSERT TABLE 14.2 HERE]

Table 14.2: Temperature and precipitation projections by the CMIP5 global models. Averages over SREX (Seneviratne et al., 2012) regions of the projections by a set of [xx] [this number is consistent with the models used in the Atlas] global models for the RCP4.5 scenario. The mean temperature and precipitation responses are first averaged for each model over the 1986–2005 period from the historical simulations and the 2016–2035, 2046–2065 and 2081–2100 periods of RCP4.5. Computing the difference between these two periods, the table shows the 25, 50 and 75 percentiles and the lowest and highest response among the [xx] models, for temperature in degrees Celsius and precipitation as a per cent change. The regions are defined by latitude/longitude boxes as specified in SREX. Information is provided for land areas contained in the boxes unless otherwise indicated. Where appropriate, the numbers refer to Figure 14.32. The

temperature responses are averaged over the boreal winter and summer seasons; December, January and February (DJF) and June, July and August (JJA) respectively, whereas the precipitation responses are averaged over half year periods, boreal winter; October, November, December, January, February and March (ONDJFM) and summer; April, May, June, July, August and September (AMJJAS). [PLACEHOLDER FOR FINAL DRAFT: Final version of this table will also include annual mean values. Regions in which the middle half (25–75%) of the distribution is all of the same sign in the precipitation response will be coloured light brown for decreasing and light blue for increasing precipitation as was the case in AR4, Table 11.1.]

14.7.2 Arctic

In this section, a brief overview of Arctic climate variability and change is presented, with references to the many other places in the report where climate change in this region is discussed in greater detail.

Arctic climate is affected by three modes of climate variability: NAO, PDO, and the AMO. These modes all have their greatest temperature impact at the region's margins. For example, the NAO index is positively correlated with temperatures in the northeastern Eurasian sector, and adjacent coastal Arctic, and negatively correlated with temperatures in the Baffin Bay and Canadian Archipelago, but exhibits little relationship with temperature in the central Arctic (Polyakov et al., 2003). The PDO, meanwhile, plays a large role in temperature variability of Alaska and the Yukon (Hartmann and Wendler, 2005), being positive correlated with temperatures there. The AMO is positively associated with SST throughout the Arctic (Chylek et al., 2010; Chylek et al., 2009), especially as far north as the Barents Sea (Levitus et al., 2009). The significance of the NAO for Arctic climate may be more in its impact on sea ice through the associated surface wind field: Positive NAO anomalies result in detectable ice advection anomalies that would lead to ice thinning (Rigor et al., 2002). Other more analyses more confined to the Arctic have revealed atmospheric variability patterns unrelated to the NAO, PDO, or AMO, but directly linked to sea ice advection, thinning, and export out of the Arctic (Overland et al., 2008; Overland and Wang, 2005; Wu et al., 2006; Zhang et al., 2008b).

The surface and lower troposphere in Arctic and Pan-Arctic land areas have shown warming over the past three decades that is significantly larger than the global mean (Figures 2.8 and 2.13). Pan-Arctic temperature reconstructions based on proxy records from lake sediments, ice cores, and tree rings reveal that the observed warming is also highly unusual, and that Arctic temperatures over the past few decades have been significantly higher than any temperatures seen during the past 2000 years (Kaufman et al., 2009). Finally, the warm temperatures have been sustained in pan-Arctic land areas affected by the NAO and PDO as described above, despite the fact that both the PDO and the NAO have trended negative over the past decade. The absence of a connection between overall Arctic warming and NAO variability is particularly well-documented in the literature (Semenov, 2007; Turner et al., 2007b). Thus three factors all point towards a likely role for anthropogenic forcing in the warming of the Arctic region over the past few decades: The pattern match of anthropogenic and observed warming in the Arctic, the large magnitude of the warming compared with estimates of natural variability, and the difficulty in reconciling recent trends in known modes of natural variability with the observed warming trends. Observations have also shown an increase in winter cyclone activity over the Canadian Arctic over the last 50 years (Section 2.6.4). Because of a dearth of quality precipitation data, it is very difficult to assess whether precipitation trends over the past few decades in the Arctic drainage areas also show an increase (ACIA, 2005). However, river gauge observations do show consistent runoff increases of approximately 10% in rivers draining into the Arctic since about the mid-20th century (Richter-Menge and Overland, 2009). This could be driven partly by the indirect effects of warming, including permafrost and snow melt (Section 2.5.2) in addition to undetected precipitation increases. The Arctic has of course also experienced a dramatic and well-documented decline in sea ice (see Figure 9.24).

The CMIP3 models exhibited common biases in the Arctic region, including a cold bias in surface air temperature of 1–2°C, and a small positive bias in sea level pressure in the eastern Arctic (Chapman and Walsh, 2007a). There is a robust relationship between the temperature response and the model biases in both CMIP3 and CMIP5 that can be exploited to give more precise predictions of Arctic warming (Bracegirdle and Stephenson, 2012a; Bracegirdle and Stephenson, 2012b). There has been substantial progress in adapting community-based regional climate models for polar climate applications (Wilson et al., 2012). These models have been extensively evaluated, particularly with regard to their ability to simulate Arctic clouds, surface heat fluxes, and boundary layer processes (Inoue et al., 2006; Rinke et al., 2006; Tjernstrom et al., 2004). Such models have been used to improve simulations of Arctic-specific climate processes, such as glacial

mass balance (Zhang et al., 2007a). However, there has not been a systematic effort to use regional climate models to project Arctic climate change, as with some other regions.

The CMIP5 model simulations show an ensemble-mean polar amplification warming that is quantitatively very similar to previous CMIP3 model simulations (Bracegirdle and Stephenson, 2012b). The warming is greatest in DJF, due in large part to a thinning of sea ice and an increase in heat flux from the relatively warm ocean to the lowest atmospheric layers (e.g., Boé et al., 2009). For RCP4.5, ensemble wintertime warming rises to 5°C over pan-Arctic land areas by the end of the 21st century, and about 8°C over the Arctic Ocean. Throughout the 21st century, the warming exceeds simulated estimates of internal variability (Figure AI.8). The RCP4.5 ensemble-mean warming is more modest in JJA (Figure AI.9), reaching about 3.5°C by the end of the century over land, and a little over 2°C over the ocean. The summertime warming exceeds internal variability estimates by about the middle of the 21st century. The overall Arctic warming is much larger than in the tropics or mid-latitudes, exhibiting the so-called "polar amplification" pattern (see Box 5.1). These simulated anthropogenic seasonal warming patterns match qualitatively the observed warming patterns over the past six decades (AMAP, 2011). This indicates that the future temperature evolution of Arctic climate on decadal time scales and longer will likely continue to be dominated by the signals of anthropogenic climate change.

Increasing precipitation is another important manifestation of Arctic climate change. The CMIP5 models robustly project increased moisture flux convergence and precipitation in the pan-Arctic region over the 21st century, as did their AR4 counterparts (Kattsov et al., 2007; Rawlins et al., 2010). Under the RCP4.5 scenario, the cold-season, ensemble-mean precipitation increases roughly 20–30% by the end of the 21st century (Figure AI.10). However, this signal does not rise consistently above the noise of simulated internal precipitation variability until mid-century. During the warm season, the precipitation increases are somewhat smaller, on the order of 10%, though these signals also rise above variability at roughly mid-century (Figure AI.11). Throughout the year, the precipitation increase is generally larger over the Arctic itself than over the adjacent land areas. The inter-model spread in the precipitation increase is generally as large as the ensemble-mean signal itself. The CMIP3 models also diverged widely in the quantitative details of projected Arctic hydrologic change (Holland and Webster, 2007). However, since nearly all models project a large precipitation increase rising above the variability year-round, it is likely the pan-Arctic region will experience a statistically-significant increase in precipitation by mid-century.

There is extensive discussion of Arctic sea ice loss, including the origin of the recent observed loss (Section 5.4.1.5, Chapter 10), projections of sea ice change (Chapters 11 and 12) and their quality (Sections 9.4.3 and 9.8.3 and Chapter 11). Here we simply note that internal variability processes also strongly affect sea ice anomalies on interannual time scales in both positive and negative senses. These processes include Arctic-centred atmospheric circulation anomalies (noted above), cloud variations (Kay et al., 2008), and ocean circulation (Smedsrud et al., 2008). Therefore, ice loss or gain in any particular year cannot be taken as an indication of a trend due to anthropogenic forcing, or lack thereof.

In summary, there is high confidence that future temperature evolution of Arctic climate on decadal time scales and longer will likely continue to be dominated by the signals of anthropogenic climate change. It is likely the pan-Arctic region will experience a significant increase in precipitation by mid-century. There is high confidence that Arctic sea ice anomalies exhibit substantial interannual variability, so that ice loss or gain in any particular year cannot be taken as an indication or absence of a long-term trend due to anthropogenic forcing.

14.7.3 North America

The climate of North America (NA) is mainly affected by the following modes of variability: NAO, ENSO, PNA, PDO, and the NAMS. The NAO affects Eastern NA during winter. Positive NAO brings warmer temperatures to this zone, and a northward shift of the storm track (Hurrell et al., 2003). Positive PNA also affects wintertime climate, and brings warmer temperatures to northern Western NA and Alaska, cooler temperatures to the southern part of Eastern NA, and dry conditions to much of Eastern NA (Nigam, 2003). The PNA can also be excited by ENSO-related SST anomalies, providing a link between ENSO and NA climate (HOREL and WALLACE, 1981; Nigam, 2003). Storm track disturbances over North America may link the PNA and NAO patterns (Li and Lau, 2011; Li and Lau, 2012a). The PDO is associated with NA

climate anomalies that resemble those of the PNA, though the PDO is associated with much longer time scale variability. Positive anomalies of the NAMS bring excess rainfall to the northern portion of Central America and Mexico and the southern portion of Western NA during summer (Gutzler, 2004). Tropical cyclones also have a significant impact on the Gulf Coast and the seaboard of Eastern NA (see Box 14.3). Atlantic SST and the modes shaping it (AMM and AMO) may affect the frequency and intensity of such disturbances (Cassou et al., 2007; Emanuel, 2007; Goldenberg et al., 2001; Landsea et al., 1999; Smirnov and Vimont, 2011; Vimont and Kossin, 2007).

Assessment of historical trends in this region is complicated somewhat by systematic changes in spatial coverage, especially the small number of stations in Western NA early in the 20th century (Shen et al., 2012). Nonetheless, a general surface warming trend has been documented over NA in the last century, particularly in the last 50 years (see Chapter 2). This warming is particularly large over Alaska and northern Western NA during winter and spring (i.e., MAM) and the northern part of Eastern NA during summer (i.e., JJA) (Zhang et al., 2011c). There is also a cooling tendency over Central and Eastern NA (i.e., the "warming hole" discussed in Section 2.7.1 of Chapter 2) during spring (Bukovsky, 2012) which is absent in lower tropospheric temperature (cf. Chapter 2, Figure 2.13). Land-use and land-cover change could also play in a role in these surface temperature changes; however, investigations of this effect have not led to a clear consensus (Avila et al., 2012; Fall et al., 2010). The warming has also been associated with a systematic decline in the North American snowpack (Brown and Mote, 2009; McCabe and Wolock, 2010), though the snowpack decline may also stem partly from increasing black carbon deposition on snow (Qian et al., 2009b). While these regionally coherent trends toward earlier spring melt across Western NA are influenced in part by PDO phase, the trend spans PDO phases (Stewart et al., 2005). The decline is particularly large in the late spring, when temperatures rise enough above freezing that warming ought to cause additional snowmelt (Kapnick and Hall, 2011). Reductions in Western NA snowpack over the last 50 years of the 20th century exceed model estimates of trends expected to occur by chance due to internal variability alone (Pierce et al., 2008). In addition, tree-ring evidence reveals that the size and geographical coherence of late 20th century western North American snowpack reductions have no precedent in the last thousand years (Pederson, 2011). Thus both model and observational evidence indicate anthropogenic changes in snowpack are already underway.

Consistent with the trends of mean surface temperature, extremes defined with reference to the lower 10th and upper 90th percentiles also exhibit secular changes. Cold days and nights have been shown to decrease in the last half century over NA, while warm days and nights have increased (see Chapter 2). These trends are especially apparent for nightly extremes (Vincent et al., 2007). It is unclear whether there have been trends in mean precipitation over the last 50 years. For example, some studies have significant positive trends over Eastern and northern Western NA while others have found none over NA (Chapter 2, Zhang et al., 2011b). The extremes in precipitation have been found to be increasing overall in NA, especially over Central and Eastern NA (see Chapter 2 and SREX).

Since the AR4, numerous regional modeling experiments have been performed over NA, with the aim of reducing model biases partly through increased resolution. In general, these experiments have focused on reproducing the climate record of the past few decades, and model biases have decreased as the resolutions have increased, though not always substantially. One program, the North American Regional Climate Change Assessment Program (NARCCAP), created a series of RCM-GCM simulations for the entire continent at 50-km resolution. When forced by reanalysis data, the NARCCAP suite generally reproduces the seasonal and geographical distributions of temperature and precipitation within the range of observational error, though the simulation quality for precipitation is distinctly lower, as is the case with global models (Gutowski, 2010; Mearns et al., 2012; Wang et al., 2009b). Other regional modeling experiments covering only portions of NA have demonstrated bias reductions as resolution increases (Liang et al., 2008a; Lim et al., 2011; Yeung et al., 2011). Bias reduction is especially large (e.g., compared to GCMs and NARCCAP simulations (Salzmann and Mearns, 2012)) in the case of snowpack in Western NA, as revealed by 2- to 20-km resolution regional simulations focused within Western NA (Pavelsky et al., 2011; Qian et al., 2010b; Rasmussen, 2011; Salathe Jr et al., 2010). This is virtually certain to be a reflection of the importance of resolving topography in simulating snowpack distributions accurately. In general, since the AR4 there has been substantial progress in understanding the strengths and limitations of regional modeling techniques in simulating NA climate of the past few decades. However, with the exception of changes in the snowpack over Western NA and Canada, where the higher resolution of regional models

almost certainly enhances credibility in this specific dimension of climate change, there is little progress to report in understanding the added value of using regional models to simulate climate change.

The NA warming patterns in the RCP4.5 CMIP5 projections are generally similar to those of CMIP3 (Figures AI.4 and AI.5). Land generally warms more than the oceans, an effect that is particularly apparent in the five northernmost NA regions (1-5). There is a pronounced seasonality to this pattern. In the wintertime, the warming is greatest in Alaska and Canada/Greenland (Figures AI.12 and AI.16), while in the summertime, the maximum warming shifts south, to Western, Central, and Eastern NA. Examining the early 21st century (2016–2035) CMIP5 warming projections of the less sensitive models (25th percentile, i.e., upper left maps in Figures AI.12, AI.13, AI.16, AI.17, AI.20 AI.21, AI.24, and AI.25), the near-term warming exceeds internal variability estimates in most cases. The only exceptions are Alaska, parts of Western, Central, and Eastern NA, and Canada/Greenland during winter, when internal variability due to the wintertime storm track is large enough even to overwhelm the large warming signals in some GCMs. By 2046–2065, the warming in all regions exceeds the internal variability estimate, even for the less sensitive models. Thus it is very likely that the warming signal will be large compared to internal variability in all NA regions throughout the year by mid-century. Analysis of CMIP3 models showed that this degree of warming leads to a two to four fold increase in the frequency of heat waves over the course of the 21st century (Lau and Nath, 2012). As with the CMIP3 models, projected changes in snowpack are difficult to assess with the CMIP5 models because of poorly resolved topography in Western NA.

Anthropogenic climate change may also bring with it systematic changes in the precipitation distribution over NA. As with previous generations of models, projections by CMIP5 models robustly produce an increase in wintertime precipitation over the northern half of NA (Figure AI.19). This is in part associated with increased moisture in the warmer atmosphere yielding increased moisture convergence and in part with a pole ward shift in wintertime extratropical cyclone activity (see Box 14.3) over the continent. This change is also consistent with model projections of positive NAO trends in response to increased concentrations of greenhouse gases diagnosed in AR4 (Hori et al., 2007; Karpechko, 2010; Zhu and Wang, 2010). Thus Canada/Greenland and Alaska will likely experience a substantial October to March precipitation increase over the remainder of the 21st century. The projection of positive wintertime increases extends southward into substantial portions of the USA (northern portions of SREX regions 3–5), especially in December to February (Maloney, 2012b; Neelin et al., 2012) but with increasing dependence on location and decreasing certainty as one moves southward toward the region of projected precipitation decrease in the subtropics that affects Central America and Mexico. April to September precipitation also exhibits robust increases in Alaska and northern Canada (regions 1 and 2; Figures AI.19 and AI.22) by end of century. See also Table 14.2 for details about CMIP5 results for RCP4.5.

The robustness of the precipitation change as evaluated using 20-year averages in the RCP4.5 scenario is less clear over the rest of NA (Figure AI.27), until one arrives at the Central American/Caribbean region (Section 14.7.4) where robust drying is found, consistent with CMIP3 results (Neelin et al., 2006; Rauscher et al., 2008; Seth et al., 2010). In RCP8.5, where the signal is stronger, (Maloney, 2012b) notes agreement among CMIP5 models on the sign of precipitation reduction in the northern portions of Western NA and Central NA. Assessment of CMIP3 models had noted a 21st-century decrease in precipitation across much of the southern portion of Western NA, accompanied by a robust evaporation increase characteristic of mid-latitude continental warming, leading in turn to a drying trend in regional hydro climate (Seager and Vecchi, 2010; Seager, 2007) and an increase in the occurrence of drought (Gutzler and Robbins, 2011; Sheffield and Wood, 2008). There is also broad consistency in the simulated anthropogenic patterns of hydro climate change in western NA and the patterns of hydro climate change observed over the course of the 20th century (Barnett et al., 2008), including the distinct dry period over the past decade (Cayan et al., 2010). However, there is disagreement as to whether the recent observed changes have a magnitude large enough to be attributable to anthropogenic forcing (Das et al., 2009; Seager and Vecchi, 2010) and there is some correlation between model drying and overestimates of historical precipitation (McAfee et al., 2011). Despite shifts in the boundary between mid-to-high latitude precipitation increases and subtropical decreases in CMIP5 relative to the CMIP3 ensemble in some parts of Western NA, the overall pattern remains consistent. Consistency of simulations of anthropogenic changes in Western NA hydro climate among themselves and with observations suggests the region may be particularly vulnerable to future reductions in water resource availability. A key remaining uncertainty in future hydro climate in Western NA is the impact of anthropogenic changes in tropical Pacific SST, since the region exhibits a documented precipitation

sensitivity to SST modes in the equatorial Pacific (Cayan et al., 1999; Findell and Delworth, 2010) through the PNA mode of variability; unfortunately global models do not provide consistent information regarding anthropogenic changes in the equatorial Pacific SST (Seager and Vecchi, 2010).

In summary, it is very likely that the anthropogenic warming signal will be large compared to internal variability in all NA regions throughout the year by mid-century. It is likely that the northern half of NA will experience an increase in precipitation over the 21st century, while Mexico and Central American will experience a decrease.

14.7.4 Central America and Caribbean

The annual cycle of Central American and Caribbean climate is the result of air–sea interactions over the Western Hemisphere warm pool (WHWP) in the tropical eastern north Pacific and the Intra Americas Seas (IAS) (Amador et al., 2006; Wang et al., 2007). As in many other regions, interactions between transients and the mean flow shape the mean circulation. For instance, the Caribbean Low Level Jet (CLLJ) is a key element of the region's summer climate (Cook and Vizy, 2010) and is controlled by the size and intensity of the WHWP. The mechanism linking the size of the WHWP to the atmospheric circulation is the so-called "Gill atmosphere" response to an off-equatorial warm anomaly. An anomalously large WHWP is associated with a weakened CLLJ and increased rainfall over the IAS, decreased moisture transports into the eastern North Pacific and eastern North America, increased relative humidity, and decreased vertical wind shear (Wang et al., 2008b). The opposite relationships are associated with an anomalously small WHWP.

Observational analyses point to reduced precipitation in the IAS region. Comarazamy and Gonzalez (2011) found that increased easterly surface winds over Puerto Rico from 1950 to 2000 disrupted a pattern of inland moisture advection and convergence, increasing cloud base heights and reducing total column liquid water content over high elevations. This translated into a dramatic decrease in accumulated precipitation during the early rainfall season (April to June), consistent with the stronger CLLJ found in model projections of future climate. However, interdecadal climate variations in the Mesoamerican and Caribbean region can be large, and trends in precipitation should be considered in this context. Prolonged dry or wet periods in the region are related to the combined effect of decadal variability of the Pacific and Atlantic oceans (Mendez and Magana, 2010; Mendoza et al., 2007; Seager et al., 2009).

Most CMIP3 models project a warmer and drier climate for the IAS region (IPCC, 2007), with increased vertical wind shear over the tropical North Atlantic and reduced relative humidity (Vecchi and Soden, 2007b). (Tropical Atlantic features are discussed in more detail in Section 14.3.4.) When considered solely in light of local mechanisms such as the "Gill atmosphere" response described above, such projections are apparently not consistent with the large increase in SST in the WHWP also seen in the CMIP3 models. However, the atmospheric circulation change is not determined by local SST changes, but also by the larger-scale distribution of the warming—in other words, the competition between the SST changes in the WHWP and those of the Indo-Pacific warm pool (Latif et al., 2007; Vecchi and Soden, 2007c). The tropical North Atlantic warms considerably less than the tropical Pacific in the CMIP3 models due to a reduced Atlantic meridional overturning circulation. Thus in this global context of relative SST change, the WHWP actually shrinks, explaining the reduced precipitation in the IAS region. In addition, because tropospheric humidity is reduced and vertical wind shear increased, overall tropical cyclone activity decreases in embedded models that resolve these mesoscale disturbances (Knutson et al., 2008). This may also have an important effect in reducing total precipitation in the region. The CMIP5 projections also show AMOC weakening in the 21st century (Chapter 12, Section 12.4.7.2).

There are only a few examples of dynamical and statistical downscaling covering the Mesoamerican region. Those that have been done show mid-21st century warming for the region between 2°C and 3°C, depending on location, scenario and the model under consideration (Karmalkar et al., 2011; Rauscher et al., 2008; Vergara, 2007). Most downscaling exercises project precipitation decreases over most of Mesoamerica, similar to the hydrologic response in the driving global models. However, only a few have considered the role of key elements of the region's climate, such as easterly wave activity, mesoscale phenomena such as tropical cyclones, or interannual variability mechanisms associated with ENSO (Karmalkar et al., 2011). Dynamical downscaling using the RAMS model forced by HADGEM2-ES for RCP4.5 and RCP8.5 indicated decreased annual rainfall over Caribbean and northern Central America over the 21st century

(Costa et al., 2012). Temperature changes under RCP8.5 by the end of 21st century projected by this regional model are 3.6°C for Caribbean and 4.6°C for Central America.

In Central America and the Caribbean region, CMIP5 models under RCP4.5 project an ensemble-mean warming of 1°C–3°C by the end of the 21st century for DJF and JJA (Figure AI.24 and Table 14.2). In the October to March period, the ensemble-mean precipitation change shows a decrease between 10–30% in the northern sector of Central America, including Mexico. In the Caribbean region, the precipitation projections also indicate a 10–30% reduction over most of the region, except for an increase in the northern sector over Cuba (Figure AI.26). In the April to September period, the zone of reduction in projected precipitation expands over all of Central America and the entire Caribbean region, though the reduction's magnitude remains the same, about 10–30% (Figure AI.27). The changes are larger than the standard deviation of model estimated internal variability of 20-year mean anomalies.

In summary, there is medium confidence that most of the Central American and Caribbean region will continue to experience a precipitation reduction over the coming century, as the tropical North Atlantic and Caribbean warm less than the tropical North Pacific, and atmospheric convection in the region therefore becomes less frequent.

14.7.5 South America

South America is affected by intraseasonal, interannual and multidecadal modes of variability. The Pacific Ocean (ENSO-Section 14.4) and Atlantic Ocean (Sea Surface Temperature-SST tropical gradient-Section 14.3.4) have a role in interannual variability of several regions of this continent. Teleconnections such as the Pacific South American pattern (PSA-Section 14.6.2); the Southern Annular Mode (SAM-Section 14.5.2) and the Indian Ocean Dipole (IOD-Section 14.3.3) are related to climate variability over South America. The South American Monsoon System (SAMS-Section 14.2.3.2) is responsible for the rainy season in large areas of the continent. The South Atlantic Convergence Zone (SACZ- Section 14.3.1.3) and Atlantic Intertropical Convergence Zone (ITCZ-Section 14.3.1.1) also affect precipitation in large areas.

ENSO is one of the main sources of interannual variability. Northeast Brazil is affected by droughts in El Niño and floods in La Niña, while large areas of La Plata basin (LPB; southeastern South America) have the opposite signal.

Aside from Pacific Ocean influences on South America, tropical Atlantic SST anomalies also affect precipitation over northern and northeastern South America through position and intensity of the ITCZ. The ITCZ shifts southwards due to increased aerosol over North Atlantic, reducing North Atlantic SST (Chang et al., 2011). The Atlantic thermohaline circulation (Stouffer et al., 2006) can affect precipitation over Northeast Brazil. Changes in the North Atlantic Oscillation (NAO-Section 14.5.1) affect Atlantic SST and the ITCZ position (Souza and Cavalcanti, 2009). The north-south Atlantic SST gradient has high negative correlation with precipitation over Amazonia and Northeast Brazil (Good et al., 2008). North Atlantic SST anomalies in 2005 and 2010 were related to extreme droughts in Amazonia, considered the worst since 1950 (Marengo et al., 2008). AGCM (Harris et al., 2008) and CGCM experiments under a 1% CO_2 increase (Good et al., 2008) indicated a relationship between the Atlantic SST gradient and precipitation in southern Amazonia (see also Chapter 12). Precipitation over southeastern South America and southeastern Brazil is influenced by the Southern Annular Mode (Section 14.5.2; (Reboita et al., 2009); (Vasconcellos and Cavalcanti, 2010)) and PSA (Section 14.6.2),via changes in storm tracks, jet stream position and intensification of anomalous circulation centres.

Extreme droughts and floods have occurred more frequently in recent years in several regions of the globe (SREX-Chapter 3). Positive extreme precipitation trends have been identified in several regions of South America, mainly in southeastern South America, central-northern Argentina, and northwestern Peru and Ecuador. Negative trends were observed in southern Chile (Chapter 2, Section 2.7; Dufek et al., 2008; Marengo et al., 2009; Re and Barros, 2009).

Positive trends in minimum temperature have been observed in several areas of southeastern South America (Marengo and Camargo, 2008; Marengo et al., 2009; Rusticucci and Barrucand, 2004; Rusticucci and Renom, 2008; SREX Chapter 3). Significant correlations were found between number of summertime cold

nights in Uruguay and the negative phase of the SAM between 1949 and 1975, but the correlation was not seen in the period 1976 to 2005 (Renom et al., 2011).

CMIP5 models reproduce the annual cycle of precipitation over South America, although the multi-model mean underestimates rainfall over large areas of the continent (Chapter 9). The main features of precipitation were reproduced by a set of regional models, such as the rainfall minimum in Northeast Brazil and central Argentina, and the maximum over western Amazonia extending to the SACZ region (Solman et al., 2011).

Comparison of extreme temperature indices from CMIP3 20th century simulations with observations indicates that the number of warm nights is better represented than the number of frost days (Rusticucci et al., 2010). Trends toward warmer nights in CMIP3 models (Rusticucci et al., 2010; Marengo et al., 2010b) are also obtained in regional models (Marengo et al., 2009) and are consistent with global-scale results of SREX (Chapter 3, Section 3.3). In general, models results are consistent with the observed tendencies of the last few decades (e.g., Haylock et al., 2006). CMIP3 models are able to simulate precipitation indices over South America, such as R95t, but have difficulty simulating R10 or CDD (Rusticucci et al., 2010).

Ensemble-mean temperature projections for the RCP4.5 scenario of CMIP5 models show higher temperatures for all four SREX sub-regions (Amazonas: AMZ, Northeast Brazil: NEB, West Coast: WSA, Southeastern South America: SESA) at the end of 21st century compared to the 1986–2005 period. The median model temperature (°C) values increase from (DJF: 1.0, 1.0, 0.9, 0.9; JJA: 1.1, 1.1, 1.0, 0.8) in RCP2.8 to (DJF: 4.2, 3.8, 3.8, 3.9; JJA: 4.7, 4.9, 4.2, 3.5) in RCP8.5. In RCP4.5, based on the 25% and 75% percentiles, the projected temperature (°C) change in DJF varies between (AMZ: 1.8 and 2.9; NEB: 1.6 and 2.5; WSA: 1.6 and 2.3; SESA: 1.4 and 2.3) and in JJA between (AMZ: 1.8 and 2.9; NEB: 1.7 and 2.6; WSA: 1.7 and 2.5; SESA: 1.3 and 2.0) (see Table 14.2, Figures AI.28–AI.29 and AI.32–AI.33, and the Supplementary Material for different time windows and four different RCPs). The RCP4.5 changes are larger in southeastern Amazonia (up to 3.5°C in the austral winter season), and the northwestern region (up to 3°C in the summer season, see Figures AI.40–AI.42.) In the AR4, the largest warming was in central Amazonia in austral winter, up to 4°C in scenario A1B (AR4 Chapter11). Changes in temperature projected by a set of regional climate models (RCMs) forced by a range of CMIP3 models (A1B scenario) agree that the largest warming at the end of the 21st century is found over the southern Amazon during winter, but the warming is greater than that of both the CMIP3 and CMIP5 global models—between 4°C and 5°C (Figure 14.33). During summer, though all RCM models project temperature increases, the spatial distribution and magnitude of the warming vary from model to model. Land-surface processes, which become more relevant during summer, are treated differently by each RCM, explaining this large spread. Solman et al. (2012) also showed that regional models have larger biases and larger uncertainty over tropical than subtropical regions. Regional models project greater frequency of warm nights over South America, except in parts of Argentina, and a reduction of cold nights over the whole continent (Marengo et al., 2009). Results for South America presented in SREX Chapter 3 indicate a likely increase of warm days and nights, and a reduction of cold days and nights in all regions of South America. Finally, it is likely that heat waves will become more frequent in Amazonia, Northeast and the west coast of South America.

The precipitation projections for this century show distinct sub-regional and seasonally-dependent differences. In October to March, all regions are projected to receive practically unaltered precipitation amounts by the end of the century, with median model values between –3% – 3% in RCP2.6 as well as RCP8.5, with the exception of SESA, where a more clear change in RCP8.5 of an 11% increase is seen. The 25% and 75% percentile range for the end of century projection in RCP4.5 are for AMZ: –3% – 2%, NEB: –5% – 6%, WSA: 1% – 5%; SESA: 0% – 5%, respectively. In the half year (April to September), the projected changes are remain small in both RCP2.6 and RCP8.5, but with a reduction of –9% and –18% in RCP8.5 for AMZ and NEB. The percentile ranges in RCP4.5 are for AMZ: –4% – 1%, NEB: –15% – –3%, WSA: –2%–3%; SESA: 0% – 8%, respectively (see Table 14.2, Figures AI.30–AI.31 and AI.34–AI.35, and the Supplementary Material for different time windows and four different RCPs). This suggest that only the reduction in NEB in April to September is a robust multi-model result, although the inter-model spread is relatively high in both half year periods.

The RCP4.5 CMIP5 precipitation projections for the end of the 21st century show an increase (5–20%) for October to March over the southern sector of Southeast Brazil and LPB, over the northwest coast of South America and in the Atlantic ITCZ, extending to a small area of northeastern Brazil coast (Atlas Figures

AI.49–AI.51). These are the regions also projected by CMIP3 models to have an end-of-century precipitation increase in December to February. In the CMIP5 ensemble-mean, reduced October to March rainfall is projected to the extreme northern region of South America (20–40%), in eastern Brazil (10–20%) and in Chile (5–20%). There is also decreased December to February rainfall in these regions in the CMIP3 projections (AR4, Chapter 11), except in eastern Brazil. From April to September under RCP4.5, precipitation is projected to increase in the northeastern sector of the LPB (10–20%) and northwestern South America near the coast (5–20%). In contrast, a reduction is projected for nearly the entire tropical region, including Northeast Brazil (20-40%), and eastern Amazonia (10–20%). The reduction in Chile extends to Patagonia (10–40%). The areas with maximum changes are consistent with results from CMIP3 in JJA (Chapter 11, AR4). All the CMIP5 changes discussed above are significant and larger than the standard deviation of the internal variability of 20-year mean anomalies.

[INSERT FIGURE 14.33 HERE]

Figure 14.33: Precipitation changes (2071–2100) – (1961–1990) projected by three members of RCA, LMDZ, REMO, REgCM3,PROMES, ETA, and the ensemble mean.

Precipitation changes projected by a set of regional models forced by a suite of CMIP3 models suggests some projected changes discussed above are robust, such as the precipitation increase over the LPB region during summer, and the decrease over central Chile and northern South America (Figure 14.33). A winter precipitation increase over southern Brazil and Uruguay is also projected by some RCMs, as in CMIP5 models. Increased precipitation in the LPB was projected by CMIP3 models and RCMs (Bombardi and Carvalho, 2009; Marengo et al., 2009; Nunez et al., 2009; Seth et al., 2010). However, the summer precipitation decrease in the Northeastern region in the RCMs is seen only in the winter in CMIP3 and CMIP5 models. RCM projections show a rainfall reduction over Northeast Brazil, central-eastern and southern Amazonia, and an increase over the Peruvian coast and Ecuador (Marengo et al., 2010b; Marengo et al., 2011). A relevant result from an RCM is the precipitation decrease over most of South America north of 20°S in austral spring, suggesting a longer dry season (Sörensson et al., 2010). This is consistent with some results assessed in Section 14.2.3.2. Over the Amazon basin, the agreement among RCMs (Figure 14.33) is not so clear, even if the models are driven by the same global model. These anomalies, driven by changes in the main circulation patterns affecting South American climate, vary in location and intensity depending on the RCM and the forcing global model.

Ensemble projections of the end of the 21st century with 20- and 60-km meshes using the MRI AGCM show an increase in precipitation intensity over almost the entire continent, especially in the southeast and north (Kitoh et al., 2011). At the same time, a large increase in consecutive dry days is projected over the western part of the Amazon and Central Brazil. Extreme precipitation events increase in the LPB during all seasons but spring. The annual-mean maximum number of consecutive dry days (CDD index) increases over central Brazil and eastern Amazon, but decreases in western Amazonia, the Bolivian lowland and northwestern Argentina. No clear pattern of change for this index was found over the LPB (Sörensson et al., 2010). The number of consecutive dry days increases in northeastern South America in the projections (Marengo et al., 2009). However, in the SREX report, there was low to medium confidence in South America precipitation trends. There was medium confidence that heavy rainfall events will occur with increasing frequency in the Northeast, the northern sector of the Southeast, and west coast of tropical South America. Medium confidence was also associated with an increase of dry days in Northeast Brazil.

Precipitation changes over South America projected by some models are consistent with El Niño influences, e.g., a rainfall increase over southeastern and northwestern South America and a decrease over the Northeast (Marengo et al., 2009). A study with the ECHAM5-O model indicated that the ENSO connection with southeastern South America could weaken in the future (Grimm and Natori, 2006; Grimm, 2011). However, there is no consensus about future ENSO behavior (Coelho and Goddard, 2009; Chapter 10; Section 14.4). Trends in Pacific SST and east –west SST gradients show different results depending on the dataset used (Chapter 2).

The precipitation increase in the southern center of the South America dipole (Section 14.3.3) can be related to a strengthening and displacement of the PSA in future projections (Junquas et al., 2011). The precipitation increase in the southern sector may have also a contribution from a more frequent Low Level Jet (LLJ) (Soares and Marengo, 2009). An increase in low-level meridional winds over the continent (Nunez et al.,

2009) could represent an increase in LLJ frequency. Increased moisture flux from the Amazon to the LPB is consistent with the precipitation increase in the southern regions.

The CMIP3 projections indicate an increase of Sea Level Pressure in the South Atlantic (Seth et al., 2010) as the Subtropical High is displaced polewards, related to the positive trend of the SAM and a poleward shift of the storm tracks. This shift has an impact on zones of cyclogenesis activity off the Southeast South American coast, where future climate simulations indicate they would be displaced to the south (Kruger et al., 2011). Analyses of CMIP3 models show little impact on extreme precipitation over South Hemisphere continents from SAM changes during the last thirty years of the 21st century, except in Patagonia and southern Australia (Menendez et al., 2010).

Chile becomes drier in CMIP3, RCM, and CMIP5 future projections (AR4 and Annex I: Atlas). The pole ward shift of the storm tracks is consistent with this projected precipitation decrease. Several CMIP3 projections and a projection from an RCM indicate an increase in southerly winds close to the southwestern South America coast and an extension of the upwelling region southward (Garreaud and Falvey, 2009). These changes lead to coastal SST decrease and reduced temperatures in coastal areas. A multi-model analysis of 11 CMIP3 models under the A2 scenario shows a summertime increase in mid and upper level westerly flow over the central Andes, resulting in a moisture transport decrease from the interior of the continent towards the Altiplano, This reduces precipitation there by 10-30% relative to current values (Minvielle and Garreaud, 2011).

In summary, based on the agreement of several studies and models, it is very likely that precipitation will increase in La Plata basin and northwestern coast of South America and will decrease in Northeastern Brazil, eastern Amazonia and Chile. There is medium confidence in extreme precipitation trends in Northeast, northern sector of Southeast and west coast of tropical South America. It is very likely that temperatures will increase over the whole continent, with greatest warming projected in southern Amazonia. It is very likely there will be an increase of extremely warm days and nights, and a reduction of extremely cold days and nights in most regions of South America. It is likely that the heat waves will become more frequent in Amazonia, Northeast and west coast of South America.

14.7.6 Europe and Mediterranean

This region includes the whole European territory along with the North Africa and West Asia rims of the Mediterranean basin, and is here divided into three sub-regions named as Northern Europe (NE), Central Europe (CE) and Mediterranean (MD).

14.7.6.1 Modes of Variability

The most relevant phenomena affecting climate variability in diverse periods and time-scales are those related to the extratropical large-scale atmospheric circulation: NAO (see Section 14.5.1) and blocking (see Section 14.6.3). Other patterns such as the East-Atlantic (EA) pattern are also required to describe the strength and position of the North Atlantic jet and storm track, which strongly influence weather and climate in the region (Seierstad et al., 2007; Woollings et al., 2010). The EA pattern resembles the NAO but displaced and enhanced over the MD (Krichak and Alpert, 2005).These variability modes in turn seem to be modulated by interactions with Atlantic SST (AMO pattern) and tropical phenomena, in particular ENSO, MJO and Indian summer Monsoon (see Sections 14.5 and 14.6).

Cold season precipitation (October to March) variations are strongly associated with NAO. In the positive (negative) phase higher (lower) than normal precipitation prevails in the NE and CE sub-regions while in the MD an opposite behavior is observed, possibly with the exception of the eastern and south-eastern rims of the basin (Feliks et al., 2010). There is evidence that the NAO-precipitation teleconnection patterns have changed in the past (Hirschi and Seneviratne, 2010) and that the relationships are scenario-dependent in climate simulations (Vicente-Serrano and López-Moreno, 2008). The summertime NAO has a more northerly position and a smaller extent and thus a weaker but still perceptible influence on the region. In its positive (negative) phase higher (lower) than normal summer temperatures are experienced all over Europe, except in the eastern MD, and less (more) than normal rainfall in NE and CE (Folland et al., 2009; Mariotti and Dell'Aquila, 2011).

Europe is among the regions with most frequent blocking events in the world (Woollings, 2010). The persistence of this phenomenon leads to strong climate anomalies of different sign depending on the location of the high-pressure centre that diverts the westerly storms around. When it is located over Scandinavia-West Russia higher than normal precipitation (dry, cold) prevails over the MD (NE and CE) in the winter half, while the opposite occurs when the blocking forms over west-central Europe (Barriopedro et al., 2006). In the summer season heat-waves mostly occur during blocking situations (Dole et al., 2011).

Several studies have shown that the NAO and Blocking phenomena non-locally interact with other phenomena (Küttel and Lutterbacher, 2011; Pinto and Raible, 2012). For example Marullo et al. (2011b) showed that winter NAO anti-correlates with AMO and Folland et al. (2009) found a significant relationship between AMO and summer NAO variations, while other authors concluded that summer western European and MD heat waves are related to AMO (Della-Marte et al., 2007; Mariotti and Dell'Aquila, 2011). Through a complex chain of air-sea interactions Bulic and Kucharski (2012) explain the often observed time-lagged anomalies that ENSO events induce in large-scale circulation over the North-Atlantic European region: a positive (negative) ENSO event in winter leads to positive (negative) spring precipitation anomalies in Europe (Brönnimann, 2007; Shaman and Tziperman, 2011). Also Cassou (2008) showed that the diverse phases of MJO affects the wintertime daily NAO regimes with a time-lag of few days by an interaction mechanism between tropical forced Rossby waves and mid-latitude transient eddies. A similar mechanism is proposed between a strong Indian summer monsoon and above normal rainfall and below normal temperature over CE and the western NE along with positive temperature anomalies in the eastern MD, being the opposite situation during a weak monsoon (Lin and Wu, 2012).

14.7.6.2 Observed Changes

Deduced from the GHCN V3 global data set, the averages of annual temperature trends over the last decades (1979–2010) in each sub-region (NE: 0.48°C per decade; CE: 0.44°C per decade; MD: 0.34°C per decade) are all higher than the global 0.28°C per decade (Chapter 2, Table 2.1). In wintertime (DJF) the highest averaged trend was observed in NE (0.81°C per decade) while in summer (JJA) it was reached in CE and MD (above 0.58°C per decade). Although some of the winter trend in NE might be attributed to the well known positive NAO phase from the 1980's to the 1990's (Pinto and Raible, 2012) and for the summer trend to soil moisture deficit in CE and MD (Seneviratne et al., 2010), there is growing evidence that radiative forcing is *likely* the main contributor to such trends (Cattiaux et al., 2012). Furthermore climate models generally underestimate recent observed warming in the region (van Oldenborgh et al., 2009).

The precipitation trends in Europe (1970–2010) derived from GPCC data base present a large spatial variability albeit in average slight negative trends result in MD and positive in NE throughout the year while in CE there is a positive trend only in the warm half year. However most of these trends are not statistically significant, as commented in Chapter 2, Section 2.3.1.2.

Supporting AR4 conclusions, recent analyses of extreme events point to a *very likely* decreasing of the number of cold days and nights and an increase number of warm days and nights since 1950 in Europe (see Chapter 2). Heat waves can also be amplified by pre-existing dry soil conditions resulting from a precipitation deficit (Della-Marte et al., 2007; Vautard et al., 2007). This amplification of soil moisture-temperature feedbacks is suggested to have enhanced the duration of extreme summer heat waves in eastern MD during the latter part of the last Century (Hirschi et al., 2011).

Several studies for European countries indicate general increases in the intensity and frequency of extreme precipitation especially in winter during the last four decades however there are inconsistencies between studies, regions and seasons (Chapter 2).Extreme daily winter precipitation appears to have increased in NE and CE (Moberg and al., 2006; Zolina et al., 2008), albeit the trend in summer precipitation is weak or not spatially coherent (Bartholy and Pongracz, 2007; Pavan et al., 2008; Rodda et al., 2010), while uncertainties are larger in MD where there is a low confident in the trends (Chapter 2). A rather complete view on climate extremes over NE, CE and MD is presented in Seneviratne et al. (2012).

14.7.6.3 Model Quality GCMs and RCMs

There is encouraging evidence that since AR4 improved models, for example by increasing resolution, leads to improvements in the ability of models to simulate European climate. There are however, still significant differences between model simulations that prevent substantial uncertainty reduction (Woollings, 2010). The ability of climate models to simulate historical climate, its change, and its variability, has improved in many important respects since the AR4 (see Chapter 9). Particular examples relevant for Europe include: the large-scale circulation related modes, such as the NAO and blocking events, are better represented after the increasing of resolution in models (Marti et al., 2010); the improvements in the land surface and land-atmosphere coupling have led to a better representation of the soil-moisture impacts on temperature extremes in Europe (Hirschi et al., 2011) though some refinement is still needed; new coordinated RCM experiments and ensembles afforded an added value to coarser-resolution global model providing realistic spatial detail and improved representation of climate extremes (Christensen et al., 2010; Kjellstrom et al., 2011).

The errors and biases in global models are often related to smaller-scale features and higher-order statistics such as correlations and teleconnections while those in RCM mostly come from imperfections in boundary conditions (see Chapter 9). Therefore some systematic errors are still present to various degree like a tendency towards an enhanced warm bias in the warmer months of the year (Boberg and Christensen, 2012) or to underestimate precipitation trends (Christensen et al., 2008; van Haren et al., 2012). Nevertheless, climate models taken together provide realistic simulations of the large-scale features of the climate system but reproduce observed historical change with varying degree of fidelity over Europe and the Mediterranean (Lorenz and Jacob, 2010; van Oldenborgh et al., 2009).

14.7.6.4 Projected Changes and Uncertainties

The AR4 assessed that the projections at the time indicated that annual mean temperatures in Europe are likely to increase more than the global mean with the largest warming in NE in winter and in MD in summer (Christensen et al., 2007). The lowest winter temperatures in NE will likely increase more than the average, while maximum summer temperatures are likely to increase more than the average summer temperature in CE and MD. Annual precipitation is very likely to increase in NE and decrease in MD. Precipitation in CE will increase in winter but decrease in summer.

Recent studies have updated the assessment of the AR4 with more regional information for Europe based on analyses of multi-model ensembles of GCMs as well as RCMs or in combination. In general regional climate change amplitudes for temperature and precipitation follow the global warming amplitude (Kjellstrom et al., 2011), which confirms findings in AR4. Some new investigations have focused on the uncertainties associated with such projections. Based on a large ensemble of RCM-GCMs (Dequé et al., 2012) conclude that the temperature response is robust in spite of a considerable uncertainty related to choice of model combination (GCM/RCM) and sampling (natural variability), even for the near-future 2021-2050 time frame. For near future, based on an ensemble of CMIP3 21st century SRES A1B emission scenario simulations, Mariotti et al. (2008) show that the observed twentieth century precipitation decrease in the MD (Chapter 2) would be followed by a rapid drying from 2020 onwards. A recent investigation, also based on CMIP3 projections, suggests that in the MD “forced” changes are likely to become distinguishable from the “noise” created by internal decadal variations in decades beyond 2020–2030 (Giorgi and Bi, 2009). Hence, at least in the short term (roughly 10–30 years out), regional decadal anomalies and any potential for decadal predictability is likely to be critically dependant on the regional impacts of decadal modes of variability “internal” to the climate system. However, studies have also shown that NAO trends do not account for a large fraction of the future change in mean temperature or precipitation over Europe (Stephenson et al., 2006). Furthermore, since diverse modelling studies have clearly identified a possible amplification of temperature extremes by soil moisture state (Hirschi et al., 2011; Jaeger and Seneviratne, 2010), this mechanism could further magnifies the intensity and frequency of heat waves in the MR given the projected enhance of summer drying conditions in all of the global warming scenarios. Although there is a certain degree of inter-model consistency regarding MD temperature extremes, uncertainties need to be carefully evaluated. These include general evaluations of other forcing, such as land use change. In fact, land use change has been demonstrated to influence surface temperature extremes in a afforestation-deforestation study (Anav et al., 2010). Changes in land surface conditions may be as important or possibly more so in the summer season, as non-local phenomena affects in determining mean regional climate (Findell et al., 2009).

Recent assessment of projected changes in temperature and precipitation extremes generally confirmed AR4 (Seneviratne et al., 2012): The length, frequency, and/or intensity of warm spells or heat waves (defined with respect to present regional climate) were assessed to be *very likely* to increase over most Europe with the possible exception of Scandinavia. It is *very likely* that the frequency and intensity of winter precipitation will increase in the 21st century over NE and large part of CE but there is a notably inconsistency and low confidence over the MD since changes largely depend on region and model considered.

14.7.6.5 CMIP5 Model Projections

The projection for this century is further warming in all seasons and in the considered three sub-regions (NE, CE, MD) with median model temperature (°C) values increasing from (DJF: 1.7, 1.5, 1.1; JJA: 1.3, 1.5, 1.6) in RCP2.6 to (DJF: 6.1, 5.0, 3.9; JJA: 4.6, 5.6, 6.1) in RCP8.5. In RCP4.5, by the end of the century (2080–2099), based on the 25% and 75% percentiles the projected temperature (°C) change in DJF varies between (NE: 2.3 and 4.2; CE: 1.8 and 3.3; MD: 1.5 and 2.4) and in JJA between (NE: 1.6 and 3.1; CE: 2.1 and 3.4; MD: 2.5 and 3.6) (see Table 14.2, Figures AI.36–AI.37 and AI.40–AI.41, and the Supplementary Material for different time windows and four different RCPs).

The projection for this century shows some distinct sub-regional and seasonally dependent differences. In the winter half year (October to March), by the end of the century, NE and CE are projected to receive increased precipitation amounts with median model values increasing from 5% and 3% in RCP2.6 to 20% and 11% in RCP8.5, respectively, while MD will experience no change in RCP2.6 or a moderate reduction of –12% in RCP8.5 by the end of the century. The 25% and 75% percentile range for the end of century projection in RCP4.5 are for NE: 7% – 13%, CE: 3% – 12%, and ME: –8% – –1%, respectively. In the summer half year (April to September), the projected changes are relatively small for both NE and CE with a projected increase of 4% for both sub-regions in RCP2.6 to 7% and –9% in RCP8.5, but with a quite notable reduction in MD ranging from –2% in RCP2.6 to -25% in RCP8.5. The percentile ranges in RCP4.5 are for NE: 2% – 8%, CE: –8% – 5%, and ME: –18% – –6%, respectively (see Table 14.2, Figures AI.38–AI.39 and AI.42–AI.43, and the Supplementary Material for different time windows and four different RCPs).

In summary, since AR4 climate models appear to have improved fidelity in simulating aspects of large scale climate phenomena influencing regional climates over Europe and the Mediterranean. Multi-model experiments including CMIP5 still suffer from various limitations that challenge the interpretation of detailed regional changes. Model spread in projections of the future has not decreased substantially, which is partly a result of internal variability partly due to varying degrees of model deficiencies. When taking into account the limited role of climate phenomena in controlling changes in the mean, there is generally *high confidence* in models ability to project regional temperature changes, particularly for a specific climate scenario. It is therefore *virtually certain* that temperatures will show a positive trend throughout the century over all of Europe and the Mediterranean region and will be enhanced with the intensity of the anthropogenic radiative forcing. It is *very likely* that winter temperature will raise more in NE than in CE or MD sub-regions, while in summer the warming will be more intense in MD and CE than in NE. The length, frequency, and/or intensity of warm spells or heat waves are assessed to be *very likely* to increase throughout the region.

Projected precipitation changes show less clear signal given its characteristic high temporal variability, but there is *medium confidence* in an annual increase in NE and CE, while a decrease is *likely* in MD during the summer half year. It is *very likely* that the frequency and intensity of winter precipitation will increase in the 21st century over NE and CE but there is a notably inconsistency and *low confidence* over the MD since changes depend on region and model considered.

14.7.7 Africa

The African continent encompasses a variety of climatic zones. To the north of the Sahara desert, the Mediterranean coast experiences dry summers and receives its rain from mid-latitude systems during winter. In tropical latitudes, rainfall by and large follows insulation (although this simplified picture is modified by the presence of orography, especially in the Great Horn of Africa, the geography of the coastline, and by the influence of the oceans). Equatorial regions experience rainfall year round, with clear double peaks

corresponding to the equinoctial seasons, when the sun is overhead. Away from the equator, semi-arid regions receive rainfall only during the summer monsoon.

Sub-Saharan Sahelian climate is dominated by the monsoonal system that brings rainfall to the region during only one season and has been studied in detail during the last decade by the AMMA (African Monsoon Multidisciplinary Analysis) program (Polcher et al., 2011). This season, which goes from May/June to September, provides all the water needed by the region for the vegetation, agriculture and other human activities. The rainfall during these 4 months is brought by 10 to 20 systems of large extent and very strong intensity that travel from the horn of Africa to the Atlantic Ocean. The onset of the rainy season in West Africa is one of the key parameters as it triggers changes in the vegetation and surface properties. The length and frequency of dry spells is another of the critical parameters defining the quality of monsoon season. These parameters, as well as the length or cumulated rainfall of the season, are affected by a large inter-annual variability. (Janicot et al., 2011) As they are intimately linked to the large convective systems bringing the rainfall their variability needs to relate to the large scale conditions and local surface states which govern their life cycle. The droughts of the 20th century in West Africa, which were the largest and most intense observed (Chapter 2), were characterized by fewer convective systems but systems of the same intensity as during the wet years (LeBarbe and Lebel, 1997; Lebel and Ali, 2009; Lebel et al., 2010). It is particularly critical when evaluating the sensitivity of models to take into account their ability to reproduce these characteristics of the African Monsoon. A large effect of natural multi-decadal SST and global warming of the oceans on Sahel rainfall seems beyond doubt (Hoerling et al., 2006; Mohino et al., 2011; Rodriguez-Fonseca et al., 2011; Ting et al., 2009b; Ting et al., 2011).

East Africa experiences a semi-annual rainfall cycle, driven by the seasonal migration of the ITCZ across the equator. Two peaks in annual rainfall occur: the “long rains” during MAM and the “short rains” which peak during SOND (Black et al., 2003; Shongwe et al., 2011). The short rains exhibit greater interannual variability than the long rains (Black et al., 2003) and the drivers of this variability can be largely attributed to coupled interactions between ENSO, Indian Ocean SSTs and the atmospheric Walker circulation. Direct links between the region's rainfall and ENSO have been demonstrated (Giannini et al., 2008) and references therein), but variations in Indian Ocean SST have become more widely recognised as the dominant driver of east African rainfall variability (Marchant et al., 2007). Warmer (cooler) SSTs in the western tropical (south-eastern) Indian Ocean correspond to a positive phase of the Indian Ocean Dipole mode (IOD, Black et al., 2003; Marchant et al., 2007). This feature acts to enhance rainfall through either anomalous low-level easterly flow of moist air into the continent (Shongwe et al., 2011), or a weakening of the low-level westerly flow over the northern Indian Ocean that transports moisture away from the continent (Black et al., 2003). While the effect of the IOD is evident in the short rainy season, Shongwe et al. (2011) do not find a similar relationship for the long rains. (Williams and Funk, 2011), however, argue for a reduction in the long rains over Kenya and Ethiopia in response to warmer Indian Ocean SSTs, which cause an enhancement of the Walker circulation and increased subsidence over tropical east Africa.

Variability in Southern Africa's climate is strongly influenced by its adjacent oceans (Hansingo and Reason, 2008; Hansingo and Reason, 2009; Hermes and Reason, 2009; Rouault et al., 2003) as well as remote phenomena such as ENSO (Pohl et al., 2010; Vigaud et al., 2009). Although it is generally observed that El Niño events correspond to conditions of below-average rainfall over much of southern Africa (Giannini et al., 2008; Manatsa et al., 2008; Mason, 2001) the ENSO teleconnection is not linear, but rather has complex influence in which a number of regimes of local rainfall response can be identified (Fauchereau et al., 2009). In a dynamic sense, weakened westerly flow throughout the troposphere between 15º and 40º S and stronger tropical easterly flow up to a height of 500 hPa tend to enhance rainfall over southern Africa (Boulard et al.)

The extreme south-western parts of southern Africa receive rainfall in the winter months (JJA) brought by mid-latitude frontal systems, but the majority of the region experiences a single summer rainfall season occurring between November and April. A semi-permanent zone of sub-tropical convergence, the South Indian Convergence Zone (SICZ)—a southeast oriented rain band analogous to SPCZ and SACZ (see Section 14.3.1)—extends from the eastern parts of the continent to the south-western Indian Ocean and connects tropical easterly flow to baroclinic westerly flow in the mid-latitudes (Cook, 2000; Fauchereau et al., 2009; Vigaud et al., 2012). Within this zone, synoptic-scale Tropical-Temperate Troughs (TTTs) develop, which are major contributors to summer rainfall in sub-tropical southern Africa (Fauchereau et al., 2009; Vigaud et al., 2012). The development of these TTTs are controlled largely by the phasing of mid-

latitude waves and are also influenced by localized low-level moisture advection over the Agulhas current (Vigaud et al., 2012).

14.7.7.1 Model Quality GCMs and RCMs

Because of its exceptional magnitude and its clear link to global SST, 20th century decadal rainfall variability in the Sahel is a test of GCMs ability to produce realistic long-term changes in tropical precipitation. Despite substantial biases in the region (Cook and Vizy, 2006) the CMIP3 coupled models overall can capture the observed correlation between Sahel rainfall and basin-wide area averaged SST variability (Biasutti et al., 2008) even though individual models may fail, especially at interannual time-scales (Joly et al., 2007; Lau et al., 2006a). In response to centennial changes in the tropical Atlantic meridional gradient of SST and in Indo-Pacific SST, the CMIP3 ensemble produces a robust drying of the Sahel in simulations of the 20th century, leading (Biasutti and Giannini, 2006) to estimate that at least 30% of the 1930–1999 drying trend in the Sahel could be attributed to anthropogenic forcings. More recently, (Ackerley et al., 2011) used a perturbed physics ensemble and reached a similar estimate for the role of sulphate. These ensemble results confirm previous studies that had simulated drought in the Sahel in response to either just the indirect effect of sulphate aerosols (Rotstayn and Lohmann, 2002) or both historical aerosols and greenhouse gases (Held et al., 2005).

A challenge for quantifying the true role played by 20th century anthropogenic forcing in the Sahel drought is that the amplitude of simulated rainfall anomalies at all timescales is much smaller than observed (Scaife et al., 2009) Furthermore models are unable to reproduce the observation that the droughts were caused by fewer convective systems but with unchanged intensities. The inability of GCMs to produce the intense systems bringing most of the rainfall to the region is hypothesized for this limitation of the 20th century simulations (Ruti and Dell'Aquila, 2010). This suggests that some processes (for example, mesoscale organization of convection or feedbacks between climate, vegetation, and dust) and forcings (for example, aerosols produced by biomass burning, or land use changes) that are poorly represented or altogether missing in the CMIP3 generation of models might be critical for this region). Previous studies have identified West Africa as an area where the feedback between atmospheric and continental processes might be key in the rainfall generating systems (Koster et al., 2004) and the AMMA experiment showed that local soil moisture gradients are as important as topography for generating the convective systems which bring most of the rain to the region (Taylor et al., 2011a; Taylor et al., 2011b).

14.7.7.2 Projected Changes and Uncertainties

In projections of the 21st century, as the effect of anthropogenic aerosols fades and the effect of GHG becomes dominant, changes in annual mean Sahel rainfall become less certain: the CMIP3 models produced both significant drying and significant moistening (Biasutti and Giannini, 2006; Cook and Vizy, 2006; Held et al., 2005; Lau et al., 2006a), and the mechanisms by which a model dries or wets the Sahel are not fully understood (Cook, 2008). At least qualitatively, the CMIP3 ensemble simulates a more robust response during the pre-onset and the demise portion of the rainy season (Biasutti and Sobel, 2009; Seth et al., 2011). Rainfall is projected to decrease in the early phase of the seasons—implying a small delay in the main rainy season; but is projected to increase at the end of the season—implying an intensification of late-season rains (d'Orgeval et al., 2006). Projections of a change in the timing of the rains is common to other monsoon regions (Biasutti and Sobel, 2009; Li et al., 2006; Seth et al., 2011), including Southern Africa (Shongwe et al., 2009). Biasutti et al. (2008) have shown that simulated 21st century changes in Sahel rainfall cannot be linearly derived from changes in tropical SST indices in the same way as interannual variations or 20th century trends can. Different patterns of SST change might be responsible for the 21st century trend (some non-stationarity in the Sahel/SST relationship has been noted at interannual time scales (Seth et al., 2011; Mohino et al., 2011) but it is also evident that there is uncertainty in the direct response to GHGs (which affect precipitation independently of SST).

The relevance of a local effect is supported by several lines of evidence. First, since the AMMA experiment there is observational evidence that local soil moisture gradients can trigger convective systems and that these surface contrasts are as important as topography for generating these systems, which bring most of the rain to the region (Taylor et al., 2011a; Taylor et al., 2011b). The second evidence comes from simulations of future rainfall changes in West Africa by regional climate models (RCMs) subject to coupled model-

derived boundary conditions. (Patricola and Cook, 2010) choose one RCM and create an ensemble by running it with boundary conditions from nine different coupled models from the CMIP3 archive; in a complementary experiment Paeth et al., (2011) compare the projections of different RCMs driven by the same CGCMs. In both cases, the choice of RCM appears crucial: in (Patricola and Cook, 2010) using the same RCM reduces the spread in projections from that of the original CGCM simulations, in (Paeth et al., 2011) different RCMs fundamentally modify the trend seen in the driving CGCM simulation. This behaviour indicates that local processes internal to the RCM have enough influence to change the Sahel response to global forcings (Ibrahim et al., 2012). (Patricola and Cook, 2011) document a wetting response of the Sahel to increased GHG in the absence of other forcings, but the relative importance of this effect versus the response to SST trends is not well quantified, mostly due to the limitation of using a single RCM. Rowell (2011) compares a measure of the effect of modelling uncertainty in rainfall projections to the strength of the rainfall/SST relationship in two CGCM ensembles (CMIP3 and a perturbed physics ensemble) and concludes that while differences in the projected SST matter, considerable additional uncertainty arises from the varied modelling of the direct link between changes in atmospheric constituents and changes in precipitation. A second line of evidence comes from the analysis of changes in Sahel surface energy budgets in coupled model simulations. (Giannini, 2010) notes that radiation in different models, either terrestrial or solar radiation is his as the result of one of two dominant for surface warming, indicating the dominance of either local or remote forcings of rainfall. In the first case, anthropogenic greenhouse gases increase net terrestrial radiation at the surface, which both warms the land and increases evaporation, favouring low-level vertical instability, near-surface convergence, and increased precipitation (the terrestrial radiation input is amplified via water vapour feedback). In the second case, tropical SST warming acts as a source of free-troposphere moist static energy that increases upper level stability, decreasing rainfall and evaporation, and warming the surface through increased net solar radiation.

Analysis of a coupled model in which SST has little influence on Sahel rainfall has shown that warming by GHG enhances the development of the Sahara heat low and induces a stronger monsoon (Fontaine et al., 2010; Haarsma et al., 2005). To some degree, this mechanism is present in all CMIP3 models, but while the relationship between a stronger Sahara Low and a stronger monsoon is robust, the relationship between Saharan temperature and the strength of the Sahara Low is not (Biasutti et al., 2009; Chauvin et al., 2010) have shown that variability in the Sahara Low is linked to mid latitude dynamics.

Temperature projections are of course more robust than the precipitation projections, although the amount of warming depends in part on whether precipitation will decrease or increase (dryer land would permit less evaporation and lead to warmer surface temperatures). Battisti and Naylor (2009) show that in a middle-of-the-road the A1B scenario, the CMIP3 models indicate that by the end of the century, summer temperatures in the Sahel will be hotter than any in the historical data. Biasutti and Sobel (2009) suggest that the warming will be strongest in early summer, when rainfall anomalies are negative and (Patricola and Cook, 2010) combine temperature and humidity data to estimate (in the A2 scenario) that the Sahel will see 160 days a year with a high risk of heat stroke (heat index above 314 K).

It is not clear whether the CMIP3 projections for 2100 can be of guidance for climate change in the Sahel in the next few decades. One reason is the aforementioned large effect of natural variability, the other is the effect of projected land-use changes---which are not included in the CMIP3 integrations but, under the assumption of significant vegetation loss, might be a dominant cause of warming and drying in the near future (Paeth et al., 2009; Paeth and Thamm, 2007). Whether such an assumption is warranted is controversial (Larwanou and Saadou, 2011; Tougiani et al., 2009). Furthermore the coarse resolution of models used for the CMIP simulations as well as in current RCMs, do not allow to represent properly the rain generating systems in the Sahel and their interactions with the processes on the continents. For the moment only model running at a few kilometres resolutions could reproduce the atmospheric processes responsible for the life cycle of these convective systems (Kohler et al., 2010).

An evaluation of six GCMs over East Africa by Conway et al. (2007) reveals no clear multi-model trend in mean annual rainfall by the 2080s, but some indications of increased SON and decreased MAM rainfall are noted. They find inconsistency in how the models represent changes in the IOZM and consequent changes in rainfall over East Africa. (Shongwe et al., 2011) analyse a larger ensemble of 12 CMIP3 GCMs (forced with A1B emissions) for 4 homogeneous rainfall zones covering Tanzania, Kenya, Rwanda, Burundi and Uganda. They find widespread increases in short season (OND) rainfall across the region, with statistically significant

ensemble mean increases of 8–22% for all 4 zones. The ensemble mean magnitude of the 10-year driest OND season is shown to increase by 14% over Tanzania and 32% for western Kenya and northern Uganda, thus indicating a decrease in the severity of extremely dry years in the short rain season. For wet extremes, increases in ensemble mean magnitude of 10-year wettest OND of between 9% and 15% are shown across region. For the long rains (MAM), (Shongwe et al., 2011) find similar changes in the sign and magnitude of mean and extreme seasonal rainfall, but note that model skill in simulating the MAM season is relatively poor. The changes shown for the short rains are consistent with a differential warming of 21st century Indian Ocean SSTs, which leads to a positive IOD-like state. The atmospheric consequence of this is a weakening of the descending branch of the East African Walker cell and enhancement of low-level moisture convergence over east Africa (Shongwe et al., 2011; Vecchi and Soden, 2007b).

In an assessment of 19 CMIP3 models run with the A1B emissions forcing, (Giannini et al., 2008) note a tendency toward a persistent El Niño-like state in the equatorial Pacific along with a decrease in rainfall over southern Africa. Dynamical downscaling of a single GCM by (Engelbrecht et al., 2011) shows—for the austral winter—an intensification of the southern edge of the sub-tropical high pressure belt resulting in southward displacement of the mid-latitude systems that bring frontal rain to the south western parts of the continent, thus resulting in a 10–40% decrease in rainfall in that region. For the austral summer, (Engelbrecht et al., 2011) show a general drying over most of the region, with the exception of the western interior, which is linked to an intensification of the sub-tropical high pressure system at 500 hPa. The decrease in summer rainfall is consistent with high-resolution (18 km) RCM simulations done by (Haensler et al., 2011) which indicate widespread reductions in rainfall over Namibia and Botswana and much of Zimbabwe and the Republic of South Africa (RSA) under the A1B scenario. A strong regional temperature signal is evident over the central interior, with most of Botswana and north east Namibia experiencing warming of over 5ºC by the end of the 21st century (Haensler et al., 2011).

Shongwe et al. (2009) analyse an ensemble of 12 CMIP3 A1B model projections. They find consistent reduction in spring (SON) rainfall throughout the eastern parts of southern Africa, with multi-model mean decreases ranging from 10 to 35% across 5 sub-regions. There is good consensus amongst the 12 models, with the spring anomalies indicating a trend toward later onset of the summer rainy season. Autumn (MAM) reductions of 10-17% are shown for Zimbabwe, Botswana, southern and central Mozambique, southern Zambia and western RSA, while eastern RSA (including Lesotho and Swaziland) experiences no change and northern Zambia, Malawi and northern Mozambique show a 10% increase. Projections for summer (DJF) show little discernible change over most of the region, but there are some significant increases (4%) over northern Zambia, Malawi and northern Mozambique, and decreases (11%) over Botswana and western RSA. There are indications of a dipole pattern in DJF rainfall anomalies similar to an El Niño signal. Summer extreme events, here defined as the 10-year wettest and driest events, show some significant changes: 14% decrease in dry events for western RSA and Botswana, 5% increase in wet events for eastern RSA and 10% increase in wet events for northern Zambia, Malawi and northern Mozambique. In terms of regional atmospheric circulation, (Shongwe et al., 2009) highlight changes in vertically integrated moisture flux that show anomalous anticylonic circulation over much of south eastern Africa. This has two primary consequences: 1. a weakened influx of moisture from the Indian Ocean causing late onset of rains in southern Africa, and 2. increased moisture advection into East Africa along northern edge of South Indian Anticyclone.

14.7.7.3 CMIP5 Model Projections

The projection for this century is further warming in months of the year and in the considered four sub-regions (Sahara: SH, West Africa: WA, East Africa: EA, Southern Africa: SA) with median model temperature (°C) values increasing from (DJF: 1.2, 1.0, 0.9, 1.1; JJA: 1.3, 1.0, 1.0, 1.0) in RCP2.8 to (DJF: 4.4, 4.1, 4.1; JJA: 5.1, 3.9, 4.1, 4.6) in RCP8.5. In RCP4.5, by the end of the century (2080–2099), based on the 25% and 75% percentiles the projected temperature (°C) change in DJF varies between (SH: 1.8 and 2.6; WA: 1.7 and 2.6; EA: 1.6 and 2.4; SA: 1.7 and 2.7) and in JJA between (SH: 2.2 and 3.2; WA: 1.6 and 2.7; EA: 1.7 and 2.5; SA: 1.8 and 2.6) (see Table 14.2, Figures AI.40–AI.41, AI.44–AI.45, AI.48–AI.49 and the Supplementary Material for different time windows and four different RCPs).

The projection for this century shows some distinct sub-regional and seasonally dependent differences. In the half year (October to March), by the end of the century, all regions are projected to receive practically

unaltered precipitation amounts with median model values of 0% – 3% in RCP2.6 but with more clear changes in RCP8.5, SH: –4%; WA: 7%; EA: 16% and SA: –5%, respectively. The 25% and 75% percentile range for the end of century projection in RCP4.5 are for SH: –15% – 8%, WA: 1% – 6%, EA: 0% – 11%; SA: –6% – 1%, respectively. In the half year (April to September), the projected changes are relatively small for both SH and EA with a projected increase of less than 3% for both sub-regions in RCP2.6 but 10% and 5% in RCP8.5, but with a quite notable reduction in SA ranging from –9% in RCP2.6 to –17% in RCP8.5. WA is projected to have an increase of 9% in RCP2.8, but only 3% in RCP8.5. The percentile ranges in RCP4.5 are for SH: -17% – 14%, WA: 0% – 4%, EA: -5% – 5%; SA: –15% – 4%, respectively (see Table 14.2, Figures AI.42–AI.43, AI.46–AI.47, AI.50–AI.51 and the Supplementary Material for different time windows and four different RCPs). This suggest that only the reduction in SA is a robust multi-model result, while almost all other changes are either small or with a large inter-model spread (e.g., SH in April to September).

In summary, due to the physical understanding of the processes involved and models ability to capture large scale climate evolution, there is *high confidence* that it is *virtually certain* that all of Africa will continue to warm during the 21st century. Sahara already very dry is *very likely* to remain dry. Because of models overall inability to capture the physical processes of the monsoonal rain in West Africa and a large full model spread in the projections, there is *low confidence* in projection statements about drying or wetting of West Africa. There is *medium confidence* in projections with *likely* little change in mean precipitation in East Africa, while Southern Africa is *likely* to receive reduced precipitation in the Austral winter. There is a *high confidence* of a *likely* increase in rainfall for the East African short rainy season, but *low confidence* in projections regarding drying or wetting in the long rainy season. There is *medium confidence* of a *likely* decrease in spring and summer rainfall over much of Southern Africa.

14.7.8 Central and North Asia

Observational temperature records indicate that some of the strongest warming trends during winter (>2°C per 50 years) in the second half of the 20th century are found in the northern Asian sector (40°N–70°N 50°E–140°E). The warming trend was particularly strong in the cold season (November to March), with an increase of 2.4°C in the mid-latitude semi-arid area of Asia (20°N–60°N, 60°E–180°E, where the annual rainfall is within the range of 200–600 mm) over the period of 1901–2009 (Huang et al., 2012). The variability and long-term change of the climate system in the central Asia and northern Asia are closely related to variations of the NAO and NAM (Takaya and Nakamura, 2005; Knutson et al., 2006; Popova and Shmakin, 2010; Sung et al., 2010). For instance, the recent warming over northern Asia may partly be attributed to the prominent positive trend of the AO index during the 1980s and early 1990s. Hence model simulations that do not take the natural variability of the AO/NAO/NAM into account are not expected to replicate the full extent of the observed warming in northern Asia. The climate change in this region is likely the consequence of both anthropogenic and natural causes. The observed pattern of precipitation trends is less spatially homogeneous, and exhibits both wet and dry tendencies in various locations within this region. The observations indicate some increasing trends of heavy precipitation events in northern Asia, but no spatially coherent trends in central Asia (Seneviratne et al., 2012).

The model projections presented in AR4 indicated strong warming in northern Asia during winter and in central Asia during summer. Precipitation was projected to increase throughout the year in northern Asia with largest fractional increase during winter. For central Asia, a majority of the models contributing to AR4 project decreased precipitation during spring and summer. A high resolution model projected a significant increase of extreme precipitation events in central and northern Asia (Kamiguchi et al., 2006). The model projections assessed in Seneviratne et al. (2012) also indicate increases in all precipitation extreme indices for northern Asia, and in the 20-year return value of annual maximum daily precipitation for central Asia. These projections are supported by output from CMIP5 models subject to various RCP scenarios (see Annex I).

A climate change 'hot spots' analysis was conducted by (Xu et al., 2009) on the basis of regional temperature and precipitation indices, as computed using output from 14 CMIP3 simulations under the SRES B1, A1B and A2 scenarios. Their results reveal that hot spots firstly emerge in northwestern China and Mongolia. The northeastern China hot spot is evident in the middle of the 21st century and become the most prominent area by the end of the century. These investigators also noted that hot spots should emerge in the Tibetan Plateau

and northwestern China even in the lowest scenario B1. (Sato et al., 2007) applied two types of dynamical downscaling methods with a RCM. Both method yield precipitation decreases over northern Mongolia and increases over southern Mongolia in July. Soil moisture over Mongolia also decreases in July as a result of the combined effect of decreased precipitation and increased potential evaporation due to rising surface temperature. This drying trend of the land surface would lead to more frequent severe droughts in this region.

Projected temperature increase in Central Asia (30°N–50°N, 60°E–75°E) is larger in JJA than in DJF. The CMIP5 model median values are 2.7°C in DJF and 3.0°C in JJA in RCP4.5 scenario. In North Asia (50°N–70°N, 40°E–180°E), temperature increases more in DJF than in JJA. The CMIP5 model median values are 3.9°C in DJF and 2.7°C in JJA in RCP4.5 scenario. There are large scatter among models in projected values in North Asia. For example, DJF temperature change in RCP4.5 varies between 2.7°C at 25%-ile and 5.0°C at 75%-ile (see Table 14.2, Figures AI.12–AI.13 and the Supplementary Material for different time windows and four different RCPs).

All models projected an increase in precipitation in winter half year in North Asia, where summer half year precipitation will also very likely increase. In Central Asia, model agreement is very less both in winter and summer precipitation changes.

In summary, a stronger warming trend is projected for northern Asia during winter. For central Asia, warming magnitude is similar between winter and summer. Precipitation in northern Asia will very likely increase, whereas the precipitation trend over central Asia is less certain. Extreme precipitation events will likely increase in both regions.

14.7.9 East Asia

The East Asian summer climate and its variability are associated with water vapour flux along the periphery of the western North Pacific subtropical high (Bonin High) (Zhou and Yu, 2005). The intensity and pole ward extension of the Bonin High is positively correlated with convective activity around the Philippines (Pacific-Japan or PJ pattern) (Kosaka and Nakamura, 2010). The latter is related to tropical cyclone (typhoon) activity. ENSO affects the subtropical high through modulation of convection in the western tropical Pacific (Wang et al., 2000; Wang and Zhang, 2002). The Meiyu-Changma-Baiu rain band appears in early summer season from eastern China through western and central Japan (Ding and Chan, 2005; Zhou et al., 2009c). There is a tight collocation between the rain band and mid-tropospheric warm advection by the SW-NE oriented subtropical jet (Sampe and Xie, 2010). The wintertime circulation is characterized by monsoonal northerlies between the Siberian High and the Aleutian Low.

CMIP3 multi-model ensemble scenario projections of future climate indicate an increased summertime rainfall over eastern Asia due to enhanced moisture convergence under the warmer climate. CMIP3 models reveal an increase of precipitation intensity over almost all regions of East Asia at the end of the 21st century (Chen et al., 2011b; Ding et al., 2007; Kusunoki and Arakawa, 2012; Sun and Ding, 2010). CMIP3 models also project an intensification of East Asian summer monsoon rainfall interannual variability in the twenty-first century (Lu and Fu, 2010). Projection of future (2011-2050) climate change along the Yangtze River of China (Xu et al., 2010) found that the mean precipitation would increase under the SRES A1B and B1 scenarios but decrease under the A2 scenario (Tao et al., 2011) Analysis of effective drought index simulated by 15 CMIP3 models found that South Asia and East Asia showed a greater increase in the standard deviation of precipitation than the mean precipitation, with an amplified seasonal precipitation cycle. This amplified seasonal precipitation cycle suggests future drought as well as flood under global warming scenario (Kim and Byun, 2009). By statistical downscaling, the annual number of rain days in Hong Kong is expected to decrease while the daily rainfall intensity will increase in the 21st century, concurrent with the expected increase in annual rainfall (Tsz-cheung et al., 2011). CMIP3 models show no clear information about the change of the rain amount around the tropical Pacific Ocean (Ninomiya, 2012). The rain amount around the mid to the eastern Pacific will increase through the weakening of the Walker circulation (HIROTA and TAKAYABU, 2012). But the change of SLP around the northern Pacific region shows large uncertainty among the models (OSHIMA et al., 2012). The CMIP5 projections suggest a likely increase of summer precipitation over the entire East Asia in the last 20 years of 21st century under both RCP4.5 and RCP8.5 scenarios (Figure 14.34). For precipitation changes, all CMIP5 models projected an increase in the

summer half year, while 90% of models projected an increase in the winter half year (see Figures AI.56–AI.59 and the Supplementary Material for different time windows and four different RCPs).

[INSERT FIGURE 14.34 HERE]

Figure 14.34: June to August precipitation anomalies over East Asia. RCP4.5 (left column) and RCP8.5 (right column) simulations (2080–2099) relative to historical simulation (1980–1999) by 15 CMIP5 model ensembles are shown in 10th, 50th and 90th percentile.

The surface air temperature over East Asia is projected to increase substantially by the end of the twenty-first century under the SRES A1B scenario, with larger magnitude over northern China and in winter (Chen et al., 2011a). The CMIP5 projections suggest temperature increase in Eastern Asia (0°–50°N, 100°E–145°E) similar in magnitude to that averaged over land grid points over the globe, and is similar between winter and summer, with CMIP5 model median value being 2.6°C in DJF and 2.5°C in JJA in RCP4.5 scenario in 2100. Unusually cold and cloudy summers over northeastern Japan are associated with northeasterly winds blowing from the North Pacific (‘Yamase’ in Japanese). Most of the CMIP3 AO-GCMs project increases of the Yamase frequency in August in future, for which a weakening of mean tropical circulation, including the Walker circulation, is considered to be responsible (Endo, 2012).

Over the Far East region, wintertime storm track activity shows peculiar characteristics, such as midwinter suppression (Nakamura, 1992). In late winter through early spring, events of strong southerlies occur over Japan associated with synoptic cyclones developing to the north. The first of such events is called "Haru-Ichiban", the first storm of the spring. Reanalysis data shows that its early occurrence tends to follow the enhanced winter storm-track activity with less apparent minimum in midwinter, and vice versa, in the course of the seasonal march. (Nishii et al., 2009) indicates that the future enhancement is likely in the midwinter storm-track activity associated with the weakening of the East Asian winter monsoon, implying that Haru-Ichiban is likely to occur earlier in the late 21st century than that in the 20th century.

The CMIP3 models project an increase of both mean and extreme precipitation over eastern China associated with a warmer climate (Li et al., 2011a; Li et al., 2011b), the change of precipitation intensity projected by a global 40-km mesh AGCM is larger than that of CMIP3 models (Feng et al., 2011a). A combination of a warming projection experiment with a 20-km mesh AGCM and ensemble simulations with the 60-km resolution model is utilized by Kusunoki et al. (2011) to assess the East Asian summer rainfall changes. In the future climate simulation by the 20-km model, precipitation increases over the Yangtze River valley (Meiyu) in May through July, Korean peninsula (Changma) in May, and Japan (Baiu) in July. Simulations by the 20-km and 60-km models consistently show that in the future climate the termination of rainy season over Japan tends to be delayed until August (Kusunoki and Mizuta, 2008). This is in accord with the CMIP3 multi-model analysis by Kitoh and Uchiyama (2006), who suggested that the El Niño-like SST response in the future tropical Pacific and associated circulation changes are responsible for these late withdrawal of Baiu. Endo (2010) noted a similar observed tendency of delayed Baiu withdrawal from the 109 years station data in eastern and western Japan.

Regional climate model simulations show mean temperature increases similar to those simulated by AOGCM, and daily maximum and minimum temperatures are very likely to increase, resulting more severe warm but less severe cold extremes; For precipitation, regional climate model simulations show the Meiyu-Changma-Baiu rainfall increases over the Yangtze River valley, the East China Sea and western Japan, and the intense precipitation events are very likely to increase (Christensen et al., 2007).

RCM simulations in China in the recent years (Gao et al., 2012a; Gao et al., 2008; Gao et al., 2012b) further proved the importance of model resolution in better reproducing the present climate over the area. The simulated warming patterns in the future by RCM essentially follow those of the driving GCMs. The pattern of precipitation changes simulated by RCM are also consistent with those by the GCMs during cold season except the more regional detail as provided by the RCM. However large differences exist in the monsoon seasons. While a predominant increase of monsoon precipitation is found in most CMIP3 and CMIP5 models (see Chapter 12), the RCM usually shows extended areas of decrease (Gao et al., 2012a; Gao et al., 2008). The inconsistent change of precipitation between GCM and RCM is found in the dynamical downscaling of near future (2015–2045) projection under RCP8.5 scenario with a RCM over CORDEX East Asia domain (Zou et al., 2012). The difference is mostly caused by the stronger and more realistic topographic forcing and

the resulting circulation changes in the RCM. In addition, comparison of precipitation changes simulated by one RCM driven by different GCMs show similar signal in western China but different signal in eastern China, indicating the large uncertainties in the projection there (Gao et al., 2012b). Kawase et al. (2009) showed an increase in precipitation over the Baiu rain band and a southward shift of the Baiu rain band. The surface air temperature increases rapidly around the high latitude continental region than the low latitude maritime region during 2090–2100 under A2 scenario, and the precipitation around the Eastern China increases large in summer but decrease in winter, following to the change of the synoptic climate condition (Liu et al., 2011b). The annual and winter mean wind speeds over China are projected to decrease based on two RCMs that downscale two different GCMs under A2/B2/B1 scenario (Jiang et al., 2010) .

The results of multi RCM down-scaling, indicate that the summer rainfall around Japan Islands are projected to increase through the end of this century (IIZUMI et al., 2012b). Iizumi et al. (2012a) showed that both the CDD (maximum numbers of consecutive dry days) and 90th percentile value of daily precipitation amount in wet days) increase till the end of 21st century around Japan Islands area. The future projection is downscaled around three main metropolitan areas in Japan (Tokyo, Nagoya, and Osaka) (Kusaka et al., 2012).Their results indicate that in all three metropolitan areas, in 2070's, the mean summer temperature will be the same as the record breaking hot summer in 2010. The local climate around Vietnam during 2000-2050 has been downscaled (Ngo-Duc et al., 2012). Their results indicate large surface mean temperature increases in summer season, and large precipitation increases around the coastal of the middle Vietnam region. Both the strength and the frequency of the extreme precipitation increase around the south to the middle Vietnam's coastal region. By using one RCM downscaling, there are many researches discussing the future regional climate change projection around Korean Peninsula under SRES B2 scenario (Im et al., 2011) A1B scenario (Im et al., 2011; Murakami et al., 2012). The change in seasonal precipitation has large uncertainty depending on scenarios, RCMs and the inclusion of air-sea coupling processes (Qian et al., 2012; Suxiang and Yaocun, 2010; Zou and Zhou, 2011; Zou and Zhou, 2012). The extreme value of the three hourly or 24 hourly precipitation is projected to increase till the end of this century (Im et al., 2008; Murakami et al., 2012).

The regional 30-year return period of daily precipitation in the region is likely to increase by 7%-29% in southern part of Japan in the late 21stcentury (Ishihara, 2010). There is a significant increase for mean, daily-maximum and minimum temperature in the southeast China, associated with a decrease in the number of frost days and an increase in the heat wave duration, precipitation extremes are also projected to increase over most of southeast China in all seasons (Chen et al., 2011b). The projection of extreme climate in China by CMIP3 models show that both frost days and annual extreme temperature range show decreasing trends, while growing season length, heat wave duration and warm nights show increasing trends. The increases are especially manifested in the Tibetan Plateau and in Southwest China. For extreme precipitation indices, the end of the twenty-first century is expected to have more frequent and more intense extreme precipitation (Jiang et al., 2011). A 20-km mesh AGCM shows that heavy precipitation increases notably in Bangladesh, the Yangtze River basin (Kamiguchi et al., (2006) and East Asia (Kusunoki and Mizuta, 2008) due to intensified convergence of water vapour flux in summer at the end of the 21st century.

Future projections of heavy precipitation were performed with a 5-km mesh regional climate model for the Japanese summer rainy season (Kitoh et al., 2009). They showed the frequency of heavy precipitation increasing in the future for hourly as well as daily precipitation. In particular, the heaviest hourly precipitation is projected to increase even in the near future (2030s) when temperature increase is modest. A southwest extension of the subtropical anticyclone over the northwestern Pacific Ocean associated with El Niño-like mean state changes and a dry air intrusion at the mid-troposphere from the Asian continent to the northwest Japan gives a favourable condition for intense precipitation in the Baiu season in Japan (Kanada et al., 2010). Increase of water vapour supply from the southern side of the Baiu front and an intensified frontal zone with intense mean updrafts contribute to the projected increase in the occurrence of intense daily precipitation during the late Baiu season (Kanada et al., 2012). Future changes in this region depend on changes in the tropical Pacific, i.e., whether precipitation shifts eastward (El Niño-like) or not, and thus models' ability to reproduce the relationship among SST, convection and circulation changes in the tropics. Extremely high summertime daily minimum or maximum temperatures are projected to occur over some regions at leeside of mountains over Japan in the late 21stcentury (Murata et al., 2012). They show that the Foehn phenomenon explain this extreme temperature events in addition to background temperature increases.

14.7.9.1 CMIP5 Model Projections

The projection for this century is further warming in all months of the year with median model temperature (°C) values over land increasing from 1.4 and 1.2 in DJF and JJA, respectively in RCP2.8 to 5.4 and 4.9 in RCP8.5. In RCP4.5, by the end of the century (2080-2099), based on the 25% and 75% percentiles the projected temperature (°C) change in DJF varies between 2.1 and 3.1 and in JJA between 1.8 and 3.0 (see Table 14.2, Figures AI.60–AI.61 and the Supplementary Material for different time windows and four different RCPs).

In the two half years (October to March and April to September), by the end of the century, the region is projected to receive weakly enhanced precipitation amounts with median model values of 7% and 5% in RCP2.6 increasing to 13% and 11% in RCP8.5. The 25% and 75% percentile range for the end of century projection in RCP4.5 are 6% – 16% in (October to March). In the half year (April to September), the projected changes are 5% – 12% (see Table 14.2, Figures AI.62–AI.63 and the Supplementary Material for different time windows and four different RCPs). This suggests that the region is likely to receive an increase in total precipitation amounts associated with the monsoon season but also more generally throughout the year.

In summary, it is very likely that temperatures will increase by the end of the century, more in summer than in winter, related to a decrease in soil moisture, and that there will be a decrease in precipitation, mainly in winter, since there is very little precipitation in summer under present-day conditions. As a consequence, it is likely that there will be more pronounced drought periods. There is medium confidence, that an increase of East Asian summer monsoon intensity throughout the 21st century and of summer precipitation over the whole of East Asia is likely. Precipitation increase is likely over the Yangtze River Valley, Korean peninsula and Japan during the Meiyu-Changma-Baiu season in May to July. Precipitation extremes are very likely to increase over most of southeastern China in all seasons, and over Japan in summer. There is high confidence that surface air temperature over East Asia virtually certain will increase significantly by the end of the 21st century, with larger magnitude over northern China and in winter.

14.7.10 West and South Asia

This region extends from just to the east of the Mediterranean along southern Asia to the Southeast Asia peninsula, approximately from Iraq in the west to Myanmar in the east, and includes both the Arabian Peninsula and the Indian subcontinent. The region spans a wide range of climates, from arid and semi-arid areas in the western part of the domain, which receive their limited (but societal-critical) precipitation primarily in the cold season and include large areas of barren desert, to areas which receive their precipitation primarily in the summer from the Indian monsoon, and record some of the heaviest rainfall totals anywhere in the world. The northernmost part of South Asia is characterized by a variety of climatic conditions from tropical to alpine, and the central and eastern parts receive 60–90% of the annual precipitation during summer monsoon.

Broadly, the western part of the region is on the margin of Atlantic and Mediterranean influences, primarily the NAO (Section 14.5.1), and the entire region is influenced by Indian and Pacific Ocean variability, especially the IOD (Section 14.3.3.3), ENSO (Section 14.4), and the MJO (Section 14.3.2). The Indian summer monsoon exhibits variability across a wide spectrum of time scales and is discussed in Section 14.2.2.1. The winter precipitation and hydrology in the West Asia are influenced by the NAO (e.g., Cullen and deMenocal, 2000; Cullen et al., 2002), the North African–West Asia pattern (Paz et al., 2003) and the North Sea – Caspian pattern (Kutiel and Benaroch, 2002), and also the hemisphere-spanning circumglobal teleconnection (Feldstein and Dayan, 2008). Through moisture transport (Barlow and Tippett, 2008; Evans and Smith, 2006) and vertical motion (Hoell et al., 2012) the cold season precipitation and hydrology variability in the western part are influenced by ENSO. The MJO modulates the sub-seasonal rainfall during the cold season (Barlow, 2011). During summer, the west and northwestern part are also influenced by ISM variability through large-scale descent (Saini et al., 2011). Occasionally, tropical cyclones makes landfall on the coasts of the Arabian Sea. During the last 5-6 decades, the unprecedented increase in anthropogenic forcing may be attributed to changes in rainfall and temperature over this region.

14.7.10.1 Observed Trends in Mean and Extremes of Temperature and Precipitation

During northern summer (June through September), the ISM dominates the climate over Southern Asia while the winter or northeast monsoon contributes to annual rainfall over southeastern parts of India and Sri Lanka. The winter weather systems are also important in northern parts of South Asian region i.e., Hindukush Himalayas (particularly over the western Himalaya). The ISM rainfall index shows interdecadal variability on which a declining tendency with more frequent and stronger deficit monsoons (Kulkarni, 2012), particularly after about 1960 is noticeable (Figure 14.35). The significance of this weakening in all-India index is rather masked by regional inhomogeneity (Annamalai et al., 2012; Bollasina et al., 2011; Konwar et al., 2012), and amplitude inconsistency over the entire country (Jain et al., 2012) while various land-based precipitation products suggest a significant decline over central India or along the monsoon trough (Annamalai et al., 2012; Bollasina et al., 2011). Various factors are attributed to this recent weakening tendency (Section 14.2.2) including black carbon and/or sulphate aerosols (Bollasina et al., 2011; Chung and Ramanathan, 2007), land-use changes (Niyogi et al., 2010) and SST rise over the Indo-Pacific warm pool (Annamalai et al., 2012). Long-term tendencies in seasonal mean rainfall in other regions indicate for an increasing tendency over northern Pakistan (Farooq and Khan, 2004), decreasing tendency (~10–15%) over the coastal belt and hyper arid plains of northwestern parts of Pakistan, weakening tendency over the West Asia (AlSarmi and Washington, 2011; Tanarhte et al., 2012), no detectable signal over northern parts of South Asia (Shrestha, 2005), increasing trend in winter and decreasing trend in summer over southern parts of South Asia (Chandrapala, 1996), and decadal anomalies dominating over long-term trends since 1960s over Bangladesh (Mirza, 2002). The factors responsible for the tendencies noted in regional rainfall are rather unclear, and statistical significance of the tendencies is low, perhaps masked by interdecadal variations.

[INSERT FIGURE 14.35 HERE]

Figure 14.35: Inter-annual variability of Indian summer monsoon rainfall (1871–2011). The smooth curve is the 11-year moving average filtered series which shows epochal variability. The fitted trend lines are also shown : green (entire period) and red (post 1950s). The dotted lines depict ±10% departures from long-term mean. X-axis denotes years and Y-axis the percentage departures from long-term mean.

At sub-seasonal timescales over India, observations during the last 5–6 decades suggest for an increase in the number of monsoon break days (Dash et al., 2009), and a decline in the number of monsoon depressions (Krishnamurthy and Ajayamohan, 2010) that are consistent with overall weakening tendency of seasonal mean rainfall. Statistics of extreme (Goswami et al., 2006) and heavy precipitation events are increasing (Krishnamurthy et al., 2009; Pattanaik and Rajeevan, 2010; Rajeevan et al., 2008; Sen Roy, 2009) while light rain events are decreasing (Goswami et al., 2006). Over the West Asia too, extreme events appear to be increasing (Alpert et al., 2002; Yosef et al., 2009). In a warmer world, enhanced atmospheric moisture content is expected to influence the occurrence of extreme and heavy rainfall events but lack of sustained three dimensional moisture observations over South Asia precludes any firm attributions.

The sub-seasonal variability on monthly to daily time scale has also shown some changes in recent period. The contribution of monsoon ISOs to seasonal rainfall appears to be decreasing in post 1970 period (Goswami et al., 2006; Kulkarni et al., 2009). The predictability on weather scales is also shown to have reduced in recent warmer period (Mani et al., 2009) due to increased potential instability of the atmosphere.

Consistent with declining tendency in regional rainfall observed temperatures indicate robust warming that is particularly accelerated in post-1970 period. Over India, during 1971–2007, large areas of the country showed significant warming trend of about 0.2°C per decade (Kothawale et al., 2010) that may be associated with anthropogenic influence (e.g., Jain et al., 2012; Kumar et al., 2011a). In the adjoining Arabian Sea, the increase in tropical cyclones is linked with local SST warming (Kumar et al., 2009); see also discussion of tropical cyclones in Box 14.2. Observed temperature records in other regions also indicate for warming tendencies. Quantitatively, an increase of about 0.04°C–0.09^{o}C per year during winter over Himalaya, about 1°C in May and 0.5°C rise over Bangladesh during 1985–1998, and 0.016°C per year rise over Sri Lanka during 1961–1990 have been noted. Over the West Asia, upward temperature trends are notable and robust (Alpert et al., 2008; AlSarmi and Washington, 2011; Tanarhte et al., 2012; Zhang et al., 2005).

Considering the entire region, during recent 5-6 decades robust signatures in temperature rise is observed while due to its localized nature and other physical processes involved rainfall changes vary across sub-regions, although there is a general weakening tendency in many sub-regions.

14.7.10.2 Projected Changes and Uncertainties

At regional scales, while systematic errors noted in the simulation of seasonal mean rainfall over the monsoon regions in CMIP3 models such as dry bias over continent India and weakened low-level circulation are also apparent in CMIP5 models (Sperber et al., 2012), certain robust features are noticeable across models' projections in the time-mean rainfall with uncertainties in magnitude. Over the Indian monsoon region, CMIP3 models (Annamalai et al., 2007; Kumar et al., 2011a; May, 2011; Turner and Annamalai, 2012; Turner et al., 2007a; Ueda et al., 2006)) as well as CMIP5 models (Wang et al., 2012b) simulate increased "time-mean" rainfall over parts of India but weakened cross-equatorial monsoon circulation (Kripalani et al., 2007b; Sabade et al., 2011; Stowasser et al., 2009). While intermodal spreads in intensity are model or scenario dependent (Annamalai et al., 2007; Kumar et al., 2011a; Sabade et al., 2011) or due to dynamical feedbacks, the general agreements in the "sign" support the expected changes due to thermodynamic effect in a warmer climate (Held and Soden, 2006). The changes in the regional circulation may be a part of the changes to global circulation (Vecchi and Soden, 2007b) or due to changes in regional distribution of rainfall (Stowasser et al., 2009). Elsewhere in the region, CMIP3 models project rainfall increase over northern parts of South Asia, Bangladesh, Sri Lanka but decrease over Pakistan (Turner and Annamalai, 2012). Under A2 scenario, ensemble of six GCMs show that around mid of the 21st century seasonal rainfall over Northern (Southern) Pakistan may increase by 2.7% (41.3%). while it is 2% (52%) at the end of the century. Under B2 scenario, precipitation during the monsoon season over Bangladesh may increase by 4% in 2030s to 11% in 2080s. The CMIP5 models' projections are generally in agreement with those from CMIP3 models (Chaturvedi et al., 2012; Wang et al., 2012b).

Further quantification at regional scales can be obtained through dynamical downscaling wherein regional climate models (RCMs) are driven with lateral and surface boundary conditions from global models. Apart from uncertainties in the driving fields from global models, the imbalances in physical parameterizations between RCMs and global models are expected to introduce further uncertainties in regional model projections (Wang et al., 2008; Stowasser et al., 2009). Very high-resolution projections indicate for increase rainfall over plains of India (Kumar et al., 2011b; Rajendran and Kitoh, 2008; Stowasser et al., 2009) reduction in rainfall along the orographic regions of Southern and eastern India are noted (Rajendran and Kitoh, 2008) and even over southern Peninsular parts of India (Kumar et al., 2011b). An exception to the above projections is suppression of the ISM precipitation in one particular regional model (Ashfaq et al., 2009). Over Nepal, GCMs project a wide range of precipitation changes, especially during the monsoon: from a decrease of 14% to an increase of 40% by the 2030s and from a decrease of 52% to an increase of 135% by the 2090s. For the West Asia, recent downscaling results (Dai, 2011; Evans, 2009; Jin et al., 2011; Lionello et al., 2008) suggest that Eastern Mediterranean will experience a decrease in precipitation during the rainy season due to a northward displacement of the storm tracks. A northward shift in the ITCZ results in more precipitation in the southern part. Based on model analysis, about 25% reduction in winter precipitation and an increase of drought duration by up to 60% are expected based on the A1B scenario (Kim and Byun, 2009). These authors also predict a northward expansion of the Arabian Desert and an increase of autumn precipitation over the Fertile Crescent by up to 50%. Some projections suggest that the Fertile Crescent may dry up by the end of the century (Kitoh et al., 2008). While precipitation is generally projected to decrease in the future, the large number of interacting dynamical influences on the precipitation of the region, which models have difficulty accurately capturing even in the current climate, results in considerable uncertainty in both the patterns and magnitude of future precipitation change.

At sub-seasonal time scales, future projections in certain models suggest that both active and break events will become wetter and drier respectively, heaviest rainfall events will increase potentially beyond those predicted by thermodynamic arguments alone (Turner and Slingo, 2009), break episodes will become more intense (Mandke et al., 2007) while others have shown inconsistencies even between different scenarios for a given model. This suggests that attention must be paid to the level of skill at which a model can simulate monsoon intraseasonal variability that are typically poorly represented in climate models (Lin et al., 2008b; Sperber and Annamalai, 2008), while CMIP5 models appear to represent them more realistically (Sperber et al., 2012). Even from best reanalysis products, large uncertainties or residuals exist in the identified

processes involved in prolonged monsoon breaks (Prasanna and Annamalai, 2012) posing a challenge for modeling the monsoon ISOs in climate models.

The AR4 concluded that it was *very likely* that heavy precipitation events, that is, the frequency of heavy precipitation or proportion of total precipitation from heavy precipitation, would increase over most areas of the globe. The projections in number of rainy days are highly uncertain however based on the simple argument that enhanced moisture content will result in higher intensity rainfall events (Kumar et al., 2011a; Revadekar et al., 2011). In RCP6.0 and RCP8.5 scenarios in CMIP5 models, frequency of extreme precipitation days shows consistent increasing trends for decades 2060 and beyond (Chaturvedi et al., 2012). The quantitative estimates still have large uncertainties associated with them due to limited number of high-resolution model simulations available at this stage. However, it is unknown whether the extreme rainfall events in GCMs are caused by monsoon depressions, because even in the 'reasonable' models these depressions do not penetrate far enough inland from their genesis over the Bay of Bengal (Stowasser et al., 2009). Our lack of understanding and modeling the relevant processes make projections of sub-seasonal variability such as prolonged breaks and extreme rainfall events hugely uncertain in the future (Turner and Annamalai, 2012). For the West Asia, precipitation statistics for an area consisting of the western part of the Arab Peninsula indicated statistically significant decrease in the number of rainy days, both following a dry or a wet day, and a general decrease of winter rainfall (Black, 2009). Future projections of synoptic systems such as monsoon depressions during summer, and tropical cyclones during late spring and fall-winter seasons have large uncertainties, perhaps due to coarse-resolution in GCMs. While high-resolution simulations suggest for intense storms to be more intense, lack of consensus among the simulations preclude any definitive assessment. Bangladesh and coastal regions of southern India are vulnerable to tropical storms.

Regarding temperature projections while all scenarios and models indicate for a warming tendency in the entire region, particularly the nighttime and winter season temperature, uncertainties in amplitude still exist. Quantitatively, A1B scenario simulations in CMIP3 models project a median increase of 3.3°C in annual mean temperature by the end of the 21st century over India, with particular seasonal dependency, 2.7°C in summer to 3.6°C in winter (Ashrit et al., 2003; Douville et al., 2000; Lal and Harasawa, 2001; Lal et al., 2001; May, 2004; Rupa Kumar and Ashrit, 2001; Rupa Kumar et al., 2002), and in the diurnal time scale, warmer nights than days (Kumar et al., 2011b). Additionally, the northern parts of India may experience maximum warming at the end of the 21st century (Kulkarni et al., 2012). In both RCP6.5 and RCP8.5 scenarios, CMIP5 models project temperature rise by 3.3°C to 5°C over India (Chaturvedi et al., 2012). Over the West Asia, analysis from GCMs (Christensen et al., 2007) and RCM experiments (Onol and Semazzi, 2009) for A1B scenario project a rise of 2°C, temperatures in winter and up to 6°C in inland regions in summer. GCM projections indicate that the temperature over Nepal will increase between 0.5°C and 2.0°C with a multi-model mean of 1.4°C, by the 2030s and between 3.0°C and 6.3°C, with a multi-model mean of 4.7°C, by the 2090s. Additionally, extremely hot days and nights (the hottest 5% of days and nights in the period from 1970 to 1999) are projected to increase by up to 55% by the 2060s and up to 70% by the 2090s, and by up to 77% by the 2060s and 93% by the 2090s, respectively. Over Bangladesh and under B2 scenario, annual temperature is projected to be warmer by 1°C in 2030s to 2.4°C in 2080s (Agrawala et al., 2003). Future climate projections indicate that at least 5°C rise in temperature over the Indus Delta by the end of 21st century (Rasul et al., 2012). Over northwestern parts of South Asia, under A2 scenario, ensemble of six GCMs show that around mid of the 21st century the temperature would rise by 2.7 (2.5) °C in Northern (Southern) Pakistan, while it is 5 (4.3) °C at the end of the century.

14.7.10.3 CMIP5 Model Projections

The projection for this century is further warming in all months of the year and in the considered two sub-regions (West Asia: WAS and South Asia: SAS) with median model temperature (°C) values increasing from (DJF: 1.4 and 1.2; JJA: 1.4, 1.0) in RCP2.8 to (DJF: 4.6 and 4.7; JJA: 5.5 and 3.7) in RCP8.5. In RCP4.5, by the end of the century (2080–2099), based on the 25% and 75% percentiles the projected temperature (°C) change in DJF varies between (WAS: 1.9 and 2.9; SAS: 2.1 and 3.0) and in JJA between (WAS: 2.1 and 3.4; SAS: 1.4 and 2.4) (see Table 14.2, Figures AI.52–AI.53 and AI.60–AI.61, and the Supplementary Material for different time windows and four different RCPs).

The projection for this century shows some clear sub-regional differences. In the half year (October to March), by the end of the century, both regions are projected to receive weakly enhanced precipitation amounts with median model values of 3% – 5% in RCP2.6 but with more clear changes in RCP8.5, WAS: 5%; SAS: 12%, respectively. The 25% and 75% percentile range for the end of century projection in RCP4.5 is for WAS: –3% – 12%, SAS: –1% – 14%, respectively. In the other half-year (April to September), the projected changes are quite similar in both sub-regions in RCP2.6 with 3% and 6% respectively, but -6% and 17% in RCP8.5. The percentile ranges in RCP4.5 are for WAS: -8% – 5%, SAS: 7% – 14%, respectively (see Table 14.2, Figures AI.54–AI.55 and AI.62–AI.63, and the Supplementary Material for different time windows and four different RCPs). This suggest that only the reduction in SA is a robust multi-model result, while almost all other changes are either small or with a large inter-model spread (e.g., SH in April to September).

In summary, there is *high confidence* in assessment of temperature projections. It is *virtually certain* that temperatures will increase in both sub-regions. Projected regional rainfall changes are broadly consistent with physical arguments "wet gets wetter and dry becomes drier". However, large uncertainties in the projected amplitude changes make the assessment difficult. There is *low to medium confidence* in quantitative assessment of precipitation changes, but it is *likely* that West Asia will receive less precipitation in the April to September half year and South Asia will receive more than at present.

14.7.11 Southeast Asia

14.7.11.1 General Characterization of Observed Temperature and Rainfall Trend

Southeast Asia features complex terrain and land-water contrasts, and consists of two geographic regions: a mainland section consisting of Myanmar, Cambodia, Laos, Thailand, Vietnam and Peninsular Malaysia, and a maritime section consisting of Brunei, East Malaysia, East Timor, Indonesia, the Philippines, and Singapore. Mean temperature for the region has been increasing at a rate of 0.135°C to 0.2°C per decade since 1960s (Tangang et al., 2007), and the increase in mean temperatures is mainly manifested in a rising number of hot days and warm nights, and a decline in cooler weather (Caesar et al., 2011; Manton et al., 2001). There are no consistent rainfall trends across the region, but the number of rain days (with at least 2 mm of rain) has decreased significantly in many countries (Manton et al., 2001), yet the proportion of annual rainfall contributed by extreme events has increased at a majority of stations (Caesar et al., 2011). Consistently, there has been a significant shift in the probability distribution functions of tropical rainfall, featuring a positive trend in the occurrence of heavy (top 10% by rain amount) and light (bottom 5%) rain events and a negative trend in moderate (25–75%) rain events (Lau and Wu, 2007). Annual total wet-day rainfall over the region has increased by 21.61 mm per decade, while rainfall from the extreme rain days has increased by 9.84 mm per decade (Caesar et al., 2011). In general, there are no significant trends in the intensity of the wettest rainfall events averaged across the region (Manton et al., 2001).

14.7.11.2 Regional Differences and Seasonality

These general trends do not preclude strong regional differences. For example, there have been no significant trends in the extreme rainfall frequency and intensity in Indonesia (Manton et al., 2001), but there has been an increased ratio of rainfall between the wet and dry season (Aldrian and Djamil, 2008). In Vietnam, Laos, Northeast Thailand and Peninsular Malaysia, an increasing frequency of extreme events has been reported, in contrast to Myanmar, where there has been a decreasing trend of such events (Chang, 2011).

For a given region, strong seasonality in the change is observed. One good example is Peninsular Malay. There, during the southwest monsoon season, there is a declining trend in total rainfall and in the frequency of wet days, leading to an increase in rainfall intensity in most of the sub-regions (Deni et al., 2010). In contrast, a trend of significantly increasing total rainfall and an increase in frequencies of extreme rainfall events during the northeast monsoon caused a significantly increasing trend in rainfall intensity over the Peninsula to be observed. However, no significant trend was observed with respect to extreme intensity during both monsoons over the Peninsula, although the intensity of extreme rainfall events displays no trend (Suhaila et al., 2010). Consistently, an increasing frequency of Borneo Vortices is observed (Juneng and Tangang, 2010), conducive to extreme rainfall events (Juneng et al., 2007).

Regions like Vietnam, Laos, Northeast Thailand and Peninsular Malaysia have shown an increasing trend in the frequency of extreme event, while places like archipelago Southeast Asia and Myanmar have shown a decreasing trend (Chang, 2011). For the period between 1979 and 2003, the total accumulated precipitation for the maritime continent region has increased (Lau and Wu, 2007). Further, Lau and Wu (2007) reported that the extreme high (top 10%) and low (bottom 5%) precipitation events are occurring more often than before. During the same period, moderate precipitation events have reduced (Lau and Wu, 2007). The same study also proposed that there is increase in amounts and frequency of high precipitation experienced over the Inter-tropical Convergence Zone, the Indian Ocean and monsoon regions during the 1980s and 1990s (Chang, 2011; Lau and Wu, 2007). For the Western Pacific (East Java region in Indonesia), precipitation data from 1955 to 2005 indicated that there has been an increased ratio of precipitation between the wet and dry season and the signal of monsoon strength weakening (Aldrian and Djamil, 2008). Amounts of heavy rain and their frequency of occurrence were found to be on the rise since the early 1980s in the cores of deep convection in the ITCZ, SPCZ, the Indian Ocean, and monsoon regions, but were found to be reduced over the maritime continent. Intermediate rains reduced over the warm pool regions and the ITCZ and SPCZ adjacent regions, but enhanced over the maritime continent (Lau and Wu, 2007).

Among many previous studies, Alexander et al. (2006) provided the latest, most comprehensive analysis regarding global-scale changes in extreme climate events through combining results obtained by many regional meetings on extreme climates (Choi et al., 2009a). A preliminary investigation of the relationship between the extremes indices and SST indicates that the interannual variability of temperature extremes may be related to local SSTs. However, the inter-annual variability of the regional series also seems to indicate that the peaks in the frequency of 'warm extremes' may coincide with large El Nino events (Caesar et al., 2011) Annual total wet-day precipitation of the Southeast Asia has increase by 21.61 mm per decade, while the extreme rain days has increase by 9.84 mm per decade. There is significant increase of warm night and significant decrease of cool day over the Southeast Asia (Caesar et al., 2011).

14.7.11.3 Climate Projections

Because of complex terrain and land-water contrasts, the low-resolution of CGCMs (typically at a scale of 200–500 km), renders that their simulation of the regional climate is poor for variables that depend highly on regional topography such as rainfall and temperature. Dynamical downscaling using regional climate models is an essential tool for filling the gap between CGCM projections and regional applications (Giorgi et al., 2004). A recent dynamical downscaling experiment at a 60-km horizontal resolution using a host CGCM under the SRES A1B emissions scenario was carried out to project changes for the region from 1990–1999 to 2045–2054 (Chotamonsak et al., 2011). The result shows a warming that varies from 0.1°C to 3°C depending on the location and season. Large changes in maximum temperature (1.0°C–1.5°C) are simulated over Cambodia, Southern Vietnam, and southern Thailand, whereas slight warming (<0.5°C) is simulated in elevated areas such as northern Myanmar and southern China. There is a greater warming at night-time than daytime for all seasons, with a decreasing diurnal temperature range. Rainfall is projected to increase averaged across the region, with local decreases in the dry season, but the spatial pattern of changes largely follows that based on outputs from CGCMs (Meehl et al., 2007a). The rainfall projection is less reliable given that the general lack of consensus commonly seen in a multi-model ensemble, and that, in the present case, it is based on one simulation forced by outputs from a host model. Further, this is a region where many CGCMs are notoriously poor at simulating the present-day climatology and the large biases inevitably carry over to the regional model. Other downscaling experiments (Nguyen et al., 2012) show that with the biases corrected, projected rainfall changes in many places could be opposite in direction to that of the host model (see discussion in Section 14.2.2.4).

14.7.11.4 CMIP5 Model Projections

The projection for this century is further warming in all months of the year with median model temperature (°C) values over land increasing from 0.8 in both DJF and JJA in RCP2.8 to 3.2 and 3.3 in RCP8.5 in DJF and JJA, respectively. In RCP4.5, by the end of the century (2080–2099), based on the 25% and 75% percentiles the projected temperature (°C) change in DJF varies between 1.5 and 2.2 and in JJA between 1.4 and 2.2 (see Table 14.2, Figures AI.64–AI.65 and the Supplementary Material for different time windows and four different RCPs).

In the half year (October to March), by the end of the century, the region is projected to receive weakly enhanced precipitation amounts with median model values of 3% in RCP2.6 increasing to 9% in RCP8.5. The 25% and 75% percentile range for the end of century projection in RCP4.5 are 4% – 10%. In the half year (April to September), the projected changes are almost identical (see Table 14.2, Figures AI.66–AI.67 and the Supplementary Material for different time windows and four different RCPs). This suggests that the region will receive a moderate increase in total precipitation amounts associated within the monsoon season.

In summary, there is high confidence that warming is very likely to continue through this century. It is likely that the warming will show substantial sub-regional differences. It is very likely that there will be a greater warming at night-time than daytime for all seasons. It is very likely that the rising temperatures will continue to be manifested in a rising number of hot days and warm nights, and a decline in cooler weather. There is medium confidence that rainfall is likely to increase averaged across the region, but the direction of change has strong geographical variations.

14.7.12 Australia and New Zealand

The climate of Australia is a mix of tropical and extra-tropical influences. Northern Australia lies in the tropics and is strongly affected by the Australian monsoon circulation, the IOD, the MJO and ENSO. Southern Australia extends into the extra-tropical westerly circulation and is also affected by the middle latitude storm track, the SAM, and mid-latitude transient wave propagation. Since New Zealand lies in the middle latitudes, its climate is most strongly affected by the mid-latitude storm track and the SAM. However, New Zealand climate is also significantly affected by the ENSO cycle.

Eastern Australian rainfall is strongly modulated by the ENSO cycle, with La Niña years typically associated with wet conditions and El Niño years with drier than normal conditions in the eastern half of the country, most notably in spring (McBride and Nicholls, 1983). The SAM also plays a significant role in modulating southern Australian rainfall, with the positive SAM associated with generally above-normal rainfall during summer (Hendon et al., 2007; Thompson et al., 2011).

On seasonal to decadal timescales, New Zealand precipitation is modulated by the SAM (Kidston et al., 2009; Thompson et al., 2011), ENSO (Kidson and Renwick, 2002; Ummenhofer and England, 2007), and the IPO (Griffiths, 2007; Salinger et al., 2001) Increased westerly flow across New Zealand, associated with negative SAM and with El Niño events, leads in western regions to increased rainfall and generally lower than normal temperatures. The positive SAM and La Niña conditions are generally associated with increased rainfall in the north and east of the country, and warmer than normal conditions.

Significant trends have been observed in Australian precipitation over recent decades, varying widely between seasons. Especially prominent is a decline in austral winter rainfall in Southwest Western Australia (SWWA; Cai and Cowan, 2006; IOCI, 2001) and autumn to winter rainfall over Southeast Australia (SEA; Murphy and Timbal, 2008). Since the 1970s, a decrease of about 20% has occurred in autumn and early-winter rainfall, associated with an even bigger (~40%) drop in stream inflow into dams. The rainfall decline in SWWA has been linked to changes in large-scale mean SLP (IOCI, 2001), shifts in synoptic systems (Hope et al., 2006), reduction in extreme wet conditions (Li et al., 2005), changes in baroclinicity (Frederiksen and Frederiksen, 2007), the SAM (Cai and Cowan, 2006; Hendon et al., 2007; Meneghini et al., 2007), natural multidecadal variability (Cai et al., 2005), land cover changes (Timbal and Arblaster, 2006), and anthropogenic forcing (Timbal et al., 2006). England et al. (2006) suggested that recent IOD-related warming trends across the eastern Indian Ocean basin bias the SST distribution to a pattern that corresponds to anomalous dry conditions for SWWA.

Recent drought in SEA has been accompanied by sustained long-term declines in precipitation across southern regions of Australia, with the majority of the decrease over SEA occurring during late austral autumn (Murphy and Timbal, 2008). The decrease has been associated with ENSO variability and long-term Indian Ocean warming (Cai and Cowan, 2008a). Other related factors include the pole ward shift of the storm track associated with the positive SAM trend, and expansion of the subtropical dry zone and pressure rises over Australia (Cai and Cowan, 2012; Hope et al., 2010; Murphy and Timbal, 2008; Nicholls, 2010). For winter and spring, Ummenhofer et al. (2009a) and Cai et al. (2009a) have related recent and historical droughts over SEA with trends and variability in the IOD.

It is without doubt that recent higher air temperatures have exacerbated the drought situation over SEA, in addition to substantial rainfall deficits. Nicholls (2004) found that both the mean maximum and minimum temperatures in the latest drought period are higher than in previous droughts due to continued continental-scale warming since the mid-20th century, almost certainly caused by increased greenhouse gas concentrations (Karoly and Braganza, 2005). Cai and Cowan (2008b) reported a 15% reduction in annual inflow into the MDB associated with a 1°C rise in temperatures.

Ummenhofer et al. (2009b) found the drying trend since 1979 across much of New Zealand during austral summer to be consistent with recent trends in the SAM and to a lesser extent to ENSO. A trend towards increased heavy rainfall in western regions and drying in the east has been linked to an increase in westerly winds over New Zealand (Griffiths, 2007). The increasing westerlies are related largely to ENSO and IPO variability since the mid-20th century.

Temperatures over New Zealand have risen by just under 1°C over the past century (Dean and Stott, 2009). The upward trend has been modulated by an increase in the frequency of cool southerly wind flows over the country since the 1950s. Once the southerly trend is taken account of, the warming observed over New Zealand is consistent with large-scale anthropogenic forcing (Dean and Stott 2009).

CMIP5-era climate models generally simulate the climate of Australia well (Watterson et al., 2012), in terms of the annual mean temperature and rainfall distribution, and show an improvement on CMIP3-era model simulations. Since ENSO has a strong effect on Australian climate, deficiencies in model simulation of ENSO (see Chapter 9) will have an impact on the simulation of interannual variability in Australian climate. Climate model simulations under enhanced greenhouse forcing project further reductions in rainfall over much of the country (Hope, 2006).

For New Zealand, future climate projections suggest further increases in the westerlies in winter and spring, though model biases in jet latitude in the present climate reduce confidence in the detail of future projections (Barnes et al., 2010). In summer and autumn, the increased frequency of the positive SAM, and the influence of pole ward expansion of the subtropical high pressure belt, is projected to lead to drier conditions in many parts of the country, and a decrease in westerly wind strength in northern regions. Such projections imply increased seasonality of rainfall in many parts of the country (Reisinger et al., 2010). Both flood and drought risk is projected to approximately double over New Zealand during the 21st century, under the SRES A1B scenario. Temperatures are projected to rise at about 70% of the global rate, because of the buffering effect of the oceans around New Zealand. The median (from a range of SRES emissions scenarios and global models) increase in mean temperatures over New Zealand is expected to be around 2°C, compared to the late 20th century, for a global mean warming of around 3°C. Temperature rises are projected to be smallest in spring (SON) while the season of greatest warming varies by region around the country. Continued decreases in frost frequency, and increases in the frequency of high temperature extremes, are expected, but have not been quantified. Sea level rise is projected to continue at close to the global rate, as has been observed over the past century (Reisinger et al., 2010).

14.7.12.1 CMIP5 Model Projections

The projection for this century is further warming in all months of the year and in the considered two sub-regions (North Australia: NAU and South Australia/New Zealand: SANZ) with median model temperature (°C) values increasing from (DJF: 1.2 and 1.1; JJA: 1.0 and 0.8) in RCP2.8 to (DJF: 4.1 and 4.0; JJA: 4.5 and 3.4) in RCP8.5. In RCP4.5, by the end of the century (2080–2099), based on the 25% and 75% percentiles the projected temperature (°C) change in DJF varies between (NAU: 1.7 and 2.7; SANZ: 1.6 and 2.4) and in JJA between (NAU: 1.7 and 2.6; SANZ: 1.3 and 1.8) (see Table 14.2, Figures AI.68–AI.69 and the Supplementary Material for different time windows and four different RCPs).

The projection for this century shows some clear sub-regional differences. In the half year (October to March), by the end of the century, both regions are projected to receive weakly reduced precipitation amounts with median model values of about –5% in RCP2.6 and with basically no changes in RCP8.5. The 25% and 75% percentile range for the end of century projection in RCP4.5 is for NAU: –6% – 4%, SANZ: –7% – 2%, respectively. In the other half-year (April to September), the projected changes is a reduction in

NAU in RCP2.6 with –5% and no change in SANZ, but –13% and –8% in RCP8.5. The percentile ranges in RCP4.5 are for NAU: –20% – 3%, SANZ: –9% – 2%, respectively (see Table 14.2, Figures AI.70–AI.71 and the Supplementary Material for different time windows and four different RCPs). This suggests that only the reductions in April to September are relatively robust multi-model results, while the other changes are insignificant.

In summary, based on analysis of observed trends, and simulations of future climate change from CMIP5 models, it is likely that cool season precipitation will continue to decrease over southern Australia (Cai et al., 2011a; Cai et al., 2011c; Shi et al., 2008b) associated with trends in the SAM and the IOD. Decreases on the order of 10% are projected for southern Australia by the end of the century, under RCP4.5. Associated with this, dry spells are likely to become more persistent over southern Australia (IPCC, 2012). Moreover, it is very likely that the Australian continent will continue to warm through the 21st century, at a rate similar to the global land-surface mean. Temperature rises of between 3°C and 4°C are projected for central and northern Australia by late-century, with slightly less warming in the south of the country (RCP4.5). The frequency of very warm days is virtually certain to increase through this century, across the whole country. For an arid to semi-arid country such as Australia, this will put further stress on already strained water resources.

Based on downscaled CMIP3 model results and global-scale CMIP5 model output, it is very likely that temperatures will continue to rise over New Zealand, at somewhat less than the global rate through the 21st century. Precipitation is likely to increase in western regions in winter and spring, but the magnitude of change is likely to remain comparable to that of natural climate variability through the rest of the century (on the order of 10%, RCP4.5). In summer and autumn, it is as likely as not that precipitation amounts will change.

14.7.13 Pacific Islands Region

In addition to the impact from ENSO, there are several important processes that influence climate in the Pacific countries (see Figure 14.36, taken from Hennessy et al., 2011). A key component of the regional climate is the South Pacific Convergence Zone (SPCZ, Section 14.3.1). Fluctuations in the position of the SPCZ are a major cause of seasonal changes in rainfall, winds and tropical cyclone risk in Solomon Islands, Tuvalu, Vanuatu, Fiji, Tonga, Samoa, Niue and the Cook Islands, and in some years Nauru and Kiribati. The ITCZ (Section 14.3.1) affects the rainfall climate of Palau, Federated States of Micronesia (FSM), Marshall Islands, and in some years Papua New Guinea, Nauru and Kiribati. Rainfall totals in the ITCZ region (defined here as 160°E–120°W, 0°–15°N) peak in September to November at values around 50% higher than those of the (late) southern summer, January to March.

The West Pacific Monsoon (WPM) is the eastern edge of the broader Australian-Asian Monsoon system that moves from the Northern Hemisphere across the equator into the tropical regions of the Southern Hemisphere during austral summer months (Section 14.2.2). The WPM extends into the transition region of both the SPCZ and the ITCZ and can be characterised by the seasonal reversal of the prevailing winds (Kim et al., 2008; Smith et al., 2012). In the Northern Hemisphere, a seasonal wind reversal is experienced in Palau and parts of the FSM, and in some years as far east as the Marshall Islands. Other countries affected include Papua New Guinea, Solomon Islands, and on the outer edges, Tuvalu and Vanuatu. The peak monsoonal rain in both hemispheres decreases during El Niño.

[INSERT FIGURE 14.36 HERE]

Figure 14.36: Locations of the Pacific Climate Change Science Program (PCCSP) partner countries (all of which are labelled) and the dominant features of the regional climate in the western Pacific Ocean. Grey dashed lines indicate the boundary of the 'PCCSP region' used in much of the analysis, and orange arrows indicate the dominant wind flows. This is taken from the BoM-CSIRO Report (2011).

Climate in the northwestern tropical Pacific (Marshall Islands, Palau, and the FSM) is mainly influenced by the ITCZ and the WPM (Smith et al., 2012). The main rainfall months are June to August for Palau, and May to November for the Marshall Island and the FSM when both the ITCZ (September to November) and the WPM (June to August) bring heavy rainfall. ENSO has a strong influence through an impact on the Pacific warm pool, the WPM and the ITCZ. El Niño events typically bring very dry conditions to this region (Brown

et al., 2012; Cai et al., 2009b). During El Niño, the WPM extends to the western FSM and the associated rainfall increase offsets a rainfall reduction induced by an equatorward shift of the ITCZ, resulting in a net rainfall increase in the wet season for the western states (Smith et al., 2012). During La Niña, the FSM experiences above-average numbers of tropical cyclones, similar to the situation in northern Australia (Lavender and Walsh, 2011; Nicholls et al., 1998). The WPM rarely extends to the Marshall Islands. During El Niño, as the ITCZ moves to the equator, rainfall decreases, often resulting in droughts four to six months after an El Niño event (Philander, 1990). More intense cyclones tend to occur during El Niño as ocean water to the east is anomalously warm (Hennessy et al., 2011).

Climate in the near-equatorial countries of Papua New Guinea (PNG), Nauru and Kiribati is affected by a combination of the ITCZ, the SPCZ and the WPM. Most of the rainfall in PNG comes from the WPM but is also influenced by the SPCZ (Smith et al., 2012), with higher-than normal rainfall typical during La Niña (Brown et al., 2012). Southern PNG experiences tropical cyclones, which tend to occur more during the neutral phase of ENSO (Kuleshov et al., 2010a; Kuleshov et al., 2010b). Nauru's wet season is affected by the SPCZ and ITCZ, which sit to the south and north of the country, respectively. Being close to the Equator, Nauru does not experience tropical cyclones (Kuleshov et al., 2010a; Kuleshov et al., 2010b) but does experience droughts during La Niña as the SPCZ and ITCZ move to the west (Brown et al., 2012). Climate in Kiribati is similarly influenced by the SPCZ and the ITCZ, and drought can be very severe during La Niña.

The seasonal evolution of the SPCZ has a strong influence on the seasonality of the climate of the southern tropical Pacific (Cook Islands, Fiji, Niue, Samoa, Tonga, Tuvalu, Vanuatu, Solomon Islands) , particularly during the austral summer wet season (Vincent, 1994). The SPCZ moves a few degrees northward during moderate El Niño events and southward during La Niña events (Folland et al., 2002; Vincent et al., 2011). During El Niño events, most of the southwest Pacific Island nations (listed above) experience forest fires and droughts (Kumar et al., 2006; Salinger et al., 2001), as well as an increased probability of tropical cyclone damage, because tropical cyclogenesis tends to reside within 6°–10° south of the SPCZ (Vincent et al., 2011). The reverse is generally true during La Niña. During strong El Niño events (e.g., 1982/1983, 1997/1998) the SPCZ undergoes an extreme swing of up to 10 degrees towards the equator and collapses to a more zonally-oriented structure (Vincent et al., 2011, Section 14.3.2). The impacts from these zonal SPCZ events are much more severe than those from moderate El Niño events (Cai et al., 2012; Vincent et al., 2011), and can include massive droughts and food shortages (Barnett, 2011).

The Cook Islands span a large latitudinal range, and ENSO has an opposite effect on the Northern to that on the Southern Group: in Rarotonga (in the south), El Niño events tend to bring drier conditions than normal, while in Penrhyn (in the north), El Niño usually brings wetter conditions (Brown et al., 2012). In Vanuatu, El Niño tends to reduce rainfall as the SPCZ moves eastward and northward, but once a threshold position is passed, further El Niño development has no influence. As such, there is no linkage between tropical cyclones affecting the country and El Niño (Basher and Zheng, 1995), similar to the situation in northeast Australia Cai et al. (2010). The number of tropical cyclones passing within 400 km of Port Vila (Vanuatu) has decreased markedly since mid-1985 - the only country where a strong trend is observed (Hennessy et al., 2011).

Analyses of data recorded by the respective national meteorological services show that temperatures generally increased throughout the Pacific Islands during the 20th century (Folland et al., 2003). Changes in temperature extremes have tended to follow those of mean temperatures, with most stations showing an increase in the occurrence of hot days and warm nights, and a decline in the number of milder days and cooler nights over the last four decades of the 20th century (Griffiths et al., 2005; Manton et al., 2001). During 1961–2000, locations to the north-east of the SPCZ became wetter, with the largest trends occurring in the eastern Pacific Ocean (east of 160°W), while locations to the south-west of the SPCZ became drier (Griffiths et al., 2003), indicative of a northeast shift of the SPCZ. Trends in the frequency of rain days were generally similar to those of total annual rainfall (Griffiths et al., 2003; Manton et al., 2001). Since 1980, WPM and ITCZ-related rain during June to August has decreased (Hennessy et al., 2011).

Since 1950, maximum temperatures have increased at a rate of around 0.1°C per decade at most sites in Palau the FSM, and the A decreasing rainfall trend is observed in Kwajalein of the Marshall Islands and in

Pohnpei of the FSM. It is not clear to what extent these decreasing rainfall trends are associated with a change in the ITCZ and/or the WPM (Smith et al., 2012).

Since 1950, annual maximum and minimum temperatures have also increased at around 0.1°C per decade in Port Moresby (PNG), and at the higher rate of 0.15°C–0.25°C per decade in Nauru, and 0.2°C per decade in Kiribati. There are no clear trends in annual or seasonal rainfall in Port Moresby or Nauru, but a well-defined increasing trend is seen in annual and wet season Kiribati rainfall. The rainfall increase in Kiribati is consistent with a SPCZ moving eastwards (Griffiths et al., 2003). There is no clear trend detected in the number of tropical cyclones for Southern Papua New Guinea (Kuleshov et al., 2010b).

Farther south, average temperatures have increased by up to 0.2°C per decade. In most countries, there are no clear trends in annual or seasonal rainfall, except in Vanuatu and Nuku'alofa of Tonga, where wet season rainfall has decreased slightly, in contrast to Penrhyn (of the Northern Cook Islands) where annual rainfall has increased. These trends are consistent with a rainfall reduction within the SPCZ and a slight northeast shift of the SPCZ (Griffiths et al., 2003). There is no clear trend in the number of tropical cyclones passing within 400 km of Tonga, Samoa and Cook Island, but a small reduction in Tuvalu, Fuji, Niue, and the Solomon Islands (Kuleshov et al., 2010a; Kuleshov et al., 2010b). However, in Vanuatu, a significant reduction in the number of tropical cyclones is observed (Hennessy et al., 2011).

Future projections for te tropical Pacific Island nations are based on direct outputs from a suite of CMIP3 models, updated using CMIP5 wherever available (Brown et al., 2011; Hennessy et al., 2011; Irving et al., 2011; Moise and Delage, 2011; Perkins, 2011; Perkins et al., 2012). These projections below carry a large uncertainty, even in the direction of change. A major source of the uncertainty is discussed below.

Annual average air and sea surface temperature are projected to continue to increase for all tropical Pacific countries.. By 2055, under a high emissions scenario (A2), the increase is projected to be 1°C–2°C. A rise in the number of hot days and warm nights is also projected, and a decline in cooler weather, as already observed (Manton et al., 2001). For a low emission scenario, the lower range decreases about 0.5ºC while the upper range reduces by between 0.2°C and 0.5°C.

In northwestern and near-equatorial regions, rainfall during the wet and dry seasons is projected to increase over the course of the 21st century. Wet season increases are consistent with the expected intensification of the West Pacific Monsoon and the ITCZ (Smith et al., 2012). For the southwestern tropical Pacific, the CMIP3 and CMIP5 ensemble mean change in summer rainfall is far smaller than the inter-model trend range (Brown et al., 2012b; Widlanski and al., 2012). Based on direct outputs of CMIP5, there is a projected intensification in the western part of the SPCZ and near the equator with little mean change in the SPCZ position (Brown et al., 2012a; Brown et al., 2012b). For the Southern Group of the Cook Islands, the Solomon Islands, and Tuvalu, average rainfall during the wet season is projected to increase; and for Vanuatu, Tonga, Samoa, Niue, Fiji, a decrease in dry season is accompanied by an increase in the wet season, indicating an intensified seasonal cycle.

Model projections show extreme rainfall days are likely to occur more often in all regions (Perkins, 2011). Droughts are projected to become less frequent in many areas, although there is little consensus between models for PNG and the southwestern states. Tropical cyclone frequency is projected to decrease in most affected regions by the late 21st century, with a regional mix of decreasing or increasing proportions of more intense storms (Chattopadhyay and Abbs, 2012) (Walsh et al., 2012b).

To a large extent, the response of the ITCZ, the SPCZ, and the WPM to greenhouse warming will determine how climate will change in tropical Pacific. The above projections are based on an intensification of the ITCZ and the SPCZ. Although the intensification appears to be reproduced in CMIP5 models (Brown et al., 2012a), it has recently been questioned (Widlanski and al., 2012) (see Section 14.3.1). There are two competing mechanisms, the "wet regions getting wetter" and the "warmest getting wetter, or coldest getting dryer" paradigm. These two mechanisms compete within much of the SPCZ region. Based on a multi-model ensemble of 55 greenhouse warming experiments, in which model biases are corrected, tropical SST changes between 2°C–3^{o}C resulted in a 5% decrease of austral summer moisture convergence in the current SPCZ region (Widlanski and al., 2012). This projects a diminished rainy season for most Southwest Pacific island nations. In Samoa and other neighbour islands, for example, summer rainfall may decrease on average by

10–20% during the 21st century as simulated by the hierarchy of bias-corrected atmospheric model experiments. Less rainfall, combined with increasing surface temperatures and enhanced potential evaporation, could increase the chance for longer-term droughts in the region. Such projections are completely opposite to those based on direct model outputs.

[INSERT FIGURE 14.37 HERE]

Figure 14.37: Multi-model mean change in November to April rainfall (mm day^{-1}) in global climate models (left) and CCAM 60 km simulations (right), each consisting of the same six models, for the 30-year period centred on 2055, relative to a 30-year period centred on 1990, using the A2 (high) emissions scenario.

Recent downscaling experiments support the above conclusion regarding the impact of biases on the SPCZ change, and suggest that the projected intensification of the ITCZ may have uncertainty of a similar nature (Chapter 7, Hennessy et al., 2011). In these experiments a bias correction is applied to average sea surface temperatures, and the atmosphere is forced with the "correct" climatological seasonal cycle together with warming derived from large-scale model outputs. The results show opposite changes in much of the SPCZ and some of the ITCZ regions (Figure 14.37).

Despite the strong uncertainty highlighted above, there is a consensus in direct outputs and bias-corrected experiments regarding an increase in rainfall along the equator. This is underpinned by a strong consensus on a faster warming rate in the equatorial Pacific than the off-equatorial regions (Xie et al., 2010b). A consequence is an increase in the frequency of the zonal SPCZ events (Cai et al., 2012), implying an increased frequency of extreme droughts and tropical cyclone occurrence.

In summary, it is very likely that temperatures, including the frequency and magnitude of extreme high temperatures, will continue to increase through the 21st century (around 1.5°C–2°C increase on average by 2100, RCP4.5). Rainfall is likely to increase in equatorial regions (e.g., Kiribati, where increases of 20–50% are projected by 2100). Given the new model results and physical insights since the AR4, it now seems that the rainfall outlook is uncertain in regions directly affected by the SPCZ and western portion of the ITCZ, and it is as likely as not that rainfall will increase in many Pacific Island nations.

14.7.14 Antarctica

Much of the climate variability of Antarctica and the Southern Ocean is modulated by the Southern Annular Mode (SAM, Section 14.5.2), the high-latitude atmospheric response to ENSO (Section 14.4), and interactions between the two (Fogt et al., 2011; Stammerjohn et al., 2008). Some signatures of the two phenomena in Antarctic temperature, snow accumulation, and sea ice have been well documented by observational and modelling studies (Bromwich et al., 2004; Genthon et al., 2003; Guo et al., 2004; Kaspari et al., 2004; Kwok and Comiso, 2002; Marshall, 2007; van den Broeke and van Lipzig, 2004). Observation-based investigations have often focused on East Antarctica and the Antarctic Peninsula, with little insight into West Antarctica owing to the lack of continuous, long-term instrumental records. However, since the AR4, several Antarctic temperature reconstructions have been completed that have shed new light on multi-decadal atmospheric variability in this part of the continent (Bromwich et al., 2012; Chapman and Walsh, 2007b; Monaghan et al., 2008; Schneider et al., 2012; Steig et al., 2009).

The positive SAM is typically associated with warmer (colder) conditions over the Peninsula (East Antarctica), with a mixed and generally non-significant impact over West Antarctica (Kwok and Comiso, 2002; Thompson and Solomon, 2002; van den Broeke and van Lipzig, 2004). In contrast, ENSO influence in high southern latitudes is manifested by mean sea level pressure anomalies over the southeast Pacific that primarily affect West Antarctic climate (Bromwich et al., 2004; Guo et al., 2004; Turner, 2004). ENSO variability tends to produce out-of-phase variations between the western and eastern sectors of West Antarctica in various atmospheric fields (Bromwich et al., 2004; Kaspari et al., 2004). This signal is part of the Pacific South American (PSA) pattern (see Section 14.6.2).

The positive trend in the SAM index in recent decades during austral summer and autumn (see Section 14.5.2) has been related to the contrasting temperature trend patterns observed in these two seasons, with warming on the eastern coast and northern tip of the Antarctic Peninsula region and cooling (or no significant temperature change) over much of East Antarctica (Thompson and Solomon, 2002; Thompson et

al., 2011; Turner et al., 2005). The high polarity of the SAM is also consistent with the significant increase in snow accumulation observed in the southern part of the Peninsula (Thomas et al., 2008). For the other seasons, and for West Antarctica, our interpretation of observed changes is more complex.

Unlike the eastern Antarctic Peninsula, its western coast shows maximum warming in austral winter (when the SAM does not exhibit any significant trend), which has been attributed to reduced sea-ice concentrations in the Bellingshausen Sea. Recent studies have emphasized the role of tropical SST forcing not directly linked to ENSO to explain the prominent spring- and wintertime atmospheric warming in West Antarctica (Ding et al., 2011; Schneider et al., 2012). There is further evidence of tropical SST influence on Antarctic temperatures and precipitation on decadal to inter-decadal time scales (Monaghan and Bromwich, 2008; Okumura et al., 2012).

The atmospheric variability associated with SAM and ENSO affects Antarctic sea ice through changes in surface wind stress (Massom and Stammerjohn, 2010). Strong circumpolar westerlies act to enhance the Ekman drift, promoting sea-ice formation near the coast, northward transport near the sea-ice edge, and greater sea ice extent (Thompson et al., 2011). This mechanism and the recent positive trend in the SAM is consistent with the small but significant increase in total Antarctic sea ice extent since 1979 (most pronounced in austral spring), despite a warmer Southern Ocean (Comiso and Nishio, 2008; Gille, 2008; Turner et al., 2009a; Turner et al., 2009b). The largest trends are seen in the South Pacific sector, with increasing (decreasing) sea ice extent in the Ross Sea (Bellingshausen Sea). This dipole-like pattern has been explained by an enhanced zonal wave number 3 pattern in the mean sea level pressure field around Antarctica, with the deepest low over the Amundsen Sea and enhanced southerly (northerly) surface winds in the Ross Sea (Bellingshausen Sea) (Turner et al., 2009b). Decadal variability in both the SAM and ENSO has been invoked to explain these changes (Sigmond and Fyfe, 2010; Stammerjohn et al., 2008; Turner and Overland, 2009). Among other far-reaching consequences of changes in the SAM, a strengthening of the circumpolar westerlies has been linked to a reduction in CO_2 uptake by the Southern Ocean (Le Quéré et al., 2007).

Since the AR4, the effects of atmospheric variability upon the Southern Ocean have received increasing attention because ice shelf basal melting and thinning are suspected to be the main causes for the acceleration of coastal glaciers in West Antarctica (Jacobs et al., 2011; Pritchard et al., 2012; Thoma et al., 2008). Anomalous melting is thought to result from upwelling of relatively warm Circumpolar Deep Water brought about by atmospheric circulation anomalies linked to changes in the SAM and tropical SST forcing (Pritchard et al., 2012; Steig et al., 2012; Thompson et al., 2011).

Modelling of Antarctic climate remains challenging, in part because of the nature of the high-elevation ice sheet in the east Antarctic and its effects on regional climate (Chapter 9, section 9.4.1.1). Moreover, modelling ice properties themselves, for both land ice and sea ice, is an area that is still developing despite improvements in recent years (Picard et al., 2012; Vancoppenolle et al., 2009; Chapter 9, Section 9.1.3.2.4). Modelling the role of the stratosphere and of ozone recovery is important for Antarctic climate, as stratospheric change is intimately linked to trends in the SAM (Section 14.5.2).

The strong reduction in Antarctic sea ice extent projected for the 21st century (Arzel et al., 2006; Bracegirdle et al., 2008) suggests that the positive SAM effect on sea ice will not be sufficient to compensate for the added thermal and radiative forcings from the atmosphere and ocean (Turner et al., 2009a). Our confidence in future climate model simulations hinges on the ability of GCMs to properly simulate the SAM pattern and temporal variability. Large disparity in model skills have been found in AR4 simulations (Fogt et al., 2009), a number of which did not feature any ozone depletion and/or recovery. Moreover, Austin et al. (2010) used an ensemble of coupled-chemistry climate models to simulate the future evolution of the Antarctic ozone hole and found a relatively wide range of results.

Recent improvements in the modelling of stratospheric chemistry and dynamical processes have had a major impact on the projection of future SAM trends and related climate changes over Antarctica and the southern oceans (Section 14.5.2, Chapter 9). During the rest of this century, recovery of the ozone hole and increasing atmospheric greenhouse gas concentrations are likely to influence the SAM in opposite directions, leading to a decrease in the positive trend seen in recent decades and possibly leading to increased warming over the Antarctic continent.

It is unclear what effect ENSO will have on future Antarctic climate change as the ENSO response to GHG emission scenarios was found to be highly model-dependent (Meehl et al., 2007b), with no indication of a significant shift in the amplitude or frequency of ENSO variability (see Section 14.4). The representation of the ENSO phenomenon has proved particularly challenging in AR4 models (Lin, 2007).

Seasonally, changes in the strength of the circumpolar westerlies are also expected during the twenty-first century as a result of changes in the semi-annual oscillation (SAO) caused by alterations in the meridional temperature gradient between the mid- and high latitudes of the Southern Hemisphere. Bracegirdle et al. (2008) considered modelled circulation changes over the Southern Ocean and found a more pronounced strengthening of the autumn peak of the SAO compared with the spring peak.

Future changes in surface temperature over Antarctica are likely to be smaller than the global mean, and much smaller than those projected for the Arctic, because of the buffering effect of the southern oceans, and the thermal mass of the east Antarctic ice sheet (Chapter 12.4.1). Future projections of precipitation over Antarctica remain uncertain.

In summary, it is very likely that Antarctic temperatures will increase through the rest of the century, but more slowly than the global mean rate of increase (average continental temperature rises of around 2°C by 2100, RCP4.5). Sea surface temperatures over the oceans around Antarctica are likely to rise more slowly, closer to 1°C rise by 2100 (RCP4.5). As temperatures rise, it is also likely that precipitation will increase, up to 20% or more over the east Antarctic (CMIP5 RCP4.5 projections). However, given known difficulties associated with correctly modelling Antarctic climate, and uncertainties associated with future SAM and ENSO trends and the extent of Antarctic sea ice, precipitation projections have only moderate confidence.

[START FAQ 14.1 HERE]

FAQ 14.1: How are Projected Changes in Regional and Global Climate Related?

Regional climates are strongly affected by regional processes, and by the effects of climate phenomena which move heat from one region to another. Such natural variations in climate can add to, or weaken, global-scale trends for years to decades. As the globe warms, climate change is likely to alter the way natural phenomena are expressed, which may further affect the rate of change of regional climates around the globe.

Because the sun's energy is not distributed evenly over the globe, regional climates vary, while the effects of topography, land-sea contrast and land cover all help to create still more localised climates. For similar reasons, the effects of climate change are not distributed evenly, but vary by region, according to latitude and geographical variation, regional land use changes and other factors.

Global average climate change is a signature of the overall increase of energy in the climate system—a result of increased emissions of greenhouse gases (which themselves are distributed roughly uniformly around the globe). Regional climate changes are related not only to latitude and geographical differences, but also the structure of the climate system, and the actions of various climate phenomena, such as patterns of variability, or regional feedback processes.

Near-equatorial latitudes are projected to become wetter, while regions on the poleward edges of the subtropics are projected to get drier, as the subtropical high pressure belts continue to expand towards the poles. Regions still farther poleward are likely to experience more rain—and winter snowfall—as the atmosphere warms, and its average moisture content increases. The largest temperature increases, meanwhile, are projected to occur in the Arctic, while lower latitudes and the Southern Hemisphere warm at rates closer to the global mean (FAQ14.1, Figure 1, left). Moreover, the rate of change of extremes of weather and climate varies regionally, influenced by large-scale change and regional effects.

[INSERT FIGURE FAQ14.1, FIGURE 1 HERE]

FAQ 14.1, Figure 1: (Left) Average pattern of surface warming projected for the final decade of the 21st century from a suite of Coupled Model Intercomparison Project Phase 5 models (taken from Chapter 12, Figure 12.40). Units are

change per degree of global warming. (Right) Change during December to February in the 90th percentile of daily maximum temperature, as a fraction of the globally and annually averaged increase of median maximum temperature (from Orlowsky and Seneviratne, 2012).

The polar regions provide good case studies of some of the factors at play. Climate change is evolving quite differently in each, because of the influences of contrasting climate patterns. In the Arctic, warming is happening considerably faster than the global average, mostly because the melting of ice and snow produces a regional feedback by allowing more sunlight to be absorbed. That gives rise to further warming, which encourages more ice and snow melt.

Many parts of the Antarctic continent—especially the east Antarctic—and surrounding ocean surface have seen little warming in recent decades. Some have even cooled, while Antarctic sea-ice extent is gradually increasing. This is largely because the westerly wind belt over the southern oceans has sped up in the last few decades, driven by the loss of stratospheric ozone, and from changes in the atmosphere's temperature structure related to increased greenhouse gas concentrations. That westerly increase has the effect of isolating the Antarctic continent and reducing heat transport from lower latitudes. It is also thought to draw sea ice northwards. The Antarctic Peninsula, however, is warming rapidly, because it is extends far enough northwards to lie under the westerly wind belt.

Natural climate phenomena, such as the El Niño-Southern Oscillation (ENSO), transport heat between one region and another, and between the atmosphere and the oceans. During an El Niño, the eastern tropical Pacific warms, while regions in the north and south Pacific tend to cool, for several months at a time (FAQ14.1, Figure 2). Such natural cycles overlie the century-scale warming pattern related to human activity (FAQ14.1, Figure 1, left panel), and add a lot of seasonal and annual variability to regional climates. The evolution through time of temperatures (and other aspects of the climate) arises from a combination of ENSO and other natural effects, plus the longer-term, human-induced trend.

Changes in the behaviour of phenomena such as ENSO would cause changes to this regional heating and cooling, on top of any background warming trend. In some areas, those changes would help reinforce the background global trend; in others, they would tend to damp it out. The future of the ENSO cycle remains uncertain, because its behaviour will depend upon how the oceanic and atmospheric circulations evolve across the tropical Pacific. The details of such evolution, however, are not consistently represented in current climate models.

[INSERT FIGURE FAQ14.1, FIGURE 2 HERE]

FAQ 14.1, Figure 2: Pattern of covariance between seasonal surface temperature anomalies and the Southern Oscillation Index (SOI). Colours show the average temperature anomaly pattern for an SOI value of –1 (El Niño event). Units are °C.

Phenomena that play out over longer time frames, such as the Pacific Decadal Oscillation (PDO) and the Atlantic Multi-decadal Oscillation (AMO), play an important role, as they can affect climate trends over decades. In different regions, they also can mask or amplify climate change signals for many years at a time. Because they directly influence regional climates, and are often associated with climate extremes such as drought, floods and heat waves, it is critical to intimately understand how such climate phenomena work, and how they are changing in response to anthropogenic warming of the climate system

[END FAQ 14.1 HERE]

[START FAQ 14.2 HERE]

FAQ 14.2: How is Climate Change Affecting Monsoons?

The monsoons are critical to the climate of many tropical regions. Their strength and timing is related to air moisture content, land-sea temperature contrast, land cover and use, atmospheric aerosol loadings, and other factors. Overall, monsoons are projected to become more intense in future, and to affect larger areas, because atmospheric moisture content increases with temperature, and the land surface is generally warming faster than the ocean surface. Regionally, however, many other factors come in to play, so the localised effects of climate change upon monsoon strength and variability remain uncertain.

Monsoons are the most important mode of seasonal climate variation in the tropics, responsible for a large fraction of annual rainfall in many regions. Monsoon rains fall over all tropical continents: Asia, Australia, the Americas, and Africa. The monsoon circulation is driven by the difference in temperature between land and sea, which varies seasonally with the distribution of solar heating. The duration and amount of rainfall depends on the moisture content of the air, and on the configuration and strength of the atmospheric circulation. The regional distribution of land and ocean also play a role, as does topography. For example, the Tibetan Plateau—along with variations in its snow cover and surface heating—modulates the strength of the Asian monsoon. Where moist on-shore winds rise over mountains, as they do in southwest India, monsoon rainfall is intensified. In the lee of such mountains, it lessens.

The East Asian summer monsoon has been weakening and not extending as far north since the late 1970s, as a result of changes in the atmospheric circulation. That in turn has led to increasing drought in northern China, but floods in the Yangtze river valley farther south. The Indo-Australian and Western Pacific monsoon systems show no coherent trends since the mid-20th century, but are strongly modulated by the El Niño-Southern Oscillation (ENSO) cycle. Similarly, changes observed in the South American monsoon system over the last few decades are strongly related to ENSO variability, rather than to longer-term human influences on the climate. Evidence of trends in the North American monsoon is limited, but a tendency towards heavier rainfalls on the northern side of the main monsoon region has been observed. No systematic trends have been observed in the behaviour of the Indian or the African monsoons.

Human activity can influence the monsoons by affecting atmospheric moisture (water vapour) content, and surface heating. Because moisture content varies strongly with air temperature, it is affected by greenhouse gas-induced warming. The land surface warms more rapidly than the ocean surface, so that temperature contrast—which drives the monsoons—is increasing in most regions. Surface heating varies with the intensity of solar radiation absorbed, which is itself affected by any land use changes that alter the albedo (reflectivity) of the land surface. Also, changing atmospheric aerosol loadings, such as air pollution, affect how much solar radiation reaches the ground, which can weaken the monsoon circulation by reducing summer solar heating of the land surface. Climate change is also associated with changes to the atmospheric circulation—such as the distribution and strength of tropical winds—which can lead to regional changes in monsoon intensity, area, and timing.

[INSERT FAQ14.2, FIGURE 1 HERE]

FAQ 14.2, Figure 1: Schematic diagram illustrating the main ways that human activity influences monsoon circulations. As the climate warms, the basic driver of the summer monsoon, land-sea temperature difference, is increasing since the land surface warms faster than the ocean. Also, warmer air contains more water vapour, increasing the potential for heavy rainfalls. Land use change and atmospheric aerosol loading can affect the amount of solar radiation that is absorbed. Other effects (not illustrated here) include warming-related changes in large-scale circulation that influence the strength and extent of the overall monsoon circulation.

The strongest effect of climate change upon the monsoons is the increase in atmospheric moisture associated with warming of the atmosphere. For every 1°C of warming, the maximum atmospheric moisture content increases by around 7%, implying an increase in total monsoon rainfall. However, rainfall increases much more slowly than does the total moisture content of the atmosphere, because overall precipitation changes are constrained by slower changes in the atmospheric radiation balance. This implies that the atmospheric circulation slows as the climate warms. Such slowing of the tropical overturning circulation has seen the whole tropical latitude band expand polewards in recent decades.

Climate model projections through the 21st century tend to show an increase in total monsoon rainfall, largely due to increasing atmospheric moisture content. The total surface area affected by the monsoons is projected to increase, along with the general poleward expansion of the tropical regions. HFowever, even as total tropical monsoon rainfall increases, some areas will receive less monsoon rain, thanks to weakening tropical wind circulations over a larger area.

The regional distribution of rainfall increase and decrease, and changes in monsoon timing, remain uncertain, as they depend on localised atmospheric circulation changes and heating contrasts. Year-to-year variations in the monsoons in many tropical regions are affected by ENSO. How ENSO will change in future—and how its effects on monsoon variability will change—also remains uncertain. However, the

projected overall increase in monsoon rainfall signals a corresponding increase in the risk of extreme rains in most regions.

Future regional trends in monsoon intensity and timing remain uncertain in many parts of the world. However, climate model projections suggest increased precipitation in the Asian monsoon, along with a rise in interannual season-averaged precipitation variability, and a delay in the timing of the West African monsoon.

References

Abram, N.J., Gagan, M.K., Cole, J.E., Hantoro, W.S. and Mudelsee, M., 2008. Recent intensification of tropical climate variability in the Indian Ocean. Nature Geoscience, **1**(12): 849-853.

ACIA, 2005. Arctic Climate Impact Assessment. Cambridge University Press, 1042 pp.

Ackerley, D., Booth, B.B.B., Knight, S.H.E., Highwood, E.J., Frame, D.J., Allen, M.R. and Rowell, D.P., 2011. Sensitivity of 20 thCentury Sahel Rainfall to Sulfate Aerosol and CO 2Forcing. Journal of Climate: 110506142853088.

Agrawala, S., Ota, T., Ahmed, A.U., Smith, J. and van Aalst, M., 2003. Development and climate change in Bangladesh: focus on coastal flooding and the sundarbans. OECD, Paris.

Aldrian, E. and Djamil, Y.S., 2008. Spatio-temporal climatic change of rainfall in east Java Indonesia. International Journal of Climatology, **28**(4): 435-448.

Aldrian, E., Gates, L.D. and Widodo, F.H., 2007. Seasonal variability of Indonesian rainfall in ECHAM4 simulations and in the reanalyses: The role of ENSO. Theoretical and Applied Climatology, **87**(1-4): 41-59.

Aldrian, E., Sein, D., Jacob, D., Gates, L.D. and Podzun, R., 2005. Modelling Indonesian rainfall with a coupled regional model. Climate Dynamics, **25**(1): 1-17.

Aldrian, E. and Susanto, R.D., 2003. Identification of three dominant rainfall regions within Indonesia and their relationship to sea surface temperature. International Journal of Climatology, **23**(12): 1435-1452.

Alexander, L.V., Zhang, X., Peterson, T.C., Caesar, J., Gleason, B., Tank, A., Haylock, M., Collins, D., Trewin, B., Rahimzadeh, F., Tagipour, A., Kumar, K.R., Revadekar, J., Griffiths, G., Vincent, L., Stephenson, D.B., Burn, J., Aguilar, E., Brunet, M., Taylor, M., New, M., Zhai, P., Rusticucci, M. and Vazquez-Aguirre, J.L., 2006. Global observed changes in daily climate extremes of temperature and precipitation. Journal of Geophysical Research-Atmospheres, **111**(D5).

Alexander, M., Blade, I., Newman, M., Lanzante, J., Lau, N. and Scott, J., 2002. The atmospheric bridge: The influence of ENSO teleconnections on air-sea interaction over the global oceans. Journal of Climate, **15**(16): 2205-2231.

Alexander, M., Vimont, D., Chang, P. and Scott, J., 2010. The Impact of Extratropical Atmospheric Variability on ENSO: Testing the Seasonal Footprinting Mechanism Using Coupled Model Experiments. Journal of Climate, **23**(11): 2885-2901.

Alexander, M.A., 2010. Extratropical air-sea interaction, SST variability and the Pacific Decadal Oscillation (PDO). In: D.S.a.F. Bryan (Editor), Climate Dynamics: Why Does Climate Vary? Geophysical Monograph Series. American Geophysical Union, Washington, D. C., pp. 123 - 148.

Allan, R. and Soden, B., 2008. Atmospheric warming and the amplification of precipitation extremes. Science, **321**(5895): 1481-1484.

Alory, G., Wijffels, S. and Meyers, G., 2007. Observed temperature trends in the Indian Ocean over 1960-1999 and associated mechanisms. Geophysical Research Letters, **34**(2): -.

Alpert, P., Ben-Gai, T., Baharad, A., Benjamini, Y., Yekutieli, D., Colacino, M., Diodato, L., Ramis, C., Homar, V., Romero, R., Michaelides, S. and Manes, A., 2002. The paradoxical increase of Mediterranean extreme daily rainfall in spite of decrease in total values. Geophysical Research Letters, **29**(11).

Alpert, P., Krichak, S., Shafir, H., Haim, D. and Osetinsky, I., 2008. Climatic trends to extremes employing regional modeling and statistical interpretation over the E. Mediterranean. Global and Planetary Change, **63**(2-3): 163-170.

AlSarmi, S. and Washington, R., 2011. Recent observed climate change over the Arabian Peninsula. Journal of Geophysical Research-Atmospheres, **116**.

Amador, J.A., Alfaro, E.J., Lizano, O.G. and Magana, V.O., 2006. Atmospheric forcing of the eastern tropical Pacific: A review. Progress in Oceanography, **69**(2-4): 101-142.

AMAP, 2011. Snow, Water, Ice and Permafrost in the Arctic., Arctic Monitoring and Assessment Programme (AMAP), Oslo.

Ambaum, M., Hoskins, B. and Stephenson, D., 2001. Arctic oscillation or North Atlantic oscillation? Journal of Climate, **14**(16): 3495-3507.

Ambaum, M.H.P., 2008. Unimodality of wave amplitude in the northern hemisphere. Journal of the Atmospheric Sciences, **65**(3): 1077-1086.

An, S.-I., Kim, J.-W., Im, S.-H., Kim, B.-M. and Park, J.-H., 2011. Recent and future sea surface temperature trends in the tropical Pacific warm pool and cold tongue regions. Climate Dynamics.

An, S.I. and Jin, F.F., 2000. An Eigen analysis of the interdecadal changes in the structure and frequency of ENSO mode. Geophysical Research Letters, **27**(16): 2573-2576.

An, S.I. and Wang, B., 2000. Interdecadal change of the structure of the ENSO mode and its impact on the ENSO frequency. Journal of Climate, **13**(12): 2044-2055.

Anav, A., Ruti, P., Artale, V. and Valentini, R., 2010. Modelling the effects of land-cover changes on surface climate in the Mediterranean region. Climate Research, **41**(2): 91-104.

Anderson, B., Wang, J., Salvucci, G., Gopal, S. and Islam, S., 2010. Observed Trends in Summertime Precipitation over the Southwestern United States, Journal of Climate, pp. 1937-1944.

Anderson, B.T., 2003. Tropical Pacific sea surface temperatures and preceding sea level pressure anomalies in the subtropical North Pacific. Journal of Geophysical Research Atmospheres, **108**(D 23).

Anderson, B.T., 2011. Near-term increase in frequency of seasonal temperature extremes prior to the 2 degree C global warming target. Climatic Change: 1-9.
Annamalai, H., Hafner, J., Sooraj, K.P. and Pillai, P., 2012. Global warming shifts monsoon circulation, drying South Asia. Journal of Climate, **revised**.
Annamalai, H., Hamilton, K. and Sperber, K.R., 2007. The South Asian summer monsoon and its relationship with ENSO in the IPCC AR4 simulations. Journal of Climate, **20**(6): 1071-1092.
Annamalai, H., Kida, S. and Hafner, J., 2010. Potential Impact of the Tropical Indian Ocean-Indonesian Seas on El Nino Characteristics. Journal of Climate, **23**(14): 3933-3952.
Annamalai, H., Xie, S., McCreary, J. and Murtugudde, R., 2005. Impact of Indian Ocean sea surface temperature on developing El Nino. Journal of Climate, **18**(2): 302-319.
Anstey, J.A. and Shepherd, T.G., 2008. Response of the northern stratospheric polar vortex to the seasonal alignment of QBO phase transitions. Geophysical Research Letters, **35**(L22810).
Arblaster, J.M., Meehl, G.A. and Karoly, D.J., 2011. Future climate change in the Southern Hemisphere: Competing effects of ozone and greenhouse gases. Geophysical Research Letters, **38**(2): L02701.
Arias, P.A., Fu, R. and Kingtse, C.M., 2012. Decadal Variation of Rainfall Seasonality in the North American Monsoon Region and Its Potential Causes. Journal of Climate, **25**: 4258-4274.
Arriaga-Ramirez, S. and Cavazos, T., 2010. Regional trends of daily precipitation indices in northwest Mexico and southwest United States. Journal of Geophysical Research, **115**: D144111.
Arzel, O., Fichefet, T. and Goosse, H., 2006. Sea ice evolution over the 20th and 21st centuries as simulated by current AOGCMs. Ocean Modelling, **12**(3–4): 401-415.
Ashfaq, M., Ying, S., Wen-wen, T., Trapp, R.J., Xueijie, G., Pal, J.S. and Diffenbaugh, N.S., 2009. Suppression of South Asian summer monsoon precipitation in the 21st century. Geophysical Research Letters: L01704 (5 pp.).
Ashok, K., Behera, S.K., Rao, S.A., Weng, H.Y. and Yamagata, T., 2007. El Nino Modoki and its possible teleconnection. Journal of Geophysical Research-Oceans, **112**(C11): -.
Ashrit, R.G., Douville, H. and Kumar, K.R., 2003. Response of the Indian monsoon and ENSO-monsoon teleconnection to enhanced greenhouse effect in the CNRM coupled model. Journal of the Meteorological Society of Japan, **81**(4): 779-803.
Athanasiadis, P.J., Wallace, J.M. and Wettstein, J.J., 2010. Patterns of Wintertime Jet Stream Variability and Their Relation to the Storm Tracks. Journal of the Atmospheric Sciences, **67**(5): 1361-1381.
Austin, J., Struthers, H., Scinocca, J., Plummer, D.A., Akiyoshi, H., Baumgaertner, A.J.G., Bekki, S., Bodeker, G.E., Braesicke, P., Brühl, C., Butchart, N., Chipperfield, M.P., Cugnet, D., Dameris, M., Dhomse, S., Frith, S., Garny, H., Gettelman, A., Hardiman, S.C., Jöckel, P., Kinnison, D., Kubin, A., Lamarque, J.F., Langematz, U., Mancini, E., Marchand, M., Michou, M., Morgenstern, O., Nakamura, T., Nielsen, J.E., Pitari, G., Pyle, J., Rozanov, E., Shepherd, T.G., Shibata, K., Smale, D., Teyssèdre, H. and Yamashita, Y., 2010. Chemistry-climate model simulations of spring Antarctic ozone. J. Geophys. Res., **115**: D00M11.
Avila, F.B., Pitman, A.J., Donat, M.G., Alexander, L.V. and Abramowitz, G., 2012. Climate model simulated changes in temperature extremes due to land cover change. Journal of Geophysical Research-Atmos, **117**.
Bader, J. and Latif, M., 2003. The impact of decadal-scale Indian Ocean sea surface temperature anomalies on Sahelian rainfall and the North Atlantic Oscillation. Geophysical Research Letters, **30**(22): -.
Bader, J., Mesquita, M.D.S., Hodges, K.I., Keenlyside, N., Osterhus, S. and Miles, M., 2011. A review on Northern Hemisphere sea-ice, storminess and the North Atlantic Oscillation: Observations and projected changes. Atmospheric Research, **101**(4): 809-834.
Baldwin, M., Stephenson, D. and Jolliffe, I., 2009. Spatial Weighting and Iterative Projection Methods for EOFs. Journal of Climate, **22**(2): 234-243.
Baldwin, M.P., Gray, J.J., Dunkerton, T.J., Hamilton, K., Haynes, P.H., Randel, W.J., Holton, J.R., Alexander, M.J., Hirota, I., Horinouchi, T., Jones, D.B.A., Kinnersley, J.S., Marquardt, C., Sato, K. and Takahashi, M., 2001. The quasi-biennial oscillation. Reviews of Geophysics, **39**(2): 179-229.
Baldwin, M.P. and Thompson, D.W.J., 2009. A critical comparison of stratosphere-troposphere coupling indices. Quarterly Journal of the Royal Meteorological Society, **135**(644): 1661-1672.
Barlow, M., 2011. The Madden-Julian Oscillation influence on Africa and West Asia. In: W. Lau and D. Waliser (Editors), In Intraseasonal Variability in the Coupled Tropical Ocean-Atmosphere System, Praxis, 2nd edition.
Barlow, M.A. and Tippett, M.K., 2008. Variability and Predictability of Central Asia River Flows: Antecedent Winter Precipitation and Large-Scale Teleconnections. Journal of Hydrometeorology, **9**(6): 1334-1349.
Barnes, E. and Polvani, L.M., 2012. Response of the midlatitude jets and their variability to increased greenhouse gases in the CMIP5 ensemble. J. of Climate.
Barnes, E.A., Hartmann, D.L., Frierson, D.M.W. and Kidston, J., 2010. Effect of latitude on the persistence of eddy-driven jets. Geophysical Research Letters, **37**(L11804).
Barnes, E.A., Slingo, J. and Woollings, T., 2011. A methodology for the comparison of blocking climatologies across indices, models and climate scenarios., Climate Dynamics (in press).
Barnett, J., 2011. Dangerous climate change in the Pacific Islands: food production and food security. Regional Environmental Change, **11**: S229-S237.

Barnett, T., Pierce, D., Hidalgo, H., Bonfils, C., Santer, B., Das, T., Bala, G., Wood, A., Nozawa, T., Mirin, A., Cayan, D. and Dettinger, M., 2008. Human-induced changes in the hydrology of the western United States. Science: 1080-1083.
Barriopedro, D., Garcia-Herrera, R., Lupo, A.R. and Hernandez, E., 2006. A climatology of northern hemisphere blocking. Journal of Climate, **19**(6): 1042-1063.
Barriopedro, D., Garcia-Herrera, R. and Trigo, R.M., 2010. Application of blocking diagnosis methods to General Circulation Models. Part I: a novel detection scheme. Climate Dynamics, **35**(7-8): 1373-1391.
Bartholy, J. and Pongracz, R., 2007. Regional analysis of extreme temperature and precipitation indices for the Carpathian Basin from 1946 to 2001., Global and Planetary Change, pp. 83-95.
Basher, R.E. and Zheng, X., 1995. Tropical cyclones in the southwest Pacific: Spatial patterns and relationships to Southern Oscillation and sea surface temperature. Journal of Climate, **8**(5, Part II): 1249-1260.
Bates, S.C., 2010. Seasonal Influences on Coupled Ocean-Atmosphere Variability in the Tropical Atlantic Ocean. Journal of Climate, **23**(3): 582-604.
Battisti, D. and Naylor, R.L., 2009. Historical Warnings of Future Food Insecurity with Unprecedented Seasonal Heat. Science, **323**(5911): 240.
Behera, S., Luo, J. and Yamagata, T., 2008. Unusual IOD event of 2007. Geophysical Research Letters, **35**(14): -.
Bell, C.J., Gray, L.J., Charlton-Perez, A.J., Joshi, M.M. and Scaife, A.A., 2009. Stratospheric Communication of El Nino Teleconnections to European Winter. Journal of Climate, **22**(15): 4083-4096.
Bender, M.A., Knutson, T.R., Tuleya, R.E., Sirutis, J.J., Vecchi, G.A., Garner, S.T. and Held, I.M., 2010. Modeled impact of anthropogenic warming on the frequency of intense Atlantic hurricanes. Science, **327**(5964): 454-458.
Benedict, J. and Randall, D., 2009. Structure of the Madden-Julian Oscillation in the Superparameterized CAM. Journal of the Atmospheric Sciences, **66**(11): 3277-3296.
Benedict, J.J., Lee, S. and Feldstein, S.B., 2004. Synoptic view of the North Atlantic Oscillation. Journal of the Atmospheric Sciences, **61**(2): 121-144.
Bengtsson, L., Hodges, K., Esch, M., Keenlyside, N., Kornblueh, L., Luo, J. and Yamagata, T., 2007. How may tropical cyclones change in a warmer climate? Tellus, **59A**: 539-561.
Bengtsson, L., Hodges, K.I. and Keenlyside, N., 2009. Will Extratropical Storms Intensify in a Warmer Climate? Journal of Climate, **22**(9): 2276-2301.
Bengtsson, L., Hodges, K.I. and Roeckner, E., 2006. Storm tracks and climate change. Journal of Climate, **19**(15): 3518-3543.
Berrisford, P., Hoskins, B.J. and Tyrlis, E., 2007. Blocking and Rossby wave-breaking on the dynamical tropopause in the Southern hemisphere., Journal of Atmospheric Sciences, pp. 2881-2898.
Bhend, J. and von Storch, H., 2008. Consistency of observed winter precipitation trends in northern Europe with regional climate change projections. Climate Dynamics, **31**(1): 17-28.
Biasutti, M. and Giannini, A., 2006. Robust Sahel drying in response to late 20th century forcings. Geophysical Research Letters: -.
Biasutti, M., Held, I., Sobel, A. and Giannini, A., 2008. SST forcings and Sahel rainfall variability in simulations of the twentieth and twenty-first centuries. Journal of Climate, **21**(14): 3471-3486.
Biasutti, M. and Sobel, A.H., 2009. Delayed seasonal cycle and African monsoon in a warmer climate. Geophys Res Lett, **36**: L23707.
Biasutti, M., Sobel, A.H. and Camargo, S.J., 2009. The role of the Sahara Low in summertime Sahel rainfall variability and change in the CMIP3 models. Journal of Climate, **22**: 5755-5771.
Bjerknes, J., 1966. A POSSIBLE RESPONSE OF ATMOSPHERIC HADLEY CIRCULATION TO EQUATORIAL ANOMALIES OF OCEAN TEMPERATURE. Tellus, **18**(4): 820-&.
Bjerknes, J., 1969. ATMOSPHERIC TELECONNECTIONS FROM EQUATORIAL PACIFIC. Monthly Weather Review, **97**(3): 163-&.
Black, E., 2009. The impact of climate change on daily precipitation statistics in Jordan and Israel. Atmospheric Science Letters, **10**(3): 192-200.
Black, E., Slingo, J. and Sperber, K., 2003. An observational study of the relationship between excessively strong short rains in coastal East Africa and Indian Ocean SST. Monthly Weather Review, **131**(1): 74-94.
Blackmon, M.L., Wallace, J.M., Lau, N.C. and Mullen, S.L., 1977. An observational study of the Northern Hemisphere winter circulation., Journal of Atmospheric Sciences, pp. 1040–1053.
Bluthgen, J., Gerdes, R. and Werner, M., 2012. Atmospheric response to the extreme Arctic sea ice conditions in 2007. Geophysical Research Letters, **39**.
Boberg, F. and Christensen, J.H., 2012. Overestimation of Mediterranean summer temperature projections due to model deficiencies. Nature Climate Change, pp. doi:10.1038/NCLIMATE1454.
Boé, J., Hall, A. and Qu, X., 2009. Current GCMs' unrealistic negative feedback in the Arctic. Journal of Climate, **22**: 4682-4695.
Boer, G., 2009. Changes in Interannual Variability and Decadal Potential Predictability under Global Warming. Journal of Climate, **22**(11): 3098-3109.
Boer, G.J. and Hamilton, K., 2008. QBO influence on extratropical predictive skill. Climate Dynamics, **31**(7-8): 987-1000.

Bollasina, M., Ming, Y. and Ramaswamy, V., 2011. Anthropogenic Aerosols and the Weakening of the South Asian Summer Monsoon. Science, **334**(6055): 502-505.
Bollasina, M. and Nigam, S., 2009. Absorbing aerosols and pre-summer monsoon hydroclimate variability over the Indian subcontinent: The challenge in investigating links. Atmospheric Research, **94**(2): 338-344.
Bombardi, R.J. and Carvalho, L.M.V., 2009. IPCC global coupled model simulations of the South America monsoon system. Climate Dynamics, **33**(7-8): 893-916.
Boo, K.O., Martin, G., Sellar, A., Senior, C. and Byun, Y.H., 2011. Evaluating the East Asian monsoon simulation in climate models. Journal of Geophysical Research, **116**(D1): D01109.
Booth, B.B.B., Dunstone, N.J., Halloran, P.R., Andrews, T. and Bellouin, N., 2012. Aerosols implicated as a prime driver of twentieth-century North Atlantic climate variability. Nature, **484**: 228-232.
Boulard, D., Pohl, B., Crétat, J., Vigaud, N. and Pham-Xuan, T., Downscaling large-scale climate variability using a regional climate model: the case of ENSO over Southern Africa. Climate Dynamics: 1-28.
Boyer, D., Boyer, H., Fossen, I. and Kreiner, A., 2001. Changes in abundance of the northern Benguela sardine stock during the decade 1990-2000, with comments on the relative importance of fishing and the environmment. South African Journal of Marine Science-Suid-Afrikaanse Tydskrif Vir Seewetenskap, **23**: 67-84.
Bracegirdle, T.J., Connolley, W.M. and Turner, J., 2008. Antarctic climate change over the Twenty First Century. Journal of Geophysical Research, **113**(D03103).
Bracegirdle, T.J., Shuckburgh, E., Sallee, J.-B., Wang, Z., Meijers, A.J.S., Bruneau, N., Phillips, T. and Wilcox, L.J., 2012. Assessment of surface winds over the Atlantic, Indian and Pacific Ocean sectors of the Southern Hemisphere in CMIP5 models: historical bias, forcing response, and state dependence. Journal of Climate: submitted.
Bracegirdle, T.J. and Stephenson, D.B., 2012a. Higher precision estimates of regional 6 polar warming by ensemble regression of climate model projections. Climate Dynamics.
Bracegirdle, T.J. and Stephenson, D.B., 2012b. On the robustness of emergent constraints used in multi-model climate change projections of Arctic warming. J. of Climate(Submitted 31 July 2012).
Braconnot, P., Otto-Bliesner, B., Harrison, S., Joussaume, S., Peterchmitt, J., Abe-Ouchi, A., Crucifix, M., Driesschaert, E., Fichefet, T., Hewitt, C., Kageyama, M., Kitoh, A., Loutre, M., Marti, O., Merkel, U., Ramstein, G., Valdes, P., Weber, L., Yu, Y. and Zhao, Y., 2007. Results of PMIP2 coupled simulations of the Mid-Holocene and Last Glacial Maximum - Part 2: feedbacks with emphasis on the location of the ITCZ and mid- and high latitudes heat budget. Climate of the Past, **3**(2): 279-296.
Braganza, K., Gergis, J., Power, S., Risbey, J. and Fowler, A., 2009. A multiproxy index of the El Nino-Southern Oscillation, AD 1525-1982. Journal of Geophysical Research-Atmospheres, **114**.
Brandefelt, J., 2006. Atmospheric modes of variability in a changing climate. Journal of Climate, **19**(22): 5934-5943.
Branstator, G. and Selten, F., 2009. "Modes of Variability" and Climate Change. Journal of Climate, **22**(10): 2639-2658.
Brayshaw, D.J., Hoskins, B. and Blackburn, M., 2009. The Basic Ingredients of the North Atlantic Storm Track. Part I: Land-Sea Contrast and Orography. Journal of the Atmospheric Sciences, **66**(9): 2539-2558.
Breugem, W., Hazeleger, W. and Haarsma, R., 2006. Multimodel study of tropical Atlantic variability and change. Geophysical Research Letters: -.
Breugem, W., Hazeleger, W. and Haarsma, R., 2007. Mechanisms of northern tropical Atlantic variability and response to CO2 doubling. Journal of Climate: 2691-2705.
Broccoli, A., Dahl, K. and Stouffer, R., 2006. Response of the ITCZ to Northern Hemisphere cooling. Geophysical Research Letters, **33**(1): -.
Bromwich, D.H., Monaghan, A.J. and Guo, Z.C., 2004. Modeling the ENSO modulation of Antarctic climate in the late 1990s with the polar MM5. Journal of Climate, **17**(1): 109-132.
Bromwich, D.H., Nicolas, J.P., Monaghan, A.J., Lazzara, M.E., Keller, L.M., Weidner, G.A. and Wilson, A.B., 2012. Central West Antarctica among most rapidly warming regions on Earth. Nature Geoscience: submitted.
Bronnimann, S., 2007. Impact of El Nino Southern Oscillation on European climate. Reviews of Geophysics, **45**(2).
Brönnimann, S., 2007. Impact of El Niño-Southern oscillation on European climate, Review of Geophysics, pp. doi:10.1029/2006RG000199.
Brown, J., et al., 2012. Implications of CMIP3 model biases and uncertainties for climate projections in the western Tropical Pacific. . Climatic Change: in press.
Brown, J., Moise, A. and Colman, R., 2012a. The South Pacific Convergence Zone in CMIP5 simulations of historical and future climate. Climate Dynamics: submitted.
Brown, J., Moise, A. and Delage, F., 2012b. Changes in the South Pacific Convergence Zone in IPCC AR4 future climate projections. Climate Dynamics, **39**(1-2): 1-19.
Brown, J., Power, S., Delage, F., Colman, R., Moise, A. and Murphy, B., 2011. Evaluation of the South Pacific Convergence Zone in IPCC AR4 Climate Model Simulations of the Twentieth Century. Journal of Climate, **24**(6): 1565-1582.
Brown, R. and Mote, P., 2009. The Response of Northern Hemisphere Snow Cover to a Changing Climate. Journal of Climate: 2124-2145.
Budikova, D., 2009. Role of Arctic sea ice in global atmospheric circulation: A review. Global and Planetary Change, **68**(3): 149-163.

Buehler, T., Raible, C.C. and Stocker, T.F., 2011. The relationship of winter season North Atlantic blocking frequencies to extreme cold and dry spells in the ERA-40., Tellus Series A, pp. 212-222.
Bukovsky, M.S., 2012. Temperature trends in the NARCCAP regional climate models. Journal of Climate, **25**: 3985-3991.
Bulic, I., Brankovic, C. and Kucharski, F., 2012. Winter ENSO teleconnections in a warmer climate. Climate Dynamics, **38**(7-8): 1593-1613.
Bulic, I. and Kucharski, F., 2012. Delayed ENSO impact on spring precipitation over the North/Atlantic European region, Climate Dynamics, pp. 2593-2612.
Bunge, L. and Clarke, A.J., 2009. A Verified Estimation of the El Nino Index Nino-3.4 since 1877. Journal of Climate, **22**(14): 3979-3992.
Butchart, N., Scaife, A.A., Bourqui, M., de Grandpré, J., Hare, S.H.E., Kettleborough, J., Langematz, U., Manzini, E., Sassi, F., Shibata, K., Shindell, D. and Sigmond, M., 2006. Simulations of anthropogenic change in the strength of the Brewer-Dobson circulation. Climate Dynamics, **27**: 727-741.
Butler, A.H., Thompson, D.W.J. and Heikes, R., 2010. The Steady-State Atmospheric Circulation Response to Climate Change-like Thermal Forcings in a Simple General Circulation Model. Journal of Climate, **23**(13): 3474-3496.
Caesar, J., Alexander, L.V., Trewin, B., Tse-Ring, K., Sorany, L., Vuniyayawa, V., Keosavang, N., Shimana, A., Htay, M.M., Karmacharya, J., Jayasinghearachchi, D.A., Sakkamart, J., Soares, E., Hung, L.T., Thuong, L.T., Hue, C.T., Dung, N.T.T., Hung, P.V., Cuong, H.D., Cuong, N.M. and Sirabaha, S., 2011. Changes in temperature and precipitation extremes over the Indo-Pacific region from 1971 to 2005. International Journal of Climatology, **31**(6): 791-801.
Cagnazzo, C. and Manzini, E., 2009. Impact of the Stratosphere on the Winter Tropospheric Teleconnections between ENSO and the North Atlantic and European Region. Journal of Climate, **22**(5): 1223-1238.
Cai, W. and Cowan, T., 2008a. Dynamics of late autumn rainfall reduction over southeastern Australia. Geophysical Research Letters, **35**(9): -.
Cai, W. and Cowan, T., 2012. Southeast Australia autumn rainfall reduction: A climate-change induced poleward shift of ocean-atmosphere circulation. Journal of Climate: in press.
Cai, W., Cowan, T. and Sullivan, A., 2009a. Recent unprecedented skewness towards positive Indian Ocean Dipole occurrences and its impact on Australian rainfall. Geophysical Research Letters, **36**: -.
Cai, W., Cowan, T., Sullivan, A., Ribbe, J. and Shi, G., 2011a. Are Anthropogenic Aerosols Responsible for the Northwest Australia Summer Rainfall Increase? A CMIP3 Perspective and Implications. Journal of Climate, **24**(10): 2556-2564.
Cai, W., Lengaigne, M., Borlace, S., Collins, M., Cowan, T., McPhaden, M.J., Timmermann, A., Power, S., Brown, J., Menkes, C., Ngari, A., Vincent, E.M. and Widlansky, M.J., 2012. More extreme swings of the South Pacific Convergence Zone due to greenhouse warming. Nature: submitted.
Cai, W., Sullivan, A., Cowan, T., Ribbe, J. and Shi, G., 2011b. Simulation of the Indian Ocean Dipole: A relevant criterion for selecting models for climate projections. Geophysical Research Letters, **38**: -.
Cai, W., van Rensch, P., Cowan, T. and Hendon, H.H., 2011c. Teleconnection Pathways of ENSO and the IOD and the Mechanisms for Impacts on Australian Rainfall. Journal of Climate, **24**(15): 3910-3923.
Cai, W.J. and Cowan, T., 2006. SAM and regional rainfall in IPCC AR4 models: Can anthropogenic forcing account for southwest Western Australian winter rainfall reduction? Geophysical Research Letters, **33**(24): -.
Cai, W.J. and Cowan, T., 2008b. Evidence of impacts from rising temperature on inflows to the Murray-Darling Basin. Geophysical Research Letters, **35**(7): -.
Cai, W.J., Shi, G. and Li, Y., 2005. Multidecadal fluctuations of winter rainfall over southwest Western Australia simulated in the CSIRO Mark 3 coupled model. Geophysical Research Letters, **32**(12): -.
Cai, W.J., Sullivan, A. and Cowan, T., 2009b. Rainfall Teleconnections with Indo-Pacific Variability in the WCRP CMIP3 Models. Journal of Climate, **22**(19): 5046-5071.
Cai, W.J., Sullivan, A. and Cowan, T., 2011d. Interactions of ENSO, the IOD, and the SAM in CMIP3 Models. Journal of Climate, **24**(6): 1688-1704.
Cai, W.J. and van Rensch, P., 2012. The 2011 southeast Queensland extreme summer rainfall: A confirmation of a negative Pacific Decadal Oscillation phase? Geophysical Research Letters, **39**.
Cai, W.J., van Rensch, P., Cowan, T. and Sullivan, A., 2010. Asymmetry in ENSO Teleconnection with Regional Rainfall, Its Multidecadal Variability, and Impact. Journal of Climate, **23**(18): 4944-4955.
Callaghan, J. and Power, S., 2010. A reduction in the frequency of severe land-falling tropical cyclones over eastern Australia in recent decades. Climate Dynamics.
Camargo, S., Robertson, A., Barnston, A. and Ghil, M., 2008. Clustering of eastern North Pacific tropical cyclone tracks: ENSO and MJO effects. Geochemistry Geophysics Geosystems, **9**.
Camargo, S., Ting, M. and Kushnir, Y., 2012. Influence of local and remote SST on North Atlantic tropical cyclone potential intensity Climate Dynamics, **In review.**
Camargo, S.J., Robertson, A.W., Gaffney, S.J., Smyth, P. and Ghil, M., 2007. Cluster analysis of typhoon tracks. Part I: General properties. Journal of Climate, **20**: 3635-3653.
Cane, M.A., Clement, A.C., Kaplan, A., Kushnir, Y., Pozdnyakov, D., Seager, R., Zebiak, S.E. and Murtugudde, R., 1997. Twentieth-century sea surface temperature trends. Science, **275**(5302): 957-960.

CARTON, J. and HUANG, B., 1994. WARM EVENTS IN THE TROPICAL ATLANTIC. Journal of Physical Oceanography: 888-903.
Carvalho, L., Jones, C. and Liebmann, B., 2002. Extreme precipitation events in Southeastern South America and Large-Scale convective patterns in the South Atlantic Convergence Zone. Journal of Climate, **15**: 2377-2393.
Carvalho, L.M.V., Jones, C. and Ambrizzi, T., 2005. Opposite phases of the antarctic oscillation and relationships with intraseasonal to interannual activity in the tropics during the austral summer. Journal of Climate, **18**(5): 702-718.
Carvalho, L.M.V., Silva Dias, M.A.F., Bookhagen, B. and Silva, A.E., 2012. Changes in the South American Monsoon System during 1948-2010. Journal of Climate-submitted.
Cassou, C., 2008. Intraseasonal interaction between the Madden-Julian Oscillation and the North Atlantic Oscillation. Nature, **455**(7212): 523-527.
Cassou, C., Deser, C. and Alexander, M.A., 2007. Investigating the impact of reemerging sea surface temperature anomalies on the winter atmospheric circulation over the North Atlantic. Journal of Climate, **20**: 3510-3526.
Cassou, C. and Terray, L., 2001. Dual influence of Atlantic and Pacific SST anomalies on the North Atlantic/Europe winter climate. Geophysical Research Letters, **28**: 3195–3198.
Castro, C.L., Pielke Sr., R.A. and Adegoke, J.O., 2007. Investigation of the Summer Climate of the Contiguous United States and Mexico Using the Regional Atmospheric Modeling System (RAMS). Part I: Model Climatology (1950-2002). Journal of Climate, **20**: 3844-3865.
Casty, C., Raible, C.C., Stocker, T.F., Wanner, H. and Luterbacher, J., 2007. A European pattern climatology 1766-2000. Climate Dynamics, **29**(7-8): 791-805.
Cattiaux, J., Yiou, P. and Vautard, R., 2012. Dynamics of future seasonal temperature trends and extremes in Europe: a multi-model analysis from CMIP3, Climate Dynamics, pp. 1949-1964.
Catto, J.L., Shaffrey, L.C. and Hodges, K.I., 2011. Northern Hemisphere Extratropical Cyclones in a Warming Climate in the HiGEM High-Resolution Climate Model. Journal of Climate, **24**(20): 5336-5352.
Cavalcanti, I.F.A. and Shimizu, M.H., 2012. Simulations and Projections of South America Features in CMIP5-HADGEM2-ES. American Journal of Climate Change.
Cavazos, T., Turrent, C. and Lettenmaier, D., 2008. Extreme precipitation trends associated with tropical cyclones in the core of the North American monsoon. Geophysical Research Letters, **35**(21): -.
Cayan, D., Das, T., Pierce, D.W., Barnett, T.P., Tyree, M. and Gershunov, A., 2010. Climate Change and Water in Southwestern North America Special Feature: Future dryness in the southwest US and the hydrology of the early 21st century drought. Proceedings of the National Academy of Sciences, **107**(50): 21271-21276.
Cayan, D.R., Redmond, K.T. and Riddle, L.G., 1999. ENSO and hydrologic extremes in the Western United States. **12**(9): 2881-2893.
Ceballos, L., Di Lorenzo, E., Schneider, N. and Taguchi, B., 2009. North Pacific gyre oscillation synchronizes climate fluctuations in the eastern and western North Pacific. Journal of Climate, **22**(19): 5163-5174.
Cerezo-Mota, R., Allen, M. and Jones, R., 2011. Mechanisms Controlling Precipitation in the Northern Portion of the North American Monsoon. Journal of Climate, **24**: 2771-2783.
Chan, J.C.L. and Xu, M., 2009. Inter-annual and inter-decadal variations of landfalling tropical cyclones in East Asia. Part I: Time series analysis. *International Journal of Climatology*, **29**: 1285-1293.
Chand, S.S. and Walsh, K.J.E., 2009. Tropical cyclone activity in the Fiji region: Spatial patterns and relationship to large-scale circulation. Journal of Climate, **22**: 3877-3893.
Chandrapala, L., 1996. Long term trends of rainfall and temperature in Sri Lanka. In: Y.P. Abrol, S. Gadgil and G.B. Pant (Editors), Climate variability and agriculture. Narosa Publishing House, New Delhi, India.
Chang, C.-H., 2011. Preparedness and storm hazards in a global warming world: lessons from Southeast Asia. Natural Hazards, **56**(3): 667-679.
Chang, C., Chiang, J., Wehner, M., Friedman, A. and Ruedy, R., 2011. Sulfate Aerosol Control of Tropical Atlantic Climate over the Twentieth Century. Journal of Climate, **24**(10): 2540-2555.
Chang, C. and Li, T., 2000. A theory for the tropical tropospheric biennial oscillation. Journal of the Atmospheric Sciences, **57**(14): 2209-2224.
Chang, C.P., Wang, Z., McBride, J. and Liu, C.H., 2005. Annual cycle of Southeast Asia - Maritime continent rainfall and the asymmetric monsoon transition. Journal of Climate, **18**(2): 287-301.
Chang, E.K.M. and Guo, Y., 2007. Is the number of North Atlantic tropical cyclones significantly underestimated prior to the availability of satellite observations? *Geophysical Research Letters*, **34**: L14801.
Chang, E.K.M., Guo, Y. and Xia, X., 2012a. CMIP5 Multi-Model Ensemble Projection of Storm Track Change Under Global Warming. J. Geophysical Research.
Chang, E.K.M., Guo, Y., Xia, X. and Zheng, M., 2012b. Storm Track Activity in IPCC AR4/CMIP3 Model Simulations. J. of Climate.
Chang, P., Fang, Y., Saravanan, R., Ji, L. and Seidel, H., 2006a. The cause of the fragile relationship between the Pacific El Nino and the Atlantic Nino. Nature: 324-328.
Chang, P., Ji, L. and Li, H., 1997. A decadal climate variation in the tropical Atlantic Ocean from thermodynamic air-sea interactions. Nature: 516-518.
Chang, P., Yamagata, T., Schopf, P., Behera, S.K., Carton, J., Kessler, W.S., Meyers, G., Qu, T., Schott, F., Shetye, S. and Xie, S.P., 2006b. Climate fluctuations of tropical coupled systems - The role of ocean dynamics. Journal of Climate, **19**(20): 5122-5174.

Chang, P., Zhang, R., Hazeleger, W., Wen, C., Wan, X.Q., Ji, L., Haarsma, R.J., Breugem, W.P. and Seidel, H., 2008. Oceanic link between abrupt changes in the North Atlantic Ocean and the African monsoon. Nature Geoscience, **1**(7): 444-448.

Chapman, W.L. and Walsh, J.E., 2007a. Simulations of Arctic Temperature and Pressure by Global Coupled Models. Journal of Climate, **20**: 609-632.

Chapman, W.L. and Walsh, J.E., 2007b. A Synthesis of Antarctic Temperatures. Journal of Climate, **20**(16): 4096-4117.

Chattopadhyay, M. and Abbs, D., 2012. On the variability of projected tropical cyclone genesis in GCM ensembles. Tellus Series a-Dynamic Meteorology and Oceanography, **64**.

Chaturvedi, R.K., Joshi, J., Jayaraman, M., Bala, G. and Ravindranath, N.H., 2012. Multi-model climate change projections for India under Representative Concentration Pathways (RCPs): A preliminary analysis **submitted**.

Chauvin, F., Roehrig, R. and Lafore, J.-P., 2010. Intraseasonal variability of the Saharan heat low and its link with mid-latitudes. Journal of Climate, **23**: 2544-2561.

Chauvin, F., Royer, J.-F. and Déqué, M., 2006. Response of hurricane-type vortices to global warming as simulated by ARPEGE-Climat at high resolution. Climate Dynamics, **27**: 377-399.

Che, H., Zhang, X., Li, Y., Zhou, Z. and Qu, J., 2007. Horizontal visibility trends in China 1981-2005. Geophysical Research Letters, **34**(24).

Chen, D., 2003. A comparison of wind products in the context of ENSO prediction. Geophysical Research Letters, **30**(3).

Chen, G., Held, I.M. and Robinson, W.A., 2007. Sensitivity of the latitude of the surface westerlies to surface friction. Journal of the Atmospheric Sciences, **64**(8): 2899-2915.

Chen, G., Lu, J. and Frierson, D.M.W., 2008. Phase Speed Spectra and the Latitude of Surface Westerlies: Interannual Variability and Global Warming Trend. Journal of Climate, **21**(22): 5942-5959.

Chen, H., Zhou, T., Neale, R.B., Wu, X. and Zhang, G.J., 2010. Performance of the new NCAR CAM3. 5 in East Asian summer monsoon simulations: Sensitivity to modifications of the convection scheme. Journal of Climate, **23**(13): 3657-3675.

Chen, W., Jiang, Z. and Li, L., 2011a. Probabilistic projections of climate change over China under the SRES A1B scenario using 28 AOGCMs. Journal of Climate, **24**: 4741-4756.

Chen, W., Jiang, Z., Li, L. and Yiou, P., 2011b. Simulation of regional climate change under the IPCC A2 scenario in southeast China. Climate Dynamics, **36**(3): 491-507.

Cheng, W., Chiang, J.C.H. and Bitz, C.M., 2007. Adjustment of the global climate to an abrupt slowdown of the Atlantic meridional overturning circulation. Ocean Circulation: Mechanisms and Impacts, Geophysical Monograph of the American Geophysical Union, **173**: 295–314.

Cherchi, A., Alessandri, A., Masina, S. and Navarra, A., 2011. Effects of increased CO2 levels on monsoons. Climate Dynamics, **37**: 83-101.

Cherchi, A. and Navarra, A., 2007. Sensitivity of the Asian summer monsoon to the horizontal resolution: differences between AMIP-type and coupled model experiments. Climate Dynamics, **28**(2-3): 273-290.

Chiang, J. and Vimont, D., 2004. Analogous Pacific and Atlantic meridional modes of tropical atmosphere-ocean variability. Journal of Climate: 4143-4158.

Chiang, J.C.H., Cheng, W. and Bitz, C.M., 2008. Fast teleconnections to the tropical Atlantic sector from Atlantic thermohaline adjustment. Geophysical Research Letters, **35**(L07704).

Choi, D.H., Kug, J.S., Kwon, W.T., Jin, F.F., Baek, H.J. and Min, S.K., 2010. Arctic Oscillation responses to greenhouse warming and role of synoptic eddy feedback. Journal of Geophysical Research-Atmospheres, **115**.

Choi, G., Collins, D., Ren, G., Trewin, B., Baldi, M., Fukuda, Y., Afzaal, M., Pianmana, T., Gomboluudev, P., Huong, P.T.T., Lias, N., Kwon, W.-T., Boo, K.-O., Cha, Y.-M. and Zhou, Y., 2009a. Changes in means and extreme events of temperature and precipitation in the Asia-Pacific Network region, 1955-2007. International Journal of Climatology, **29**(13): 1906-1925.

Choi, J., An, S.-I., Kug, J.-S. and Yeh, S.-W., 2011. The role of mean state on changes in El Nio's flavor. Climate Dynamics, **37**(5-6): 1205-1215.

Choi, J., An, S. and Yeh, S., 2012. Decadal amplitude modulation of two types of ENSO and its relationship with the mean state. Climate Dynamics, **38**(11-12): 2631-2644.

Choi, J., An, S.I., Dewitte, B. and Hsieh, W.W., 2009b. Interactive Feedback between the Tropical Pacific Decadal Oscillation and ENSO in a Coupled General Circulation Model. Journal of Climate, **22**(24): 6597-6611.

Chotamonsak, C., Salathe, E.P., Jr., Kreasuwan, J., Chantara, S. and Siriwitayakorn, K., 2011. Projected climate change over Southeast Asia simulated using a WRF regional climate model. Atmospheric Science Letters, **12**(2): 213-219.

Chou, C. and Chen, C.-A., 2010. Depth of Convection and the Weakening of Tropical Circulation in Global Warming. Journal of Climate, **23**: 3019-3030.

Chowdary, J., Xie, S., Tokinaga, H., Okumura, Y., Kubota, H., Johnson, N. and Zheng, X., 2012. Interdecadal Variations in ENSO Teleconnection to the Indo-Western Pacific for 1870-2007. Journal of Climate, **25**(5): 1722-1744.

Christensen, J.H., Boberg, F., Christensen, O.B. and Lucas-Picher, P., 2008. On the need for bias correction of regional climate change projections of temperature and precipitation. Geophysical Research Letters, **35**(20).

Christensen, J.H., Hewitson, B., Busuioc, A., Chen, A., Gao, X., Held, I., Jones, R., Kolli, R.K., Kwon, W.-T., Laprise, R., Rueda, V.M., Mearns, L., Menendez, C.G., Räisänen, J., Rinke, A., Sarr, A. and Whetton, P., 2007. Regional Climate Projections. In: S. Solomon, D. Qin, M. Manning, Z. Chen, M. Marquis, K.B. Averyt, M. Tignor and H.L. Miller (Editors), Climate Change 2007: The Physical Science Basis. Contribution of Working Group I to the Fourth Assessment Report of the Intergivernmental Panel on Climate Change. Cambridge University Press, Cambridge, United Kingdom and New York, NY, USA.

Christensen, J.H., Kjellstrom, E., Giorgi, F., Lenderink, G. and Rummukainen, M., 2010. Weight assignment in regional climate models. Climate Research, **44**(2-3): 179-194.

Christiansen, B., 2005. The shortcomings of nonlinear principal component analysis in identifying circulation regimes. Journal of Climate, **18**(22): 4814-4823.

Chu, P., Kim, J. and Chen, Y., 2012. Have steering flows in the western North Pacific and the South China Sea changed over the last 50 years? Geophysical Research Letters, **39**.

Chung, C.E. and Ramanathan, V., 2006. Weakening of North Indian SST gradients and the monsoon rainfall in India and the Sahel. Journal of Climate, **19**(10): 2036-2045.

Chung, C.E. and Ramanathan, V., 2007. Relationship between trends in land precipitation and tropical SST gradient. Geophysical Research Letters, **34**(16).

Chylek, P., Folland, C.K., Lesins, G. and Dubey, M., 2010. The 20th century bipolar seesaw of the Arctic and Antarctic surface air temperatures. Geophysical Research Letters, **37**(L08703).

Chylek, P., Folland, C.K., Lesins, G., Dubey, M. and Wang, M., 2009. Arctic air temperature change amplification and the Atlantic Multidecadal Oscillation. Geophysical Research Letters, **36**.

Chylek, P. and Lesins, G., 2008. Multidecadal variability of Atlantic hurricane activity: 1851–2007. J. Geophys. Res., **113**(D22): D22106.

Clarke, A., Liu, X. and Van Gorder, S., 1998. Dynamics of the biennial oscillation in the equatorial Indian and far western Pacific Oceans. Journal of Climate, **11**(5): 987-1001.

Clement, A.C., Seager, R., Cane, M.A. and Zebiak, S.E., 1996. An ocean dynamical thermostat. Journal of Climate, **9**(9): 2190-2196.

Cloern, J., Hieb, K.A., Jacobson, T., Sanso, B., Di Lorenzo, E. and al., e., 2010. Biological communities in San Francisco Bay track a North Pacific climate shift. Geophysical Research Letters, **37**(L21602): 6 pages.

Cobb, K.M., Charles, C.D., Cheng, H. and Edwards, R.L., 2003. El Nino/Southern Oscillation and tropical Pacific climate during the last millennium. Nature, **424**(6946): 271-276.

Coelho, C.A.S. and Goddard, L., 2009. El Nino-Induced Tropical Droughts in Climate Change Projections. Journal of Climate, **22**(23): 6456-6476.

Collier, J.C. and Zhang, G.J., 2009. Aerosol direct forcing of the summer Indian monsoon as simulated by the NCAR CAM3. Climate Dynamics, **32**(2-3): 313-332.

Collins, M., An, S.-I., Cai, W., Ganachaud, A., Guilyardi, E., Jin, F.-F., Jochum, M., Lengaigne, M., Power, S., Timmermann, A., Vecchi, G. and Wittenberg, A., 2010. The impact of global warming on the tropical Pacific ocean and El Nino. Nature Geoscience, **3**(6).

Collins, M., Booth, B.B., Bhaskaran, B., Harris, G.R., Murphy, J.M., Sexton, D.M.H. and Webb, M.J., 2011. Climate model errors, feedbacks and forcings: a comparison of perturbed physics and multi-model ensembles. Climate Dynamics, **36**(9-10): 1737-1766.

Colman, R.A., Moise, A.F. and Hanson, L.I., 2011. Tropical Australian climate and the Australian monsoon as simulated by 23 CMIP3 models. Journal of Geophysical Research-Atmospheres, **116**.

Comarazamy, D.E. and Gonzalez, J.E., 2011. Regional long-term climate change (1950-2000) in the midtropical Atlantic and its impacts on the hydrological cycle of Puerto Rico. Journal of Geophysical Research-Atmospheres, **116**.

Comiso, J.C. and Nishio, F., 2008. Trends in the sea ice cover using enhanced and compatible AMSR-E, SSM/I, and SMMR data. J. Geophys. Res., **113**(C2): C02S07.

Compo, G.P. and Sardeshmukh, P.D., 2010. Removing ENSO-Related Variations from the Climate Record. Journal of Climate, **23**(8): 1957-1978.

Conroy, J. and Overpeck, J., 2011. Regionalization of Present-Day Precipitation in the Greater Monsoon Region of Asia. Journal of Climate, **24**(15): 4073-4095.

Conway, D., Hanson, C., Doherty, R. and Persechino, A., 2007. GCM simulations of the Indian Ocean dipole influence on East African rainfall: Present and future. Geophysical Research Letters, **34**(3).

Cook, K., 2000. The South Indian convergence zone and interannual rainfall variability over southern Africa. Journal of Climate, **13**(21): 3789-3804.

Cook, K., 2008. CLIMATE SCIENCE The mysteries of Sahel droughts. Nature Geoscience, **1**(10): 647-648.

Cook, K.H. and Vizy, E.K., 2006. Coupled model simulations of the west African monsoon system: Twentieth- and Twenty-First-century simulations. Journal of Climate, **19**(15): 3681-3703.

Cook, K.H. and Vizy, E.K., 2010. Hydrodynamics of the Caribbean Low-Level Jet and Its Relationship to Precipitation. Journal of Climate, **23**(6): 1477-1494.

Coppola, E., Kucharski, F., Giorgi, F. and Molteni, F., 2005. Bimodality of the North Atlantic Oscillation in simulations with greenhouse gas forcing. Geophysical Research Letters, **32**(23).

Costa, A.A., Sales, D.C., Coutinho, M.M., Vasconcellos, F.C., Araujo, L.M. and Silva, E.M., 2012. Climate Change Simulations over the Tropical Americas using a Regional Model. Climate Dynamics.
Cravatte, S., Delcroix, T., Zhang, D., McPhaden, M. and Leloup, J., 2009. Observed freshening and warming of the western Pacific Warm Pool. Climate Dynamics, **33**(4): 565-589.
Croci-Maspoli, M., Schwierz, C. and Davies, H.C., 2007. A multifaceted climatology of atmospheric blocking and its recent linear trend. Journal of Climate, **20**(4): 633-649.
Crompton, R., Pielke, R. and McAneney, K., 2011. Emergence timescales for detection of anthropogenic climate change in US tropical cyclone loss data. Environmental Research Letters, **6**(1).
Cubasch, U., Meehl, G.A., Boer, G.J., Stouffer, R.G., Dix, M., Noda, A., Senior, C.A., Raper, S. and Yap, K.S., 2001. Projections of future climate change. Intergovernmental Panel on Climate Change, Climate change 2001: The Scientific basis.
Cullen, H. and deMenocal, P., 2000. North Atlantic influence on Tigris-Euphrates streamflow. International Journal of Climatology, **20**(8): 853-863.
Cullen, H., Kaplan, A., Arkin, P. and Demenocal, P., 2002. Impact of the North Atlantic Oscillation on Middle Eastern climate and streamflow. Climatic Change, **55**(3): 315-338.
Cunningham, C.A.C. and Cavalcanti, I.F.D., 2006. Intraseasonal modes of variability affecting the South Atlantic Convergence Zone. International Journal of Climatology, **26**(9): 1165-1180.
Curtis, S. and Hastenrath, S., 1999. Long-term trends and forcing mechanisms of circulation and climate in the equatorial Pacific. Journal of Climate, **12**(4): 1134-1144.
Curtis, S., Salahuddin, A., Adler, R.F., Huffman, G.J., Gu, G. and Hong, Y., 2007. Precipitation extremes estimated by GPCP and TRMM: ENSO relationships. Journal of Hydrometeorology, **8**(4): 678-689.
d'Orgeval, T., Polcher, J. and Li, L., 2006. Uncertainties in modelling future hydrological change over West Africa. Climate Dynamics, **26**(1): 93-108.
Dacre, H.F. and Gray, S.L., 2009. The Spatial Distribution and Evolution Characteristics of North Atlantic Cyclones. Monthly Weather Review, **137**(1): 99-115.
Dai, A., 2006. Precipitation characteristics in eighteen coupled climate models. Journal of Climate, **19**(18): 4605-4630.
Dai, A., 2011. Drought under global warming: a review. Wiley Interdisciplinary Reviews-Climate Change, **2**(1): 45-65.
Das, T., Hidalgo, H., Dettinger, M., Cayan, D., Pierce, D., Bonfils, C., Barnett, T., Bala, G. and Mirin, A., 2009. Structure and Detectability of Trends in Hydrological Measures over the Western United States. Journal of Hydrometeorology: 871-892.
Das, T., Pierce, D.W., Cayan, D.R., Vano, J.A. and Lettenmaier, D.P., 2011. The importance of warm season warming to western U.S. streamflow changes. Geophysical Research Letters, **38**: L23403.
Dash, S.K., Jenamani, R.K., Kalsi, S.R. and Panda, S.K., 2007. Some evidence of climate change in twentieth-century India. Climatic Change, **85**(3-4): 299-321.
Dash, S.K., Kulkarni, M.A., Mohanty, U.C. and Prasad, K., 2009. Changes in the characteristics of rain events in India. Journal of Geophysical Research-Atmospheres, **114**.
De Szoeke, S. and Xie, S., 2008. The tropical eastern Pacific seasonal cycle: Assessment of errors and mechanisms in IPCC AR4 coupled ocean - Atmosphere general circulation models. Journal of Climate, **21**(11): 2573-2590.
Dean, S. and Stott, P., 2009. The Effect of Local Circulation Variability on the Detection and Attribution of New Zealand Temperature Trends. Journal of Climate, **22**(23): 6217-6229.
DeFries, R., Bounoua, L. and Collatz, G., 2002. Human modification of the landscape and surface climate in the next fifty years. Global Change Biology: 438-458.
Della-Marta, P.M. and Pinto, J.G., 2009. Statistical uncertainty of changes in winter storms over the North Atlantic and Europe in an ensemble of transient climate simulations. Geophysical Research Letters, **36**.
Della-Marte, F., Lutterbacher, J., von Weissenfluh, H., Xoplaki, E., Brunet, M. and Wanner, H., 2007. Summer heat waves over western Europe 1880–2003, their relationship to large-scale forcings and predictability, Climate Dynamics, pp. 251-275.
Delworth, T. and Dixon, K., 2006. Have anthropogenic aerosols delayed a greenhouse gas-induced weakening of the North Atlantic thermohaline circulation? Geophysical Research Letters, **33**(2): -.
Deni, S.M., Suhaila, J., Zin, W.Z.W. and Jemain, A.A., 2010. Spatial trends of dry spells over Peninsular Malaysia during monsoon seasons. Theoretical and Applied Climatology, **99**(3-4): 357-371.
Deo, A., Ganer, D. and Nair, G., 2011. Tropical cyclone activity in global warming scenario. Natural Hazards: 1-16.
Dequé, M., Somot, S., Sánchez-Gómez, E., Goodess, C.M., Jacob, D., Lenderink, G. and Christensen, O.B., 2012. The spread amongst ENSEMBLES regional scenarios: regional climate models, driving general circulation models and interannual variability, Climate Dynamics, pp. 951-964.
Deser, C., Alexander, M.A., Xie, S.-P. and Phillips, A.S., 2010a. Sea Surface Temperature Variability: Patterns and Mechanisms. Annual Review of Marine Science, **2**: 115-143.
Deser, C., Phillips, A., Bourdette, V. and Teng, H., 2011. Uncertainty in climate change projections: the role of internal variability. Climate Dynamics.
Deser, C., Phillips, A., Bourdette, V. and Teng, H., 2012. Uncertainty in climate change projections: the role of internal variability, Climate Dynamics, pp. 527-546.
Deser, C., Phillips, A.S. and Alexander, M.A., 2010b. Twentieth century tropical sea surface temperature trends revisited. Geophysical Research Letters, **37**.

Deser, C., Tomas, R., Alexander, M. and Lawrence, D., 2010c. The Seasonal Atmospheric Response to Projected Arctic Sea Ice Loss in the Late Twenty-First Century. Journal of Climate, **23**(2): 333-351.
Di Lorenzo, E., Cobb, K.M., Furtado, J.C., Schneider, N., Anderson, B.T., Bracco, A., Alexander, M.A. and Vimont, D.J., 2010. Central Pacific El Nino and decadal climate change in the North Pacific Ocean. Nature Geoscience, **3**(11): 762-765.
Di Lorenzo, E., Fiechter, J., Schneider, N., Bracco, A., Miller, A., Franks, P., Bograd, S., Moore, A., Thomas, A., Crawford, W., Pena, A. and Hermann, A., 2009. Nutrient and salinity decadal variations in the central and eastern North Pacific. Geophysical Research Letters, **36**: -.
Diffenbaugh, N.S. and Ashfaq, M., 2010. Intensification of hot extremes in the United States. Geophysical Research Letters, **37**: L15701.
DiNezio, P., Kirtman, B., Clement, A., Lee, S.-K., Vecchi, G. and Wittenberg, A., 2012. Mean climate controls on the simulated response of ENSO to increasing greenhouse gases. Journal of Climate.
DiNezio, P.N., Clement, A.C., Vecchi, G.A., Soden, B.J. and Kirtman, B.P., 2009. Climate Response of the Equatorial Pacific to Global Warming. Journal of Climate, **22**(18): 4873-4892.
Ding, Q., Steig, E., Battisti, D. and Kuttel, M., 2011. Winter warming in West Antarctica caused by central tropical Pacific warming. Nature Geoscience, **4**(6): 398-403.
Ding, Q.H. and Wang, B., 2009. Predicting Extreme Phases of the Indian Summer Monsoon. Journal of Climate, **22**(2): 346-363.
Ding, Y. and Chan, J.C.L., 2005. The East Asian summer monsoon: an overview. Meteorology and Atmospheric Physics, **89**: 117-142.
Ding, Y., Ren, G., Zhao, Z., Xu, Y., Luo, Y., Li, Q. and Zhang, J., 2007. Detection, causes and projection of climate change over China: An overview of recent progress. Advances in Atmospheric Sciences: 954-971.
Ding, Y., Sun, Y., Wang, Z., Zhu, Y. and Song, Y., 2009. Inter-decadal variation of the summer precipitation in China and its association with decreasing Asian summer monsoon Part II: Possible causes. International Journal of Climatology, **29**(13): 1926-1944.
Ding, Y., Wang, Z. and Sun, Y., 2008. Inter-decadal variation of the summer precipitation in East China and its association with decreasing Asian summer monsoon. Part I: Observed evidences. International Journal of Climatology, **28**(9): 1139-1161.
Dole, R., Hoerling, M., Perlwitz, J., Eischeid, J. and Pegion, P., 2011. Was there a basis for anticipating the 2010 Russian heat wave?. Geophys. Res. Lett., L06702, pp. doi 10.1029/2010GL046582.
Donat, M.G., Leckebusch, G.C., Wild, S. and Ulbrich, U., 2011. Future changes in European winter storm losses and extreme wind speeds inferred from GCM and RCM multi-model simulations. Natural Hazards and Earth System Sciences, **11**(5): 1351-1370.
Dong, B., Sutton, R.T. and Woollings, T., 2011. Changes of interannual NAO variability in response to greenhouse gases forcing. Climate Dynamics, **37**(7-8): 1621-1641.
Dong, B.W., Sutton, R.T. and Scaife, A.A., 2006. Multidecadal modulation of El Nino-Southern Oscillation (ENSO) variance by Atlantic Ocean sea surface temperatures. Geophysical Research Letters, **33**(8).
Dong, L., Vogelsang, T.J. and Colucci, S.J., 2008. Interdecadal trend and ENSO-related interannual variability in Southern Hemisphere blocking. Journal of Climate, **21**(12): 3068-3077.
Douglas, A.V. and Englehart, P.J., 2007. A climatological perspective of transient synoptic features during NAME 2004. Journal of Climate, **20**(9): 1947-1954.
Douville, H., Royer, J.F., Polcher, J., Cox, P., Gedney, N., Stephenson, D.B. and Valdes, P.J., 2000. Impact of CO2 doubling on the Asian summer monsoon: Robust versus model-dependent responses. Journal of the Meteorological Society of Japan, **78**(4): 421-439.
DU, Y. and XIE, S., 2008. Role of atmospheric adjustments in the tropical Indian Ocean warming during the 20th century in climate models. GEOPHYSICAL RESEARCH LETTERS, **35**(8).
Du, Y., Xie, S.P., Huang, G. and Hu, K.M., 2009. Role of Air-Sea Interaction in the Long Persistence of El Nino-Induced North Indian Ocean Warming. Journal of Climate, **22**(8): 2023-2038.
Du, Y., Yang, L. and Xie, S., 2011. Tropical Indian Ocean Influence on Northwest Pacific Tropical Cyclones in Summer following Strong El Nino. Journal of Climate: 315-322.
Duan, A. and Wu, G., 2008. Weakening trend in the atmospheric heat source over the Tibetan Plateau during recent decades. Part I: Observations. Journal of Climate, **21**(13): 3149-3164.
Dufek, A.S., Ambrizzi, T. and Rocha, R.P., 2008. **Are Reanalysis Data Useful for Calculating Climate Indices over South America?** Annals of the New York Academy of Sciences, **1146**: 87-104.
Duffy, P.B. and Tebaldi, C., 2012. Increasing prevalence of extreme summer temperatures in the U.S. Climatic Change, **111**: 487-495.
Dunion, J., 2011. Rewriting the Climatology of the Tropical North Atlantic and Caribbean Sea Atmosphere. Journal of Climate, **24**(3): 893-908.
Dunion, J. and Marron, C., 2008. A Reexamination of the Jordan Mean Tropical Sounding Based on Awareness of the Saharan Air Layer: Results from 2002. Journal of Climate, **21**(20): 5242-5253.
Dunion, J. and Velden, C., 2004. The impact of the Saharan air layer on Atlantic tropical cyclone activity. Bulletin of the American Meteorological Society, **85**(3): 353-+.

Elsner, J.B., Kossin, J.P. and Jagger, T.H., 2008. The increasing intensity of the strongest tropical cyclones. Nature, **455**(7209): 92-95.
Emanuel, K., 2005. Increasing destructiveness of tropical cyclones over the past 30 years. Nature, **436**(7051): 686-688.
Emanuel, K., 2007. Environmental factors affecting tropical cyclone power dissipation. Journal of Climate, **20**(22): 5497-5509.
Emanuel, K., 2010. Tropical Cyclone Activity Downscaled from NOAA-CIRES Reanalysis, 1908-1958. Journal of Advances in Modeling Earth Systems, **2**: 12.
Emanuel, K., 2011. Global Warming Effects on US Hurricane Damage. Weather Climate and Society, **3**(4): 261-268.
Emanuel, K., Oouchi, K., Satoh, M., Tomita, H. and Yamada, Y., 2010. Comparison of Explicitly Simulated and Downscaled Tropical Cyclone Activity in a High-Resolution Global Climate Model. Journal of Advances in Modeling Earth Systems, **2**.
Emanuel, K., Solomon, S., Folini, D., Davis, S. and Cagnazzo, C., 2012. Influence of tropical tropopause layer cooling on Atlantic hurricane activity. Journal of Climate, **in review.**
Emanuel, K., Sundararajan, R. and Williams, J., 2008. Hurricanes and global warming: results from downscaling IPCC AR4 simulations. Bulletin of the American Meteorological Society, **89**: 347-367.
Emanuel, K.A., 1987. Dependence of hurricane intensity on climate. Nature, **326**: 483-485.
Emanuel, K.A., 2000. A statistical analysis of tropical cyclone intensity. Monthly Weather Review, **128**(4): 1139-1152.
Endo, H., 2010. Long-Term Changes of Seasonal Progress in Baiu Rainfall Using 109 Years (1901-2009) Daily Station Data. Sola: 5-8.
Endo, H., 2012. Future changes of Yamase bringing unusually cold summers over northeastern Japan in CMIP3 multi-models. Journal of the Meteorological Society of Japan: (in press).
Engelbrecht, C.J., Engelbrecht, F.A. and Dyson, L.L., 2011. High-resolution model-projected changes in mid-tropospheric closed-lows and extreme rainfall events over southern Africa. International Journal of Climatology: n/a-n/a.
England, M.H., Ummenhofer, C.C. and Santoso, A., 2006. Interannual rainfall extremes over southwest Western Australia linked to Indian ocean climate variability. Journal of Climate, **19**(10): 1948-1969.
Englehart, P.J. and Douglas, A.V., 2006. Defining intraseasonal rainfall variability within the North American monsoon. Journal of Climate, **19**(17): 4243-4253.
Evan, A., 2012. Atlantic hurricane activity following two major volcanic eruptions. Journal of Geophysical Research-Atmospheres, **117**.
Evan, A., Foltz, G. and Zhang, D., 2012. Physical response of the tropical-subtropical North Atlantic Ocean to decadal-multidecadal forcing by African dust. Journal of Climate, **in press.**
Evan, A., Foltz, G., Zhang, D. and Vimont, D., 2011a. Influence of African dust on ocean-atmosphere variability in the tropical Atlantic. Nature Geoscience, **4**(11): 762-765.
Evan, A.T., Kossin, J.P., Chung, C.E. and Ramanathan, V., 2011b. Arabian Sea tropical cyclones intensified by emissions of black carbon and other aerosols. Nature, **479**: 94-97.
Evan, A.T., Vimont, D.J., Heidinger, A.K., Kossin, J.P. and Bennartz, R., 2009. The Role of Aerosols in the Evolution of Tropical North Atlantic Ocean Temperature Anomalies. Science, **324**(5928): 778-781.
Evans, J. and Smith, R., 2006. Water vapor transport and the production of precipitation in the eastern fertile crescent. Journal of Hydrometeorology, **7**(6): 1295-1307.
Evans, J.P., 2009. 21st century climate change in the Middle East. Climatic Change, **92**(3-4): 417-432.
Fall, S., Niyogi, D., Gluhovsky, A., Pielke, R.A., Kalnay, E. and Rochon, G., 2010. Impacts of land use land cover on temperature trends over the continental United States: assessment using the North American Regional Reanalysis. International Journal of Climatology, **30**: 1980-1993.
Farooq, A.B. and Khan, A.H., 2004. Climate change perspective in Pakistan., Proceedings of the Capacity Building APN Workshop on Global Change Research, Islamabad, pp. 39-46.
Fauchereau, N., Pohl, B., Reason, C., Rouault, M. and Richard, Y., 2009. Recurrent daily OLR patterns in the Southern Africa/Southwest Indian Ocean region, implications for South African rainfall and teleconnections. Climate Dynamics, **32**(4): 575-591.
Fedorov, A., Harper, S., Philander, S., Winter, B. and Wittenberg, A., 2003. How predictable is El Nino? Bulletin of the American Meteorological Society, **84**(7): 911-+.
Fedorov, A. and Philander, S., 2001. A stability analysis of tropical ocean-atmosphere interactions: Bridging measurements and theory for El Nino. Journal of Climate, **14**(14): 3086-3101.
Fedorov, A.V. and Philander, S.G., 2000. Is El Nino changing? Science, **288**(5473): 1997-2002.
Feldstein, S. and Dayan, U., 2008. Circumglobal teleconnections and wave packets associated with Israeli winter precipitation. Quarterly Journal of the Royal Meteorological Society, **134**(631): 455-467.
Feldstein, S.B. and Franzke, C., 2006. Are the North Atlantic Oscillation and the Northern Annular Mode distinguishable? Journal of the Atmospheric Sciences, **63**(11): 2915-2930.
Feliks, Y., Ghil, M. and Robertson, A.W., 2010. Oscillatory Climate Modes in the Eastern Mediterranean and Their Synchronization with the North Atlantic Oscillation. Journal of Climate, **23**(15): 4060-4079.
Feng, J. and Li, J.P., 2011. Influence of El Nino Modoki on spring rainfall over south China. Journal of Geophysical Research-Atmospheres, **116**.

Feng, J., Wang, L., Chen, W., Fong, S. and Leong, K., 2010. Different impacts of two types of Pacific Ocean warming on Southeast Asian rainfall during boreal winter. Journal of Geophysical Research-Atmospheres, **115**.

Feng, L., Zhou, T.J., Wu, B., Li, T. and Luo, J.J., 2011a. Projection of Future Precipitation Change over China with a High-Resolution Global Atmospheric Model. Advances in Atmospheric Sciences, **28**(2): 464-476.

Feng, S. and Hu, Q., 2008. How the North Atlantic Multidecadal Oscillation may have influenced the Indian summer monsoon during the past two millennia?, Geophys. Res. Lett., 35, L01707., pp. doi:10.1029/2007GL032484.

Feng, S., Hu, Q. and Oglesby, R., 2011b. Influence of Atlantic sea surface temperatures on persistent drought in North America. Climate Dynamics, **37**(3-4): 569-586.

Fereday, D.R., Knight, J.R., Scaife, A.A., Folland, C.K. and Philipp, A., 2008. Cluster analysis of North Atlantic-European circulation types and links with tropical Pacific sea surface temperatures. Journal of Climate, **21**(15): 3687-3703.

Findell, K.L. and Delworth, T.L., 2010. Impact of Common Sea Surface Temperature Anomalies on Global Drought and Pluvial Frequency. Journal of Climate: 485-503.

Findell, K.L., Pitman, A.J., England, M.H. and Pegion, P.J., 2009. Regional and Global Impacts of Land Cover Change and Sea Surface Temperature Anomalies. Journal of Climate, **22**(12): 3248-3269.

Fink, A., Pohle, S., Pinto, J. and Knippertz, P., 2012. Diagnosing the influence of diabatic processes on the explosive deepening of extratropical cyclones. Geophysical Research Letters, **39**.

Fink, A.H., Bruecher, T., Ermert, V., Krueger, A. and Pinto, J.G., 2009. The European storm Kyrill in January 2007: synoptic evolution, meteorological impacts and some considerations with respect to climate change. Natural Hazards and Earth System Sciences, **9**(2): 405-423.

Fischer-Bruns, I., Banse, D.F. and Feichter, J., 2009. Future impact of anthropogenic sulfate aerosol on North Atlantic climate. Climate Dynamics, **32**(4): 511-524.

Flanner, M.G., Shell, K.M., Barlage, M., Perovich, D.K. and Tschudi, M.A., 2011. Radiative forcing and albedo feedback from the Northern Hemisphere cryosphere between 1979 and 2008. Nature Geoscience, **4**(3): 151-155.

Fogt, R., Bromwich, D. and Hines, K., 2011. Understanding the SAM influence on the South Pacific ENSO teleconnection. Climate Dynamics, **36**(7-8): 1555-1576.

Fogt, R.L. and Bromwich, D.H., 2006. Decadal variability of the ENSO teleconnection to the high-latitude South Pacific governed by coupling with the Southern Annular Mode. Journal of Climate, **19**: 979–997.

Fogt, R.L., Jones, J.M. and Renwick, J.A., 2012. Seasonal zonal asymmetries in the Southern Annular Mode and their impact on regional temperature anomalies. Journal of Climate: in press.

Fogt, R.L., Perlwitz, J., Monaghan, A.J., Bromwich, D.H., Jones, J.M. and Marshall, G.J., 2009. Historical SAM Variability. Part II: Twentieth-Century Variability and Trends from Reconstructions, Observations, and the IPCC AR4 Models. Journal of Climate, **22**(20): 5346-5365.

Folland, C., Salinger, M., Jiang, N. and Rayner, N., 2003. Trends and variations in South Pacific island and ocean surface temperatures. Journal of Climate, **16**(17): 2859-2874.

Folland, C.K., Knight, J., Linderholm, H.W., Fereday, D., Ineson, S. and Hurrell, J.W., 2009. The Summer North Atlantic Oscillation: Past, Present, and Future. Journal of Climate, **22**(5): 1082-1103.

Folland, C.K., Renwick, J.A., Salinger, M.J. and Mullan, A.B., 2002. Relative influences of the Interdecadal Pacific Oscillation and ENSO on the South Pacific Convergence Zone. Geophysical Research Letters, **29 (13): 10.1029/2001GL014201**(13): 4pp.

Fontaine, B., Garcia-Serrano, J., Roucou, P., Rodriguez-Fonseca, B., Losada, T., Chauvin, F., Gervois, S., Sijikumar, S., Ruti, P. and Janicot, S., 2010. Impacts of warm and cold situations in the Mediterranean basins on the West African monsoon: observed connection patterns (1979-2006) and climate simulations. Climate Dynamics, **35**(1): 95-114.

Forster, P., Ramaswamy, V., Artaxo, P., Berntsen, T., Betts, R., Fahey, D.W., Haywood, J., Lean, J., Lowe, D.C., Myhre, G., Nganga, J., Prinn, R., Raga, G., Schulz, M. and Van Dorland, R., 2007. Changes in Atmospheric Constituents and in Radiative Forcing, Climate Change 2007: The Physical Science Basis. Contribution of Working Group I to the Fourth Assessment Report of the Intergovernmental Panel on Climate Change. Cambridge University Press, Cambridge, United Kingdom and New York, NY, USA.

Frank, W. and Roundy, P., 2006. The role of tropical waves in tropical cyclogenesis. Monthly Weather Review, **134**(9): 2397-2417.

Frederiksen, J.S. and Frederiksen, C.S., 2007. Interdecadal changes in southern hemisphere winter storm track modes. Tellus Series a-Dynamic Meteorology and Oceanography, **59**(5): 599-617.

Friedman, A.R., Hwang, Y.T., Chiang, J.C.H. and Frierson, D.M.W., 2012. The Interhemispheric Thermal Gradient over the 20th century and in Future Projections, J. Climate.

Frierson, D.M.W., Held, I.M. and Zurita-Gotor, P., 2007. A gray-radiation aquaplanet moist GCM. Part II: Energy transports in altered climates. Journal of the Atmospheric Sciences, **64**(5): 1680-1693.

FUJIBE, F., YAMAZAKI, N. and KOBAYASHI, K., 2006. Long-term changes of heavy precipitation and dry weather in Japan (1901-2004). 気象集誌, **84**(6): 1033-1046.

Furtado, J., Di Lorenzo, E., Schneider, N. and Bond, N.A., 2011. North Pacific Decadal Variability and Climate Change in the IPCC AR4 Models. Journal of Climate, **24**(12): 18.

Gao, X., Shi, Y. and Giorgi, F., 2012a. A high resolution simulation of climate change over China. Science China: Earth Science, **54**(3): 11.

Gao, X., Shi, Y., Song, R., Giorgi, F., Wang, Y. and Zhang, D., 2008. Reduction of future monsoon precipitation over China: Comparison between a high resolution RCM simulation and the driving GCM. Meteorology and Atmospheric Physics, **100**(1): 73-86.

Gao, X., Shi, Y., Zhang, D., Wu, J., Giorgi, F., Ji, Z. and Wang, Y., 2012b. Uncertainties in monsoon precipitation projections over China: results from two high-resolution RCM simulations. Climate Research, **2**: 213.

Gao, X., Xu, Y., Zhao, Z., Pal, J. and Giorgi, F., 2006. On the role of resolution and topography in the simulation of East Asia precipitation. Theoretical and Applied Climatology, **86**(1): 173-185.

Garcia, R. and Randel, W.J., 2008. Acceleration of the Brewer–Dobson circulation due to increases in greenhouse gases. Journal of the Atmospheric Sciences, **65**: 2731–2739.

Garfinkel, C.I. and Hartmann, D.L., 2011. The Influence of the Quasi-Biennial Oscillation on the Troposphere in Wintertime in a Hierarchy of Models, Part 1: Simplified Dry GCMs. Journal of the Atmospheric Sciences, **68**.

Garreaud, R.D. and Falvey, M., 2009. The coastal winds off western subtropical South America in future climate scenarios. International Journal of Climatology, **29**(4): 543-554.

Gastineau, G. and Soden, B.J., 2009. Model projected changes of extreme wind events in response to global warming. Geophysical Research Letters, **36**.

Geng, Q.Z. and Sugi, M., 2003. Possible change of extratropical cyclone activity due to enhanced greenhouse gases and sulfate aerosols - Study with a high-resolution AGCM. Journal of Climate, **16**(13): 2262-2274.

Genthon, C., Krinner, G. and Sacchettini, M., 2003. Interannual Antarctic tropospheric circulation and precipitation variability. Climate Dynamics, **21**: 289-307.

Gerber, E.P., Baldwin, M.P., Akiyoshi, H., Austin, J., Bekki, S., Braesicke, P., Butchart, N., Chipperfield, M., Dameris, M., Dhomse, S., Frith, S.M., Garcia, R.R., Garny, H., Gettelman, A., Hardiman, S.C., Karpechko, A., Marchand, M., Morgenstern, O., Nielsen, J.E., Pawson, S., Peter, T., Plummer, D.A., Pyle, J.A., Rozanov, E., Scinocca, J.F., Shepherd, T.G. and Smale, D., 2010. Stratosphere-troposphere coupling and annular mode variability in chemistry-climate models. Journal of Geophysical Research, **115**(D00M06).

Gerber, E.P., Polvani, L.M. and Ancukiewicz, D., 2008. Annular mode time scales in the Intergovernmental Panel on Climate Change Fourth Assessment Report models. Geophysical Research Letters, **35**(22).

Gerber, E.P. and Vallis, G.K., 2007. Eddy-zonal flow interactions and the persistence of the zonal index. Journal of the Atmospheric Sciences, **64**(9): 3296-3311.

Gerber, E.P. and Vallis, G.K., 2009. On the Zonal Structure of the North Atlantic Oscillation and Annular Modes. Journal of the Atmospheric Sciences, **66**(2): 332-352.

Ghosh, S., Luniya, V. and Gupta, A., 2009. Trend analysis of Indian summer monsoon rainfall at different spatial scales. Atmospheric Science Letters, **10**(4): 285-290.

Giannini, A., 2010. Mechanisms of Climate Change in the Semiarid African Sahel: The Local View. Journal of Climate, **23**(3): 743-756.

Giannini, A., Biasutti, M., Held, I. and Sobel, A., 2008. A global perspective on African climate. Climatic Change, **90**(4): 359-383.

Giannini, A., Robertson, A.W. and Qian, J.H., 2007. A role for tropical tropospheric temperature adjustment to El Nino-Southern Oscillation in the seasonality of monsoonal Indonesia precipitation predictability. Journal of Geophysical Research-Atmospheres, **112**(D16).

Giannini, A., Saravanan, R. and Chang, P., 2003. Oceanic forcing of Sahel rainfall on interannual to interdecadal time scales. Science: 1027-1030.

Giese, B. and Ray, S., 2011. El Nino variability in simple ocean data assimilation (SODA), 1871-2008. Journal of Geophysical Research-Oceans, **116**.

Gille, S.T., 2008. Decadal-Scale Temperature Trends in the Southern Hemisphere Ocean. Journal of Climate, **21**(18): 4749-4765.

Gillett, N.P. and Fyfe, J.C., 2012. Attribution of observed sea level pressure trends to greenhouse gas, aerosol and ozone changes. Nature.

Gillett, N.P., Stott, P.A. and Santer, B.D., 2008. Attribution of cyclogenesis region sea surface temperature change to anthropogenic influence. *Geophysical Research Letters*, **35**: L09707.

Ginn, W.L., Lee, T.C. and Chan, K.Y., 2010. Past and Future Changes in the Climate of Hong Kong. Acta Meteorologica Sinica, **24(2)**: 163-175.

Giorgi, F. and Bi, X., 2009. Time of emergence (TOE) of GHG-forced precipitation change hot-spots, Geophysical Research Letters, pp. doi:10.1029/2009GL037593.

Giorgi, F. and Francesco, R., 2000. Evaluating uncertainties in the prediction of regional climate change. Geophysical Research Letters, **27**: 1295-1298.

Giorgi, F., Whetton, P.H., Jones, R.G., Christensen, J.H., Mearns, L.O., Hewitson, B., vonStorch, H., Francisco, R. and Jack, C., 2001. Emerging patterns of simulated regional climatic changes for the 21st century due to anthropogenic forcings. Geophysical research Letters, **28**(17): 3317-3320.

Gochis, D.J., Castillo-Brito, L. and Shuttleworth, J., 2007. Correlations between sea-surface temperatures and warm season streamflow in northwest Mexico. International Journal of Climatology, **27**: 883-901.

Goldenberg, S.B., Landsea, C., Mestas-Nunez, A.M. and Gray, W.M., 2001. The recent increase in Atlantic hurricane activity: Causes and implications. Science: 474-479.

Gong, D.Y. and Ho, C.H., 2002. The Siberian High and climate change over middle to high latitude Asia. Theoretical and Applied Climatology, **72**(1-2): 1-9.
Gong, D.Y. and Wang, S.W., 1999. Definition of Antarctic Oscillation index. Geophysical Research Letters, **26**(4): 459-462.
Good, P., Lowe, J.A., Collins, M. and Moufouma-Okia, W., 2008. An objective tropical Atlantic sea surface temperature gradient index for studies of south Amazon dry-season climate variability and change. Philosophical Transactions of the Royal Society B-Biological Sciences, **363**(1498): 1761-1766.
Goswami, B.N., Venugopal, V., Sengupta, D., Madhusoodanan, M.S. and Xavier, P.K., 2006. Increasing trend of extreme rain events over India in a warming environment. Science, **314**(5804): 1442-1445.
Goswami, P. and Ramesh, K.V., 2008. Extreme rainfall events: Vulnerability analysis for disaster management and observation system design. Current Science, **94**(8): 1037-1044.
Graf, H. and Zanchettin, D., 2012. Central Pacific El Nino, the "subtropical bridge," and Eurasian climate. Journal of Geophysical Research-Atmospheres, **117**.
Graff, L. and LaCasce, J., 2012. Changes in the Extratropical Storm Tracks in Response to Changes in SST in an AGCM. Journal of Climate, **25**(6): 1854-1870.
Grainger, S., Frederiksen, C., Zheng, X., Fereday, D., Folland, C., Jin, E., Kinter, J., Knight, J., Schubert, S. and Syktus, J., 2011. Modes of variability of Southern Hemisphere atmospheric circulation estimated by AGCMs. Climate Dynamics: 473-490.
Grantz, K., Rajagopalan, B., Clark, M. and Zagona, E., 2007. Seasonal shifts in the North American monsoon. Journal of Climate, **20**(9): 1923-1935.
Griffiths, G., Chambers, L., Haylock, M., Manton, M., Nicholls, N., Baek, H., Choi, Y., Della-Marta, P., Gosai, A., Iga, N., Lata, R., Laurent, V., Maitrepierre, L., Nakamigawa, H., Ouprasitwong, N., Solofa, D., Tahani, L., Thuy, D., Tibig, L., Trewin, B., Vediapan, K. and Zhai, P., 2005. Change in mean temperature as a predictor of extreme temperature change in the Asia-Pacific region. International Journal of Climatology, **25**(10): 1301-1330.
Griffiths, G., Salinger, M. and Leleu, I., 2003. Trends in extreme daily rainfall across the South Pacific and relationship to the South Pacific Convergence Zone. International Journal of Climatology, **23**(8): 847-869.
Griffiths, G.M., 2007. Changes in New Zealand daily rainfall extremes 1930 - 2004. Weather and Climate, **27**: 3-44.
Grimm, A.M., 2011. Interannual climate variability in South America: impacts on seasonal precipitation, extreme events and possible effects of climate change. . Stochastic Environmental Research and Risk Assessment, **25**(4): *537-554*.
Grimm, A.M. and Natori, A.A., 2006. Climate change and interannual variability of precipitation in South America. Geophysical Research Letters, **33**: *L19706*.
Gu, D.F. and Philander, S.G.H., 1995. SECULAR CHANGES OF ANNUAL AND INTERANNUAL VARIABILITY IN THE TROPICS DURING THE PAST CENTURY. Journal of Climate, **8**(4): 864-876.
Gu, G., Adler, R., Huffman, G. and Curtis, S., 2004. African easterly waves and their association with precipitation. Journal of Geophysical Research-Atmospheres, **109**(D4).
Gu, Y., Liou, K., Xue, Y., Mechoso, C., Li, W. and Luo, Y., 2006. Climatic effects of different aerosol types in China simulated by the UCLA general circulation model. JOURNAL OF GEOPHYSICAL RESEARCH-ALL SERIES-, **111**(D15): 15201.
Gualdi, S., Scoccimarro, E. and Navarra, A., 2008. Changes in Tropical Cyclone Activity due to Global Warming: Results from a High-Resolution Coupled General Circulation Model. Journal of Climate, **21**(20): 5204-5228.
Guanghua, C. and Chi-Yung, T., 2010. Different impacts of two kinds of Pacific Ocean warming on tropical cyclone frequency over the western North Pacific. Geophysical Research Letters, **37**(1).
Guilyardi, E., Bellenger, H., Collins, M., Ferrett, S., Cai, W. and Wittenberg, A., 2012. A first look at ENSO in CMIP5, CLIVAR Exchanges.
Guo, Z.C., Bromwich, D.H. and Hines, K.M., 2004. Modeled antarctic precipitation. Part II: ENSO modulation over West Antarctica. Journal of Climate, **17**: 448-465.
Gutowski, W.J.e.a., 2010. Regional, extreme monthly precipitation simulated by NARCCAP RCMs. Journal of Hydrometeorology, **11**: 1373-1379.
Gutzler, D.S., 2004. An Index of Interannual Precipitation Variability in the Core of the North American Monsoon Region. **17**: 4473-4480.
Gutzler, D.S. and Robbins, T.O., 2011. Climate variability and projected change in the western United States: Regional downscaling and drought statistics. Climate Dynamics, **37**: 835-849.
Gutzler, D.S.a.C., 2009. Simulations of the 2004 North American Monsoon: NAMAP2. Journal of Climate, **22**: 6716-6740.
Haarsma, R., Selten, F., Weber, S. and Kliphuis, M., 2005. Sahel rainfall variability and response to greenhouse warming. Geophysical Research Letters, **32**(17): -.
Haensler, A., Hagemann, S. and Jacob, D., 2011. The role of the simulation setup in a long-term high-resolution climate change projection for the southern African region. Theoretical and Applied Climatology, **106**(1-2): 153-169.
Haerter, J., Roeckner, E., Tomassini, L. and von Storch, J., 2009. Parametric uncertainty effects on aerosol radiative forcing. Geophysical Research Letters, **36**.
Hagen, A.B. and Landsea, C.W., 2012. On the Classification of Extreme Atlantic Hurricanes Utilizing Mid-Twentieth-Century Monitoring Capabilities*. Journal of Climate, **25**(13): 4461-4475.

Hagen, A.B., Strahan-Sakoskie, D. and Luckett, C., 2012. A Reanalysis of the 1944–53 Atlantic Hurricane Seasons—The First Decade of Aircraft Reconnaissance*. Journal of Climate, **25**(13): 4441-4460.
Hagos, S. and Cook, K., 2008. Ocean warming and late-twientieth-century Sahel drought and recovery. Journal of Climate, **21**(15): 3797-3814.
Haigh, J.D. and Roscoe, H.K., 2006. Solar influences on polar modes of variability. Meteorologische Zeitschrift, **15**(3): 371-378.
Han, W., Meehl, G., Rajagopalan, B., Fasullo, J., Hu, A., Lin, J., Large, W., Wang, J., Quan, X., Trenary, L., Wallcraft, A., Shinoda, T. and Yeager, S., 2010. Patterns of Indian Ocean sea-level change in a warming climate. Nature Geoscience, **3**(8): 546-550.
Handorf, K. and Dethloff, 2009. Atmospheric teleconnections and flow regimes under future climate projections, European Physics Journal, Special Topics, pp. 237-255.
Hansen, J., Sato, M., Ruedy, R., Lo, K., Lea, D.W. and Medina-Elizade, M., 2006. Global temperature change. Proceedings of the National Academy of Sciences of the United States of America, **103**(39): 14288-14293.
Hansingo, K. and Reason, C., 2008. Modelling the atmospheric response to SST dipole patterns in the South Indian Ocean with a regional climate model. Meteorology and Atmospheric Physics, **100**(1-4): 37-52.
Hansingo, K. and Reason, C., 2009. Modelling the atmospheric response over southern Africa to SST forcing in the southeast tropical Atlantic and southwest subtropical Indian Oceans. International Journal of Climatology, **29**(7): 1001-1012.
Harris, P.P., Huntingford, C. and Cox, P.M., 2008. Amazon Basin climate under global warming: the role of the sea surface temperature. Philosophical Transactions of the Royal Society B-Biological Sciences, **363**(1498): 1753-1759.
Harrison, S.P., Kutzbach, J.E., Liu, Z., Bartlein, P.J., Otto-Bliesner, B., Muhs, D., Prentice, I.C. and Thompson, R.S., 2003. Mid-Holocene climates of the Americas: A dynamical response to changed seasonality. Climate Dynamics, **20**(7): 663-688.
Hartmann, B. and Wendler, G., 2005. The Significance of the 1976 Pacific Climate Shift in the Climatology of Alaska. Journal of Climate, **18**: 4824–4839.
Harvey, B.J., Shaffrey, L.C., Woollings, T.J., Zappa, G. and Hodges, K.I., 2012. How large are projected 21st century storm track changes? . Geophys. Res. Lett., **Submitted**
Hasegawa, A. and Emori, S., 2005. Tropical Cyclones and Associated Precipitation over the Western North Pacific: T106 Atmospheric GCM Simulation for Present-day and Doubled CO2 Climates. Sola, **1**: 145-148.
Hasegawa, A. and Emori, S., 2007. Effect of air-sea coupling in the assessment of CO2-induced intensification of tropical cyclone activity. Geophysical Research Letters, **34**(5).
Haylock, M.R., Peterson, T.C., Alves, L.M., Ambrizzi, T., Anunciacao, Y.M.T., Baez, J., Barros, V.R., Berlato, M.A., Bidegain, M., Coronel, G., Corradi, V., Garcia, V.J., Grimm, A.M., Karoly, D., Marengo, J.A., Marino, M.B., Moncunill, D.F., Nechet, D., Quintana, J., Rebello, E., Rusticucci, M., Santos, J.L., Trebejo, I. and Vincent, L.A., 2006. Trends in total and extreme South American rainfall in 1960-2000 and links with sea surface temperature. Journal of Climate, **19**(8): 1490-1512.
Held, I., Delworth, T., Lu, J., Findell, K. and Knutson, T., 2005. Simulation of Sahel drought in the 20th and 21st centuries. Proceedings of the National Academy of Sciences of the United States of America, **102**(50): 17891-17896.
Held, I. and Zhao, M., 2011. The Response of Tropical Cyclone Statistics to an Increase in CO2 with Fixed Sea Surface Temperatures. Journal of Climate, **24**(20): 5353-5364.
Held, I.M., 1993. LARGE-SCALE DYNAMICS AND GLOBAL WARMING. Bulletin of the American Meteorological Society, **74**(2): 228-241.
Held, I.M. and Soden, B.J., 2000. Water vapor feedback and global warming. Annual Review of Energy and the Environment, **25**: 441-475.
Held, I.M. and Soden, B.J., 2006. Robust responses of the hydrological cycle to global warming. Journal of Climate, **19**: 5686–5699.
Hendon, H.H., Thompson, D.W.J. and Wheeler, M.C., 2007. Australian rainfall and surface temperature variations associated with the Southern Hemisphere annular mode. Journal of Climate, **20**: 2452–2467.
Hennessy, K., Power, S. and Cambers (Eds.), G., 2011. Climate change in the Pacific: Scientific Assessment and New Research. Regional Overview (Volume 1) and Country Reports (Volume 2), Australian Bureau of Meteorology (BoM) and Commonwealth Scientific and Industrial Organisation (CSIRO).
Hermes, J. and Reason, C., 2009. Variability in sea-surface temperature and winds in the tropical south-east Atlantic Ocean and regional rainfall relationships. International Journal of Climatology, **29**(1): 11-21.
Hernandez-Deckers, D. and von Storch, J.-S., 2010. Energetics Responses to Increases in Greenhouse Gas Concentration. Journal of Climate, **23**(14): 3874-3887.
Hidayat, R. and Kizu, S., 2010. Influence of the Madden-Julian Oscillation on Indonesian rainfall variability in austral summer. International Journal of Climatology, **30**(12): 1816-1825.
Higgins, R.W., Yao, Y. and Wang, X.L., 1997. Influence of the North American Monsoon System on the U.S. Summer Precipitation. Journal of Climate, **10**(2600-2622).
Hinton, T.J., Hoskins, B.J. and Martin, G.M., 2009. The influence of tropical sea surface temperatures and precipitation on North Pacific atmospheric blocking, Climate Dynamics, pp. 549-563.

HIROTA, N. and TAKAYABU, Y.N., 2012. Inter-Model Differences of Future Precipitation Changes in CMIP3 and MIROC5 Climate Models. 気象集誌, **90**(0): 307-316.
Hirschi, M. and Seneviratne, S.I., 2010. Intra-annual link of spring and autumn precipitation over France. Climate Dynamics, **35**(7-8): 1207-1218.
Hirschi, M., Seneviratne, S.I., Alexandrov, V., Boberg, F., Boroneant, C., Christensen, O.B., Formayer, H., Orlowsky, B. and Stepanek, P., 2011. Observational evidence for soil-moisture impact on hot extremes in southeastern Europe. Nature Geoscience, **4**(1): 17-21.
Ho, C., Baik, J., Kim, J., Gong, D. and Sui, C., 2004. Interdecadal changes in summertime typhoon tracks. Journal of Climate, **17**(9): 1767-1776.
Hoell, A., Barlow, M. and Saini, R., 2012. The Leading Pattern of Intraseasonal and Interannual Indian Ocean Precipitation Variability and its Relationship with Asian Circulation During the Boreal Cold Season. Journal of Climate(2012).
Hoerling, M., Hurrell, J., Eischeid, J. and Phillips, A., 2006. Detection and attribution of twentieth-century northern and southern African rainfall change. Journal of Climate, **19**(16): 3989-4008.
Hoerling, M.P., Kumar, A. and Zhong, M., 1997. El Nino, La Nina, and the nonlinearity of their teleconnections. Journal of Climate, **10**(8): 1769-1786.
Holland, G.J. and Webster, P.J., 2007. Heightened tropical cyclone activity in the North Atlantic: Natural variability or climate trend? Philosophical Transactions of the Royal Society A, **365**: 2695-2716.
Hong, C.-C., Li, Y.-H., Li, T. and Lee, M.-Y., 2011. Impacts of central Pacific and eastern Pacific El Ninos on tropical cyclone tracks over the western North Pacific. Geophysical Research Letters, **38**.
Hope, P., Timbal, B. and Fawcett, R., 2010. Associations between rainfall variability in the southwest and southeast of Australia and their evolution through time. International Journal of Climatology, **30**(9): 1360-1371.
Hope, P.K., 2006. Projected future changes in synoptic systems influencing southwest Western Australia. Climate Dynamics, **26**(7-8): 765-780.
Hope, P.K., Drosdowsky, W. and Nicholls, N., 2006. Shifts in the synoptic systems influencing southwest Western Australia. Climate Dynamics, **26**(7-8): 751-764.
HOREL, J. and WALLACE, J., 1981. PLANETARY-SCALE ATMOSPHERIC PHENOMENA ASSOCIATED WITH THE SOUTHERN OSCILLATION. Monthly Weather Review: 813-829.
Hori, M.E., Nohara, D. and Tanaka, H.L., 2007. Influence of Arctic Oscillation towards the Northern Hemisphere surface temperature variability under the global warming scenario. Journal of the Meteorological Society of Japan, **85**(6): 847-859.
Hori, M.E. and Ueda, H., 2006. Impact of global warming on the East Asian winter monsoon as revealed by nine coupled atmosphere-ocean GCMs. Geophys. Res. Lett, **33**(3): L03713.
Hoskins, B.J. and Hodges, K.I., 2002. New perspectives on the Northern Hemisphere winter storm tracks. Journal of the Atmospheric Sciences, **59**(6): 1041-1061.
Hsieh, W.W., Wu, A. and Shabbar, A., 2006. Nonlinear atmospheric teleconnections, Geophysical Research Letters, pp. doi:10.1029/2005GL025471.
Hsu, P.-C., Li, T. and Wang, B., 2011. Trends in global monsoon area and precipitation in the past 30 years. Geophysical research Letters, **38**(L08701).
Hsu, P., Li, T., Luo, J.-J., Murakami, H., Kitoh, A. and Zhao, M., 2012a. Increase of global monsoon area and precipitation under global warming: A robust signal? Geophysical Research Letters, **39**: L06701.
Hsu, P., Li, T., Murakami, H. and Kitoh, A., 2012b. An analysis of global monsoon variability based on simulations by 19 CMIP5 models. J. Geophys. Res.: submitted.
Hu, Z., Kumar, A., Huang, B., Xue, Y., Wang, W. and Jha, B., 2011. Persistent Atmospheric and Oceanic Anomalies in the North Atlantic from Summer 2009 to Summer 2010. Journal of Climate, **24**(22): 5812-5830.
Hu, Z., Kumar, A., Jha, B. and Huang, B., 2012a. An Analysis of Forced and Internal Variability in a Warmer Climate in CCSM3. Journal of Climate, **25**(7): 2356-2373.
Hu, Z., Kumar, A., Jha, B., Wang, W., Huang, B. and Huang, B., 2012b. An analysis of warm pool and cold tongue El Nios: air-sea coupling processes, global influences, and recent trends. Climate Dynamics, **38**(9-10): 2017-2035.
Hu, Z.Z., 1997. Interdecadal variability of summer climate over East Asia and its association with 500 hPa height and global sea surface temperature. Journal of Geophysical Research-Atmospheres, **102**(D16): 19403-19412.
Hu, Z.Z. and Wu, Z.H., 2004. The intensification and shift of the annual North Atlantic Oscillation in a global warming scenario simulation. Tellus Series a-Dynamic Meteorology and Oceanography, **56**(2): 112-124.
Huang, B. and Liu, Z., 2001. Temperature trend of the last 40 yr in the upper Pacific Ocean. Journal of Climate, **14**(17): 3738-3750.
Huang, G., Hu, K. and Xie, S., 2010. Strengthening of Tropical Indian Ocean Teleconnection to the Northwest Pacific since the Mid-1970s: An Atmospheric GCM Study. Journal of Climate: 5294-5304.
Huang, J., Guan, X. and Ji, F., 2012. Enhanced cold-season warming in semi-arid regions. Atmos. Chem. Phys. Discuss., **12**: 4627-4653.
Huang, R., Chen, W., Yang, B. and Zhang, R., 2004. Recent advances in studies of the interaction between the east Asian winter and summer monsoons and ENSO cycle. Advances in Atmospheric Sciences: 407-424.
Hung, C.W., Liu, X.D. and Yanai, M., 2004. Symmetry and asymmetry of the Asian and Australian summer monsoons. Journal of Climate, **17**(12).

Hurrell, J.W. and Deser, C., 2009. North Atlantic climate variability: The role of the North Atlantic Oscillation. Journal of Marine Systems, **78**(1): 28-41.
Hurrell, J.W. and Deser, C., 2010. North Atlantic climate variability: The role of the North Atlantic Oscillation. Journal of Marine Systems, **79**(3-4): 231-244.
Hurrell, J.W., Kushnir, Y., Visbeck, M. and Ottersen, G., 2003. **An Overview of the North Atlantic Oscillation.** *The North Atlantic Oscillation: Climate Significance and Environmental Impact*. Geophysical Monograph series, 134. American Geophysical Union, Washington D.C.
Huss, M., Hock, R., Bauder, A. and Funk, M., 2010. 100-year mass changes in the Swiss Alps linked to the Atlantic Multidecadal Oscillation. Geophysical Research Letters, **37**: -.
Hwang, Y.-T. and Frierson, D.M.W., 2011. Increasing atmospheric poleward energy transport with global warming (vol 37, L24807, 2010). Geophysical Research Letters, **38**.
Ibrahim, B., Polcher, J., Karambiri, H. and Rockel, B., 2012. Characterization of the rainy season in Burkina Faso and it's representation by regional climate models. Climate Dynamics: 1-16.
Ihara, C., Kushnir, Y., Cane, M. and de la Pena, V., 2009. Climate Change over the Equatorial Indo-Pacific in Global Warming. Journal of Climate, **22**(10): 2678-2693.
Iizumi, T., Takayabu, I., Dairaku, K., Kusaka, H., Nishimori, M., Sakurai, G., Ishizaki, N.N., Adachi, S.A. and Semenov, M.A., 2012a. Future change of daily precipitation indices in Japan: A stochastic weather generator-based bootstrap approach to provide probabilistic climate information. Journal of Geophysical Research, **117**(D11): D11114.
IIZUMI, T., UNO, F. and NISHIMORI, M., 2012b. Climate Downscaling as a Source of Uncertainty in Projecting Local Climate Change Impacts. 気象集誌, **90**(0): 83-90.
Im, E., Jung, I. and Bae, D., 2011. The temporal and spatial structures of recent and future trends in extreme indices over Korea from a regional climate projection. International Journal of Climatology, **31**(1): 72-86.
Im, E.S., Ahn, J.B., Kwon, W.T. and Giorgi, F., 2008. Multi-decadal scenario simulation over Korea using a one-way double-nested regional climate model system. Part 2: future climate projection (2021–2050). Climate Dynamics, **30**(2): 239-254.
Ineson, S. and Scaife, A., 2009. The role of the stratosphere in the European climate response to El Nino. Nature Geoscience: 32-36.
Ineson, S., Scaife, A.A., Knight, J.R., Manners, J.C., Dunstone, N.J., Gray, L.J. and Haigh, J.D., 2011. Solar forcing of winter climate variability in the
Northern Hemisphere. Nature Geoscience.
Inoue, J., Liu, J. and Curry, J.A., 2006. Intercomparison of arctic regional climate models: Modeling clouds and radiation for SHEBA in May 1998. Journal of Climate, **19**(17): 4167-4178.
Inoue, T. and Ueda, H., 2009. Evaluation for the Seasonal Evolution of the Summer Monsoon over the Asian and Western North Pacific Sector in the WCRP CMIP3 Multi-model Experiments. Journal of the Meteorological Society of Japan: 539-560.
IOCI, 2001. Second research report - towards understanding climate variability in South Western Australia, Perth, Australia.
Ionita, M., Lohmann, G., Rimbu, N., Chelcea, S. and Dima, M., 2012. Interannual to decadal summer drought variability over Europe and its relationship to global sea surface temperature. Climate Dynamics, **38**(1-2): 363-377.
IPCC, 2007a. Climate Change 2007: Impacts, Adaptation and Vulnerability. Contribution of Working Group II to the Fourth Assessment Report of the Intergovernmental Panel on Climate Change (IPCC). Cambridge University Press, Cambridge, United Kingdom and New York, NY, USA, 976 pp. pp.
IPCC, 2007b. Climate Change 2007: The Physical Science Basis. Contribution of Working Group I to the Fourth Assessment Report of the Intergovernmental Panel on Climate Change (IPCC). Cambridge University Press, Cambridge, United Kingdom and New York, NY, USA, 996 pp pp.
IPCC, 2012. Managing the Risks of Extreme Events and Disasters to Advance Climate Change Adaptation. A Special Report of Working Groups I and II of the Intergovernmental Panel on Climate Change, Cambridge, United Kingdom and New York, NY, USA.
Irving, D., Perkins, S., Brown, J., Sen Gupta, A., Moise, A., Murphy, B., Muir, L., Colman, R., Power, S., Delage, F. and Brown, J., 2011. Evaluating global climate models for the Pacific island region. Climate Research, **49**(3): 169-187.
Ishihara, K., 2010. Quantifying the uncertainty range of 30-year daily precipitation change due to global warming using regional frequency analysis. Hydrological Research Letters, **4**: 90-94.
Izumo, T., et al., 2010: Influence of the state of the Indian Ocean Dipole on the following year's El Nino. Nature Geoscience, 3, 168-172.
Izumo, T., Montegut, C.D., Luo, J.J., Behera, S.K., Masson, S. and Yamagata, T., 2008. The Role of the Western Arabian Sea Upwelling in Indian Monsoon Rainfall Variability. Journal of Climate, **21**(21): 5603-5623.
Jacobs, S.S., Jenkins, A., Giulivi, C.F. and Dutrieux, P., 2011. Stronger ocean circulation and increased melting under Pine Island Glacier ice shelf. Nature Geosci, **4**(8): 519-523.
Jaeger, E.B. and Seneviratne, S.I., 2010. Impact of soil moisture–atmosphere coupling on European climate extremes and trends in a regional climate model, Climate Dynamics.

Jain, S.K., Kumar, V. and Saharia, M., 2012. Analysis of rainfall and temperature trends in northeast India. International Journal of Climatology: n/a-n/a.

Janicot, S., Caniaux, G., Chauvin, F., De Coëtlogon, G., Fontaine, B., Hall, N., Kiladis, G., Lafore, J.P., Lavaysse, C. and Lavender, S., 2011. Intraseasonal variability of the West African monsoon. Atmospheric Science Letters, **12**(1): 58-66.

Janicot, S., Moron, V. and Fontaine, B., 1996. Sahel droughts and ENSO dynamics. Geophysical Research Letters, **23**(5): 515-518.

JIANG, D., Huijun, W. and Xianmei, L., 2005. Evaluation of East Asian Climatology as Simulated by Seven Coupled Models. AAS, **22(4)**: 479-495.

Jiang, H. and Zipser, E., 2010. Contribution of Tropical Cyclones to the Global Precipitation from Eight Seasons of TRMM Data: Regional, Seasonal, and Interannual Variations. Journal of Climate, **23**: 1526–1543.

Jiang, Y., Luo, Y., Zhao, Z., Shi, Y., Xu, Y. and Zhu, J., 2010. Projections of wind changes for 21st century in China by three regional climate models. Chinese Geographical Science, **20**(3): 226-235.

Jiang, Z., Song, J., Li, L., Chen, W., Wang, Z. and Wang, J., 2011. Extreme climate events in China: IPCC-AR4 model evaluation and projection. Climatic Change: 1-17.

Jin, J.M., Wang, S.Y. and Gillies, R.R., 2011. An Improved Dynamical Downscaling for the Western United States. In: J. Blanco and H. Kheradmand (Editors), Climate Change - Research and Technology for Adaptation and Mitigation. InTech, pp. 23-38.

JMA, 2011. Climate Change Monitoring Report 2010. Japan Meteorological Agency, Tokyo, pp. 98.

Joly, M., Voldoire, A., Douville, H., Terray, P. and Royer, J.-F., 2007. African monsoon teleconnections with tropical SSTs: validation and evolution in a set of IPCC4 simulations. Climate Dynamics, **29**(1): 1-20.

Jones, C. and Carvalho, L.M.V., 2012. Climate change in the South American Monsoon System:present climate and CMIP5 projections. Journal of Climate.

Jones, J.M., Fogt, R.L., Widmann, M., Marshall, G.J., Jones, P.D. and Visbeck, M., 2009. Historical SAM Variability. Part I: Century-Length Seasonal Reconstructions. Journal of Climate, **22**(20): 5319-5345.

Joseph, R. and Nigam, S., 2006. ENSO evolution and teleconnections in IPCC's twentieth-century climate simulations: Realistic representation? Journal of Climate, **19**(17): 4360-4377.

Joshi, M.M., Charlton, A.J. and Scaife, A.A., 2006. On the influence of stratospheric water vapor changes on the tropospheric circulation. Geophysical Research Letters, **33**(9).

Jourdain, N.C., Gupta, A.S., Taschetto, A.S., Ummenhofer, C.C., Moise, A.F. and Ashok, K., 2012. The Indo-Australian monsoon and its relationship to ENSO and IOD in reanalysis data and the CMIP3/CMIP5 simulations. Climate Dynamics, **submitted**.

Juneng, L. and Tangang, F.T., 2005. Evolution of ENSO-related rainfall anomalies in Southeast Asia region and its relationship with atmosphere-ocean variations in Indo-Pacific sector. Climate Dynamics, **25**(4): 337-350.

Juneng, L. and Tangang, F.T., 2010. Long-term trends of winter monsoon synoptic circulations over the maritime continent: 1962-2007. Atmospheric Science Letters, **11**(3): 199-203.

Juneng, L., Tangang, F.T. and Reason, C.J.C., 2007. Numerical case study of an extreme rainfall event during 9-11 December 2004 over the east coast of Peninsular Malaysia. Meteorology and Atmospheric Physics, **98**(1-2): 81-98.

Jung, T., Ferranti, L. and Tompkins, A., 2006. Response to the summer of 2003 Mediterranean SST anomalies over Europe and Africa. Journal of Climate, **19**(20): 5439-5454.

Junquas, C., Vera, C., Li, L. and Le Treut, H., 2011. Summer precipitation variability over Southeastern South America in a global warming scenario. Springer-Verlag 2011, Climate Dynamics.

Kajikawa, Y., Wang, B. and Yang, J., 2010. A multi-time scale Australian monsoon index. International Journal of Climatology, **30**(8): 1114-1120.

Kamiguchi, K., A. Kitoh, T. Uchiyama, and, R.M. and Noda, A., 2006. Changes in precipitation-based extremes indices due to global warming projected by a global 20-km-mesh atmospheric model. **2**: 64-67.

Kanada, S., and, M.N. and Kato, T., 2010. Changes in mean atmospheric structures around Japan during July due to global warming in regional climate experiments using a cloud resolving model. **4**: 11-14.

Kanada, S., Nakano, M. and Kato, T., 2012. Projections of future changes in precipitation and the vertical structure of the frontal zone during the Baiu season in the vicinity of Japan using a 5-km-mesh regional climate model. Journal of the Meteorological Society of Japan, **90A**: 65-86.

Kang, S., Held, I., Frierson, D. and Zhao, M., 2008. The response of the ITCZ to extratropical thermal forcing: Idealized slab-ocean experiments with a GCM. Journal of Climate, **21**(14): 3521-3532.

Kang, S.M., Frierson, D.M.W. and Held, I.M., 2009. The Tropical Response to Extratropical Thermal Forcing in an Idealized GCM: The Importance of Radiative Feedbacks and Convective Parameterization. Journal of the Atmospheric Sciences, **66**(9): 2812-2827.

Kao, H.Y. and Yu, J.Y., 2009. Contrasting Eastern-Pacific and Central-Pacific Types of ENSO. Journal of Climate, **22**(3): 615-632.

Kapnick, S. and Hall, A., 2011. Causes of recent changes in western North American snowpack, Climate Dynamics.

Karmalkar, A.V., Bradley, R.S. and Diaz, H.F., 2011. Climate change in Central America and Mexico: regional climate model validation and climate change projections. Climate Dynamics, **37**(3-4): 605-629.

Karnauskas, K.B., Seager, R., Kaplan, A., Kushnir, Y. and Cane, M.A., 2009. Observed Strengthening of the Zonal Sea Surface Temperature Gradient across the Equatorial Pacific Ocean. Journal of Climate, **22**(16): 4316-4321.
Karoly, D.J. and Braganza, K., 2005. Attribution of recent temperature changes in the Australian region. Journal of Climate, **18**(3): 457-464.
Karoly, D.J. and Wu, Q.G., 2005. Detection of regional surface temperature trends. Journal of Climate, **18**: 4337-4343.
Karpechko, A.Y., 2010. Uncertainties in future climate attributable to uncertainties in future Northern Annular Mode trend. Geophysical research Letters, **37**.
Karpechko, A.Y., Gillett, N.P., Gray, L.J. and Dall'Amico, M., 2010. Influence of ozone recovery and greenhouse gas increases on Southern Hemisphere circulation. J. Geophys. Res., **115**(D22): D22117.
Kaspari, S., Mayewski, P.A., Dixon, D.A., Spikes, V.B., Sneed, S.B., Handley, M.J. and Hamilton, G.S., 2004. Climate variability in West Antarctica derived from annual accumulation-rate records from ITASE firn/ice cores. Annals of Glaciology, **39**(1): 585-594.
Kattsov, V.M., Walsh, J.E., Chapman, W.L., Govorkova, V.A., Pavlova, T.V. and Zhang, X.D., 2007. Simulation and projection of arctic freshwater budget components by the IPCC AR4 global climate models. Journal of Hydrometeorology, **8**: 571-589.
Katzfey, J.J., McGregor, J., Nguyen, K. and Thatcher, M., 2009. Dynamical downscaling techniques: Impacts on regional climate change signals. 18th World Imacs Congress and Modsim09 International Congress on Modelling and Simulation: Interfacing Modelling and Simulation with Mathematical and Computational Sciences: 3942-3947.
Kaufman, D.S., Schneider, D.P., McKay, N.P., Ammann, C.M., Bradley, R.S., Briffa, K.R., Miller, G.H., Otto-Bliesner, B.L., Overpeck, J.T., Vinther, B.M. and Members, A.L.k.P., 2009. Recent warming reverses long-term Arctic cooling. Science, **325**: 1236-1239.
Kawase, H., Yoshikane, T., Hara, M., Kimura, F., Yasunari, T., Ailikun, B., Ueda, H. and Inoue, T., 2009. Intermodel variability of future changes in the Baiu rainband estimated by the pseudo global warming downscaling method. Journal of Geophysical Research, **114**(D24110).
Kawatani, Y., Hamilton, K. and Noda, A., 2012. The Effects of Changes in Sea Surface Temperature and CO2 Concentration on the Quasi-Biennial Oscillation. Journal of the Atmospheric Sciences, **69**(5): 1734-1749.
Kawatani, Y., Hamilton, K. and Watanabe, S., 2011. The Quasi-Biennial Oscillation in a double CO2 climate. Journal of the Atmospheric Sciences, **68**: 265–283.
Kay, J.E., L'Ecuyer, T., Gettelman, A., Stephens, G. and O'Dell, C., 2008. The contribution of cloud and radiation anomalies to the 2007 Arctic sea ice extent minimum. Geophysical Research Letters, **35**: L08503.
Keenlyside, N. and Latif, M., 2007. Understanding equatorial Atlantic interannual variability. Journal of Climate: 131-142.
Keenlyside, N., Latif, M., Jungclaus, J., Kornblueh, L. and Roeckner, E., 2008. Advancing decadal-scale climate prediction in the North Atlantic sector. Nature, **453**(7191): 84-88.
Khain, A., Cohen, N., Lynn, B. and Pokrovsky, A., 2008. Possible Aerosol Effects on Lightning Activity and Structure of Hurricanes. Journal of the Atmospheric Sciences, **65**(12): 3652-3677.
Khain, A., Lynn, B. and Dudhia, J., 2010. Aerosol Effects on Intensity of Landfalling Hurricanes as Seen from Simulations with the WRF Model with Spectral Bin Microphysics. Journal of the Atmospheric Sciences, **67**(2): 365-384.
Kidson, J.W. and Renwick, J.A., 2002. Patterns of convection in the tropical Pacific and their influence on New Zealand weather. International Journal of Climatology, **22**: 151-174.
Kidston, J. and Gerber, E.P., 2010. Intermodel variability of the poleward shift of the austral jet stream in the CMIP3 integrations linked to biases in 20th century climatology. Geophysical Research Letters, **37**.
Kidston, J., Renwick, J.A. and McGregor, J., 2009. Hemispheric-scale seasonality of the Southern Annular Mode and impacts on the climate of New Zealand. Journal of Climate, **22**(18): 4759-4770.
Kidston, J., Vallis, G.K., Dean, S.M. and Renwick, J.A., 2011. Can the Increase in the Eddy Length Scale under Global Warming Cause the Poleward Shift of the Jet Streams? Journal of Climate, **24**(14): 3764-3780.
Kiehl, J.T., 2007. Twentieth century climate model response and climate sensitivity. Geophysical Research Letters, **34**: L22710, doi:10.1029/2007GL031383.
Kim, B.M. and An, S.I., 2011. Understanding ENSO Regime Behavior upon an Increase in the Warm-Pool Temperature Using a Simple ENSO Model. Journal of Climate, **24**(5): 1438-1450.
Kim, D. and Byun, H., 2009. Future pattern of Asian drought under global warming scenario. Theoretical and Applied Climatology: 137-150.
Kim, D., Choi, K. and Byun, H., 2012. Effects of El Nino Modoki on winter precipitation in Korea. Climate Dynamics, **38**(7-8): 1313-1324.
Kim, H.-J., Takata, K., Wang, B., Watnabe, M., Kimoto, M., Toyohata, T. and Yasunari, T., 2011a. Global Monsoon, El Niño, and their interannual linkage simulated by MIROC5 and the CMIP3 CGCMs, Journal of Climate, pp. 5604-5618.
Kim, H.J., Wang, B. and Ding, Q.H., 2008. The Global Monsoon Variability Simulated by CMIP3 Coupled Climate Models. Journal of Climate, **21**(20): 5271-5294.
Kim, H.M., Webster, P.J. and Curry, J.A., 2009. Impact of Shifting Patterns of Pacific Ocean Warming on North Atlantic Tropical Cyclones. Science, **325**(5936): 77-80.

Kim, H.M., Webster, P.J. and Curry, J.A., 2011b. Modulation of North Pacific Tropical Cyclone Activity by Three Phases of ENSO. Journal of Climate, **24**(6): 1839-1849.
Kim, M.K., Lau, W.K.M., Kim, K.M. and Lee, W.S., 2007. A GCM study of effects of radiative forcing of sulfate aerosol on large scale circulation and rainfall in East Asia during boreal spring. Geophysical Research Letters, **34**(24): L24701.
Kim, S. and Yu, J.-Y., 2012. The two types of ENSO in CMIP5 models. Geophysical Researcher Letters.
Kitoh, A., Endo, H., Krishna Kumar, K., Cavalcanti, I.F.A., Goswami, P. and Zhou, T., 2012. Global monsoon rainfall - what the future holds? Nature Climate Change: submitted.
Kitoh, A. and Kusunoki, S., 2008. East Asian summer monsoon simulation by a 20-km mesh AGCM. Climate Dynamics, **31**(4): 389-401.
Kitoh, A., Kusunoki, S. and Nakaegawa, T., 2011. Climate change projections over South America in the late 21st century with the 20 and 60 km mesh Meteorological Research Institute atmospheric general circulation model (MRI-AGCM). Journal of Geophysical Research-Atmospheres, **116**: -.
Kitoh, A., Kusunoki, S., Sato, Y., Ferdousi, N., Rahman, M., Makmur, E., Solis, A., Chaowiwat, W. and Trong, T., 2010. Climate Change Projections in Some Asian Countries. In: **R. Fujikura** and **M. Kawanishi** (Editors), Climate Change Adaptation and International Development. Earthscan Taylor & Francis Groups, Amsterdam, pp. 416.
Kitoh, A., T. Ose, K. Kurihara, S. Kusunoki, and, M.S. and Group, K.T.-M., 2009. Projection of changes in future weather extremes using super-high-resolution global and regional atmospheric models in the KAKUSHIN Program: Results of preliminary experiments. **3**: 49-53.
Kitoh, A. and Uchiyama, T., 2006. Changes in onset and withdrawal of the East Asian summer rainy season by multi-model global warming experiments. Journal of the Meteorological Society of Japan: 247-258.
Kitoh, A., Yatagai, A. and Alpert, P., 2008. First super-high-resolution model projection that the ancient “Fertile Crescent” will disappear in this century. Hydrological Research Letters, **2**: 1-4.
Kjellstrom, E., Nikulin, G., Hansson, U., Strandberg, G. and Ullerstig, A., 2011. 21st century changes in the European climate: uncertainties derived from an ensemble of regional climate model simulations. Tellus Series a-Dynamic Meteorology and Oceanography, **63**(1): 24-40.
Klein, S., Soden, B. and Lau, N., 1999. Remote sea surface temperature variations during ENSO: Evidence for a tropical atmospheric bridge. Journal of Climate: 917-932.
Klingaman, N., Woolnough, S., Weller, H. and Slingo, J., 2011. The Impact of Finer-Resolution Air-Sea Coupling on the Intraseasonal Oscillation of the Indian Monsoon. Journal of Climate, **24**(10): 2451-2468.
Knapp, K.R. and Kruk, M.C., 2010. Quantifying inter-agency differences in tropical cyclone best track wind speed estimates. Monthly Weather Review, **138**(4): 1459-1473.
Knight, J., 2009. The Atlantic Multidecadal Oscillation Inferred from the Forced Climate Response in Coupled General Circulation Models. Journal of Climate, **22**(7): 1610-1625.
Knutson, T. and Manabe, S., 1998. Model assessment of decadal variability and trends in the tropical Pacific Ocean. Journal of Climate, **11**(9): 2273-2296.
Knutson, T., Tuleya, R., Shen, W. and Ginis, I., 2001. Impact of CO2-induced warming on hurricane intensities as simulated in a hurricane model with ocean coupling. Journal of Climate, **14**(11): 2458-2468.
Knutson, T.R., Delworth, T.L., Dixon, K.W., Held, I.M., Lu, J., Ramaswamy, V., Schwarzkopf, M.D., Stenchikov, G. and Stouffer, R.J., 2006. Assessment of twentieth-century regional surface temperature trends using the GFDL CM2 coupled models. Journal of Climate, **19**(9): 1624-1651.
Knutson, T.R., McBride, J.L., Chan, J., Emanuel, K., Holland, G., Landsea, C., Held, I., Kossin, J.P., Srivastava, A.K. and Sugi, M., 2010. Tropical cyclones and climate change. Nature Geoscience, **3**(3): 157-163.
Knutson, T.R., Sirutis, J.J., Garner, S.T., Vecchi, G.A. and Held, I.M., 2008. Simulated reduction in Atlantic hurricane frequency under twenty-first-century warming conditions (vol 1, pg 359, 2008). Nature Geoscience, **1**(7): 479-479.
Knutson, T.R. and Tuleya, R.E., 2004. Impact of CO2-Induced Warming on Simulated Hurricane Intensity and Precipitation: Sensitivity to the Choice of Climate Model and Convective Parameterization. Journal of Climate, **17**(18): 3477-3495.
Kobayashi, C. and Sugi, M., 2004. Impact of horizontal resolution on the simulation of the Asian summer monsoon and tropical cyclones in the JMA global model. Climate Dynamics, **23**(2): 165-176.
Kodama, C. and Iwasaki, T., 2009. Influence of the SST Rise on Baroclinic Instability Wave Activity under an Aquaplanet Condition. Journal of the Atmospheric Sciences, **66**(8): 2272-2287.
Kodera, K., Hori, M.E., Yukimoto, S. and Sigmond, M., 2008. Solar modulation of the Northern Hemisphere winter trends and its implications with increasing CO2. Geophysical Research Letters, **35**(3).
Kohler, M., Kalthoff, N. and Kottmeier, C., 2010. The impact of soil moisture modifications on CBL characteristics in West Africa: A case-study from the AMMA campaign. Quarterly Journal of the Royal Meteorological Society, **136**: 442-455.
Koldunov, N.V., Stammer, D. and Marotzke, J., 2010. Present-Day Arctic Sea Ice Variability in the Coupled ECHAM5/MPI-OM Model. Journal of Climate, **23**(10): 2520-2543.
Konwar, M., Parekh, A. and Goswami, B., 2012. Dynamics of east-west asymmetry of Indian summer monsoon rainfall trends in recent decades. Geophysical Research Letters, **39**.

Kosaka, Y. and Nakamura, H., 2010. Mechanisms of meridional teleconnection observed between a summer monsoon system and a subtropical anticyclone. Part I: The Pacific-Japan pattern. J.Climate, **23**: 5085-5108.
Kossin, J., Knapp, K., Vimont, D., Murnane, R. and Harper, B., 2007. A globally consistent reanalysis of hurricane variability and trends. Geophysical Research Letters, **34**(4).
Kossin, J.P. and Camargo, S.J., 2009. Hurricane track variability and secular potential intensity trends. Climatic Change, **97**: 329-337.
Kossin, J.P., Camargo, S.J. and Sitkowski, M., 2010. Climate Modulation of North Atlantic Hurricane Tracks. Journal of Climate, **23**(11): 3057-3076.
Koster, R., Dirmeyer, P., Guo, Z., Bonan, G., Chan, E., Cox, P., Gordon, C., Kanae, S., Kowalczyk, E., Lawrence, D., Liu, P., Lu, C., Malyshev, S., McAvaney, B., Mitchell, K., Mocko, D., Oki, T., Oleson, K., Pitman, A., Sud, Y., Taylor, C., Verseghy, D., Vasic, R., Xue, Y., Yamada, T. and Team, G., 2004. Regions of strong coupling between soil moisture and precipitation. Science, **305**(5687): 1138-1140.
Kothawale, D.R., Munot, A.A. and Kumar, K.K., 2010. Surface air temperature variability over India during 1901-2007, and its association with ENSO. Climate Research, **42**(2): 89-104.
Krichak, S.O. and Alpert, P., 2005. Signatures of the NAO in the atmospheric circulation during wet winter months over the Mediterranean region. Theoretical and Applied Climatology, **82**(1-2): 27-39.
Kripalani, R., Oh, J. and Chaudhari, H., 2007a. Response of the East Asian summer monsoon to doubled atmospheric CO2: Coupled climate model simulations and projections under IPCC AR4. Theoretical and Applied Climatology, **87**: 1-28.
Kripalani, R.H., Oh, J.H., Kulkarni, A., Sabade, S.S. and Chaudhari, H.S., 2007b. South Asian summer monsoon precipitation variability: Coupled climate model simulations and projections under IPCC AR4. Theoretical and Applied Climatology, **90**(3-4): 133-159.
Krishna, K.M., 2009. Intensifying tropical cyclones over the North Indian Ocean during summer monsoon – Global warming. Global and Planetary Change, **65**: 12-16.
Krishna Kumar, K., Rajagopalan, B., Hoerling, M., Bates, G. and Cane, M., 2006. Unraveling the mystery of Indian monsoon failure during El Nino. Science, **314**(5796): 115-19.
Krishnamurthy, C.K.B., Lall, U. and Kwon, H.H., 2009. Changing Frequency and Intensity of Rainfall Extremes over India from 1951 to 2003. Journal of Climate, **22**(18): 4737-4746.
Krishnamurthy, V. and Ajayamohan, R.S., 2010. Composite Structure of Monsoon Low Pressure Systems and Its Relation to Indian Rainfall. Journal of Climate, **23**(16): 4285-4305.
Krishnamurti, T.N., Chakraborty, A., Martin, A., Lau, W.K., Kim, K.M., Sud, Y. and Walker, G., 2009. Impact of Arabian Sea pollution on the Bay of Bengal winter monsoon rains. Journal of Geophysical Research-Atmospheres, **114**.
Kruger, L.F., da Rocha, R.P., Reboita, M.S. and Ambrizzi, T., 2011. RegCM3 nested in the HadAM3 scenarios A2 and B2: projected changes in cyclogeneses, temperature and precipitation over South Atlantic Ocean., Climatic Change.
Kubota, H. and Chan, J.C.L., 2009. Interdecadal variability of tropical cyclone landfall in the Philippines from 1902 to 2005. *Geophysical Research Letters*, **36**: L12802.
Kucharski, F., Bracco, A., Yoo, J., Tompkins, A., Feudale, L., Ruti, P. and Dell'Aquila, A., 2009a. A Gill-Matsuno-type mechanism explains the tropical Atlantic influence on African and Indian monsoon rainfall. Quarterly Journal of the Royal Meteorological Society, **135**(640): 569-579.
Kucharski, F., Molteni, F. and Yoo, J., 2006. SST forcing of decadal Indian Monsoon rainfall variability. Geophysical Research Letters, **33**(3): -.
Kucharski, F., Scaife, A.A., Yoo, J.H., Folland, C.K., Kinter, J., Knight, J., Fereday, D., Fischer, A.M., Jin, E.K., Kroger, J., Lau, N.C., Nakaegawa, T., Nath, M.J., Pegion, P., Rozanov, E., Schubert, S., Sporyshev, P.V., Syktus, J., Voldoire, A., Yoon, J.H., Zeng, N. and Zhou, T., 2009b. The CLIVAR C20C project: skill of simulating Indian monsoon rainfall on interannual to decadal timescales. Does GHG forcing play a role? Climate Dynamics, **33**(5): 615-627.
Küttel, M. and Lutterbacher, J., 2011. Multidecadal changes in winter circulation-climate relationship in Europe: frequency variations, within-type modifications, and long-term trends, Climate Dynamics.
Kug, J.-S., Jin, F.-F. and An, S.-I., 2009. Two Types of El Nino Events: Cold Tongue El Nino and Warm Pool El Nino. Journal of Climate, **22**(6): 1499-1515.
Kug, J.S., An, S.I., Ham, Y.G. and Kang, I.S., 2010a. Changes in El Nio and La Nia teleconnections over North Pacific-America in the global warming simulations. Theoretical and Applied Climatology, **100**(3-4): 275-282.
Kug, J.S., Choi, J., An, S.I., Jin, F.F. and Wittenberg, A.T., 2010b. Warm Pool and Cold Tongue El Nino Events as Simulated by the GFDL 2.1 Coupled GCM. Journal of Climate, **23**(5): 1226-1239.
Kuleshov, Y., et al., 2010a. On developing a tropical cyclone archive and climatology for the South Indian and South Pacific Oceans. Indian Ocean Tropical Cyclones and Climate Change Springer.
Kuleshov, Y., et al., 2010b. Trends in tropical cyclones in the South Indian Ocean and the South Pacific Ocean. Journal of Geophysical Research, **115**(D01101).
Kulkarni, A., 2012. Weakening of Indian summer monsoon rainfall in warming environment. Theoretical and Applied Climatology.

Kulkarni, A., Patwardhan, S., Krishna Kumar, K., Ashok, K. and Krishnan, R., 2012. Projected Climate Change over Hindukush-Himalayan Region using high Resolution Regional Climate Model PRECIS. Mountain research development, **submitted**.

Kulkarni, A., Sabade, S.S. and Kripalani, R.H., 2009. Spatial variability of intra-seasonal oscillations during extreme Indian monsoons. International Journal of Climatology, **29**(13): 1945-1955.

Kumar, K., Kamala, K., Rajagopalan, B., Hoerling, M., Eischeid, J., Patwardhan, S., Srinivasan, G., Goswami, B. and Nemani, R., 2011a. The once and future pulse of Indian monsoonal climate. Climate Dynamics, **36**(11-12): 2159-2170.

Kumar, K., Patwardhan, S., Kulkarni, A., Kamala, K., Rao, K. and Jones, R., 2011b. Simulated projections for summer monsoon climate over India by a high-resolution regional climate model (PRECIS). Current Science, **101**(3): 312-326.

Kumar, K.K., Rajagopalan, B. and Cane, M.A., 1999. On the weakening relationship between the Indian monsoon and ENSO. Science, **284**(5423): 2156-2159.

Kumar, M.R.R., Krishnan, R., Sankar, S., Unnikrishnan, A.S. and Pai, D.S., 2009. Increasing Trend of "Break-Monsoon" Conditions Over India-Role of Ocean-Atmosphere Processes in the Indian Ocean. Ieee Geoscience and Remote Sensing Letters, **6**(2): 332-336.

Kumar, P., Kumar, K.R., Rajeevan, M. and Sahai, A.K., 2007. On the recent strengthening of the relationship between ENSO and northeast monsoon rainfall over South Asia. Climate Dynamics, **28**(6): 649-660.

Kumar, V., Deo, R. and Ramachandran, V., 2006. Total rain accumulation and rain-rate analysis for small tropical Pacific islands: a case study of Suva, Fiji. Atmospheric Science Letters, **7**(3): 53-58.

Kunkel, K.E. and al., e., 2008. Observed Changes in Weather and Climate Extremes. In: Weather and Climate Extremes in a Changing Climate. Regions of Focus: North America,
Hawaii, Caribbean, and U.S. Pacific Islands., Washington DC.

KUSAKA, H., HARA, M. and TAKANE, Y., 2012. Urban Climate Projection by the WRF Model at 3-km Horizontal Grid Increment: Dynamical Downscaling and Predicting Heat Stress in the 2070's August for Tokyo, Osaka, and Nagoya Metropolises. 気象集誌, **90**(0): 47-63.

Kusunoki, S. and Arakawa, O., 2012. Change in the precipitation intensity of the East Asian summer monsoon projected by CMIP3 models. Climate Dynamics, **38**: 2055-2072.

Kusunoki, S. and Mizuta, R., 2008. Future changes in the Baiu rain band projected by a 20-km mesh global atmospheric model: sea surface temperature dependence. Sola, **4**: 85-88.

Kutiel, H. and Benaroch, Y., 2002. North Sea-Caspian Pattern (NCP) - an upper level atmospheric teleconnection affecting the Eastern Mediterranean: Identification and definition. Theoretical and Applied Climatology, **71**(1-2): 17-28.

Kuzmina, S.I., Bengtsson, L., Johannessen, O.M., Drange, H., Bobylev, L.P. and Miles, M.W., 2005. The North Atlantic Oscillation and greenhouse-gas forcing. Geophysical Research Letters, **32**(4).

Kvamsto, N., Skeie, P. and Stephenson, D., 2004. Impact of labrador sea-ice extent on the North Atlantic oscillation. International Journal of Climatology, **24**(5): 603-612.

Kwok, R. and Comiso, J.C., 2002. Southern ocean climate and sea ice anomalies associated with the Southern Oscillation. Journal of Climate, **15**(5): 487-501.

L'Heureux, M. and Higgins, R., 2008. Boreal winter links between the Madden-Julian oscillation and the Arctic oscillation. Journal of Climate, **21**(12): 3040-3050.

L'Heureux, M.L. and Thompson, D.W.J., 2006. Observed relationships between the El Niño–Southern Oscillation and the extratropical zonal-mean circulation. Journal of Climate, **19**(2): 276-287.

Laine, A., Kageyama, M., Salas-Melia, D., Ramstein, G., Planton, S., Denvil, S. and Tyteca, S., 2009. An Energetics Study of Wintertime Northern Hemisphere Storm Tracks under 4 x CO(2) Conditions in Two Ocean-Atmosphere Coupled Models. Journal of Climate, **22**(3): 819-839.

Lal, M. and Harasawa, H., 2001. Future climate change scenarios for Asia as inferred from selected coupled atmosphere-ocean global climate models. Journal of the Meteorological Society of Japan, **79**(1): 219-227.

Lal, M., Nozawa, T., Emori, S., Harasawa, H., Takahashi, K., Kimoto, M., Abe-Ouchi, A., Nakajima, T., Takemura, T. and Numaguti, A., 2001. Future climate change: Implications for Indian summer monsoon and its variability. Current Science, **81**(9): 1196-1207.

Lam, H., Kok, M.H. and Shum, K.K.Y., 2012. Benefits from typhoons – the Hong Kong perspective. Weather, **67**: 16-21.

Lambert, S.J. and Fyfe, J.C., 2006. Changes in winter cyclone frequencies and strengths simulated in enhanced greenhouse warming experiments: results from the models participating in the IPCC diagnostic exercise. Climate Dynamics, **26**(7-8): 713-728.

Landsea, C., Feuer, S., Hagen, A., Glenn, D., Sms, J., Perez, R., Chenoweth, M. and Anderson, N., 2012. A Reanalysis of the 1921-30 Atlantic Hurricane Database. Journal of Climate, **25**(3): 865-885.

Landsea, C., Vecchi, G., Bengtsson, L. and Knutson, T., 2010. Impact of Duration Thresholds on Atlantic Tropical Cyclone Counts. Journal of Climate, **23**(10): 2508-2519.

Landsea, C.W., 2007. Counting Atlantic tropical cyclones back to 1900. *Eos Transactions (AGU)*, **88**(18): 197-202.

Landsea, C.W., Harper, B.A., Hoarau, K. and Knaff, J.A., 2006. Can We Detect Trends in Extreme Tropical Cyclones? Science, **313**(5786): 452-454.

Landsea, C.W., Pielke, R.A., Mestas-Nunez, A. and Knaff, J.A., 1999. Atlantic basin hurricanes: Indices of climatic changes. Climatic Change: 89-129.
Lapp, S.L., St. Jacques, J.M., Barrow, E.M. and Sauchyn, D.J., 2011. GCM projections for the Pacifi Decadal Oscillation under greenhouse forcing for the early 21st century. International Journal of Climatology.
Larkin, N.K. and Harrison, D.E., 2005. On the definition of El Nino and associated seasonal average US weather anomalies. Geophysical Research Letters, **32**(13).
Larwanou, M. and Saadou, M., 2011. The role of human interventions in tree dynamics and environmental rehabilitation in the Sahel zone of Niger. Journal of Arid Environments, **75**(2): 194-200.
Latif, M. and Grotzner, A., 2000. The equatorial Atlantic oscillation and its response to ENSO. Climate Dynamics: 213-218.
Latif, M., Keenlyside, N. and Bader, J., 2007. Tropical sea surface tempera- ture, vertical wind shear, and hurricane development. Geophysical Research Letters, **34**: L01710.
Latif, M., Kleeman, R. and Eckert, C., 1997. Greenhouse warming, decadal variability, or El Nino? An attempt to understand the anomalous 1990s. Journal of Climate, **10**(9): 2221-2239.
Lau, K. and Kim, K., 2006. Observational relationships between aerosol and Asian monsoon rainfall, and circulation. Geophysical Research Letters, **33**(21): -.
Lau, K., Ramanathan, V., Wu, G., Li, Z., Tsay, S., Hsu, C., Sikka, R., Holben, B., Lu, D., Tartari, G., Chin, M., Koudelova, R., Chen, H., Ma, Y., Huang, J., Taniguchi, K. and Zhang, R., 2008. The Joint Aerosol-Monsoon Experiment - A new challenge for monsoon climate research. Bulletin of the American Meteorological Society: 369-383.
Lau, K., Shen, S., Kim, K. and Wang, H., 2006a. A multimodel study of the twentieth-century simulations of Sahel drought from the 1970s to 1990s. Journal of Geophysical Research-Atmospheres, **111**(D7): -.
Lau, K. and Weng, H., 1999. Interannual, decadal-interdecadal, and global warming signals in sea surface temperature during 1955-97. Journal of Climate, **12**(5): 1257-1267.
Lau, K. and Wu, H., 2001. Principal modes of rainfall-SST variability of the Asian summer monsoon: A reassessment of the monsoon-ENSO relationship. Journal of Climate, **14**(13): 2880-2895.
Lau, K.M., Kim, M.K. and Kim, K.M., 2006b. Asian summer monsoon anomalies induced by aerosol direct forcing: the role of the Tibetan Plateau. Climate Dynamics, **26**(7-8): 855-864.
Lau, K.M. and Wu, H.T., 2007. Detecting trends in tropical rainfall characteristics, 1979-2003. International Journal of Climatology, **27**(8): 979-988.
Lau, K.M. and Wu, H.T., 2010. Characteristics of Precipitation, Cloud, and Latent Heating Associated with the Madden-Julian Oscillation. Journal of Climate, **23**(3): 504-518.
Lau, N.-C. and Nath, M.-J., 2012. A model study of heat waves over North America: Meteorological aspects and projections for the 21st century. Journal of Climate, **25**(submitted).
Lau, W.K.M., Kim, M.K., Kim, K.M. and Lee, W.S., 2010. Enhanced surface warming and accelerated snow melt in the Himalayas and Tibetan Plateau induced by absorbing aerosols. Environmental Research Letters, **5**(2).
Lavender, S. and Walsh, K., 2011. Dynamically downscaled simulations of Australian region tropical cyclones in current and future climates. Geophysical Research Letters, **38**.
Le Quéré, C., Rodenbeck, C., Buitenhuis, E.T., Conway, T.J., Langenfelds, R., Gomez, A., Labuschagne, C., Ramonet, T., Nakazawa, T., Metzl, N., Gillett, N.P. and Heimann, M., 2007. Saturation of the Southern Ocean CO_2 sink due to recent climate change. Science, **316**: 1735-1738.
LeBarbe, L. and Lebel, T., 1997. Rainfall climatology of the HAPEX-Sahel region during the years 1950-1990. Journal of Hydrology, **189**(1-4): 43-73.
Lebel, T. and Ali, A., 2009. Recent trends in the Central and Western Sahel rainfall regime (1990-2007). Journal of Hydrology, **375**(1-2): 52-64.
Lebel, T., Parker, D., Flamant, C., Bourles, B., Marticorena, B., Mougin, E., Peugeot, C., Diedhiou, A., Haywood, J., Ngamini, J., Polcher, J., Redelsperger, J. and Thorncroft, C., 2010. The AMMA field campaigns: Multiscale and multidisciplinary observations in the West African region. Quarterly Journal of the Royal Meteorological Society, **136**: 8-33.
Leckebusch, G.C., Koffi, B., Ulbrich, U., Pinto, J.G., Spangehl, T. and Zacharias, S., 2006. Analysis of frequency and intensity of European winter storm events from a multi-model perspective, at synoptic and regional scales. Climate Research, **31**(1): 59-74.
Leckebusch, G.C., Ulbrich, U., Froehlich, L. and Pinto, J.G., 2007. Property loss potentials for European midlatitude storms in a changing climate. Geophysical Research Letters, **34**(5).
Lee, J.N., Hameed, S. and Shindell, D.T., 2008. The northern annular mode in summer and its relation to solar activity variations in the GISS ModelE. Journal of Atmospheric and Solar-Terrestrial Physics, **70**(5): 730-741.
Lee, S.-K., Wang, C. and Enfield, D.B., 2010a. On the impact of central Pacific warming events on Atlantic tropical storm activity. Geophysical Research Letters, **37**.
Lee, T., Hobbs, W., Willis, J., Halkides, D., Fukumori, I., Armstrong, E., Hayashi, A., Liu, W., Patzert, W. and Wang, O., 2010b. Record warming in the South Pacific and western Antarctica associated with the strong central-Pacific El Nino in 2009-10. Geophysical Research Letters, **37**.
Lee, T. and McPhaden, M.J., 2010. Increasing intensity of El Nino in the central-equatorial Pacific. Geophysical Research Letters, **37**.

Lei, Y., Hoskins, B. and Slingo, J., 2011. Exploring the Interplay between Natural Decadal Variability and Anthropogenic Climate Change in Summer Rainfall over China. Part I: Observational Evidence. Journal of Climate, **24**(17): 4584-4599.
Lengaigne, M., Boulanger, J.-P., Menkes, C., Delecluse, P. and Slingo, J., 2004. Westerly wind events in the tropical Pacific and their influence on the coupled ocean-atmosphere system: A review. GEOPHYSICAL MONOGRAPH SERIES, **147**: 49-69.
Leslie, L., Karoly, D., Leplastrier, M. and Buckley, B., 2007. Variability of tropical cyclones over the southwest Pacific Ocean using a high-resolution climate model. Meteorology and Atmospheric Physics, **97**(1-4): 171-180.
Levine, R.C. and Turner, A.G., 2011. Dependence of Indian monsoon rainfall on moisture fluxes across the Arabian Sea and the impact of coupled model sea surface temperature biases, Climate Dynamics.
Levitus, S., Matishov, G., Seidov, D. and Smolyar, I., 2009. Barents Sea multidecadal variability. Geophysical Research Letters, **36**: L19604.
Li, B. and Zhou, T.J., 2011. El Nino-Southern Oscillation-related principal interannual variability modes of early and late summer rainfall over East Asia in sea surface temperature-driven atmospheric general circulation model simulations. Journal of Geophysical Research-Atmospheres, **116**: 15.
Li, C., Lu, R. and Dong, B., 2012a. Predictability of the western North Pacific summer climate demonstrated by the coupled models of ENSEMBLES. Climate Dynamics: 1-18.
Li, G. and Ren, B., 2011. Evidence for strengthening of the tropical Pacific ocean surface wind speed during 1979-2001. Theoretical Applied Climatology.
Li, G., Ren, B.H., Yang, C.Y. and Zheng, J.Q., 2010a. Indices of El Nio and El Nio Modoki: An improved El Nio Modoki index. Advances in Atmospheric Sciences, **27**(5): 1210-1220.
Li, H., Dai, A., Zhou, T. and Lu, J., 2010b. Responses of East Asian summer monsoon to historical SST and atmospheric forcing during 1950–2000. Climate dynamics, **34**(4): 501-514.
Li, H.M., Feng, L. and Zhou, T.J., 2011a. Multi-model Projection of July-August Climate Extreme Changes over China under CO2 Doubling. Part I: Precipitation. Advances in Atmospheric Sciences, **28**(2): 433-447.
Li, H.M., Feng, L. and Zhou, T.J., 2011b. Multi-Model Projection of July-August Climate Extreme Changes over China under CO2 Doubling. Part II: Temperature. Advances in Atmospheric Sciences, **28**(2): 448-463.
Li, J., Feng, J. and Li, Y., 2012b. A possible cause of decreasing summer rainfall in northeast Australia. International Journal of Climatology, **32**(7): 995-1005.
Li, J. and Wang, J., 2003. A modified zonal index and its physical sense. Geophysical Research Letters, **30**(12).
Li, J., Wu, Z., Jiang, Z. and He, J., 2010c. Can Global Warming Strengthen the East Asian Summer Monsoon? Journal of Climate, **23**(24): 6696-6705.
Li, J., Yu, R., Yuan, W. and Chen, H., 2011c. Changes in duration-related characteristics of late-summer precipitation over eastern China in the past 40 years. Journal of Climate.
Li, J.B., Xie, S.P., Cook, E.R., Huang, G., D'Arrigo, R., Liu, F., Ma, J. and Zheng, X.T., 2011d. Interdecadal modulation of El Nino amplitude during the past millennium. Nature Climate Change, **1**(2): 114-118.
Li, L., Wang, B. and Zhou, T., 2007. Contributions of natural and anthropogenic forcings to the summer cooling over eastern China: An AGCM study. Geophysical Research Letters, **34**(18).
Li, T., Kwon, M., Zhao, M., Kug, J., Luo, J. and Yu, W., 2010d. Global warming shifts Pacific tropical cyclone location. Geophysical Research Letters, **37**.
Li, T., Liu, P., Fu, X., Wang, B. and Meehl, G., 2006. Spatiotemporal structures and mechanisms of the tropospheric biennial oscillation in the Indo-Pacific warm ocean regions. Journal of Climate, **19**(13): 3070-3087.
Li, T., Tham, C. and Chang, C., 2001. A coupled air-sea-monsoon oscillator for the tropospheric biennial oscillation. Journal of Climate, **14**(5): 752-764.
Li, W., Zhang, P., Ye, J., Li, L. and Baker, P., 2011 Impact of two different types of El Nino events on the Amazon climate and ecosystem productivity. Journal of Plant Ecology, **4**: 91-99.
Li, Y., Cai, W. and Campbell, E.P., 2005. Statistical Modeling of Extreme Rainfall in Southwest Western Australia. Journal of Climate, **18**(6): 852-863.
Li, Y. and Lau, N.-C., 2011. Impact of ENSO on the atmospheric variability over the North Atlantic in late winter-Role of transient eddies. Journal of Climate, **24**(in press).
Li, Y. and Lau, N.-C., 2012a. Contributions of downstream eddy development to the teleconnection between ENSO and atmospheric circulation over the North Atlantic. Journal of Climate, **25**(Submitted).
Li, Y. and Lau, N., 2012b. Impact of ENSO on the Atmospheric Variability over the North Atlantic in Late Winter-Role of Transient Eddies. Journal of Climate, **25**(1): 320-342.
Lian, T. and Chen, D., An evaluation of rotated EOF analysis and its application to tropical Pacific SST variability. Journal of climate.
Lian, T. and Chen, D., 2012. An Evaluation of Rotated EOF Analysis and Its Application to Tropical Pacific SST Variability. Journal of Climate, **25**.
Liang, X.-Z., Kunkel, K.E., Meehl, G.A., Jones, R.G. and Wang, J.X.L., 2008a. Geophysical Research Letters, **35**: L08709.
Liang, X.-Z., Zhu, J., Kunkel, K.E., Ting, M. and Wang, J.X.L., 2008b. Do GCMs Simulate the North American Monsoon Precipitation Seasonal-Interannual Variability? Journal of Climate, **21**: 4424-4448.

Liberato, M.L.R., Pinto, J.G., Trigo, I.F. and Trigo, R.M., 2011. Klaus – an exceptional winter storm over northern Iberia and southern France, Weather.

Liebmann, B., Camargo, S.J., Seth, A., Marengo, J.A., Carvalho, L.M.V., Allured, D., Fu, R. and Vera, C.S., 2007. Onset and end of the rainy season in South America in observations and the ECHAM 4.5 atmospheric general circulation model. Journal of Climate, **20**(10): 2037-2050.

Lienert, F., Fyfe, J.C. and Marryfield, W.J., 2011. Do Climate Models Capture the Tropical Influences on North Pacific sea surface temperature variability? Journal of Climate, **in press**.

Lim, E.-P. and Simmonds, I., 2009. Effect of tropospheric temperature change on the zonal mean circulation and SH winter extratropical cyclones. Climate Dynamics, **33**(1): 19-32.

Lim, Y.-K., Stefanova, L.B., Chan, S.C., Schubert, S.D. and O'Brien, J.J., 2011. High-resolution subtropical summer precipitation derived from dynamical downscaling of the NCEP/DOE reanalysis:how much small-scale information is added by a regional model? Climate Dynamics, **37**: 1061-1080.

Lin, H., Brunet, G. and Derome, J., 2009. An Observed Connection between the North Atlantic Oscillation and the Madden-Julian Oscillation. Journal of Climate, **22**(2): 364-380.

Lin, H. and Wu, Z., 2012. Indian summer monsoon influence on the climate in the North Atlantic–European region, Climate Dynamics, pp. doi:10.1007/s00382-011-1286-8.

Lin, J., 2007. The double-ITCZ problem in IPCC AR4 coupled GCMs: Ocean-atmosphere feedback analysis. Journal of Climate, **20**(18): 4497-4525.

Lin, J., Kiladis, G., Mapes, B., Weickmann, K., Sperber, K., Lin, W., Wheeler, M., Schubert, S., Del Genio, A., Donner, L., Emori, S., Gueremy, J., Hourdin, F., Rasch, P., Roeckner, E. and Scinocca, J., 2006. Tropical intraseasonal variability in 14 IPCC AR4 climate models. Part I: Convective signals. Journal of Climate, **19**(12): 2665-2690.

Lin, J.L., Mapes, B.E., Weickmann, K.M., Kiladis, G.N., Schubert, S.D., Suarez, M.J., Bacmeister, J.T. and Lee, M.I., 2008a. North American monsoon and convectively coupled equatorial waves simulated by IPCC AR4 coupled GCMs. Journal of Climate, **21**(12): 2919-2937.

Lin, J.L., Weickman, K.M., Kiladis, G.N., Mapes, B.E., Schubert, S.D., Suarez, M.J., Bacmeister, J.T. and Lee, M.I., 2008b. Subseasonal variability associated with Asian summer monsoon simulated by 14 IPCC AR4 coupled GCMs. Journal of Climate, **21**(18): 4541-4567.

Linkin, M. and Nigam, S., 2008. The north pacific oscillation-west Pacific teleconnection pattern: Mature-phase structure and winter impacts. Journal of Climate, **21**(9): 1979-1997.

Lintner, B. and Neelin, J., 2008. Eastern margin variability of the South Pacific Convergence Zone. Geophysical Research Letters, **35**.

Lionello, P., Platon, S. and Rodo, X., 2008. Preface: Trends and climate change in the Mediterranean region. Global and Planetary Change, **63**(2-3): 87-89.

Liu, B., Xu, M. and Henderson, M., 2011a. Where have all the showers gone? Regional declines in light precipitation events in China, 1960–2000. International Journal of Climatology, **31**(8): 1177-1191.

Liu, C.M., Wu, M.C., Paul, S., Chen, Y.C., Lin, S.H., Lin, W.S., Lee, Y.C., Hsu, H.H., Tseng, R.Y. and Chen, C.T., 2011b. Super-ensemble of three RCMs for climate projection over East Asia and Taiwan. Theoretical and Applied Climatology, **103**(1): 265-278.

Liu, H.W., Zhou, T.J., Zhu, Y.X. and Lin, Y.H., 2012. The strengthening East Asia summer monsoon since the early 1990s. Chinese Science Bulletin, **57**(13): 1553-1558.

Liu, J., Wang, B., Ding, Q.H., Kuang, X.Y., Soon, W.L. and Zorita, E., 2009a. Centennial Variations of the Global Monsoon Precipitation in the Last Millennium: Results from ECHO-G Model. Journal of Climate, **22**(9): 2356-2371.

Liu, J.P. and Curry, J.A., 2006. Variability of the tropical and subtropical ocean surface latent heat flux during 1989-2000. Geophysical Research Letters, **33**(5).

Liu, Y., Sun, J. and Yang, B., 2009b. The effects of black carbon and sulfate aerosols in China regions on East Asian monsoon. Tellus, **61B**: 642-656.

Liu, Z. and Huang, B., 2000. Cause of tropical Pacific warming trend. Geophysical Research Letters, **27**(13): 1935-1938.

Liu, Z., Vavrus, S., He, F., Wen, N. and Zhong, Y., 2005. Rethinking tropical ocean response to global warming: The enhanced equatorial warming. Journal of Climate, **18**(22): 4684-4700.

Lockwood, M., Harrison, R.G., Woollings, T. and Solanki, S.K., 2010. Are cold winters in Europe associated with low solar activity? Environmental Research Letters, **5**(2).

Loeptien, U., Zolina, O., Gulev, S., Latif, M. and Soloviov, V., 2008. Cyclone life cycle characteristics over the Northern Hemisphere in coupled GCMs. Climate Dynamics, **31**(5): 507-532.

Long, Z., Perrie, W., Gyakum, J., Laprise, R. and Caya, D., 2009. Scenario changes in the climatology of winter midlatitude cyclone activity over eastern North America and the Northwest Atlantic. Journal of Geophysical Research-Atmospheres, **114**.

Lorenz, D.J. and DeWeaver, E.T., 2007. Tropopause height and zonal wind response to global warming in the IPCC scenario integrations. Journal of Geophysical Research-Atmospheres, **112**(D10).

Lorenz, D.J. and Hartmann, D.L., 2003. Eddy-zonal flow feedback in the Northern Hemisphere winter. Journal of Climate, **16**(8): 1212-1227.

Lorenz, P. and Jacob, D., 2010. Validation of temperature trends in the ENSEMBLES regional climate model runs driven by ERA40. Climate Research, **44**(2-3): 167-177.

Loschnigg, J., Meehl, G., Webster, P., Arblaster, J. and Compo, G., 2003. The Asian monsoon, the tropospheric biennial oscillation, and the Indian Ocean zonal mode in the NCAR CSM. Journal of Climate, **16**(11): 1617-1642.

Lu, J., 2009. The dynamics of the Indian Ocean sea surface temperature forcing of Sahel drought. Climate Dynamics, **33**(4): 445-460.

Lu, J., Chen, G. and Frierson, D.M.W., 2008. Response of the Zonal Mean Atmospheric Circulation to El Nino versus Global Warming. Journal of Climate, **21**(22): 5835-5851.

Lu, J., Chen, G. and Frierson, D.M.W., 2010. The Position of the Mid latitude Storm Track and Eddy-Driven Westerlies in Aquaplanet AGCMs. Journal of the Atmospheric Sciences, **67**(12): 3984-4000.

Lu, J., Vecchi, G.A. and Reichler, T., 2007. Expansion of the Hadley cell under global warming. Geophysical Research Letters, **34**(6).

Lu, R. and Fu, Y., 2010. Intensification of East Asian Summer Rainfall Interannual Variability in the Twenty-First Century Simulated by 12 CMIP3 Coupled Models. Journal of Climate: 3316-3331.

Lucarini, V. and Ragone, F., 2011. ENERGETICS OF CLIMATE MODELS: NET ENERGY BALANCE AND MERIDIONAL ENTHALPY TRANSPORT. Reviews of Geophysics, **49**.

Luebbecke, J.F., Boening, C.W., Keenlyside, N.S. and Xie, S.-P., 2010. On the connection between Benguela and equatorial Atlantic Ninos and the role of the South Atlantic Anticyclone. Journal of Geophysical Research-Oceans, **115**.

Luo, Y. and Rothstein, L.M., 2011. Response of the Pacific ocean circulation to climate change. Atmosphere-ocean, **49**: 235-244.

Ma, J. and Xie, S.-P., 2012. Regional patterns of sea surface temperature change: A source of uncertainty in future projections of precipitation and atmospheric circulation, J. Climate.

Madden, R.A. and Julian, P.R., 1994. Observations of the 40-50-day Tropical oscillation-A review. Monthly Weather Review, **122**(5): 814-837.

Magnusdottir, G., Deser, C. and Saravanan, R., 2004. The effects of North Atlantic SST and sea ice anomalies on the winter circulation in CCM3. Part I: Main features and storm track characteristics of the response. Journal of Climate, **17**(5): 857-876.

Mahmood, R. and Li, S., 2012. Asian Black Carbon Influence on East Asian Summer Monsoons. Geophysical Research Abstracts, EGU General Assembly 2012, **14**.

Mahowald, N., 2007. Anthropocene changes in desert area: Sensitivity to climate model predictions. Geophysical Research Letters, **34**(18).

Maloney, E.D., 2012a. Sensitivity of MJO activity to the pattern of climate warming. In: S.-P. Xie (Editor), *J. Adv. Model. Earth Syst.*

Maloney, E.D. and Shaman, J., 2008. Intraseasonal variability of the West African monsoon and Atlantic ITCZ. Journal of Climate, **21**(12): 2898-2918.

Maloney, E.D.a.C., 2012b. North American Climate in CMIP5 Experiments: Part III: Assessment of 21st century Projections. Journal of Climate, **submitted**.

Manatsa, D., Chingombe, W., Matsikwa, H. and Matarira, C.H., 2008. The superior influence of Darwin Sea level pressure anomalies over ENSO as a simple drought predictor for Southern Africa. Theoretical and Applied Climatology, **92**(1): 1-14.

Mandke, S.K., Sahai, A.K., Shinde, M.A., Joseph, S. and Chattopadhyay, R., 2007. Simulated changes in active/break spells during the Indian summer monsoon due to enhanced CO2 concentrations: assessment from selected coupled atmosphere-ocean global climate models. International Journal of Climatology, **27**(7): 837-859.

Mani, N.J., Suhas, E. and Goswami, B.N., 2009. Can global warming make Indian monsoon weather less predictable? Geophysical Research Letters, **36**.

Mann, M.E. and Emanuel, K.A., 2006. Atlantic hurricane trends linked to climate change. Eos Transactions (AGU), **87**(24): 233-241.

Mann, M.E., Emanuel, K.A., Holland, G.J. and Webster, P.J., 2007a. Atlantic tropical cyclones revisited. *Eos Transactions (AGU)*, **88**: 349-350.

Mann, M.E., Sabbatelli, T.A. and Neu, U., 2007b. Evidence for a modest undercount bias in early historical Atlantic tropical cyclone counts. *Geophysical Research Letters*, **34**: L22707.

Manton, M.J., Della-Marta, P.M., Haylock, M.R., Hennessy, K.J., Nicholls, N., Chambers, L.E., Collins, D.A., Daw, G., Finet, A., Gunawan, D., Inape, K., Isobe, H., Kestin, T.S., Lefale, P., Leyu, C.H., Lwin, T., Maitrepierre, L., Ouprasitwong, N., Page, C.M., Pahalad, J., Plummer, N., Salinger, M.J., Suppiah, R., Tran, V.L., Trewin, B., Tibig, I. and Yee, D., 2001. Trends in extreme daily rainfall and temperature in Southeast Asia and the South Pacific: 1961-1998. International Journal of Climatology, **21**(3): 269-284.

Mantua, N.J., Hare, S.R., Zhang, Y., Wallace, J.M. and Francis, R.C., 1997. A Pacific interdecadal climate oscillation with impacts on salmon production. Bulletin of the American Meteorological Society: 1069-1079.

Marchant, R., Mumbi, C., Behera, S. and Yamagata, T., 2007. The Indian Ocean dipole - the unsung driver of climatic variability in East Africa. African Journal of Ecology, **45**(1): 4-16.

Marengo, J., B. Liebmann, A. M. Grimm, V. Misra, P. L. Silva Dias, I. F. A. Cavalcanti, L. M. V. Carvalho, E. H. Berbery, T. Ambrizzi, C. S. Vera, A. C. Saulo, J. Nogues-Paegle, E. Zipser, and, A.S. and Alves, L.M., 2010a. Recent developments on the South American Monsoon system. International Journal of Climatology, **32**(1): 1-21.

Marengo, J.A. and Camargo, C.C., 2008. Surface air temperature trends in Southern Brazil for 1960-2002. International Journal of Climatology, **28**(7): 893-904.

Marengo, J.A., Chou, S.C., Kay, G., Alves, L., Pesquero, J.F., Soares, W.R., Santos, D.C., Lyra, A.A., Sueiro, G., Betts, R., Chagas, D.J., Gomes, J.L., Bustamante, J.F. and Tavares, P., 2011. Development of regional future climate change scenarios in South America using the Eta CPTEC/HadCM3 climate change projections: climatology and regional analyses for the Amazon, São Francisco and the Paraná River basins
Climate Dynamics, **38**(9-10): 1829-1848.

Marengo, J.A., Jones, R., Alves, L.M. and Valverde, M.C., 2009. Future change of temperature and precipitation extremes in South America as derived from the PRECIS regional climate modeling system. International Journal of Climatology, **29**(15): 2241-2255.

Marengo, J.A., Nobre, C.A., Tomasella, J., Oyama, M.D., De Oliveira, G.S., De Oliveira, R., Camargo, H., Alves, L.M. and Brown, I.F., 2008. The drought of Amazonia in 2005. Journal of Climate, **21**(3): 495-516.

Marengo, J.A., Rusticucci, M., Penalba, O. and Renom, M., 2010b. An intercomparison of observed and simulated extreme rainfall and temperature events during the last half of the twentieth century: part 2: historical trends. Climatic Change, **98**(3-4): 509-529.

Mariotti, A. and Dell'Aquila, A., 2011. Decadal climate variability in the Mediterranean region: roles of large-scale forcings and regional processes., Clim. Dyn., pp. doi 10.1007/s00382-011-1056-7.

Mariotti, A., Zeng, N., Yoon, J., Artale, V., Navarra, A., Alpert, P. and Li, L., 2008. Mediterranean water cycle changes: transition to drier 21st century conditions in observations and CMIP3 simulations. Environmental Research Letters, **3**(4).

Marshall, A.G. and Scaife, A.A., 2009. Impact of the QBO on surface winter climate. Journal of Geophysical Research, **114**(D18110).

Marshall, A.G. and Scaife, A.A., 2010. Improved predictability of stratospheric sudden warming events in an atmospheric general circulation model with enhanced stratospheric resolution. Journal of Geophysical Research-Atmospheres, **115**.

Marshall, G.J., 2007. Half-century seasonal relationships between the Southern Annular Mode and Antarctic temperatures. International Journal of Climatology, **27**: 373–383.

Marshall, G.J., di Battista, S., Naik, S.S. and Thamban, M., 2011. Analysis of a regional change in the sign of the SAM-temperature relationship in Antarctica. Climate Dynamics, **36**: 277–287.

Marti, O., Braconnot, P., Dufresne, J.L., Bellier, J., Benshila, R., Bony, S., Brockmann, P., Cadule, P., Caubel, A., Codron, F., de Noblet, N., Denvil, S., Fairhead, L., Fichefet, T., Foujols, M.A., Friedlingstein, P., Goosse, H., Grandpeix, J.Y., Guilyardi, E., Hourdin, F., Idelkadi, A., Kageyama, M., Krinner, G., Levy, C., Madec, G., Mignot, J., Musat, I., Swingedouw, D. and Talandier, C., 2010. Key features of the IPSL ocean atmosphere model and its sensitivity to atmospheric resolution. Climate Dynamics, **34**(1): 1-26.

Marullo, S., Artale, V. and Santoleri, R., 2011a. The SST Multidecadal Variability in the Atlantic-Mediterranean Region and Its Relation to AMO. Journal of Climate, **24**(16): 4385-4401.

Marullo, S., Artale, V. and Santoleri, R., 2011b. The SST Multidecadal Variability in the Atlantic–Mediterranean Region
and Its Relation to AMO, Journal of Climate, pp. 4385-4401.

Mason, S., 2001. El Nino, climate change, and Southern African climate. Environmetrics, **12**(4): 327-345.

Massom, R.A. and Stammerjohn, S.E., 2010. Antarctic sea ice change and variability – Physical and ecological implications. Polar Science, **4**(2): 149-186.

Matsueda, M., Endo, H. and Mizuta, R., 2010. Future change in Southern Hemisphere summertime and wintertime atmospheric blocking simulated using a 20-km-mesh AGCM., Geophysical Research Letters, pp. L02803.

Matsueda, M., Mizuta, R. and Kusunoki, S., 2009. Future change in wintertime atmospheric blocking simulated using a 20-km-mesh atmospheric global circulation model, Journal of Geophysical Research, pp. doi:10.1029/2009JD011919.

Maue, R., 2011. Recent historically low global tropical cyclone activity. Geophysical Research Letters, **38**.

May, W., 2004. Potential future changes in the Indian summer monsoon due to greenhouse warming: analysis of mechanisms in a global time-slice experiment. Climate Dynamics, **22**(4): 389-414.

May, W., 2011. The sensitivity of the Indian summer monsoon to a global warming of 2 degrees C with respect to pre-industrial times. Climate Dynamics, **37**(9-10): 1843-1868.

McAfee, S.A., Russell, J.L. and Goodman, P.J., 2011. Evaluting IPCC AR4 cool-season precipitation simulations and projections for impacts assessment over North America. Climate Dynamics, **37**: 2271-2287.

McBride, J.L. and Nicholls, N., 1983. Seasonal Relationships between Australian Rainfall and the Southern Oscillation. Monthly Weather Review, **111**(10): 1998-2004.

McCabe, G. and Wolock, D., 2010. Long-term variability in Northern Hemisphere snow cover and associations with warmer winters. Climatic Change: 141-153.

McDonald, R., Bleaken, D., Cresswell, D., Pope, V. and Senior, C., 2005. Tropical storms: representation and diagnosis in climate models and the impacts of climate change. Climate Dynamics, **25**(1): 19-36.
McDonald, R.E., 2011. Understanding the impact of climate change on Northern Hemisphere extra-tropical cyclones, Climate Dynamics, pp. 1399-1425.
McKee, D.C., Yuan, X., Gordon, A.L., Huber, B.A. and Dong, Z., 2011. Climate impact on interannual variability of Weddell Sea Bottom Water. Journal of Geophysical Research, **116**(C05020).
McLandress, C. and Shepherd, T.G., 2009. Simulated anthropogenic changes in the Brewer–Dobson circulation, including its extension to high latitudes. Journal of Climate, **22**(6): 1516–1540.
McPhaden, M.J., Lee, T. and McClurg, D., 2011. El Nino and its relationship to changing background conditions in the tropical Pacific Ocean. Geophysical Research Letters, **38**.
Mearns, L.O., Arritt, R., Biner, S., Bukovsky, M., Stain, S. and al., e., 2012. The North American Regional Climate Change Assessment Program: Overview of Phase I Results. Bulletin of the American Meteorological Society, **in press, to appear very soon**.
MEEHL, G., 1987. THE ANNUAL CYCLE AND INTERANNUAL VARIABILITY IN THE TROPICAL PACIFIC AND INDIAN-OCEAN REGIONS. Monthly Weather Review, **115**(1): 27-50.
MEEHL, G., 1994a. COUPLED LAND-OCEAN-ATMOSPHERE PROCESSES AND SOUTH ASIAN MONSOON VARIABILITY. Science, **266**(5183): 263-267.
MEEHL, G., 1994b. INFLUENCE OF THE LAND-SURFACE IN THE ASIAN SUMMER MONSOON - EXTERNAL CONDITIONS VERSUS INTERNAL FEEDBACKS. Journal of Climate, **7**(7): 1033-1049.
Meehl, G. and Arblaster, J., 2002a. Indian monsoon GCM sensitivity experiments testing tropospheric biennial oscillation transition conditions. Journal of Climate, **15**(9): 923-944.
Meehl, G. and Arblaster, J., 2002b. The tropospheric biennial oscillation and Asian-Australian monsoon rainfall. Journal of Climate, **15**(7): 722-744.
Meehl, G. and Arblaster, J., 2011. Decadal Variability of Asian-Australian Monsoon-ENSO-TBO Relationships. Journal of Climate, **24**(18): 4925-4940.
Meehl, G., Arblaster, J. and Collins, W., 2008. Effects of Black Carbon Aerosols on the Indian Monsoon. Journal of Climate, **21**: 2869-2882.
Meehl, G., Arblaster, J. and Loschnigg, J., 2003. Coupled ocean-atmosphere dynamical processes in the tropical Indian and Pacific Oceans and the TBO. Journal of Climate, **16**(13): 2138-2158.
Meehl, G., Hu, A. and Tebaldi, C., 2010. Decadal Prediction in the Pacific Region. Journal of Climate, **23**(11): 2959-2973.
Meehl, G. and Teng, H., 2007. Multi-model changes in El Nino teleconnections over North America in a future warmer climate. Climate Dynamics, **29**(7-8): 779-790.
Meehl, G., Teng, H. and Branstator, G., 2006. Future changes of El Nino in two global coupled climate models. Climate Dynamics, **26**(6): 549-566.
Meehl, G.A., 1997. The south Asian monsoon and the tropospheric biennial oscillation. Journal of Climate, **10**(8): 1921-1943.
Meehl, G.A. and Arblaster, J.M., 2012. Relating the strength of the tropospheric biennial oscillation (TBO) to the phase of the Interdecadal Pacific Oscillation (IPO). Geophysical Research Letters, **submitted**.
Meehl, G.A., Stocker, T.F., Collins, W.D., Friedlingstein, P., Gaye, A.T., Gregory, J.M., Kitoh, A., Knutti, R., Murphy, J.M., Noda, A., Raper, S.C.B., Watterson, I.G., Weaver, A.J. and Zhao, Z.-C., 2007a. Global Climate Projections. In: S. Solomon, D. Qin, M. Manning, Z. Chen, M. Marquis, K.B. Averyt, M. Tignor and H.L. Miller (Editors), Climate Change 2007: The Physical Science Basis. Contribution of Working Group I to the Fourth Assessment Report of the Intergovernmental Panel on Climate Change. Cambridge University Press, Cambridge, United Kingdom and New York, NY, USA.
Meehl, G.A., Stocker, T.F., Collins, W.D., Friedlingstein, P., Gaye, A.T., Gregory, J.M., Kitoh, A., Knutti, R., Murphy, J.M., Noda, A., Raper, S.C.B., Watterson, I.G., Weaver, A.J. and Zhao, Z.-C., 2007b. Global climate projections. Contribution of Working Group I to the Fourth Assessment Report of the Intergovernmental Panel on Climate Change, Climate change 2007: The physical science basis.
Meehl, G.A., Washington, W.M., Arblaster, J.M., Hu, A.X., Teng, H.Y., Tebaldi, C., Sanderson, B.N., Lamarque, J.F., Conley, A., Strand, W.G. and White, J.B., 2012. Climate System Response to External Forcings and Climate Change Projections in CCSM4. Journal of Climate, **25**(11): 3661-3683.
Menary, M., Park, W., Lohmann, K., Vellinga, M., Palmer, M., Latif, M. and Jungclaus, J., 2012. A multimodel comparison of centennial Atlantic meridional overturning circulation variability. Climate Dynamics, **38**(11-12): 2377-2388.
Mendelsohn, R., Emanuel, K., Chonabayashi, S. and Bakkensen, L., 2012. The impact of climate change on global tropical cyclone damage. Nature Climate Change, **2**(3): 205-209.
Mendez, M. and Magana, V., 2010. Regional Aspects of Prolonged Meteorological Droughts over Mexico and Central America. Journal of Climate, **23**(5): 1175-1188.
Mendoza, B., Garcia-Acosta, V., Velasco, V., Jauregui, E. and Diaz-Sandoval, R., 2007. Frequency and duration of historical droughts from the 16th to the 19th centuries in the Mexican Maya lands, Yucatan Peninsula. Climatic Change, **83**(1-2): 151-168.

Meneghini, B., Simmonds, I. and Smith, I.N., 2007. Association between Australian rainfall and the Southern Annular Mode. International Journal of Climatology, **27**(1): 109-121.
Menendez, C.G., de Castro, M., Boulanger, J.P., D'Onofrio, A., Sanchez, E., Sorensson, A.A., Blazquez, J., Elizalde, A., Jacob, D., Le Treut, H., Li, Z.X., Nunez, M.N., Pessacg, N., Pfeiffer, S., Rojas, M., Rolla, A., Samuelsson, P., Solman, S.A. and Teichmann, C., 2010. Downscaling extreme month-long anomalies in southern South America. Climatic Change, **98**(3-4): 379-403.
Metcalfe, S.E., Jones, M.D., Davies, S.J., Noren, A. and MacKenzie, A., 2010. Climate variability over the last two millennia in the North American Monsoon, recorded in laminated lake sediments from Laguna de Juanacatlan, Mexico. The Holocene, **20**(8): 1195-1206.
Miller, R.L., Schmidt, G.A. and Shindell, D.T., 2006. Forced annular variations in the 20th century intergovernmental panel on climate change fourth assessment report models. Journal of Geophysical Research-Atmospheres, **111**(D18).
Ming, Y. and Ramaswamy, V., 2009. Nonlinear Climate and Hydrological Responses to Aerosol Effects. Journal of Climate: 1329-1339.
Minvielle, M. and Garreaud, R.D., 2011. Projecting Rainfall Changes over the South American Altiplano. Journal of Climate, **24**(17): 4577-4583.
Mirza, M.M.Q., 2002. Global warming and changes in the probability of occurrence of floods in Bangladesh and implications. Global Environmental Change-Human and Policy Dimensions, **12**(2): 127-138.
Mitas, C.M. and Clement, A., 2005. Has the Hadley cell been strengthening in recent decades? Geophysical Research Letters, **32**(3).
Mitas, C.M. and Clement, A., 2006. Recent behavior of the Hadley cell and tropical thermodynamics in climate models and reanalyses. Geophysical Research Letters, **33**(1).
Mitchell, T.P. and Wallace, J.M., 1996. ENSO seasonality: 1950-78 versus 1979-92. Journal of Climate, **9**(12): 3149-3161.
Mizuta, R., 2012. Intensification of extratropical cyclones associated with the polar jet change in the CMIP5 global warming projections. Geophys. Res. Lett.
Mizuta, R., Matsueda, M., Endo, H. and Yukimoto, S., 2011. Future Change in Extratropical Cyclones Associated with Change in the Upper Troposphere. Journal of Climate, **24**(24): 6456-6470.
Mo, K.C., 2010. Interdecadal Modulation of the Impact of ENSO on Precipitation and Temperature over the United States. Journal of Climate, **23**(13): 3639-3656.
Mo, K.C. and Higgins, R.W., 1998. The Pacific-South American modes and tropical convection during the Southern Hemisphere winter. Monthly Weather Review, **126**(6): 1581–1596.
Moberg, A. and al., e., 2006. Indices for daily temperature and precipitation extremes in Europe analyzed for the period 1901-2000, Journal of Geophysical Research-Atmospheres.
Mock, C.J. and Brunelle-Daines, A.R., 1999. A modern analogue of western United States summer palaeoclimate at 6000 years before present. The Holocene, **9**(5): 541-545.
Mohapatra, M., Bandyopadhyay, B.K. and Tyagi, A., 2011. Best track parameters of tropical cyclones over the North Indian Ocean: a review. Natural Hazards.
Mohino, E., Janicot, S. and Bader, J., 2011. Sahel rainfall and decadal to multi-decadal sea surface temperature variability. Climate Dynamics, **37**(3-4): 419-440.
Moise, A. and Delage, F., 2011. New climate model metrics based on object-orientated pattern matching of rainfall. Journal of Geophysical Research-Atmospheres, **116**.
Moise, A.F., Colman, R.A. and Brown, J.R., 2012. Behind uncertainties in projections of Australian tropical climate: Analysis of 19 CMIP3 models. Journal of Geophysical Research-Atmospheres, **117**.
Moise, A.F., Colman, R.A., Zhang, H. and participating, C.m.g., 2005. Coupled model simulations of current Australian surface climate and its changes under greenhouse warming: an analysis of 18 CMIP2 models. Australian Meteorological Magazine, **54**(4): 291-307.
Monaghan, A.J. and Bromwich, D.H., 2008. Advances in Describing Recent Antarctic Climate Variablity. Bulletin of the American Meteorological Society, **89**(9): 1295-1306.
Monaghan, A.J., Bromwich, D.H., Chapman, W. and Comiso, J.C., 2008. Recent variability and trends of Antarctic near-surface temperature. J. Geophys. Res., **113**(D4): D04105.
Monahan, A.H., Fyfe, J.C., Ambaum, M.H.P., Stephenson, D.B. and North, G.R., 2009. Empirical Orthogonal Functions: The Medium is the Message. Journal of Climate, **22**(24): 6501-6514.
Monahan, A.H., Pandolfo, L. and Fyfe, J.C., 2001. The preferred structure of variability of the Northern Hemisphere atmospheric circulation. Geophysical Research Letters, **28**: 1019–1022.
MOOLEY, D. and PARTHASARATHY, B., 1983. VARIABILITY OF THE INDIAN-SUMMER MONSOON AND TROPICAL CIRCULATION FEATURES. Monthly Weather Review, **111**(5): 967-978.
Morgenstern, O., Akiyoshi, H., Bekki, S., Braesicke, P., Butchart, N., Chipperfield, M.P., Cugnet, D., Deushi, M., Dhomse, S.S., Garcia, R.R., Gettelman, A., Gillett, N.P., Hardiman, S.C., Jumelet, J., Kinnison, D.E., Lamarque, J.F., Lott, F., Marchand, M., Michou, M., Nakamura, T., Olivie, D., Peter, T., Plummer, D., Pyle, J.A., Rozanov, E., Saint-Martin, D., Scinocca, J.F., Shibata, K., Sigmond, M., Smale, D., Teyssedre, H., Tian, W., Voldoire, A. and Yamashita, Y., 2010. Anthropogenic forcing of the Northern Annular Mode in CCMVal-2 models. Journal of Geophysical Research-Atmospheres, **115**.

Moron, V., Robertson, A.W. and Boer, R., 2009. Spatial Coherence and Seasonal Predictability of Monsoon Onset over Indonesia. Journal of Climate, **22**(3): 840-850.
Moron, V., Robertson, A.W. and Qian, J.-H., 2010. Local versus regional-scale characteristics of monsoon onset and post-onset rainfall over Indonesia. Climate Dynamics, **34**(2-3): 281-299.
Moss, R.H., Edmonds, J.A., Hibbard, K.A., Manning, M.R., Rose, S.K., van Vuuren, D.P., Carter, T.R., Emori, S., Kainuma, M., Kram, T., Meehl, G.A., Mitchell, J.F.B., Nakicenovic, N., Riahi, K., Smith, S.J., Stouffer, R.J., Thomson, A.M., Weyant, J.P. and Wilbanks, T.J., 2010. The next generation of scenarios for climate change research and assessment. Nature, **463**(7282): 747-756.
Müller, W.A. and Roeckner, E., 2008. ENSO teleconnections in projections of future climate in ECHAM5/MPI-OM, Climate Dynamics, pp. 533-549.
Muller, W.A. and Roeckner, E., 2006. ENSO impact on midlatitude circulation patterns in future climate change projections. Geophysical Research Letters, **33**(5).
Mumby, P., Vitolo, R. and Stephenson, D., 2011. Temporal clustering of tropical cyclones and its ecosystem impacts. Proceedings of the National Academy of Sciences of the United States of America, **108**(43): 17626-17630.
Murakami, H., Mizuta, R. and Shindo, E., 2011a. Future changes in tropical cyclone activity projected by multi-physics and multi-SST ensemble experiments using the 60-km-mesh MRI-AGCM. Climate Dynamics.
Murakami, H. and Sugi, M., 2010. Effect of Model Resolution on Tropical Cyclone Climate Projections. Sola, **6**: 73-76.
Murakami, H. and Wang, B., 2010. Future Change of North Atlantic Tropical Cyclone Tracks: Projection by a 20-km-Mesh Global Atmospheric Model. Journal of Climate, **23**(10): 2699-2721.
Murakami, H., Wang, B. and Kitoh, A., 2011b. Future Change of Western North Pacific Typhoons: Projections by a 20-km-Mesh Global Atmospheric Model. Journal of Climate, **24**(4): 1154-1169.
Murakami, H., Wang, Y., Yoshimura, H., Mizuta, R., Sugi, M., Shindo, E., Adachi, Y., Yukimoto, S., Hosaka, M., Kusunoki, S., Ose, T. and Kitoh, A., 2012. Future Changes in Tropical Cyclone Activity Projected by the New High-Resolution MRI-AGCM. Journal of Climate, **25**(9): 3237-3260.
Murata, A., Nakano, M., Kanada, S., Kurihara, K. and Sasaki, H., 2012. Summertime temperature extremes over Japan in the late 21st century projected by a high-resolution regional climate model. Journal of the Meteorological Society of Japan, **90A**: 101-122.
Murphy, B.F. and Timbal, B., 2008. A review of recent climate variability and climate change in southeastern Australia. International Journal of Climatology, **28**(7): 859-879.
Na, H., Jang, B.-G., Choi, W.-M. and Kim, K.-Y., 2011. Statistical simulations of the future 50-year statistics of cold-tongue El Niño and warm-pool El Niño. Asia-Pacific Journal of Atmospheric Sciences, **47**: 223-233.
Nakamura, H., 1992. Midwinter Suppression of Baroclinic Wave Activity in the Pacific. **49 (17)**: 1629-1642.
Nanjundiah, R., Vidyunmala, V. and Srinivasan, J., 2005. The impact of increase in CO2 on the simulation of tropical biennial oscillations (TBO) in 12 coupled general circulation models. Atmospheric Science Letters, **6**(3): 183-191.
Naylor, R.L., Battisti, D.S., Vimont, D.J., Falcon, W.P. and Burke, M.B., 2007. Assessing risks of climate variability and climate change for Indonesian rice agriculture. Proceedings of the National Academy of Sciences of the United States of America, **104**(19): 7752-7757.
Neale, R. and Slingo, J., 2003. The maritime continent and its role in the global climate: A GCM study. Journal of Climate, **16**(5).
Neelin, J., Chou, C. and Su, H., 2003. Tropical drought regions in global warming and El Nino teleconnections. Geophysical Research Letters, **30**(24): -.
Neelin, J.D., Langenbrunner, B., Meyerson, J.E., Hall, A. and Berg, N., 2012. California winter precipitation change under global warming in CMIP5 models. Journal of Climate, **submitted**.
Neelin, J.D., Munnich, M., Su, H., Meyerson, J.E. and Holloway, C.E., 2006. Tropical drying trends in global warming models and observations. Proceedings of the National Academy of Sciences, **103**: 6110-6115.
Newman, M., Shin, S. and Alexander, M., 2011. Natural variation in ENSO flavors. Geophysical Research Letters, **38**.
Newton, A., Thunell, R. and Stott, L., 2006. Climate and hydrographic variability in the Indo-Pacific Warm Pool during the last millennium. Geophysical Research Letters, **33**(19): -.
Ngo-Duc, T., Kieu, C., Phan-Van, T. and Thatcher, M., 2012. Evaluating performance of three regional climate models and their ensemble combination in projecting future climate in Vietnam. Climate Research: submitted.
Nguyen, K., Katzfey, J. and McGregor, J., 2012. Global 60 km simulations with CCAM: evaluation over the tropics. *Climate Dynamics*, **39**, 637-654.
NICHOLLS, N., 1978. AIR-SEA INTERACTION AND QUASI-BIENNIAL OSCILLATION. Monthly Weather Review, **106**(10): 1505-1508.
Nicholls, N., 2004. The changing nature of Australian droughts. Climatic Change, **63**(3): 323-336.
Nicholls, N., 2010. Local and remote causes of the southern Australian autumn-winter rainfall decline, 1958-2007. Climate Dynamics, **34**(6): 835-845.
Nicholls, N., Landsea, C. and Gill, J., 1998. Recent trends in Australian region tropical cyclone activity. Meteorology and Atmospheric Physics, **65**(3-4): 197-205.
Nieto-Ferreira, R. and Rickenbach, T., 2010. Regionality of monsoon onset in South America: A three-stage conceptual model. International Journal of Climatology(DOI: 10.1002/joc.2161).

Nigam, S., 2003. Teleconnections. In: J.A.P. J. R. Holton, and J. A. Curry, Eds. (Editor), *Encyclop*edia of Atmospheric Sciences,. Academic Press, pp. 2243–2269.
Ninomiya, K., 2012. Characteristics of intense rainfalls over southwestern Japan in the Baiu season in the CMIP3 20th century simulation and 21st century projection. Journal of the Meteorological Society of Japan, **90A**: 327-338.
Nishii, K., Miyasaka, T., Kosaka, Y. and Nakamura, H., 2009. Reproducibility and Future Projection of the Midwinter Storm-Track Activity over the Far East in the CMIP3 Climate Models in Relation to "Haru-Ichiban" over Japan. Journal of the Meteorological Society of Japan: 581-588.
Niyogi, D., Kishtawal, C., Tripathi, S. and Govindaraju, R.S., 2010. Observational evidence that agricultural intensification and land use change may be reducing the Indian summer monsoon rainfall. Water Resources Research, **46**.
Nogués-Paegle, J., Byerle, L.A. and Mo, K.C., 2000. Intraseasonal modulation of South American summer precipitation. Monthly Weather Review, **128**: 837-849.
Nunez, M.N., Solman, S.A. and Cabre, M.F., 2009. Regional climate change experiments over southern South America. II: Climate change scenarios in the late twenty-first century. Climate Dynamics, **32**(7-8): 1081-1095.
O'Gorman, P.A., 2010. Understanding the varied response of the extratropical storm tracks to climate change. Proceedings of the National Academy of Sciences of the United States of America, **107**(45): 19176-19180.
O'Gorman, P.A. and Schneider, T., 2008. Energy of Midlatitude Transient Eddies in Idealized Simulations of Changed Climates. Journal of Climate, **21**(22): 5797-5806.
Ogasawara, N., Kitoh, A., Yasunari, T. and Noda, A., 1999. Tropospheric biennial oscillation of ENSO-monsoon system in the MRI coupled GCM. Journal of the Meteorological Society of Japan, **77**(6): 1247-1270.
Okamoto, K., Sato, K. and Akiyoshi, H., 2011. A study on the formation and trend of the Brewer-Dobson circulation. Journal of Geophysical Research, **116**(D10117).
Okumura, Y. and Xie, S.P., 2006. Some overlooked features of tropical Atlantic climate leading to a new Nino-like phenomenon. Journal of Climate, **19**(22): 5859-5874.
Okumura, Y.M., Ohba, M., Deser, C. and Ueda, H., 2011. A Proposed Mechanism for the Asymmetric Duration of El Niño and La Niña. Journal of Climate.
Okumura, Y.M., Schneider, D., Deser, C. and Wilson, R., 2012. Decadal-interdecadal climate variability over Antarctica and linkages to the tropics: Analysis of ice core, instrumental, and tropical proxy data. Journal of Climate: in press.
Onol, B. and Semazzi, F., 2009. Regionalization of Climate Change Simulations over the Eastern Mediterranean. Journal of Climate, **22**(8): 1944-1961.
Oouchi, K., Yoshimura, J., Yoshimura, H., Mizuta, R., Kusunoki, S. and Noda, A., 2006. Tropical cyclone climatology in a global-warming climate as simulated in a 20 km-mesh global atmospheric model: Frequency and wind intensity analyses. Journal of the Meteorological Society of Japan, **84**(2): 259-276.
Ose, T. and Arakawa, O., 2011. Uncertainty of Future Precipitation Change Due to Global Warming Associated with Sea Surface Temperature Change in the Tropical Pacific. Journal of Meteorological Society of Japan, **89**(5): 539-552.
OSHIMA, K., TANIMOTO, Y. and XIE, S.P., 2012. Regional patterns of wintertime SLP change over the North Pacific and their uncertainty in CMIP3 multi-model projections. 気象集誌, **90**(0): 385-396.
Ouzeau, G., Cattiaux, J., Douville, H., Ribes, A. and Saint-Martin, D., 2011. European cold winter 2009-2010: How unusual in the instrumental record and how reproducible in the ARPEGE-Climat model? Geophysical research Letters, **38**: 6.
Overland, J.E., Wang, M. and Salo, S., 2008. The recent Arctic warm period. Tellus Series A, **60**: 589-597.
Overland, J.E. and Wang, M.Y., 2005. The third Arctic climate pattern: 1930s and early 2000s. Geophysical Research Letters, **32**: L23808.
Paeth, H., Born, K., Girmes, R., Podzun, R. and Jacob, D., 2009. Regional Climate Change in Tropical and Northern Africa due to Greenhouse Forcing and Land Use Changes. Journal of Climate, **22**(1): 114-132.
Paeth, H., Hall, N., Gaertner, M., Alonso, M., Moumouni, S., Polcher, J., Ruti, P., Fink, A., Gosset, M., Lebel, T., Gaye, A., Rowell, D., Moufouma-Okia, W., Jacob, D., Rockel, B., Giorgi, F. and Rummukainen, M., 2011. Progress in regional downscaling of west African precipitation. Atmospheric Science Letters, **12**(1): 75-82.
Paeth, H. and Thamm, H., 2007. Regional modelling of future African climate north of 15 degrees S including greenhouse warming and land degradation. Climatic Change, **83**(3): 401-427.
Palmer, T.N., 1999. A nonlinear dynamical perspective on climate prediction. Journal of Climate, **12**: 575–591.
Parker, D., Folland, C., Scaife, A., Knight, J., Colman, A., Baines, P. and Dong, B., 2007. Decadal to multidecadal variability and the climate change background. J. Geophys. Res., **112**(D18): D18115.
Patricola, C. and Cook, K., 2010. Northern African climate at the end of the twenty-first century: an integrated application of regional and global climate models. Climate Dynamics, **35**(1): 193-212.
Patricola, C. and Cook, K., 2011. Sub-Saharan Northern African climate at the end of the twenty-first century: forcing factors and climate change processes. Climate Dynamics, **37**(5-6): 1165-1188.
Pattanaik, D.R. and Rajeevan, M., 2010. Variability of extreme rainfall events over India during southwest monsoon season. Meteorological Applications, **17**(1): 88-104.
Pavan, V., Tomozeiu, R., Cacciamani, C. and Di Lorenzo, M., 2008. Daily precipitation observations over Emilia-Romagna: mean values and extremes., International Journal of Climatology, pp. 2065-2079.

Pavelsky, T., Kapnick, S. and Hall, A., 2011. Accumulation and melt dynamics of snowpack from a multiresolution regional climate model in the central Sierra Nevada, California. Journal of Geophysical Research-Atmospheres, **116**: D16115.
Paz, S., Tourre, Y. and Planton, S., 2003. North Africa-West Asia (NAWA) sea-level pressure patterns and their linkages with the Eastern Mediterranean (EM) climate. Geophysical Research Letters, **30**(19).
Pederson, e.a., 2011. The unusual nature of recent snowpack declines in the North American Cordillera. Science, **333**: 332-335.
Peduzzi, P., Chatenoux, B., Dao, H., De Bono, A., Herold, C., Kossin, J., Mouton, F. and Nordbeck, O., 2012. Global trends in tropical cyclone risk. Nature Climate Change, **2**(4): 289-294.
Perkins, S., 2011. Biases and Model Agreement in Projections of Climate Extremes over the Tropical Pacific. Earth Interactions, **15**.
Perkins, S., Irving, D., Brown, J., Power, S., Moise, A., Colman, R. and Smith, I., 2012. CMIP3 ensemble climate projections over the western tropical Pacific based on model skill. Climate Research, **51**(1): 35-58.
Perlwitz, J., Pawson, S., Fogt, R.L., Nielsen, J.E. and Neff, W.D., 2008. Impact of stratospheric ozone hole recovery on Antarctic climate. Geophysical Research Letters, **35**(L08714).
Petersen, K.L., 1994. A Warm and Wet Little Climatic Optimum and a Cold and Dry Little Ice Age in the Southern Rocky Mountains, U.S.A. Climatic Change, **26**: 243-269.
Pezzulli, S., Stephenson, D. and Hannachi, A., 2005. The variability of seasonality. Journal of Climate, **18**(1): 71-88.
Philander, S., 1990. El Niño, La Niña, and the Southern Oscillation. Academic Press, 289 pp.
Philip, S. and Van Oldenborgh, G., 2006. Shifts in ENSO coupling processes under global warming. Geophysical Research Letters, **33**(11).
Picard, G., Domine, F., Krinner, G., Arnaud, L. and Lefebvre, E., 2012. Inhibition of the positive snow-albedo feedback by precipitation in interior Antarctica Nature Climate Change.
Pierce, D., Barnett, T., Hidalgo, H., Das, T., Bonfils, C., Santer, B., Bala, G., Dettinger, M., Cayan, D., Mirin, A., Wood, A. and Nozawa, T., 2008. Attribution of Declining Western US Snowpack to Human Effects. Journal of Climate: 6425-6444.
Pinto, J. and Raible, C., 2012. Past and recent changes in the North Atlantic oscillation, Climate Change, pp. 79-90.
Pinto, J.G., Karreman, M.K., Born, K., Della-Marta, P.M. and Klawa, M., 2012. Loss potentials associated with European windstorms under future climate conditions. Climate Research, **In press**.
Pinto, J.G., Ulbrich, U., Leckebusch, G.C., Spangehl, T., Reyers, M. and Zacharias, S., 2007. Changes in storm track and cyclone activity in three SRES ensemble experiments with the ECHAM5/MPI-OM1 GCM. Climate Dynamics, **29**(2-3): 195-210.
Plumb, R.A., 1977. The interaction of two internal waves with the mean flow: Implications for the theory of the quasi-biennial oscillation. Journal of the Atmospheric Sciences, **34**: 1847-1858.
Pohl, B., Fauchereau, N., Reason, C. and Rouault, M., 2010. Relationships between the Antarctic Oscillation, the Madden - Julian Oscillation, and ENSO, and Consequences for Rainfall Analysis. Journal of Climate, **23**(2): 238-254.
Polcher, J., Parker, D.J., Gaye, A., Diedhiou, A., Eymard, L., Fierli, F., Genesio, L., Höller, H., Janicot, S., Lafore, J.-P., Karambiri, H., Lebel, T., Redelsperger, J.-L., Reeves, C.E., Ruti, P., Sandholt, I. and Thorncroft, C., 2011. AMMA's contribution to the evolution of prediction and decision-making systems for West Africa. Atmospheric Science Letters, **12**(1): 2-6.
Polvani, L.M., Previdi, M. and Deser, C., 2011. Large cancellation, due to ozone recovery, of future Southern Hemisphere atmospheric circulation trends. Geophysical Research Letters, **38**(L04707).
Polyakov, I., Alexeev, V., Bhatt, U., Polyakova, E. and Zhang, X., 2010. North Atlantic warming: patterns of long-term trend and multidecadal variability. Climate Dynamics, **34**(2-3): 439-457.
Polyakov, I.V., Bekryaev, R.V., Alekseev, G.V., Bhatt, U.S., Colony, R.L., Johnson, M.A., Maskshtas, A.P. and Walsh, D., 2003. Variability and Trends of Air Temperature and Pressure in the Maritime Arctic, 1875–2000. Journal of Climate, **16**: 2067-2077.
Poore, R.Z., Pavich, M.J. and Grissino-Mayer, H.D., 2005. Record of the North American southwest monsoon from Gulf of Mexico sediment cores. Geology, **33**: 209-212.
Popova, V.V. and Shmakin, A.B., 2010. Regional structure of surface-air temperature fluctuatoons in Northern Eurasia in the latter half of the 20th and early 21st centuries. Izvestiya Atmospheric and Oceanic Physics, **46**: 144-158.
Power, S., Casey, T., Folland, C., Colman, A. and Mehta, V., 1999a. Inter-decadal modulation of the impact of ENSO on Australia. Climate Dynamics, **15**(5): 319-324.
Power, S. and Colman, R., 2006. Multi-year predictability in a coupled general circulation model. Climate Dynamics, **26**(2-3): 247-272.
Power, S., Haylock, M., Colman, R. and Wang, X., 2006. The predictability of interdecadal changes in ENSO activity and ENSO teleconnections. Journal of Climate, **19**(19): 4755-4771.
Power, S.B., Caey, T., Folland, C., Colman, A. and Mehta, V., 1999b. Interdecadal modulation of the Impact of ENSO on Australia. Climate Dynamics, **15**: 5.
Power, S.B. and Smith, I.N., 2007. Weakening of the Walker Circulation and apparent dominance of El Nino both reach record levels, but has ENSO really changed? Geophysical Research Letters, **34**(18): L18702.

Prasanna, V. and Annamalai, H., 2012. Moist Dynamics of Extended Monsoon Breaks over South Asia. Journal of Climate, **25**(11): 3810-3831.
Previdi, M. and Liepert, B.G., 2007. Annular modes and Hadley cell expansion under global warming. Geophysical Research Letters, **34**(L22701): 5.
Pritchard, H.D., Ligtenberg, S.R.M., Fricker, H.A., Vaughan, D.G., van den Broeke, M.R. and Padman, L., 2012. Antarctic ice-sheet loss driven by basal melting of ice shelves. Nature, **484**(7395): 502-505.
Qian, H., Suxiang, Y. and Yaocun, Z., 2012. Analysis of local air-sea interaction in East Asia using a regional air-sea coupled model. J Climate, **25(2)**: 767-776.
Qian, J.-H., 2008. Why precipitation is mostly concentrated over islands in the Maritime Continent. Journal of the Atmospheric Sciences, **65**(4): 1428-1441.
Qian, J.-H., Robertson, A.W. and Moron, V., 2010a. Interactions among ENSO, the Monsoon, and Diurnal Cycle in Rainfall Variability over Java, Indonesia. Journal of the Atmospheric Sciences, **67**(11): 3509-3524.
Qian, J.-H. and Zubair, L., 2010. The effects of grid spacing and domain size on the quality of ensemble regional climate downscaling over South Asia during the northeasterly monsoon. Monthly Weather Review, **138**: 2780-2802.
Qian, W., Fu, J. and Yan, Z., 2007a. Decrease of light rain events in summer associated with a warming environment in China during 1961–2005. Geophysical Research Letters, **34**(11): L11705.
Qian, Y., Flanner, M.G., Leung, L.R. and Wang, W., 2011. Sensitivity studies on the impacts of Tibetan Plateau snowpack pollution on the Asian hydrological cycle and monsoon climate. Atmospheric Chemistry and Physics, **11**(5): 1929-1948.
Qian, Y., Ghan, S.J. and Leung, L.R., 2010b. Downscaling hydroclimate changes over the Western US based on CAM subgrid scheme and WRF regional climate simulations. International Journal of Climatology, **30**: 675-693.
Qian, Y., Gong, D., Fan, J., Leung, L.R., Bennartz, R., Chen, D. and Wang, W., 2009a. Heavy pollution suppresses light rain in China: Observations and modeling. J. Geophys. Res, **114**: D00K02.
Qian, Y., Kaiser, D., Leung, L. and Xu, M., 2006. More frequent cloud-free sky and less surface solar radiation in China from 1955 to 2000. Geophysical Research Letters: -.
Qian, Y., L.R., G., Leung, L.R. and Ghan, S.J., 2009b. Journal of Geophysical Research, **114**.
Qian, Y., Wang, W., Leung, L. and Kaiser, D., 2007b. Variability of solar radiation under cloud-free skies in China: The role of aerosols. Geophysical Research Letters: -.
Quadrelli, R. and Wallace, J.M., 2004. A simplified linear framework for interpreting patterns of Northern Hemisphere wintertime climate variability. Journal of Climate, **17**(19): 3728-3744.
R, B., Fan, J., Rausch, J., Leung, L. and Heidinger, A., 2011. Pollution from China increases cloud droplet number, suppresses rain over the East China Sea. Geophysical Research Letters, **38**(Article No. L09704).
Raia, A. and Cavalcanti, I.F.A., 2008. The Life Cycle of the South American Monsoon System. Journal of Climate, **21**(23): 6227-6246.
Raible, C., 2007. On the relation between extremes of midlatitude cyclones and the atmospheric circulation using ERA40. Geophysical Research Letters, **34**(7).
Raible, C.C., Della-Marta, P.M., Schwierz, C., Wernli, H. and Blender, R., 2008. Northern hemisphere extratropical cyclones: A comparison of detection and tracking methods and different reanalyses. Monthly Weather Review, **136**(3): 880-897.
Raible, C.C., Ziv, B., Saaroni, H. and Wild, M., 2010. Winter synoptic-scale variability over the Mediterranean Basin under future climate conditions as simulated by the ECHAM5. Climate Dynamics, **35**(2-3): 473-488.
Rajeevan, M., Bhate, J. and Jaswal, A.K., 2008. Analysis of variability and trends of extreme rainfall events over India using 104 years of gridded daily rainfall data. Geophysical Research Letters, **35**(18).
Rajendran, K. and Kitoh, A., 2008. Indian summer monsoon in future climate projection by a super high-resolution global model. **95**: 1560-1569.
Ramanathan, V. and Carmichael, G., 2008. Global and regional climate changes due to black carbon. Nature Geoscience, **1**(4): 221-227.
Ramanathan, V., Chung, C., Kim, D., Bettge, T., Buja, L., Kiehl, J., Washington, W., Fu, Q., Sikka, D. and Wild, M., 2005. Atmospheric brown clouds: Impacts on South Asian climate and hydrological cycle. Proceedings of the National Academy of Sciences of the United States of America: 5326-5333.
Ramesh, K.V. and Goswami, P., 2007a. Reduction in temporal and spatial extent of the Indian summer monsoon. Geophysical Research Letters, **34**(23).
Ramesh, K.V. and Goswami, P., 2007b. The shrinking Indian summer monsoon. CSIR Centre for Mathematical Modelling and Computer Simulation. Research Report RR CM 0709.
Ramsay, H.A. and Sobel, A.H., 2011. The effects of relative and absolute sea surface temperature on tropical cyclone potential intensity using a single column model. Journal of Climate: In press.
Randel, W., Garcia, R., Calvo, N. and Marsh, D., 2009. ENSO influence on zonal mean temperature and ozone in the tropical lower stratosphere. Geophysical Research Letters, **36**.
Randles, C.A. and Ramaswamy, V., 2008. Absorbing aerosols over Asia: A Geophysical Fluid Dynamics Laboratory general circulation model sensitivity study of model response to aerosol optical depth and aerosol absorption. Journal of Geophysical Research-Atmospheres, **113**(D21).

Rao, V.B., Ferreira, C.C., Franchito, S.H. and Ramakrishna, S.S.V.S., 2008. In a changing climate weakening tropical easterly jet induces more violent tropical storms over the north Indian Ocean. Geophysical Research Letters, **35**: L15710.

Raphael, M. and Holland, M., 2006. Twentieth century simulation of the southern hemisphere climate in coupled models. Part 1: large scale circulation variability. Climate Dynamics: 217-228.

Rappin, E.D., Nolan, D.S. and Emanuel, K.A., 2010. Thermodynamic control of tropical cyclogenesis in environments of radiative-convective equilibrium with shear. Quarterly Journal of the Royal Meteorological Society, **136**: 1954-1971.

Rasmussen, R.J.a.C., 2011. High-resolution coupled climate runoff simulations of seasonal snowfall over Colorado; A process study of current and warmer climate. Journal of Climate, **24**: 3015-3048.

Rasul, G., A, Mahmood, A.S. and Khan, S.I., 2012. Vulnerability of the Indus Delta to Climate Change in Pakistan. Journal of Meteorology, **8**(6).

Rauniyar, S.P. and Walsh, K.J.E., 2011. Scale Interaction of the Diurnal Cycle of Rainfall over the Maritime Continent and Australia: Influence of the MJO. Journal of Climate, **24**(2): 325-348.

Rauscher, S.A., Giorgi, F., Diffenbaugh, N.S. and Seth, A., 2008. Extension and Intensification of the Meso-American mid-summer drought in the twenty-first century. Climate Dynamics, **31**(5): 551-571.

Rawlins, M.A., et al., 2010. Analysis of the Arctic System for Freshwater Cycle Intensification: Observations and Expectations. Journal of Climate, **23**: 5715-5737.

Re, M. and Barros, V., 2009. Extreme rainfalls in SE South America. Climatic Change, **96**: 119-136.

Reason, C.J.C., Florenchie, **P.**, Rouault, M. and **V**eitch, J., 2006. Influences of large scale climate modes and Agulhas System variability on the BCLME region. Elsevier, Amsterdam, *Benguela: Predicting a Large Marine Ecosystem*, pp. 225–241.

Reboita, M.S., Ambrizzi, T. and da Rocha, R.P., 2009. Relationship between the southern annular mode and southern hemisphere atmospheric systems, Revista Brasileira de Meteorologia.

Reisinger, A., Mullan, A.B., Manning, M., Wratt, D. and Nottage, R., 2010. Global & local climate change scenarios to support adaptation in New Zealand. In: R.A.C. Nottage, D.S. Wratt, J.F. Bornman and K. Jones (Editors), Climate Change Adaptation in New Zealand: Future scenarios and some sectoral perspectives. VUW Press, Wellington, pp. 26-43.

Ren, R., Cai, M., Xiang, C. and Wu, G., 2012. Observational evidence of the delayed response of stratospheric polar vortex variability to ENSO SST anomalies. Climate Dynamics, **38**(7-8): 1345-1358.

Renom, M., Rusticucci, M. and Barreiro, M., 2011. Multidecadal changes in the relationship between extreme temperature events in Uruguay and the general atmospheric circulation. (DOI 10.1007/s00382-010-0986-9).

Revadekar, J.V., Patwardhan, S.K. and Rupa Kumar, K., 2011. Characteristic Features of Precipitation Extremes over India in the Warming Scenarios. Advances in Meteorology.

Richter-Menge, J. and Overland, J.E., 2009. Arctic Report Card 2009. NOAA, pp. 103.

Richter, I. and Xie, S., 2008. On the origin of equatorial Atlantic biases in coupled general circulation models. Climate Dynamics: 587-598.

Rigor, I.G., Wallace, J.M. and Colony, R.L., 2002. Response of Sea Ice to the Arctic Oscillation. Journal of Climate, **15**: 2648-2663.

Rind, D., 2008. The consequences of not knowing low-and high-latitude climate sensitivity. Bulletin of the American Meteorological Society, **89**(6): 855-864.

Rinke, A., Dethloff, J., Cassano, J.J., Christensen, J.H., Curry, J.A., Du, P., Girard, E., Haugen, J.-E., Jacob, D., Jones, C.G., Koltzow, M., Laprise, R., Lynch, A.H., Pfeifer, S., Serreze, M.C., Shaw, M.J., Tjernstrom, M., Wyser, K. and Zagar, M., 2006. Evaluation of an ensemble of Arctic regional climate models: Spatiotemporal fields during the SHEBA year. Climate Dynamics, **26**: 459-472.

Riviere, G., 2011. A Dynamical Interpretation of the Poleward Shift of the Jet Streams in Global Warming Scenarios. Journal of the Atmospheric Sciences, **68**(6): 1253-1272.

Robertson, A., Moron, V., Qian, J., Chang, C., Tangang, F., Aldrian, E., Koh, T. and Juneng, L., 2011. The Maritime Continent monsoon. In: *C. Chang*, *Y. Ding*, *N.* L*au*, *R. J*ohn*son*, B. *Wan*g and T. *Yasuna*ri (Editors), The Global Monsoon System: Research and Forecast. *World Scientific Publication Company*, Singapore, pp. 594.

Robinson, W.A., 2006. On the self-maintenance of midlatitude jets. Journal of the Atmospheric Sciences, **63**(8): 2109-2122.

Rodda, J., Little, M., Rodda, H. and McSharry, P., 2010. A comparative study of the magnitude, frequency and distribution of intense rainfall in the United Kingdom., International Journal of Climatology, pp. 176-1783.

Rodgers, K., Friederichs, P. and Latif, M., 2004. Tropical pacific decadal variability and its relation to decadal modulations of ENSO. Journal of Climate, **17**(19): 3761-3774.

Rodriguez-Fonseca, B., Janicot, S., Mohino, E., Losada, T., Bader, J., Caminade, C., Chauvin, F., Fontaine, B., Garcia-Serrano, J., Gervois, S., Joly, M., Polo, I., Ruti, P., Roucou, P. and Voldoire, A., 2011. Interannual and decadal SST-forced responses of the West African monsoon. Atmospheric Science Letters, **12**(1): 67-74.

Rogers, J.C., 1981. The North Pacific Oscillation. Journal of Climatology, **1**: 19.

Rosenfeld, D., Clavner, M. and Nirel, R., 2011. Pollution and dust aerosols modulating tropical cyclones intensities. Atmospheric Research, **102**(1-2): 66-76.

Rotstayn, L. and Lohmann, U., 2002. Tropical rainfall trends and the indirect aerosol effect. Journal of Climate: 2103-2116.

Rotstayn, L.D., Cai, W.J., Dix, M.R., Farquhar, G.D., Feng, Y., Ginoux, P., Herzog, M., Ito, A., Penner, J.E., Roderick, M.L. and Wang, M.H., 2007. Have Australian rainfall and cloudiness increased due to the remote effects of Asian anthropogenic aerosols? Journal of Geophysical Research-Atmospheres, **112**(D9): -.

Rouault, M., Florenchie, P., Fauchereau, N. and Reason, C., 2003. South East tropical Atlantic warm events and southern African rainfall. Geophysical Research Letters, **30**(5).

Rouault, M. and Richard, Y., 2003. Intensity and spatial extension of drought in South Africa at different time scales. Water Sa: 489-500.

Rowell, D., 2003. The impact of Mediterranean SSTs on the Sahelian rainfall season. Journal of Climate, **16**(5): 849-862.

Rowell, D., 2011. Sources of uncertainty in future changes in local precipitation. Climate Dynamics: 1-22.

Rowell, D.P., 2001. Teleconnections between the tropical Pacific and the Sahel. Quarterly Journal of the Royal Meteorological Society, **127**(575): 1683-1706.

Rupa Kumar, K. and Ashrit, R.G., 2001. Regional aspects of global climate change simulations: validation and assessment of climate response over Indian monsoon region to transient increase of greenhouse gases and sulfate aerosols. Mausam, **52**: 229-244.

Rupa Kumar, K., Ashrit, R.G. and Pant, G.B., 2002. Indian summer monsoon: Past, Present and Future. Science and Culture, **68**: 217-224.

Rusticucci, M. and Barrucand, M., 2004. Observed trends and changes in temperature extremes over Argentina. Journal of Climate, **17**(20): 4099-4107.

Rusticucci, M., Marengo, J., Penalba, O. and Renom, M., 2010. An intercomparison of model-simulated in extreme rainfall and temperature events during the last half of the twentieth century. Part 1: mean values and variability. Climatic Change, **98**(3-4): 493-508.

Rusticucci, M. and Renom, M., 2008. Variability and trends in indices of quality-controlled daily temperature extremes in Uruguay. International Journal of Climatology, **28**(8): 1083-1095.

Ruti, P. and Dell'Aquila, A., 2010. The twentieth century African easterly waves in reanalysis systems and IPCC simulations, from intra-seasonal to inter-annual variability. Climate Dynamics, **35**(6): 1099-1117.

S, K., R, M. and M, M., 2011. Future changes in the East Asian rain band projected by global atmospheric models with 20-km and 60-km grid size. (DOI 10.1007/s00382-011-1000-x).

Sabade, S., Kulkarni, A. and Kripalani, R., 2011. Projected changes in South Asian summer monsoon by multi-model global warming experiments. Theoretical and Applied Climatology: 543-565.

Saenger, C., Cohen, A., Oppo, D., Halley, R. and Carilli, J., 2009. Surface-temperature trends and variability in the low-latitude North Atlantic since 1552. Nature Geoscience, **2**(7): 492-495.

Sahu, S., Beig, G. and Sharma, C., 2008. Decadal growth of black carbon emissions in India. Geophysical Research Letters, **35**(2).

Saini, R., Barlow, M. and Hoell, A., 2011. Dynamics and Thermodynamics of the Regional Response to the Indian Monsoon Onset. Journal of Climate, **24**(22): 5879-5886.

Saji, N.H., Goswami, B.N., Vinayachandran, P.N. and Yamagata, T., 1999. A dipole mode in the tropical Indian Ocean. Nature, **401**(6751): 360-363.

Salahuddin, A. and Curtis, S., 2011. Climate extremes in Malaysia and the equatorial South China Sea. Global and Planetary Change, **78**(3-4): 83-91.

Salathe Jr, E.P., Leung, L.R., Qian, Y. and Zhang, Y., 2010. Regional climate model projections for the State of Washington. Climatic Change, **102**: 51-75.

Salinger, M.J., Renwick, J.A. and Mullan, A.B., 2001. Interdecadal Pacific Oscillation and South Pacific climate. International Journal of Climatology, **21**(14): 1705-1722.

Salzmann, N. and Mearns, L.O., 2012. Assessing the performance of multiple regional climate model simulations for seasonal mountain snow in the upper Colorado River Basin. Journal of Hydrometeorology, **13**: 539-556.

Sampe, T. and Xie, S.-P., 2010. Large-scale dynamics of the Meiyu-Baiu rainband: Environmental forcing by the westerly jet. J. Climate, **23**: 113-134.

Sansom, P.G., Stephenson, D.B., Ferro, C.A.T., Zappa, G. and Shaffrey, L., 2012. A simple framework for weighting climate change projections in multi-model ensembles. Journal of Climate, **Submitted**.

Santer, B., Wigley, T., Gleckler, P., Bonfils, C., Wehner, M., AchutaRao, K., Barnett, T., Boyle, J., Bruggemann, W., Fiorino, M., Gillett, N., Hansen, J., Jones, P., Klein, S., Meehl, G., Raper, S., Reynolds, R., Taylor, K. and Washington, W., 2006. Forced and unforced ocean temperature changes in Atlantic and Pacific tropical cyclogenesis regions. Proceedings of the National Academy of Sciences of the United States of America, **103**(38): 13905-13910.

Sato, T., Kimura, F. and Kitoh, A., 2007. Projection of global warming onto regional precipitation over Mongolia using a regional climate model. Journal of Hydrology: 144-154.

Scaife, A., Kucharski, F., Folland, C., Kinter, J., Bronnimann, S., Fereday, D., Fischer, A., Grainger, S., Jin, E., Kang, I., Knight, J., Kusunoki, S., Lau, N., Nath, M., Nakaegawa, T., Pegion, P., Schubert, S., Sporyshev, P., Syktus, J., Yoon, J., Zeng, N. and Zhou, T., 2009. The CLIVAR C20C project: selected twentieth century climate events. Climate Dynamics, **33**(5): 603-614.

Scaife, A., Spangehl, T., Fereday, D., Cubasch, U., Langematz, U., Akiyoshi, H., Bekki, S., Braesicke, P., Butchart, N., Chipperfield, M., Gettelman, A., Hardiman, S., Michou, M., Rozanov, E. and Shepherd, T., 2011a. Climate change projections and stratosphere–troposphere interaction. Climate Dynamics.

Scaife, A.A., Copsey, D., Gordon, C., Harris, C., Hinton, T., Keeley, S., O'Neil, A., Roberts, M. and Williams, K., 2011b. Improved Atlantic winter blocking ina a climate model., Geophysical Research Letters, pp. doi:10.1029/2011GL049573.

Scaife, A.A., Folland, C.K., Alexander, L.V., Moberg, A. and Knight, J.R., 2008. European climate extremes and the North Atlantic Oscillation. Journal of Climate, **21**(1): 72-83.

Scaife, A.A., Knight, J.R., Vallis, G.K. and Folland, C.K., 2005. A stratospheric influence on the winter NAO and North Atlantic surface climate. Geophysical Research Letters, **32**(18).

Scaife, A.A., Wollings, T., Knight, J., Martin, G. and Hinton, T., 2010. Atmospheric blocking and mean biases in 18 climate models., Journal of Climate, pp. 6143-6152.

Schimanke, S., Koerper, J., Spangehl, T. and Cubasch, U., 2011. Multi-decadal variability of sudden stratospheric warmings in an AOGCM. Geophysical Research Letters, **38**.

Schneider, D., Deser, C. and Okumura, Y., 2011. An assessment and interpretation of the observed warming of West Antarctica in the austral spring. Climate Dynamics: 1-25.

Schneider, D., Deser, C. and Okumura, Y., 2012. An assessment and interpretation of the observed warming of West Antarctica in the austral spring. Climate Dynamics, **38**(1-2): 323-347.

Schneider, N. and Cornuelle, B., 2005. The forcing of the Pacific decadal oscillation. Journal of Climate, **18**(21): 4355-4373.

Schneider, T., O'Gorman, P.A. and Levine, X.J., 2010. WATER VAPOR AND THE DYNAMICS OF CLIMATE CHANGES. Reviews of Geophysics, **48**.

Schott, F., Xie, S. and McCreary, J., 2009. INDIAN OCEAN CIRCULATION AND CLIMATE VARIABILITY. Reviews of Geophysics: -.

Schubert, J.J., Stevens, B. and Crueger, T., 2012. The Madden-Julian Oscillation as Simulated by the MPI Earth System Model: Over the Last and Into the Next Millennium, JAMES.

Screen, J.A., Deser, C., Simmonds, I. and Tomas, R., 2012. The atmospheric response to three decades of observed Arctic sea ice loss. J. of Climate.

Seager, R., Kushnir, Y., Ting, M., Cane, M., Naik, N. and Miller, J., 2008. Would advance knowledge of 1930s SSTs have allowed prediction of the dust bowl drought? Journal of Climate, **21**(13): 3261-3281.

Seager, R. and Murtugudde, R., 1997. Ocean dynamics, thermocline adjustment, and regulation of tropical SST. Journal of Climate, **10**(3): 521-534.

Seager, R., Naik, N. and Vogel, L., 2012. Does Global Warming Cause Intensified Interannual Hydroclimate Variability? Journal of Climate, **25**(9).

Seager, R., Ting, M., Davis, M., Cane, M., Naik, N., Nakamura, J., Li, C., Cook, E. and Stahle, D.W., 2009. Mexican drought: an observational modeling and tree ring study of variability and climate change. Atmosfera, **22**: 1-31.

Seager, R. and Vecchi, G., 2010. Greenhouse warming and the 21st century hydroclimate of southwestern North America. Proceedings of the National Academy of Sciences, **107**(50): 21277-21282.

Seager, R.e.a., 2007. Model projections of an imminent transition to a more arid climate in southwestern North America. Science, **316**(5828): 1181-1184.

Seierstad, I., Stephenson, D. and Kvamsto, N., 2007. How useful are teleconnection patterns for explaining variability in extratropical storminess ? Tellus Series a-Dynamic Meteorology and Oceanography, **59**(2): 170-181.

Seierstad, I.A. and Bader, J., 2009. Impact of a projected future Arctic Sea Ice reduction on extratropical storminess and the NAO. Climate Dynamics, **33**(7-8): 937-943.

Semenov, V.A., 2007. Structure of temperature variability in the high latitudes of the Northern Hemisphere. Izvestiya Atmospheric and Oceanic Physics, **43**(6): 687-695.

Semmler, T., Varghese, S., McGrath, R., Nolan, P., Wang, S., Lynch, P. and O'Dowd, C., 2008. Regional climate model simulations of North Atlantic cyclones: frequency and intensity changes. Climate Research, **36**(1): 1-16.

Sen Roy, S., 2009. A spatial analysis of extreme hourly precipitation patterns in India. International Journal of Climatology, **29**(3): 345-355.

Seneviratne, S., Corti, T., Davin, E., Hirschi, M., Jaeger, E., Lehner, I., Orlowsky, B. and Teuling, A., 2010. Investigating soil moisture-climate interactions in a changing climate: A review, Earth Science Reviews, pp. 125-161.

Seneviratne, S.I., Nicholls, N., Easterling, D., Goodess, C.M., Kanae, S., Kossin, J., Luo, Y., Marengo, J., McInnes, K., Rahimi, M., Reichstein, M., Sorteberg, A., Vera, C. and Zhang, X., 2012. Changes in climate extremes and their impacts on the natural physical environment. In: *Managing the Risks of Extreme Events and Disasters to Advance Climate Change Adaptation*. In: C.B. Field, V. Barros, T. F. Stocker, D. Qin, D. J. Dokken, K. L. Ebi, M. D. Mastrandrea, K. J. Mach, G. -K. Plattner, S. K. Allen, M. Tignor, and P. M. Midgley (Editor), A Special Report of Working Groups I and II of the Intergovernmental Panel on Climate Change (IPCC), Cambridge, UK, and New York, NY, USA, pp. pp. 109-230.

Servain, J., Wainer, I., McCreary, J. and Dessier, A., 1999. Relationship between the equatorial and meridional modes of climatic variability in the tropical Atlantic. Geophysical Research Letters: 485-488.

Seth, A., Rauscher, S.A., Rojas, M., Giannini, A. and Camargo, S.J., 2011. Enhanced spring convective barrier for monsoons in a warmer world? Climatic Change, **104**: 403-414.
Seth, A., Rojas, M. and Rauscher, S.A., 2010. CMIP3 projected changes in the annual cycle of the South American Monsoon. Climatic Change, **98**(3-4): 331-357.
Shaman, J. and Tziperman, E., 2011. An atmospheric teleconnection linking ENSO and Southwestern European precipitation, Journal of Climate, pp. 124-139.
Sheffield, J. and Wood, E.F., 2008. Projected changes in drought occurrence under future global warming from multi-model, multi-scenario, IPCC AR4 simulations. Climate Dynamics, **31**(1): 79-105.
Shen, S.S.P., Lee, C.K. and Lawrimore, J., 2012. Uncertainties, trends and hottest and coldest years of the U.S. surface air temperature since 1895: an update based on the USHCN V2 TOB data. Journal of Climate, **25**: 4185-4203.
Shi, G., Cai, W., Cowan, T., Ribbe, J., Rotstayn, L. and Dix, M., 2008a. Variability and trend of North West Australia rainfall: Observations and coupled climate modeling. Journal of Climate, **21**(12): 2938-2959.
Shi, G., Ribbe, J., Cai, W. and Cowan, T., 2008b. An interpretation of Australian rainfall projections. Geophys. Res. Lett., **35**(2): L02702.
Shongwe, M., van Oldenborgh, G., van den Hurk, B. and van Aalst, M., 2011. Projected Changes in Mean and Extreme Precipitation in Africa under Global Warming. Part II: East Africa. Journal of Climate, **24**(14): 3718-3733.
Shongwe, M.E., van Oldenborgh, G.J., van den Hurk, B., de Boer, B., Coelho, C.A.S. and van Aalst, M.K., 2009. Projected Changes in Mean and Extreme Precipitation in Africa under Global Warming. Part I: Southern Africa. Journal of Climate, **22**(13): 3819-3837.
Shrestha, K.L., 2005. Global change impact assessment for Himalayan mountain regions for environmental management and sustainable development. . Global Environmental Research, **9**(1): 69-81.
Sigmond, M. and Fyfe, J.C., 2010. Has the ozone hole contributed to increased Antarctic sea ice extent? Geophys. Res. Lett., **37**(18): L18502.
Sillman, J., Croci-Maspoli, M., Kallache, M. and Katz, R.W., 2011. Extreme clod winter temperatures in Europe under the influence of North Atlantic Atmospheric blocking., Journal of Climate, pp. 5899-5913.
Silva, A.E. and Carvalho, L.M.V., 2007. Large-scale index for South America Monsoon (LISAM). Atmospheric Science Letters, **8**: 51-57.
Silvestri, G. and Vera, C., 2009. Nonstationary Impacts of the Southern Annular Mode on Southern Hemisphere Climate. Journal of Climate, **22**(22): 6142-6148.
Simpson, I.R., Blackburn, M., Haigh, J.D. and Sparrow, S.N., 2010. The Impact of the State of the Troposphere on the Response to Stratospheric Heating in a Simplified GCM. Journal of Climate, **23**(23): 6166-6185.
Singh, A., Delcroix, T. and Cravatte, S., 2011. Contrasting the flavors of El Nino-Southern Oscillation using sea surface salinity observations. Journal of Geophysical Research-Oceans, **116**.
Smedsrud, L.H., Sorteberg, A. and Kloster, K., 2008. Recent and future changes of the Arctic sea-ice cover. Geophysical Research Letters, **35**: L20503.
Smirnov, D. and Vimont, D., 2011. Variability of the Atlantic Meridional Mode during the Atlantic Hurricane Season. Journal of Climate, **24**(5): 1409-1424.
Smith, I.N., Moise, A.F. and Colman, R., 2012. Large scale circulation features in the tropical Western Pacific and their representation in climate models. Journal of Geophysical Research, **117**(D04109).
Smith, I.N., Wilson, L. and Suppiah, R., 2008. Characteristics of the northern Australian rainy season. Journal of Climate, **21**(17): 4298-4311.
Soares, W.R. and Marengo, J.A., 2009. Assessments of moisture fluxes east of the Andes in South America in a global warming scenario. International Journal of Climatology, **29**(10): 1395-1414.
Sobel, A. and Camargo, S., 2011. Projected Future Seasonal Changes in Tropical Summer Climate. Journal of Climate, **24**(2): 473-487.
Sobel, A.H., Held, I.M. and Bretherton, C.S., 2002. The ENSO Signal in Tropical Tropospheric Temperature. Journal of Climate, **15**: 2702-2706.
Sohn, B. and Park, S., 2010. Strengthened tropical circulations in past three decades inferred from water vapor transport. Journal of Geophysical Research-Atmospheres, **115**.
Solman, S., Sanches, E., Samuelsson, P., Berbery, E.H., Recca-Remedio, A., Rocha, R.P., Chou, S.C. and Li, L., 2011. CLARIS LPB WP5: Regional Climate Change assessments for La Plata Basin. Clivar Exchanges, **16**(57): 19-21.
Solman, S., Sanchez, E., Samuelsson, P., Rocha, R.P., Marengo, J., Pessacg, N., Remedio, A., Chou, S.C., Berbery, H., Le Treut, H., de Castro, M. and Jacob, D., 2012. Evaluation of an ensemble of regional climate model simulations over South America driven by the ERA-Interim reanalysis: Models' performance and uncertainties. Climate Dynamics.
Solman, S.A. and Le Treut, H., 2006. Climate change in terms of modes of atmospheric variability and circulation regimes over southern South America. Climate Dynamics, **26**(7-8): 835-854.
Solomon, A., Goddard, L., Kumar, A., Carton, J., Deser, C., Fukumori, I., Greene, A., Hegerl, G., Kirtman, B., Kushnir, Y., Newman, M., Smith, D., Vimont, D., Delworth, T., Meehl, G., Stockdale, T., W, U.C.D.P. and W, U.C.D.P., 2011. DISTINGUISHING THE ROLES OF NATURAL AND ANTHROPOGENICALLY FORCED DECADAL CLIMATE VARIABILITY Implications for Prediction. Bulletin of the American Meteorological Society, **92**(2): 141-+.

Solomon, A. and Newman, M., 2011. Decadal predictability of tropical Indo-Pacific Ocean temperature trends due to anthropogenic forcing in a coupled climate model. Geophysical Research Letters, **38**.

Son, S.W., Gerber, E.P., Perlwitz, J., Polvani, L.M., Gillett, N.P., Seo, K.H., Eyring, V., Shepherd, T.G., Waugh, D., Akiyoshi, H., Austin, J., Baumgaertner, A., Bekki, S., Braesicke, P., Brühl, C., Butchart, N., Chipperfield, M.P., Cugnet, D., Dameris, M., Dhomse, S., Frith, S., Garny, H., Garcia, R., Hardiman, S.C., Jöckel, P., Lamarque, J.F., Mancini, E., Marchand, M., Michou, M., Nakamura, T., Morgenstern, O., Pitari, G., Plummer, D.A., Pyle, J., Rozanov, E., Scinocca, J.F., Shibata, K., Smale, D., Teyssèdre, H., Tian, W. and Yamashita, Y., 2010. Impact of stratospheric ozone on Southern Hemisphere circulation change: A multimodel assessment. J. Geophys. Res., **115**: D00M07.

Son, S.W. and Lee, S.Y., 2005. The response of westerly jets to thermal driving in a primitive equation model. Journal of the Atmospheric Sciences, **62**(10): 3741-3757.

Song, J., Wang, Y. and Wu, L., 2010. Trend discrepancies among three best track data sets of western North Pacific tropical cyclones. Journal of Geophysical Research-Atmospheres, **115**.

Sörensson, A.A., Menéndez, C., Ruscica, R., Alexander, P., Samuelsson, P. and Willén, U., 2010. Projected precipitation changes in South America: a dynamical downscaling within CLARIS. . Meteorologische Zeitschrift, **19**(4): 347-355.

Souza, P. and Cavalcanti, I.F.A., 2009. Atmospheric centres of action associated with the Atlantic ITCZ position. International Journal of Climatology, **29**(14): 2091-2105.

Sperber, K. and Annamalai, H., 2008. Coupled model simulations of boreal summer intraseasonal (30-50 day) variability, Part 1: Systematic errors and caution on use of metrics. Climate Dynamics, **31**(2-3): 345-372.

Sperber, K.R., Annamalai, H., Kang, I.S., Kitoh, A., Moise, A., Turner, A., Wang, B. and Zhou, T., 2012. The Asian summer monsoon: An intercomparison of CMIP5 vs CMIP3 simulations of the late 20th century. Climate Dynamics, **submitted**.

Stammerjohn, S.E., Martinson, D.G., Smith, R.C., Yuan, X. and Rind, D., 2008. Trends in Antarctic annual sea ice retreat and advance and their relation to El Niño–Southern Oscillation and Southern Annular Mode variability. J. Geophys. Res., **113**(C3): C03S90.

Steffensen, J., Andersen, K., Bigler, M., Clausen, H., Dahl-Jensen, D., Fischer, H., Goto-Azuma, K., Hansson, M., Johnsen, S., Jouzel, J., Masson-Delmotte, V., Popp, T., Rasmussen, S., Rothlisberger, R., Ruth, U., Stauffer, B., Siggaard-Andersen, M., Sveinbjornsdottir, A., Svensson, A. and White, J., 2008. High-resolution Greenland Ice Core data show abrupt climate change happens in few years. Science, **321**(5889): 680-684.

Steig, E.J., Ding, Q., Battisti, D.S. and Jenkins, A., 2012. Tropical forcing of Circumpolar Deep Water inflow and outlet glacier thinning in the Amundsen Sea Embayment, West Antarctica. Annals of Glaciology, **53**: 19–28.

Steig, E.J., Schneider, D.P., Rutherford, S.D., Mann, M.E., Comiso, J.C. and Shindell, D.T., 2009. Warming of the Antarctic ice-sheet surface since the 1957 International Geophysical Year. Nature, **457**(7228): 459-462.

Stephenson, D., Hannachi, A. and O'Neill, A., 2004. On the existence of multiple climate regimes. Quarterly Journal of the Royal Meteorological Society, **130**(597): 583-605.

Stephenson, D., Pavan, V., Collins, M., Junge, M. and Quadrelli, R., 2006. North Atlantic Oscillation response to transient greenhouse gas forcing and the impact on European winter climate: a CMIP2 multi-model assessment. Climate Dynamics, **27**(4): 401-420.

Stephenson, D.B. and Pavan, V., 2003. The North Atlantic Oscillation in coupled climate models: a CMIP1 evaluation. Climate Dynamics, **20**(4): 381-399.

Stevenson, S., 2012. Significant Changes to ENSO Strength and Impacts in the Twenty-First Century: Results from CMIP5. Geophysical Research Letters.

Stevenson, S., Fox-Kemper, B., Jochum, M., Neale, R., Deser, C. and Meehl, G., 2012. Will There Be a Significant Change to El Nino in the Twenty-First Century? Journal of Climate, **25**(6): 2129-2145.

Stewart, I.T., Cayan, D.R. and Dettinger, M.D., 2005. Changes toward earlier streamflow timing across western North America. Journal of Climate, **18**: 1136-1155.

Stoner, A.M.K., Hayhoe, K. and Wuebbles, D.J., 2009. Assessing General Circulation Model Simulations of Atmospheric Teleconnection Patterns. Journal of Climate, **22**(16): 4348-4372.

Stouffer, R., Yin, J., Gregory, J., Dixon, K., Spelman, M., Hurlin, W., Weaver, A., Eby, M., Flato, G., Hasumi, H., Hu, A., Jungclaus, J., Kamenkovich, I., Levermann, A., Montoya, M., Murakami, S., Nawrath, S., Oka, A., Peltier, W., Robitaille, D., Sokolov, A., Vettoretti, G. and Weber, S., 2006. Investigating the causes of the response of the thermohaline circulation to past and future climate changes. Journal of Climate, **19**(8): 1365-1387.

Stowasser, M., Annamalai, H. and Hafner, J., 2009. Response of the South Asian Summer Monsoon to Global Warming: Mean and Synoptic Systems. Journal of Climate, **22**(4): 1014-1036.

Stowasser, M., Wang, Y. and Hamilton, K., 2007. Tropical cyclone changes in the western North Pacific in a global warming scenario. Journal of Climate, **20**(11): 2378-2396.

Straus, D. and Shukla, J., 2002. Does ENSO force the PNA? Journal of Climate: 2340-2358.

Strong, C., Magnusdottir, G. and Stern, H., 2009. Observed Feedback between Winter Sea Ice and the North Atlantic Oscillation. Journal of Climate, **22**(22): 6021-6032.

Sugi, M., Murakami, H. and Yoshimura, J., 2009. A Reduction in Global Tropical Cyclone Frequency due to Global Warming. Sola, **5**: 164-167.

Sugi, M., Noda, A. and Sato, N., 2002. Influence of the global warming on tropical cyclone climatology: An experiment with the JMA global model. Journal of the Meteorological Society of Japan, **80**(2): 249-272.
Suhaila, J., Deni, S.M., Zin, W.Z.W. and Jemain, A.A., 2010. Spatial patterns and trends of daily rainfall regime in Peninsular Malaysia during the southwest and northeast monsoons: 1975-2004. Meteorology and Atmospheric Physics, **110**(1-2): 1-18.
Sun, D., 2003. Possible effect of an increase in the warm-pool SST on the magnitude of El Nino warming. Journal of Climate, **16**(2): 185-205.
Sun, D. and Zhang, T., 2006. A regulatory effect of ENSO on the time-mean thermal stratification of the equatorial upper ocean. Geophysical Research Letters, **33**(7).
Sun, D.Z. and Liu, Z.Y., 1996. Dynamic ocean-atmosphere coupling: A thermostat for the tropics. Science, **272**(5265): 1148-1150.
Sun, Y. and Ding, Y.H., 2010. A projection of future changes in summer precipitation and monsoon in East Asia. Science China Earth Sciences, **53**(2): 284-300.
Sung, M.-K., Lim, G.-H. and Kug, J.-S., 2010. Phase asymmetric downstream development of the North Atlantic Oscillation and its impact on the East Asian winter monsoon. J. Geophys. Res., **115**(D09105).
Suxiang, Y. and Yaocun, Z., 2010. Simulation of China Summer Precipitation Using a Regional Air-Sea Coupled Model. 气象学报, **24**(2).
Takahashi, K. and Battisti, D.S., 2007. Processes Controlling the Mean Tropical Pacific Precipitation Pattern. Part II: The SPCZ and the Southeast Pacific Dry Zone. Journal of Climate, **20**(23): 5696-5706.
Takahashi, K., Montecinos, A., Goubanova, K. and Dewitte, B., 2011. ENSO regimes: Reinterpreting the canonical and Modoki El Nino. Geophysical Research Letters, **38**.
Takaya, K. and Nakamura, H., 2005. Mechanisms of intraseasonal amplification of the cold Siberian high. Journal of the Atmospheric Sciences, **62**: 4423-4440.
Tanarhte, M., Hadjinicolaou, P. and Lelieveld, J., 2012. Intercomparison of temperature and precipitation data sets based on observations in the Mediterranean and the Middle East. Journal of Geophysical Research-Atmospheres, **117**.
Tangang, F.T., Juneng, L. and Ahmad, S., 2007. Trend and interannual variability of temperature in Malaysia: 1961-2002. Theoretical and Applied Climatology, **89**(3-4): 127-141.
Tangang, F.T., Juneng, L., Salimun, E., Vinayachandran, P.N., Seng, Y.K., Reason, C.J.C., Behera, S.K. and Yasunari, T., 2008. On the roles of the northeast cold surge, the Borneo vortex, the Madden-Julian Oscillation, and the Indian Ocean Dipole during the extreme 2006/2007 flood in southern Peninsular Malaysia. Geophysical Research Letters, **35**(14): 6.
Tao, H., Gemmer, M., Jiang, J., Lai, X. and Zhang, Z., 2011. Assessment of CMIP3 climate models and projected changes of precipitation and temperature in the Yangtze River Basin, China. Climatic Change: 1-15.
Taschetto, A.S. and England, M.H., 2009. El Nino Modoki Impacts on Australian Rainfall. Journal of Climate, **22**(11): 3167-3174.
Taschetto, A.S., Ummenhofer, C.C., Sen Gupta, A. and England, M.H., 2009. Effect of anomalous warming in the central Pacific on the Australian monsoon. Geophysical Research Letters, **36**.
Taylor, C., Gounou, A., Guichard, F., Harris, P., Ellis, R., Couvreux, F. and De Kauwe, M., 2011a. Frequency of Sahelian storm initiation enhanced over mesoscale soil-moisture patterns. Nature Geoscience, **4**(7): 430-433.
Taylor, C., Parker, D., Kalthoff, N., Gaertner, M., Philippon, N., Bastin, S., Harris, P., Boone, A., Guichard, F., Agusti-Panareda, A., Baldi, M., Cerlini, P., Descroix, L., Douville, H., Flamant, C., Grandpeix, J. and Polcher, J., 2011b. New perspectives on land-atmosphere feedbacks from the African Monsoon Multidisciplinary Analysis. Atmospheric Science Letters, **12**(1): 38-44.
Taylor, K.E., Stouffer, R.J. and Meehl, G.A., 2011c. An Overview of CMIP5 and the Experiment Design. Bulletin of the American Meteorological Society, **93**(4): 485-498.
Thoma, M., Jenkins, A., Holland, D. and Jacobs, S., 2008. Modelling Circumpolar Deep Water intrusions on the Amundsen Sea continental shelf, Antarctica. Geophys. Res. Lett., **35**(18): L18602.
Thomas, E.R., Marshall, G.J. and McConnell, J.R., 2008. A doubling in snow accumulation in the western Antarctic Peninsula since 1850. Geophys. Res. Lett., **35**(1): L01706.
Thompson, D. and Solomon, S., 2009. Understanding Recent Stratospheric Climate Change. Journal of Climate, **22**(8): 1934-1943.
Thompson, D.W.J. and Solomon, S., 2002. Interpretation of recent Southern Hemisphere climate change. Science, **296**(5569): 895-899.
Thompson, D.W.J., Solomon, S., Kushner, P.J., England, M.H., Grise, K.M. and Karoly, D.J., 2011. Signatures of the Antarctic ozone hole in Southern Hemisphere surface climate change. Nature Geoscience, **4**(11): 741-749.
Thompson, D.W.J. and Wallace, J.M., 1998. The Arctic Oscillation signature in the wintertime geopotential height and temperature fields. Geophysical Research Letters, **25**(9): 1297-1300.
Thompson, D.W.J. and Wallace, J.M., 2000. Annular modes in the extratropical circulation. Part I: Month-to-month variability. Journal of Climate, **13**(5): 1000-1016.
Thompson, D.W.J., Wallace, J.M., Kennedy, J.J. and Jones, P.D., 2010. An abrupt drop in Northern Hemisphere sea surface temperature around 1970. Nature, **467**(7314): 444-447.
Tibaldi, S. and Molteni, F., 1990. On the operational predictability of blocking., Tellus, pp. 343-365.

Timbal, B. and Arblaster, J.M., 2006. Land cover change as an additional forcing to explain the rainfall decline in the south west of Australia. Geophysical Research Letters, **33**(7): -.
Timbal, B., Arblaster, J.M. and Power, S., 2006. Attribution of the late-twentieth-century rainfall decline in southwest Australia. Journal of Climate, **19**(10): 2046-2062.
Timmermann, A., Jin, F.F. and Abshagen, J., 2003. A nonlinear theory for El Nino bursting. Journal of the Atmospheric Sciences, **60**(1): 152-165.
Timmermann, A., Menviel, L., Okumura, Y., Schilla, A., Merkel, U., Timm, O., Hu, A.X., Otto-Bliesner, B. and Schulz, M., 2010. Towards a quantitative understanding of millennial-scale Antarctic warming events. Quaternary Science Reviews, **29**(1-2): 74-85.
Timmermann, A., Okumura, Y., An, S.I., Clement, A., Dong, B., Guilyardi, E., Hu, A., Jungclaus, J.H., Renold, M., Stocker, T.F., Stouffer, R.J., Sutton, R., Xie, S.P. and Yin, J., 2007. The influence of a weakening of the Atlantic meridional overturning circulation on ENSO. Journal of Climate, **20**(19): 4899-4919.
Ting, M., Kushnir, Y., Seager, R. and Li, C., 2009a. Forced and Internal 20th century SST Trends in the North Atlantic. Journal of Climate, **22**.
Ting, M., Kushnir, Y., Seager, R. and Li, C., 2009b. Forced and Internal Twentieth-Century SST Trends in the North Atlantic. Journal of Climate, **22**(6): 1469-1481.
Ting, M., Kushnir, Y., Seager, R. and Li, C., 2011. Robust features of Atlantic multi-decadal variability and its climate impacts. Geophysical Research Letters, **38**: -.
Tjernstrom, M., Zagar, M., Svensson, G., Cassano, J., Pfeifer, S., Rinke, A., Wyser, K., Dethloff, K., Jones, C. and Semmier, T., 2004. Modeling the Arctic boundary layer: An evalutation of six ARCMIP regional-scale models with data from the SHEBA project. Boundary-Layer Meteorology, **117**: 337-381.
Tokinaga, H. and Xie, S., 2011. Weakening of the equatorial Atlantic cold tongue over the past six decades. Nature Geoscience, **4**(4): 222-226.
Tokinaga, H., Xie, S., Timmermann, A., McGregor, S., Ogata, T., Kubota, H. and Okumura, Y., 2012. Regional Patterns of Tropical Indo-Pacific Climate Change: Evidence of the Walker Circulation Weakening. Journal of Climate, **25**(5): 1689-1710.
Tougiani, A., Guero, C. and Rinaudo, T., 2009. Community mobilisation for improved livelihoods through tree crop management in Niger. GeoJournal, **74**(5): 377-389.
TRENBERTH, K., 1975. QUASI-BIENNIAL STANDING WAVE IN SOUTHERN-HEMISPHERE AND INTERRELATIONS WITH SEA-SURFACE TEMPERATURE - REPLY. Quarterly Journal of the Royal Meteorological Society, **101**(427): 174-176.
Trenberth, K., Davis, C. and Fasullo, J., 2007a. Water and energy budgets of hurricanes: Case studies of Ivan and Katrina. Journal of Geophysical Research-Atmospheres, **112**(D23).
Trenberth, K. and Fasullo, J., 2010. Simulation of Present-Day and Twenty-First-Century Energy Budgets of the Southern Oceans. Journal of Climate, **23**(2): 440-454.
Trenberth, K., Fasullo, J. and Smith, L., 2005a. Trends and variability in column-integrated atmospheric water vapor. Climate Dynamics, **24**(7-8): 741-758.
Trenberth, K.E. and Hurrell, J.W., 1994. Decadal atmosphere-ocean vairations in the Pacific. Climate Dynamics, **9**: 17.
Trenberth, K.E., Jones, P.D., Ambenje, P., Bojariu, R., Easterling, D., Klein Tank, A., Parker, D., Rahimzadeh, F., Renwick, J.A., Rusticucci, M., Soden, B. and Zhai, P., 2007b. Observations: Surface and Atmospheric Climate Change, Climate Change 2007: The Physical Science Basis. Contribution of Working Group I to the Fourth Assessment Report of the Intergovernmental Panel on Climate Change. Cambridge University Press, Cambridge, United Kingdom and New York, NY, USA.
Trenberth, K.E., Stepaniak, D.P. and Caron, J.M., 2000. The global monsoon as seen through the divergent atmospheric circulation. Journal of Climate, **13**: 3969-3993.
Trenberth, K.E., Stepaniak, D.P. and Smith, L., 2005b. Interannual variability of patterns of atmospheric mass distribution. Journal of Climate, **18**(15): 2812-2825.
Trenberth, K.E. and Tepaniak, D.P., 2001. Indices of El Nino evolution. Journal of Climate, **14**(8): 1697-1701.
TROUP, A., 1965. SOUTHERN OSCILLATION. Quarterly Journal of the Royal Meteorological Society, **91**(390): 490-&.
Tsz-cheung, L., Kin-yu, C., Ho-sun, C. and Mang-hin, K., 2011. Projections of Extreme Rainfall in Hong Kong in the 21st century. Acta Meteor. Sinica, **25(6)**: 691–709.
Tu, J., Chou, C. and Chu, P., 2009. The Abrupt Shift of Typhoon Activity in the Vicinity of Taiwan and Its Association with Western North Pacific-East Asian Climate Change. Journal of Climate, **22**(13): 3617-3628.
Tung, K.K. and Zhou, J.S., 2010. The Pacific's Response to Surface Heating in 130 Yr of SST: La Nina-like or El Nino-like? Journal of the Atmospheric Sciences, **67**(8): 2649-2657.
Turner, A., Sperber, K., Slingo, J., Meehl, G.A., Mechoso, C.R., Kimoto, M. and Giannini, A., 2011. Modelling monsoons: Understanding and predicting current and future behaviour. World Scientific Series on Asia-Pacific Weather and Climate, Vol. 5. In: C.P. Chang, Y. Ding, N.-C. Lau, R.H. Johnson, B. Wang and T. Yasunari (Editors), The Global Monsoon System: Research and Forecast (2nd Edition). World Scientific Publication Company, Hackensack, NJ, USA, pp. 608.
Turner, A.G. and Annamalai, H., 2012. Climate change and the south asian summer monsoon. Nature Climate Change, **2**: 587-595.

Turner, A.G., Inness, P.M. and Slingo, J.M., 2007a. The effect of doubled CO2 and model basic state biases on the monsoon-ENSO system. I: Mean response and interannual variability. Quarterly Journal of the Royal Meteorological Society, **133**(626): 1143-1157.
Turner, A.G. and Slingo, J.M., 2009. Uncertainties in future projections of extreme precipitation in the Indian monsoon region. Atmospheric Science Letters, **10**(3): 152-158.
Turner, J., 2004. The El Niño–southern oscillation and Antarctica. International Journal of Climatology, **24**(1): 1-31.
Turner, J., Bindschadler, R.A., Convey, P., Di Prisco, G., Fahrbach, E., Gutt, J., Hodgson, D.A., Mayewski, P.A. and Summerhayes (Eds.), C.P., 2009a. Antarctic Climate Change and the Environment. SCAR, Cambridge, 526 pp.
Turner, J., Colwell, S.R., Marshall, G.J., Lachlan-Cope, T.A., Carleton, A.M., Jones, P.D., Lagun, V., Reid, P.A. and Iagovkina, S., 2005. Antarctic climate change during the last 50 years. International Journal of Climatology, **25**(3): 279-294.
Turner, J., Comiso, J.C., Marshall, G.J., Lachlan-Cope, T.A., Bracegirdle, T., Maksym, T., Meredith, M.P., Wang, Z. and Orr, A., 2009b. Non-annular atmospheric circulation change induced by stratospheric ozone depletion and its role in the recent increase of Antarctic sea ice extent. Geophys. Res. Lett., **36**: L08502, doi:10.1029/2009GL037524.
Turner, J. and Overland, J., 2009. Contrasting climate change in the two polar regions. Polar Research, **28**(2): 146-164.
Turner, J., Overland, J.E. and Walsh, J.E., 2007b. An Arctic and Antarctic perspective on recent climate change. International Journal of Climatology, **27**(3): 277-293.
Tyrlis, E. and Hoskins, B.J., 2008. Aspects of a Northern Hemisphere atmospheric blocking climatology. Journal of the Atmospheric Sciences, **65**(5): 1638-1652.
Ueda, H., Iwai, A., Kuwako, K. and Hori, M.E., 2006. Impact of anthropogenic forcing on the Asian summer monsoon as simulated by eight GCMs. Geophysical Research Letters, **33**(6).
Ueda, H., Ohba, M. and Xie, S.P., 2009. Important Factors for the Development of the Asian-Northwest Pacific Summer Monsoon. Journal of Climate, **22**(3): 649-669.
Ulbrich, U. and Christoph, M., 1999. A shift of the NAO and increasing storm track activity over Europe due to anthropogenic greenhouse gas forcing. Climate Dynamics, **15**(7): 551-559.
Ulbrich, U., Leckebusch, G.C. and Pinto, J.G., 2009. Extra-tropical cyclones in the present and future climate: a review. Theoretical and Applied Climatology, **96**(1-2): 117-131.
Ulbrich, U., Pinto, J.G., Kupfer, H., Leckebusch, G.C., Spangehl, T. and Reyers, M., 2008. Changing northern hemisphere storm tracks in an ensemble of IPCC climate change simulations. Journal of Climate, **21**(8): 1669-1679.
Ummenhofer, C.C. and England, M.H., 2007. Interannual extremes in New Zealand precipitation linked to modes of Southern Hemisphere climate variability. Journal of Climate, **20**(21): 5418-5440.
Ummenhofer, C.C., England, M.H., McIntosh, P.C., Meyers, G.A., Pook, M.J., Risbey, J.S., Gupta, A.S. and Taschetto, A.S., 2009a. What causes southeast Australia's worst droughts? Geophysical Research Letters, **36**: -.
Ummenhofer, C.C., Sen Gupta, A. and England, M.H., 2009b. Causes of Late Twentieth-Century Trends in New Zealand Precipitation. Journal of Climate, **22**(1): 3-19.
van den Broeke, M.R. and van Lipzig, N.P.M., 2004. Changes in Antarctic temperature, wind and precipitation in response to the Antarctic Oscillation. Annals of Glaciology, **39**(1): 119-126.
van Haren, R., van Oldenborgh, G.J., Lenderink, G., Collins, M. and Hazeleger, W., 2012. SST and circulation trend biases cause an understimation of European precipitation trends, Climate Dynamics, pp. doi: 10.1007/s00382-012-1401-5.
van Loon, H., Meehl, G.A. and Arblaster, J.M., 2004. A decadal solar effect in the tropics in July-August. Journal of Atmospheric and Solar-Terrestrial Physics, **66**: 1767-1178.
van Oldenborgh, G., Drijfhout, S., van Ulden, A., Haarsma, R., Sterl, A., Sverijns, C., Hazeleger, W. and Dijkstra, H., 2009. Western Europe is warming much faster than expected, Climate Past, pp. 1-12.
van Oldenborgh, G., Philip, S. and Collins, M., 2005. El Nino in a changing climate: A multi-model study. Ocean Sci, **1**: 81-95.
Vancoppenolle, M., Fichefet, T., Goosse, H., Bouillon, S., Madec, G. and Maqueda, M.A.M., 2009. Simulating the mass balance and salinity of arctic and antarctic sea ice. 1. model description andvalidation. Ocean Modelling, **27**: 33-53.
Vasconcellos, F.C. and Cavalcanti, I.F.A., 2010. Extreme precipitation over Southeastern Brazil in the austral summer and relations with the Southern Hemisphere annular mode. Atmospheric Science Letters, **11**(1): 21-26.
Vautard, R., Yiou, P., D'Andrea, F., de Noblet, N., Viovy, N., Cassou, C., J, P., Ciais, P., Kageyama, M. and Fan, Y., 2007. Summertime European heat and drought waves induced by wintertime Mediterranean 1 rainfall deficit, Geophysical Research Letters, pp. doi:10.1029/2006GL028001.
Vecchi, G. and Knutson, T., 2011. Estimating Annual Numbers of Atlantic Hurricanes Missing from the HURDAT Database (1878-1965) Using Ship Track Density. Journal of Climate, **24**(6): 1736-1746.
Vecchi, G. and Wittenberg, A., 2010. El Nino and our future climate: where do we stand? Wiley Interdisciplinary Reviews-Climate Change, **1**(2): 260-270.
Vecchi, G.A. and Knutson, T.R., 2008. On Estimates of Historical North Atlantic Tropical Cyclone Activity. Journal of Climate, **21**(14): 3580-3600.

Vecchi, G.A. and Soden, B.J., 2007a. Effect of remote sea surface temperature change on tropical cyclone potential intensity. Nature, **450**(7172): 1066-U9.
Vecchi, G.A. and Soden, B.J., 2007b. Global warming and the weakening of the tropical circulation. Journal of Climate, **20**(17): 4316-4340.
Vecchi, G.A. and Soden, B.J., 2007c. Increased tropical Atlantic wind shear in model projections of global warming. Geophysical Research Letters, **34**(8).
Vecchi, G.A., Soden, B.J., Wittenberg, A.T., Held, I.M., Leetmaa, A. and Harrison, M.J., 2006. Weakening of tropical Pacific atmospheric circulation due to anthropogenic forcing. Nature, **441**(7089): 73-76.
Vecchi, G.A., Swanson, K.L. and Soden, B.J., 2008. Whither hurricane activity. Science, **322**(5902).
Vera, C., Higgins, W., Amador, J., Ambrizzi, T., Garreaud, R., Gochis, D., Gutzler, D., Lettenmaier, D., Marengo, J., Mechoso, C.R., Nogues-Paegle, J., Dias, P.L.S. and Zhang, C., 2006a. Toward a unified view of the American Monsoon Systems. Journal of Climate, **19**(20): 4977-5000.
Vera, C. and Silvestri, G., 2009. Precipitation interannual variability in South America from the WCRP-CMIP3 multi-model dataset. Climate Dynamics, **32**(7-8): 1003-1014.
Vera, C., Silvestri, G., Liebmann, B. and Gonzalez, P., 2006b. Climate change scenarios for seasonal precipitation in South America from IPCC-AR4 models. Geophysical Research Letters, **33**(13).
Vergara, 2007. Visualizing Future Climate in Latin America: Results from the application of the Earth Simulator.
Vial, J. and Osborn, T.J., 2011. Assessment of atmosphere-ocean general circulation model simulations of winter Northern Hemisphere atmospheric blocking., Climate Dynamics, pp. doi:10.1007/s00382-011-1177-z.
Vicente-Serrano, S. and López-Moreno, J., 2008. Nonstationary influence of the North Atlantic Oscillation on European precipitation., J. Geophys. Res., pp. doi 10.1029/2008JD010382.
Vigaud, N., Pohl, B. and Crétat, J., 2012. Tropical-temperate interactions over southern Africa simulated by a regional climate model. Climate Dynamics: 1-22.
Vigaud, N., Richard, Y., Rouault, M. and Fauchereau, N., 2009. Moisture transport between the South Atlantic Ocean and southern Africa: relationships with summer rainfall and associated dynamics. Climate Dynamics, **32**(1): 113-123.
Villarini, G., Vecchi, G., Knutson, T., Zhao, M. and Smith, J., 2011. North Atlantic Tropical Storm Frequency Response to Anthropogenic Forcing: Projections and Sources of Uncertainty. Journal of Climate, **24**(13): 3224-3238.
Villarini, G. and Vecchi, G.A., 2012. Twenty-first-century projections of North Atlantic tropical storms from CMIP5 models. Nature Clim. Change, **advance online publication**.
Vimont, D., Alexander, M. and Fontaine, A., 2009. Midlatitude Excitation of Tropical Variability in the Pacific: The Role of Thermodynamic Coupling and Seasonality. Journal of Climate, **22**(3): 518-534.
Vimont, D. and Kossin, J., 2007. The Atlantic Meridional Mode and hurricane activity. Geophysical Research Letters: .
Vincent, D., 1994. The South Pacific Convergence Zone (SPCZ): A review. Monthly Weather Review, **122**: 1949-1970.
Vincent, E., Lengaigne, M., Menkes, C., Jourdain, N., Marchesiello, P. and Madec, G., 2011. Interannual variability of the South Pacific Convergence Zone and implications for tropical cyclone genesis. Climate Dynamics, **36**(9-10): 1881-1896.
Vincent, L.A., van Wijngaarden, W.A. and Ropkinson, R., 2007. Surface temperature and humidity trends in Canda for 1953-2005. Journal of Climate, **20**: 5100-5113.
Vizy, E. and Cook, K., 2002. Development and application of a mesoscale climate model for the tropics: Influence of sea surface temperature anomalies on the West African monsoon. Journal of Geophysical Research-tmospheres:.
Walker, G.T., 1924. Correlation in seasonal variations of wether. IX. A further study of world weather.
Wallace, J.M. and Gutzler, D.S., 1981. Teleconnections in the geopotential height field during the Northern Hemisphere winter. Monthly Weather Review, **109**: 784-812.
Walsh, K., Lavender, S., Scoccimarro, E. and Murakami, H., 2012a. Resolution dependence of tropical cyclone formation in CMIP3 and finer resolution models. Climate Dynamics, **in press.**
Walsh, K., McInnes, K. and McBride, J., 2012b. Climate change impacts on tropical cyclones and extreme sea levels in the South Pacific - A regional assessment. Global and Planetary Change, **80-81**: 149-164.
Walsh, K., Nguyen, K. and McGregor, J., 2004. Fine-resolution regional climate model simulations of the impact of climate change on tropical cyclones near Australia. Climate Dynamics, **22**(1): 47-56.
Wang, B., 1995. INTERDECADAL CHANGES IN EL-NINO ONSET IN THE LAST 4 DECADES. Journal of Climate, **8**(2): 267-285.
Wang, B. and An, S.I., 2001. Why the properties of El Nino changed during the late 1970s. Geophysical Research Letters, **28**(19): 3709-3712.
Wang, B. and An, S.I., 2002. A mechanism for decadal changes of ENSO behavior: roles of background wind changes. Climate Dynamics, **18**(6): 475-486.
Wang, B. and Ding, Q., 2006. Changes in global monsoon precipitation over the past 56 years. Geophysical Research Letters, **33**: L06711.
Wang, B. and Ding, Q., 2008. Global monsoon: Dominant mode of annual variation in the tropics. Dynamics of Atmospheres and Oceans, **44**(3-4): 165-183.

Wang, B., Ding, Q. and Jhun, J., 2006. Trends in Seoul (1778-2004) summer precipitation. Geophysical Research Letters, **33**(L15803).
Wang, B., Kang, I.S. and Lee, J.Y., 2004. Ensemble Simulations of Asian-Australian Monsoon Variability by 11 AGCMs. Journal of Climate, **17**(4): 803-818.
Wang, B. and LinHo, 2002. Rainy season of the Asian-Pacific summer monsoon. J. Climate, **15**: 386-398.
Wang, B., Liu, J., Kim, H.-J., Webster, P.J. and Yim, S.-Y., 2012a. Recent change of the global monsoon precipitation (1979-2008). Climate Dynamics.
Wang, B. and Wang, Y., 1996. Temporal structure of the Southern Oscillation as revealed by waveform and wavelet analysis. Journal of Climate, **9**(7): 1586-1598.
Wang, B., Wu, R.G. and Fu, X.H., 2000. Pacific-East Asian teleconnection: how does ENSO affect East Asian climate? Journal of Climate, **13**(9): 1517-1536.
Wang, B., Wu, R.G. and Li, T., 2003. Atmosphere-warm ocean interaction and its impacts on Asian-Australian monsoon variation. Journal of Climate, **16**(8): 1195-1211.
Wang, B., Yang, J. and Zhou, T.J., 2008a. Interdecadal changes in the major modes of Asian-Australian monsoon variability: Strengthening relationship with ENSO since the late 1970s. Journal of Climate, **21**(8): 1771-1789.
Wang, B., Yang, Y., Ding, Q., Murakami, H. and Huang, F., 2010a. Climate control of the global tropical storm days (1965-2008). Geophysical Research Letters, **37**.
Wang, B., Yim, S.-Y., Lee, J.-Y., Liu, J. and Ha, K.-J., 2012b. Future change of Asian-Australian monsoon. Climate Dynamics: submitted.
Wang, B. and Zhang, Q., 2002. Pacific-east Asian teleconnection. Part II: How the Philippine Sea anomalous anticyclone is established during El Nino development. Journal of Climate, **15**(22): 3252-3265.
Wang, C., Kim, D., Ekman, A., Barth, M. and Rasch, P., 2009a. Impact of anthropogenic aerosols on Indian summer monsoon. Geophysical Research Letters, **36**.
Wang, C. and Lee, S., 2008. Global warming and United States landfalling hurricanes. Geophysical Research Letters, **35**(2).
Wang, C., Lee, S.K. and Enfield, D.B., 2007. Impact of the Atlantic warm pool on the summer climate of the Western Hemisphere. Journal of Climate, **20**: 5021-5040.
Wang, C., Lee, S.K. and Enfield, D.B., 2008b. Climate response to anomalously large and small Atlantic warm pools during the summer. Journal of Climate, **21**: ***2437–2450***.
Wang, C., Liang, X.Z. and Samel, A.N., 2011a. AMIP GCM Simulations of Precipitation Variability over the Yangtze River Valley. Bulletin of the American Meteorological Society.
Wang, G. and Hendon, H.H., 2007. Sensitivity of Australian rainfall to inter-El Nino variations. Journal of Climate, **20**(16): 4211-4226.
Wang, H., 2001. The weakening of the Asian monsoon circulation after the end of 1970's. Advances in Atmospheric Sciences: 376-386.
Wang, S.Y., Gillies, R.R., Takle, E.S. and Gutowski, W.J., 2009b. Evaluation of precipitation in the Intermountain Region as simulated by the NARCCAP regional climate models. Geophysical Research Letters, **36**: L11704.
Wang, X., Wang, C., Zhou, W., Wang, D. and Song, J., 2011b. Teleconnected influence of North Atlantic sea surface temperature on the El Nio onset. Climate Dynamics, **37**(3-4): 663-676.
Wang, Y., Yan, Z. and Chandler, R.E., 2010b. An analysis of mid‐summer rainfall occurrence in eastern China and its relationship with large‐scale warming using generalized linear models. International Journal of Climatology, **30**(12): 1826-1834.
Wang, Y. and Zhou, L., 2005. Observed trends in extreme precipitation events in China during 1961–2001 and the associated changes in large-scale circulation. Geophys. Res. Lett, **32**(9): L09707.
Wanner, H., Bronnimann, S., Casty, C., Gyalistras, D., Luterbacher, J., Schmutz, C., Stephenson, D. and Xoplaki, E., 2001. North Atlantic Oscillation - Concepts and studies. Surveys in Geophysics, **22**(4): 321-382.
Ward, P., Marfai, M., Poerbandono and Aldrian, E., 2011. Climate adaptation in the city of Jakarta. In: J. Aerts, W. Botzen, M. Bowman, P. Ward and P. Dircke (Editors), Climate Adaptation and Flood Risk in Coastal Cities. Routledge - Earthscan, Amsterdam, pp. 352.
Watanabe, S. and Kawatani, Y., 2012. Sensitivity of the QBO to mean tropical upwelling under a changing climate simulated with an Earth System Model. Journal of the Meteorological Society of Japan, Series II, **90A**: 351-360.
Watterson, I., Hirst, A.C. and Rotstayn, L.D., 2012. A skill-score based evaluation of simulated Australian climate. Australian Meteorological and Oceanographic Journal: submitted.
Watterson, I.G., 2009. Components of precipitation and temperature anomalies and change associated with modes of the Southern Hemisphere. International Journal of Climatology, **29**(6): 809-826.
Weare, B.C., Cagnazzo, C., Fogli, P.G., Manzini, E. and Navarra, A., 2012. Madden-Julian Oscillation in a climate model with a well-resolved stratosphere. J. Geophys. Res., **117**(D1): D01103.
Webster, P., Holland, G., Curry, J. and Chang, H., 2005. Changes in tropical cyclone number, duration, and intensity in a warming environment. Science, **309**(5742): 1844-1846.
Webster, P.J., 2006. The coupled monsoon system. In: B. Wang (Editor), The Asian Monsoon. Springer Praxis Publishing, New York, pp. 3-66.
Webster, P.J., Moore, A.M., Loschnigg, J.P. and Leben, R.R., 1999. Coupled ocean-atmosphere dynamics in the Indian Ocean during 1997-98. Nature, **401**(6751): 356-360.

Weinkle, J., Maue, R. and Pielke, R., 2012. Historical Global Tropical Cyclone Landfalls. Journal of Climate, **25**(13): 4729-4735.
Weiss, J.L., Castro, C.L. and Overpeck, J.T., 2009. Distinguishing Pronounced Droughts in the Southwestern United States: Seasonality and Effects of Warmer Temperatures. Journal of Climate, **22**: 5918-5932.
Widlanski and al., e., 2012. Changes in South Pacific rainfall bands in a warming climate. Nature Climate Change, **submitted**.
Widlansky, M., Webster, P. and Hoyos, C., 2011. On the location and orientation of the South Pacific Convergence Zone. Climate Dynamics, **36**(3): 561-578.
Wiedenmann, J.M., Lupo, A.R., Mokhov, I.I. and Tikhonova, E.A., 2002. The climatology of blocking anticyclones for the Northern and Southern Hemispheres: Block intensity as a diagnostic. Journal of Climate, **15**(23): 3459-3473.
Wilcox, L.J., Charlton-Perez, A.J. and Gray , L.J., 2012. Trends in Austral jet position in ensembles of high- and low-top CMIP5 models. Journal of Geophysical Research: in press.
Williams, A. and Funk, C., 2011. A westward extension of the warm pool leads to a westward extension of the Walker circulation, drying eastern Africa. Climate Dynamics, **37**(11-12): 2417-2435.
Williams, K., Jones, A., Roberts, D., Senior, C. and Woodage, M., 2001. The response of the climate system to the indirect effects of anthropogenic sulfate aerosol. Climate Dynamics: 845-856.
Wilson, A.B., Bromwich, D.H. and Hines, K.M., 2012. Evaluation of Polar WRF forecasts on the Arctic System Reanalysis domain:2. Atmopsheric hydrologic cycle. Journal of Geophysical Research, **17**: D04107.
Wing, A.A., Sobel, A.H. and Camargo, S.J., 2007. Relationship between the potential and actual intensities of tropical cyclones on interannual time scales. *Geophysical Research Letters*, **34**: L08810.
Wittenberg, A., 2004. Extended wind stress analyses for ENSO. Journal of Climate, **17**(13): 2526-2540.
Wittenberg, A.T., 2009. Are historical records sufficient to constrain ENSO simulations? Geophysical Research Letters, **36**.
Wong, M., Mok, H. and Lee, T., 2011. Observed changes in extreme weather indices in Hong Kong. International Journal of Climatology, **31**(15): 2300-2311.
Woollings, T., 2008. Vertical structure of anthropogenic zonal-mean atmospheric circulation change. Geophysical research Letters, **35**(19).
Woollings, T., 2010. Dynamical influences on European climate: an uncertain future. Philosophical Transactions of the Royal Society a-Mathematical Physical and Engineering Sciences, **368**(1924): 3733-3756.
Woollings, T., Gregory, J., Pinto, J., Reyers, M. and Brayshaw, D., 2012. Response of the North Atlantic storm track to climate change shaped by ocean-atmosphere coupling. Nature Geoscience, **5**(5): 313-317.
Woollings, T., Hannachi, A., Hoskins, B. and Turner, A., 2010. A Regime View of the North Atlantic Oscillation and Its Response to Anthropogenic Forcing. Journal of Climate, **23**(6): 1291-1307.
Wu, B., Li, T. and Zhou, T., 2010. Asymmetry of Atmospheric Circulation Anomalies over the Western North Pacific between El Niño and La Niña*. Journal of Climate, **23**(18): 4807-4822.
Wu, B. and Zhou, T., 2012. The relationship between ENSO and western North Pacific-East Asian monsoon: An Intercomparison of CMIP-5 climate system models. J. Climate, **Submitted**.
Wu, B.Y., Wang, J. and Walsh, J.E., 2006. Dipole anomaly in the winter Arctic atmosphere and its association with sea ice motion. Journal of Climate, **19**: 210-225.
Wu, G., Liu, Y., He, B., Bao, Q., Duan, A. and Jin, F.-F., 2012. Thermal controls on the Asian summer monsoon. Sci. Rep., **2**(404).
Wu, L., 2007. Impact of Saharan air layer on hurricane peak intensity. Geophysical Research Letters, **34**(9).
Wu, L., Wang, B. and Geng, S., 2005. Growing typhoon influence on east Asia. Geophysical Research Letters, **32**(18).
Wu, Q. and Zhang, X., 2010. Observed forcing-feedback processes between Northern Hemisphere atmospheric circulation and Arctic sea ice coverage. Journal of Geophysical Research-Atmospheres, **115**.
Wu, Q.G. and Karoly, D.J., 2007. Implications of changes in the atmospheric circulation on the detection of regional surface air temperature trends. Geophysical Research Letters, **34**(8).
Wu, R. and Kirtman, B., 2004. Impacts of the Indian Ocean on the Indian summer monsoon-ENSO relationship. Journal of Climate, **17**(15): 3037-3054.
Wu, R., Kirtman, B. and Krishnamurthy, V., 2008. An asymmetric mode of tropical Indian Ocean rainfall variability in boreal spring. Journal of Geophysical Research-Atmospheres, **113**(D5): -.
Wu, Y., Ting, M., Seager, R., Huang, H.-P. and Cane, M.A., 2011. Changes in storm tracks and energy transports in a warmer climate simulated by the GFDL CM2.1 model. Climate Dynamics, **37**(1-2): 53-72.
Xavier, P.K., Duvel, J.-P., Braconnot, P. and Doblas-Reyes, F.J., 2010. An Evaluation Metric for Intraseasonal Variability and its Application to CMIP3 Twentieth-Century Simulations. Journal of Climate, **23**(13): 3497-3508.
XIE, S. and PHILANDER, S., 1994. A COUPLED OCEAN-ATMOSPHERE MODEL OF RELEVANCE TO THE ITCZ IN THE EASTERN PACIFIC. Tellus Series a-Dynamic Meteorology and Oceanography: 340-350.
Xie, S.P. and Carton, J.A., 2004. Tropical Atlantic variability: Patterns, mechanisms, and impacts. American Geophysical Union, Geophysical Monograph, pp. 121–142.
Xie, S.P., Du, Y., Huang, G., Zheng, X.T., Tokinaga, H., Hu, K.M. and Liu, Q.Y., 2010a. Decadal Shift in El Nino Influences on Indo-Western Pacific and East Asian Climate in the 1970s. Journal of Climate, **23**(12): 3352-3368.

Xie, S.P., Hu, K., Hafner, J., Tokinaga, H., Du, Y., Huang, G. and Sampe, T., 2009. Indian Ocean capacitor effect on Indo-western Pacific climate during the summer following El Nino. Journal of Climate, **22**(3): 730-747.

Xie, S.P.D., Deser, C., Vecchi, G.A., Ma, J., Teng, H. and Wittenberg, A.T., 2010b. Global Warming Pattern Formation: Sea Surface Temperature and Rainfall. Journal of Climate, **23**: 966-986.

Xin, X.G., Zhou, T.J. and Yu, R.C., 2010. Increased Tibetan Plateau snow depth: An indicator of the connection between enhanced winter NAO and late-spring tropospheric cooling over East Asia. Advances in Atmospheric Sciences, **27**(4): 788-794.

Xu, M., Chang, C., Fu, C., Qi, Y., Robock, A., Robinson, D. and Zhang, H., 2006. Steady decline of east Asian monsoon winds, 1969-2000: Evidence from direct ground measurements of wind speed. Journal of Geophysical Research-Atmospheres: -.

Xu, Y., Gao, X.-J. and Giorgi, F., 2009. Regional variability of climate change hot-spots in East Asia. Adv. Atmos. Sci., **26**: 783-792.

Xu, Y., Gao, X. and Giorgi, F., 2010. Upgrades to the reliability ensemble averaging method for producing probabilistic climate-change projections. Climate Research, **41**: 61-81.

Xue, Y. and others, 2010. Intercomparison and analyses of the climatology of the West African Monsoon in the West African Monsoon Modeling and Evaluation project (WAMME) first model intercomparison experiment. Climate Dynamics, **35**: 3-27.

Yamada, Y., Oouchi, K., Satoh, M., Tomita, H. and Yanase, W., 2010. Projection of changes in tropical cyclone activity and cloud height due to greenhouse warming: Global cloud-system-resolving approach. Geophysical Research Letters, **37**.

Yamagata, T., Behera, S.K., Luo, J.-J., Masson, S., Jury, M. and Rao, S.A., 2004. Coupled ocean-atmosphere variability in the tropical Indian Ocean. American Geophysical Union, *Earth Climate: The Ocean-Atmosphere Interaction*, pp. 189–212.

Yan, H., Sun, L.G., Wang, Y.H., Huang, W., Qiu, S.C. and Yang, C.Y., 2011. A record of the Southern Oscillation Index for the past 2,000 years from precipitation proxies. Nature Geoscience, **4**(9): 611-614.

Yasunari, T.J., Koster, R.D., Lau, K.M., Aoki, T., Sud, Y.C., Yamazaki, T., Motoyoshi, H. and Kodama, Y., 2011. Influence of dust and black carbon on the snow albedo in the NASA Goddard Earth Observing System version 5 land surface model. Journal of Geophysical Research-Atmospheres, **116**.

Ye, Z.Q. and Hsieh, W.W., 2008. Changes in ENSO and Associated Overturning Circulations from Enhanced Greenhouse Gases by the End of the Twentieth Century. Journal of Climate, **21**(22): 5745-5763.

Yeh, S.-W., Kirtman, B.P., Kug, J.-S., Park, W. and Latif, M., 2011. Natural variability of the central Pacific El Nino event on multi-centennial timescales. Geophysical Research Letters, **38**.

Yeh, S.W. and Kirtman, B.P., 2005. Pacific decadal variability and decadal ENSO amplitude modulation. Geophysical Research Letters, **32**(5).

Yeh, S.W., Kug, J.S., Dewitte, B., Kwon, M.H., Kirtman, B.P. and Jin, F.F., 2009a. El Nino in a changing climate. Nature, **461**(7263): 511-U70.

Yeh, S.W., Kug, J.S., Dewitte, B., Kwon, M.H., Kirtman, B.P. and Jin, F.F., 2009b. El Nino in a changing climate (vol 461, pg 511, 2009). Nature, **462**(7273).

Yeung, J.K., Smith, J.A., Villarini, G., A.N., A., Baeck, M.L. and Krajewski, W.F., 2011. Analyses of the warm season rainfall climatology of the northeastern US using regional climate model simulations and radar rainfall fields. Advances in Water Resources, **34**: 184-204.

Yin, J.H., 2005. A consistent poleward shift of the storm tracks in simulations of 21st century climate. Geophysical Research Letters, **32**(18): 4.

Yokoi, S. and Takayabu, Y., 2009. Multi-model Projection of Global Warming Impact on Tropical Cyclone Genesis Frequency over the Western North Pacific. Journal of the Meteorological Society of Japan: 525-538.

Yosef, Y., Saaroni, H. and Alpert, P., 2009. Trends in daily rainfall intensity over Israel 1950.

Yoshimura, J., Sugi, M. and Noda, A., 2006. Influence of greenhouse warming on tropical cyclone frequency. Journal of the Meteorological Society of Japan, **84**(2): 405-428.

Yu, B. and Zwiers, F.W., 2010. Changes in equatorial atmospheric zonal circulations in recent decades. Geophysical Research Letters, **37**.

Yu, J., Wang, Y. and Hamilton, K., 2010a. Response of Tropical Cyclone Potential Intensity to a Global Warming Scenario in the IPCC AR4 CGCMs. Journal of Climate, **23**(6): 1354-1373.

Yu, J.Y., Kao, H.Y. and Lee, T., 2010b. Subtropics-Related Interannual Sea Surface Temperature Variability in the Central Equatorial Pacific. Journal of Climate, **23**(11): 2869-2884.

Yu, J.Y., Kao, H.Y., Lee, T. and Kim, S.T., 2011. Subsurface ocean temperature indices for Central-Pacific and Eastern-Pacific types of El Nio and La Nia events. Theoretical and Applied Climatology, **103**(3-4): 337-344.

Yu, R., Li, J., Yuan, W. and Chen, H., 2010c. Changes in characteristics of late-summer precipitation over eastern China in the past 40 years revealed by hourly precipitation data. Journal of Climate, **23**(12): 3390-3396.

Yu, R.C., Wang, B. and Zhou, T.J., 2004. Tropospheric cooling and summer monsoon weakening trend over East Asia. Geophysical Research Letters, **31**(22): 4.

Yu, R.C. and Zhou, T.J., 2007. Seasonality and three-dimensional structure of interdecadal change in the East Asian monsoon. Journal of Climate, **20**(21): 5344-5355.

Zahn, M. and Allan, R., 2011. Changes in water vapor transports of the ascending branch of the tropical circulation. Journal of Geophysical Research-Atmospheres, **116**.
Zahn, M. and von Storch, H., 2010. Decreased frequency of North Atlantic polar lows associated with future climate warming. Nature, **467**(7313): 309-312.
Zanchettin, D., Rubino, A. and Jungclaus, J., 2010. Intermittent multidecadal-to-centennial fluctuations dominate global temperature evolution over the last millennium. Geophysical Research Letters, **37**: -.
Zappa, G., Shaffrey, L. and Hodges, K., 2012a. The ability of CMIP5 models to simulate North Atlantic extratropical cyclones. Journal of Climate, **Submitted**.
Zappa, G., Shaffrey, L., Hodges, K., Sansom, P. and Stephenson, D.B., 2012b. A CMIP5 multi-model assessment of future projections in North Atlantic and European cyclones. Journal of Climate, **Submitted**.
ZEBIAK, S., 1993. AIR-SEA INTERACTION IN THE EQUATORIAL ATLANTIC REGION. Journal of Climate: 1567-1568.
Zhai, P., Zhang, X., Wan, H. and Pan, X., 2005. Trends in total precipitation and frequency of daily precipitation extremes over China. Journal of Climate, **18**(7): 1096-1108.
Zhang, C., 2005. Madden-Julian Oscillation. Reviews of Geophysics, **43**(2): RG2003.
Zhang, C., Dong, M., Gualdi, S., Hendon, H., Maloney, E., Marshall, A., Sperber, K. and Wang, W., 2006a. Simulations of the Madden-Julian oscillation in four pairs of coupled and uncoupled global models. Climate Dynamics, **27**(6): 573-592.
Zhang, G.J. and Wang, H., 2006. Toward mitigating the double ITCZ problem in NCAR CCSM3. Geophysical Research Letters, **33**(L06709).
Zhang, H., 2010. Diagnosing Australia-Asian monsoon onset/retreat using large-scale wind and moisture indices. Climate Dynamics, **35**(4): 601-618.
Zhang, H., Liang, P., Moise, A. and Hanson, L., 2012. The response of summer monsoon onset/retreat in Sumatra-Java and tropical Australia region to global warming in CMIP3 models. . Climate Dynamics, **37**.
Zhang, H., Wang, Z. and Guo, P., 2009. A modeling study of the effects of direct radiative forcing due to carbonaceous aerosol on the climate in East Asia. Advances in Atmospheric Sciences, **26**(1): 57-66.
Zhang, J., Bhatt, U.S., Tangborn, W.V. and Lingle, C.S., 2007a. Climate downscaling for estimating glacier mass balances in northwestern North America: Validation with a USGS benchmark glacier. Geophysical Research Letters, **34**: L21505.
Zhang, L., Wu, L. and Yu, L., 2011a. Oceanic origin of a recent La Nia-like trend in the tropical Pacific. Advances in Atmospheric Sciences, **28**(5): 1109-1117.
Zhang, L. and Zhou, T., 2011a. An assessment of monsoon precipitation changes during 1901–2001. Climate Dynamics.
Zhang, L.X. and Zhou, T.J., 2011b. An assessment of monsoon precipitation changes during 1901-2001. Climate Dynamics, **37**(1-2): 279-296.
Zhang, M.H. and Song, H., 2006. Evidence of deceleration of atmospheric vertical overturning circulation over the tropical Pacific. Geophysical Research Letters, **33**(12).
Zhang, Q., Guan, Y. and Yang, H., 2008a. ENSO amplitude change in observation and coupled models. Advances in Atmospheric Sciences: 361-366.
Zhang, R. and Delworth, T.L., 2009. A new method for attributing climate variations over the Atlantic Hurricane Basin's main development region. Geophysical Research Letters, **36**: L06701.
Zhang, R., Kang, S. and Held, I., 2010. Sensitivity of Climate Change Induced by the Weakening of the Atlantic Meridional Overturning Circulation to Cloud Feedback. Journal of Climate, **23**(2): 378-389.
Zhang, S. and Wang, B., 2008. Global summer monsoon rainy seasons. International Journal of Climatology, **28**(12): 1563-1578.
Zhang, X., Aguilar, E., Sensoy, S., Melkonyan, H., Tagiyeva, U., Ahmed, N., Kutaladze, N., Rahimzadeh, F., Taghipour, A., Hantosh, T., Albert, P., Semawi, M., Ali, M., Al-Shabibi, M., Al-Oulan, Z., Zatari, T., Khelet, I., Hamoud, S., Sagir, R., Demircan, M., Eken, M., Adiguzel, M., Alexander, L., Peterson, T. and Wallis, T., 2005. Trends in Middle East climate extreme indices from 1950 to 2003. Journal of Geophysical Research-Atmospheres, **110**(D22).
Zhang, X., Brown, R., Vincent, L., Skinner, W., Feng, Y. and Mekis, E., 2011b. Canadian climate trends, 1950-2007. Canadian Bioversity: Ecosystem Status and Trends 2010, Technical Thematic Report No. 5., Canadian Councils of Resource Ministers, Ottawa, ON.
Zhang, X., Brown, R., Vincent, L., Skinner, W., Feng, Y. and Mekis, E., 2011c. Canadian climate trends, 1950-2007. Canadian Bioversity: Ecosystem Status and Trends 2012, Technical Thematic Report No. 5., Canadian Councils of Resource Ministers, Ottawa, ON.
Zhang, X., Lin, W. and Zhang, M., 2007b. Toward understanding the double Intertropical Convergence Zone pathology in coupled ocean-atmosphere general circulation models. Journal of Geophysical Research-Atmospheres, **112**(D12): -.
Zhang, X.B., Zwiers, F.W. and Stott, P.A., 2006b. Multimodel multisignal climate change detection at regional scale. Journal of Climate, **19**(17): 4294-4307.
Zhang, X.D., Sorteberg, A., Zhang, J., Gerdes, R. and Comiso, J.C., 2008b. Recent radical shifts of atmospheric circulations and rapid changes in Arctic climate system. Geophysical Research Letters, **35**: L22701.

Zhang, Y., Li, T. and Wang, B., 2004. Decadal Change of the Spring Snow Depth over the Tibetan Plateau: The Associated Circulation and Influence on the East Asian Summer Monsoon*. Journal of Climate, **17**(14): 2780-2793.

Zhang, Y.C., Kuang, X.Y., Guo, W.D. and Zhou, T.J., 2006c. Seasonal evolution of the upper-tropospheric westerly jet core over East Asia. Geophysical Research Letters, **33**(11): 4.

Zhao, M. and Held, I., 2010. An Analysis of the Effect of Global Warming on the Intensity of Atlantic Hurricanes Using a GCM with Statistical Refinement. Journal of Climate, **23**(23): 6382-6393.

Zhao, M. and Held, I., 2012. TC-Permitting GCM Simulations of Hurricane Frequency Response to Sea Surface Temperature Anomalies Projected for the Late-Twenty-First Century. Journal of Climate, **25**(8): 2995-3009.

Zhao, M., Held, I., Lin, S. and Vecchi, G., 2009. Simulations of Global Hurricane Climatology, Interannual Variability, and Response to Global Warming Using a 50-km Resolution GCM. Journal of Climate, **22**(24): 6653-6678.

Zheng, X.-T., Xie, S.-P. and Liu, Q., 2011. Response of the Indian Ocean basin mode and its capacitor effect to global warming. Journal of Climate, **24**.

Zheng, X., Xie, S., Vecchi, G., Liu, Q. and Hafner, J., 2010. Indian Ocean Dipole Response to Global Warming: Analysis of Ocean-Atmospheric Feedbacks in a Coupled Model. Journal of Climate: 1240-1253.

Zhou, T., Wu, B. and Wang, B., 2009a. How well do atmospheric general circulation models capture the leading modes of the interannual variability of the Asian-Australian monsoon? Journal of Climate, **22**(5): 1159-1173.

Zhou, T., Wu, B., Wen, X., Li, L. and Wang, B., 2008a. A fast version of LASG/IAP climate system model and its 1000-year control integration. Advances in Atmospheric Sciences, **25**(4): 655-672.

Zhou, T., Yu, R., Chen, H., Dai, A. and Pan, Y., 2008b. Summer precipitation frequency, intensity, and diurnal cycle over China: A comparison of satellite data with rain gauge observations. Journal of Climate, **21**(16): 3997-4010.

Zhou, T., Yu, R., Zhang, J., Drange, H., Cassou, C., Deser, C., Hodson, D.L.R., Sanchez-Gomez, E., Li, J., Keenlyside, N., Xin, X. and Okumura, Y., 2009b. Why the Western Pacific Subtropical High Has Extended Westward since the Late 1970s. Journal of Climate, **22**(8): 2199-2215.

Zhou, T. and Zhang, J., 2009. Harmonious Inter-decadal Changes of July-August Upper Tropospheric Temperature Across the North Atlantic, Eurasian Continent, and North Pacific. Advances in Atmospheric Sciences, **26**(4): 656-665.

Zhou, T.J., Gong, D.Y., Li, J. and Li, B., 2009c. Detecting and understanding the multi-decadal variability of the East Asian Summer Monsoon - Recent progress and state of affairs. Meteorologische Zeitschrift, **18**(4): 455-467.

Zhou, T.J., Wu, B., Scaife, A.A., Bronnimann, S., Cherchi, A., Fereday, D., Fischer, A.M., Folland, C.K., Jin, K.E., Kinter, J., Knight, J.R., Kucharski, F., Kusunoki, S., Lau, N.C., Li, L.J., Nath, M.J., Nakaegawa, T., Navarra, A., Pegion, P., Rozanov, E., Schubert, S., Sporyshev, P., Voldoire, A., Wen, X.Y., Yoon, J.H. and Zeng, N., 2009d. The CLIVAR C20C project: which components of the Asian-Australian monsoon circulation variations are forced and reproducible? Climate Dynamics, **33**(7-8): 1051-1068.

Zhou, T.J. and Yu, R.C., 2005. Atmospheric water vapor transport associated with typical anomalous summer rainfall patterns in China. Journal of Geophysical Research-Atmospheres, **110**(D8): 12.

Zhou, T.J. and Yu, R.C., 2006. Twentieth-century surface air temperature over China and the globe simulated by coupled climate models. Journal of Climate, **19**(22): 5843-5858.

Zhou, T.J., Zhang, L.X. and Li, H.M., 2008c. Changes in global land monsoon area and total rainfall accumulation over the last half century. Geophysical Research Letters, **35**(16): 6.

Zhou, T.J. and Zou, L.W., 2010. Understanding the Predictability of East Asian Summer Monsoon from the Reproduction of Land-Sea Thermal Contrast Change in AMIP-Type Simulation. Journal of Climate, **23**(22): 6009-6026.

Zhu, C., Wang, B., Qian, W. and Zhang, B., 2012. Recent weakening of northern East Asian summer monsoon: A possible response to global warming. Geophysical Research Letters, **39**(9): L09701.

Zhu, Y., Wang, H., Zhou, W. and Ma, J., 2011. Recent changes in the summer precipitation pattern in East China and the background circulation. Climate Dynamics, **36**(7-8): 1463-1473.

Zhu, Y.L. and Wang, H.J., 2010. The Arctic and Antarctic Oscillations in the IPCC AR4 Coupled Models. Acta Meteorologica Sinica, **24**(2): 176-188.

Zolina, O., Simmer, C., Kapala, A., Bachner, S., Gulev, S. and Maechel, H., 2008. Seasonally dependent changes of precipitation extremes over Germany since 1950 from a very dense observational network., Journal of Geophysical Research-Atmospheres,.

Zou, L., Zhou, T. and Han, Z., 2012. Near Future (2016-2040) summer precipitation changes over China under RCP8.5 emission scenario projected by a regional climate model: A Comparison between RCM downscaling and driving GCM. Advance in Atmospheric Science, **Submitted**.

Zou, L.W. and Zhou, T.J., 2011. Sensitivity of a regional ocean-atmosphere coupled model to convection parameterization over western North Pacific. Journal of Geophysical Research-Atmospheres, **116**: 11.

Zou, L.W. and Zhou, T.J., 2012. Development and evaluation of a regional ocean-atmosphere coupled model with focus on the western North Pacific summer monsoon simulation: Impacts of different atmospheric components. Science China-Earth Sciences, **55**(5): 802-815.

Zubair, L. and Ropelewski, C.F., 2006. The strengthening relationship between ENSO and northeast monsoon rainfall over Sri Lanka and southern India. Journal of Climate, **19**(8): 1567-1575.

Tables

Box 14.1, Table 1: Regional impacts of modes of variability.

Mode	Regional Impacts of Modes of Variability
ENSO	Global impact on interannual variability in global mean temperature. Influences severe weather and tropical cyclone activity worldwide. The diverse El Niño flavours present different teleconnection patterns that induce large impacts in numerous regions from polar to tropical latitudes (see Section 14.4).
PDO	Influences surface air temperature and precipitation over the entire North American continent and extratropical North Pacific. Modulates ENSO rainfall teleconnections e.g., Australian climate.
IPO	Modulates decadal variability in Australian rainfall, and ENSO teleconnections to rainfall, surface temperature, river flow and flood risk over Australia, New Zealand and the SPCZ.
NAO	Influences the N. Atlantic jet stream, storm tracks and blocking and thereby affects climate in over the N. Atlantic and surrounding landmasses.
NPO	Influences winter air temperature and precipitation over much of western North America as well as Arctic sea ice in the Pacific sector.
SAM	Influences temperature over Antarctica, Australia, Argentina, Tasmania and the south of New Zealand and precipitation over southern South America, New Zealand, Tasmania, Australia and South Africa
PNA	Influences the jet stream and storm tracks over the Pacific and North American sectors, exerting notable influences on the temperature and precipitation in these regions on intraseasonal and interannual time scales.
PSA	Influences atmospheric circulation over South America and thereby has impacts on precipitation over the continent.
AMO	Influences air temperatures and rainfall over much of the Northern Hemisphere, in particular, North America and Europe. It is associated with multidecadal variations in Indian, East-Asian and West-African monsoons, the North-African Sahel and North-east Brazil rainfall, the frequency of North American droughts and Atlantic hurricanes.
AMM	Influences seasonal hurricane activity in the tropical Atlantic on both decadal and interannual time scales. Its variability is strongly influenced by other modes, particularly ENSO and NAO.
AN	Affects the West African Monsoon, the oceanic forcing of Sahel rainfall on interannual to interdecadal time-scales and the spatial extension of drought in South Africa
IOB	Associated with the intensity of Northwest Pacific monsoon, the tropical cyclone activity over the Northwest Pacific and anomalous rainfall over East Asia
IOD	Associated with droughts in Indonesia, reduced rainfall over Australia, intensified Indian summer monsoon, floods in East Africa, hot summers over Japan, and anomalous climate in the extratropical Southern Hemisphere
TBO	Modulates the strength of the Indian and West Pacific monsoons. Affects droughts and floods over large areas of south Asia and Australia
MJO	Modulates the intensity of monsoon systems around the globe and tropical cyclone activity in the Indian, Pacific and Atlantic Oceans, enhanced rainfall in Western North America, Northeast Brazil, Southeast Africa and Indonesia during boreal winter and Central America/Mexico and Southeast Asia during boreal summer.
QBO	Strongly affects the strength of the northern stratospheric polar vortex as well as the extratropical troposphere circulation particularly in boreal winter.
BLC	Associated with cold air outbreaks, heat-waves, floods and droughts in middle and high latitudes of both hemispheres
EAP	Influences wintertime storminess and regional temperature and precipitation in western Europe e.g., southern England, western France and the Iberian peninsula.

Notes:
AMM: Atlantic Meridional Mode
AMO: Atlantic Multi-decadal Oscillation
AN: Atlantic Niño pattern
BLC: Blocking events
EAP: East Atlantic pattern
ENSO: El Niño-Southern Oscillation
IOB: Indian Ocean Basin pattern

IOD: Indian Ocean Dipole pattern
IPO: Interdecadal Pacific Oscillation
MJO: Madden-Julian Oscillation
NAO: North Atlantic Oscillation
NPO: North Pacific Oscillation
PDO: Pacific Decadal Oscillation
PNA: Pacific North America pattern
PSA: Pacific South America pattern
QBO: Quasi-Biennial Oscillation
SAM: Southern Annular Mode
TBO: Tropospheric Biennial Oscillation

Table 14.1: Lists of years for Eastern Pacific and Central Pacific El Nino events. A: Types based on EOF by (Ashok et al., 2007), B: Types based on the relative ration between NINO3 and NINO4 SST index by (Yeh et al., 2009a), C: similar to (Yeh et al., 2009a) but 1982-2010 climatology by (Lee and McPhaden, 2010), D: As in C but 1948-2006 climatology by(Li et al., 2011), E: similar to B but including 'Mixed type, M' by (Kug et al., 2009), F: Types based on subsurface temperature by (Yu et al., 2011), G: Types based on sea surface salinity for 1977-2008 by (Singh et al., 2011), H: Modified (Ashok et al., 2007) by (Li et al., 2010a), I: Similar to (Yeh et al., 2009a) but 1950-2008 climatology by (Hu et al., 2012b). CP indicates 'Central Pacific El Nino', 'date line El Nino', or 'El Nino-Modoki' events; EP indicates 'Eastern Pacific El Nino' or 'conventional El Nino'; M indicates the mixed type that belongs to neither EP nor CP type. Each paper uses different terminology but here EP, CP and M instead of various names.

El Nino	A	B	C	D	E	F	G	H	I
1950–1951		EP							
1957–1958		EP		EP					EP
1963–1964	CP	EP		EP		CP			
1965–1966		EP		EP		M			EP
1968–1969	CP	CP		CP		CP			CP
1969–1970		EP		EP		CP			EP
1972–1973		EP		EP	EP	M			EP
1976–1977		EP		EP	EP	M			
1977–1978	CP	CP		CP	CP	CP	CP		
1979–1980	CP	EP		EP					
1982–1983		EP	EP	EP	EP	M	EP	EP	EP
1986–1987		EP		EP	M	M	CP	EP	EP
1987–1988	CP	EP	EP	EP	M	M			CP
1990–1991	CP	CP		CP	CP		CP	CP	
1991–1992	CP	EP	CP	EP	M	M	EP	EP	EP
1992–1993	CP	CP					CP		
1994–1995	CP	CP	CP	CP	CP	M	CP	CP	CP
1997–1998		EP	EP	EP	EP	EP	EP	EP	EP
2001–2002		CP							
2002–2003	CP	EP	CP	CP	CP		CP	CP	CP
2003–2004		EP							
2004–2005	CP	CP	CP	CP	CP		CP	CP	
2006–2007		EP	EP	EP			CP		CP
2009–2010		CP	CP		CP				

Box 14.2, Table 1: Projections of tropical storm frequency. Projected change in frequency of tropical storms in warm climate runs relative to control run in percent. Red and blue numbers/text denote projected increases and decreases, respectively. Bold text denotes where a statistical significance test was reported that showed significance. The frequency projections from Emanuel et al. (2008) been computed slightly differently from those shown in Figure 8 of the original paper in order to facilitate intercomparison with projection results from other studies.

Reference	**Model/Type**	**Resolution**	**Experiment**	**Basin**								
				Global	**NH**	**SH**	**N Atl.**	**NW Pac.**	**NE Pac.**	**N Ind.**	**S. Ind.**	**SW Pac.**
(Sugi et al., 2002)	JMATimeslice	T106 L21 (~120km)	10y 1xCO2, 2xCO2	**-34**	**-28**	**-39**	**+61**	**-66**	-67	+9	**-57**	**-31**
(McDonald et al., 2005)	HadAM3 Timeslice	N144 L30 (~100km)	15y IS95a 1979-1994 2082-2097	**-6**	-3	**-10**	**-30**	**-30**	**+80**	**+42**	+10	**-18**
(Hasegawa and Emori, 2005)	CCSR/NIES/FRCGC Timeslice	T106 L56 (~120km)	5x20y at 1xCO2 7x20y at 2xCO2					-4				
(Yoshimura et al., 2006)	JMA Timeslice	T106 L21 (~120km)	10y 1xCO2, 2xCO2	**-15**								
(Oouchi et al., 2006)	MRI/JMA Timeslice	TL959 L60 (~20km)	10y A1B 1982-1993 2080-2099	**-30**	**-28**	**-32**	**+34**	**-38**	**-34**	**-52**	**-28**	**-43**
(Chauvin et al., 2006)	ARPEGE Climat Timeslice	~50 km	Downscale CNRM B2 Downscale Hadley A2				**+18** **-25**					
(Stowasser et al., 2007)	IPRC Regional		Downscale NCAR CCSM2, 6xCO2					+19				
(Bengtsson et al., 2007)	ECHAM5 Timeslice	T213 (~60 km)	2071-2100, A1B		-13		-8	-20	+4	-26		
(Bengtsson et al., 2007)	ECHAM5 Timeslice	T319 (~40 km)	2071-2100, A1B		-19		-13	-28	+7	-51		
(Emanuel et al., 2008)	Statistical-deterministic	---	Downscale 7 CMIP3 mods.: A1B, 2180-2200 Average over 7 models	-7	+2	-13	+4	+6	-5	-7	-12	-15
(Knutson et al., 2008)	GFDL Zetac regional	18 km	Downscale CMIP3 ens. A1B, 2080-2100				-27					
(Leslie et al., 2007)	OU-CGCM with high-res. window	Up to 50 km	2000 to 2050 control and IS92a (6 members)									~0
(Gualdi et al., 2008)	SINTEX-G coupled model	T106 (~120 km)	30 yr 1xCO2, 2xCO2, 4xCO2	**-16** (2x) **-44** (4x)			-14	-20	-3	-13	-14	**-22**

(Semmler et al., 2008)	Rossby Centre regional model	28 km	16 yr control and A2, 2085-2100				-13					
(Zhao et al., 2009)	GFDL HIRAM Timeslice	50 km	Downscale A1B: CMIP3 n=18 ens. GFDL CM2.1 HadCM3 ECHAM5	 **-20** **-20** **-11** **-20**	 **-14** **-14** +5 **-17**	 **-32** **-33** **-42** **-27**	 **-39** -5 **-62** -1	 **-29** -5 **-12** **-52**	 +15 **-23** **+61** **+35**	 -2 **-43** -2 -25	 **-30** **-33** **-41** **-13**	 **-32** **-31** **-42** **-48**
(Sugi et al., 2009)	JMA/MRI global AGCM Timeslice	 20 km 20 km 20 km 20 km 60 km 60 km 60 km 60 km	Downscale A1B: MRI CGCM2.3 MRI CGCM2.3 MIROC-H CMIP3 n=18 ens. MRI CGCM2.3 MIROC-H CMIP3 n=18 ens. CSIRO	 **-29** **-25** **-27** **-20** **-20** -6 **-21** **-22**	 **-31** **-25** **-15** **-21** **-21** 0 **-19** **-29**	 **-27** **-25** **-42** **-19** **-17** **-16** **-25** -11	 +22 +23 -18 +5 **+58** +6 +4 **-37**	 **-36** **-29** **+28** **-26** **-36** **+64** -14 +13	 **-39** **-30** **-50** **-25** **-31** **-42** **-33** **-49**	 **-39** -29 +32 -15 -12 **+79** +33 -7	 **-28** **-25** **-24** -5 **-22** +10 -18 **-22**	 **-22** **-27** **-90** **-42** -8 **-69** **-36** +10
(Murakami et al., 2012)	JMA/MRI global AGCM Timeslice	V3.1 20 km V3.2 20 km V3.1 60 km V3.2 60 km	Downscale CMIP3 multi-model ens. A1B change (2075-2099 minus control)	**-23** **-15** **-23** **-24**	**-20** **-14** **-23** **-23**	**-25** **-18** **-24** **-25**	+8 **-29** -2 **-39**	**-27** **-23** -20 **-28**	**-24** +1 **-32** -10	-14 -2 +21 -14	-10 **-23** **-15** **-24**	**-45** -15 **-39** **-27**
(Murakami et al., 2011a)	JMA/MRI global AGCM Timeslice	V3.2 60 km	Downscale A1B: YS, CMIP3 ens. YS, Cluster 1 YS, Cluster 2 YS, Cluster 3 KF, CMIP3 ens. KF, Cluster 1 KF, Cluster 2 KF, Cluster 3 AS, CMIP3 ens. AS, Cluster 1 AS, Cluster 2 AS, Cluster 3	 **-27** **-25** **-28** **-14** **-20** **-20** **-21** **-14** **-20** **-22** **-13** **-14**	 **-27** **-25** **-30** -3 **-24** **-27** **-28** **-12** -11 **-22** **-11** 0	 **-27** **-27** **-26** **-35** **-16** **-10** **-12** **-15** **-33** **-24** **-17** **-32**	 **-44** -24 -23 **-31** **-39** **-40** -21 **-53** +1 -27 +28 -24	 **-33** **-32** **-42** -2 **-28** **-33** **-44** -8 -19 -19 **-32** +8	 -11 **-30** -9 +6 -3 -15 +5 +17 -22 **-42** +24 +15	 -16 +19 -21 +1 **-42** **-28** **-50** **-48** +1 **-20** -5 -15	 **-29** **-24** **-20** **-46** **-24** **-20** -10 **-26** **-31** **-25** **-27** **-44** **-48**	 **-31** **-37** **-42** **-25** -11 -6 **-24** -6 **-43** **-27** **-44** -11
(Villarini et al., 2011)	Statistical downscale of CMIP3 models	---	24 CMIP3 model mean and ±1 σ range; A1B scenario, 21st century trend				Basin: -10 ± 29% US land: -3 ±26					

(Emanuel et al., 2010)	Statistical-deterministic	--	Timeslice using CMIP3 model mean SST change, 1990-2090, NICAM model 14 km		+45 (global but June - Oct only)							
(Yamada et al., 2010)	NICAM	14 km	Timeslice using CMIP3 model mean SST change, 1990-2090		-35 (global but June - Oct only)		-80	0	0	-77		
(Lavender and Walsh, 2011)	CSIRO CCAM regional model nested in a suite of GCMs	15 km	A2 1990, 2090 GFDL CM2.1 MPI ECHAM5 CSIRO Mk3.5									-38 -33 -27

1
2
3

Box 14.2, Table 2: Projections of intense TC frequency. Projected change in frequency of intense tropical cyclones (i.e., more intense than tropical storms) in warm climate runs relative to control run in percent. The rows of reported results are ordered from top to bottom generally in order of decreasing model horizontal resolution. Red and blue numbers/text denote projected increases and decreases, respectively. Bold text denotes where a statistical significance test was reported that showed significance.

Reference	**Model/type**	**Resolution: high to low**	**Experiment**	**Basin**								
				Global	**NH**	**SH**	**N Atl.**	**NW Pac.**	**NE Pac.**	**N Ind.**	**S. Ind.**	**SW Pac.**
(Bender et al., 2010)	GFDL Hurricane model	9 km	Downscale TCs from ref 22 18-mod ensemble: (range over 4 indiv. models)				cat 4-5 freq: +100% (-66 to +138%)					
(Knutson et al., 2008)	GFDL Zetac regional	18 km	Downscale CMIP3 ens. A1B, 2080-2100				+140% (12 vs 5) # w/ V_{sfc}>45m/s					
(Murakami et al., 2012)	JMA/MRI global AGCM Timeslice	V3.2 20 km	Downscale CMIP3 multi-model ens. A1B change (2075-2099 minus control)	# Cat 4-5: +4% # Cat. 5: +56%	+9% +60%	-7% +43%	+15% +287%	-4% +45%	+179% Increase from 0	+35% +100%	+45% +261%	-54% -61%
(Oouchi et al., 2006)	MRI/JMA Timeslice	TL959 L60 (~20km)	10y A1B 1982-1993 2080-2099	Signif. Increase, # V_{850} of 55-60 m/s								
(Walsh et al., 2004)	CSIRO DARLAM regional model	30 km	3xCO2; 2061-2090 minus 1961-1990									+26% P<970 mb
(Bengtsson et al., 2007)	ECHAM5 Timeslice	T319 (~40 km)	2071-2100, A1B		+42%, #>50m/s							
(Zhao and Held, 2010)	GFDL HIRAM Timeslice with statistical refinement of intensity	50 km	Downscale A1B: CMIP3 n=7 ens. GFDL CM2.0 GFDL CM2.1 HadCM3 HadGem1 ECHAM5 MRI_CGCM2.3 MIROC High				cat 3-5 hurr % -13 +9 +5 -28 -53 +24 0 -27					
(Zhao and Held, 2012)	GFDL HIRAM timeslice	50 km	Downscale A1B:	#>33m/s, %	#>33	#>33	#>33m/s	#>33m/s	#>33	#>33	#>33	#>33

			CMIP3 n=8 ens. GFDL CM2.0 GFDL CM2.1 HadCM3 HadGem1 ECHAM5 CCCMA MRI_CGCM2.3 MIROC High	-15 -6 -11 +6 -11 -14 -22 -16 -5	-16 -1 -5 +17 -3 -13 -24 -18 -6	-13 -21 -26 -26 -31 -16 -16 -10 -4	-20 +16 -4 -51 -84 +25 -42 +20 -31	-30 -19 +9 -11 -29 -49 -37 -33 -17	+14 +30 -34 +121 +115 +58 +17 -3 +44	+6 +20 -31 +39 -35 -21 -21 -12 -40	-11 -14 -30 -20 -46 +9 -2 -12 +16	-14 -30 -19 -35 -9 -56 -37 -7 -34
(Leslie et al., 2007)	OU-CGCM with high-res. window	Up to 50 km	2000 to 2050 control and IS92a (6 members)									+100% #>30m/s by 2050
(Bengtsson et al., 2007)	ECHAM5 Timeslice	T213 (~60 km)	2071-2100, A1B		+32%, #>50m/s							
(McDonald et al., 2005)	HadAM3 Timeslice	N144 L30 (~100km)	15y IS95a 1979-1994 2082-2097	Increase In # strong TCs (vort > 24-30 x 10^{-5}/s)								
(Sugi et al., 2002)	JMA Timeslice	T106 L21 (~120km)	10y 1xCO2, 2xCO2	~0 # >40 m/s								
(Gualdi et al., 2008)	SINTEX-G coupled model	T106 (~120 km)	30 yr 1xCO2, 2xCO2, 4xCO2	~0								
(Hasegawa and Emori, 2007)	CCSR/NIES/FRC coupled model	T106 L56 (~120km)	20yr control Vs +1%/yr CO2 (yr 61-80)	Rel. freq. of Pc < 985mb +21 couple +59 uncoup								
(Yoshimura et al., 2006)	JMA Timeslice	T106 L21 (~120km)	10y 1xCO2, 2xCO2	Mixed changes: # > 25 m/s								

Box 14.2, Table 3: Tropical cyclone intensity change projections (percent change in maximum wind speed or central pressure fall, except as noted in the table. The dynamical model projections are ordered from top to bottom in order of decreasing model horizontal resolution. Red and blue colors denote increases and decreases, respectively. Pairs of numbers in parentheses denote ranges obtained using different models as input to a downscaling model or theory. The potential intensity change projections from Emanuel et al. (2008), Knutson and Tuleya (2004), and Vecchi and Soden (2007) in the table include some results that are adapted from the original papers but have been modified in order to facilitate intercomparison of methods and projection results from different studies. In some cases, ACE or PDI changes are reported, which depend on intensity, frequency, and lifetime.

Metric / Reference	**Technique / Model**	**Resolution / Metric Type**	**Climate Change Scenario**	**Global**	**NH**	**SH**	**NAtl, NW Pac, NE Pac**	**N Atl.**	**NW Pac.**	**NE Pac.**	**N Ind.**	**S. Ind.**	**SW Pac.**
Dynamical or Stat/Dyn. Model Projections (Max wind speed % change)								Avg (low, high)					
(Emanuel et al., 2008)	Stat./Dyn. Model	Max Wind speed (%)	CMIP3 7-model A1B (2181-2200 minus 1981-2000)	1.7	3.1	0.2	3.3	2.0	4.1	-0.1	0.2	0.5	-0.8
(Bender et al., 2010)	GFDL Hurricane model	9 km; Max Wind speed (%)	Downscale TCs from ref 22 18-mod ensemble: CMIP3 A1B; yrs 2081-2100 minus 2001-2020					+0.7 (trop. storms) +6 (hurri-canes)					
(Knutson and Tuleya, 2004)	GFDL Hurricane Model	9 km grid inner nest; Max Wind speed (%)	CMIP2+ +1%/yr CO2 80-yr trend				5.9	5.5 (1.5, 8.1)	5.4 (3.3, 6.7)	6.6 (1.1, 10.1)			
(Knutson and Tuleya, 2004)	GFDL Hurricane Model	9 km grid inner nest; Pressure fall (%)	CMIP2+ +1%/yr CO2 80-yr trend				13.8	13.0 (3.2, 21.6)	13.6 (8.0, 16.5)	14.8 (3.6, 25.0)			
(Lavender and Walsh, 2011)	CCAM regional model nested in a suite of GCMs	15 km Max winds	A2 1990, 2090										+5 to +10%
(Knutson et al., 2001)	GFDL Hurricane Model	18 km grid w./ ocean coupling; Max Wind speed (%)	GFDL R30 downscale, +1%/yr CO2 yr 71-120 avg	6									
(Knutson et al., 2008)	GFDL Zetac regional	18 km; Max Wind speed (%)	Downscale CMIP3 ens. A1B, 2080-2100					+2.9					
(Murakami et al., 2012)	JMA/MRI global AGCM timeslice	V3.1 20 km V3.2 20 km Avg. lifetime max	Downscale CMIP3 multi-model ens. A1B change (2075-2099	13 3	12 5	14 -1		2 9	16 6	13 6	8 5	15 7	7 -10

		winds	minus control)										
(Murakami et al., 2012)	JMA/MRI global AGCM timeslice	V3.1 20 km V3.2 20 km; Avg. max winds over lifetime of all TCs	Downscale CMIP3 multi-model ens. A1B change (2075-2099 minus control)	11 4	12 6	10 0		5 10	18 7	12 6	5 7	10 7	8 -10
(Oouchi et al., 2006)	MRI/JMA Timeslice	TL959 L60 (~20km) Avg. lifetime max windspeed	10y A1B 1982-1993 2080-2099	10.7	8.5	14.1		11.2	4.2	0.6	-12.8	17.3	-2.0
(Oouchi et al., 2006)	MRI/JMA Timeslice	TL959 L60 (~20km) Avg. annual max winds	10y A1B 1982-1993 2080-2099	13.7	15.5	6.9		20.1	-2.0	-5.0	-16.7	8.2	-22.5
(Semmler et al., 2008)	Rossby Centre regional model	28 km; Max winds	16 yr control and A2, 2085-2100					+4					
(Chauvin et al., 2006)	ARPEGE Climat Timeslice	~50 km Max winds	Downscale - CNRM B2 - Hadley A2					 ~0 ~0					
(Sugi et al., 2002)	JMA Timeslice	T106 L21 (~120km) Max winds	10y 1xCO2, 2xCO2	~0									
(Gualdi et al., 2008)	SINTEX-G coupled model	T106 (~120 km); Max winds	30 yr 1xCO2, 2xCO2, 4xCO2	~0									
(Hasegawa and Emori, 2005)	CCSR/NIES/FRCG C timeslice	T106 L56 (~120km) Max winds	5x20y at 1xCO2 7x20y at 2xCO2						Decrease				
(Yoshimura et al., 2006)	JMA Timeslice	T106 L21 (~120km) Max winds	10y 1xCO2, 2xCO2	~0									
(Hasegawa and Emori, 2007)	CCSR/NICS/FRC Coupled GCM	T106 L56 (~120 km) Max winds	20yr control Vs +1%/yr CO2 (yr 61-80)	~0 for Pc < 985 mb									
Potential intensity theory projections of intensity (% Change)								Avg (low, high)					
(Vecchi and Soden, 2007a)	Emanuel PI, reversible w/ diss. heating	Max Wind speed (%)	CMIP3 18-model A1B (100yr trend)	2.6	2.7	2.4	2.1	0.05 (-8.0, 4.6)	2.9 (-3.1, 12.6)	3.5 (-6.4 16.1)	4.4 (-3.3, 16.0)	3.7 (-7.6, 17.1)	0.99 (-8.6, 8.6)

(Knutson and Tuleya, 2004)	Potential Intensity Emanuel, reversible	Pressure fall (%)	CMIP2+ +1%/yr CO2 80-yr trend				5.0	2.6 (-5.6, 12.6)	7.0 (-1.0, 19.6)	5.4 (-5.0, 21.9)			
(Knutson and Tuleya, 2004)	Potential Intensity, Emanuel, pseudoadiabatic	Pressure fall (%)	CMIP2+ +1%/yr CO2 80-yr trend				7.6	6.0 (1.6, 13.2)	8.5 (2.8, 25.2)	8.2 (-3.3, 28.0)			
(Knutson and Tuleya, 2004)	Potential Intensity, Holland	Pressure fall (%)	CMIP2+ +1%/yr CO2 80-yr trend				15.2	12.4 (-4.0, 28.9)	17.3 (9.4, 30.6)	15.8 (3.4, 42.5)			
(Yu et al., 2010a)	Emanuel PI modified by vertical wind shear	Max Wind speed (%)	CMIP3 18 model ensemble 1%/yr CO2, 70-year trend					-0.1 to 2.3	2.3	2.4	3.3	3.4	1.0
ACE or PDI (% change) using Dynamical or Stat/Dyn. Models													
(Emanuel et al., 2010)	Stat./Dyn. Model	Power Dissipation Index (%)	Timeslice using CMIP3 ens. mean SST change, 1990-2090, and NICAM model 14 km fields		+65% in PDI,; (global but June to Oct only)								
(Yamada et al., 2010)	NICAM GCM	14 km Metric: ACE (Accum. Cyclone Energy)	Timeslice using CMIP3 model mean SST change, 1990-2090		-14% (ACE) (global but June to Oct only)			-88% (ACE)	+17% (ACE)	+65% (ACE)	-86% ACE	-14% ACE	
(Stowasser et al., 2007)	IPRC Regional model	~50 km PDI	Downscale NCAR CCSM2, 6xCO2						+50% in PDI,; incr. intensity				

Box 14.2, Table 4: Tropical cyclone-related precipitation projected changes (%) for the late 21st century (relative to present day).

Reference	Model/type	Resolution/	Experiment	Basins	Radius Around Storm Center	Percent Change
(Hasegawa and Emori, 2005)	CCSR/NIES/FRCGC Timeslice	T106 L56 (~120km)	5x20y at 1xCO2 7x20y at 2xCO2	NW Pacific	1000 km	+8.4 (all TC periods)
(Yoshimura et al., 2006)	JMA GSM8911 Timeslice	T106 L21 (~120km)	10y 1xCO2, 2xCO2	Global	300 km	+10 (all TC periods) Arakawa-Schubert +15 (all TC periods) Kuo
(Chauvin et al., 2006)	ARPEGE Climat Timeslice	~50 km	Downscale CNRM B2 Downscale Hadley A2	Atlantic	n/a	Substantial increase
(Bengtsson et al., 2007)	ECHAM5 Timeslice	T213 (~60 km)	2071-2100, A1B	Northern Hemisphere	550 km Accum. Along path	+21 (all TCs) +30 (TC > 33 m/s intensity)
(Knutson et al., 2008)	GFDL Zetac regional	18 km	Downscale CMIP3 ens. A1B, 2080-2100	Atlantic	50 km 100 km 400 km	+37 (all hurricane periods) +23 “ +10 “
(Knutson and Tuleya, 2004)	GFDL Hurricane Model (idealized)	9 km inner nest	CMIP2+ +1%/yr CO2 80-yr trend	Atlantic, NE Pacific, NW Pacific	~100 km	+22 (at time of max hurricane intensity)
(Gualdi et al., 2008)	SINTEX-G coupled model	T106 (~120 km)	30 yr 1xCO2, 2xCO2	Global	100 km 400 km 100 km 400 km	+6.1 (all TC periods) +2.8 (all TC periods) +11 (at time of max winds) +4.9 (at time of max winds)

Table 14.2: Temperature and precipitation projections by the CMIP5 global models. Averages over SREX (Seneviratne et al., 2012) regions of the projections by a set of [xx] [this number is consistent with the models used in the Atlas] global models for the RCP4.5 scenario. The mean temperature and precipitation responses are first averaged for each model over the 1986–2005 period from the historical simulations and the 2016–2035, 2046–2065 and 2081–2100 periods of RCP4.5. Computing the difference between these two periods, the table shows the 25, 50 and 75 percentiles and the lowest and highest response among the [xx] models, for temperature in degrees Celsius and precipitation as a per cent change. The regions are defined by latitude/longitude boxes as specified in SREX. Information is provided for land areas contained in the boxes unless otherwise indicated. Where appropriate, the numbers refer to Figure 14.32. The temperature responses are averaged over the boreal winter and summer seasons; December, January and February (DJF) and June, July and August (JJA) respectively, whereas the precipitation responses are averaged over half year periods, boreal winter; October, November, December, January, February and March (ONDJFM) and summer; April, May, June, July, August and September (AMJJAS). [PLACEHOLDER FOR FINAL DRAFT: Final version of this table will also include annual mean values. Regions in which the middle half (25–75%) of the distribution is all of the same sign in the precipitation response will be coloured light brown for decreasing and light blue for increasing precipitation as was the case in AR4, Table 11.1.]

Region		**Temperature Response**						**Precipitation Response**					
Artic	**YR**	**MONTH**	**MIN**	**25**	**50**	**75**	**MAX**	**MONTH**	**MIN**	**25**	**50**	**75**	**MAX**
Land	2035	DJF	0,5	1,4	1,7	2,1	3,4	ONDJFM	1%	6%	9%	13%	22%
	2065		0,3	2,8	3,2	4,3	5,6		3%	14%	17%	22%	38%
	2100		-1,2	3,5	4,6	6,1	7,1		-4%	17%	24%	35%	52%
	2035	JJA	0,3	0,8	1,0	1,5	3,3	AMJJAS	-1%	3%	5%	7%	20%
	2065		0,6	1,3	1,9	2,7	5,2		0%	6%	10%	13%	36%
	2100		0,4	1,8	2,3	3,4	6,5		-4%	10%	14%	18%	43%
Sea	2035	DJF	0,1	2,4	2,9	3,3	7,1	ONDJFM	-1%	6%	9%	14%	27%
	2065		-0,8	4,2	5,1	6,9	12,2		-4%	13%	18%	26%	41%
	2100		-2,6	5,6	7,4	9,6	16,3		-12%	19%	26%	39%	51%
	2035	JJA	0,2	0,4	0,6	0,7	1,4	AMJJAS	-1%	4%	6%	8%	16%
	2065		-0,1	0,8	1,1	1,4	2,4		-2%	8%	11%	15%	21%
	2100		-0,4	1,3	1,5	2,1	3,4		-4%	12%	16%	19%	28%
North America	**YR**	**MONTH**	**MIN**	**25**	**50**	**75**	**MAX**	**MONTH**	**MIN**	**25**	**50**	**75**	**MAX**
1 Alaska/	2035	DJF	0,2	1,1	1,6	2,6	3,4	ONDJFM	-1%	3%	5%	9%	11%
NW Canada	2065		1,9	2,7	3,7	5,0	7,4		4%	9%	12%	18%	29%
	2100		2,3	3,7	4,9	6,2	9,7		7%	11%	16%	21%	34%
	2035	JJA	0,3	0,7	1,0	1,4	2,8	AMJJAS	-1%	2%	4%	7%	16%
	2065		0,7	1,3	1,8	2,4	4,9		-2%	7%	10%	12%	29%
	2100		0,9	1,7	2,3	3,3	5,2		-2%	10%	12%	17%	34%
2 Canada/	2035	DJF	-0,2	1,2	1,6	2,1	3,1	ONDJFM	0%	4%	6%	9%	12%
Greenland/	2065		0,6	2,8	3,4	4,0	6,6		3%	9%	12%	16%	21%
Iceland	2100		-0,5	3,2	4,6	5,8	8,1		-2%	11%	15%	24%	29%

	2035	JJA	0,1	0,6	1,0	1,3	3,0	AMJJAS	0%	2%	3%	4%	8%
	2065		0,5	1,3	1,8	2,4	4,5		2%	4%	7%	9%	16%
	2100		0,2	1,7	2,4	3,2	5,6		1%	6%	9%	13%	20%
3 West North	2035	DJF	-0,4	0,7	1,2	1,5	2,5	ONDJFM	-2%	0%	3%	4%	7%
America	2065		0,9	1,8	2,3	2,7	4,0		-3%	2%	5%	6%	11%
	2100		1,3	2,3	2,9	3,5	5,2		-4%	4%	6%	8%	17%
	2035	JJA	0,3	1,0	1,1	1,4	2,0	AMJJAS	-6%	-2%	0%	4%	9%
	2065		0,8	1,7	2,2	2,8	3,4		-7%	-1%	1%	5%	10%
	2100		0,9	2,1	2,8	3,7	4,6		-8%	-1%	3%	6%	10%
4 Central North	2035	DJF	-0,1	0,8	1,2	1,6	2,9	ONDJFM	-8%	-1%	1%	5%	8%
America	2065		0,9	1,6	2,4	2,8	4,2		-7%	0%	3%	7%	17%
	2100		1,2	2,0	2,7	3,6	4,9		-6%	-2%	4%	9%	18%
	2035	JJA	0,3	0,9	1,2	1,4	2,3	AMJJAS	-7%	-2%	0%	3%	9%
	2065		0,9	1,8	2,2	2,7	3,5		-16%	-1%	2%	5%	12%
	2100		1,0	2,1	2,8	3,4	4,6		-13%	-1%	2%	4%	13%
5 Eastern North	2035	DJF	0,0	0,8	1,1	1,6	2,1	ONDJFM	-3%	0%	3%	7%	12%
America	2065		0,9	1,7	2,4	2,9	4,1		-2%	4%	7%	10%	18%
	2100		0,7	2,2	3,0	3,9	4,6		-4%	6%	9%	12%	20%
	2035	JJA	0,1	0,8	1,1	1,3	1,9	AMJJAS	-4%	1%	3%	5%	9%
	2065		0,8	1,5	2,1	2,5	3,9		-6%	2%	3%	6%	14%
	2100		1,0	2,0	2,7	3,2	4,8		-7%	3%	5%	7%	14%

Central America	**YR**	**MONTH**	**MIN**	**25**	**50**	**75**	**MAX**	**MONTH**	**MIN**	**25**	**50**	**75**	**MAX**
6 Central	2035	DJF	0,3	0,7	0,8	0,9	1,3	ONDJFM	-8%	-4%	-1%	3%	10%
America	2065		0,7	1,2	1,5	1,9	2,1		-15%	-5%	-1%	3%	10%
	2100		1,0	1,6	1,9	2,4	2,7		-22%	-5%	-1%	3%	11%
	2035	JJA	0,5	0,8	0,9	1,0	1,4	AMJJAS	-8%	-3%	-1%	3%	7%
	2065		1,1	1,4	1,7	2,0	2,5		-15%	-6%	-2%	2%	6%
	2100		1,2	1,6	2,0	2,5	3,2		-17%	-6%	-2%	1%	12%
Caribbean	2035	DJF	0,3	0,6	0,6	0,8	1,0	ONDJFM	-13%	-3%	-1%	3%	11%
(land and sea)	2065		0,6	1,0	1,2	1,5	1,9		-13%	-6%	-1%	3%	20%
	2100		0,7	1,2	1,5	2,0	2,4		-27%	-7%	0%	4%	19%
	2035	JJA	0,4	0,5	0,6	0,7	1,1	AMJJAS	-18%	-10%	-5%	1%	16%
	2065		0,7	0,9	1,2	1,4	2,1		-31%	-16%	-11%	-3%	15%

	2100		0,7	1,2	1,5	1,9	2,5		-37%	-17%	-8%	-3%	15%

South America	YR	MONTH	MIN	25	50	75	MAX	MONTH	MIN	25	50	75	MAX
7 Amazon	2035	DJF	0,4	0,7	0,8	0,9	1,6	ONDJFM	-12%	-2%	0%	2%	4%
	2065		0,8	1,3	1,6	2,0	3,0		-22%	-3%	0%	2%	6%
	2100		0,7	1,7	2,1	2,6	3,7		-22%	-3%	0%	2%	7%
	2035	JJA	0,5	0,8	1,0	1,1	1,8	AMJJAS	-14%	-2%	0%	1%	5%
	2065		1,0	1,5	1,8	2,2	3,3		-25%	-4%	-1%	2%	11%
	2100		1,3	1,8	2,4	2,9	4,2		-31%	-4%	-1%	1%	9%
8 North East Brazil	2035	DJF	0,4	0,6	0,8	1,0	1,3	ONDJFM	-10%	-2%	1%	4%	17%
	2065		0,8	1,2	1,5	1,8	2,3		-15%	-3%	2%	5%	21%
	2100		0,8	1,6	1,9	2,5	2,9		-17%	-5%	1%	6%	25%
	2035	JJA	0,3	0,7	0,8	1,0	1,7	AMJJAS	-12%	-6%	-4%	2%	15%
	2065		0,8	1,4	1,7	1,9	3,0		-29%	-10%	-5%	3%	18%
	2100		0,9	1,7	2,0	2,6	3,3		-39%	-15%	-10%	-3%	27%
9 West Coast South America	2035	DJF	0,5	0,7	0,8	0,9	1,2	ONDJFM	-4%	0%	1%	3%	6%
	2065		0,9	1,3	1,5	1,7	2,1		-7%	-1%	2%	4%	7%
	2100		1,0	1,6	1,9	2,3	2,9		-8%	1%	3%	5%	9%
	2035	JJA	0,5	0,7	0,9	1,0	1,3	AMJJAS	-9%	-2%	0%	2%	7%
	2065		1,1	1,3	1,6	1,9	2,5		-10%	-3%	-1%	2%	11%
	2100		1,2	1,7	2,0	2,5	3,0		-11%	-2%	0%	3%	9%
10Southeastern South America	2035	DJF	0,4	0,6	0,6	0,9	1,4	ONDJFM	-3%	0%	2%	4%	10%
	2065		0,7	1,1	1,4	1,7	2,4		-6%	0%	2%	6%	13%
	2100		1,0	1,4	1,8	2,3	3,0		-6%	0%	3%	5%	15%
	2035	JJA	0,0	0,5	0,6	0,9	1,2	AMJJAS	-12%	-1%	2%	6%	19%
	2065		0,4	1,1	1,3	1,6	2,1		-13%	-3%	4%	6%	17%
	2100		0,9	1,3	1,6	2,0	2,7		-18%	0%	3%	8%	27%

Europe	YR	MONTH	MIN	25	50	75	MAX	MONTH	MIN	25	50	75	MAX
11North Europe	2035	DJF	-0,3	0,6	1,1	2,2	3,0	ONDJFM	-4%	2%	4%	7%	12%
	2065		-0,5	1,8	2,2	3,2	5,7		-1%	3%	7%	11%	24%
	2100		-3,2	2,3	3,4	4,2	6,0		2%	7%	10%	13%	25%
	2035	JJA	0,2	0,6	1,0	1,3	2,6	AMJJAS	-6%	0%	4%	6%	11%
	2065		0,0	1,2	1,8	2,6	3,6		-10%	0%	3%	8%	18%

	2100		-1,1	1,6	2,2	3,1	4,7		-4%	2%	4%	8%	23%
12 Central	2035	DJF	-0,4	0,6	1,1	1,6	2,5	ONDJFM	-4%	-2%	2%	4%	11%
Europe	2065		0,3	1,4	1,9	2,7	3,6		-3%	2%	5%	10%	17%
	2100		-0,8	1,8	2,6	3,3	5,1		-4%	3%	7%	12%	18%
	2035	JJA	0,3	0,9	1,2	1,6	2,4	AMJJAS	-10%	-3%	0%	3%	9%
	2065		0,4	1,7	2,1	2,8	4,3		-17%	-4%	0%	3%	8%
	2100		0,4	2,1	2,8	3,4	4,6		-16%	-8%	0%	5%	13%
13South Europe	2035	DJF	-0,1	0,5	0,7	1,1	1,5	ONDJFM	-11%	-5%	-2%	2%	8%
Mediterranean	2065		0,1	1,2	1,4	1,8	2,3		-15%	-7%	-4%	-1%	7%
	2100		-0,2	1,5	2,0	2,4	3,0		-19%	-8%	-4%	-1%	9%
	2035	JJA	0,6	0,9	1,3	1,5	2,9	AMJJAS	-16%	-7%	-4%	-2%	4%
	2065		1,0	1,9	2,3	2,7	4,3		-24%	-12%	-10%	-5%	2%
	2100		1,2	2,5	2,9	3,6	5,5		-28%	-18%	-12%	-6%	2%

Africa	**YR**	**MONTH**	**MIN**	**25**	**50**	**75**	**MAX**	**MONTH**	**MIN**	**25**	**50**	**75**	**MAX**
14 Sahara	2035	DJF	0,1	0,7	0,9	1,2	1,5	ONDJFM	-43%	-11%	-1%	7%	33%
	2065		0,6	1,5	1,7	1,9	2,4		-29%	-14%	-4%	8%	92%
	2100		0,7	1,8	2,2	2,6	3,1		-31%	-15%	-4%	8%	98%
	2035	JJA	0,4	0,9	1,1	1,2	2,0	AMJJAS	-25%	-5%	2%	10%	45%
	2065		0,9	1,7	2,0	2,5	3,5		-31%	-11%	3%	14%	70%
	2100		1,1	2,2	2,5	3,2	4,5		-27%	-17%	0%	14%	108%
15 West Africa	2035	DJF	0,4	0,8	0,9	1,1	1,5	ONDJFM	-5%	-2%	2%	4%	9%
	2065		0,9	1,4	1,6	1,9	2,7		-10%	0%	4%	5%	8%
	2100		1,3	1,7	2,0	2,6	3,6		-4%	1%	4%	6%	11%
	2035	JJA	0,6	0,7	0,8	1,0	1,2	AMJJAS	-4%	-1%	1%	2%	6%
	2065		1,1	1,3	1,5	2,0	2,6		-9%	-1%	1%	3%	5%
	2100		1,0	1,6	1,9	2,7	3,3		-12%	0%	2%	4%	9%
16 East Africa	2035	DJF	0,4	0,7	0,8	1,0	1,4	ONDJFM	-4%	-1%	3%	6%	10%
	2065		0,8	1,3	1,5	1,9	2,4		-3%	1%	5%	9%	19%
	2100		1,0	1,6	2,0	2,4	3,2		-4%	0%	7%	12%	25%
	2035	JJA	0,6	0,7	0,9	1,0	1,2	AMJJAS	-8%	-3%	0%	2%	12%
	2065		1,0	1,3	1,6	2,0	2,5		-10%	-5%	1%	3%	18%
	2100		0,9	1,7	2,0	2,5	3,2		-12%	-5%	1%	5%	19%
17 Southern	2035	DJF	0,5	0,7	0,9	1,1	1,2	ONDJFM	-6%	-4%	-1%	0%	3%

Africa	2065		1,0	1,4	1,7	2,0	2,4		-11%	-5%	-2%	0%	6%
	2100		1,1	1,7	2,2	2,7	3,1		-13%	-6%	-2%	1%	5%
	2035	JJA	0,5	0,8	0,9	1,0	1,5	AMJJAS	-18%	-8%	-4%	0%	9%
	2065		1,1	1,5	1,7	2,0	2,5		-29%	-12%	-7%	-2%	4%
	2100		1,5	1,8	2,2	2,6	3,3		-29%	-15%	-10%	-4%	12%

Asia	**YR**	**MONTH**	**MIN**	**25**	**50**	**75**	**MAX**	**MONTH**	**MIN**	**25**	**50**	**75**	**MAX**
18 North Asia	2035	DJF	0,5	1,0	1,5	2,1	4,0	ONDJFM	2%	4%	7%	9%	22%
	2065		1,2	2,4	2,9	4,0	6,0		5%	10%	13%	18%	34%
	2100		0,2	3,0	3,9	5,0	7,8		5%	13%	18%	22%	44%
	2035	JJA	0,1	0,7	1,2	1,5	2,5	AMJJAS	1%	2%	4%	5%	16%
	2065		0,8	1,4	2,1	2,7	4,4		-1%	5%	6%	9%	21%
	2100		0,8	2,1	2,7	3,7	5,1		-3%	5%	9%	12%	30%
20 Central Asia	2035	DJF	-0,1	0,7	1,0	1,5	2,4	ONDJFM	-6%	0%	3%	7%	19%
	2065		0,6	1,6	2,2	2,8	4,0		-9%	-2%	4%	8%	19%
	2100		1,0	2,3	2,7	3,3	5,4		-12%	-2%	3%	10%	25%
	2035	JJA	0,3	0,9	1,2	1,5	2,1	AMJJAS	-13%	-3%	2%	5%	19%
	2065		1,1	1,7	2,1	2,8	4,3		-22%	-5%	1%	5%	10%
	2100		0,9	2,2	3,0	3,6	5,0		-16%	-3%	1%	4%	18%
21 Tibetan	2035	DJF	0,0	0,8	1,1	1,5	2,2	ONDJFM	-3%	1%	4%	7%	15%
Plateau	2065		0,9	1,9	2,3	3,0	3,6		-1%	5%	8%	12%	18%
	2100		1,4	2,3	2,8	3,5	5,5		2%	6%	10%	19%	25%
	2035	JJA	0,5	0,9	1,1	1,3	2,3	AMJJAS	-5%	1%	3%	6%	12%
	2065		1,0	1,7	2,2	2,5	4,4		-2%	2%	5%	8%	25%
	2100		0,9	2,2	2,9	3,3	5,4		-4%	5%	9%	13%	37%
22 Eastern Asia	2035	DJF	0,3	0,8	0,9	1,2	2,3	ONDJFM	-9%	-1%	2%	4%	10%
	2065		0,8	1,6	2,0	2,6	3,1		-5%	3%	6%	10%	16%
	2100		0,9	2,1	2,6	3,1	4,7		-9%	6%	9%	16%	30%
	2035	JJA	0,4	0,7	0,9	1,1	1,6	AMJJAS	-3%	0%	2%	3%	6%
	2065		0,7	1,4	1,9	2,4	3,1		-1%	3%	6%	8%	18%
	2100		0,7	1,8	2,5	3,0	3,9		1%	5%	8%	12%	24%
19 West Asia	2035	DJF	0,0	0,7	1,0	1,3	1,6	ONDJFM	-7%	0%	3%	7%	20%
	2065		0,5	1,4	1,9	2,3	2,8		-10%	-1%	3%	8%	21%
	2100		0,6	1,9	2,4	2,9	3,8		-14%	-3%	3%	12%	20%

	2035	JJA	0,2	0,9	1,2	1,4	2,1	AMJJAS	-10%	-4%	1%	6%	55%
	2065		1,1	1,8	2,2	2,6	4,0		-20%	-6%	-2%	2%	51%
	2100		1,2	2,1	2,8	3,4	4,7		-29%	-8%	-3%	5%	60%
23 South Asia	2035	DJF	0,1	0,7	0,9	1,1	1,4	ONDJFM	-18%	-5%	-1%	3%	8%
	2065		0,6	1,5	1,8	2,3	2,6		-17%	-3%	5%	7%	13%
	2100		1,4	2,1	2,4	3,0	3,7		-9%	-1%	9%	14%	28%
	2035	JJA	0,3	0,5	0,7	0,9	1,3	AMJJAS	-3%	1%	2%	6%	9%
	2065		0,7	1,1	1,4	1,7	2,6		-3%	5%	8%	11%	14%
	2100		0,5	1,4	1,8	2,4	3,3		-7%	7%	11%	14%	19%
24 Southeast	2035	DJF	0,3	0,5	0,7	0,8	1,1	ONDJFM	-2%	1%	2%	4%	12%
Asia (land)	2065		0,6	1,1	1,3	1,7	2,2		-1%	2%	4%	8%	13%
	2100		0,8	1,5	1,7	2,2	3,0		-5%	4%	7%	10%	16%
	2035	JJA	0,3	0,6	0,7	0,8	1,2	AMJJAS	-3%	0%	1%	4%	7%
	2065		0,7	1,1	1,2	1,6	2,2		-2%	2%	4%	7%	12%
	2100		0,9	1,4	1,6	2,2	2,7		-2%	3%	6%	10%	19%
Southeast	2035	DJF	0,3	0,5	0,6	0,7	1,0	ONDJFM	-4%	0%	2%	4%	13%
Asia (sea)	2065		0,6	1,0	1,2	1,3	1,9		-4%	0%	3%	7%	13%
	2100		0,9	1,2	1,5	1,7	2,6		-4%	0%	3%	7%	13%
	2035	JJA	0,3	0,5	0,6	0,7	1,0	AMJJAS	-2%	0%	2%	3%	10%
	2065		0,7	1,0	1,1	1,3	1,9		-2%	2%	3%	5%	9%
	2100		0,9	1,2	1,5	1,7	2,5		-1%	3%	4%	7%	16%

Australia	**YR**	**MONTH**	**MIN**	**25**	**50**	**75**	**MAX**	**MONTH**	**MIN**	**25**	**50**	**75**	**MAX**
25 North	2035	DJF	0,2	0,6	0,9	1,1	1,9	ONDJFM	-20%	-5%	-2%	3%	9%
Australia	2065		0,9	1,2	1,5	2,1	3,4		-18%	-5%	1%	5%	12%
	2100		1,1	1,7	2,1	2,7	4,0		-31%	-6%	-3%	4%	9%
	2035	JJA	0,2	0,7	0,9	1,1	1,4	AMJJAS	-48%	-11%	-2%	2%	15%
	2065		0,9	1,4	1,6	1,9	2,3		-53%	-16%	-7%	-1%	17%
	2100		0,8	1,8	2,1	2,6	2,9		-46%	-20%	-7%	3%	9%
26 S. Australia/	2035	DJF	0,3	0,6	0,8	1,0	1,2	ONDJFM	-27%	-6%	-2%	2%	8%
New Zealand	2065		0,8	1,2	1,5	1,9	2,2		-18%	-5%	0%	3%	11%
	2100		1,1	1,6	1,9	2,4	3,0		-17%	-7%	-3%	2%	8%
	2035	JJA	0,1	0,6	0,6	0,8	1,0	AMJJAS	-22%	-4%	-1%	1%	4%
	2065		0,6	1,0	1,2	1,4	1,6		-21%	-8%	-3%	2%	11%
	2100		0,7	1,4	1,6	1,8	2,3		-20%	-9%	-3%	2%	7%

Antarctica	YR	MONTH	MIN	25	50	75	MAX	MONTH	MIN	25	50	75	MAX
Land	2035	DJF	0,1	0,5	0,6	0,8	1,3	ONDJFM	-4%	1%	3%	5%	10%
	2065		0,2	1,1	1,4	1,6	2,3		-8%	3%	6%	8%	17%
	2100		0,5	1,5	1,9	2,3	3,1		-6%	6%	8%	12%	22%
	2035	JJA	-0,5	0,6	0,8	0,9	1,8	AMJJAS	-3%	3%	5%	7%	11%
	2065		-0,1	1,1	1,4	1,8	2,5		0%	6%	9%	14%	18%
	2100		-0,3	1,6	2,0	2,6	3,8		-3%	9%	13%	18%	25%
Sea	2035	DJF	-0,3	0,2	0,4	0,5	0,7	ONDJFM	-1%	1%	3%	3%	5%
	2065		-0,4	0,5	0,6	0,9	1,3		1%	3%	5%	5%	8%
	2100		-0,3	0,6	0,9	1,3	1,9		1%	4%	6%	8%	11%
	2035	JJA	-0,7	0,4	0,6	1,0	1,9	AMJJAS	0%	2%	2%	4%	5%
	2065		-0,6	0,7	1,1	1,7	3,3		2%	4%	5%	7%	10%
	2100		-0,8	1,1	1,6	2,6	3,8		3%	5%	7%	10%	13%

Chapter 14: Climate Phenomena and their Relevance for Future Regional Climate Change

Coordinating Lead Authors: Jens Hesselbjerg Christensen (Denmark), Krishna Kumar Kanikicharla (India)

Lead Authors: Edvin Aldrian (Indonesia), Soon-Il An (Korea), Iracema Fonseca Albuquerque Cavalcanti (Brazil), Manuel de Castro (Spain), Wenjie Dong (China), Prashant Goswami (India), Alex Hall (USA), Joseph Katongo Kanyanga (Zambia), Akio Kitoh (Japan), James Kossin (USA), Ngar-Cheung Lau (USA), James Renwick (New Zealand), David Stephenson (UK), Shang-Ping Xie (USA), Tianjun Zhou (China)

Contributing Authors: Tercio Ambrizzi, Bruce Anderson, Osamu Arakawa, Raymond Arritt, Mark Baldwin, Mathew Barlow, David Barriopedro, Michela Biasutti, Sebastien Biner, David Bromwich, Josephine Brown, Wenju Cai, Leila V. Carvalho, Ping Chang, Ole Bøssing Christensen, Clara Deser, Kerry Emanuel, Hirokazu Endo, David Enfield, Amato Evan, Belen Rodriguez de Fonseca, Alessandra Giannini, Annamalai Hariharasubramanian, Ashok Karumuri, Jack Katzfey, Erik Kjellström, Jeff Knight, Thomas Knutson, Ashwini Kulkarni, Ashok Karumuri, William K. Lau, Geert Lenderink, Chris Lennard, Renping Lin, Neil Mackellar, Victor Magnana, Gareth Marshall, Linda Mearns, Jerry Meehl, Claudio Menendez, Hiroyuki Murakami, David Neelin, Geert Jan van Oldenborgh, Martin Olesen, Jan Polcher, Yun Qian, Paulo Ruti, James Screen, Jan Sedlacek, Silvina Solman, Martin Stendel, Izuru Takayabu, John Turner, Caroline Ummenhofer, Kevin Walsh, Bin Wang, Chunzai Wang, Ian Watterson, Matthew Widlansky, Andrew Wittenberg, Tim Woollings, Sang-Wook Yeh, Chidong Zhang, Lixia Zhang, Xiaotong Zheng, Liwei Zou

Review Editors: John Fyfe (Canada), Won-Tae Kwon (Korea), Kevin Trenberth (USA), David Wratt (New Zealand)

Date of Draft: 5 October 2012

Notes: TSU Compiled Version

Figures

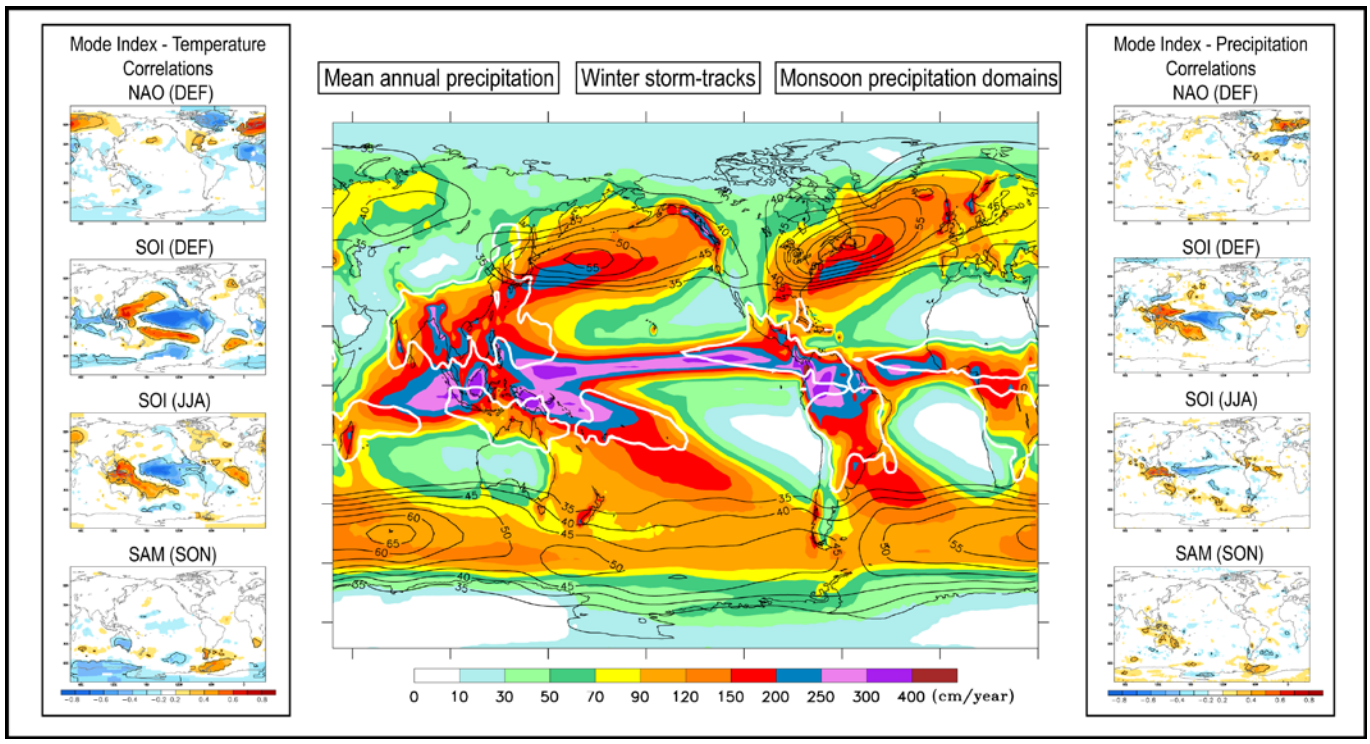

Box 14.1, Figure1: Global distribution of average annual rainfall (in cm/year) from 1979-2010 GPCP data base, monsoon precipitation domain (white contours) as defined by (Kim et al., 2011a) and winter storm-tracks in both hemispheres (black contours) depicted by contours of band-pass filtered root-mean-square of 500 hPa geopotential height in m (as proposed by (Blackmon et al., 1977) from 1979–2010 NCEPv1 reanalysis (reference here). In left (right) column seasonal correlation maps of NAO, SOI (the atmospheric component of ENSO) and SAM mode indexes vs. monthly temperature (precipitation) anomalies in boreal winter (DJF) and austral winter (JJA) or spring (SON). Grey contours indicate a 99% significance level. The mode indexes were taken from NOAA (http://www.esrl.noaa.gov/psd/data/climateindices/list/), global temperatures from NASA GISTEMP (http://data.giss.nasa.gov/gistemp/) and global precipitations from GPCP (http://www.esrl.noaa.gov/psd/data/gridded/data.gpcp.html).

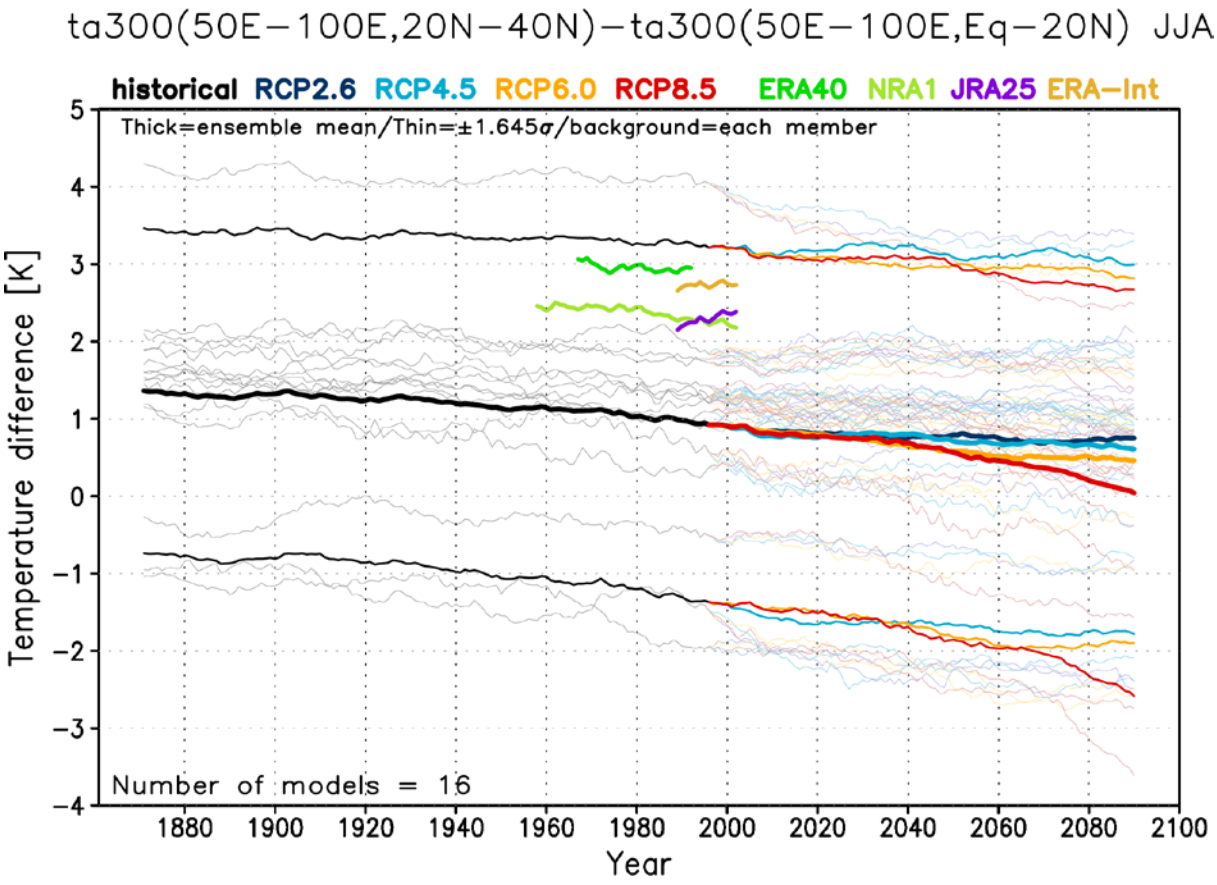

Figure 14.1: Time series of meridional temperature difference of June to August mean 300 hPa temperature between 50°E–100°E, 20°N–40°N and 50°E–100°E, 0°N–20°N (20 years running mean). Thin black, dark blue, warm blue, warm yellow and bright red lines denote each CMIP5 model results of historical, RCP2.6, RCP4.5, RCP6.0 and RCP8.5 runs, respectively. Thick lines are ensemble means of 16 CMIP5 models. 90%-range (±1.65 standard deviation) is also plotted. Four reanalysis data are shown by green (ERA40), yellow-green (NRA1), purple (JRA25) and oragne (ERA-Int) lines.

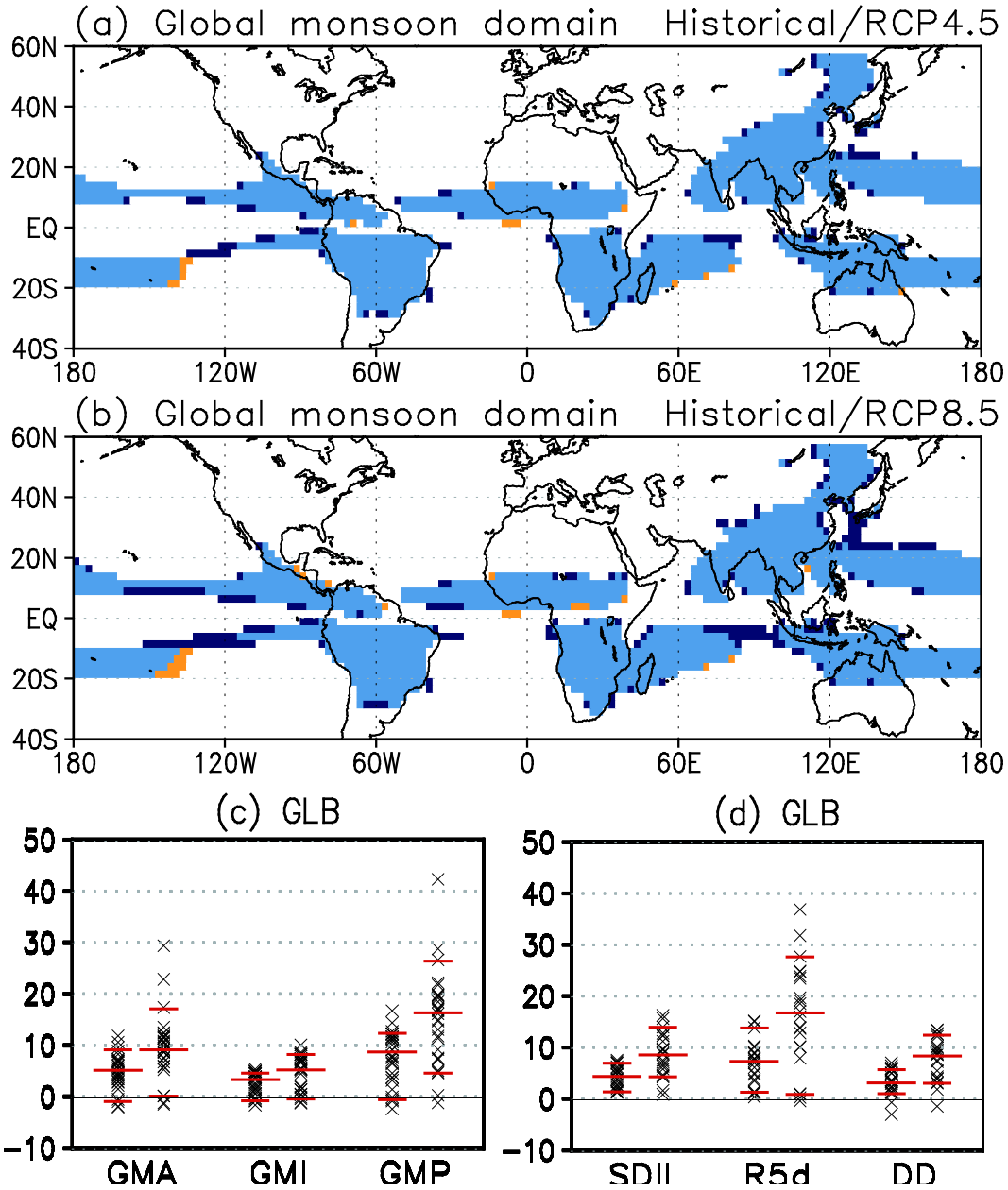

Figure 14.2: (a) Monsoon precipitation domain based on 29 CMIP5 multi-model mean precipitation during 1986–2005 and 2080–2099 for RCP4.5 scenario, based on the definition by Wang et al. (2011). Warm Yellow (dark blue) shading: monsoon domain only in the present (future). Blue shading: monsoon domain in the both periods. (b) As in (a), but for RCP8.5. (c) Future change ratio (%) in global monsoon area (GMA), global monsoon total precipitation (GMP), and global monsoon intensity (GMI), defined by Hsu et al. (2012), over monsoon domain defined by every model and scenario, based on monthly data by the 29 models. Left (right) sides: RCP4.5 (RCP8.5) scenario. Red line: 10th, 50th, and 90th percentile. (d) As in (c), but for simple precipitation daily intensity index (SDII), annual maximum 5-day precipitation total (R5d), and dry days (DD), based on daily data by 21 CMIP5 models. All these indices are calculated for the summer season (NH: MJJAS, SH: NDJFM).

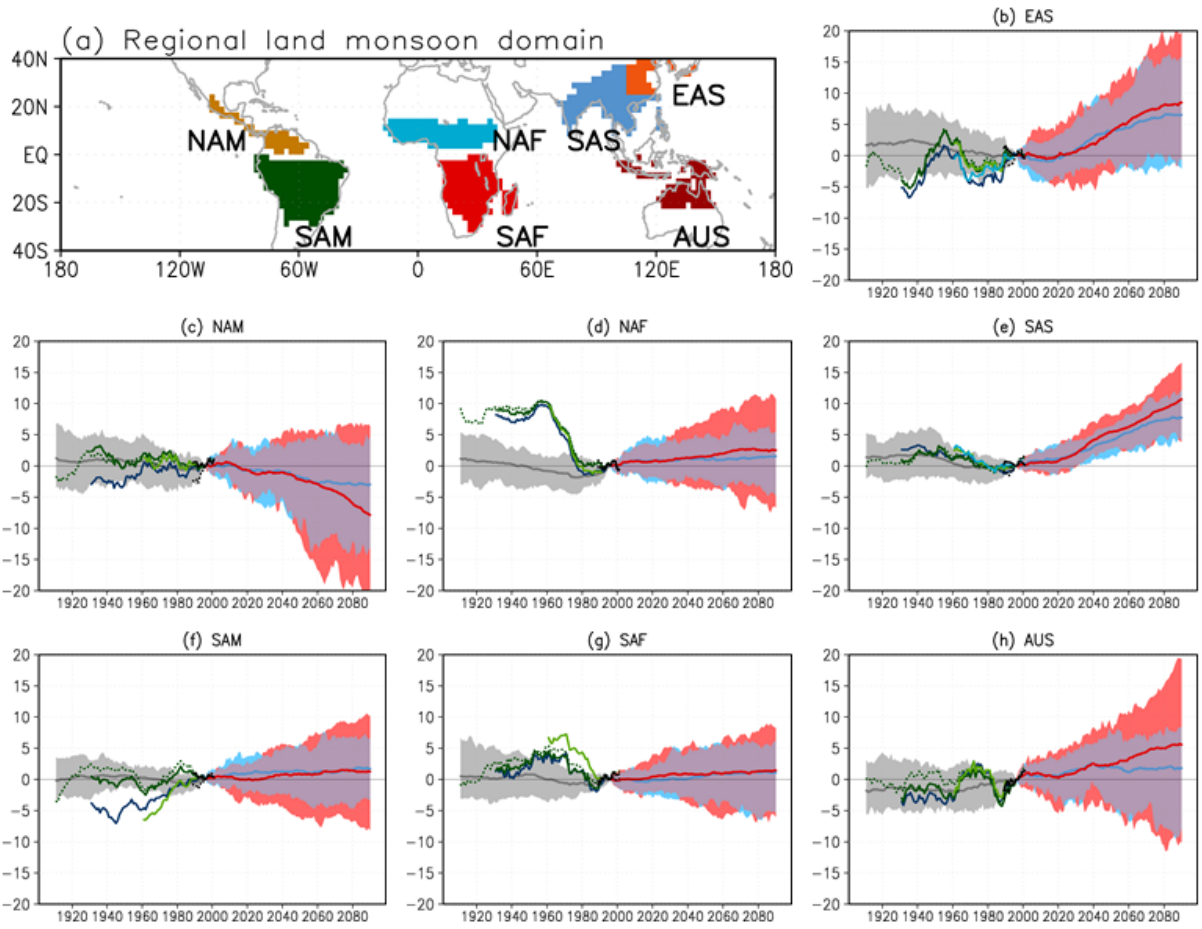

Figure 14.3: Time series of observed and simulated summer precipitation anomalies (%; 20 years running mean) relative to the base period average (1986–2005, except GPCC VASClimO (1986–2000)) over land global monsoon domain. The monsoon domains defined for the base period are fixed for the whole period. For the time series of simulations, Historical (grey), RCP4.5 (blue), and RCP8.5 (red) simulations by 29 CMIP5 model ensembles are shown in 10th and 90th percentile (shading), and in all model average (thick line). For the time series of observations, CRU TS3.1 (dark blue), APHRODITE (light blue), and GPCC v.6 (deep green with solid line) are calculated using only grid boxes (2.5 degree in lon./lat.) where at least an observation site exists for more than 80% of the whole period (1921–2005 for CRU TS3.1 and GPCC v.6; 1951–2005 for APHRODITE); GPCC VASClimO (light green), GPCC v.6 (deep green with dot), GPCP (black) and CMAP (black with dot) are calculated using all grids for the period (1901–2010 for GPCC v.6; 1951-2000 for GPCC VASClimO; 1979–2010 for GPCP and CMAP). (a) Land monsoon domains with regional division. (b) EAS. (c) NAM. (d) NAF. (e) SAS. (f) SAM. (g) SAF. (h) AUS.

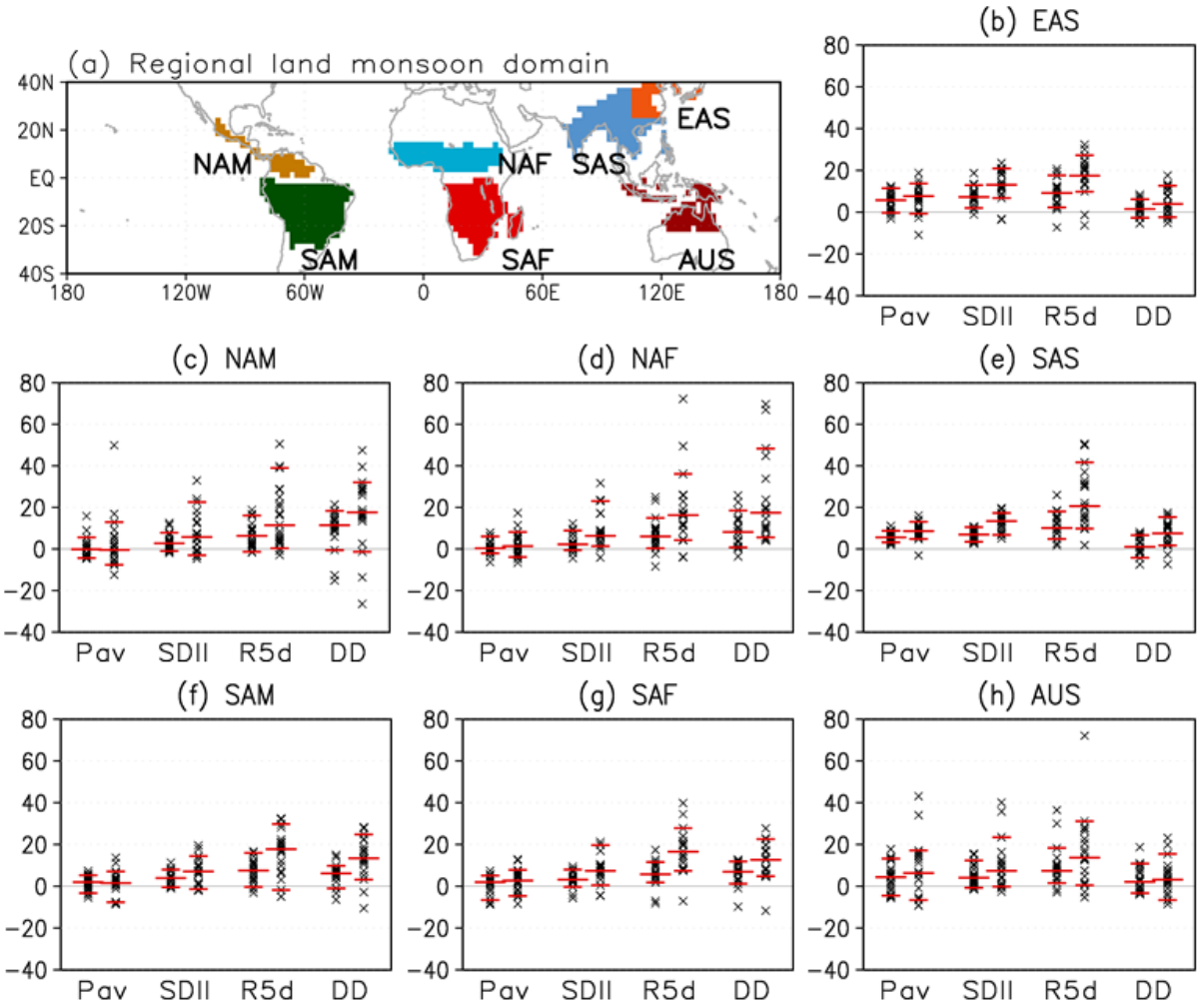

Figure 14.4: Change ratio (%) in averaged precipitation (Pav), simple precipitation daily intensity index (SDII), annual maximum 5-day precipitation total (R5d), and dry days (DD) over each regional land monsoon domain, based on daily data by 21 CMIP5 models. All these indices are calculated over monsoon domains determined by each model and each scenario for the summer season (NH: MJJAS, SH: NDJFM). Left (right) side plots are for RCP4.5 (RCP8.5) scenario. Red lines indicate 10th, 50th, and 90th percentile. (a) Land monsoon domains with regional division. (b) EAS. (c) NAM. (d) NAF. (e) SAS. (f) SAM. (g) SAF. (h) AUS.

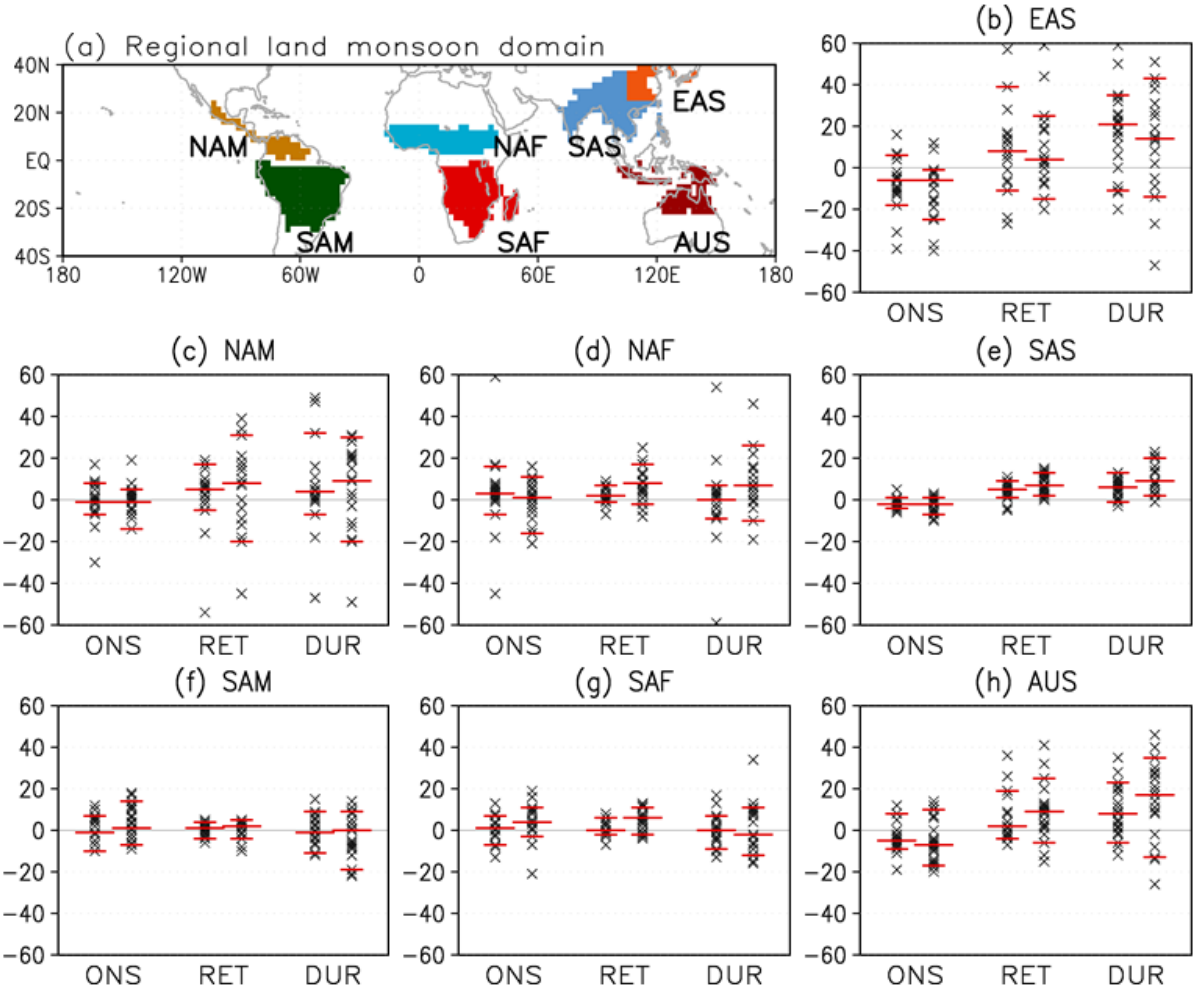

Figure 14.5: As for Figure 14.4, but for future changes (days) in monsoon onset date, retreat date and duration. The calculation is based on the definition by Wang and LinHo (2002)using daily precipitation climatology (filtered with 12 harmonics) averaged over regional monsoon domain. It is noted that for EAS the threshold value of the relative precipitation is adjusted from 5.0 to 4.0 mm day^{-1}.

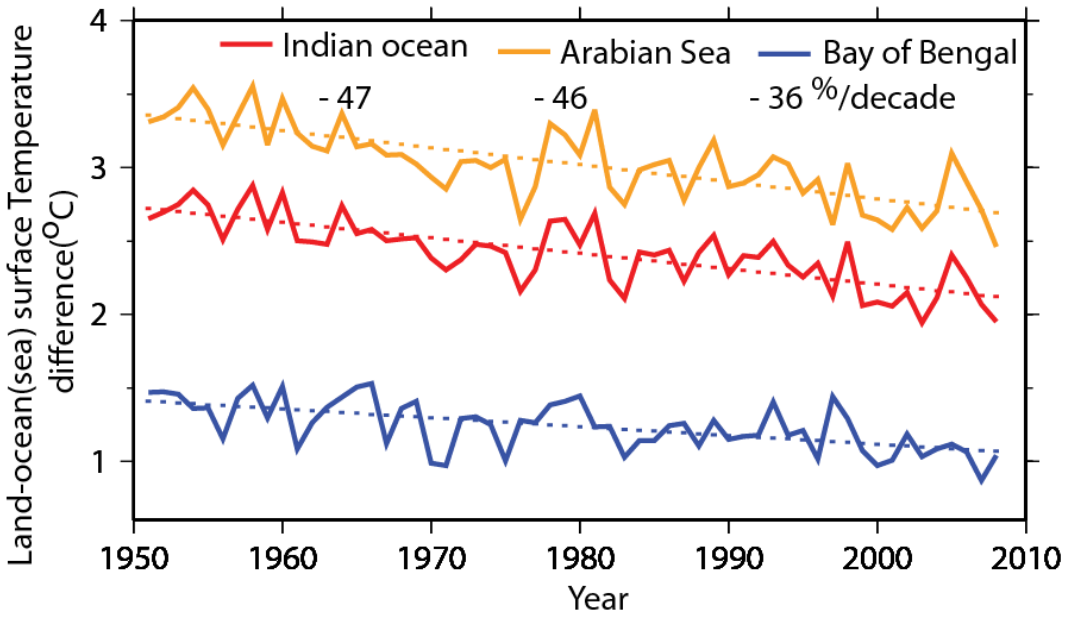

Figure 14.6: Inter annual variability and linear trend in the difference between area averaged surface temperature over the Indian land mass and the adjoining seas (Indian Ocean, Arabian sea and Bay of bengal) for the period 1951–2010 (adopted from, Ramesh and Goswami, 2007a). The linear trends have been expressed as % of standard deviation over the period.

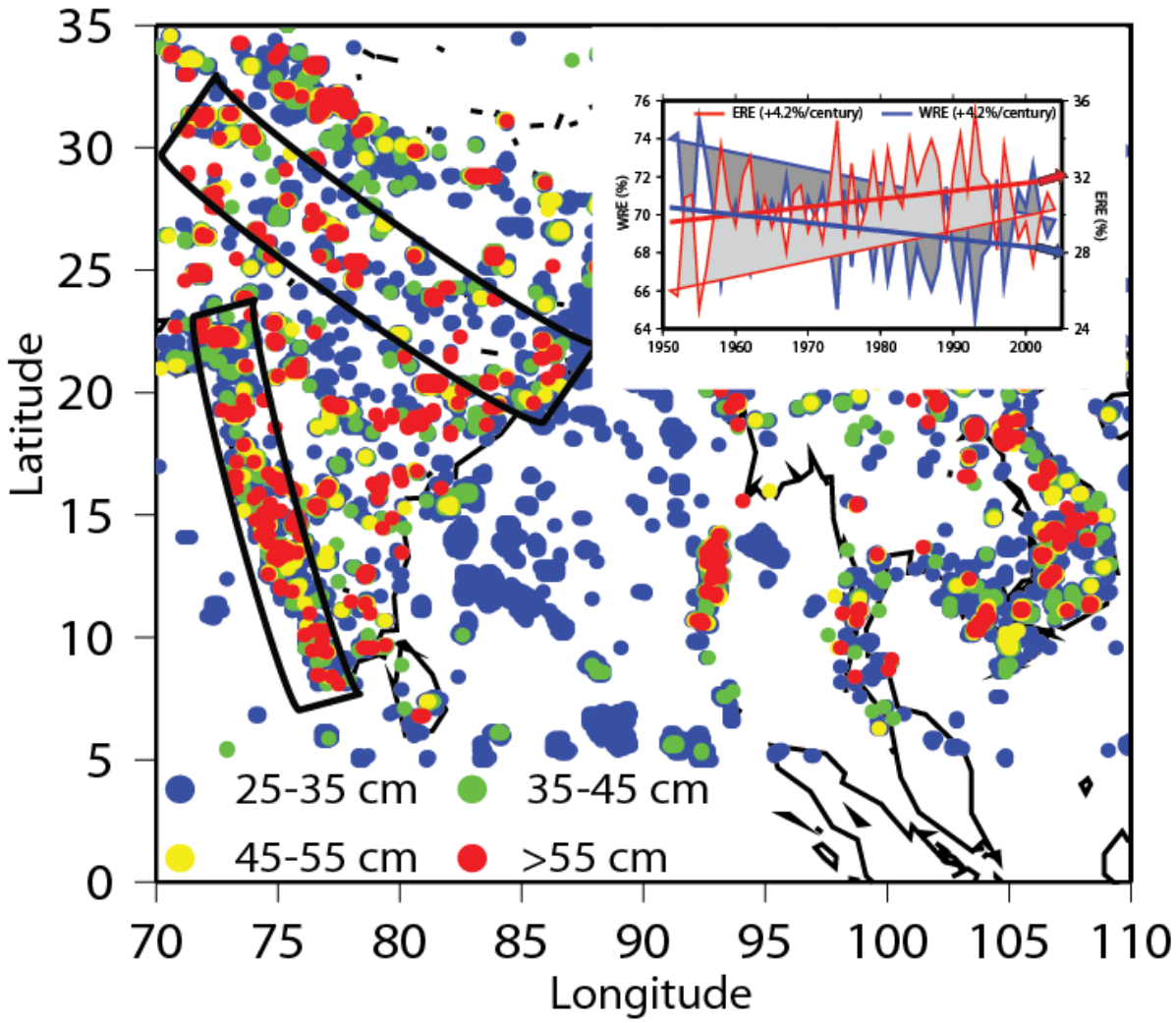

Figure 14.7: Spatial distribution of ERE of different categories accumulated over five years (2001–2005). The high density of ERE over the west coast and along the flanks of the monsoon trough is prominent.Inter-annual variations in the percentage contribution of ERE (light grey shaded)/ WRE (dark grey shaded) to seasonal (June-September) rainfall over India (black) and the linear trend line (red). The percentage contribution of ERE has grown in the recent years; the linear trend of ERE component is +0.042% yr^{-1} (inset). The analysis is based on daily rainfall data from IMD for the period 1951–2004 (adopted from, Goswami and Ramesh, 2008; Ramesh and Goswami, 2007a).

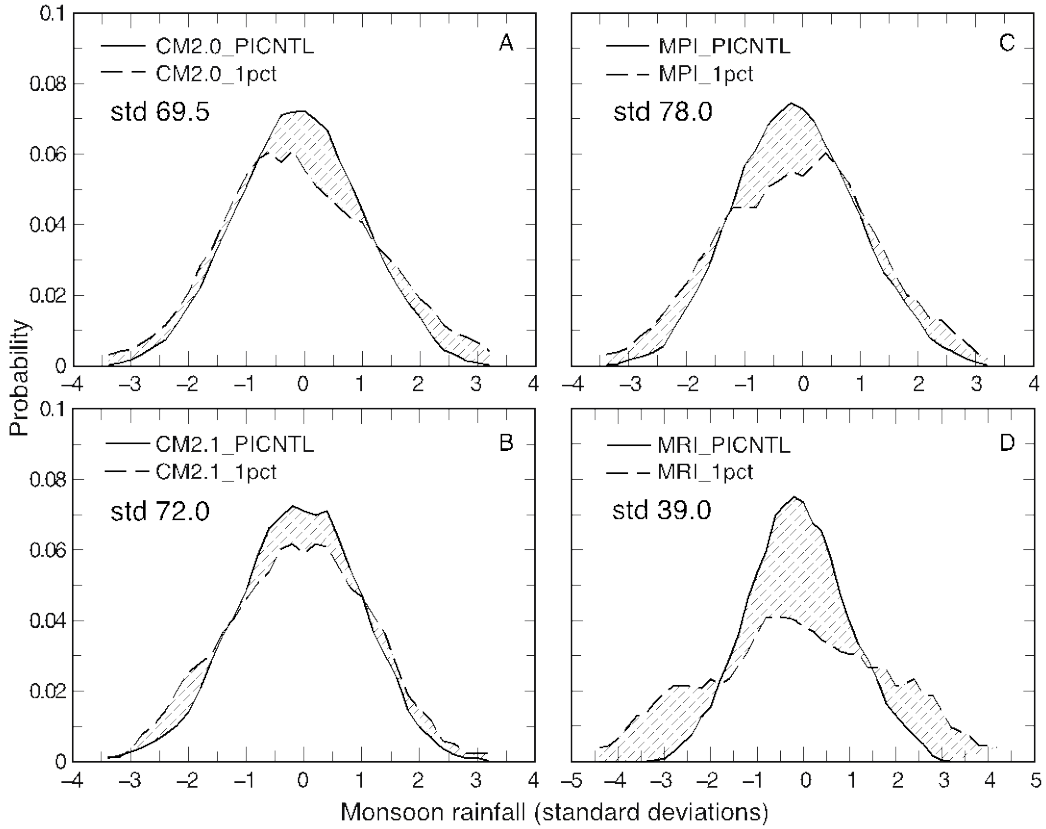

Figure 14.8: Climate scenarios. Normalized probability of occurrences (number of occurrences divided by the total number of years) of interannual variability of South Asian monsoon rainfall from four CMIP3 models that depict realistic mean monsoon precipitation and ENSO–monsoon association. a, gfdl_cm2_0. b, gfdl_cm2_1. c, mpi_echam5. d, mri_cgcm2_3_2a. Pre-industrial control probability density function (PDF; solid line) and future climate (1% per year increase in carbon dioxide experiments, 1pctto2x) PDF (dashed line) are shown. The future variations are scaled by the pre-industrial control interannual standard deviations whose values (in mm) are also shown (std). The differences in the shape of the PDFs have been tested for significance based on a Kolmogorov–Smirnov test. Although all models suggest a reduction in the occurrence of normal monsoon years (± one standard deviation in monsoon rainfall) the changes in the tails of the distribution are significant in only one model, mri_cgcm2_3_21 (d). The caveat is that this particular model has the least agreement in terms of mean and interannual standard deviation with observed rainfall). In the model that has the best agreement with observations, gfdl_cm2_1 (b), changes in the tails are not significant.

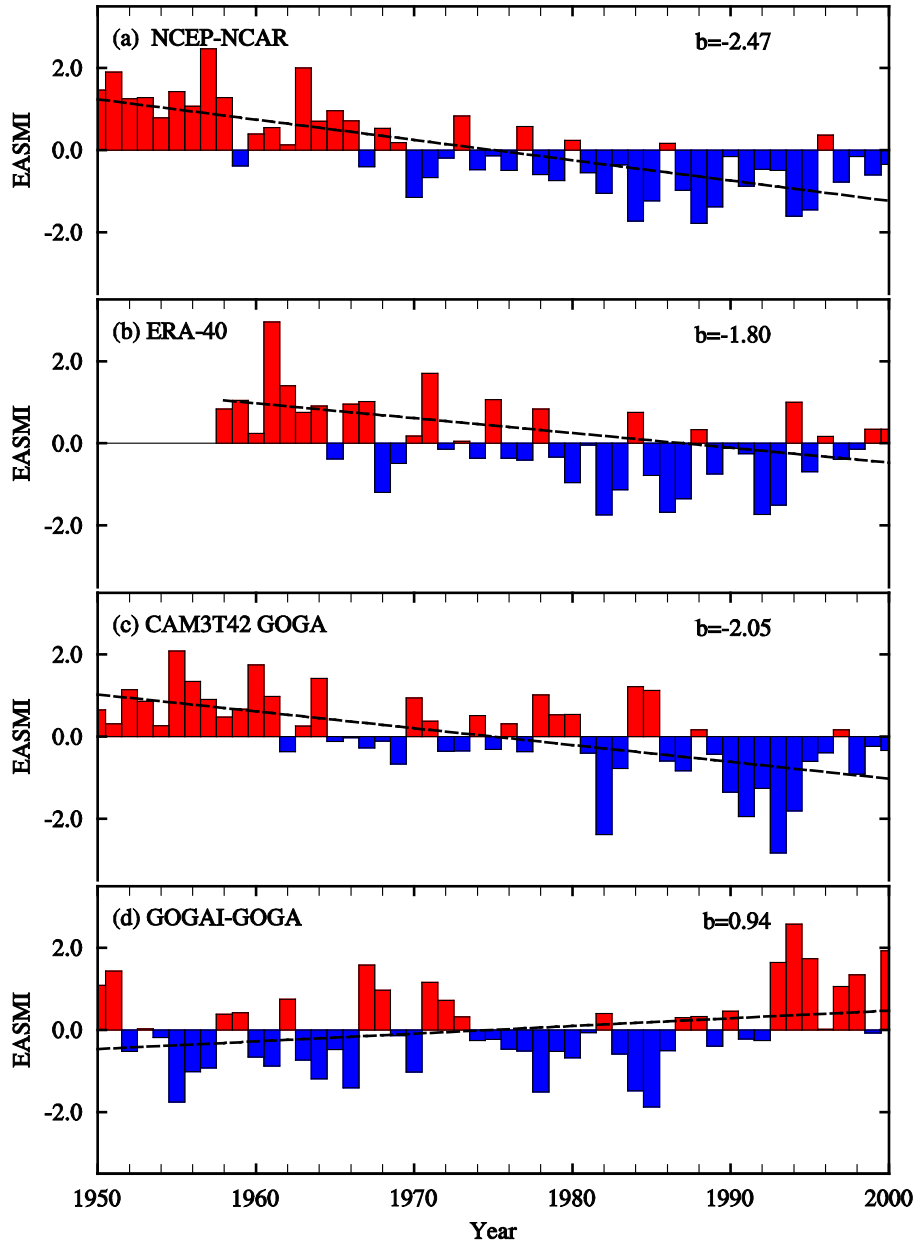

Figure 14.9: Time series of EASM indices (bars) and their trend line (dashed line) from NCEP/NCAR reanalysis, (b) ERA-40 reanalysis, (c) GOGA run of CAM3, (d) difference between GOGAI and GOGA run of CAM3. Also shown are the slope of the trends (b, change per 50-year). The EASM index is defined as the normalized zonal wind shear between 850 and 200 hPa averaged over 20°N–40°N and 110°E–140°E. GOGA run is forced by observed monthly SSTs over the global oceans from 1950 to 2000, while GOGAI is driven by global SST plus IPCC 20th century atmospheric (primarily greenhouse gases and direct aerosol) forcings (Li et al., 2010b).

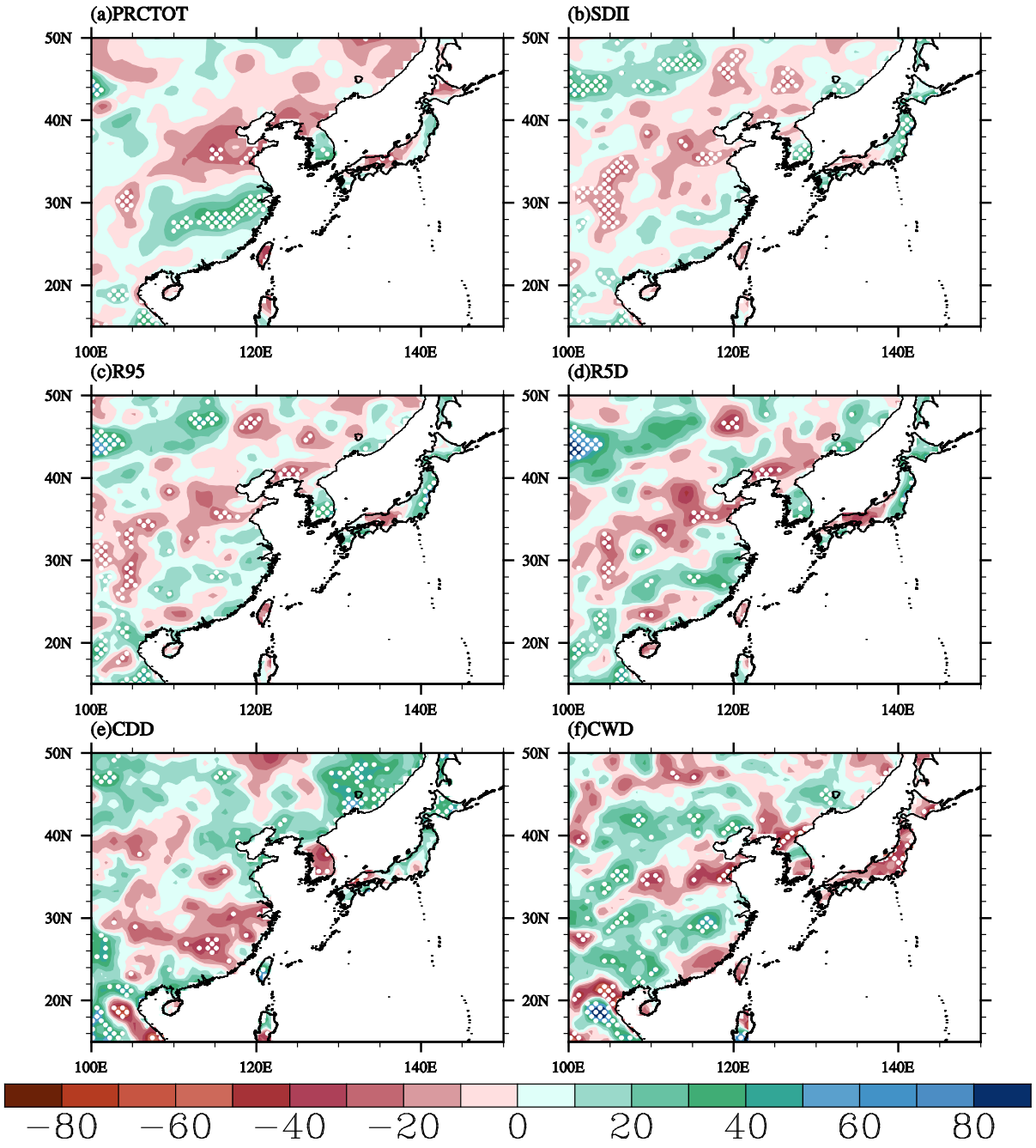

Figure 14.10: Linear trend for summer (a) total precipitation (b) SDII, (c) R95 (summer total precipitation when PR >95th percentile), (d) R5d, (e) CDD (maximum number of consecutive days with PR <1 mm)and (f) CWD (maximum number of consecutive days with PR >1mm) in percent per 50-year for summer precipitation from the APHRODITE data set for 1951–2000. The trends statistically significant at 5% level are dotted.

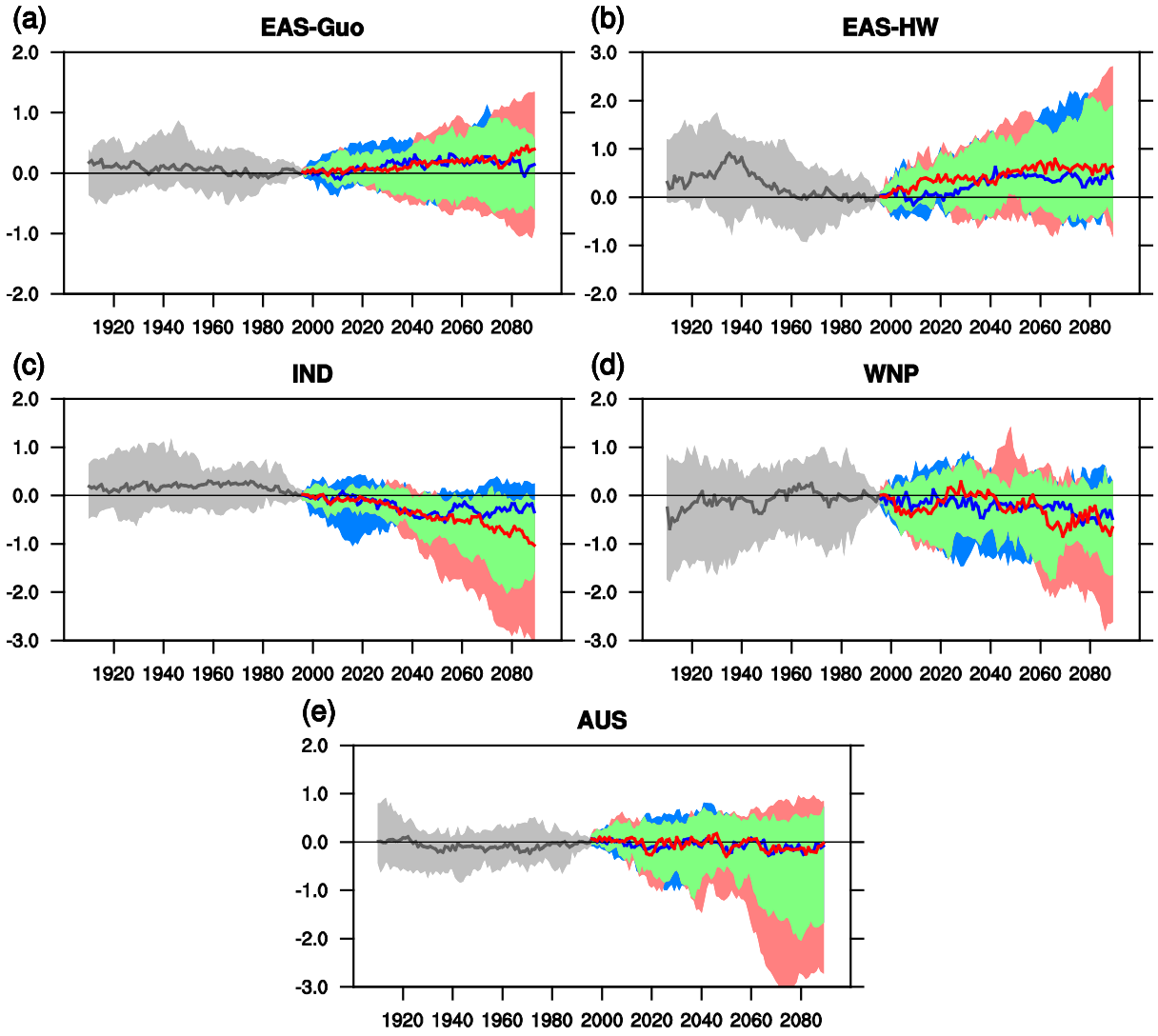

Figure 14.11: Time series of summer monsoon indices (21-year running mean) relative to the base period average (1986-2005). Historical (gray), RCP4.5 (blue) and RCP8.5 (Red) simulations by 15 CMIP5 model ensembles are shown in 10th and 90th (shading), and 50th (thick line) percentile. (a) East Asian monsoon zonal thermal contrast index, (b) East Asian summer monsoon meridional thermal contrast index, (c) Indian monsoon index, (d) western North Pacific summer monsoon index, (e) Australian monsoon index (see Zhou et al. (2009) for indices definitions)

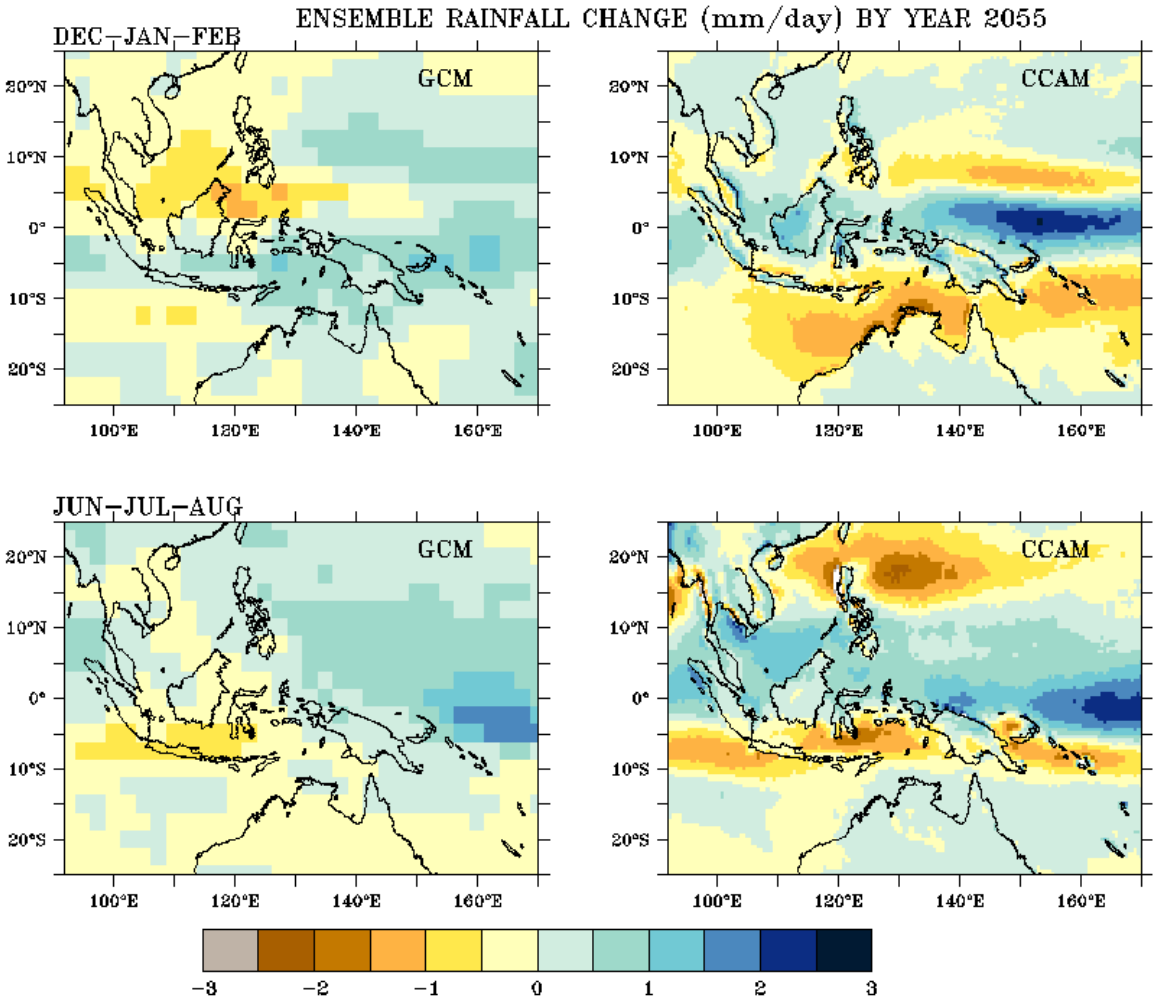

Figure 14.12: Multi-model mean rainfall change in DJF (upper row) and JJA (lower row) (mm day^{-1}) in global climate models (left) and a regional downscaling model 60 km simulations (right, (Nguyen et al., 2012)), each consisting of the same six models, for the 30-year period centred on 2055, relative to a 30-year period centred on 1990, using the A2 (high) emissions scenario.

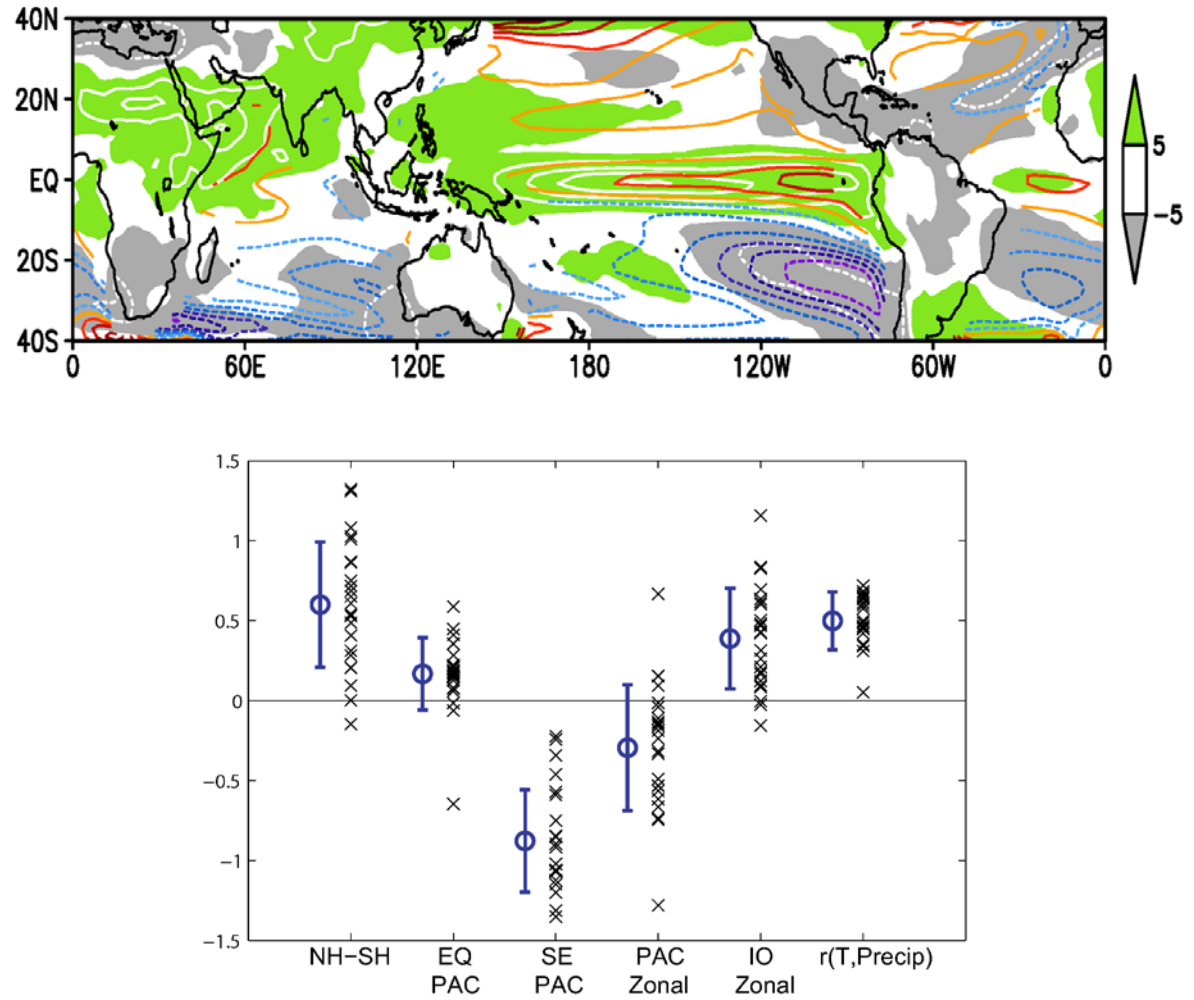

Figure 14.13: Upper panel: Annual-mean precipitation percentage change (δP/P in green/gray shade and white contours at 20% intervals), and relative SST change (color contours at intervals of 0.2°C; negative dashed) to the tropical (20°S–20°N) mean warming in RCP8.5 projections, shown as 23 CMIP5 model ensemble mean. Lower panel: SST warming pattern indices in 23-model RCP8.5 ensemble, shown as the 2050–2099 minus 1900–1949 difference. From left: Northern (EQ-60°N) minus Southern (60°S-EQ) Hemisphere; equatorial (120°E–60°W, 5°S–5°N) and Southeast (130°W–70°W, 30°S–15°S) Pacific relative to the tropical mean warming; zonal SST gradient in the equatorial Pacific (120°E–180°E minus 150°W–90°W, 5°S–5°N) and Indian (50°E–70°E, 10°S–10°N minus 90°E–110°E, 10°S-EQ) Oceans. Rightmost: spatial correlation between relative SST change and precipitation percentage change (δP/P) in the tropics (20°S–20°N). (The spatial correlation for the multi-model ensemble mean fields in the upper panel is 0.61). The circle and error bar indicate the ensemble mean and ±1 standard deviation, respectively.

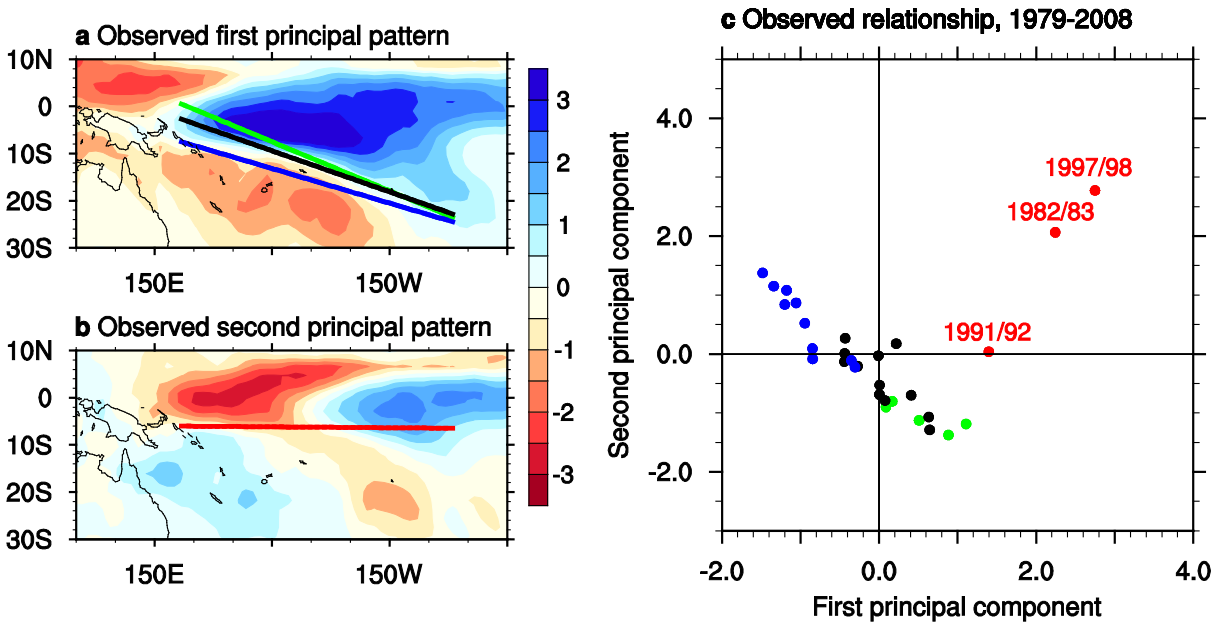

Figure 14.14: (a) and (b) – the two leading principal component patterns of rainfall (Global Precipitation Climatology Project version 2) in the SPCZ region (Eq.–30°S, 160°E–80°W), during December to February (units are mm day^{-1}). Lines superimposed in (a) show the average SPCZ position during El Niño (green), La Niña (blue) and neutral (black) states. The red line in (b) shows the average SPCZ position during zonal-SPCZ events. The SPCZ position is defined as the position where the maximum of rainfall greater than 6 mm per day5 is situated and a linear fit is applied. (c) illustrates the nonlinear relationship between the leading principal component time series. La Niña, neutral and moderate El Niño years are indicated with blue, black and green dots, respectively. A zonal SPCZ event (red dots) is defined as when the first principal component is greater than one standard deviation, and when the second principal component is positive. (from Cai et al., 2012).

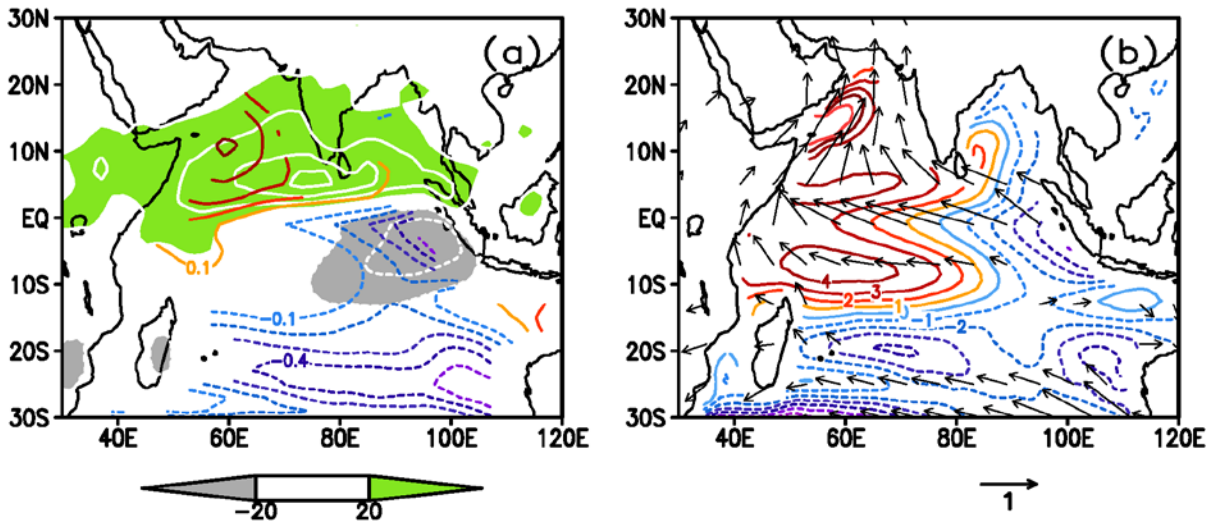

Figure 14.15: September to November changes in a 22-model CMIP5 ensemble (2050–2099 in RCP8.5 minus 1900–1949 in historical run). (a) SST (colour contours at 0.1°C intervals) relative to the tropical mean (20°S–20°N), and precipitation (shading and white contours at 20 mm per month intervals). (b) Surface wind velocity (m/s), and SSH deviation from the global mean (contours, cm). Over the equatorial Indian Ocean, ocean-atmospheric changes are in positive Bjerknes feedback, with the reduced SST warming and suppressed convection in the east.

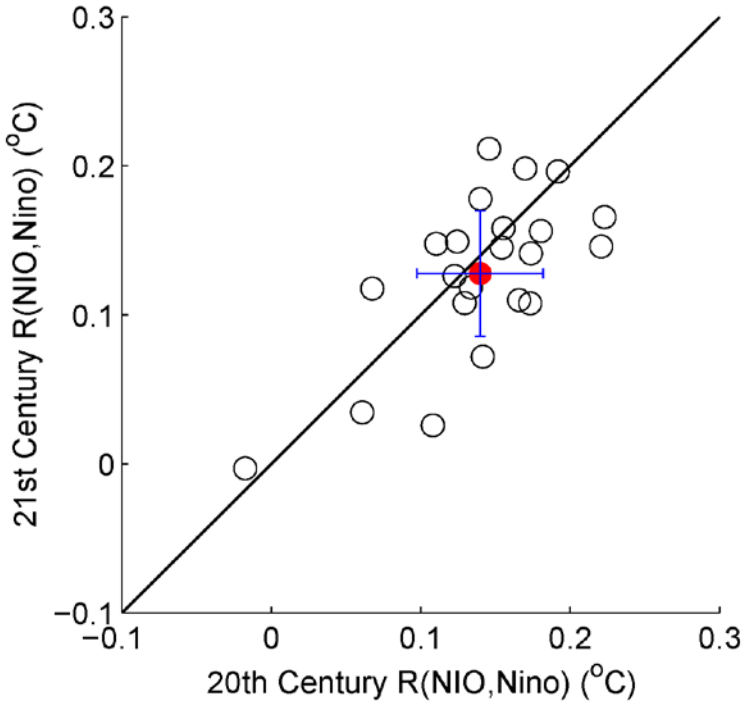

Figure 14.16: Scatter plot comparing the IOB mode in 22 CMIP5 models between the 20th century historical and 21st century RCP8.5 simulations: regression of North Indian Ocean (40°E–100°E, 0–20°N) SST during July to September upon the preceding November to January Nino3.4 (170°W–120°W, 5°S–5°N) SST. The red dot denotes the multi-model ensemble mean, and the error bar the standard deviation of inter-model variability.

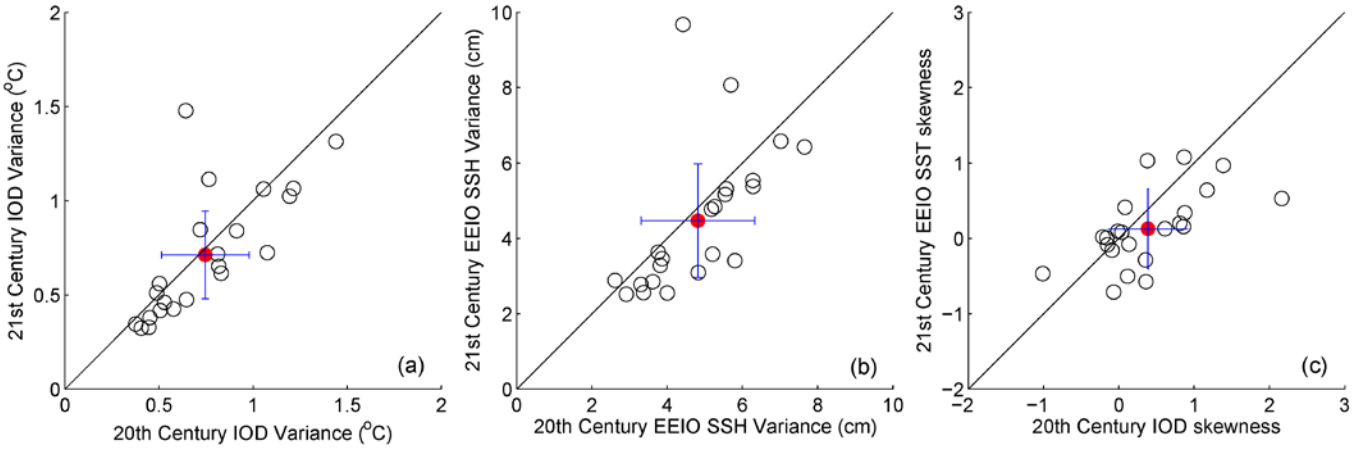

Figure 14.17: Scatter plots comparing IOD properties in 22 CMIP5 models between the 20th century historical and 21st century RCP8.5 simulations: (a) standard deviation and skewness of the dipole mode index defined as the western (50°E–70°E, 10°S–10°N) minus eastern (90°E–110°E, 10°S–0°) SST difference; and (b) SSH standard deviation in the eastern equatorial Indian Ocean (90°E–110°E, 10°S–0°). September to November interannual anomalies are used. The red dot denotes the multi-model ensemble mean, and the error bar the standard deviation of inter-model variability. Most models show little change in IOD variance but a decrease in both SSH variance and IOD skewness.

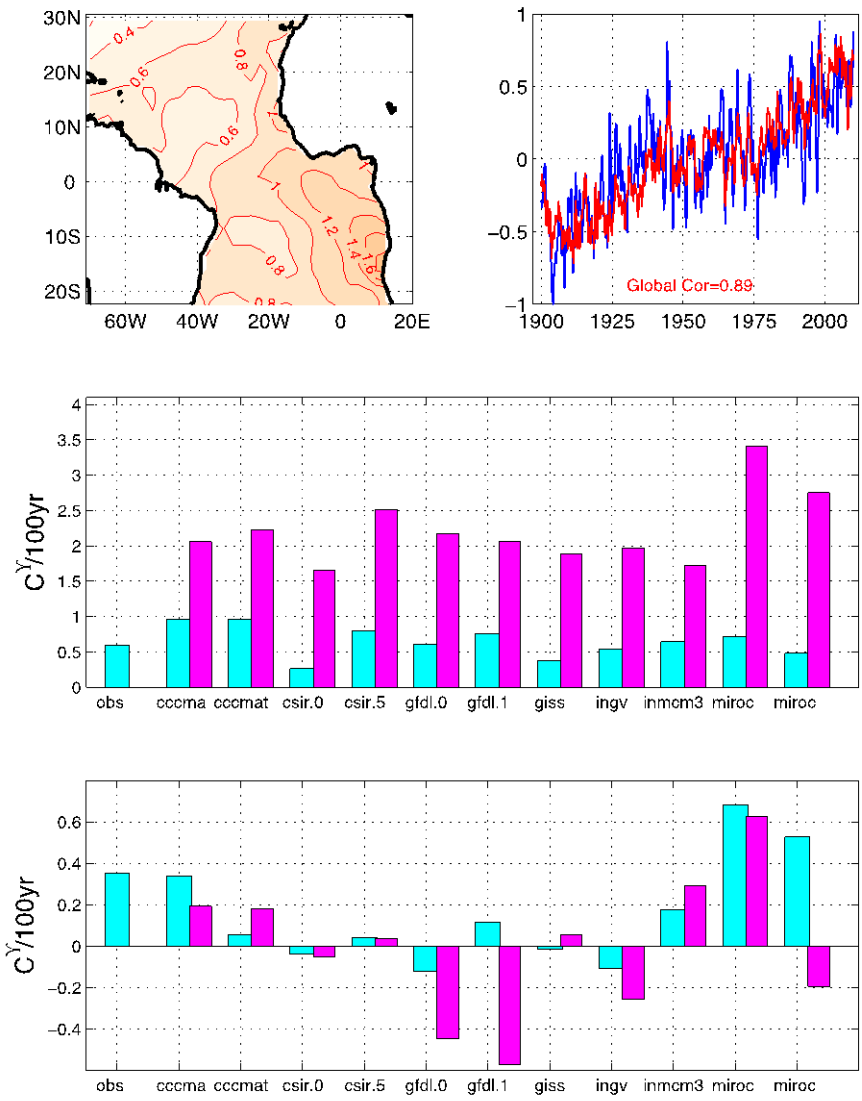

Figure 14.18: The leading EOF (left) of a gridded observed monthly mean SST record from Hadley Centre sea ice and SST version 1 (HadISST1) data set (Rayner et al., 2003), which explains 36% of the SST variance, and the associated monthly mean time series (right) normalized by its maximum absolute value (blue) overlaid by the globally averaged SST (red). The middle and bottom panel show the observed and modeled linear trend values for SST averaged in the tropical Atlantic basin and for an interhemispheric SST index, respectively, in the 20th century simulation (cyan) and the A1B simulation (magenta).

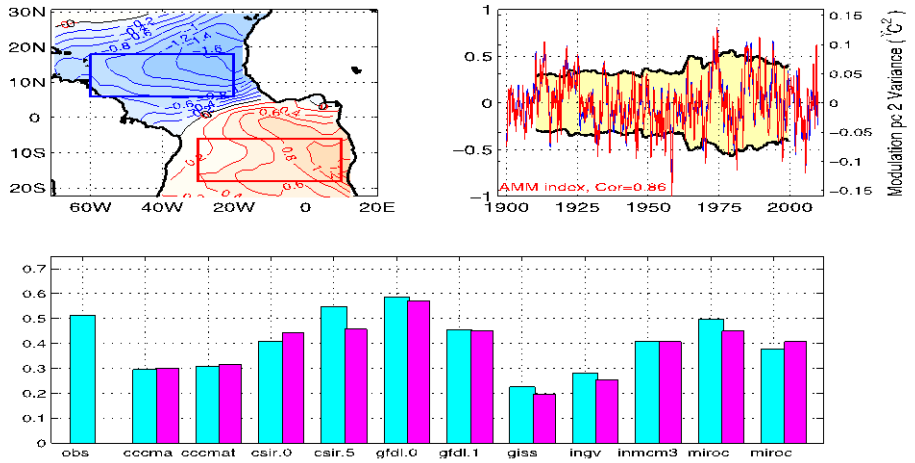

Figure 14.19: Same as Figure 14.18, except for the 2nd EOF (left), which explains 14% of the monthly mean SST variance. The associated time variation(blue in right panel) is overlaid by a detrended interhemispheric SST gradient index derived by differencing the SSTs averaged in the two boxes shown in the left panel. The two time series are correlated at r = 0.86. The yellow shade and black lines show the amplitude modulation of the PC time series using a 21-year moving window. Standard deviations of the observed and modeled March-April-May interhemispheric SST gradient time series are shown in the bottom panel for the 20th century simulation (cyan) and the A1B simulation (magenta), respectively.

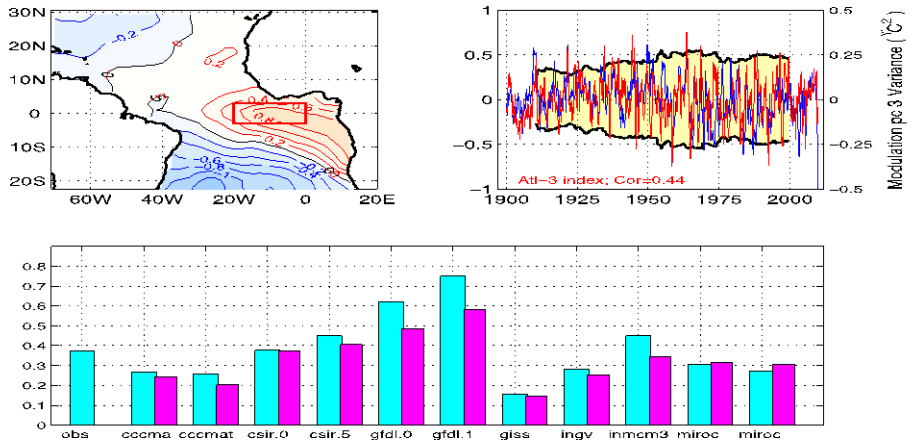

Figure 14.20: Same as Figure 14.18, except for the 3rd EOF (upper left), which explains 9% of the monthly mean SST variance. The associated time series (blue in upper right panel) is overlaid by a detrended Atl-3 index derived by averaging the monthly mean SST in the box shown in the left panel. The two time series are correlated at r = 0.5. The yellow shade and black lines show the amplitude modulation of the Atl-3 index using a 21-year moving window. Standard deviations of the observed and modeled September-October-November detrended Atl-3 SST time series are shown in the bottom panel for the 20th century simulation (cyan) and the A1B simulation (magenta).

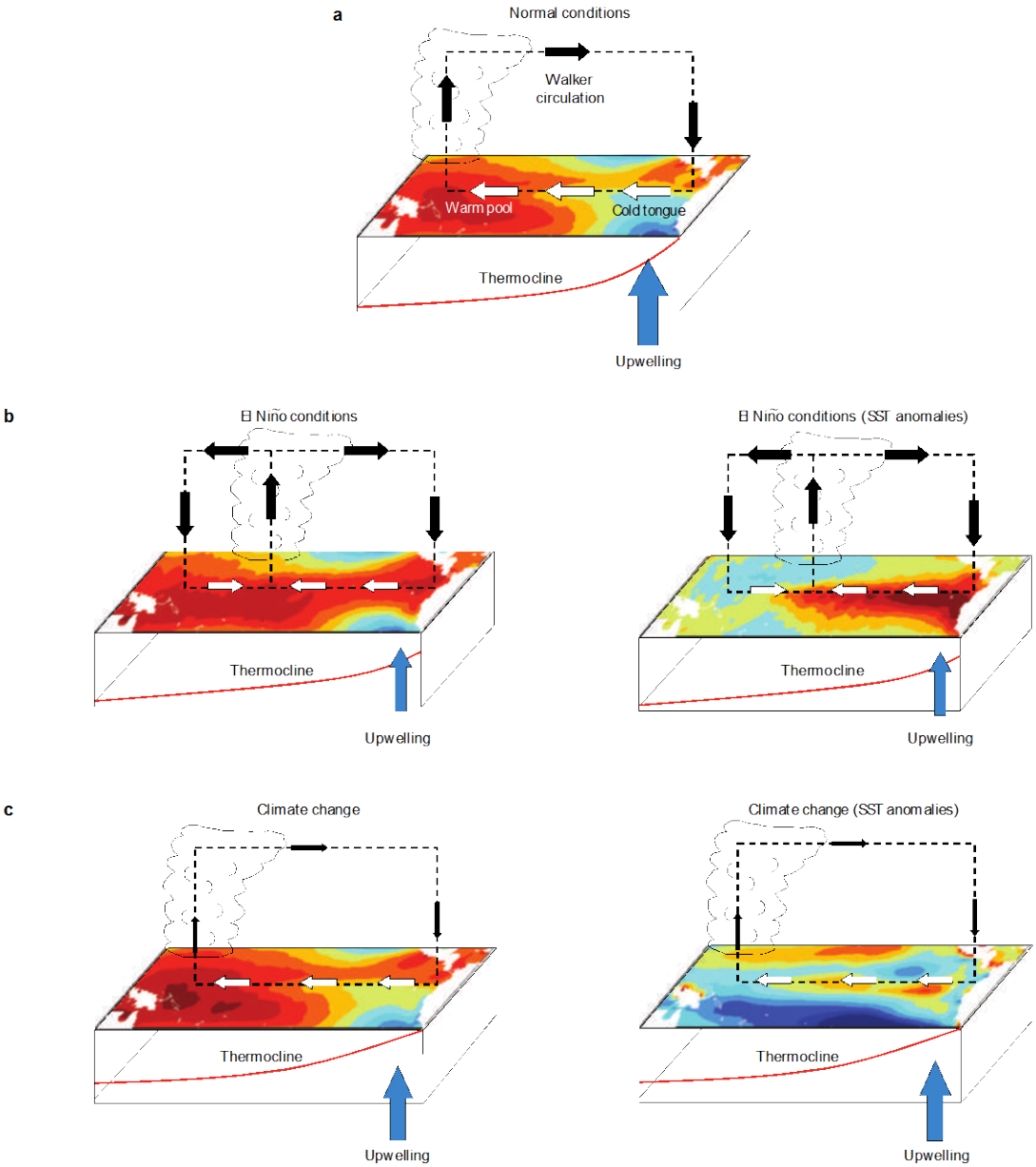

Figure 14.21: Idealized schematic showing atmospheric and oceanic conditions of the tropical Pacific region and their interactions during normal conditions, El Niño conditions, and in a warmer world. a, Mean climate conditions in the tropical Pacific, indicating SSTs, surface wind stress and associated Walker circulation, the mean position of convection, and the mean upwelling and position of the thermocline. b, Typical conditions during an El Niño event. SSTs are anomalously warm in the east; convection moves into the central Pacific; the trade winds weaken in the east and the Walker circulation is disrupted; the thermocline flattens and the upwelling is reduced. c, The likely mean conditions under climate change derived from observations, theory and CGCMs. The trade winds weaken; the thermocline flattens and shoals; the upwelling is reduced although the mean vertical temperature gradient is increased; and SSTs (shown as anomalies with respect to the mean tropical-wide warming) increase more on the equator than off. Diagrams with absolute SST fields are shown on the left, diagrams with SST anomalies are shown on the right. For the climate change fields, anomalies are expressed with respect to the basin average temperature change so that blue colors indicate a warming smaller than the basin mean, not a cooling (Collins et al., 2010).

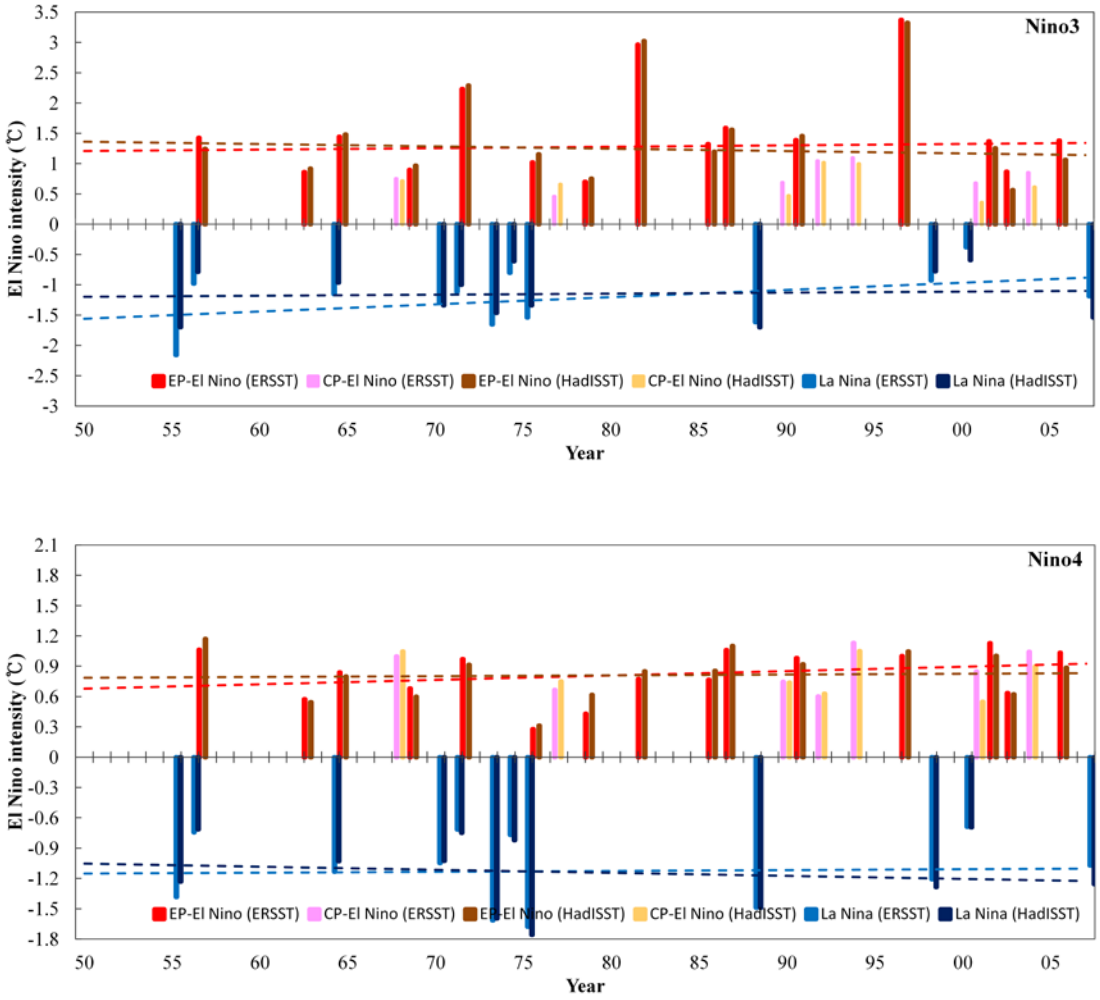

Figure 14.22: Intensities of El Niño and La Niña events in the eastern equatorial Pacific (Niño3 region; upper) and in the central equatorial Pacific (Niño4 region; lower) the estimated linear trends, obtained from ERSST and HadISST (upper). Red and blue lines from ERSST, and dark red and dark blue lines from HadISST. EP and CP events are selected based on B case of Table 14.1.

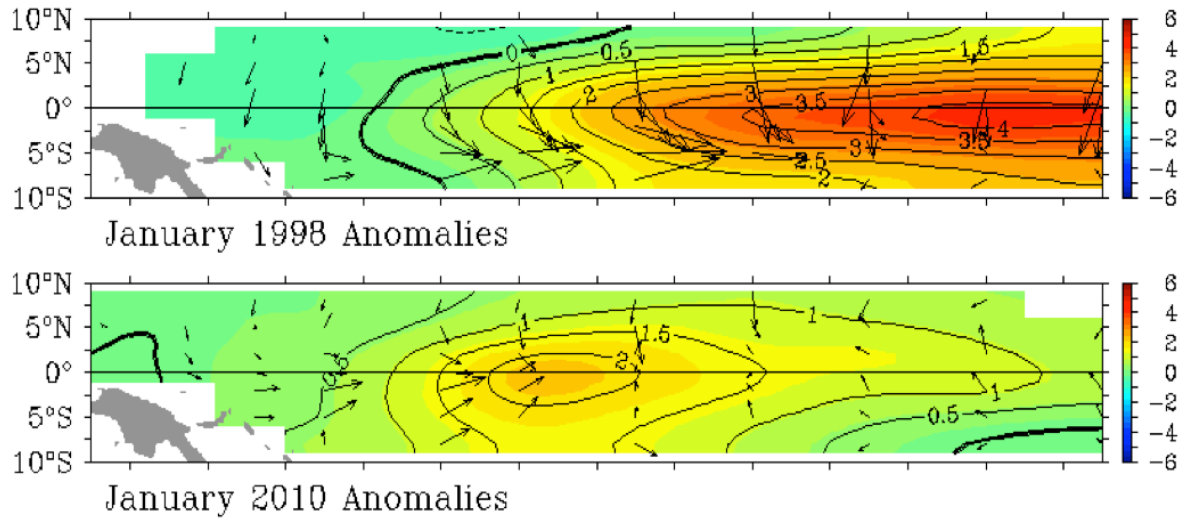

Figure 14.23: Sea surface temperature anomalies and anomalous surface wind vectors on January 1998 and January 2010. Former and latter events are one of the biggest Eastern Pacific El Nino and Central Pacific El Nino in 20th century, respectively. Contour intervals are 0.5 degrees. Courtesy of TOGA TAO.

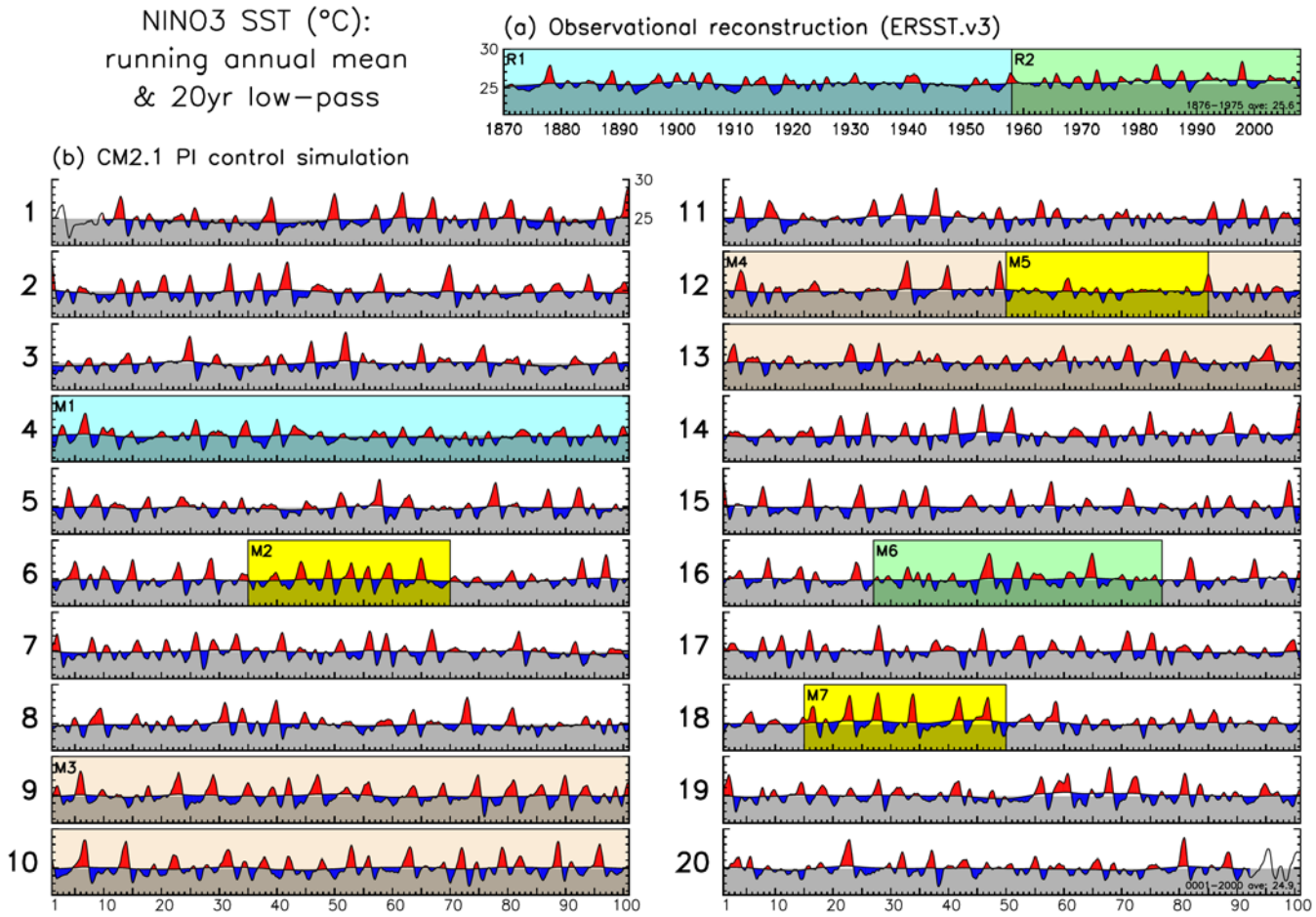

Figure 14.24: SST (°C) averaged over the Niño3 region (150°W–90°W, 5°S–5°N), for (a) the ERSST.v3 historical reconstruction of Smith et al. (2008), and (b) the 20 consecutive centuries (numbered) from the GFDL CM2.1 pre-industrial control run. Red/blue shading highlights departures of the running annual-mean SST from the multidecadal background state, where the latter is obtained via a 211-month triangle smoother which transmits (25, 50, 75)% of the time series amplitude at periods of (15, 20, 30) year. Unshaded time series ends in Figure 14.24 indicate the half-width of the triangle smoother; ends of the observed time series in panel (a) are zero-padded prior to smoothing. The top of the grey bar is the long-term mean, indicated at the bottom right of each plot (Wittenberg, 2009).

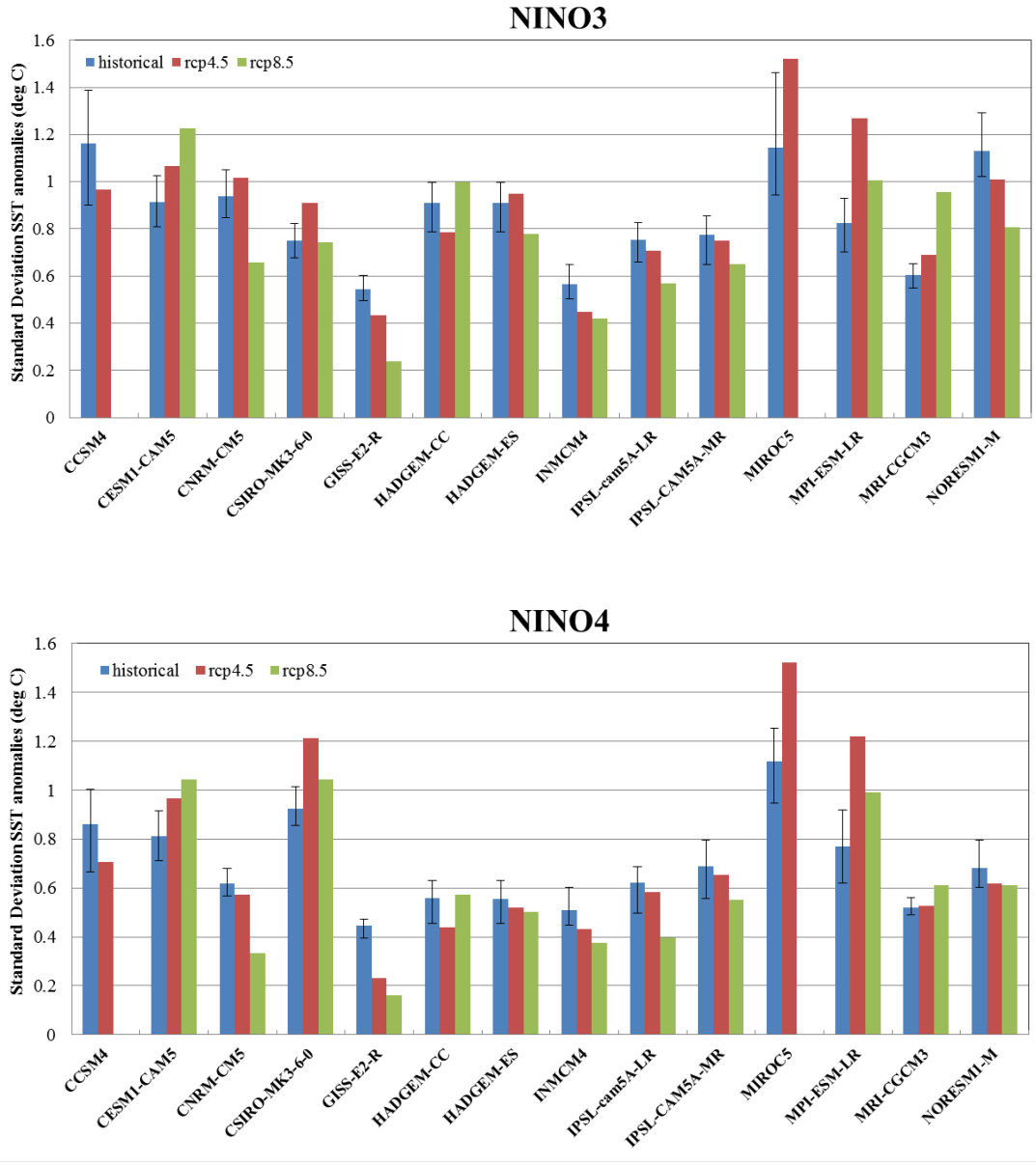

Figure 14.25: Standard deviation of Niño3 (upper) and Niño4 (lower) SST anomalies for CMIP5 model experiments. Blue bars, pre-industrial control experiments, dark red bars, last half of 21 century from the RCP4.5 experiments, yellow green bars, last half of 21 century from RCP8.5 experiments. Calculations are performed for the models indicated on the x-axis, and the linear trend has been removed in RCP4.5 and RCP8.5. The black 'error bar' indicates the minimum and maximum of 50-year windowed standard deviation of Niño index anomalies computed from the pre-industrial control experiments.

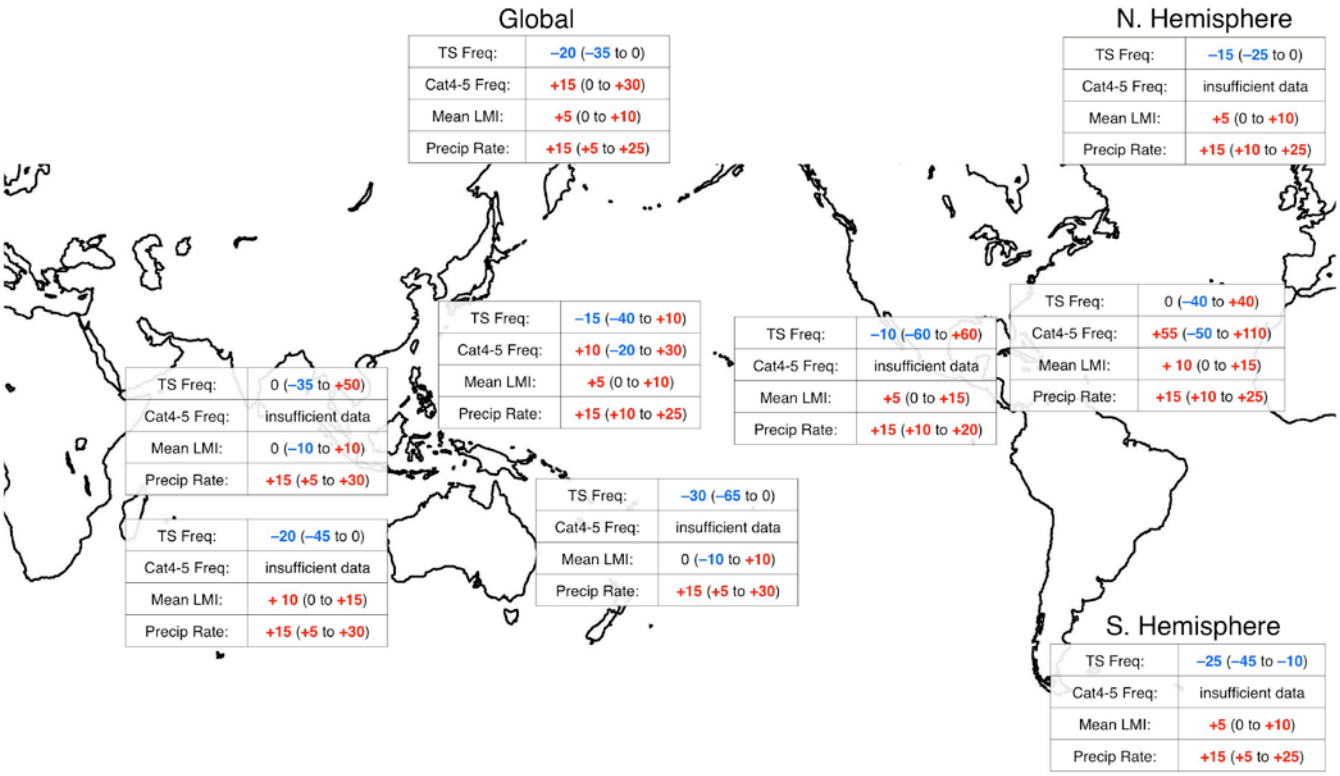

Box 14.2, Figure 1: General consensus assessment of the numerical experiments described in Box 14.2, Tables 1-4. All values represent *expected percent change* (year 2100 relative to 2000) under an A1B-like scenario, based on expert judgment after subjective normalisation of the model projections. Four metrics were considered: the percent change in 1) the total annual frequency of tropical storms, 2) the annual frequency of Category 4 and 5 storms, 3) the mean Lifetime Maximum Intensity (LMI; the maximum intensity achieved during a storm's lifetime), and 4) the precipitation rate within 200 km of storm center at the time of LMI. For each metric, the first numeric value is the best guess of the expected percent change, and the range in parentheses is the 67% (*likely*) confidence interval for this value. There are nine regions considered: Global, Northern Hemisphere, Southern Hemisphere, Eastern North Pacific, North Atlantic, Northern Indian, Southern Indian, Western North Pacific, and South Pacific.

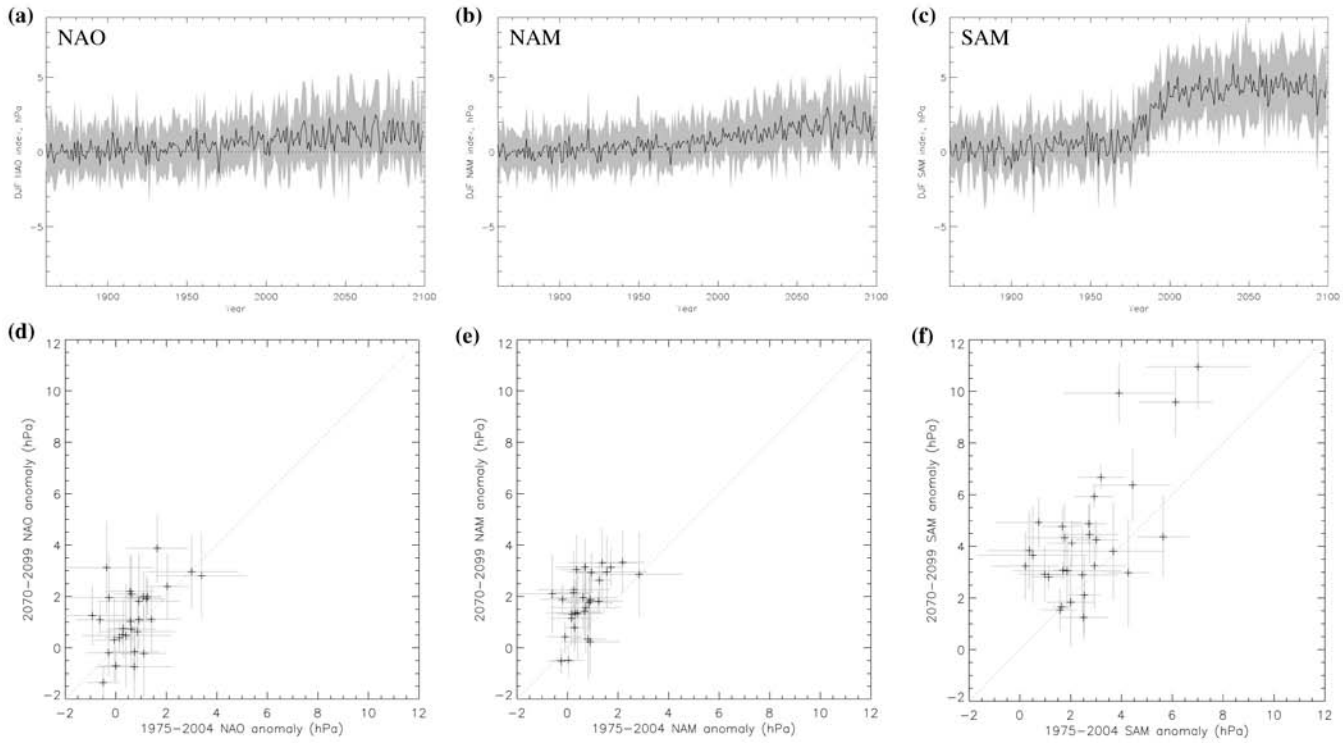

Figure 14.26: Summary of multi-model ensemble simulations of wintertime mean NAO, NAM and SAM sea-level pressure indices for historical and RCP4.5 scenarios produced by 30 climate models participating in CMIP5. Panels a-c) show time series of the ensemble mean (black line) and inter-quartile range (grey shading) of the mean index for each model. Panels d-f) show scatter plots of individual model 2070–2099 time means versus 1975–2004 time means (black crosses) together with (–2,+2) standard error bars. The NAO index is defined here as the difference of regional averages: (90°W–60°E, 20°N–55°N) minus (90°W–60°E, 55°N–90N) (Stephenson and Pavan, 2003). The NAM and SAM are defined as zonal indices: NAM as the difference in zonal mean SLP at 35°N and 65°N (Li and Wang, 2003) and SAM as the difference in zonal mean SLP at 40°S and 65°S (Gong and Wang, 1999). All indices have been centered to have zero time mean from 1861–1900. Comparison of simulated and observed trends from 1961–2011 is shown in Figure 10.11.

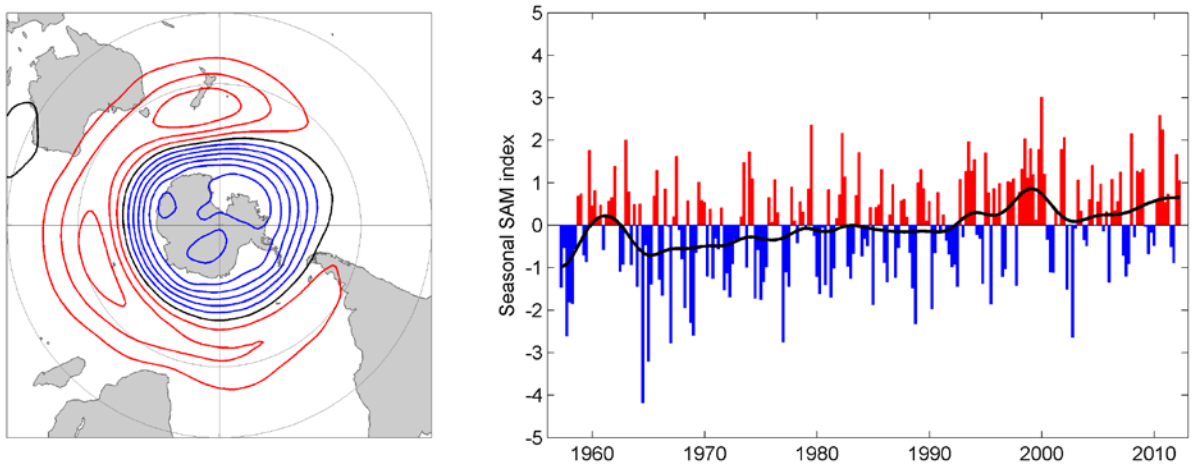

Figure 14.27: Left – the annual mean pattern of the positive SAM in the 850 hPa monthly height anomaly field (average height anomalies when the amplitude time series is +1 standard deviation). Positive contours are red, negative are blue and zero is black. The contour interval is 5 m. Right – the seasonal-mean amplitude of the SAM pattern, taken from station data (courtesy G. Marshall, British Antarctic Survey, http://www.antarctica.ac.uk/met/gjma/sam.html). The black line illustrates the long-term trend, calculated by heavily smoothing the raw seasonal amplitude time series with seven applications of a 13-point binomial filter (Trenberth et al., 2007b, Appendix 3A).

(a)

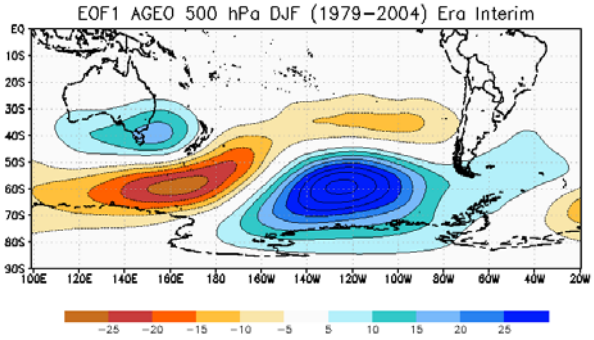

(c)

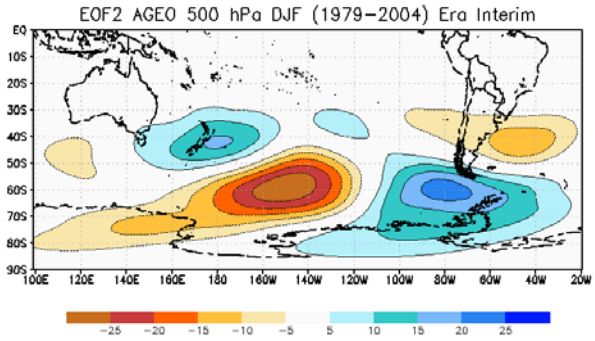

(b)

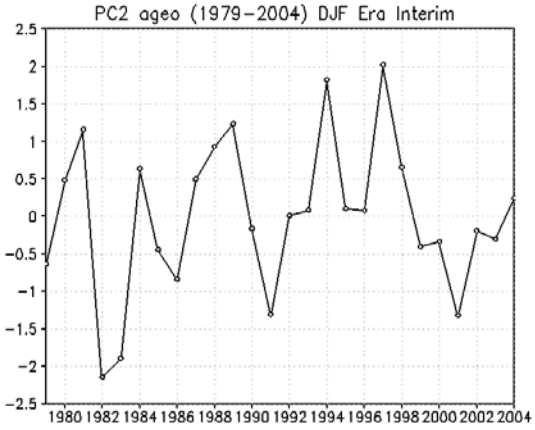

(d)

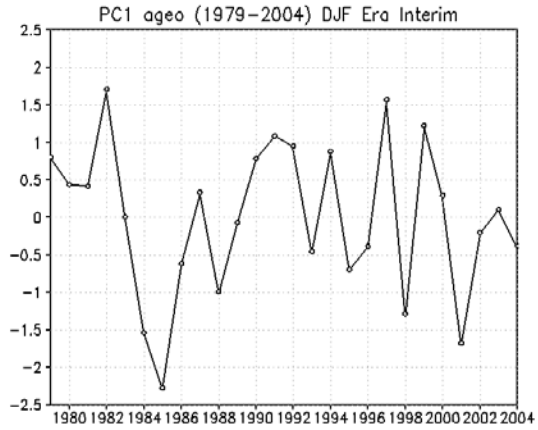

Figure 14.28: (a) PSA1 in DJF from zonal asymmetric geopotential anomaly at 500 hPa (Era Interim); (b) C1 amplitudes series (1979–2004); (c) PSA2 in DJF from zonal asymmetric geopotential anomaly at 500 hPa (Era Interim); (d) PC2 amplitudes series (1979–2004).

(a)

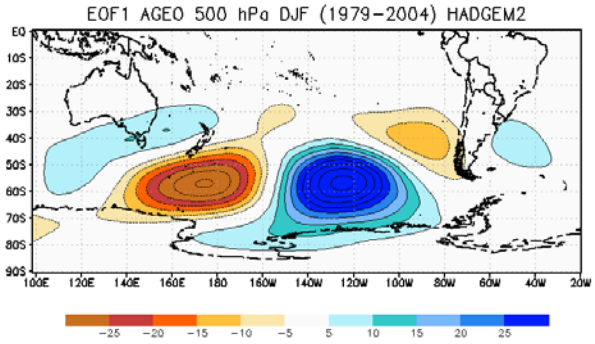

(c)

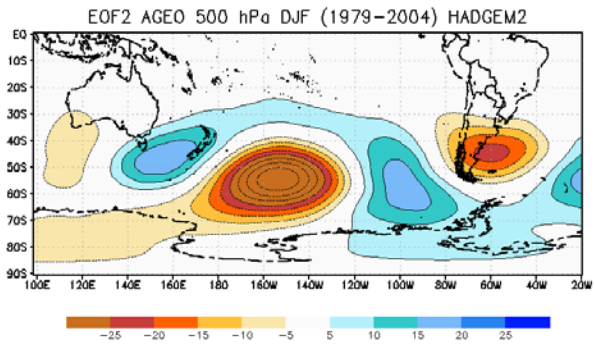

(b)

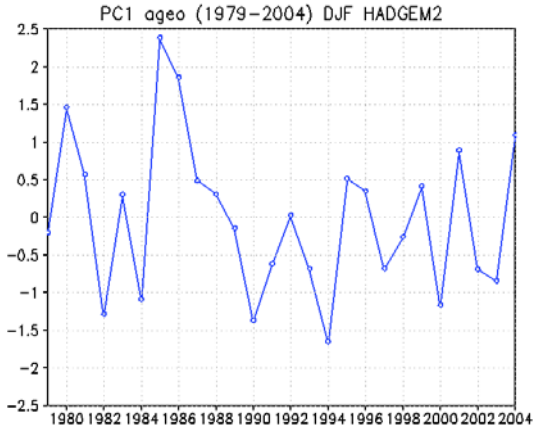

(d)

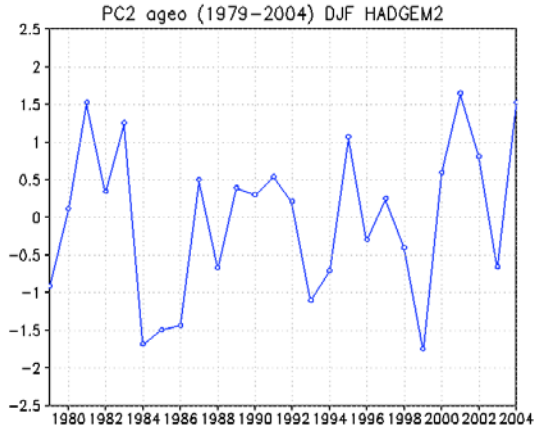

Figure 14.29: (a) PSA1 in DJF from zonal asymmetric geopotential anomaly at 500 hPa (HADGEM2-historical); (b) PC1 amplitudes series (1979–2004); (c) PSA2 in DJF from zonal asymmetric geopotential anomaly at 500 hPa (HADGEM2-historical); (d) PC2 amplitudes series (1979–2004).

(a)

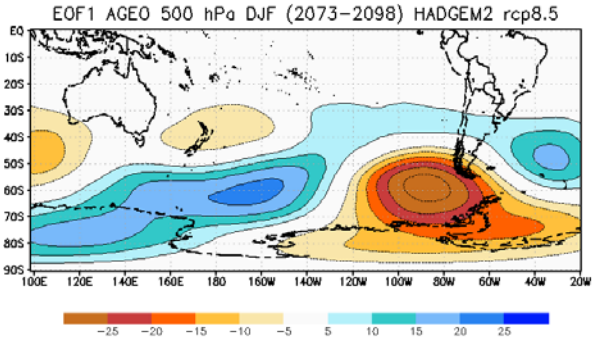

(c)

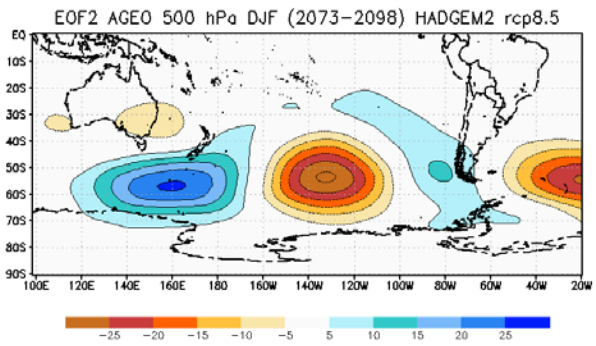

(b)

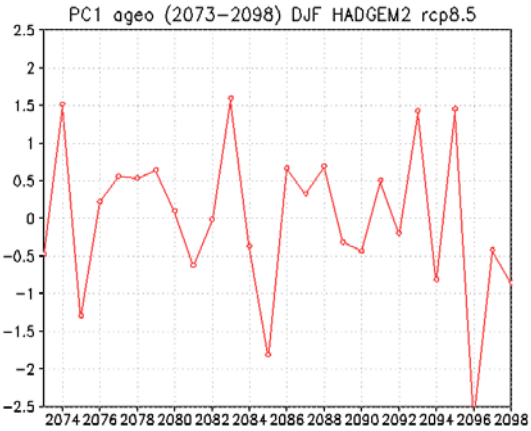

(d)

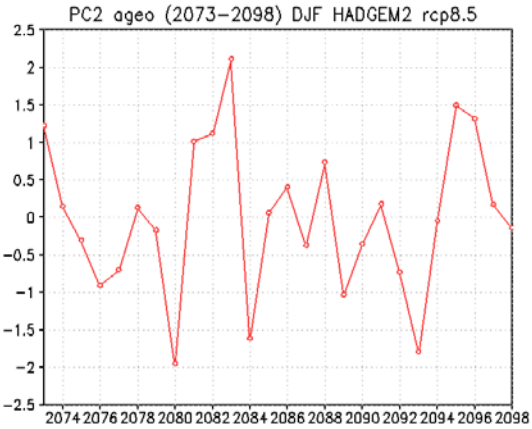

Figure 14.30: (a) PSA1 in DJF from zonal asymmetric geopotential anomaly at 500 hPa (HADGEM2-CP8.5); (b) PC1 amplitudes series (2073–2098); (c) PSA2 in DJF from zonal asymmetric geopotential anomaly at 500 hPa (HADGEM2-RCP8.5); (d) PC2 amplitudes series (2073–2098).

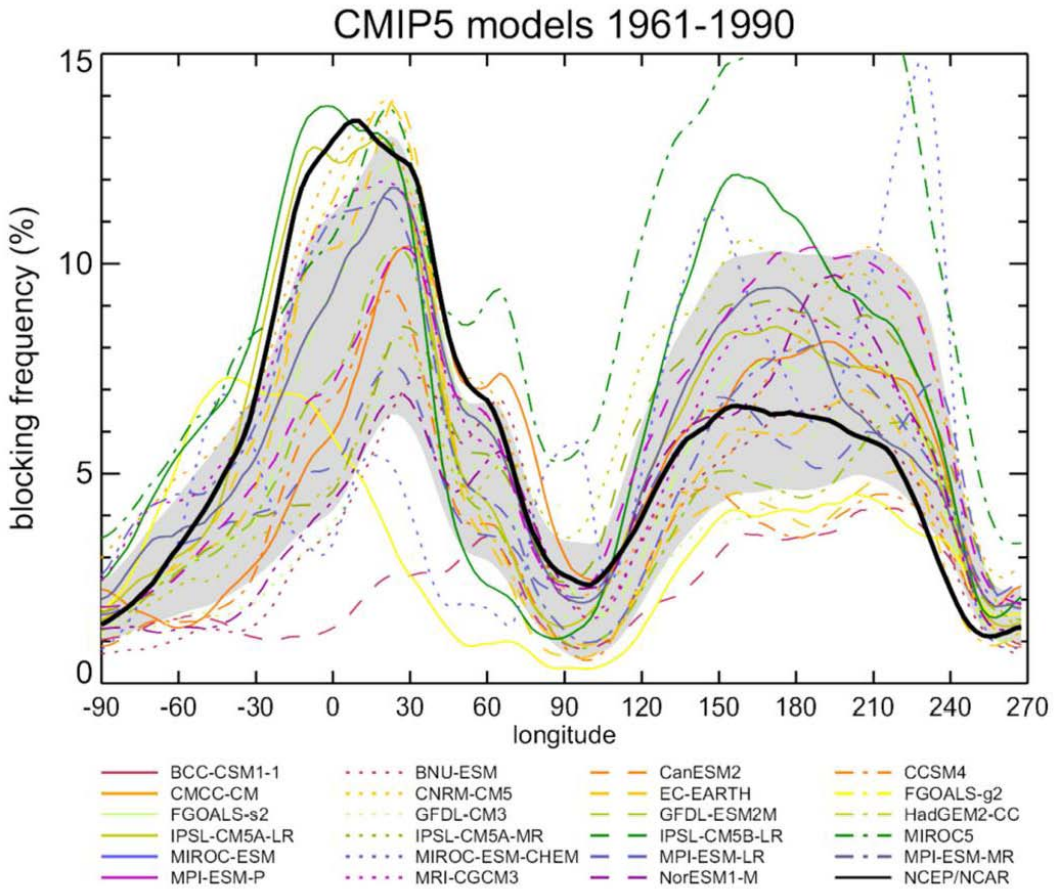

Figure 14.31: Annual mean blocking frequency in the Northern Hemisphere (expressed in % of time, i.e., 1% means ~4 days per year) as simulated by a suite of CMIP5 models (color lines) for the 1961–1990 period of one run of the historical simulation. Grey shading shows the mean model result plus/minus one standard deviation. Black thick line indicates the observed blocking frequency derived from the NCEP/NCAR reanalysis. Only CMIP5 models with available 500 hPa geopotential height daily data at http://pcmdi3.llnl.gov/esgcet/home.htm have been used. Blocking is defined as in (Barriopedro et al., 2006), which uses a modified version of the (Tibaldi and Molteni, 1990) index. Daily data was interpolated to a common regular 2.5° × 2.5° longitude-latitude grid before detecting blocking.

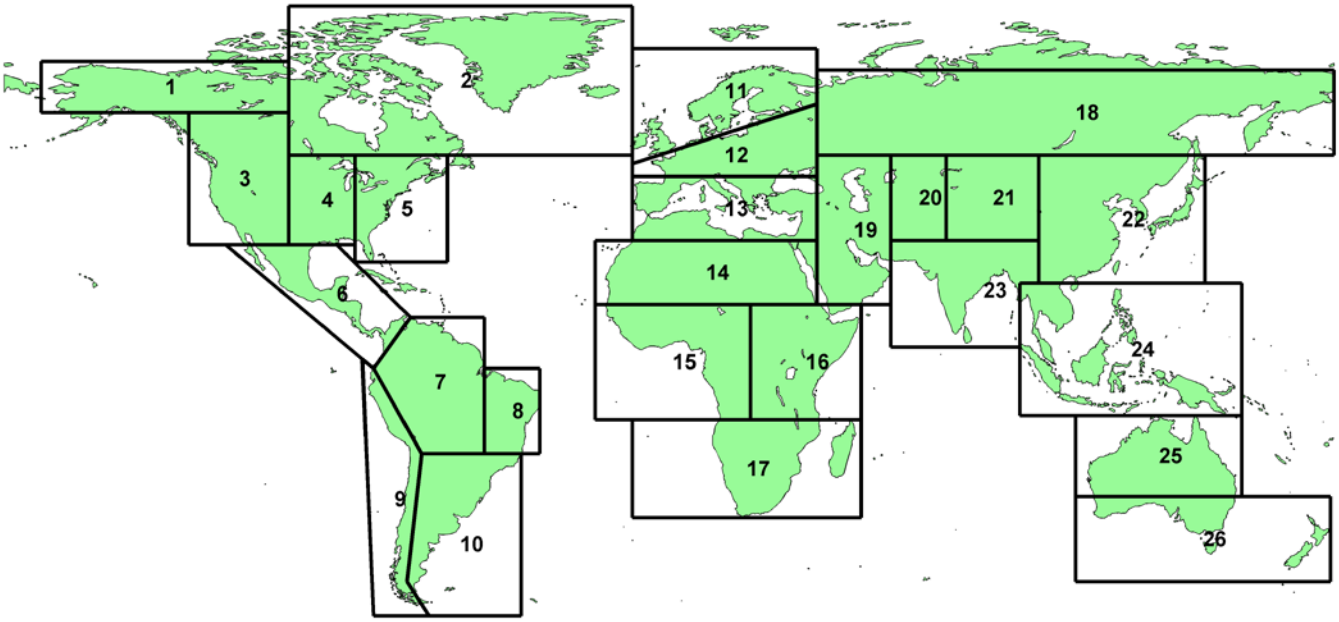

Figure 14.32: Spatial extent of 26 sub-regions covering different climate zones. Analyses in this chapter are performed for land grid points only, unless stated otherwise in the text. Region names and coordinates are given in Table 14.2. See also Seneviratne et al. (2012). [To be updated and confirmed with Atlas].

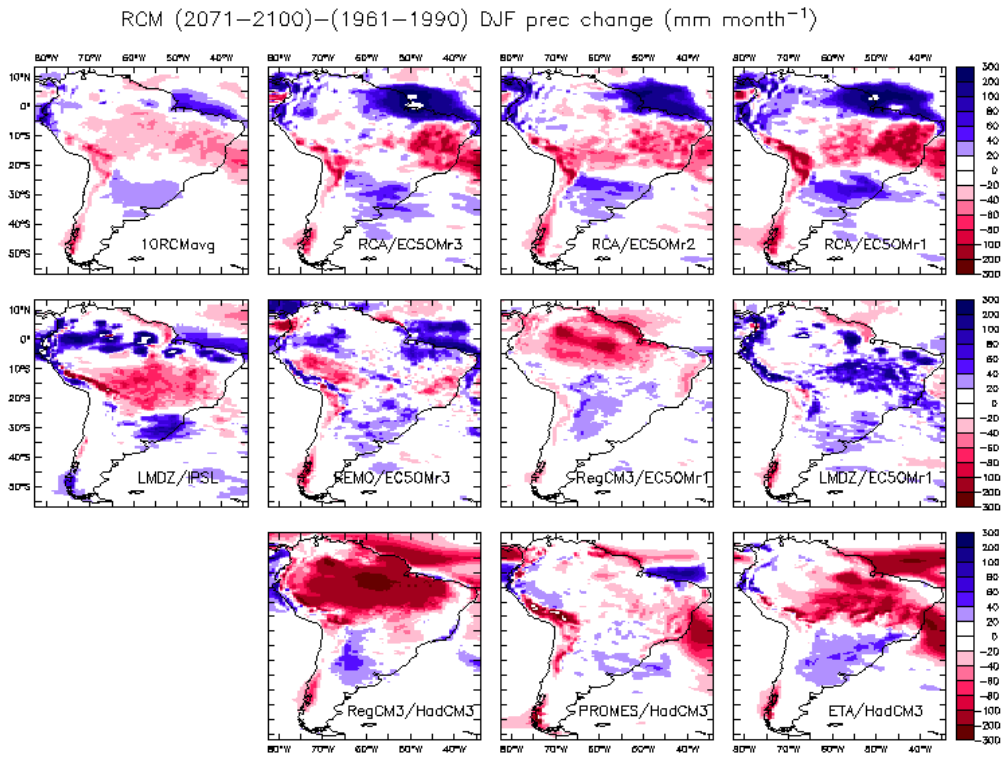

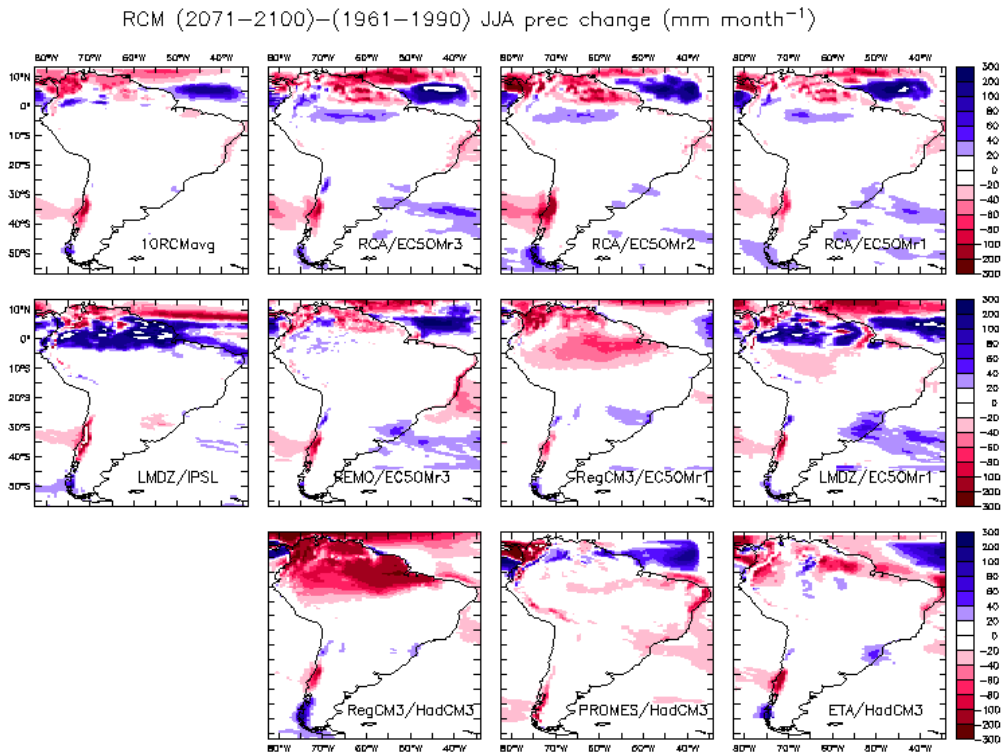

Figure 14.33: Precipitation changes (2071–2100) – (1961–1990) projected by three members of RCA, LMDZ, REMO, REgCM3,PROMES, ETA, and the ensemble mean.

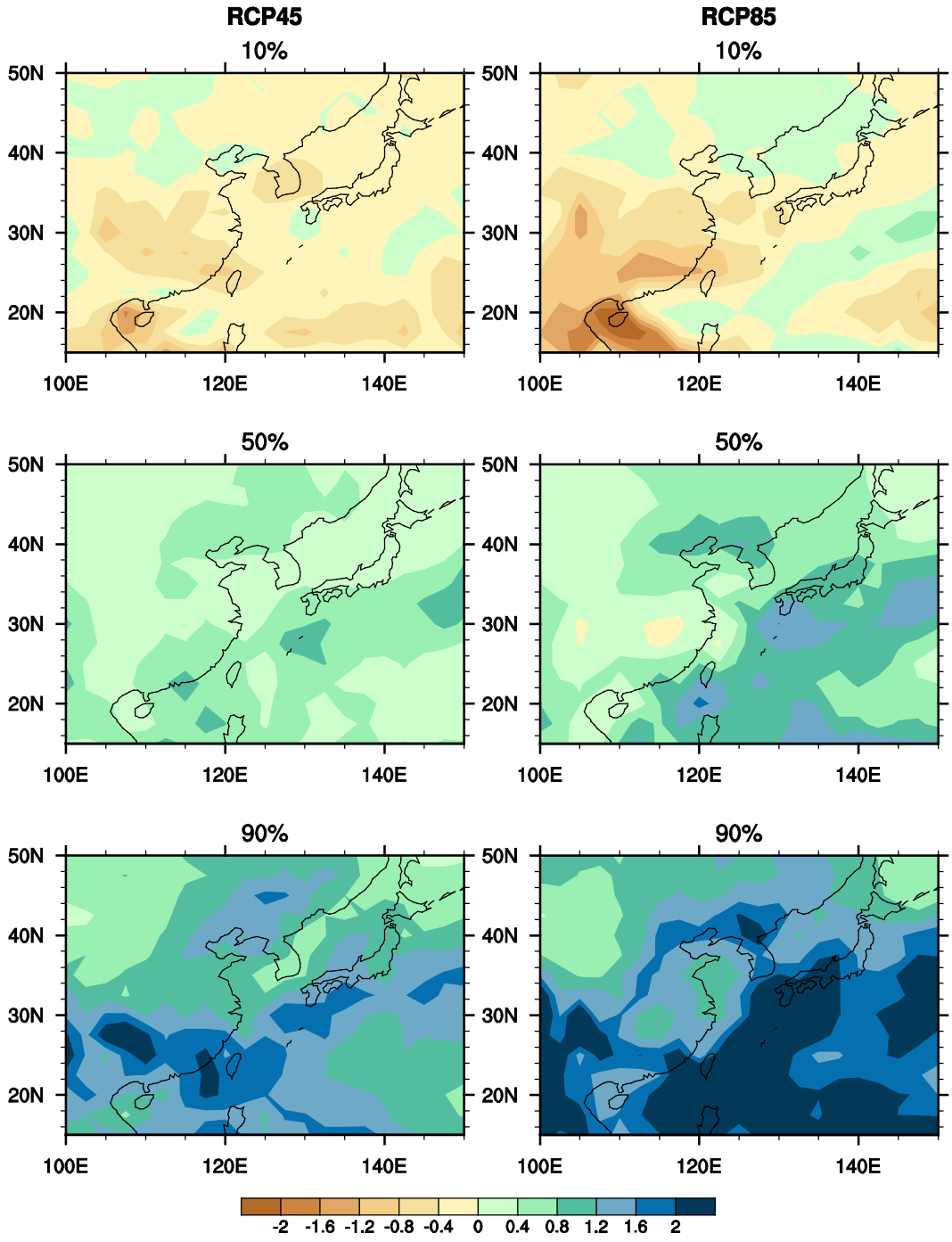

Figure 14.34: June to August precipitation anomalies over East Asia. RCP4.5 (left column) and RCP8.5 (right column) simulations (2080–2099) relative to historical simulation (1980–1999) by 15 CMIP5 model ensembles are shown in 10th, 50th and 90th percentile.

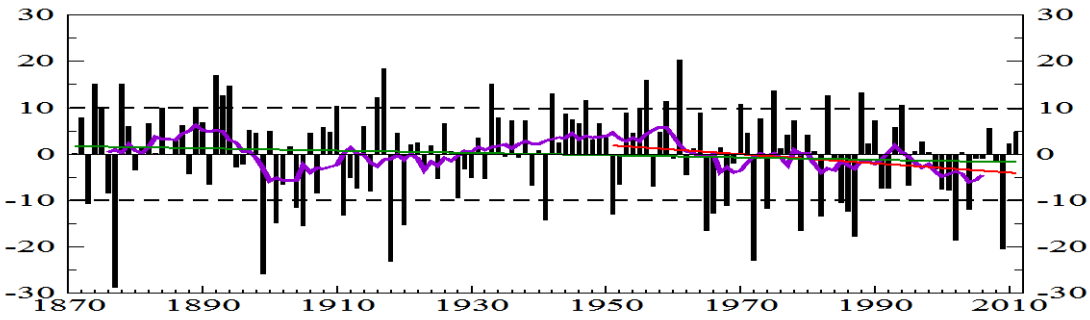

Figure 14.35: Inter-annual variability of Indian summer monsoon rainfall (1871–2011). The smooth curve is the 11-year moving average filtered series which shows epochal variability. The fitted trend lines are also shown : green (entire period) and red (post 1950s). The dotted lines depict ±10% departures from long-term mean. X-axis denotes years and Y-axis the percentage departures from long-term mean.

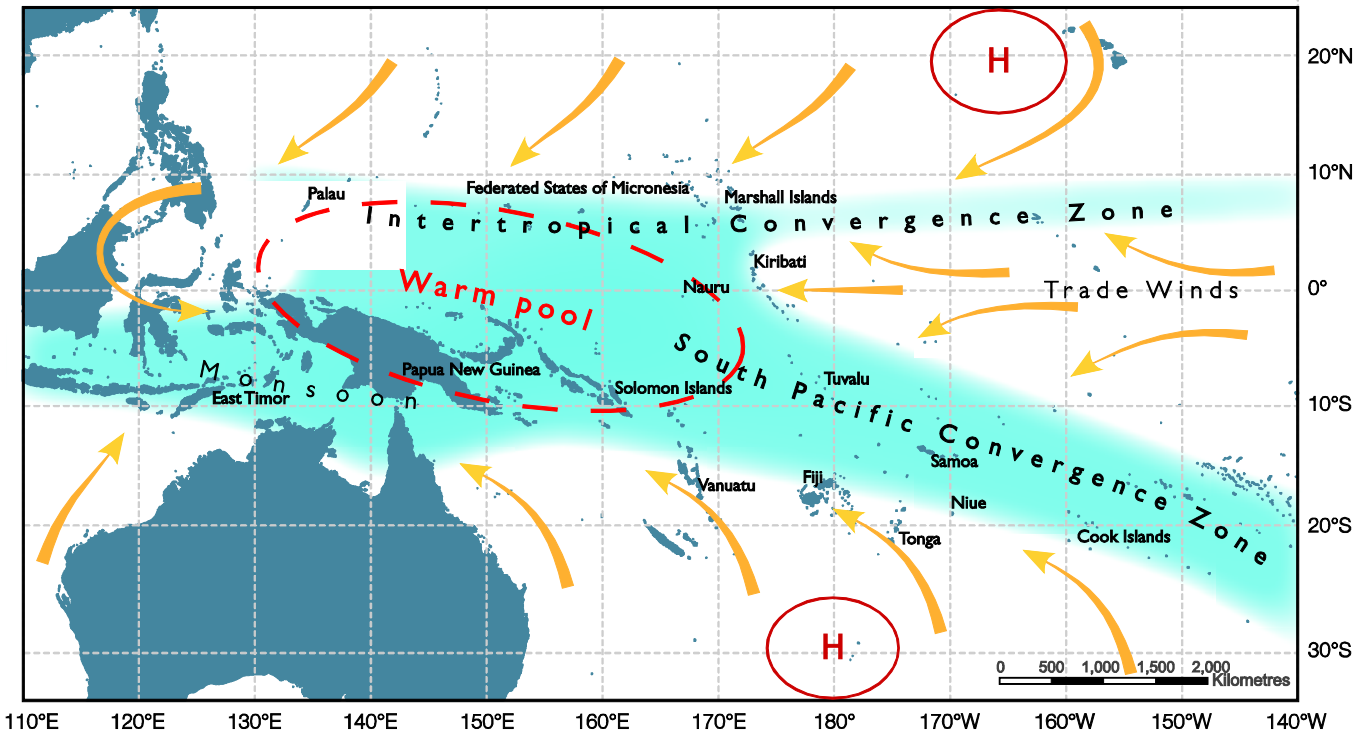

Figure 14.36: Locations of the Pacific Climate Change Science Program (PCCSP) partner countries (all of which are labelled) and the dominant features of the regional climate in the western Pacific Ocean. Grey dashed lines indicate the boundary of the 'PCCSP region' used in much of the analysis, and orange arrows indicate the dominant wind flows. This is taken from the BoM-CSIRO Report (2011).

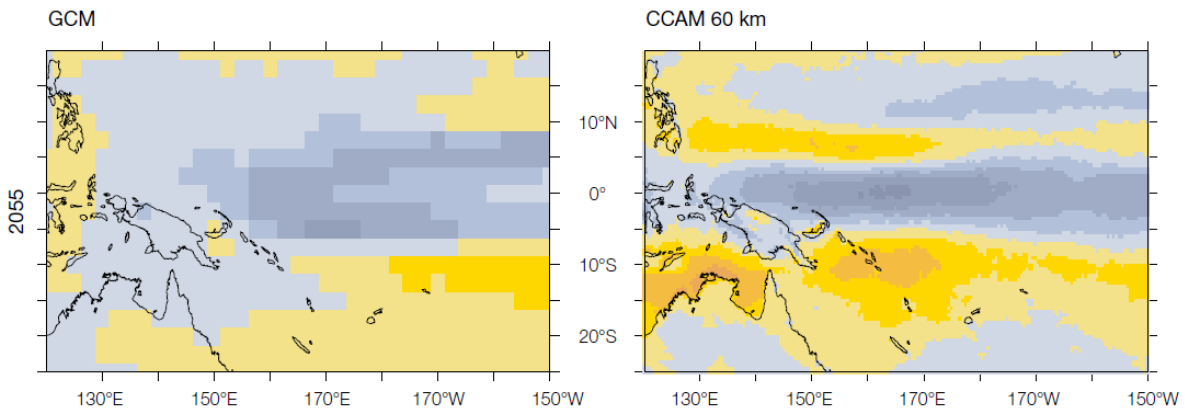

Figure 14.37: Multi-model mean change in November to April rainfall (mm day^{-1}) in global climate models (left) and CCAM 60 km simulations (right), each consisting of the same six models, for the 30-year period centred on 2055, relative to a 30-year period centred on 1990, using the A2 (high) emissions scenario.

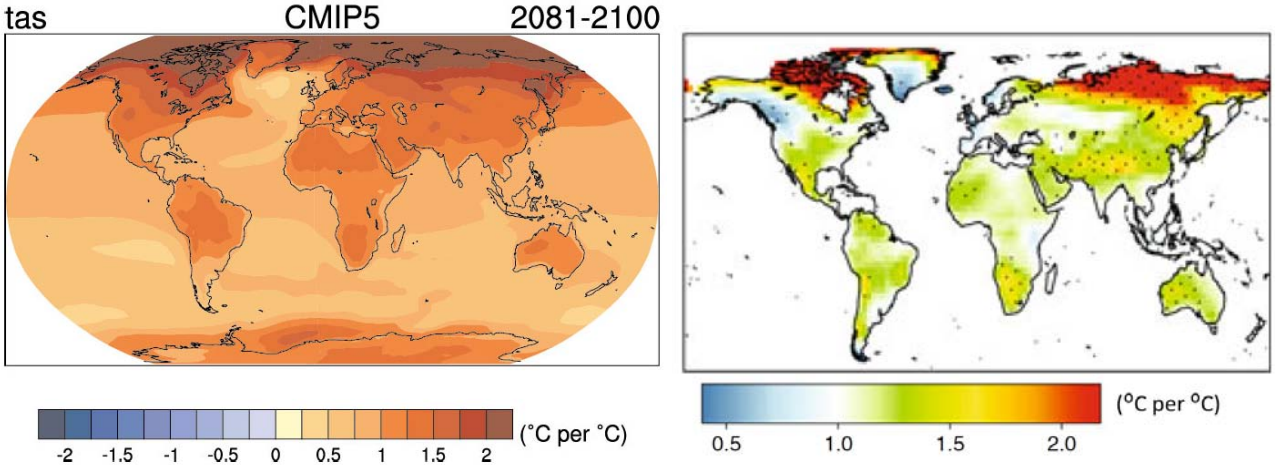

FAQ 14.1, Figure 1: (Left) Average pattern of surface warming projected for the final decade of the 21st century from a suite of Coupled Model Intercomparison Project Phase 5 models (taken from Chapter 12, Figure 12.40). Units are change per degree of global warming. (Right) Change during December to February in the 90th percentile of daily maximum temperature, as a fraction of the globally and annually averaged increase of median maximum temperature (from Orlowsky and Seneviratne, 2012).

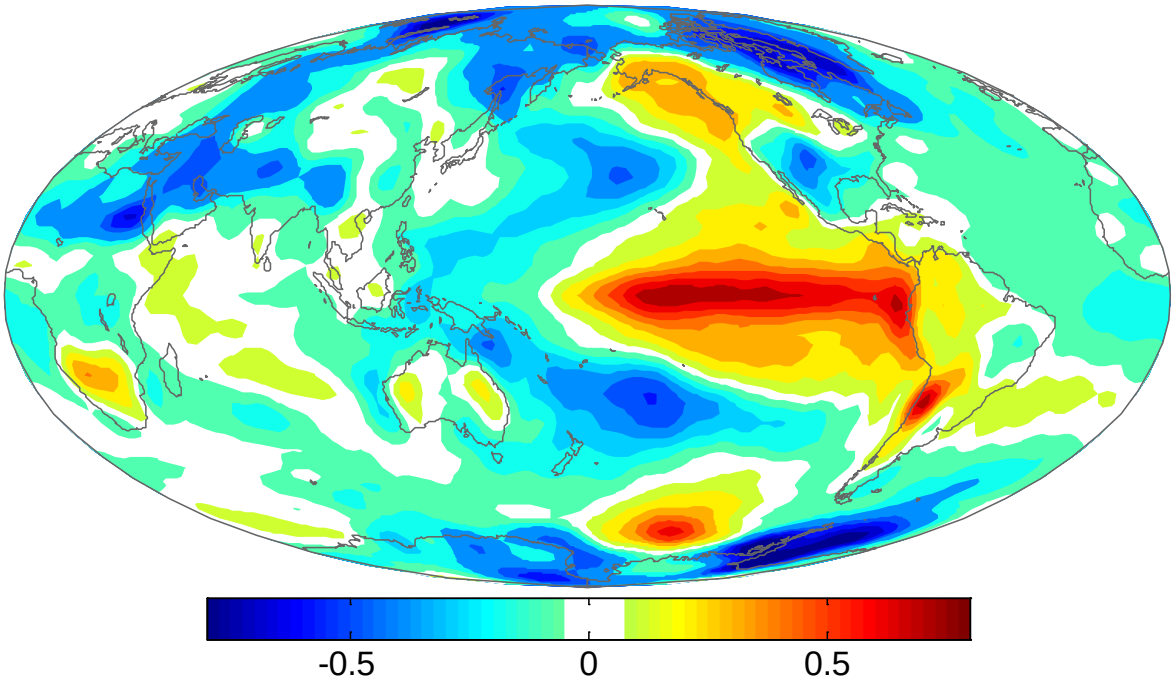

FAQ 14.1, Figure 2: Pattern of covariance between seasonal surface temperature anomalies and the Southern Oscillation Index (SOI). Colours show the average temperature anomaly pattern for an SOI value of –1 (El Niño event). Units are °C.

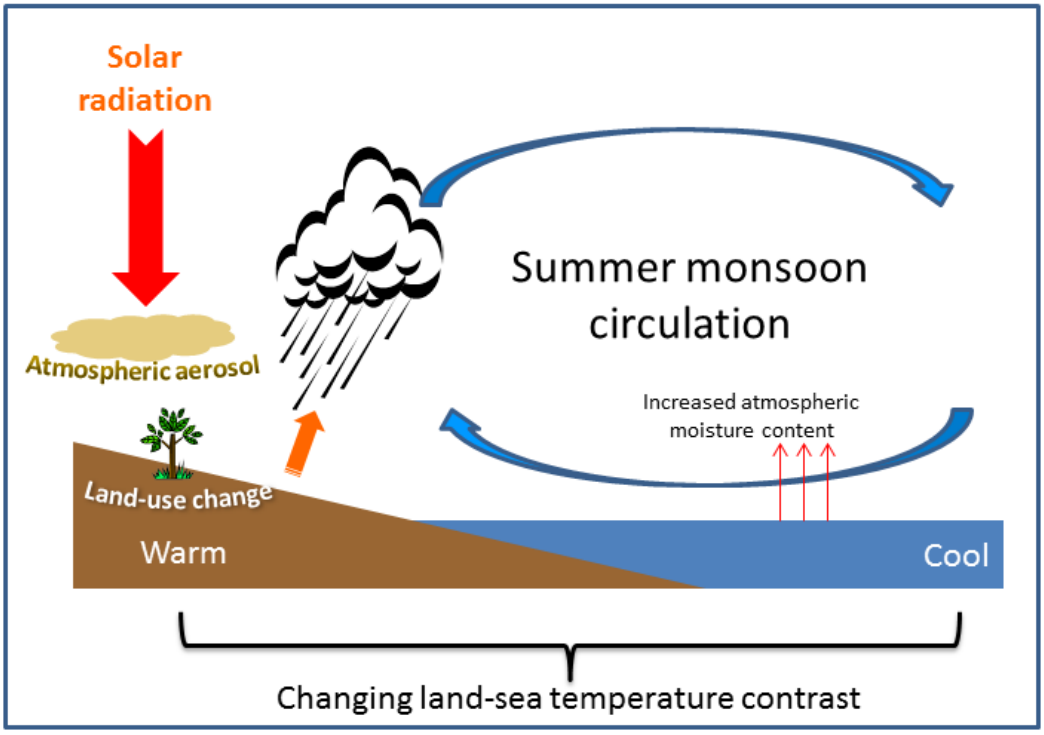

FAQ 14.2, Figure 1: Schematic diagram illustrating the main ways that human activity influences monsoon circulations. As the climate warms, the basic driver of the summer monsoon, land-sea temperature difference, is increasing since the land surface warms faster than the ocean. Also, warmer air contains more water vapour, increasing the potential for heavy rainfalls. Land use change and atmospheric aerosol loading can affect the amount of solar radiation that is absorbed. Other effects (not illustrated here) include warming-related changes in large-scale circulation that influence the strength and extent of the overall monsoon circulation.